STOMATAL BIOLOGY AND BEYOND

EDITED BY: Wenxiu Ye, Juan Dong and Toshinori Kinoshita

PUBLISHED IN: Frontiers in Plant Science

frontiers Research Topics

ISSN 1664-8714
ISBN 978-2-88974-620-0
DOI 10.3389/978-2-88974-620-0

About Frontiers

Frontiers is more than just an open-access publisher of scholarly articles: it is a pioneering approach to the world of academia, radically improving the way scholarly research is managed. The grand vision of Frontiers is a world where all people have an equal opportunity to seek, share and generate knowledge. Frontiers provides immediate and permanent online open access to all its publications, but this alone is not enough to realize our grand goals.

Frontiers Journal Series

The Frontiers Journal Series is a multi-tier and interdisciplinary set of open-access, online journals, promising a paradigm shift from the current review, selection and dissemination processes in academic publishing. All Frontiers journals are driven by researchers for researchers; therefore, they constitute a service to the scholarly community. At the same time, the Frontiers Journal Series operates on a revolutionary invention, the tiered publishing system, initially addressing specific communities of scholars, and gradually climbing up to broader public understanding, thus serving the interests of the lay society, too.

Dedication to Quality

Each Frontiers article is a landmark of the highest quality, thanks to genuinely collaborative interactions between authors and review editors, who include some of the world's best academicians. Research must be certified by peers before entering a stream of knowledge that may eventually reach the public - and shape society; therefore, Frontiers only applies the most rigorous and unbiased reviews.
Frontiers revolutionizes research publishing by freely delivering the most outstanding research, evaluated with no bias from both the academic and social point of view. By applying the most advanced information technologies, Frontiers is catapulting scholarly publishing into a new generation.

What are Frontiers Research Topics?

Frontiers Research Topics are very popular trademarks of the Frontiers Journals Series: they are collections of at least ten articles, all centered on a particular subject. With their unique mix of varied contributions from Original Research to Review Articles, Frontiers Research Topics unify the most influential researchers, the latest key findings and historical advances in a hot research area! Find out more on how to host your own Frontiers Research Topic or contribute to one as an author by contacting the Frontiers Editorial Office: frontiersin.org/about/contact

STOMATAL BIOLOGY AND BEYOND

Topic Editors:
Wenxiu Ye, Shanghai Jiao Tong University, China
Juan Dong, The State University of New Jersey, United States
Toshinori Kinoshita, Nagoya University, Japan

Citation: Ye, W., Dong, J., Kinoshita, T., eds. (2022). Stomatal Biology and Beyond. Lausanne: Frontiers Media SA. doi: 10.3389/978-2-88974-620-0

Table of Contents

frontiers in Plant Science

EDITORIAL
published: 11 February 2022
doi: 10.3389/fpls.2022.848811

Editorial: Stomatal Biology and Beyond

Wenxiu Ye[1,2]*, *Juan Dong*[3,4]* and *Toshinori Kinoshita*[5,6]*

[1] Shanghai Collaborative Innovation Center of Agri-Seeds, Center for Viticulture and Enology, School of Agriculture and Biology, Shanghai Jiao Tong University, Shanghai, China, [2] Shanghai Urban Forest Ecosystem Research Station, National Forestry and Grassland Administration, Shanghai, China, [3] Waksman Institute of Microbiology, Rutgers, The State University of New Jersey, Piscataway, NJ, United States, [4] Department of Plant Biology, Rutgers, The State University of New Jersey, New Brunswick, NJ, United States, [5] Institute of Transformative Bio-Molecule, Nagoya University, Nagoya, Japan, [6] Graduate School of Science, Nagoya University, Nagoya, Japan

Keywords: stomata, guard cell, biotechnology, development, signaling

Editorial on the Research Topic

Stomatal Biology and Beyond

Stomata, each surrounded by a pair of guard cells, are microscopic pores in the shoot epidermis of plants, which serve as a low-resistance pathway for the diffusional movement of gas and water vapor between a plant and the environment. On the other hand, as natural openings in the leaf, stomata are exploited as a convenient entry route by a wide range of pathogens. In adaption to the ever-changing environment, guard cells have acquired sensing mechanisms to a variety of internal and external stimuli resulting in the change of turgor pressure in guard cells. As a result, stomata open and close, by which the plant actively regulates gas exchange with the environment including CO_2 uptake and over 90% water transpiration, and wards off pathogens. Therefore, stomata have a central impact on regulating plant photosynthesis, water status, and stress resistance at the plant physiology level, and on crop production as well as the global carbon and water cycle at the social-ecological level. Stomatal biology has been consistently one of the major research fields of plant science and develops rapidly as evidenced by several research collections on this Research Topic (Blatt et al., 2017; Raghavendra and Murata, 2017; McAdam et al., 2021) as well as the 15 articles in this Research Topic. These Research Topics have provided great insights into the fundamental mechanisms underlying stomatal movement, development, and patterning at both the molecular and systemic levels, making guard cell one of the best-characterized model systems for plant cell and developmental biology. There is also increasing interest in the translation of the knowledge to crop production. The present Frontiers Research Topic covers recent research and review papers on the Research Topics of stomatal development, stomatal dynamics in response to environmental cues, and stomatal manipulation technologies.

Stomate is a fascinating model for developmental biology, not only for its highly specialized division and differentiation processes, also for the formation of isolated guard cells without plasmodesmata. The asymmetric divisional behavior and seemingly random yet one-cell-spaced distribution pattern provide an ideal system for studying cell polarity and cell-division orientation (Pillitteri and Dong, 2013). In this Research Topic, Han et al. overview the recent advances in understanding the molecular basis of cell fate and dynamics of stomatal lineage cells at the cell state- or single-cell level and the regulation of stomatal development by environmental cues. Xiao et al. performed a comprehensive functional analysis of *Arabidopsis* guard cell-enriched GDSLs Lipases (GGLs) and determined several GGLs are involved in regulating stomatal density and

Edited and reviewed by:
Yuree Lee,
Seoul National University,
South Korea

***Correspondence:**
Wenxiu Ye
yewenxiu@sjtu.edu.cn
Juan Dong
dong@waksman.rutgers.edu
Toshinori Kinoshita
kinoshita@bio.nagoya-u.ac.jp

Specialty section:
This article was submitted to Plant Cell Biology, a section of the journal Frontiers in Plant Science

Received: *05 January 2022*
Accepted: *19 January 2022*
Published: *11 February 2022*

Citation:
Ye W, Dong J and Kinoshita T (2022) Editorial: Stomatal Biology and Beyond. Front. Plant Sci. 13:848811. doi: 10.3389/fpls.2022.848811

morphology. Stomata in dicot and monocots are different in morphology with kidney shape for dicots and dumbbell shape for monocots. In addition, the monocot stomatal complex consists of two subsidiary cells surrounding two guard cells. Therefore, research on monocots is necessary to fully understand stomatal development. Based on a forward genetic screening, Yu et al. find a protein with unknown function, Rice Stomata Development Defect 1, is important for stomatal development in rice and appears to regulate proper expression of the protease gene, *Stomatal Density and Distribution 1*. Serna provides a perspective on the functions of a master regulator, the MUTE transcription factor, in the last step of stomatal development in monocots.

Stomatal movement responding to environmental stimuli including light, CO_2, and dehydration, is a major research area of stomatal biology because of their important role in photosynthesis and water use efficiency. In this Research Topic, Liu et al. find that a cyclophilin, ROC3, positively regulates the stress hormone abscisic acid-induced stomatal closure and dehydration response by regulating reactive oxygen species homeostasis and transcription of stress-response genes. Several GGLs identified by Xiao et al. are also involved in stomatal dynamics and plant water relations. In terms of light signaling in guard cells, Ye et al. identify several new genes including a vacuolar channel, Aluminum-Activated Malate Transporter 6, required for in blue light-induced stomatal opening. A pharmacological study by Wang et al. suggests that a group of proteinases are required for light signaling in guard cells. The stomatal responses are quite different in crassulacean acid metabolism (CAM) and C3 plants. A typical difference is that CAM stomata open in the dark and close in response to light, while C3 stomata operate in an opposite way. In this Research Topic, Santos et al. investigated the stomatal response to light and CO_2 in C3 and CAM plants, using *Vicia faba* and *Kalanchoë fedtschenkoi* as model plants. This elegant study provides evidence that both signals from guard cells and mesophyll contribute to the differences observed in CAM and C3 stomatal responses. Research on stomatal immune responses against pathogens has been very active these years with a focus on the short-term defenses (Thor et al., 2020; Ye et al., 2020). Here, Gahir et al. raise an interesting point on the long-term effect of stomatal closure in terms of defense against pathogen and discuss possible research directions.

One important goal of research on stomatal biology is, by developing new strategies to manipulate stomatal development, activity and/or physiology, to improve crop resilience and water use efficiency. To this end, there is also a trend shifting from using model plants to crops for research. In this Research Topic, Hayashi et al. constructed a gene expression database of *V. faba* and found ABA-dependent phosphorylation of the *V. faba* orthologs of important genes known to be involved in the stomatal movement including a basic helix–loop–helix transcription factor *VfAKS1*, an ABA importer in guard cells *VfABCG40*, and a clathrin heavy chain *VfCHC1*. These results set the basis for future research on stomatal biology in *V. faba*. Pitaloka et al. reveal the functions of rice stomatal mega-papillae in stomatal dynamics, defense against pathogens, highlighting its potential as an important trait for rice breeding. Stomatal phenotyping is critical for field study, which is greatly facilitated by the emerging machine-learning-based imaging analysis. Zhu et al. build up a method based on machine learning to automatically assess the stomatal index in wheat. Moreover, Toda et al. report the establishment of a readily available image-analysis platform to accelerate stomatal phenotyping in the field. Regarding manipulation approaches of stomatal traits, agrochemicals have been proved very effective (Kinoshita et al., 2021). The protease inhibitors (PIs) identified by Wang et al. could be the lead compounds for manipulating stomatal movement. A more efficient and environmental-friendly approach would be genetic technology. The guard cell-specific promoters identified by Ye et al. are a plus to the toolkits for designing guard cell-targeting genetic strategies. A beautiful example to show the contribution of genetic manipulation of stomata to crop production is the establishment of the "PUMP" technique short for the promotion and upregulation of plasma membrane proton-ATPase (Zhang et al., 2021). By increasing the expression level of plasma membrane H^+-ATPases in guard cells, this strategy has been proved very efficient for enhancing photosynthesis and thus plant growth. In this Research Topic, Ren et al. review the progress and synthesize the principle of this technique. Toh et al. report the technique is also efficient in enhancing photosynthesis and growth of perennial woody plants using poplar as a model.

CONCLUDING REMARKS

Stomate is an evolution success for plants to colonize land some 450 million years ago. Because of its importance to plant physiology, there is continuing scientific effort to understand its evolution path, mechanism of its biogenesis and function, and potential for translation. The current Research Topic accommodates new findings on most of these areas and is dedicated to stimulating future research on stomatal biology. More research efforts are needed on new research directions, such as guard cell metabolism, cell wall mechanics, memory mechanism, as well as on many economically important plants. Particularly, we want to highlight two research areas under development, stomatal traits influenced by biotic stimuli and pollutants from human activity, because of their importance in crop protection and climate control. Regarding stomatal biotechnology, we have witnessed striking progress as a result from combining approaches of genetics, optics, and chemistry (Papanatsiou et al., 2019; Kinoshita et al., 2021). These research findings underline the importance of incorporating knowledge from multi-disciplines to realize innovation with broad impact. We believe stomatal biotechnology is a powerful strategy to achieve sustainable development goals including crop production improving and climate control. Bearing this in mind, this Research Topic is delivered as a call for more participation of scientists from different fields.

AUTHOR CONTRIBUTIONS

WY wrote the first draft. All authors contributed to the article and approved the submitted version.

FUNDING

This work was supported by the National Natural Science Foundation of China (31901984 to WY), the National Institute of Health (GM131827 to JD), the National Science Foundation (1851907, 1952823, and 2049642 to JD), and Grants-in-Aid for Scientific Research from the Ministry of Education, Culture, Sports, Science, and Technology, Japan (20H05687 and 20H05910 to TK).

ACKNOWLEDGMENTS

We would like to thank all the authors in this Research Topic for their excellent manuscripts and working under a defined deadline and all the reviewers for providing constructive comments and suggestions.

REFERENCES

Blatt, M. R., Brodribb, T. J., and Torii, K. U. (2017). Small pores with a big impact. *Plant Physiol.* 174, 467–469. doi: 10.1104/pp.17.00642

Kinoshita, T., Toh, S., and Torii, K. U. (2021). Chemical control of stomatal function and development. *Curr. Opin. Plant Biol.* 60:102010. doi: 10.1016/j.pbi.2021.102010

McAdam, S. A. M., Chater, C. C. C., Shpak, E. D., Raissig, M. T., and Dow, G. J. (2021). Editorial: linking stomatal development and physiology: from stomatal models to non-model species and crops. *Front. Plant Sci.* 12:743964. doi: 10.3389/fpls.2021.743964

Papanatsiou, M., Petersen, J., Henderson, L., Wang, Y., Christie, J. M., and Blatt, M. R. (2019). Optogenetic manipulation of stomatal kinetics improves carbon assimilation, water use, and growth. *Science* 363, 1456–1459. doi: 10.1126/science.aaw0046

Pillitteri, L. J., and Dong, J. (2013). Stomatal development in arabidopsis. *Arabidopsis Book* 2013:e162. doi: 10.1199/tab.0162

Raghavendra, A. S., and Murata, Y. (2017). Editorial: signal transduction in stomatal guard cells. *Front. Plant Sci.* 8:114. doi: 10.3389/fpls.2017.00114

Thor, K., Jiang, S., Michard, E., George, J., Scherzer, S., Huang, S., et al. (2020). The calcium-permeable channel OSCA1.3 regulates plant stomatal immunity. *Nature* 585, 569–573. doi: 10.1038/s41586-020-2702-1

Ye, W., Munemasa, S., Shinya, T., Wu, W., Ma, T., Lu, J., et al. (2020). Stomatal immunity against fungal invasion comprises not only chitin-induced stomatal closure but also chitosan-induced guard cell death. *Proc. Natl. Acad. Sci. U. S. A.* 117, 20932–20942. doi: 10.1073/pnas.1922319117

Zhang, M., Wang, Y., Chen, X., Xu, F., Ding, M., Ye, W., et al. (2021). Plasma membrane H^+-ATPase overexpression increases rice yield *via* simultaneous enhancement of nutrient uptake and photosynthesis. *Nat. Commun.* 12:735. doi: 10.1038/s41467-021-20964-4

Conflict of Interest: The authors declare that the research was conducted in the absence of any commercial or financial relationships that could be construed as a potential conflict of interest.

Publisher's Note: All claims expressed in this article are solely those of the authors and do not necessarily represent those of their affiliated organizations, or those of the publisher, the editors and the reviewers. Any product that may be evaluated in this article, or claim that may be made by its manufacturer, is not guaranteed or endorsed by the publisher.

frontiers in Plant Science

ORIGINAL RESEARCH
published: 30 November 2020
doi: 10.3389/fpls.2020.600021

RSD1 Is Essential for Stomatal Patterning and Files in Rice

*Qi Yu, Liang Chen, Wenqi Zhou, Yanhuang An, Tengxiao Luo, Zhongliang Wu, Yuqi Wang, Yunfeng Xi, Longfeng Yan and Suiwen Hou**

Key Laboratory of Cell Activities and Stress Adaptations, Ministry of Education, School of Life Sciences, Lanzhou University, Lanzhou, China

Stomatal density is an important factor that determines the efficiency of plant gas exchange and water transpiration. Through forward genetics, we screened a mutant *rice stomata developmental defect 1* (*rsd1-1*) with decreased stomatal density and clustered stomata in rice (*Oryza sativa*). After the first asymmetric division, some of the larger sister cells undergo an extra asymmetric division to produce a small cell neighboring guard mother cell. Some of these small cells develop into stomata, which leads to stomatal clustering, and the rest arrested or developed into pavement cell. After map-based cloning, we found the protein encoded by this gene containing DUF630 and DUF632 domains. Evolutionary analysis showed that the *DUF630/632* gene family differentiated earlier in land plants. It was found that the deletion of *RSD1* would lead to the disorder of gene expression regarding stomatal development, especially the expression of *stomatal density and distribution 1* (*OsSDD1*). Through the construction of *OsSDD1* deletion mutants by CRISPR-Cas9, we found that, similar to *rsd1* mutants, the *ossdd1* mutants have clustered stomata and extra small cells adjacent to the stomata. *OsSDD1* and *RSD1* are both required for inhibiting ectopic asymmetric cell divisions (ACDs) and clustered stomata. By dehydration stress assay, the decreased stomatal density of *rsd1* mutants enhanced their dehydration avoidance. This study characterized the functions of *RSD1* and *OsSDD1* in rice stomatal development. Our findings will be helpful in developing drought-resistant crops through controlling the stomatal density.

Keywords: stomatal development, stomatal density, *RSD1*, *OsSDD1*, dehydration avoidance, rice

OPEN ACCESS

Edited by:
Juan Dong,
Rutgers, The State University of New Jersey, United States

Reviewed by:
Xingyun Qi,
Rutgers, The State University of New Jersey, United States
Jie Le,
Institute of Botany (CAS), China

****Correspondence:***
Suiwen Hou
housw@lzu.edu.cn

Specialty section:
This article was submitted to Plant Cell Biology, a section of the journal Frontiers in Plant Science

Received: *02 September 2020*
Accepted: *23 October 2020*
Published: *30 November 2020*

Citation:
Yu Q, Chen L, Zhou W, An Y, Luo T, Wu Z, Wang Y, Xi Y, Yan L and Hou S (2020) RSD1 Is Essential for Stomatal Patterning and Files in Rice. Front. Plant Sci. 11:600021. doi: 10.3389/fpls.2020.600021

INTRODUCTION

Stomata are small valves in the epidermis of plants for gas exchange between plants and the environment and play essential roles in regulating photosynthesis and water use efficiency (Hetherington and Woodward, 2003). Proper stomatal density and patterning are very important for the growth of plants. There are great differences in stomatal patterning and development processes between monocotyledons and dicotyledons. In *Arabidopsis*, stomata are constantly generated in different positions of the epidermis during leaf development. The asymmetric entry division of some protodermal cells named meristemoid mother cell (MMC) initiates the stomatal lineage and produces a larger daughter cell called stomatal lineage ground cell (SLGC) and a smaller meristemoid (M). The M can undergo asymmetrically amplifying divisions to renew itself and generate more SLGCs. Then, the

M converts into the guard mother cell (GMC). The GMC divides equally to form a pair of guard cells (GCs). The SLGCs can differentiate into pavement cells or divide asymmetrically to produce a new M oriented away from preexisting stomata or stomatal precursors (Bergmann and Sack, 2007).

Most of crops belong to grasses, and they have a great impact on food security (Godfray et al., 2010; Elert, 2014). In contrast to the scattered pattern of *Arabidopsis* leaves, stomata in graminoid grasses (monocots) are distributed in files. Stomatal development in rice consists of six stages. Epidermal cells that acquired lineage fate undergo an asymmetric entry division to produce two daughter cells, a small cell, and a large sister cell (Stages I and II) (Stebbins and Shah, 1960; Luo et al., 2012; Raissig et al., 2016; Wu et al., 2019; McKown and Bergmann, 2020). Since the absence of a stem-cell-like meristemoid stage in the rice stomatal development, the small cell is named GMC (Stebbins and Shah, 1960; Nunes et al., 2020). The GMC induces the polarization of the subsidiary mother cell (SMC), which then divides asymmetrically to produce a subsidiary cell (SC) and a pavement cell (Stage III and Stage IV) (Cartwright et al., 2009; Facette et al., 2015). After that, GMCs divide symmetrically to produce a pair of GCs (Stage V). Finally, the four-cell stomatal complex is formed (Stage VI) (Stebbins and Shah, 1960).

The stomatal lineage cell fate transformation mechanism has been well studied in *Arabidopsis*. Three basic helix-loop-helix (bHLH) family transcription factors SPEECHLESS (SPCH), MUTE, and FAMA control the consecutive MMC-M-GMC-GC cell fate transitions (Ohashi-Ito and Bergmann, 2006; MacAlister et al., 2007; Pillitteri et al., 2007; Lampard et al., 2008; Chen et al., 2020). These specified cell state transitions require another two paralogous bHLH transcription factors, INDUCER OF CBF EXPRESSION1 (ICE1) and SCREAM2 (SCRM2), to form heterodimers with SPCH, MUTE, and FAMA (Kanaoka et al., 2008). In addition, the cell fate transition from GMC to GC is regulated by FOUR LIPS (FLP) and MYB88, two partially redundant R2R3 MYB transcription factors (Lai et al., 2005; Lee et al., 2014).

Recently, the molecular mechanisms that promote stomatal development in grasses are gradually elucidated. In grasses, the new factors OsSCRs/OsSHRs control the initiation of stomatal lineage cells, and the formation of SCs has been reported recently (Schuler et al., 2018; Wu et al., 2019). The core factors regulating stomatal fate transformation have similar but different functions. OsSPCH1/2 control formation of stomatal files (Raissig et al., 2016; Wu et al., 2019). *OsMUTE* is expressed in early stage of GMCs and moves to SMC to regulate SC formation. In addition, OsMUTE is involved in the direction of GMC division (Raissig et al., 2017; Wang et al., 2019; Wu et al., 2019). OsFAMA influences SMC division and differentiation of mature stomata (Liu et al., 2009; Wu et al., 2019). OsICE1 and OsICE2 influence the initiation of stomatal lineage, GMC transition, SMC division, and the differentiation of mature stomata (Raissig et al., 2016; Wu et al., 2019). The *OsFLP* regulates the direction of GMC division (Wu et al., 2019). In addition, an A2-type cyclin; OsCYCA2;1 positive regulates entry division in stomatal file (Qu et al., 2018).

The stomatal patterning in *Arabidopsis* follows the one-cell-spacing rule; that is, two stomatal complexes are separated by at least one non-stomatal cell to ensure a reasonable stomatal density and a proper stomatal patterning in different environmental conditions (Lau and Bergmann, 2012; Dow et al., 2014; Qi and Torii, 2018). Epidermal patterning factors (EPFs) include negative regulators *EPF1/2* and *EPFL4-6*, and a positive regulator *EPFL9/STOMAGEN* regulates stomatal density (Hara et al., 2007, 2009; Hunt and Gray, 2009; Abrash and Bergmann, 2010; Sugano et al., 2010; Niwa et al., 2013). These ligands bind to the receptor complex consisting of ERECTA family receptor kinase [RLK; ER, ERECTA-LIKE1 (ERL1), and ERL2] and TOO MANY MOUTHS (TMM) (Shpak et al., 2005; Lee et al., 2012, 2015). Downstream of the receptors is a mitogen-activated protein kinase (MAPK) cascade, which is composed of YODA and MKK4/5/7/9 and MPK3/6 to inhibit SPCH activity (Bergmann et al., 2004; Wang et al., 2007; Lampard et al., 2008). The predicted serine protease STOMATAL DENSITY AND DISTRIBUTION1 (SDD1) also negatively regulate stomatal patterning and density by genetically acting upstream of TMM (Berger and Altmann, 2000; Von Groll et al., 2002). The function of SDD1 in dicotyledonous plants is conserved. Overexpression of tomato *SchSDD1-like* in cultivated tomato plants decreased the stomatal index and density (Morales-Navarro et al., 2018).

The grass stomatal patterning stands in line and also abides by the one-cell-spacing rule that two stomatal complexes are separated by at least one pavement cell. The role of EPFs is conserved in stomatal development. In rice and wheat, the overexpression of *OsEPF1/2* and *TaEPF1/2* has been shown to increase water use efficiency by reducing stomatal density (Hughes et al., 2017; Caine et al., 2019; Dunn et al., 2019). *OsEPFL9* can promote stomatal development, and knocking down *OsEPFL9* reduces stomata density in rice (Lu et al., 2019). In addition, *BdYODA1* in *Brachypodium distachyon* involved in maintaining stomatal lineage fate asymmetry and loss of *BdYODA1* results in large sister cells obtain stomatal fate (Abrash et al., 2018). In maize, the overexpression of *ZmSDD1* results in stomatal density decrease of 30% and enhances the drought resistance (Liu et al., 2015).

In this study, we identified a novel stomatal mutant from EMS mutants' library. This mutant exhibits clustered stomata and reduced stomatal file density and was named as *rice stomata developmental defect 1* (*rsd1*). Detailed analysis of stomatal development process indicated that larger sister cell of entry division underwent excessive asymmetric division in *rsd1-1*. Map-based cloning showed that *RSD1* encoded a protein also named REL2, which functions in controlling leaf rolling. The quantitative reverse transcription–quantitative polymerase chain reaction (RT-qPCR) result indicated that the expression of *OsSDD1* was significantly down-regulated in *rsd1* mutants. Knockout of *OsSDD1* produced similar stomatal phenotype with *rsd1* mutants, clustered stomata, and extra small cells adjacent to the stomata. *OsSDD1* and *RSD1* are both required for inhibiting ectopic ACDs and clustered stomata. More importantly, the looss of *RSD1* decreased stomatal density and resulted in higher dehydration avoidance.

MATERIALS AND METHODS

Plant Materials and Growth Conditions

Rice (*Oryza sativa* L. *japonica* cv. Zhonghua 11, ZH11) was used as the wild type in this study. The *rsd1-1* mutant with clustered stomata was screened from the M2 generation of EMS mutant library and then back-crossed into ZH11 three times prior to use. The *rel2* mutant was acquired from Kunming Chen's lab (**Supplementary Table 1**). The seedlings were grown initially on Murashige and Skoog (MS) medium under 16:8 h, light–dark cycles for 5–7 days and then cultivated in the glasshouse at Lanzhou University (Gansu, China), with a 12 h photoperiod, 60–80% relative humidity, and a day/night temperature of 32°C/22°C.

Dental Resin Impression and Stomatal Density

The dental resin impression method was used to screen mutants *rsd1-1*, *rsd1-2*, *rel2*, *sdd1-1*, and *sdd1-2* with clustered stomata. Fully expanded fourth and fifth rice leaves were used to impress the abaxial side, and the detailed impression procedures and stomatal density statistics were performed through methods in our previous report (Luo et al., 2012).

Imaging and Microscopy Analysis

For confocal imaging, the FM4-64 was captured using a Nikon (A1R+Ti2-E) confocal microscope. The base of the fifth leaf was cut into 0.5 cm pieces stained in FM4-64 solution. The strain method was performed according to our previous report (Wu et al., 2019). Images of the leaf were used for statistical analyses.

Map-Based Cloning of *RSD1*

Plants with the clustered stomata were isolated as recombinants from F2 plants of a cross between the *rsd1-1* (*O. sativa* L. *japonica* cv. Zhonghua 11, ZH11) and 9,311 (*O. sativa* L. *indica*) hybrids were selected using dental resin impressions for mapping. The published RM-series rice simple sequence repeat markers[1] were used to map the mutant gene. The locus was roughly mapped between RM228 and RM590 on the short arm of chromosome 10 by the primary location. Subsequently, the locus was fine mapped onto the ∼440 kb region between two new development markers X-02 and X-08 using 76 homozygote mutants (**Supplementary Table 1**). The markers were designed by Primer Premier 5.0 and the genomic sequence acquired from the Gramene. The candidate gene *RSD1* was identified by sequence analysis of all genes on the region.

Phylogenetic Tree Construction

The genes containing DUF630 and DUF632 domains were identified from the databases JGI, *Marchantia polymorpha* (Bowman et al., 2017), *Physcomitrella patens* (Lang et al., 2018), *Arabidopsis thaliana* (Lamesch et al., 2012), *Medicago truncatula* (Young et al., 2011), *Solanum lycopersicum* (Tomato Genome, 2012), *O. sativa* (Ouyang et al., 2007), *Zea mays* (Schnable et al., 2009), *B. distachyon* (Vogel et al., 2010), *Zostera marina* (Olsen et al., 2016), and *Brachypodium stacei* (Gordon et al., 2020) by using the reciprocal BLAST technique with RSD1 protein sequence. The program BLASTP had an *e*-value cutoff of 1-E30. These sequences were further verified using Simple Modular Architecture Research Tool (SMART) protein analyzing software (Letunic and Bork, 2017). Sequences that were confirmed by both methods were used for further analyses. Eventually, the genes from this species were used for phylogenetic analyses in this study. Full-length amino acid sequences were aligned using CLUSTALW2 (Larkin et al., 2007). The neighbor-joining (NJ) (Saitou and Nei, 1987) tree was constructed by using the Molecular Evolutionary Genetics Analysis version 5.0 (MEGA 5). The tree nodes were evaluated by bootstrap analysis with 1,000 replicates. Branches with bootstrap values less than 50% were collapsed. The evolutionary tree is displayed by Interactive Tree of Life[2] (Letunic and Bork, 2019).

Generation of Mutant Plants by CRISPR/Cas9

The Vector pBGK032 to construct CRISPR/Cas9 line was performed from our previous report (Wu et al., 2019). The targeting sequences of RSD1 and OsSDD1 were selected (**Supplementary Table 2**). The designed targeting sequences were inserted into pBGK032 vector to produce CRISPR/Cas9 plasmids as described previously (Wu et al., 2019). The vectors were transformed into rice cultivars ZH11 as described previously (Nishimura et al., 2006). The transgene lines were extracted genomic DNA and PCR amplification acquired target sequences (**Supplementary Table 1**). The PCR products were sequenced and analyzed by CRISPR-GE[3] (Xie et al., 2017). The mutant lines used in our experiments were predicted resulting truncated protein.

Real-Time PCR Analysis

The method used for extracting the total RNA and RT has been described previously. For quantitative real-time PCR, we used a TB Green Premix Ex Taq (Takara Bio, Inc.) and a StepOnePlus Real-Time PCR System (Applied Biosystems) running a standard programme (**Supplementary Table 1**). For each real-time PCR experiment, individual samples had three biological replicates per experiment, and all experiments were repeated at least three times.

Dehydration Response Analysis: Water Deficit Shock Treatment

For the measurement of water loss from leaves, 8 weeks old fully expanded leaves of rice wild-type plants ZH11 and *rsd1* mutants (*rsd1-1* and *rsd1-2*) were excised and placed on weighing paper with three replicates. All samples were dried slowly under 22°C and 50% relative humidity. The weight was measured every half hour. The percentage of the sample weight at each time point relative to the initial weight was the water loss weight. Three independent experiments were performed.

[1] http://www.gramene.org/

[2] https://itol.embl.de/

[3] http://skl.scau.edu.cn/

RESULTS

rsd1-1 Exhibits Clustered Stomata and Reduced Stomatal Files

By screening EMS mutants' library generated from *O. sativa japonica* cultivar ZH11, we identified a stomatal mutant with clustered stomata, decreased stomatal density, and files (**Figures 1A,B,K–N**). We named the mutant as *rice stomata developmental defect 1* (*rsd1*). In wild type, stomata strictly comply with the principle of "one-cell-spacing rule," that is, two stomatal complexes had to be separated by at least one pavement cell (**Figures 1A,C**). In *rsd1-1*, clustered stomata were observed, and some of them co-use a SC (**Figures 1B,D**). In addition, we observed small cells neighboring some stomata in stomatal file (**Figures 1B,E–G**). Some of the small cells were able to induce an extra SC, but they would not develop into mature stomata (**Figure 1E**). Some of small cells seemed to obtain the fate of pavement cell with lobes (**Figures 1F**, G). Occasionally, we observed that some GMCs exited stomatal lineage before or after inducing unilateral or bilateral SCs (**Figures 1H–J**), suggesting that *RSD1* is required for promoting GMC to differentiate into mature stomata. Statistical analysis revealed that the percentage of clustered stomata or extra small cell neighboring stomata significantly increased (**Figure 1O**). We observed that the stomatal density and stomatal file density of *rsd1-1* decreased in the same position and phyllotaxis of leaf blade (**Figures 1K–N**). Together, these results indicated that *RSD1* regulates stomatal distribution pattern and density.

RSD1 Is Essential for the Differentiation of Large Sister Cells Into Pavement Cell to Establish the Stomatal Patterning

The stomatal patterning and density of grasses are established in a very small area at the base of the leaf. Stomatal development in grasses consists of six stages (**Figures 2A–F**) (Luo et al., 2012; Raissig et al., 2016; Wu et al., 2019). At stage II, the stomatal lineage cells initiate entry division to generate a smaller GMC and a larger sister cell that will differentiate into a pavement cell (Stebbins and Shah, 1960; Raissig et al., 2016; Wu et al., 2019). The direct differentiation of large sister cells into pavement cells determines the establishment of stomatal patterning in stomatal files.

The stomatal development stages of *rsd1-1* were observed. The stomatal development of *rsd1* mutant at stages I and II were regular (**Figures 2G,H,O,P**). At stage III, some of the larger sister cells underwent an extra asymmetric division to produce an extra small cell neighboring GMC (**Figures 2I,Q**). At stage IV, a large number of extra small cells neighboring GMC were produced (**Supplementary Figure S1**). We observed that some SCs flanked a GMC and its neighboring extra small cell (**Figure 2J**). Occasionally, we also observed that the GMCs failed to induce SC formation (**Figure 2R**). At stage V, a few extra small cells neighboring GMC can divide equally to form paired GCs, resulting in clustered stomata (**Figure 2K**), and the rest of the extra small cells neighboring GMC exit stomatal linage (**Figure 2M**). In addition, the arrested GMCs were occasionally observed (**Figure 2S**). At stage VI, the abnormal stomata differentiated into mature stomata and form disrupted pattern (**Figures 2L,N,T**). These observations indicated that *RSD1* is required to prevent ACD in large sister cells' reentry stomatal lineage.

Map-Based Cloning of *RSD1* Gene

Our genetic analysis showed that the clustered stomata of *rsd1-1* were caused by a single recessive mutation. To identify the mutated gene, the map-based cloning strategy was used, and the candidate gene locus was mapped in a 440 kb region between two newly developed molecular markers (X-02 and X-08) in chromosome 10 (**Figure 3A**). Using whole-genome sequencing, we found a 1 bp deletion at the fourth exon of *LOC_Os10g41310*, resulting in a premature transcription termination (PTT) (**Figure 3B**). The rice genome contains only one copy of the *RSD1* gene, which is predicted to encode a protein consisting of 767 amino acid residues. This gene is also named *Rolled and Erect Leaf 2* (*REL2*), which is involved in the control of leaf rolling in rice (Yang et al., 2016).

To confirm whether the stomatal phenotypes of *rsd1-1* were caused by the mutation of *LOC_Os10g41310*, we created an additional frameshift mutation that is 1 bp insertion in the first exon, resulting in a PTT by clustered, regularly interspaced short palindromic repeats–associated nuclease 9 (CRISPR/Cas9). We named this mutant *rsd1-2* (**Supplementary Figure S2**). It exhibited similar stomatal phenotypes with *rsd1-1* (**Figures 3C,D,I**). In addition, similar to *rsd1-1* and *rsd1-2*, the allelic mutant *rel2* produced clustered stomatal and small cell neighboring stomata (**Figures 3E,F,I**), and the stomatal density also decreased (**Figure 3H**). F1 generation plants of a cross between *rsd1-1* and *rsd1-2* show similar phenotypes with *rsd1* mutants (**Figure 3G**). These results indicated that the mutation of the *LOC_Os10g41310* is responsible for stomatal development defects of *rsd1* mutants.

Evolutionary Analysis of RSD1 in Plants

RSD1 encodes a protein containing DUF630 and DUF632 domains (**Supplementary Figure S4**). The BLASTp analysis indicated that there was no homolog of *RSD1* in green alga *Coccomyxa subellipsoidea*. In liverwort *M. polymorpha*, there was only one copy of *RSD1*. In moss *P. patens*, there were four putative paralogs. In dicots and monocots, we found lots of homologous genes contained DUF630 and DUF632 domains, such as *M. polymorpha* (1 sequence), *P. patens* (4 sequences), *A. thaliana* (15 sequences), *M. truncatula* (17 sequences), *S. lycopersicum* (11 sequences), *O. sativa* (20 sequences), *Z. mays* (21 sequences), *B. distachyon* (17 sequences), and *B. stacei* (18 sequences). In order to determine the evolutionary relationship between the *RSD1* proteins with different species, we performed multiple sequence alignment and generated an NJ phylogenetic tree for *RSD1* proteins from nine land plants (**Figure 4**). These genes were divided into clade A containing 45 proteins and clade B containing 74 proteins. Phylogenetic analysis indicated that the homologous genes diverged early in the evolution of land plants (**Figure 4**). Pairwise sequence alignment revealed that RSD1 shows 51.1% amino acid sequence identity with *Arabidopsis AtNRG2*, which plays a key role in nitrate regulation

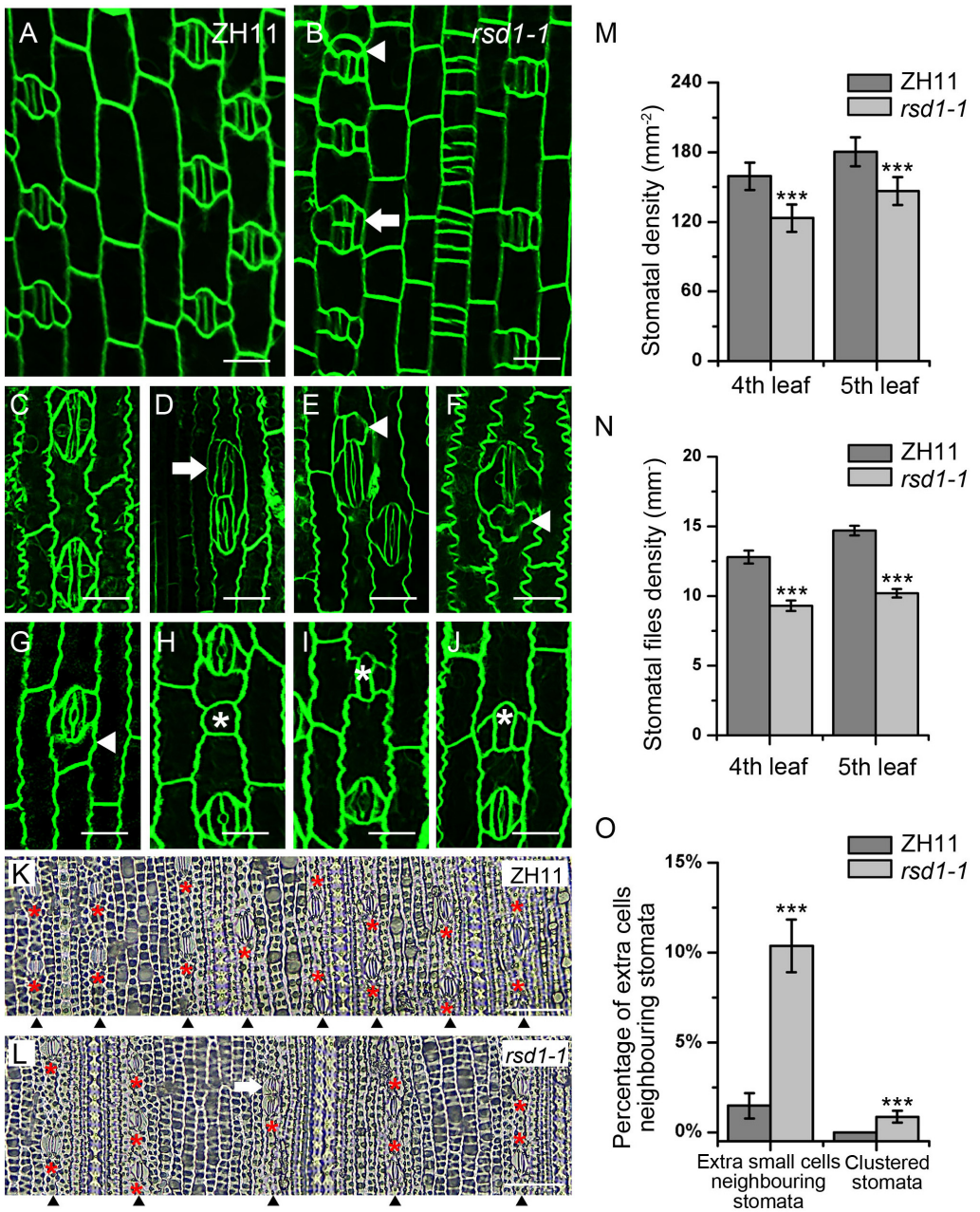

FIGURE 1 | *rsd1-1* mutant showed clustered stomata and an extra small cell neighboring stoma. **(A)** Developing stomata of ZH11. **(B)** Developing stomata of *rsd1-1*. **(C)** Mature stomata of ZH11. **(D)** Two-cluster stomata sharing one subsidiary cell. **(E)** A stoma with three subsidiary cells and a small cell. **(F)** Five-cell stomatal complex. **(G)** An extra small cell neighboring stoma. **(H)** A small cell arrested in GMC stage. **(I)** Arrested GMC with one subsidiary cell. **(J)** Arrested GMC with both sides of subsidiary cell. Bars, 10 μm. The white arrowheads indicated ectopic extra small cells neighboring stomata. The white arrows indicated clustered stomata. The white asterisks indicated arrested GMCs. The red asterisks indicated stomata. **(K)** The stomatal files of ZH11. **(L)** The stomatal files of *rsd1-1*. The white arrowheads indicated stomatal files. Bars, 50 μm. **(M)** Quantification of the stomatal density at mature stage. **(N)** Quantification of the stomatal files at mature stage. **(O)** Quantification of the extra small cells neighboring stomata and clustered stomata at the fifth leave. The error bars indicated the mean ± SEM, $n = 20$; ***$P < 0.001$ by Student's *t*-test.

(Xu et al., 2016). Another gene *APSR1* in this family is required for root meristem maintenance (Gonzalez-Mendoza et al., 2013). These limited results indicated that this gene family had important functions in the process of plant growth and development, and the exploration of the gene function of this new gene family would be able to understand the mechanism of plant growth and development.

The number of DUF630/632 family genes in angiosperm is more than liverwort and moss remarkable (**Figure 4**), indicating that this gene family is growing in richness. The high

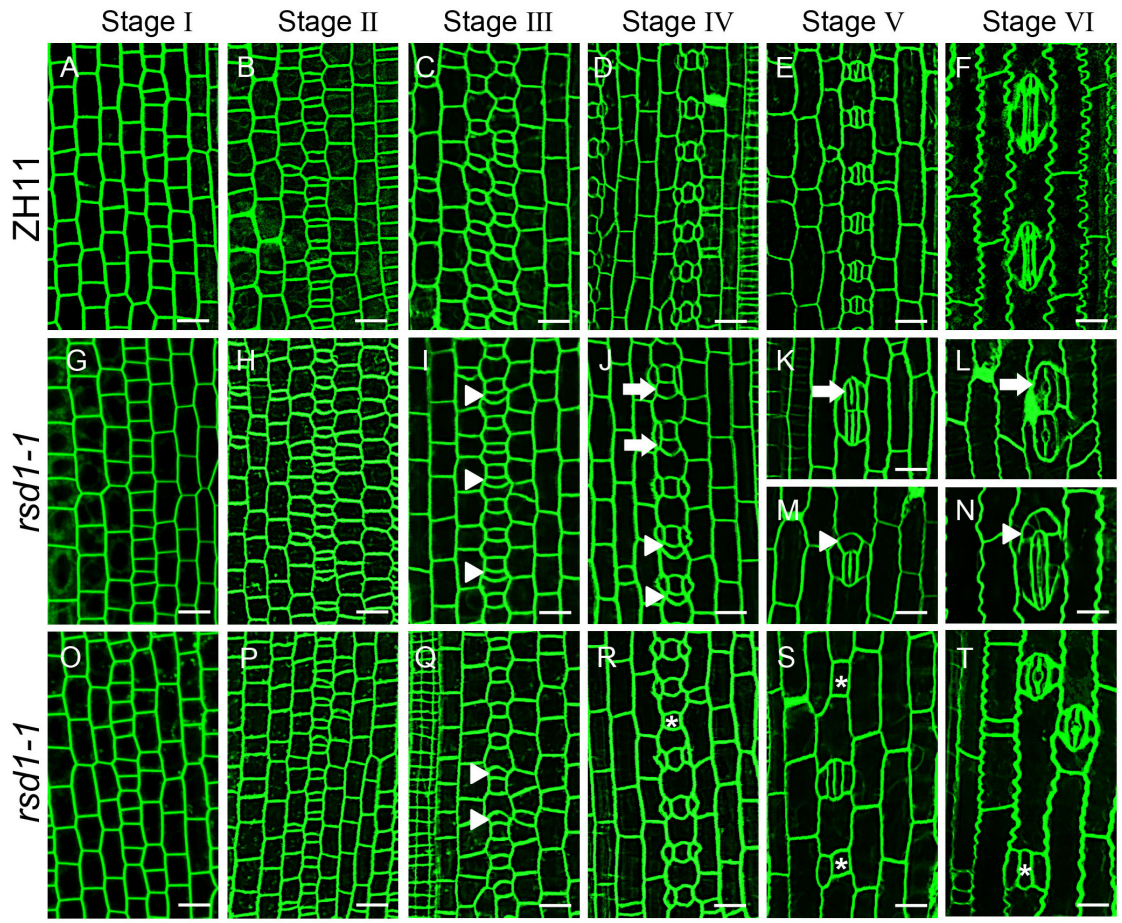

FIGURE 2 | Stomatal developmental process in *rsd1-1* mutant. **(A–T)** Confocal images of six main stomatal developmental stages in *rsd1-1* mutant. There was no significant difference between *rsd1-1* and ZH11 at stage I and stage II **(A**,**B**,**G**,**H**,**O**,**P)**. Extra divisions in large sister cells resulting in extra small cells neighboring GMCs at stage III in *rsd1-1* mutant **(I**,**Q)**. Two-cluster GMCs sharing one subsidiary cell and arrested GMC at stage IV in *rsd1-1* mutant **(J**,**R)**. Clustered stomata, five-cell stomatal complex and arrested GMCs at stage V in *rsd1-1* mutant **(K**,**M**,**S)**. Morphogenesis and differentiation of clustered stomata, five-cell stomatal complex and arrested GMC at stage VI in *rsd1-1* mutant **(L**,**N**,**T)**. The white arrowheads indicated ectopic extra small cells neighboring stomata. The white arrows indicated clustered stomata. The asterisks indicated arrested GMCs. Bars, 10 μm.

number of *DUF630/632* family genes in angiosperm indicated that *DUF630/632* gene duplication might be important, which was associated with their abundance of function. In marine angiosperm *Z. marina*, the stomatal development genes (*SPCH*, *MUTE*, *FAMA*, *FLP*, *TMM*, *SDD1*, *EPF1*, *EPF2*, *EPFL9*) are absent, consisting of its phenotype without stomata (Olsen et al., 2016). However, *Z. marina* possesses two *RSD1* genes (**Supplementary Figure S3**). These results suggest that *RSD1* is not only related to stomatal development, but also is important for plant growth.

RSD1 Is Required for Proper Expression of Stomatal Development-Related Genes

The *RSD1*/*REL2* is dominantly expressed in the younger leaf blades (**Supplementary Figure S5**; Yang et al., 2016), suggesting that this gene is involved in stomatal development.

To investigate the relationship between *RSD1* and stomatal development, we detected the transcript abundance of 18 important stomatal development genes by RT-qPCR in the base of young leaves in *rsd1-1* (**Figure 5**). The expression of *OsMUTE*, *OsEPF1*, and *OsSDD1* was down-regulated in *rsd1-1* mutant, whereas the expression of *OsICE1* and *OsEPFL9* was upregulated (**Figure 5**). There were no significant changes in other stomatal development genes (**Figure 5**). The expression of *OsMUTE* and *OsSDD1* was also significantly decreased in *rsd1-2* (**Supplementary Figure S6**). Most small cell neighboring stomata cannot develop into stomata, and some of the GMCs arrested in the mutants. Thus, we suspected that these cells may not express *OsMUTE*, which may lead to the downregulation of *OsMUTE* in the *rsd1* mutants. These results suggest that *RSD1* is required for proper expression of stomatal development-related genes.

OsSDD1 Mutants Exhibit Similar Stomatal Phenotype to *rsd1*

The significant downregulation of *OsSDD1* in *rsd1* mutants led us to investigate the role of *OsSDD1* in stomatal development. There

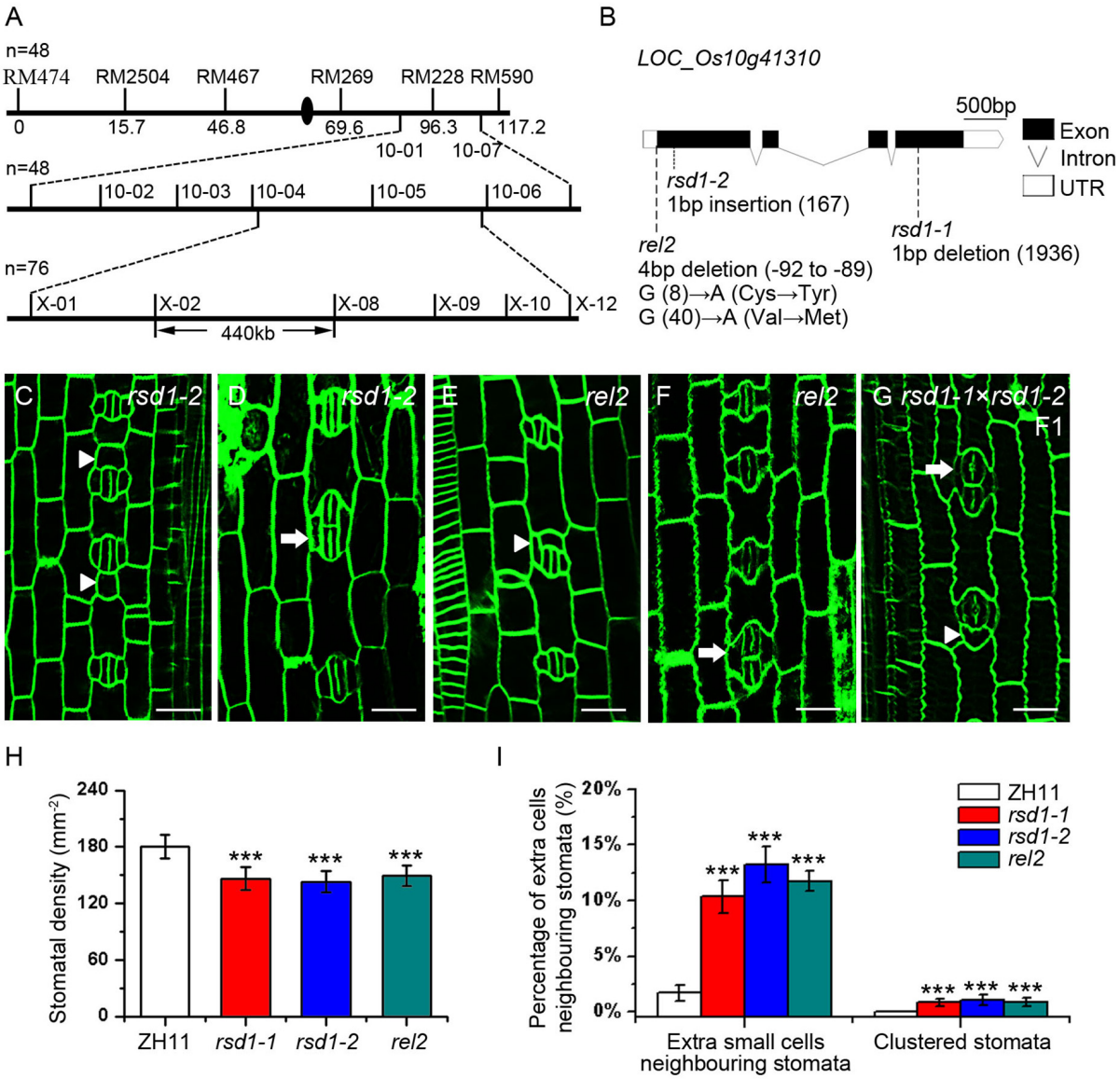

FIGURE 3 | Map-based cloning of *rsd1-1* and the phenotype of *rsd1-1* allelic mutants *rsd1-2* and *rel2*. **(A)** *RSD1* was localized between X-02 and X-08 on chromosome 10. *n* represents sample size. **(B)** Gene structure and mutant sites of candidate gene *LOC_Os10g41310* (*RSD1*). Black boxes indicated the exons, lines indicated the introns, and white boxes represented untranslated region (UTR). The *rsd1-1* had a 1 bp deletion in the fourth exon. The *rsd1-2* had a 1 bp insertion in the first exon. The *rel2* had a 4 bp (GGAG) deletion in 5′-UTR and two mutations (G to A and G to A) in the first exon. **(C–G)** Confocal images of developing stomata in *rsd1-2*, *rel2*, and F1 generation plant of a cross between *rsd1-1* and *rsd1-2*. **(C)** An extra small cell neighboring stoma in *rsd1-2*. **(D)** Two-cluster stomata sharing two subsidiary cells in *rsd1-2*. **(E)** An extra small cell neighboring stoma in *rel2*. **(F)** Two-cluster stomata sharing two subsidiary cells in *rel2*. **(G)** An extra small cell neighboring stoma and clustered stomata in F1 generation plant of a cross between *rsd1-1* and *rsd1-2*. Bars, 10 μm. The white arrowheads indicated ectopic extra small cells neighboring stomata. The white arrows indicated clustered stomata. **(H)** Quantification of the stomatal density at mature stage. **(I)** Quantification of the clustered stomata and extra small cells neighboring stomata at the fifth leaf. The error bars indicated the mean ± SEM, $n = 10$; $^{***}P < 0.001$ by Student's *t*-test.

was one copy of *SDD1* in rice named *OsSDD1* (**Supplementary Figure S7**). To explore the phenotype of *OsSDD1*, CRISPR/Cas9 genome editing was performed, and we obtained two mutants named *ossdd1-1* and *ossdd1-2* (**Supplementary Figure S8**). In *ossdd1-1*, 1 bp was inserted at nucleotide position between 131 and 132, resulting in a PTT. In *ossdd1-2*, the 131st nucleotide was deleted, which also led to a PTT (**Supplementary Figure S8**). We then observed the stomatal phenotype in mature leaves of *ZH11*, *ossdd1-1*, and *ossdd1-2* (**Figures 6A–D**). Similar to *rsd1* mutants, both *ossdd1-1* and *ossdd1-2* exhibited clustered stomata and extra small cell neighboring stomata (**Figures 6B–D,J**). In addition, we observed the stomatal development process in *ossdd1-1* (**Figures 6E–H**). Similar to *rsd1*, an extra asymmetric division was observed in some larger sister cells of the *ossdd1* mutants at stage III, producing an extra small cell neighboring GMC (**Figure 6E**). A few of extra small cells neighboring GMC could induce the

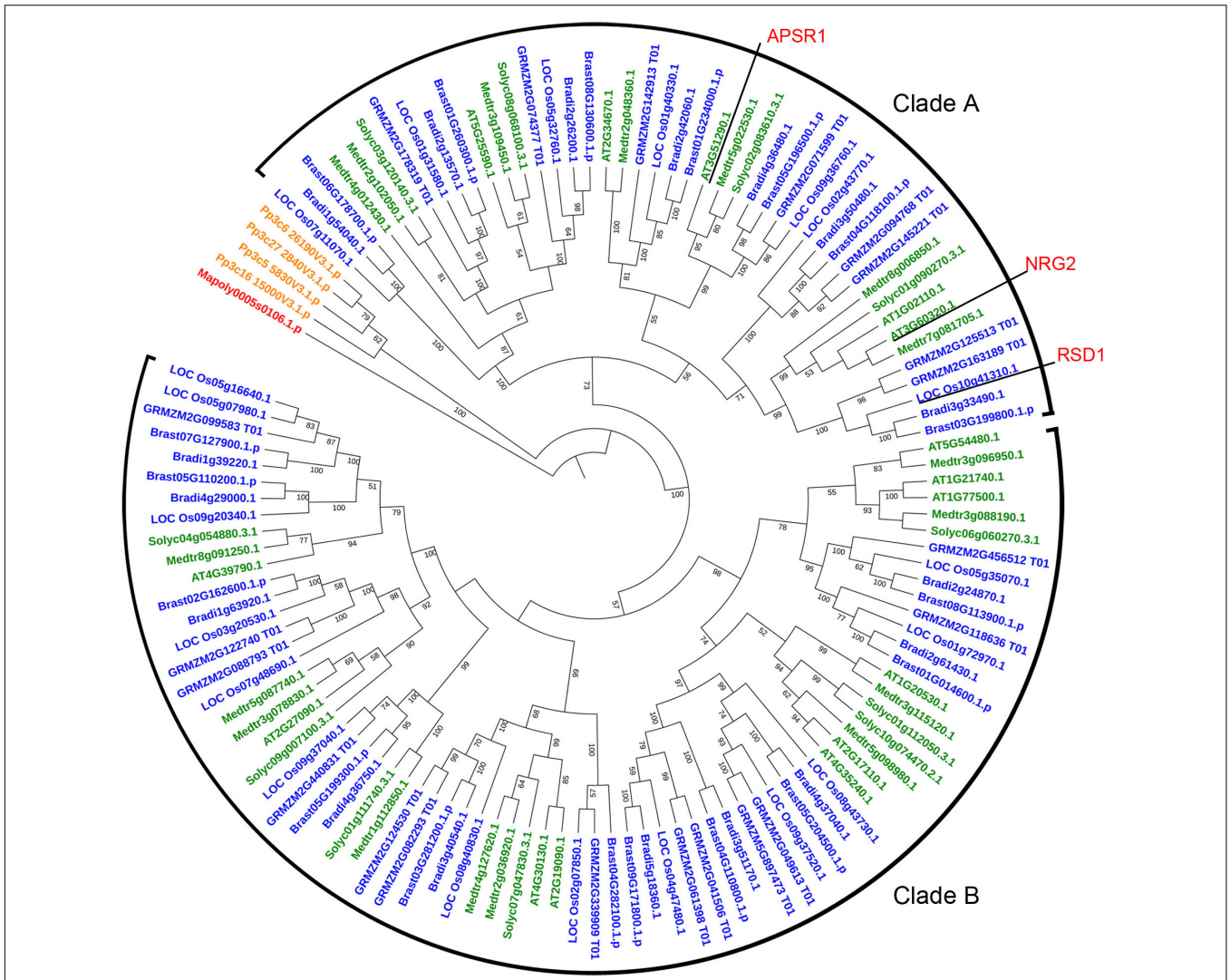

FIGURE 4 | Phylogenetic relationship of proteins containing DUF630 and DUF632 domain of RSD1 in 9 land plants. The protein sequences for constructing phylogenetic tree were identified from the databases Phytozome V12 by using the reciprocal BLAST technique with rice RSD1 protein sequence. The phylogenetic tree was constructed by the NJ method in MEGA 5. Bootstrap values for 1,000 replicates are given in nodes as percentages. Amino acid sequences were used from *Marchantia polymorpha* (1 sequence), *Physcomitrella patens* (4 sequences), *Arabidopsis thaliana* (15 sequences), *Medicago truncatula* (17 sequences), *Solanum lycopersicum* (11 sequences), *O. sativa* (20 sequences), *Zea mays* (21 sequences), *Brachypodium distachyon* (17 sequences), and *Brachypodium stacei* (18 sequences).

formation of SC at Stage V (**Figure 6G**) and may finally divide equally to form paired GCs, resulting in clustered stomata at stage VI (**Figure 6H**). The stomatal density of *ossdd1* mutants was slightly increased (**Figure 6I**), but the stomatal files had nothing different with ZH11 (**Supplementary Figure S9**). These observations suggested that *OsSDD1* is required for restricting ectopic ACDs and clustered stomata but not needed for stomatal file density in rice.

rsd1 Mutants Enhance the Dehydration Avoidance

As stomatal density was decreased in *rsd1* mutants (**Figure 1M**), we performed a dehydration shock stress assay to determine the role of *RSD1* in water deficit. In ZH11, the fresh weight was reduced to 56.62% after 2 h of water deficit shock. Compared with ZH11, the water loss rate of *rsd1* mutants was significantly lower. The fresh weight of *rsd1-1* and *rsd1-2* was reduced to 65.57 and 67.94%, respectively, under the same treatment (**Figure 7A**). This result suggested that *RSD1* is required for regulating water loss by modulating stomatal density.

DISCUSSION

Stomata are key determinants of the trade-off between photosynthetic carbon fixation and water transpiration (Franks and Farquhar, 1999). Grasses with lower stomatal

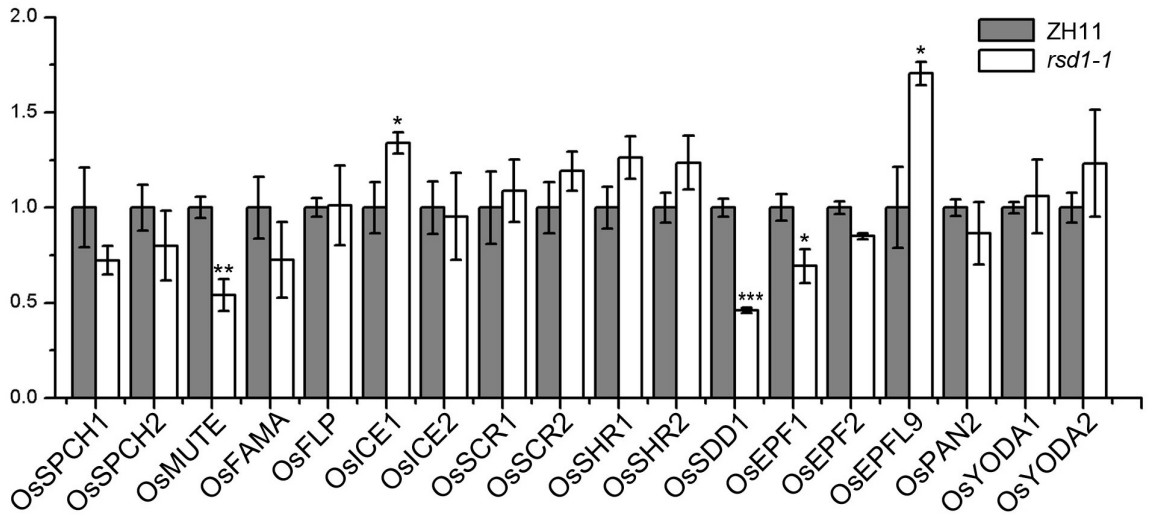

FIGURE 5 | Expression analysis of stomatal development regulation genes in *rsd1-1* mutant. Analyzing the expression of stomatal development relative genes in *rsd1-1* mutant by RT-qPCR. *OsUBQ10* was used as the internal control. The error bars indicated mean ± SD, $n = 3$; ***$P < 0.001$. **$0.001 < P < 0.01$. *$0.01 < P < 0.05$ by Student's *t*-test.

density have higher water use efficiency and greater drought tolerance than other species (Hughes et al., 2017). However, the detailed mechanisms of stomatal development in grasses were still very poorly understood. By forward genetic approach, we found *RSD1*, a new stomatal patterning regulatory gene, was required for inhibiting clustered stomata and promoting stomatal density (**Figure 7B**). Knockout of *OsSDD1* also produced clustered stomata and extra small cells adjacent to the stomata. *OsSDD1* and *RSD1* are both required for inhibiting ectopic ACDs and clustered stomata (**Figure 7C**).

In grasses, stomatal patterning is established when each stomatal precursor in a cell file divides once asymmetrically in the same orientation to produce a GMC (Facette and Smith, 2012). Therefore, there may be two ways to produce clustered stomata. One is the disruption of the division direction in neighboring stomatal precursors; another is the reentry of stomatal development in large sister cells to produce a stoma neighboring preexisting stoma. The *rsd1* mutants produce clustered stomata. Closer observation of stomatal development stages in the mutants showed that the direction of entry division was not affected. We found that the larger sister cell underwent an asymmetric division neighboring preexisting stoma or GMC, suggesting that the *RSD1* is required for inhibiting reentry division in larger sister cells. Similar causes of clustered stomatal were also observed in *ossdd1* mutants, suggesting that *OsSDD1* is also involved in preventing larger sister cells from dividing asymmetrically and promoting the differentiation of larger sister cells into pavement cells. In addition, some GMCs arrested and failed to differentiate into GC in *rsd1* mutants, suggesting a role of *RSD1* in promoting GMC to differentiate into mature stomata. These results suggest that *RSD1* promoted cell differentiation of both large sister cell and GMC.

The molecular mechanism of clustered stomata in grasses is still unknown. In *Arabidopsis*, *AtSPCH* and *AtICE1/AtSCRM2* coordinately established stomatal fate (MacAlister et al., 2007; Kanaoka et al., 2008). When they accumulated, additional stomata will be produced, and all epidermal cells will be turned into stomata in extreme conditions (MacAlister et al., 2007; Kanaoka et al., 2008). The upstream MAPK and receptor ligand signals ensure that additional stomata are not produced by limiting the accumulation of fate determination transcription factors (Bergmann et al., 2004; Lampard et al., 2008; Putarjunan et al., 2019). In grass plants, it is found that overexpression of stomatal fate factor *SPCH1/2* in *B. distachyon* could induce additional cell division in epidermal cells (Raissig et al., 2016; Wu et al., 2019). In POSTECH insertion mutant line of *osspch2*, the clustered stomata had been observed (Liu et al., 2009). Overexpression of *ICE1* and *SCRM2* produced only a small amount of extra cell division, whereas *Ubipro:BdICE1*^{scrmD} produced clustered stomata (Raissig et al., 2016). In addition, the absence of *BdYODA1* leads to the disorder of cell fate in stomatal files, which results in clustered stomata (Abrash et al., 2018). In the *rsd1-1* mutant, the expression of *ICE1* and *EPFL9* was slightly up-regulated, which might be one of the reasons of clustered stomata.

AtSDD1 is expressed in pseudo-meristem cells and GMCs, and the stomatal density of the mutant with functional deletion increased by 2–4 times and clustered, and its overexpression inhibited stomatal differentiation and decreased stomatal density (Berger and Altmann, 2000; Von Groll et al., 2002). Its function is to regulate stomatal development in the upstream of TMM but independent of EPFL gene family (Von Groll et al., 2002). Its protein function is conserved to a certain extent and has a significant effect on stomatal density in tomato and maize (Liu et al., 2015; Morales-Navarro et al., 2018). However, the function of *OsSDD1* in stomatal development is still unclear in rice. By constructing the knockout lines, we found that the *ossdd1* mutants have clustered stomata and extra small cells

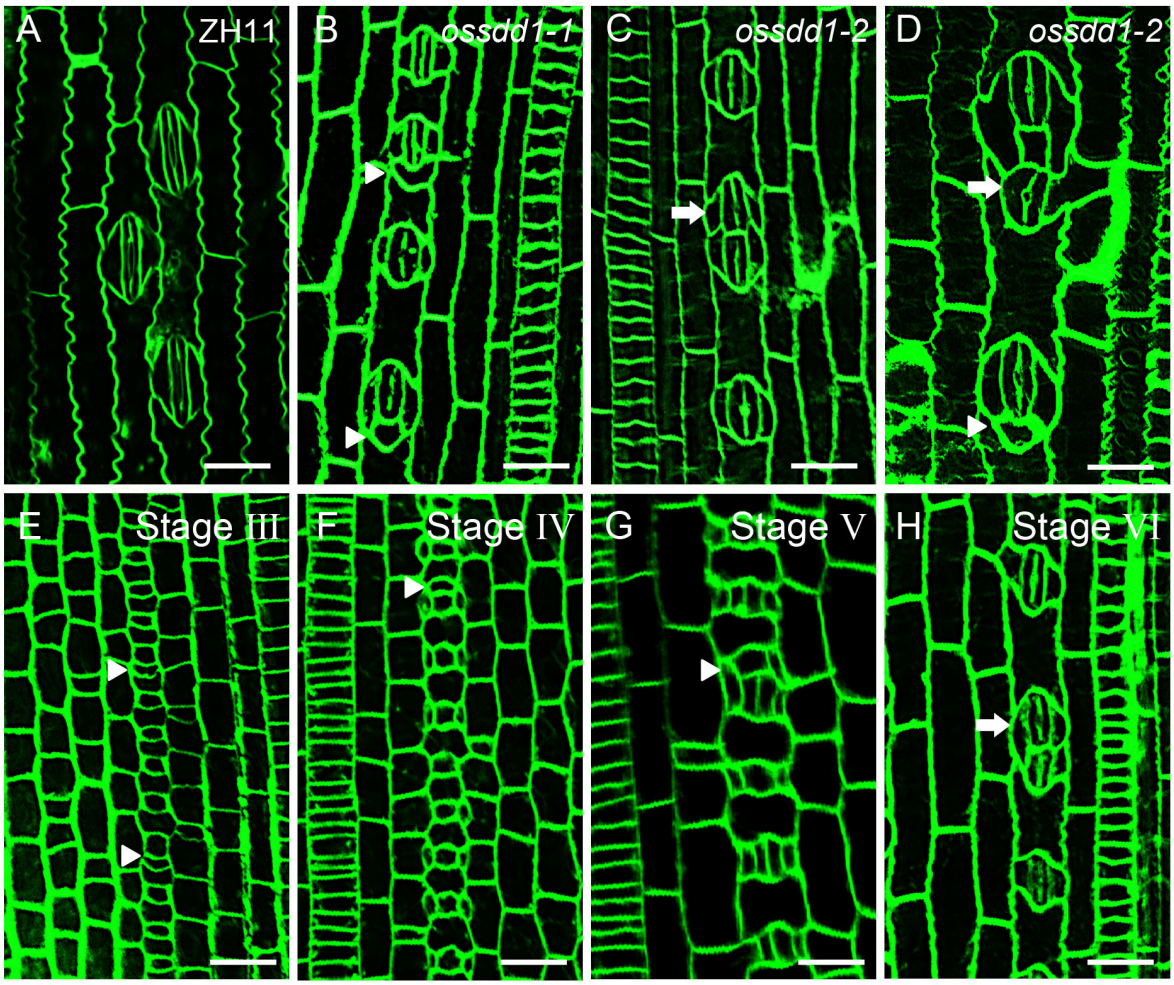

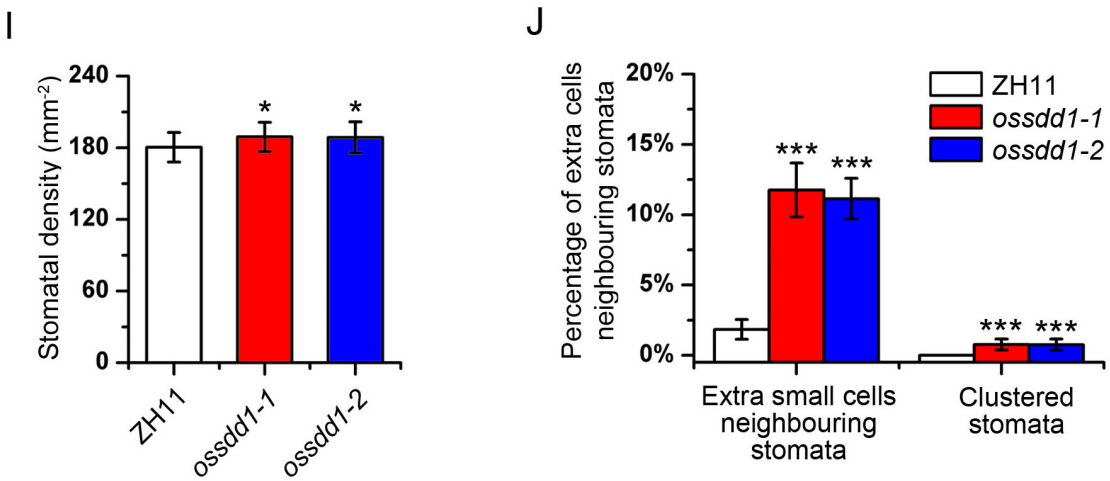

FIGURE 6 | Phenotypic analysis of *ossdd1-1* and *ossdd1-2* mutants. **(A)** Mature stomata of ZH11. **(B)** An extra small cell neighboring stoma in *ossdd1-1*. **(C)** Two-cluster stomata with four subsidiary cells in *ossdd1-2*. **(D)** Five-cell stomatal complex and ectopic stomatal patterning in *ossdd1-2*. **(E)** The extra division of large sister cell resulting in an extra small cell neighboring GMC at stage III in *ossdd1-1*. **(F)** GMC with a small cell at stage IV in *ossdd1-1*. **(G)** Stomata with a small cell sharing SC at stage V. **(H)** Morphogenesis and differentiation of clustered stomata at stage VI. Bars, 10 μm. The white arrowheads indicated extra small cells neighboring stomata. The white arrows indicated clustered stomata. **(I)** Quantification of the stomatal density at mature stage. **(J)** Quantification of the clustered stomata and extra small cells neighboring stomata at the fifth leave. The error bars indicated the mean ± SEM, $n = 10$; ***$P < 0.001$; *$0.01 < P < 0.05$ by Student's *t*-test.

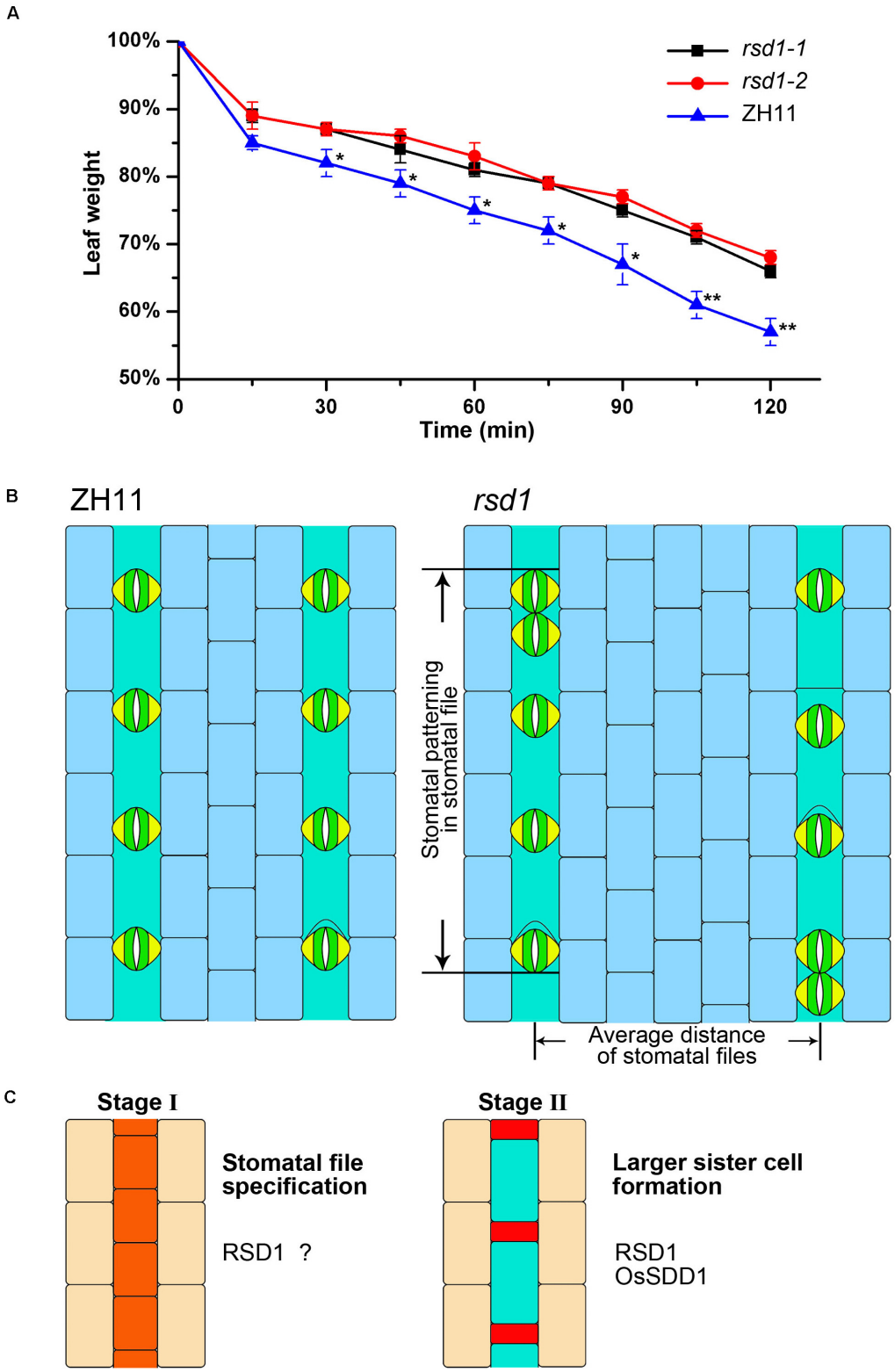

FIGURE 7 | The *rsd1* mutants increase dehydration avoidance, and the model showed *RSD1* and *OsSDD1* regulating stomatal development. **(A)** Water loss in 8 weeks old detached leaves at different time points with three replicates. Three independent experiments were performed with similar results. The error bars indicated the mean ± SEM, $n = 3$; $^{**}0.001 < P < 0.01$, $^{*}0.01 < P < 0.05$ by Student's *t*-test. **(B)** The stomatal patterning in ZH11 and *rsd1* mutants. **(C)** RSD1 and OsSDD1 required at early stage of stomatal development.

neighboring stomata (**Figures 6B–D**). The phenotype of *ossdd1* mutants is similar to *rsd1-1*. *OsSDD1* and *RSD1* are both required for inhibiting ectopic ACDs and clustered stomata.

In grasses, stomata are always arranged parallel and adjacent to leaf veins (Zwieniecki and Boyce, 2014; Nunes et al., 2020). The density of stomatal files was different in different development stages, species, or growth conditions (Stebbins and Shah, 1960). Therefore, the density of stomatal files is the key factor for stomatal density. The grass SHR/SCR is a common module that not only controls vein development and Kranz anatomy in maize (Slewinski et al., 2014; Hughes et al., 2019) but also regulates stomatal development in rice (Kamiya et al., 2003; Schuler et al., 2018; Wu et al., 2019). The deletion of *OsSHRs* will lead to the decrease of stomatal density in rice (Wu et al., 2019), while the overexpression of *ZmSHRs* in rice produces additional stomatal files far away from the vein to increase stomatal density (Schuler et al., 2018). In the *rsd1-1* mutant, we observed a decrease in the density of stomatal files in the leaf at the seedling stage (**Figure 1L**). However, the expression of *OsSHR* and *OsSCR* was not significantly changed in the *rsd1* mutants compared with ZH11 (**Figure 5**), suggesting that the decrease of stomatal files in the mutants is independent of *OsSHR*/*OsSCR*.

Rice is one of the most important food crops in the world. Although global climatic variability is a serious threat to food security, genetic engineering of stomatal development will enable us to create stress-tolerant crops (Serna and Fenoll, 2002; Korres et al., 2017). By controlling stomatal development and reducing stomatal density, rice can control water loss and make it easier to survive under drought conditions (Buckley et al., 2019). The lack of *RSD1* led to a reduction of stomatal density and the leaf water loss rate in rice. The effect of stomatal density on plants has been applied to create drought-resistant crops (Buckley et al., 2019). Recent research has shown that excessive expression of *EPF* genes in wheat and rice can significantly improve water use efficiency without affecting plant yield when stomatal density is reduced (Caine et al., 2019; Dunn et al., 2019). Therefore, RSD1 can be used as a candidate gene for breeding of drought-resistant rice.

DATA AVAILABILITY STATEMENT

The original contributions presented in the study are included in the article/**Supplementary Material**, further inquiries can be directed to the corresponding author.

AUTHOR CONTRIBUTIONS

QY and SH designed the experiments, and wrote the manuscript. QY, LC, WZ, TL, YA, ZW, YW, YX, and LY performed experiments, QY, LC, and SH revised the manuscript. All authors contributed to the article and approved the submitted version.

ACKNOWLEDGMENTS

We are grateful to Kunming Chen for kindly providing seeds of *rel2* mutant. We appreciate the help of Dr. Yangwen Qian and Biogle Genetech Corporation in generating all CRISPR/Cas9 lines. This work was supported by the Ministry of Agriculture of the People's Republic of China (Grant No. 2016ZX08009-003-002), the National Natural Science Foundation of China (NSFC) (Grant Nos. 31670185 and 31870251), the major project of Science and Technology of Gansu province (17ZD2NA016), and the Chang Jiang Scholars Program of China (2017).

SUPPLEMENTARY MATERIAL

The Supplementary Material for this article can be found online at: https://www.frontiersin.org/articles/10.3389/fpls.2020.600021/full#supplementary-material

REFERENCES

Abrash, E., Anleu Gil, M. X., Matos, J. L., and Bergmann, D. C. (2018). Conservation and divergence of YODA MAPKKK function in regulation of grass epidermal patterning. *Development* 145:dev165860. doi: 10.1242/dev.165860

Abrash, E. B., and Bergmann, D. C. (2010). Regional specification of stomatal production by the putative ligand CHALLAH. *Development* 137, 447–455. doi: 10.1242/dev.040931

Berger, D., and Altmann, T. (2000). A subtilisin-like serine protease involved in the regulation of stomatal density and distribution in *Arabidopsis thaliana*. *Genes Dev.* 14, 1119–1131. doi: 10.1101/gad.14.9.1119

Bergmann, D. C., Lukowitz, W., and Somerville, C. R. (2004). Stomatal development and pattern controlled by a MAPKK kinase. *Science* 304, 1494–1497. doi: 10.1126/science.1096014

Bergmann, D. C., and Sack, F. D. (2007). Stomatal development. *Annu. Rev. Plant Biol.* 58, 163–181.

Bowman, J. L., Kohchi, T., Yamato, K. T., Jenkins, J., Shu, S., Ishizaki, K., et al. (2017). Insights into land plant evolution garnered from the *Marchantia polymorpha* Genome. *Cell* 171, 287.e15–304.e15. doi: 10.1016/j.cell.2017.09.030

Buckley, C. R., Caine, R. S., and Gray, J. E. (2019). Pores for thought: can genetic manipulation of stomatal density protect future rice yields? *Front. Plant Sci.* 10:1783. doi: 10.3389/fpls.2019.01783

Caine, R. S., Yin, X., Sloan, J., Harrison, E. L., Mohammed, U., Fulton, T., et al. (2019). Rice with reduced stomatal density conserves water and has improved drought tolerance under future climate conditions. *New Phytol.* 221, 371–384. doi: 10.1111/nph.15344

Cartwright, H. N., Humphries, J. A., and Smith, L. G. (2009). A receptor-like protein that promotes polarization of an asymmetric cell division in maize. *Science* 323, 649–651. doi: 10.1126/science.1161686

Chen, L., Wu, Z., and Hou, S. (2020). SPEECHLESS speaks loudly in stomatal development. *Front. Plant Sci.* 11:114. doi: 10.3389/fpls.2020.00114

Dow, G. J., Berry, J. A., and Bergmann, D. C. (2014). The physiological importance of developmental mechanisms that enforce proper stomatal spacing in *Arabidopsis thaliana*. *New Phytol.* 201, 1205–1217. doi: 10.1111/nph.12586

Dunn, J., Hunt, L., Afsharinafar, M., Meselmani, M. A., Mitchell, A., Howells, R., et al. (2019). Reduced stomatal density in bread wheat leads to increased water-use efficiency. *J. Exp. Bot.* 70, 4737–4748. doi: 10.1093/jxb/erz248

Elert, E. (2014). Rice by the numbers: a good grain. *Nature* 514, S50–S51. doi: 10.1038/514S50a

Facette, M. R., Park, Y., Sutimantanapi, D., Luo, A., Cartwright, H. N., Yang, B., et al. (2015). The SCAR/WAVE complex polarizes PAN receptors and promotes division asymmetry in maize. *Nat. Plants* 1:14024. doi: 10.1038/nplants.2014.24

Facette, M. R., and Smith, L. G. (2012). Division polarity in developing stomata. *Curr. Opin. Plant Biol.* 15, 585–592. doi: 10.1016/j.pbi.2012.09.013

Franks, P. J., and Farquhar, G. D. (1999). A relationship between humidity response, growth form and photosynthetic operating point in C3 plants. *Plant Cell Environ.* 22, 1337–1349. doi: 10.1046/j.1365-3040.1999 00494. x

Godfray, H. C. J., Beddington, J. R., Crute, I. R., Haddad, L., Lawrence, D., Muir, J. F., et al. (2010). Food security: the challenge of feeding 9 billion people. *Science* 327, 812–818. doi: 10.1126/science.1185383

Gonzalez-Mendoza, V., Zurita-Silva, A., Sanchez-Calderon, L., Sanchez-Sandoval, M. E., Oropeza-Aburto, A., Gutierrez-Alanis, D., et al. (2013). *APSR1*, a novel gene required for meristem maintenance, is negatively regulated by low phosphate availability. *Plant Sci.* 205-206, 2–12. doi: 10.1016/j.plantsci.2012.12.015

Gordon, S. P., Contreras-Moreira, B., Levy, J. J., Djamei, A., Czedik-Eysenberg, A., Tartaglio, V. S., et al. (2020). Gradual polyploid genome evolution revealed by pan-genomic analysis of *Brachypodium hybridum* and its diploid progenitors. *Nat. Commun.* 11:3670. doi: 10.1038/s41467-020-17302-5

Hara, K., Kajita, R., Torii, K. U., Bergmann, D. C., and Kakimoto, T. (2007). The secretory peptide gene *EPF1* enforces the stomatal one-cell-spacing rule. *Genes Dev.* 21, 1720–1725. doi: 10.1101/gad.1550707

Hara, K., Yokoo, T., Kajita, R., Onishi, T., Yahata, S., Peterson, K. M., et al. (2009). Epidermal cell density is autoregulated via a secretory peptide, EPIDERMAL PATTERNING FACTOR 2 in *Arabidopsis* leaves. *Plant Cell Physiol.* 50, 1019–1031. doi: 10.1093/pcp/pcp068

Hetherington, A. M., and Woodward, F. I. (2003). The role of stomata in sensing and driving environmental change. *Nature* 424, 901–908. doi: 10.1038/nature01843

Hughes, J., Hepworth, C., Dutton, C., Dunn, J. A., Hunt, L., Stephens, J., et al. (2017). Reducing stomatal density in barley improves drought tolerance without impacting on yield. *Plant Physiol.* 174, 776–787. doi: 10.1104/pp.16.01844

Hughes, T. E., Sedelnikova, O. V., Wu, H., Becraft, P. W., and Langdale, J. A. (2019). Redundant *SCARECROW* genes pattern distinct cell layers in roots and leaves of maize. *Development* 146:dev.177543. doi: 10.1242/dev.177543

Hunt, L., and Gray, J. E. (2009). The signaling peptide EPF2 controls asymmetric cell divisions during stomatal development. *Curr. Biol.* 19, 864–869. doi: 10.1016/j.cub.2009.03.069

Kamiya, N., Itoh, J. I., Morikami, A., Nagato, Y., and Matsuoka, M. (2003). The *SCARECROW* gene's role in asymmetric cell divisions in rice plants. *Plant J.* 36, 45–54. doi: 10.1046/j.1365-313X.2003.01856.x

Kanaoka, M. M., Pillitteri, L. J., Fujii, H., Yoshida, Y., Bogenschutz, N. L., Takabayashi, J., et al. (2008). SCREAM/ICE1 and SCREAM2 specify three cell-state transitional steps leading to *Arabidopsis* stomatal differentiation. *Plant Cell* 20, 1775–1785. doi: 10.1105/tpc.108.060848

Korres, N., Norsworthy, J., Burgos, N., and Oosterhuis, D. (2017). Temperature and drought impacts on rice production: an agronomic perspective regarding short-and long-term adaptation measures. *Water Resour. Rural Dev.* 9, 12–27. doi: 10.1016/j.wrr.2016.10.001

Lai, L. B., Nadeau, J. A., Lucas, J., Lee, E. K., Nakagawa, T., Zhao, L., et al. (2005). The *Arabidopsis* R2R3 MYB proteins FOUR LIPS and MYB88 restrict divisions late in the stomatal cell lineage. *Plant Cell* 17, 2754–2767. doi: 10.1105/tpc.105.034116

Lamesch, P., Berardini, T. Z., Li, D., Swarbreck, D., Wilks, C., Sasidharan, R., et al. (2012). The *Arabidopsis* information resource (TAIR): improved gene annotation and new tools. *Nucleic Acids Res.* 40, D1202–D1210. doi: 10.1093/nar/gkr1090

Lampard, G. R., MacAlister, C. A., and Bergmann, D. C. (2008). *Arabidopsis* stomatal initiation is controlled by MAPK-mediated regulation of the bHLH SPEECHLESS. *Science* 322, 1113–1116. doi: 10.1126/science.1162263

Lang, D., Ullrich, K. K., Murat, F., Fuchs, J., Jenkins, J., Haas, F. B., et al. (2018). The *Physcomitrella patens* chromosome-scale assembly reveals moss genome structure and evolution. *Plant J.* 93, 515–533. doi: 10.1111/tpj.13801

Larkin, M. A., Blackshields, G., Brown, N. P., Chenna, R., McGettigan, P. A., McWilliam, H., et al. (2007). Clustal W and clustal X version 2.0. *Bioinformatics* 23, 2947–2948. doi: 10.1093/bioinformatics/btm404

Lau, O. S., and Bergmann, D. C. (2012). Stomatal development: a plant's perspective on cell polarity, cell fate transitions and intercellular communication. *Development* 139, 3683–3692. doi: 10.1242/dev.080523

Lee, E., Lucas, J. R., and Sack, F. D. (2014). Deep functional redundancy between FAMA and FOUR LIPS in stomatal development. *Plant J.* 78, 555–565. doi: 10.1111/tpj.12489

Lee, J. S., Hnilova, M., Maes, M., Lin, Y.-C. L., Putarjunan, A., Han, S.-K., et al. (2015). Competitive binding of antagonistic peptides fine-tunes stomatal patterning. *Nature* 522, 439–443. doi: 10.1038/nature14561

Lee, J. S., Kuroha, T., Hnilova, M., Khatayevich, D., Kanaoka, M. M., McAbee, J. M., et al. (2012). Direct interaction of ligand-receptor pairs specifying stomatal patterning. *Genes Dev.* 26, 126–136. doi: 10.1101/gad.179895.111

Letunic, I., and Bork, P. (2017). 20 years of the SMART protein domain annotation resource. *Nucleic Acids Res.* 46, D493–D496. doi: 10.1093/nar/gkx922

Letunic, I., and Bork, P. (2019). Interactive tree of life (iTOL) v4: recent updates and new developments. *Nucleic Acids Res.* 47, W256–W259. doi: 10.1093/nar/gkz239

Liu, T., Ohashi-Ito, K., and Bergmann, D. C. (2009). Orthologs of *Arabidopsis thaliana* stomatal bHLH genes and regulation of stomatal development in grasses. *Development* 136, 2265–2276. doi: 10.1242/dev.032938

Liu, Y., Qin, L., Han, L., Xiang, Y., and Zhao, D. (2015). Overexpression of maize *SDD1* (*ZmSDD1*) improves drought resistance in *Zea mays* L. by reducing stomatal density. *Plant Cell Tiss. Organ Cult.* 122, 147–159. doi: 10.1007/s11240-015-0757-8

Lu, J., He, J., Zhou, X., Zhong, J., Li, J., and Liang, Y. K. (2019). Homologous genes of epidermal patterning factor regulate stomatal development in rice. *J. Plant Physiol.* 23, 18–27. doi: 10.1016/j.jplph.2019.01.010

Luo, L., Zhou, W. Q., Liu, P., Li, C. X., and Hou, S. W. (2012). The development of stomata and other epidermal cells on the rice leaves. *Biol. Plant.* 56, 521–527. doi: 10.1007/s10535-012-0045-y

MacAlister, C. A., Ohashi-Ito, K., and Bergmann, D. C. (2007). Transcription factor control of asymmetric cell divisions that establish the stomatal lineage. *Nature* 445, 537–540. doi: 10.1038/nature05491

McKown, K. H., and Bergmann, D. C. (2020). Stomatal development in the grasses: lessons from models and crops (and crop models). *New Phytol.* 227, 1636–1648. doi: 10.1111/nph.16450

Morales-Navarro, S., Perez-Diaz, R., Ortega, A., de Marcos, A., Mena, M., Fenoll, C., et al. (2018). Overexpression of a *SDD1*-Like gene from wild tomato decreases stomatal density and enhances dehydration avoidance in *Arabidopsis* and cultivated Tomato. *Front. Plant Sci.* 9:940. doi: 10.3389/fpls.2018.00940

Nishimura, A., Aichi, I., and Matsuoka, M. (2006). A protocol for *Agrobacterium*-mediated transformation in rice. *Nat. Protoc.* 1, 2796–2802. doi: 10.1038/nprot.2006.469

Niwa, T., Kondo, T., Nishizawa, M., Kajita, R., Kakimoto, T., and Ishiguro, S. (2013). EPIDERMAL PATTERNING FACTOR LIKE5 peptide represses stomatal development by inhibiting meristemoid maintenance in *Arabidopsis thaliana*. *Biosci. Biotechnol. Biochem.* 77, 1287–1295. doi: 10.1271/bbb.130145

Nunes, T. D. G., Zhang, D., and Raissig, M. T. (2020). Form, development and function of grass stomata. *Plant J.* 101, 780–799. doi: 10.1111/tpj.14552

Ohashi-Ito, K., and Bergmann, D. C. (2006). *Arabidopsis* FAMA controls the final proliferation/differentiation switch during stomatal development. *Plant Cell* 18, 2493–2505. doi: 10.1105/tpc.106.046136

Olsen, J. L., Rouze, P., Verhelst, B., Lin, Y. C., Bayer, T., Collen, J., et al. (2016). The genome of the seagrass *Zostera marina* reveals angiosperm adaptation to the sea. *Nature* 530, 331–335. doi: 10.1038/nature16548

Ouyang, S., Zhu, W., Hamilton, J., Lin, H., Campbell, M., Childs, K., et al. (2007). The TIGR rice genome annotation resource: improvements and new features. *Nucleic Acids Res.* 35, D883–D887. doi: 10.1093/nar/gkl976

Pillitteri, L. J., Sloan, D. B., Bogenschutz, N. L., and Torii, K. U. (2007). Termination of asymmetric cell division and differentiation of stomata. *Nature* 445, 501–505. doi: 10.1038/nature05467

Putarjunan, A., Ruble, J., Srivastava, A., Zhao, C., Rychel, A. L., Hofstetter, A. K., et al. (2019). Bipartite anchoring of SCREAM enforces stomatal initiation by coupling MAP kinases to SPEECHLESS. *Nat. Plants* 5, 742–754. doi: 10.1038/s41477-019-0440-x

Qi, X., and Torii, K. U. (2018). Hormonal and environmental signals guiding stomatal development. *BMC Biol.* 16:21. doi: 10.1186/s12915-018-0488-5

Qu, X., Yan, M., Zou, J., Jiang, M., Yang, K., and Le, J. (2018). A2-type cyclin is required for the asymmetric entry division in rice stomatal development. *J. Exp. Bot.* 69, 3587–3599. doi: 10.1093/jxb/ery158

Raissig, M. T., Abrash, E., Bettadapur, A., Vogel, J. P., and Bergmann, D. C. (2016). Grasses use an alternatively wired bHLH transcription factor network to establish stomatal identity. *Proc. Natl. Acad. Sci. U.S.A.* 113, 8326–8331. doi: 10.1073/pnas.1606728113

Raissig, M. T., Matos, J. L., Gil, M. X. A., Kornfeld, A., Bettadapur, A., Abrash, E., et al. (2017). Mobile MUTE specifies subsidiary cells to build physiologically improved grass stomata. *Science* 355, 1215–1218. doi: 10.1126/science.aal3254

Saitou, N., and Nei, M. (1987). The neighbor-joining method: a new method for reconstructing phylogenetic trees. *Mol. Biol. Evol.* 4, 406–425. doi: 10.1093/oxfordjournals.molbev.a040454

Schnable, P. S., Ware, D., Fulton, R. S., Stein, J. C., Wei, F., Pasternak, S., et al. (2009). The B73 maize genome: complexity, diversity, and dynamics. *Science* 326:1112. doi: 10.1126/science.1178534

Schuler, M. L., Sedelnikova, O. V., Walker, B. J., Westhoff, P., and Langdale, J. A. (2018). SHORTROOT-mediated increase in stomatal density has no impact on photosynthetic efficiency. *Plant Physiol.* 176, 757–772. doi: 10.1104/pp.17.01005

Serna, L., and Fenoll, C. (2002). Reinforcing the idea of signaling in the stomatal pathway. *Trends Genet.* 18, 597–600. doi: 10.1016/s0168-9525(02)02790-7

Shpak, E. D., McAbee, J. M., Pillitteri, L. J., and Torii, K. U. (2005). Stomatal patterning and differentiation by synergistic interactions of receptor kinases. *Science* 309, 290–293. doi: 10.1126/science.1109710

Slewinski, T. L., Anderson, A. A., Price, S., Withee, J. R., Gallagher, K., and Turgeon, R. (2014). Short-root1 plays a role in the development of vascular tissue and kranz anatomy in maize leaves. *Mol. Plant* 7, 1388–1392. doi: 10.1093/mp/ssu036

Stebbins, G., and Shah, S. (1960). Developmental studies of cell differentiation in the epidermis of monocotyledons: II. Cytological features of stomatal development in the Gramineae. *Dev. Biol.* 2, 477–500. doi: 10.1016/0012-1606(60)90050-6

Sugano, S. S., Shimada, T., Imai, Y., Okawa, K., Tamai, A., Mori, M., et al. (2010). Stomagen positively regulates stomatal density in *Arabidopsis*. *Nature* 463, 241–244. doi: 10.1038/nature08682

Tomato Genome, C. (2012). The tomato genome sequence provides insights into fleshy fruit evolution. *Nature* 485, 635–641. doi: 10.1038/nature11119

Vogel, J. P., Garvin, D. F., Mockler, T. C., Schmutz, J., Rokhsar, D., Bevan, M. W., et al. (2010). Genome sequencing and analysis of the model grass *Brachypodium distachyon*. *Nature* 463, 763–768. doi: 10.1038/nature08747

Von Groll, U., Berger, D., and Altmann, T. (2002). The subtilisin-like serine protease SDD1 mediates cell-to-cell signaling during *Arabidopsis* stomatal development. *Plant Cell* 14, 1527–1539. doi: 10.1105/tpc.001016

Wang, H., Guo, S., Qiao, X., Guo, J., Li, Z., Zhou, Y., et al. (2019). BZU2/ZmMUTE controls symmetrical division of guard mother cell and specifies neighbor cell fate in maize. *PLoS Genet.* 15:e1008377. doi: 10.1371/journal.pgen.1008377

Wang, H., Ngwenyama, N., Liu, Y., Walker, J. C., and Zhang, S. (2007). Stomatal development and patterning are regulated by environmentally responsive mitogen-activated protein kinases in *Arabidopsis*. *Plant Cell* 19, 63–73. doi: 10.1105/tpc.106.048298

Wu, Z., Chen, L., Yu, Q., Zhou, W., Gou, X., Li, J., et al. (2019). Multiple transcriptional factors control stomata development in rice. *New Phytol.* 223, 220–232. doi: 10.1111/nph.15766

Xie, X., Ma, X., Zhu, Q., Zeng, D., Li, G., and Liu, Y.-G. (2017). CRISPR-GE: a convenient software toolkit for CRISPR-based genome editing. *Mol. Plant* 10, 1246–1249. doi: 10.1016/j.molp.2017.06.004

Xu, N., Wang, R., Zhao, L., Zhang, C., Li, Z., Lei, Z., et al. (2016). The *Arabidopsis* NRG2 protein mediates nitrate signaling and interacts with and regulates key nitrate regulators. *Plant Cell* 28, 485–504. doi: 10.1105/tpc.15.00567

Yang, S. Q., Li, W. Q., Miao, H., Gan, P. F., Qiao, L., Chang, Y. L., et al. (2016). *REL2*, a gene encoding an unknown function protein which contains DUF630 and DUF632 domains controls leaf rolling in rice. *Rice* 9:37. doi: 10.1186/s12284-016-0105-6

Young, N. D., Debelle, F., Oldroyd, G. E., Geurts, R., Cannon, S. B., Udvardi, M. K., et al. (2011). The Medicago genome provides insight into the evolution of rhizobial symbioses. *Nature* 480, 520–524. doi: 10.1038/nature10625

Zwieniecki, M. A., and Boyce, C. K. (2014). Evolution of a unique anatomical precision in angiosperm leaf venation lifts constraints on vascular plant ecology. *Proc. Biol. Sci.* 281:20132829. doi: 10.1098/rspb.2013.2829

Conflict of Interest: The authors declare that the research was conducted in the absence of any commercial or financial relationships that could be construed as a potential conflict of interest.

frontiers in Plant Science

ORIGINAL RESEARCH
published: 25 May 2021
doi: 10.3389/fpls.2021.668792

The Cyclophilin *ROC3* Regulates ABA-Induced Stomatal Closure and the Drought Stress Response of *Arabidopsis thaliana*

*Huiping Liu[1], Jianlin Shen[1], Chao Yuan[1], Dongxue Lu[1], Biswa R. Acharya[2], Mei Wang[1], Donghua Chen[1] and Wei Zhang[1]**

[1] Key Laboratory of Plant Development and Environmental Adaption Biology, Ministry of Education, School of Life Science, Shandong University, Qingdao, China, [2] College of Natural and Agricultural Sciences, University of California, Riverside, Riverside, CA, United States

Drought causes a major constraint on plant growth, development, and crop productivity. Drought stress enhances the synthesis and mobilization of the phytohormone abscisic acid (ABA). Enhanced cellular levels of ABA promote the production of reactive oxygen species (ROS), which in turn induce anion channel activity in guard cells that consequently leads to stomatal closure. Although Cyclophilins (CYPs) are known to participate in the biotic stress response, their involvement in guard cell ABA signaling and the drought response remains to be established. The *Arabidopsis thaliana* gene *ROC3* encodes a CYP. Arabidopsis *roc3* T-DNA mutants showed a reduced level of ABA-activated S-type anion currents, and stomatal closure than wild type (WT). Also, *roc3* mutants exhibited rapid loss of water in leaf than wild type. Two complementation lines of *roc3* mutants showed similar stomatal response to ABA as observed for WT. Both complementation lines also showed similar water loss as WT by leaf detached assay. Biochemical assay suggested that *ROC3* positively regulates ROS accumulation by inhibiting catalase activity. In response to ABA treatment or drought stress, *roc3* mutant show down regulation of a number of stress responsive genes. All findings indicate that *ROC3* positively regulates ABA-induced stomatal closure and the drought response by regulating ROS homeostasis and the expression of various stress-activated genes.

Keywords: *ROC3*, abscisic acid, stomatal closure, drought stress, anion channel, reactive oxygen species, catalase

OPEN ACCESS

Edited by:
Wenxiu Ye,
Shanghai Jiao Tong University, China

Reviewed by:
Izumi C. Mori,
Okayama University, Japan
Agnieszka Katarzyna Banas,
Jagiellonian University, Poland

***Correspondence:**
Wei Zhang
weizhang@sdu.edu.cn

Specialty section:
This article was submitted to Plant Cell Biology, a section of the journal Frontiers in Plant Science

Received: *17 February 2021*
Accepted: *28 April 2021*
Published: *25 May 2021*

Citation:
Liu H, Shen J, Yuan C, Lu D, Acharya BR, Wang M, Chen D and Zhang W (2021) The Cyclophilin ROC3 Regulates ABA-Induced Stomatal Closure and the Drought Stress Response of Arabidopsis thaliana. Front. Plant Sci. 12:668792. doi: 10.3389/fpls.2021.668792

INTRODUCTION

Drought stress causes a major constraint on plant growth, development, and productivity (Langridge and Reynolds, 2015). Stomata are surrounded by pairs of specialized epidermal cells termed guard cells, and which are essential for controlling gas exchange (carbon dioxide and oxygen) and water loss. Plants have the ability to adapt to drought stress by regulating stomatal closure (Agurla et al., 2018). The turgor and volume of the pair of guard cells determine the extent of the stomata's aperture (Schroeder et al., 2001). Various environmental cues regulate stomatal

movement, but at the cellular level the most critical factor is the phytohormone abscisic acid (ABA) (Raghavendra et al., 2010; Kollist et al., 2014; Osakabe et al., 2014; Murata et al., 2015). During moisture deficiency, ABA synthesis in the leaf vasculature is enhanced and the hormone is transported to guard cells (Seo and Koshiba, 2011; Munemasa et al., 2015). The accumulation of ABA activates S-type anion channels in guard cells, resulting in an efflux of anions and a consequent decreases in guard cells' turgor, which eventually induces stomatal closure (Li et al., 2000; Wang et al., 2001; Vahisalu et al., 2008).

The simultaneous functions of many signaling molecules in guard cells provide stomatal defense response against drought stress. Reactive oxygen species (ROS) are major secondary messengers which play a crucial role in ABA-triggered stomatal closure (Pei et al., 2000; Zhang et al., 2001; Kwak et al., 2003; Bright et al., 2006; Miao et al., 2006; Murata et al., 2015). Drought stress induces the accumulation of ABA in guard cells, subsequently that leads to the activation of NADPH oxidase and the promotion of ROS production. The elevated level of ROS can also enhance the level of NO and cytosolic calcium. As a result, plasma membrane localized anion channels in guard cells are activated, consequently that leads to the efflux of anions and stomatal closure (Pei et al., 2000; Schroeder et al., 2001; Kwak et al., 2003; Mori et al., 2006; Munemasa et al., 2015). However, oxidative stress is induced in response to high concentration of ROS that causes injuries in plant cells. Hence plant cells are equipped with the antioxidant systems composed of superoxide dismutase (SOD), glutathione peroxidase (GPX), ascorbate peroxidase (APX), catalase (CAT), and non-enzymatic antioxidants to control the homeostasis of ROS (Willekens et al., 1997; Corpas et al., 2001; Mittler, 2002; Apel and Hirt, 2004; Nyathi and Baker, 2006; Palma et al., 2009; Jannat et al., 2011). However, uncontrolled action of antioxidant systems could reduce appropriate levels of ROS that function as secondary messengers, which would negatively impact the ABA and/or drought signal transduction systems. It is unknown how antioxidant systems are regulated during ABA and drought signaling to maintain the suitable levels of ROS in plants.

The Cyclophilins (CYPs) belong to a large class of proteins, referred to as the immunophilins. This class of protein is widely distributed across both prokaryotes and eukaryotes (Handschumacher et al., 1984; Wang et al., 2005; Kim et al., 2012). Plant CYPs have been shown to participate in a diversity of physiological processes, including protein folding, transcriptional regulation, and stress response (Santos and Park, 2019). For example, the rice protein CYP18-2, regulates the transcription and post-transcriptional modification of a number of stress-related genes (Lee et al., 2015), and over-expression of rice *CYP19-4* could enhance the plant cold tolerance as well (Yoon et al., 2016). There are 29 genes predicted to encode CYP or CYP-like proteins in the *Arabidopsis thaliana* genome (He et al., 2004). The ROC3 (also known as AtCYP19-1) has been shown to boost the plant's ability to withstand infection by the pathogen *Pseudomonas syringae* (Pogorelko et al., 2014). The present experiments were designed to explore whether ROC3 also plays any roles in drought stress tolerance and ABA signaling in *A. thaliana*.

MATERIALS AND METHODS

Plant Materials and Growing Conditions

The *A. thaliana*, Columbia-0 (Col-0) was used as the wild-type (WT) for all experiments in this study. Seeds of the two T-DNA insertion mutants, *roc3-1* (SALK_063724c) and -*2* (SALK_095698c), in Columbia-0 background, were obtained from Arabidopsis Biological Resource Center (http://abrc.osu.edu/). The homozygous status of both T-DNA mutants was verified using a PCR assay (primer sequences are given in **Supplementary Table 1**). Seeds were surface sterilized in 75% v/v ethanol for 3 min, followed by 1 min in 95% v/v ethanol and then dried in air. The sterilized seeds were plated on half strength Murashige and Skoog (1962) medium (1/2 MS) containing 0.7% w/v agar. The plates were kept in the dark for 3 days at 4°C for vernalization, then transferred to a controlled growth chamber (∼70% relative humidity) for 7–10 days, with 16 h photoperiod (100 μmol $m^{-2}s^{-1}$ fluorescent lamp light) and day/night temperature regime of 22 ± 1°C/16 ± 4°C. Thereafter, the seedlings were transplanted to pots containing mixture of soil and vermiculite (2:1 (v/v), and transferred back to the growth chamber.

Generation of Transgenic Plants Harboring p*ROC3::GUS* and GUS Assay

The *ROC3* native promoter, 1854 bp fragment upstream of the initiation codon (from CTTCTCACAT to AAAAAAAGAA of WT genomic DNA), was PCR-amplified from WT genomic DNA using the primer pair *ROC3-GUS-F/R* (sequences are given in **Supplementary Table 1**) and the amplicon was inserted into the HindIII and SmaI cloning sites of the p*Cambia-ubiGUS* vector to generate the construct p*ROC3::GUS*. The recombinant plasmid was introduced into *Agrobacterium tumefaciens* strain GV3101, then transformed into *Arabidopsis* via *Agrobacterium*-mediated transformation using the floral dip technique (Clough and Bent, 1998). p*ROC3::GUS* activity was detected in seedling (2-week-old), root (2-week-old), leaf (2-week-old), flower (6-week-old), silique (8-week-old), and guard cells (4-week-old) of transgenic plants. The described plant tissues were immersed for ∼3 h at 37°C in 50 mM sodium phosphate buffer (pH 7.2) containing 2 mM X-Gluc, 2 mM $K_3Fe(CN)_6$, 2 mM $K_4Fe(CN)_6$, 0.1% v/v Triton X-100, and 10 mM EDTA. Subsequently, the samples were incubated in absolute ethanol to remove chlorophyll and then inspected under a stereomicroscope (SZX2-ILLT; OLYMPUS, Tokyo, Japan). For ABA treatment tests, the samples were treated with 50 μM ABA or absolute ethanol (solvent control) respectively for 2.5h before staining. Relative GUS activity was quantified from three independent biological replicates using ImageJ open source software (v. 1.37, https://imagej.nih.gov/ij/).

Subcellular Localization Assay of *ROC3*

To generate the construct p*35S::ROC3-GFP*, the full length cDNA of *ROC3* was PCR-amplified from WT cDNA using the primer pair *ROC3-GFP-F/R* (**Supplementary Table 1**) and the amplicon inserted into the BamHI and SalI sites of the *pBI221-GFP* vector, with the GFP in the carboxyl terminus (Lin et al., 2009). The plasmids p*35S::GFP*, p*35S::ROC3-GFP* and

p*35S::AHL22-RFP* (used as a nuclear localization marker) (Xiao et al., 2009) were isolated with NucleoBond® Xtra Midi Kit (Macherey-Nagel, Germany) and transfected into Arabidopsis mesophyll protoplasts (Sheen, 2001). The protoplast cultures were incubated in the dark for 16 h at 23°C and then fluorescence was assessed using laser scanning confocal microscopy (LSM880; Carl Zeiss, Oberkochen, Germany). The GFP signal was detected at excitation wavelengths of 488 and emission between 495 and 540 nm. The excitation of RFP was conducted at 543 nm, with emission being captured between 580 and 620 nm.

Stomatal Aperture Assay

The bioassay for stomatal aperture was performed as reported by Li et al. (2016) with a slight modification. In short, the leaves of 4-week-old plants were excised and incubated in closure buffer (20 mM KCl, 1 mM $CaCl_2$, 5 mM MES-KOH, pH 6.15) at 23°C for 2.5 h in light (100 μmol $m^{-2}s^{-1}$ fluorescent lamp light), then added ABA (1, 10, 50 μM), 20 mM 3-amino-1,2,4-triazole (AT, an inhibitor of catalase) (Jannat et al., 2011), 100 μM H_2O_2 or absolute ethanol (solvent control) respectively for an additional 2.5 h in the same incubation place and condition. Subsequently, abaxial epidermal strips were peeled off and immediately photographed by a light inverted microscope. Stomatal aperture width and length were measured by the open access software ImageJ (v1.37, https://imagej.nih.gov/ij/). Each experiment included at least three biological replicates, with no fewer than 60 guard cells that were measured per each sample. The Student's *t*-test was used to determine whether differences between mean values were statistically significant.

Drought Stress and Water Loss Experiments

Seedlings were potted into the soil/vermiculite mixture and grown for about 4 weeks in well-watered condition, then water was withheld for 3 weeks. At the end of the treatment, the plants were re-watered over a 3 d period and photographed. Water loss assay from detached rosette leaves was sampled from 4-week-old well-watered plants. Detached rosette leaves were placed on filter paper in the light at room temperature and measured by weighing the leaves every 30 min over a 3 h period to measure the rate of water loss. The entire experiment was performed at least three biological replicates in the controlled growth chamber under the same light condition.

qRT-PCR Assay

Two-week-old seedlings grown on a half-strength Murashige-Skoog (1/2 MS) medium (0.7% w/v agar) were incubated in liquid 1/2 MS for 24 h in a growth chamber (∼70% relative humidity, 16 h photoperiod, 100 μmol $m^{-2}s^{-1}$ fluorescent lamp light, 22 ± 1°C/16 ± 4°C). Then the first set of seedlings was transferred to 1/2 MS liquid medium containing ABA (final concentration 50 μM); and a second set of seedlings was exposed on filter paper for drought treatment. Both ABA and drought treated seedlings, together with their control samples, were placed in the controlled growth chamber. Treated samples and their controls were collected at the same time after treatments, and snap-frozen in liquid nitrogen. RNA extracted from the frozen seedlings using the TRIzol reagent (Sigma–Aldrich, St. Louis, United States), was used to synthesize cDNA using a 5X All-In-One MasterMIX (with an AccuRT Genomic DNA Removal Kit (ABM, Canada). A quantitative real time (qRT)-PCR assay was performed using the FastStart Universal SYBR Green master mix (Roche, Basel, Switzerland) and the *ROC3-qRT-F/R* and *ACTIN2-qRT-F/R* primer pairs (**Supplementary Table 1**). qRT-PCR was also performed to quantify the transcript abundances of various genes encoding ROS signaling enzymes and stress-responsive proteins using specific primer pairs (**Supplementary Table 1**). All the quantitative analyses included three independent biological replicates, and each replicate contained three technical duplicates. *ACTIN2* used as the internal reference. The reaction steps were firstly pre-incubated at 95°C for 300 s, then ran 40 cycles with 95°C for 15 s, 58°C for 15 s, and 72°C for 20 s. CFX Connect™ Real-Time PCR Detection System (Bio-Rad, California, U.S.A.) was used and the data was quantified by the ΔΔCt method.

Complementation of the *roc3* Loss-of-Function Mutants

The *ROC3* open reading frame was PCR-amplified from Col-0 cDNA using the primer pair *ROC3-C-F/R* (**Supplementary Table 1**). The amplicon was inserted into the SmaI and SacI cloning sites of p*ROC3::GUS* vector to generate the transgene construct p*ROC3::ROC3*. *Agrobacterium tumefaciens* (strain GV3101) was transformed using this construct. The *roc3-1* and *roc3-2* mutants were transformed via *Agrobacterium* mediated transformation using the floral dip method (Clough and Bent, 1998). Transformants were selected on 1/2 MS Agar medium containing 30 mg/L hygromycin. *ROC3* complementation lines generated from *roc3-1* and *roc3-2* mutants were named as C-1 and C-2, respectively.

Guard Cell Isolation and Electrophysiology

A. thaliana guard cell protoplasts were isolated as described previously (Zhang et al., 2008) with slight modifications. In brief, 10–12 rosette leaves from 4-week-old plants were cut off, and epidermal strips were peeled off. Then, the peeled epidermal strips were blended in a blender filled with 750 mL cold distilled water for 30 s, and filtered through a 100-μm nylon mesh and placed in a 10 mL beaker filled with 2 mL enzyme solution I [0.7% Cellulysin cellulase, 0.1% PVP-40, 0.25% BSA in 55% basic solution (5 mM MES, 0.5 mM $CaCl_2$, 0.5 mM $MgCl_2$, 0.5 mM ascorbic acid, 10 μM KH_2PO_4, 0.55 M sorbitol, pH 5.5)]. The beaker was placed in a water bath shaker and shook at 80 rpm for 30 min at 28°C, then 2 mL basic solution was added to enzyme solution I and shook for another 10 min. After that, the strips were filtered through a 100-μm nylon mesh and placed in beaker containing 2 mL enzyme solution II (1.5% Onuzuka cellulase RS, 0.01% cellulase Y-23, 0.25% BSA in 100% basic solution), and shaking was continued at 60 rpm for at least 15 min. Subsequently, the materials were mixed by pipetting up and down with a 1-mL pipette and filtered through a 30-μm nylon mesh. The protoplasts were centrifuged at 800 rpm for 5 min and washed twice with basic solution.

The whole-cell mode patch-clamp electrophysiology tests were carried out as described in the previous articles (Schroeder and Hagiwara, 1989; Pei et al., 1997; Vahisalu et al., 2008; Acharya et al., 2013). For anion current recordings, the bath solution contained 2 mM $MgCl_2$, 30 mM CsCl, 1 mM $CaCl_2$, 10 mM MES-Tris (pH 5.6) and the osmolarity of this solution was adjusted to 480 mOsm with sorbitol. The pipette solution contained 150 mM CsCl, 2 mM $MgCl_2$, 6.7 mM EDTA, 3.35 mM $CaCl_2$, and 10 mM HEPES (pH 7.5), the osmolarity of this solution was adjusted to 500 mOsm with sorbitol. ATP (10 mM Mg-ATP) and GTP (10 mM) were added to it before experiments. The whole-cell currents were recorded using the Axopath-200B amplifier (Molecular Devices, Downingtown, PA, USA) after the whole-cell configuration was achieved. The holding potential was +30 mV and voltage steps were applied from −145 to +35 mV with +30 mV increments, and each test voltage lasted 60 s. For ABA treatment tests, guard cell protoplasts were treated with 50 μM ABA for at least 1h before measurement. In order to obtain the currents and draw the current density voltage plots, pCLAMP software (version10.2; Axon Instruments, Sunnyvale, CA, USA) and SigmaPlot 12.0 (Systat Software, Richmond, CA, USA) were used respectively.

Quantification of Guard Cell ROS and Leaf H_2O_2 and Catalase Levels

Quantification ROS content of both WT and *roc3* guard cells was performed using the fluorescent dye CM-H_2DCFDA (Thermo Fisher, Waltham, MA, USA) as described previously with slight modifications (Miao et al., 2006; Zhang et al., 2011). In order to open the stomata, abaxial epidermis strips were prepared from the leaves of 4-week-old plants and immersed in 1 mM $CaCl_2$, 20 mM KCl, 5 mM MES-KOH (pH 6.15) for 2.5 h in the light; then added 50 μM ABA or absolute ethanol as solvent control and the incubation continued for an additional 2.5 h. At the end of this period, the epidermal peels were transferred to aqueous 50 μM CM-H_2DCFDA for 10 min in the dark, then rinsed at least three times in distilled water to remove excess dye. The H_2DCFDA fluorescence was captured using laser scanning confocal microscope and inverted fluorescence microscope (TI-1; NIKON, Tokyo, Japan), and the fluorescence intensity was quantified by using ImageJ software.

To measure the leaf H_2O_2 content, the leave samples (4-week-old) were first weighed and immersed in liquid buffer (20 mM KCl, 1 mM $CaCl_2$, 5 mM MES-KOH, pH 6.15) for 2.5 h, then added 50 μM ABA or absolute ethanol (solvent control), and the incubation continued for a additional 2.5 h. Snap-frozen leaf material was ground to a powder and processed using a commercial H_2O_2 content determination kit (Comin, Suzhou, China) according to the supplier's protocol. Finally, 200 μL aliquots of these reaction mix were pipetted into plates, and their absorbance at 415 nm was measured; H_2O_2 content was calculated according to the formula: H_2O_2 (μmol/g) = 2.67 × (ΔA − 0.0006) ÷ W (ΔA = A_{sample} − $-A_{blank}$, W : sample weight).

Catalase assay were performed using a CAT detection kit (Comin, Suzhou, China). The samples were treated as described above in the method of H_2O_2 content assay. Then catalase extraction was performed according to the manufacturers' instruction. To quantify catalase, 10 μL aliquot of the extract added to 190 μL of Comin catalase reaction solution in a 96-well UV plate. The reactions' absorbance at 240 nm was recorded immediately (A1) and subsequently after 1 min (A2). Catalase activity was calculated on the basis of the formula: CAT (nmol/min/g) = 918 × ΔA ÷ W (ΔA = A1 − −A2, W : sample weight).

RESULTS

The Response of *ROC3* to ABA Treatment and Drought Stress

Gene expression profiles of *ROC3* showed that the gene was induced by both ABA treatment and drought stress (**Figures 1A,B**). To test spatial expression of *ROC3* promoter, histochemical analysis was performed in transgenic plants expressing p*ROC3::GUS* construct. GUS expression was observed in seedling, leaf, flower, and silique (**Figures 1D–G**). Besides, *ROC3* promoter was mildly induced in the guard cells of plants treated with ABA (**Figures 1C,H,I**). Transient expression of GFP-tagged ROC3 (p*35S::ROC3-GFP*) in Arabidopsis mesophyll protoplasts showed that ROC3 located in both the cytoplasm and the nucleus (**Figure 1J**). To further confirm the nucleus localization of ROC3, the p*35S::ROC3-GFP* was co-transformed into protoplasts with the p*35S::AHL22-RFP* (AHL22, a known nucleus protein), and the GFP and RFP signals substantially overlapped in the nucleus (**Figure 1J**).

The Stomatal Closure in *roc3* Is Hyposensitive to ABA and *roc3* Mutants Show a Lower Tolerance to Drought Stress

Since the expression of *ROC3* could be induced by ABA (**Figure 1A**) and p*ROC3::GUS* was expressed in guard cells (**Figures 1H,I**), we hypothesized that *ROC3* may play a role in ABA-regulated stomatal movement. Two independent T-DNA insertion *roc3* mutants (**Figures 2A,B**; **Supplementary Figure 1**) were used to examine the role of ROC3 in stomatal closure. Under control conditions, stomatal apertures did not show significant difference between either of the *roc3* mutants and WT, but when leaves were treated with a range of ABA concentrations (1–50 μM), the aperture of the mutants' stomata was clearly bigger than that of WT stomata (**Figure 2C**). Similarly, the rate of water loss from *roc3* mutant excised rosette leaves was higher than WT plants (**Figure 2D**), while the survival rate of soil-grown *roc3* mutant plants was lower than that of WT plants after rehydration (**Figures 2E,F**).

The p*ROC3::ROC3* Transgene Rescues the Drought Stress Phenotype of the *roc3* Mutants

To further confirm the function of *ROC3* in stomatal regulation and drought response, we generated transgenic plants harboring p*ROC3::ROC3* in *roc3* mutant backgrounds. The abundance of *ROC3* transcript in the *ROC3* complementation lines, C1 and

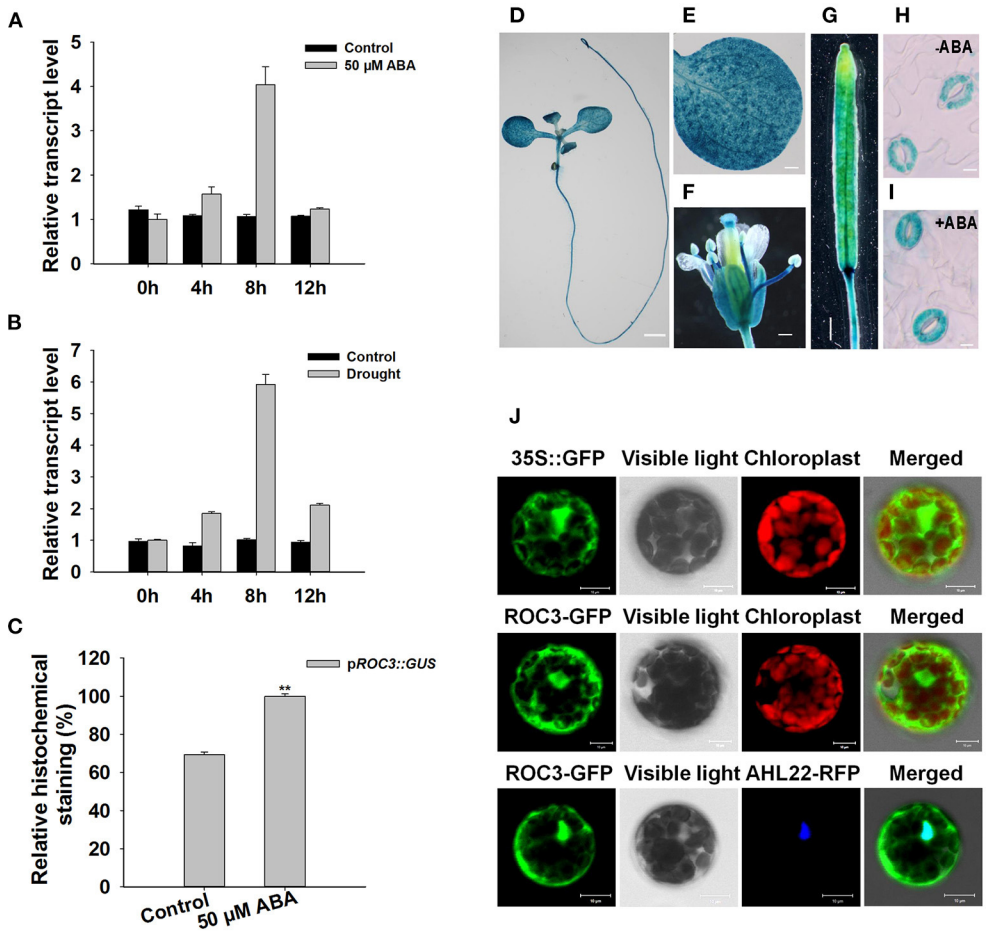

FIGURE 1 | Transcriptional and expression profiling of *ROC3*. **(A,B)** Relative transcript abundances assessed using qRT-PCR in seedlings subjected to **(A)** ABA treatment, **(B)** drought stress. **(C)** Relative GUS activity of p*ROC3::GUS* in guard cells. Error bars represent the SE ($n = 30$), **: means differed significantly from control ($P < 0.01$). The experiments were repeated three times with similar results. **(D–I)** GUS staining reveals the tissue expression of p*ROC3::GUS* transgene in **(D)** the whole seedling (bar: 1.5 mm), **(E)** the leaf (bar: 0.3 mm), **(F)** the flower (bar: 0.3 mm), **(G)** the silique (bar: 1 mm) and **(H,I)** guard cells in plants **(H)** not exposed to ABA (bar: 10μm), **(I)** exposed to 50 μM ABA (bar: 10 μm). **(J)** The topological expression of p*35S::GFP*, p*35S::ROC3-GFP*, and p*35S::AHL22-RFP* in protoplasts (bar: 10 μm).

C2, was similar as in WT plants (**Figure 3A**). When C-1 and C-2 line plants were assessed either for their water loss from detached rosette leaves or their growth response to drought stress, their performance was almost indistinguishable from that of WT plants (**Figures 3B,D,E**). Similarly, stomatal aperture was similar between *ROC3* complementation lines and WT plants upon ABA treatment (**Figure 3C**).

ROC3 Influences the Activation of S-Type Anion Channels in Plants Exposed to ABA

Previous research findings described that the activation of S-type anion channels in guard cell plasma membrane can lead to anion outflow, change in guard cell turgor, and finally promote stomatal closure (Vahisalu et al., 2008; Kim et al., 2010; Zhang et al., 2018). To investigate whether *ROC3* positively regulates ABA-induced stomatal closure through the activation of S-type anion channels, we examined the activity of S-type anion channel currents in guard cells. Under control conditions, no difference was observed for S-type anion channel currents in the guard cells of WT, *roc3* mutants and the two *ROC3* complementation lines. In contrast, in response to ABA, ABA-activated of anion currents was clearly smaller in the *roc3* mutants than in either WT or the C-1 and C-2 lines (**Figures 4A,B**).

The Accumulation of Cytosolic ROS Is Reduced by the Absence of Functional ROC3

ROS are crucial messenger molecules that participate in ABA regulation of anion channels and stomatal movement (Pei et al., 2000; Zhang et al., 2001; Munemasa et al., 2007). We wanted to know whether *ROC3* plays any regulatory roles in ABA-triggered ROS accumulation. Firstly, a fluorescence-based assay was used to measure the ROS content of WT and *roc3* guard cells. In the control condition, the guard cells of *roc3* showed reduced accumulation of ROS compared to WT. In response to ABA, the guard cells of WT showed

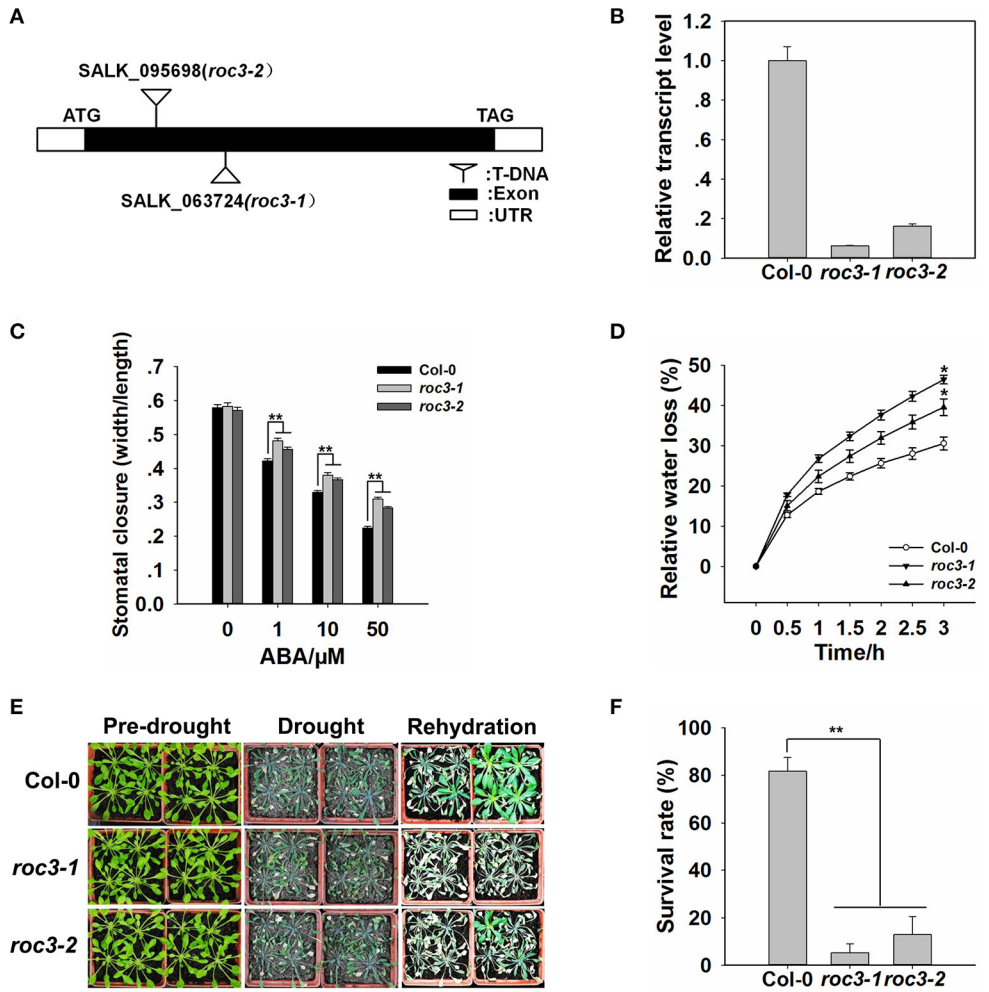

FIGURE 2 | Stomatal closure in *ROC3* knock-down mutants is induced by exposure to ABA and the plants exhibit a lesser level of drought tolerance. **(A)** The T-DNA insertion points in the two independent *roc3* mutants. **(B)** Relative *ROC3* transcript abundances assessed using qRT-PCR in WT and *roc3* seedlings. Values shown in the form mean ± SE ($n = 3$). **(C)** ABA-induced stomatal closure, as quantified by the stomatal width/length ratio measured in at least 60 stomata per genotype per replicate. Error bars represent the SE ($n = 60$), **: means differed significantly from WT ($P < 0.01$). **(D)** The rate of water loss from detached rosette leaves of WT and *roc3* mutants. Values shown in the form mean ± SE ($n = 3$), *: means differed significantly from WT ($P < 0.05$). **(E)** The appearance of WT and *roc3* mutant plants grown under conditions of drought stress. **(F)** The survival rate of WT and *roc3* mutant plants grown under conditions of moisture stress. Data are shown as means ± SE ($n = 8$).

higher accumulation of ROS compared to the guard cells of *roc3* (**Figures 5A,B**; **Supplementary Figure 2**). Similarly, H_2O_2 levels were lower in ABA-treated *roc3* than in ABA-treated WT plants (**Figure 5C**). After ABA treatment, the absence of *ROC3* had no obvious effect on the transcripts of two NADPH oxidase genes, *RbohD* and *RbohF*, which are involved in the ABA induced ROS production (**Supplementary Figure 3**). However, there was a moderate effect on the expression of both *CAT1* and *CAT2*, genes encode catalases which act as ROS scavengers: the expression of both genes was greater in *roc3* mutants than in WT plants upon ABA treatment (**Figures 5D,E**). Similarly, leaf catalase activity was higher in the mutants' leaves than WT in response to ABA treatment (**Figure 5F**).

ROS Accumulation Participates in *ROC3*-Regulated Stomatal Closure

To explore whether *ROC3* was involved in ABA-induced stomatal closure by affecting ROS accumulation, we carried out stomatal closure experiments with H_2O_2 or AT (an inhibitor of catalase) treatment, in the presence or absence of ABA. The absence of functional ROC3 had no discernible effect on H_2O_2-induced stomatal closure in leaf epidermis strips, but the genotypic difference in stomatal aperture induced by ABA treatment was abolished by addition of exogenous H_2O_2 (**Figure 6A**). AT treatment had little influence on the stomatal movement, but the presence of AT promoted ABA-induced stomatal closure and abolished the difference in ABA-promoted stomatal closure between WT and *roc3* (**Figure 6B**).

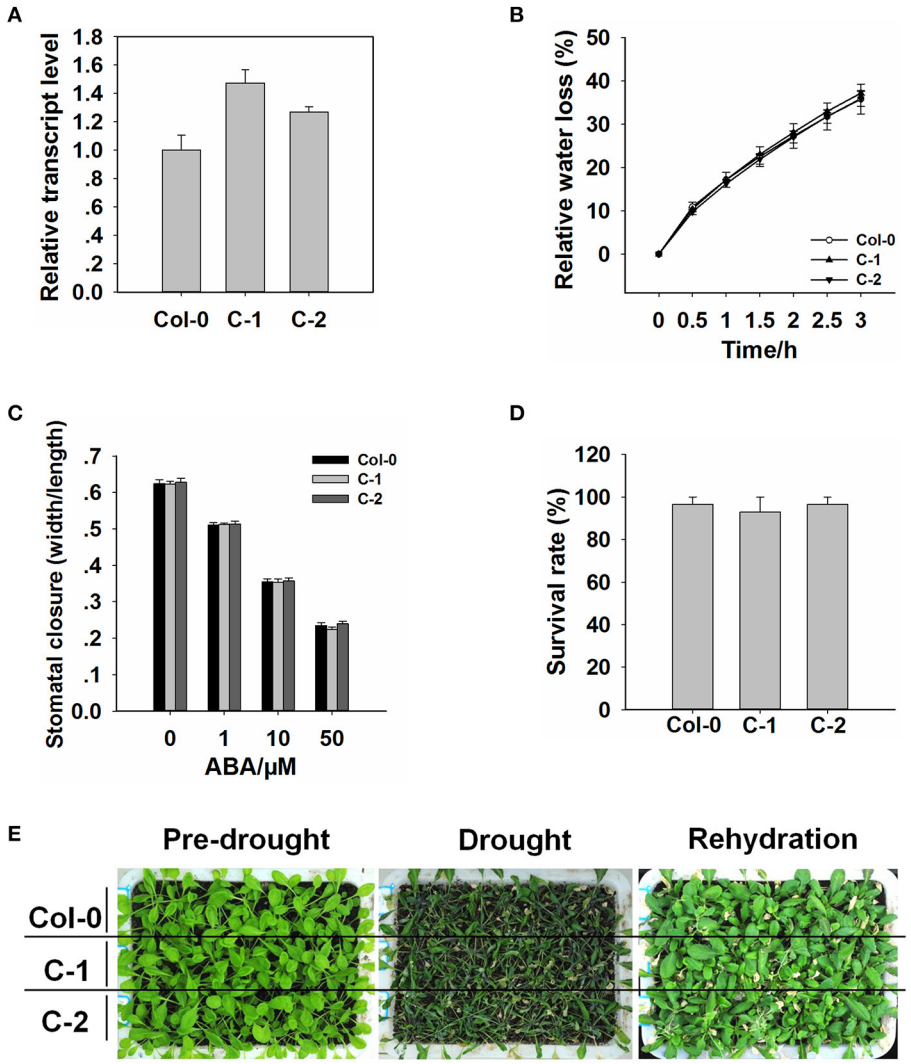

FIGURE 3 | The insertion of the p*ROC3::ROC3* transgene rescues the *roc3* mutants' phenotype. **(A)** Relative *ROC3* transcript abundances assessed using qRT-PCR in WT and the complementation lines C-1 and C-2. Error bars represent the SE ($n = 3$). **(B)** The rate of water loss from rosette leaves detached from WT, C-1, and C-2 plants. Values shown in the form mean ± SE ($n = 3$). **(C)** ABA-induced stomatal closure in the WT, C-1, and C-2 leaf epidermis, stomatal aperture width/length ratios measured in at least 60 stomata per genotype per replicate. Data are shown as means ± SE ($n = 60$). **(D)** The survival rate of WT, C-1, and C-2 plants growing under drought stress conditions. Values shown in the form mean ± SE ($n = 3$). **(E)** The appearance of drought-stressed WT, C-1, and C-2 plants.

ROC3 Influences the Expression Levels of Stress-Responsive Genes

Previous findings have shown that, ABA can induce the expression of many downstream key genes involved in plant dehydration stress (Yamaguchi-shinozaki and Shinozaki, 2006; Ju et al., 2020). An examination of the effect of ROC3 on the transcription of a series of genes known to participate in the stress response (*RD29A*, *RD29B*, *RAB18*, *ABI5*, *ABF2*, *ABF3*, *ERD10*, and *COR47*) showed that in each gene, transcript abundances were lower in *roc3* mutant than in WT plants in response to ABA treatment or drought stress (**Figure 7**).

DISCUSSION

Drought exerts significant negative effects on crop productivity (Boyer, 1982; Venuprasad et al., 2007). Attempts to increase the resilience of crop varieties to this stress via conventional breeding has achieved only a modest level of success, while the potential of transgenic technology to address this issue has also been demonstrated (Manavalan et al., 2009; Hu and Xiong, 2014). The key to the success of a transgenic-based improvement strategy for a specific stress like drought is very much dependent on the specific choice of transgene(s). Therefore, the identification of

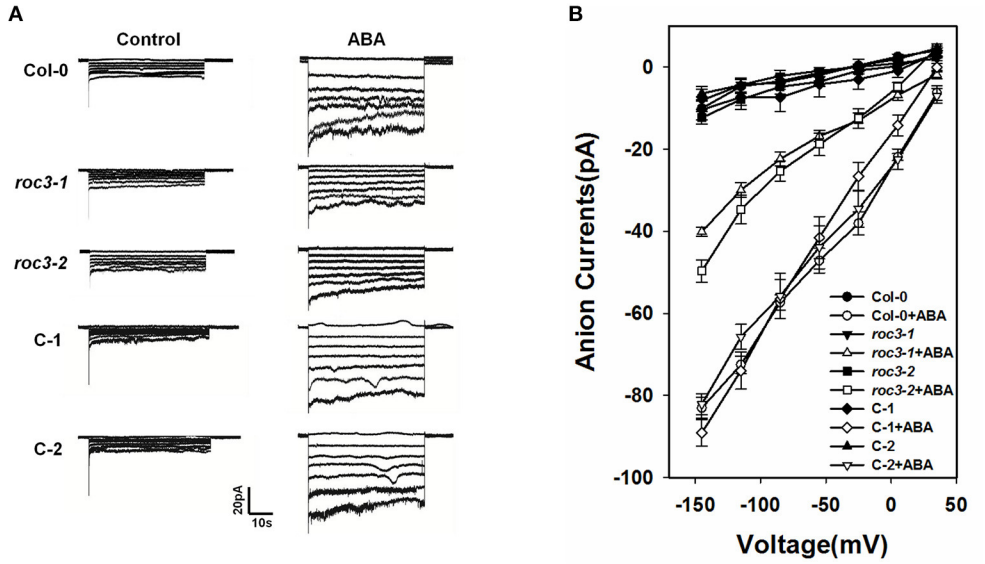

FIGURE 4 | *ROC3* is involved in the ABA-induced activation of anion channels in guard cells. **(A)** Patch-clamp whole cell recordings of S-type anion currents present in guard cell protoplasts isolated from WT, *roc3* mutants and the C-1 and C-2 complementation lines, incubated in the presence/absence of 50 μM ABA. **(B)** Average current-voltage relationships of whole cell S-type anion currents. The number of guard cells measured were: WT (5), WT+ABA (6), *roc3-1* (4), *roc3-1*+ABA (6), *roc3-2* (5), *roc3-2*+ABA (6), C-1 (4), C-1+ABA (6), C-2 (4), C-2+ABA (5). Values shown in the form mean ± SE.

genes contributing to a plant's defense against drought remains a major research priority and it is very much necessary to understand how the candidate genes affect the plant's response to the stress. Most of the water lost by plants passes through the stomata, so control on stomatal movement will have a major impact on the plant's hydration status (Schroeder et al., 2001; Martin-StPaul et al., 2017; Agurla et al., 2018). It has been established that ABA-triggered activation of guard cell anion channels results in the efflux of anions, which in turn reduces the turgor of guard cells to close the stomata (Cutler et al., 2010; Hubbard et al., 2010; Lee and Luan, 2012) and other proteins also have been implicated in this process.

The outcome of our experiments support the notion that the CYP member ROC3 of *A. thaliana* acts as a positive regulator of ABA-induced stomatal closure. *ROC3* was found to be induced by both ABA treatment and the drought stress (**Figures 1A,B**). p*ROC3::GUS* activity was detected in seedling, leaf, flower, silique, and was mildly induced in guard cells upon ABA treatment (**Figures 1C–I**), implying that *ROC3* may play a role in guard cell ABA signaling. The stomata of *roc3* mutant plants were more open than those of WT plants in ABA treatment (**Figure 2C**), and the mutants were also less tolerant of drought (**Figures 2D–F**). Supportively, *ROC3* complementation lines, C1 and C2, restored the WT phenotype (**Figure 3**), suggesting that ROC3 plays a positive regulatory role in ABA-induced stomatal closure and the drought stress response. Plasma membrane localized anion channels are activated by the accumulation of ABA in guard cells, leading to the depolarization of plasma membrane and anion outflow which causes the reduction of guard cell turgor, that ultimately leads to stomatal closure (MacRobbie, 1998; Hedrich, 2012; Roelfsema et al., 2012; Hedrich and Geiger, 2017). A patch clamp experiment demonstrated that in protoplasts exposed to ABA, S-type anion channel activity was lower in *roc3* mutants compared to WT or the *ROC3* complementation line plants (**Figure 4**), indicating that the absence of functional ROC3 causes reduced outflow of anions from the guard cells in response to ABA, hence stomatal aperture remains larger. It remains to be explored how ROC3 influences anion channel activity in response to drought stress or ABA treatment. Further research will be conducted to analyze whether *ROC3* can regulate the expression of the known genes encoding anion channels (e.g., *SLAC1*) or these channels activity regulation (e.g., *CPK3*).

It is well-known that ABA signaling in guard cells requires the participation of multiple signaling elements. Among them, ROS (notably H_2O_2) work as crucial secondary messengers in regulating ABA-induced stomatal closure (Hua et al., 2012; Gayatri et al., 2013; Song et al., 2014; Dietz et al., 2016; Li et al., 2017). A rise in leaf ABA content, due to endogenous processes or an exogenous ABA treatment, stimulates the production of ROS (Bright et al., 2006; Kreslavski et al., 2012). The concentration of ROS in the leaves of *roc3* mutant plants exposed to ABA was less than in WT leaves (**Figures 5A–C**; **Supplementary Figure 2**), consistent with the proposed positive regulatory roles of ROC3 in both stomatal closure and the drought stress response. Interestingly, the stomatal aperture of *roc3* was similar to Col-0's when simultaneously exposed to ABA and H_2O_2, and the hyposensitive phenotype of the *roc3* mutants with respect to ABA-induced stomatal closure was abolished when supplemented with exogenous H_2O_2 (**Figure 6A**). It is possible that ROS act as downstream components during

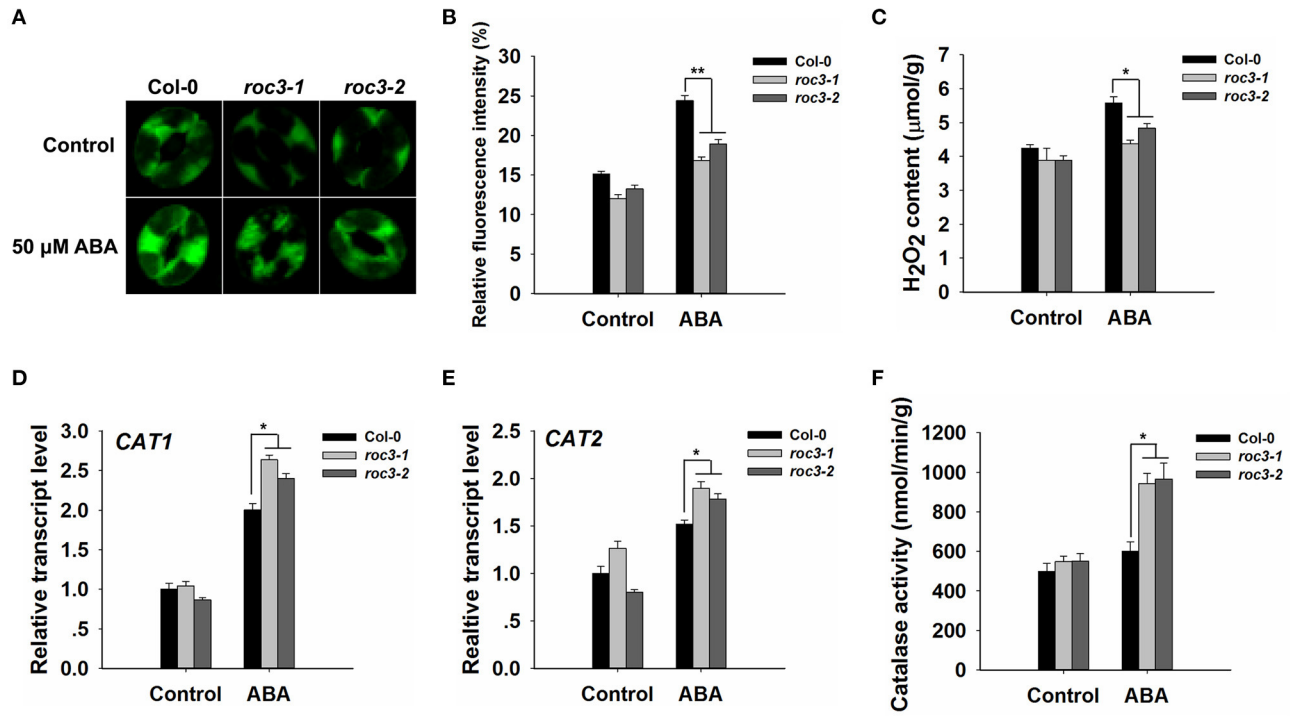

FIGURE 5 | The accumulation of ROS is less efficient in *roc3* mutants than in WT guard cells. **(A)** Laser confocal micrographs revealing the ROS content of guard cells sampled from WT or *roc3* mutant plants either exposed or not exposed to ABA; the fluorescent signal is generated from CM-H_2DCFDA. **(B)** Quantification of the fluorescence intensities shown in **(A)**. At least 100 guard cells were sampled from each genotype. Error bars represent the SE ($n = 100$). The experiments were repeated three times with similar results. **(C)** The H_2O_2 content in the leaf of WT and *roc3* plants, either exposed or not exposed to 50 μM ABA. Values shown in the form mean ± SE ($n = 3$). **(D,E)** Relative transcript abundances assessed using qRT-PCR in plants either exposed or not exposed to ABA: **(D)** *CAT1*, **(E)** *CAT2*. Data are shown as means ± SE ($n = 3$). **(F)** Quantification of catalase activity assay in WT and *roc3* mutants, either exposed or not exposed to 50 μM ABA. Values shown in the form mean ± SE ($n = 3$). *,**: values differed significantly from WT ($P < 0.05$, 0.01).

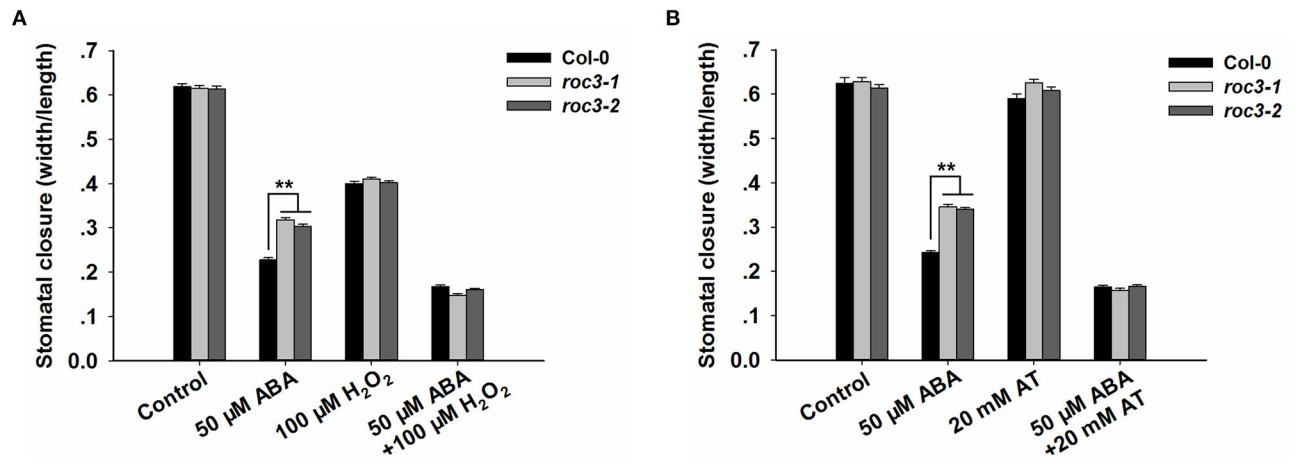

FIGURE 6 | ROC3 participates in ROS signal-regulated stomatal closure. **(A)** Stomatal closure assays of WT and *roc3* mutant leaf epidermis treated with either ABA and/or H_2O_2, and stomatal aperture width/length ratios measured in at least 60 stomata per genotype per replicate. Means shown in the form mean ± SE ($n = 60$), **: means differed significantly from WT ($P < 0.01$). **(B)** Stomatal closure assays of WT and *roc3* mutant leaf epidermis treated with ABA and/or AT, and stomatal aperture width/length ratios measured in at least 60 stomata per genotype per replicate. Values shown in the form mean ± SE ($n = 60$), **: means differed significantly from WT ($P < 0.01$). Both of the experiments were repeated three times.

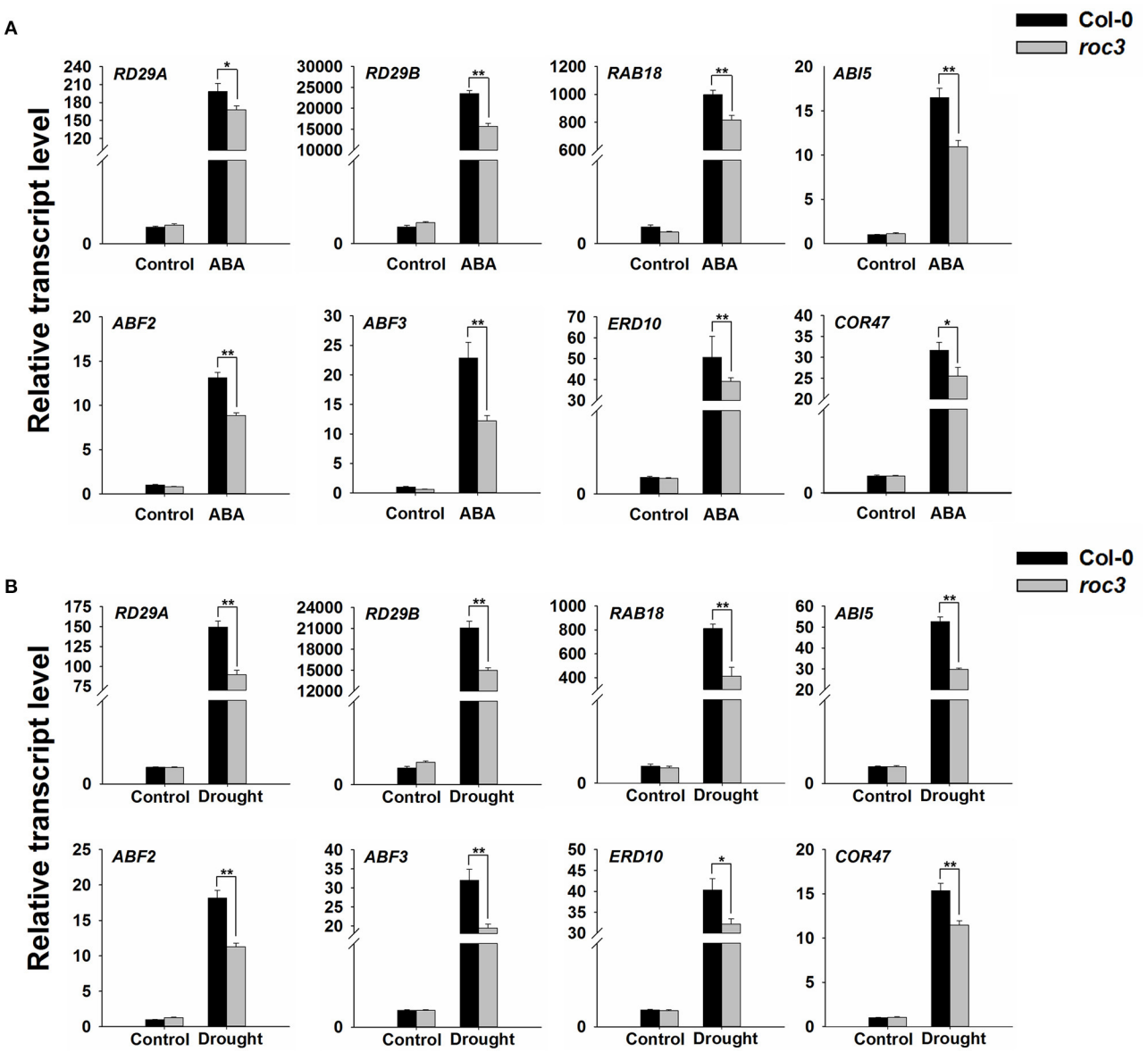

FIGURE 7 | Transcriptional profiling of the indicated genes associated with the stress response in *roc3* mutant exposed to either ABA treatment or drought stress. Relative transcript abundances assessed using qRT-PCR in plants subjected to **(A)** 6 h exposure to ABA, **(B)** 6 h exposure to drought stress. Means shown in the form mean ± SE ($n = 3$), *, **: means differed significantly from control treatment ($P < 0.05, 0.01$).

ROC3-modulated stomatal closure. Previously it has been shown that the ABA-induced production of ROS is primarily catalyzed by plasma membrane localized NADPH oxidases, while ROS neutralization is carried out by various enzymatic (notably catalase) and non-enzymatic antioxidants (Willekens et al., 1995; Zhang et al., 2001; Dietz, 2003; Kwak et al., 2003; Mittler et al., 2004; Mhamdi et al., 2010). In response to ABA, *roc3* mutants showed the upregulation of both *CAT1* and *CAT2* compared to WT plants (**Figures 5D,E**), although the *roc3* plants did not show any differences in the gene expression profile of either *RbohD* or *RbohF* (**Supplementary Figure 3**). Furthermore, higher catalase activity was observed in *roc3* mutants than in WT in response to ABA (**Figure 5F**). These findings suggested that reduced accumulation of ROS in *roc3* mutants was due to a higher level of catalase activity. This hypothesis was tested by stomatal movement experiments with a known catalase inhibitor, AT. The difference of stomatal aperture between WT and *roc3* mutants in ABA treatment was abolished when AT was combined with ABA (**Figure 6B**). Our findings propose that by unknown mechanism ROC3 suppresses catalase activity, thereby affecting the accumulation of ROS that in turn positively regulates ABA-induced stomatal closure.

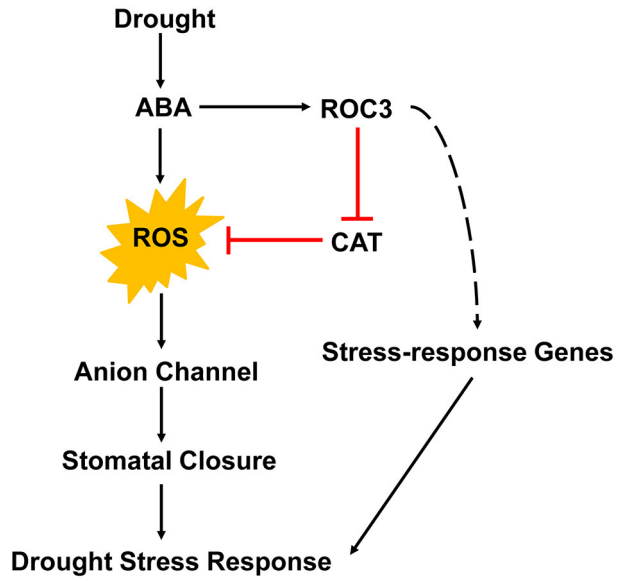

FIGURE 8 | A proposed working model for the role of ROC3 in the regulation of stomatal movement and the drought stress response of *A. thaliana*.

Many genes involved in the drought stress response are known to be induced by ABA treatment (Kang et al., 2002; Yamaguchi-shinozaki and Shinozaki, 2006; Kovacs et al., 2008; Liu and Stone, 2010; Ma et al., 2019; Ju et al., 2020). Comparisons of the profiles of the expression of some of these genes between *roc3* and WT leaves which were either treated with ABA or subjected to drought stress indicated that their expression in response to either stress was somewhat compromised in the mutant (**Figure 7**), providing an additional explanation for the reduced sensitivity of *roc3* to exogenous ABA or drought stress. The mechanistic basis of this interaction is unknown.

A working model summarizing the participation of ROC3 in ABA-induced stomatal closure and the drought stress response of *A. thaliana* is depicted in **Figure 8**. Drought stress promotes the accumulation of ABA in guard cells. Then, ABA induces the production of ROS and subsequently the activation of anion channels that leads to stomatal closure, thereby cutting off the major route by which water is lost from the plant. Our current findings suggest that ROC3 acts as a positive regulator in ABA-induced stomatal closure. ROC3 inhibits CAT activity, thereby maintaining a sufficient level of ROS in guard cells to ensure stomatal closure. At the same time, ROC3 also contributes to both ABA signaling and tolerance to drought stress by maintaining the expression of a number of genes that play important roles in plant's stress response. The present experimental findings have revealed a novel function for ROC3 beyond its known involvement in protein folding, the catalysis of *cis-trans* isomerization of proline imidic peptide bonds in oligopeptides and the response to pathogen infection. The exact mechanism remains to be elucidated how ROC3 interacts with ABA signaling machineries, how it suppresses catalase activity, and how it influences the expression of stress response genes.

DATA AVAILABILITY STATEMENT

The raw data supporting the conclusions of this article will be made available by the authors, without undue reservation.

AUTHOR CONTRIBUTIONS

WZ designed the experiments, interpreted the results, and edited the manuscript. HL performed the major experiments, analyzed the results, and wrote the manuscript. CY and DL performed a few experiments. JS, BA, MW, and DC designed a few experiments and analyzed some data. All authors contributed to the article and approved the submitted version.

FUNDING

This work was financially supported by Distinguished Young Scholar of Shandong University (61200088963137), Natural Science Foundation of Shandong Province (ZR201807100168 to WZ), and National Natural Science Foundation of China (31771353 and 31471158 to MW). Cooperation project on nutritional value and health care function of special vegetable for pregnant women and infants (61200012001902 to WZ).

ACKNOWLEDGMENTS

We thank the Arabidopsis Biological Resource Center (ABRC) for providing T-DNA insertion seeds SALK_063724c, SALK_095698c. We are also thankful to Haiyan Yu, Xiaomin Zhao, and Sen Wang from SKLMT (State Key Laboratory of Microbial Technology, Shandong University) for the assistance in microimaging of LSCM analysis.

SUPPLEMENTARY MATERIAL

The Supplementary Material for this article can be found online at: https://www.frontiersin.org/articles/10.3389/fpls.2021.668792/full#supplementary-material

Supplementary Table 1 | Primer sequences used in the experiments.

Supplementary Figure 1 | PCR screening of homozygous T-DNA mutants of *ROC3*. 1: *roc3-1*-LP+LBb1.3; 2: *roc3-1*-RP+LBb1.3; 3: *roc3-1*-LP+ *roc3-1*-RP; 4: *roc3-2*-LP+LBb1.3; 5: *roc3-2*-RP+LBb1.3; 6: *roc3-2*-LP+ *roc3-2*-RP; M: Marker.

Supplementary Figure 2 | Fluorescence micrographs revealing the ROS content of guard cells sampled from WT or *roc3* mutant plants either exposed or not exposed to ABA; the fluorescent signal is generated from CM-H_2DCFDA and captured by a conventional fluorescence microscope. There are 60 guard cells were sampled from each genotype. Error bars represent the SE ($n = 60$), **: means differed significantly from Col-0 ($P < 0.01$).

Supplementary Figure 3 | Transcriptional profiling of two genes encoding NADPH/respiratory burst oxidase proteins. Relative transcript abundances of **(A)** *RBOHD*, **(B)** *RBOHF*, assessed using qRT-PCR, in WT or *roc3* mutants either exposed or not exposed to ABA. Values shown in the form mean ± SE ($n = 3$).

REFERENCES

Acharya, B. R., Jeon, B. W., Zhang, W., and Assmann, S. M. (2013). Open Stomata 1 (OST1) is limiting in abscisic acid responses of Arabidopsis guard cells. *New phytol.* 200, 1049–1063. doi: 10.1111/nph.12469

Agurla, S., Gahir, S., Munemasa, S., Murata, Y., and Raqhavendra, A. S. (2018). Mechanism of stomatal closure in plants exposed to drought and cold stress. *Adv. Exp. Med. Biol.* 1081, 215–232. doi: 10.1007/978-981-13-1244-1_12

Apel, K., and Hirt, H. (2004). Reactive oxygen species: metabolism, oxidative stress, and signal transduction. *Annu. Rev. Plant Biol.* 55, 373–399. doi: 10.1146/annurev.arplant.55.031903.141701

Boyer, J. S. (1982). Plant productivity and environment. *Science* 218, 443–448. doi: 10.1126/science.218.4571.443

Bright, J., Desikan, R., Hancock, J. T., Weir, I. S., and Neill, S. J. (2006). ABA-induced NO generation and stomatal closure in *Arabidopsis* are dependent on H_2O_2 synthesis. *Plant J.* 45, 113–122. doi: 10.1111/j.1365-313X.2005.02615.x

Clough, S. J., and Bent, A. F. (1998). Floral dip: a simplified method for Agrobacterium-mediated transformation of *Arabidopsis thaliana*. *Plant J.* 16, 735–743. doi: 10.1046/j.1365-313x.1998.00343.x

Corpas, F. J., Barroso, J. B., and del Río, L. A. (2001). Peroxisomes as a source of reactive oxygen species and nitric oxide signal molecules in plant cells. *Trends Plant Sci.* 6, 145–150. doi: 10.1016/S1360-1385(01)01898-2

Cutler, S. R., Rodriguez, P. L., Finkelstein, R. R., and Abrams, S. R. (2010). Abscisic acid: emergence of a core signaling network. *Annu. Rev. Plant Biol.* 61, 651–679. doi: 10.1146/annurev-arplant-042809-112122

Dietz, K. J. (2003). Plant peroxiredoxins. *Annu. Rev. Plant Biol.* 54, 93–107. doi: 10.1146/annurev.arplant.54.031902.134934

Dietz, K. J., Mittler, R., and Noctor, G. (2016). Recent progress in understanding the role of reactive oxygen species in plant cell signaling. *Plant Physiol.* 171, 1535–1539. doi: 10.1104/pp.16.00938

Gayatri, G., Agurla, S., and Raghavendra, A. S. (2013). Nitric oxide in guard cells as an important secondary messenger during stomatal closure. *Front. Plant Sci.* 4:425. doi: 10.3389/fpls.2013.00425

Handschumacher, R. E., Harding, M. W., Rice, J., Drugge, R. J., and Speicher, D. W. (1984). Cyclophilin: a specific cytosolic binding protein for cyclosporin A. *Science* 226, 544–546. doi: 10.1126/science.6238408

He, Z., Li, L., and Luan, S. (2004). Immunophilins and parvulins. Superfamily of peptidyl prolyl isomerases in Arabidopsis. *Plant Physiol.* 134, 1248–1267. doi: 10.1104/pp.103.031005

Hedrich, R. (2012). Ion channels in plants. *Physiol. Rev.* 92, 1777–1811. doi: 10.1152/physrev.00038.2011

Hedrich, R., and Geiger, D. (2017). Biology of SLAC1-type anion channels-from nutrient uptake to stomatal closure. *New Phytol.* 216, 46–61. doi: 10.1111/nph.14685

Hu, H., and Xiong, L. (2014). Genetic engineering and breeding of drought-resistant crops. *Annu. Rev. Plant Biol.* 65, 715–741. doi: 10.1146/annurev-arplant-050213-040000

Hua, D. P., Wang, C., He, J. N., Liao, H., Duan, Y., Zhu, Z. Q., et al. (2012). A plasma membrane receptor kinase, GHR1, mediates abscisic acid, and hydrogen peroxide-regulated stomatal movement in *Arabidopsis*. *Plant Cell.* 24, 2546–2561. doi: 10.1105/tpc.112.100107

Hubbard, K. E., Nishimura, N., Hitomi, K., Getzoff, E. D., and Schroeder, J. I. (2010). Early abscisic acid signal transduction mechanisms: newly discovered components and newly emerging questions. *Genes Dev.* 24, 1695–1708. doi: 10.1101/gad.1953910

Jannat, R., Uraji, M., Morofuji, M., Islam, M. M., Bloom, R. E., Nakamura, Y., et al. (2011). Roles of intracellular hydrogen peroxide accumulation in abscisic acid signaling in *Arabidopsis* guard cells. *J. Plant Physiol.* 168, 1919–1926. doi: 10.1016/j.jplph.2011.05.006

Ju, Y. L., Min, Z., Yue, X. F., Zhang, Y. L., Zhang, J. X., Zhang, Z. Q., et al. (2020). Overexpression of grapevine VvNAC08 enhances drought tolerance in transgenic *Arabidopsis*. *Plant Physiol. Biochem.* 151, 214–222. doi: 10.1016/j.plaphy.2020.03.028

Kang, J. Y., Choi, H. I., Im, M. Y., and Kim, S. Y. (2002). Arabidopsis basic leucine zipper proteins that mediate stress-responsive abscisic acid signaling. *Plant Cell* 14, 343–357. doi: 10.1105/tpc.010362

Kim, S. K., You, Y. N., Park, J. C., Joung, Y., Kim, B. G., Ahn, J. C., et al. (2012). The rice thylakoid lumenal cyclophilin OsCYP20-2 confers enhanced environmental stress tolerance in tobacco and *Arabidopsis*. *Plant Cell Rep.* 31, 417–426. doi: 10.1007/s00299-011-1176-x

Kim, T. H., Böhmer, M., Hu, H., Nishimura, N., and Schroeder, J. I. (2010). Guard cell signal transduction network: advances in understanding abscisic acid, CO_2, and Ca^{2+} signaling. *Annu. Rev. Plant Biol.* 61, 561–591. doi: 10.1146/annurev-arplant-042809-112226

Kollist, H., Nuhkat, M., and Roelfsema, M. R. (2014). Closing gaps: linking elements that control stomatal movement. *New phytol.* 203, 44–62. doi: 10.1111/nph.12832

Kovacs, D., Kalmar, E., Torok, Z., and Tompa, P. (2008). Chaperone activity of ERD10 and ERD14, two disordered stress-related plant proteins. *Plant Physiol.* 147, 381–390. doi: 10.1104/pp.108.118208

Kreslavski, V. D., Los, D. A., Allakhverdiev, S. I., and Kuznetsov, V. V. (2012). Signaling role of reactive oxygen species in plants under stress. *Russ. J. Plant Physl.* 59, 141–154. doi: 10.1134/S1021443712020057

Kwak, J. M., Mori, I. C., Pei, Z. M., Leonhardt, N., Torres, M. A., Dangl, J. L., et al. (2003). NADPH oxidase *AtrbohD* and *AtrbohF* genes function in ROS-dependent ABA signaling in *Arabidopsis*. *EMBO J.* 22, 2623–2633. doi: 10.1093/emboj/cdg277

Langridge, P., and Reynolds, M. P. (2015). Genomic tools to assist breeding for drought tolerance. *Curr. Opin. Biotechnol.* 32, 130–135. doi: 10.1016/j.copbio.2014.11.027

Lee, S. C., and Luan, S. (2012). ABA signal transduction at the crossroad of biotic and abiotic stress responses. *Plant Cell Environ.* 35, 53–60. doi: 10.1111/j.1365-3040.2011.02426.x

Lee, S. S., Park, H. J., Yoon, D. H., Kim, B. G., Ahn, J. C., Luan, S., et al. (2015). Rice cyclophilin OsCYP18-2 is translocated to the nucleus by an interaction with SKIP and enhances drought tolerance in rice and *Arabidopsis*. *Plant Cell Environ.* 38, 2071–2087. doi: 10.1111/pce.12531

Li, C. L., Wang, M., Wu, X. M., Chen, D. H., Lv, H. J., Shen, J. L., et al. (2016). THI1, a thiamine thiazole synthase, interacts with Ca^{2+}-dependent protein kinase CPK33 and modulates the S-type anion channels and stomatal closure in *Arabidopsis*. *Plant Physiol.* 170, 1090–1104. doi: 10.1104/pp.15.01649

Li, J., Wang, X. Q., Watson, M. B., and Assmann, S. M. (2000). Regulation of abscisic acid-induced stomatal closure and anion channels by guard cell AAPK kinase. *Science* 287, 300–303. doi: 10.1126/science.287.5451.300

Li, J. J., Li, Y., Yin, Z. G., Jiang, J. H., Zhang, M. H., Guo, X., et al. (2017). OsASR5 enhances drought tolerance through a stomatal closure pathway associated with ABA and H_2O_2 signalling in rice. *Plant Biotechnol. J.* 15, 183–196. doi: 10.1111/pbi.12601

Lin, H., Wang, R., Qian, Q., Yan, M., Meng, X., Fu, Z., et al. (2009). DWARF27, an iron-containing protein required for the biosynthesis of strigolactones, regulates rice tiller bud outgrowth. *Plant Cell* 21, 1512–1525. doi: 10.1105/tpc.109.065987

Liu, H., and Stone, S. L. (2010). Abscisic acid increases *Arabidopsis* ABI5 transcription factor levels by promoting KEG E3 ligase self-ubiquitination and proteasomal degradation. *Plant Cell* 22, 2630–2641. doi: 10.1105/tpc.110.076075

Ma, Y., Cao, J., Chen, Q., He, J., Liu, Z., et al. (2019). The kinase CIPK11 functions as a negative regulator in drought stress response in *Arabidopsis*. *Int. J. Mol. Sci.* 20:2422. doi: 10.3390/ijms20102422

MacRobbie, E. A. (1998). Signal transduction and ion channels in guard cells. *Philos. Trans. R. Soc. Lond. B Biol. Sci.* 353, 1475–1488. doi: 10.1098/rstb.1998.0303

Manavalan, L. P., Guttikonda, S. K., Tran, L. S., and Nguyen, H. T. (2009). Physiological and molecular approaches to improve drought resistance in soybean. *Plant Cell Physiol.* 50, 1260–1276. doi: 10.1093/pcp/pcp082

Martin-StPaul, N., Delzon, S., and Cochard, H. (2017). Plant resistance to drought depends on timely stomatal closure. *Ecol. Lett.* 20, 1437–1447. doi: 10.1111/ele.12851

Mhamdi, A., Queval, G., Chaouch, S., Vanderauwera, S., Van Breusegem, F., and Noctor, G. (2010). Catalase function in plants: a focus on Arabidopsis mutants as stress-mimic models. *J. Exp. Bot.* 61, 4197–4220. doi: 10.1093/jxb/erq282

Miao, Y., Lv, D., Wang, P., Wang, X. C., Chen, J., Miao, C., et al. (2006). An *Arabidopsis* glutathione peroxidase functions as both a redox transducer and a scavenger in abscisic acid and drought stress responses. *Plant Cell* 18, 2749–2766. doi: 10.1105/tpc.106.044230

Mittler, R. (2002). Oxidative stress, antioxidants, and stress tolerance. *Trends Plant Sci.* 7, 405–410. doi: 10.1016/S1360-1385(02)02312-9

Mittler, R., Vanderauwera, S., Gollery, M., and Van Breusegem, F. (2004). Reactive oxygen gene network of plants. *Trends Plant Sci.* 9, 490–498. doi: 10.1016/j.tplants.2004.08.009

Mori, I. C., Murata, Y., Yang, Y., Munemasa, S., Wang, Y. F., Andreoli, S., et al. (2006). CDPKs CPK6 and CPK3 function in ABA regulation of guard cell S-type anion- and Ca^{2+}- permeable channels and stomatal closure. *PLoS Biol.* 4:e327. doi: 10.1371/journal.pbio.0040327

Munemasa, S., Hauser, F., Park, J., Waadt, R., Brandt, B., and Schroeder, J. I. (2015). Mechanisms of abscisic acid-mediated control of stomatal aperture. *Curr. Opin. Plant Biol.* 28, 154–162. doi: 10.1016/j.pbi.2015.10.010

Munemasa, S., Oda, K., Watanabe-Sugimoto, M., Nakamura, Y., Shimoishi, Y., and Murata, Y. (2007). The coronatine-insensitive 1 mutation reveals the hormonal signaling interaction between abscisic acid and methyl jasmonate in Arabidopsis guard cells. Specific impairment of ion channel activation and second messenger production. *Plant Physiol.* 143, 1398–1407. doi: 10.1104/pp.106.091298

Murashige, T., and Skoog, F. (1962). A revised medium for rapid growth and bioassays with tobacco tissue cultures. *Physiol. Plant.* 15, 473–472. doi: 10.1111/j.1399-3054.1962.tb08052.x

Murata, Y., Mori, I. C., and Munemasa, S. (2015). Diverse stomatal signaling and the signal integration mechanism. *Annu. Rev. Plant Biol.* 66, 369–392. doi: 10.1146/annurev-arplant-043014-114707

Nyathi, Y., and Baker, A. (2006). Plant peroxisomes as a source of signalling molecules. *Biochem. Biophys. Acta* 1763, 1478–1495. doi: 10.1016/j.bbamcr.2006.08.031

Osakabe, Y., Osakabe, K., Shinozaki, K., and Tran, L. S. (2014). Response of plants to water stress. *Front. Plant Sci.* 5:86. doi: 10.3389/fpls.2014.00086

Palma, J. M., Corpas, F. J., and del Río, L. A. (2009). Proteome of plant peroxisomes: new perspectives on the role of these organelles in cell biology. *Proteomics* 9, 2301–2312. doi: 10.1002/pmic.200700732

Pei, Z. M., Kuchitsu, K., Ward, J. M., Schwarz, M., and Schroeder, J. I. (1997). Differential abscisic acid regulation of guard cell slow anion channels in *Arabidopsis* wild-type and abi1 and abi2 mutants. *Plant Cell* 9, 409–423. doi: 10.1105/tpc.9.3.409

Pei, Z. M., Murata, Y., Benning, G., Thomine, S., Klüsener, B., Allen, G. J., et al. (2000). Calcium channels activated by hydrogen peroxide mediate abscisic acid signalling in guard cells. *Nature* 406, 731–734. doi: 10.1038/35021067

Pogorelko, G. V., Mokryakova, M., Fursova, O. V., Abdeeva, I., Piruzian, E. S., and Bruskin, S. A. (2014). Characterization of three *Arabidopsis thaliana* immunophilin genes involved in the plant defense response against *Pseudomonas syringae*. *Gene* 538, 12–22. doi: 10.1016/j.gene.2014.01.029

Raghavendra, A. S., Gonugunta, V. K., Christmann, A., and Grill, E. (2010). ABA perception and signaling. *Trends Plant Sci.* 15, 395–401. doi: 10.1016/j.tplants.2010.04.006

Roelfsema, M. R., Hedrich, R., and Geiger, D. (2012). Anion channels: master switches of stress responses. *Trends Plant Sci.* 17, 221–229. doi: 10.1016/j.tplants.2012.01.009

Santos, I. B. D., and Park, S. W. (2019). Versatility of cyclophilins in plant growth and survival: a case study in *Arabidopsis*. *Biomolecules* 9:20. doi: 10.3390/biom9010020

Schroeder, J. I., Allen, G. J., Hugouvieux, V., Kwak, J. M., and Waner, D. (2001). Guard cell signal transdution. *Annu. Rev. Plant Physiol. Plant Mol. Biol.* 52, 627–658. doi: 10.1146/annurev.arplant.52.1.627

Schroeder, J. I., and Hagiwara, S. (1989). Cytosolic calcium regulates ion channels in the plasma membrane of Vicia faba guard cells. *Nature* 338, 427–430. doi: 10.1038/338427a0

Seo, M., and Koshiba, T. (2011). Transport of ABA from the site of biosynthesis to the site of action. *J. Plant Res.* 124, 501–507. doi: 10.1007/s10265-011-0411-4

Sheen, J. (2001). Signal transduction in maize and Arabidopsis mesophyll protoplasts. *Plant Physiol.* 127, 1466–1475. doi: 10.1104/pp.010820

Song, Y., Miao, Y., and Song, C. P. (2014). Behind the scenes: the roles of reactive oxygen species in guard cells. *New Phytol.* 202, 1121–1140. doi: 10.1111/nph.12565

Vahisalu, T., Kollist, H., Wang, Y. F., Nishimura, N., Chan, W. Y., Valerio, G., et al. (2008). SLAC1 is required for plant guard cell S-type anion channel function in stomatal signalling. *Nature* 452, 487–491. doi: 10.1038/nature06608

Venuprasad, R., Lafitte, H. R., and Atlin, G. N. (2007). Response to direct selection for grain yield under drought stress in rice. *Crop Sci.* 47, 285–293. doi: 10.2135/cropsci2006.03.0181

Wang, X., Shi, X., Hao, B., Ge, S., and Luo, J. (2005). Duplication and DNA segmental loss in the rice genome: implications for diploidization. *New Phytol.* 165, 937–946. doi: 10.1111/j.1469-8137.2004.01293.x

Wang, X. Q., Ullah, H., Jones, A. M., and Assmann, S. M. (2001). G protein regulation of ion channels and abscisic acid signaling in *Arabidopsis* guard cells. *Science* 292, 2070–2072. doi: 10.1126/science.1059046

Willekens, H., Chamnongpol, S., Davey, M., Schraudner, M., Langebartels, C., Montagu, M. V., et al. (1997). Catalase is a sink for H_2O_2 and is indispensable for stress defence in C_3 plants. *EMBO J.* 16, 4806–4816. doi: 10.1093/emboj/16.16.4806

Willekens, H., Inzé, D., Van Montagu, M., and Van Camp, W. (1995). Catalases in plants. *Mol. Breed.* 1, 207–228. doi: 10.1007/BF02277422

Xiao, C., Chen, F., Yu, X., Lin, C., and Fu, Y. F. (2009). Over-expression of an AT-hook gene, AHL22, delays flowering, and inhibits the elongation of the hypocotyl in *Arabidopsis thaliana*. *Plant Mol. Biol.* 71, 39–50. doi: 10.1007/s11103-009-9507-9

Yamaguchi-shinozaki, K., and Shinozaki, K. (2006). Transcriptional regulatory networks in cellular responses and tolerance to dehydration and cold stresses. *Annu. Rev. Plant Biol.* 57, 781–803. doi: 10.1146/annurev.arplant.57.032905.105444

Yoon, D. H., Lee, S. S., Park, H. J., Lyu, J. I., Chong, W. S., Liu, J. R., et al. (2016). Overexpression of OsCYP19-4 increases tolerance to cold stress and enhances grain yield in rice (*Oryza sativa*). *J. Exp. Bot.* 67, 69–82. doi: 10.1093/jxb/erv421

Zhang, J., Wang, N., Miao, Y., Hauser, F., McCammon, J. A., Rappel, W. J., et al. (2018). Identification of SLAC1 anion channel residues required for CO_2/bicarbonate sensing and regulation of stomatal movements. *Proc. Natl. Acad. Sci. U.S.A.* 115, 11129–11137. doi: 10.1073/pnas.1807624115

Zhang, W., Jeon, B. W., and Assmann, S. M. (2011). Heterotrimeric G-protein regulation of ROS signalling and calcium currents in *Arabidopsis* guard cells. *J. Exp. Bot.* 62, 2371–2379. doi: 10.1093/jxb/erq424

Zhang, W., Nilson, S. E., and Assmann, S. M. (2008). Isolation and whole-cell patch clamping of *Arabidopsis* guard cell protoplasts. *CSH Protoc.* 2008:pdb.prot5014. doi: 10.1101/pdb.prot5014

Zhang, X., Zhang, L., Dong, F., Gao, J., Galbraith, D. W., and Song, C. P. (2001). Hydrogen peroxide is involved in abscisic acid-induced stomatal closure in *Vicia faba*. *Plant Physiol.* 126, 1438–1448. doi: 10.1104/pp.126.4.1438

Conflict of Interest: The authors declare that the research was conducted in the absence of any commercial or financial relationships that could be construed as a potential conflict of interest.

frontiers in Plant Science

ORIGINAL RESEARCH
published: 04 June 2021
doi: 10.3389/fpls.2021.677839

Rice Stomatal Mega-Papillae Restrict Water Loss and Pathogen Entry

Mutiara K. Pitaloka[1], Emily L. Harrison[2], Christopher Hepworth[3], Samart Wanchana[4], Theerayut Toojinda[4], Watchara Phetluan[5], Robert A. Brench[2], Supatthra Narawatthana[6], Apichart Vanavichit[7,8], Julie E. Gray[2], Robert S. Caine[2]* and Siwaret Arikit[7,8]**

[1] Faculty of Agriculture at Kamphaeng Saen, Kasetsart University, Nakhon Pathom, Thailand, [2] Department of Molecular Biology and Biotechnology, University of Sheffield, Sheffield, United Kingdom, [3] Department of Animal and Plant Sciences, University of Sheffield, Sheffield, United Kingdom, [4] National Center for Genetic Engineering and Biotechnology (BIOTEC), National Science and Technology Development Agency (NSTDA), Khlong Luang, Thailand, [5] Center for Agricultural Biotechnology, Kasetsart University, Kamphaeng Saen Campus, Nakhon Pathom, Thailand, [6] Thailand Rice Science Institute, Rice Department, Ministry of Agriculture and Cooperatives (MOAC), Suphanburi, Thailand, [7] Rice Science Center, Kasetsart University, Nakhon Pathom, Thailand, [8] Department of Agronomy, Faculty of Agriculture at Kamphaeng Saen, Kasetsart University Kamphaeng Saen Campus, Nakhon Pathom, Thailand

OPEN ACCESS

Edited by:
Wenxiu Ye,
Shanghai Jiao Tong University, China

Reviewed by:
Lifang Zou,
Shanghai Jiao Tong University, China
Yizhou Wang,
Zhejiang University, China

***Correspondence:**
Julie E. Gray
j.e.gray@sheffield.ac.uk
Robert S. Caine
b.caine@sheffield.ac.uk
Siwaret Arikit
siwaret.a@ku.th

Specialty section:
This article was submitted to Plant Physiology, a section of the journal Frontiers in Plant Science

Received: *08 March 2021*
Accepted: *10 May 2021*
Published: *04 June 2021*

Citation:
Pitaloka MK, Harrison EL, Hepworth C, Wanchana S, Toojinda T, Phetluan W, Brench RA, Narawatthana S, Vanavichit A, Gray JE, Caine RS and Arikit S (2021) Rice Stomatal Mega-Papillae Restrict Water Loss and Pathogen Entry. Front. Plant Sci. 12:677839. doi: 10.3389/fpls.2021.677839

Rice (*Oryza sativa*) is a water-intensive crop, and like other plants uses stomata to balance CO_2 uptake with water-loss. To identify agronomic traits related to rice stomatal complexes, an anatomical screen of 64 Thai and 100 global rice cultivars was undertaken. Epidermal outgrowths called papillae were identified on the stomatal subsidiary cells of all cultivars. These were also detected on eight other species of the *Oryza* genus but not on the stomata of any other plant species we surveyed. Our rice screen identified two cultivars that had "mega-papillae" that were so large or abundant that their stomatal pores were partially occluded; Kalubala Vee had extra-large papillae, and Dharia had approximately twice the normal number of papillae. These were most accentuated on the flag leaves, but mega-papillae were also detectable on earlier forming leaves. Energy dispersive X-Ray spectrometry revealed that silicon is the major component of stomatal papillae. We studied the potential function(s) of mega-papillae by assessing gas exchange and pathogen infection rates. Under saturating light conditions, mega-papillae bearing cultivars had reduced stomatal conductance and their stomata were slower to close and re-open, but photosynthetic assimilation was not significantly affected. Assessment of an F_3 hybrid population treated with *Xanthomonas oryzae pv. oryzicola* indicated that subsidiary cell mega-papillae may aid in preventing bacterial leaf streak infection. Our results highlight stomatal mega-papillae as a novel rice trait that influences gas exchange, stomatal dynamics, and defense against stomatal pathogens which we propose could benefit the performance of future rice crops.

Keywords: stomata, subsidiary cells, papillae, silicon, gas-exchange, bacterial pathogen

INTRODUCTION

Rice is an integral food staple that influences economic and social prosperity (Redfern et al., 2012; Pachauri et al., 2014). It is produced in dry, tropical and temperate climates, on average requiring around 2,500 liters of water to produce 1 kg of grain (Bouman, 2009). With increased temperatures and incidences of severe drought forecast, climate-proofing of rice for future environments will be critical; and as water availability for agriculture is predicted to decrease, there is a focus toward generating rice that is more water-use efficient (Jagadish et al., 2015; Wu et al., 2017; Zhou et al., 2017; Caine et al., 2019; Yang et al., 2019). At the same time, rice breeders need to consider how pathogens such as *Xanthomonas oryzae pv. oryzae* (*Xoo*), which causes bacterial blight, and *Xanthomonas oryzae pv. oryzicola (Xoc*), which causes bacterial leaf streak (BLS), will impact on future yields (Niño-Liu et al., 2006). For *Xoc,* which enters through the same microscopic stomatal pores that govern water-use, yield losses can already exceed 30% (Liu et al., 2014). Despite the potential losses caused by *Xoc*, no studies have investigated how altering stomata on rice leaves might affect *Xoc* infection rate.

For most plants, stomata consist of a pair of guard cells surrounding a central pore (Zeiger et al., 1987). Stomatal opening permits atmospheric CO_2 uptake for photosynthetic assimilation, and facilitates the diffusion of water vapor in the opposite direction. This loss of water drives a transpiration stream, permitting evaporative cooling and internal movement of solutes from roots to shoots (Hetherington and Woodward, 2003; Hepworth et al., 2015; Caine et al., 2019). Stomatal closure prevents water loss and mitigates against pathogens which enter through the pore - key traits in conserving water and protecting against disease, but it also prevents CO_2 uptake (Flexas and Medrano, 2002; Martin-StPaul et al., 2017; Ye et al., 2020). Over longer durations, plants can modulate gaseous exchanges and defense against pathogens via changes to stomatal development (Lake et al., 2001; Casson and Gray, 2008; Beerling and Franks, 2009; Dutton et al., 2019). This leads to alterations in the number and or size of stomata that form on developing leaves. By adjusting stomatal opening and stomatal development, uptake of CO_2 can be tightly balanced with water loss and defense against pathogens. These adjustments to stomatal number, size, and pore aperture help plants to thrive in otherwise adverse environments.

There is considerable morphological variation in stomata between different types of plants, with dicots typically forming pairs of kidney-shaped guard cells and monocot grasses having dumbbell-shaped guard cells (Stebbins and Shah, 1960; Hepworth et al., 2018; Nunes et al., 2020). The stomatal complexes of all grass (and some dicot) species, have subsidiary cells adjacent to their guard cells (Stebbins and Shah, 1960; Rudall et al., 2017). Subsidiary cells are suggested to improve the efficiency of turgor changes in guard cells, thereby enabling quicker opening and closing (Hetherington and Woodward, 2003; Cai et al., 2017; Bertolino et al., 2019). Due to the apparent importance of stomatal complex morphology to grass performance, the volume of associated research is growing rapidly (Liu et al., 2009; Taylor et al., 2012; Chen et al., 2017; Raissig et al., 2017; McKown and Bergmann, 2018; Chatterjee et al., 2020).

Genetic modification (GM) and gene editing have been employed to alter stomatal properties and have demonstrated improved drought tolerance and/or enhanced water-use efficiency in crops and model species (Huang et al., 2009; Yoo et al., 2010; Liu et al., 2012; Hepworth et al., 2015; Hu et al., 2017; Hughes et al., 2017; Li et al., 2017; Caine et al., 2019). This breadth of research demonstrates that there is scope to manipulate stomata to improve plant water-use. However, for many rice producing countries, the growth of crops that have undergone GM or gene editing is currently prohibited (Whitty et al., 2013). Consequently, other naturally derived or non-GM techniques are required to produce plants with stomatal-based changes that improve drought tolerance and or water-use efficiency.

Papillae are dense microscopic outgrowths formed on the epidermis of many plant species including rice (Prasad et al., 2011; Chowdhury et al., 2014; Gorb et al., 2017; Kang et al., 2017; Young et al., 2017). They are found on both earlier and later diverging plant lineages and fulfil a diverse array of functions (Banks and Davis, 1969; Haworth and McElwain, 2008; Duarte-Silva et al., 2013; Chowdhury et al., 2014). In barley (*Hordeum vulgare*) and *Arabidopsis thaliana*, papillae form in response to powdery mildew hyphae, thereby helping to prevent pathogen infection (Thordal-Christensen et al., 1997; Hückelhoven et al., 1999; Maekawa et al., 2014). On lotus leaves, they prevent films of water by reducing the contactable surface area for water droplets, which in turn improves the overall waterproofing of the leaf (Ensikat et al., 2011). In other species, including members of the Proteaceae, papillae aid in photoprotection by reducing the amount of light that passes to the underlying mesophyll (Jordan et al., 2005). Further functions include the production of mucilage and slime in certain lower land plants (Proust et al., 2016), and potentially in regulating gas exchange around stomata (Maricle et al., 2009; Sack and Buckley, 2016).

Reports of papillae developing in close proximity to stomata come from both extant and extinct plant species (Pant and Mehra, 1964; Palmer et al., 1981; Fischer et al., 2010; Prasad et al., 2011). They have been detected on epidermal pavement cells adjacent to stomata and in some instances on subsidiary cells. For grasses, subsidiary cell papillae (SCP) do not appear to be ubiquitous across all members of the Poaceae, instead evidence suggests they are limited to a relatively small number of species, including certain members of the Olyreae (includes bamboo) and Oryzeae tribes (Palmer et al., 1981, 1983; Lima et al., 2020). It has been suggested that papillae forming near stomata may restrict gas flow thereby improving water-use efficiency (Maricle et al., 2009; Lima et al., 2020). However, because papillae have also been detected in species such as rice (Luo et al., 2012; Chatterjee et al., 2020), where water availability is often plentiful, additional roles for papillae are probable. These include preventing water build-up, entry of certain fungal and bacterial pathogens, or protecting against stomatal pore occlusion, such as when volcanic dust particles are prevalent in the atmosphere (Haworth and McElwain, 2008;

McElwain and Steinthorsdottir, 2017; Lima et al., 2020). Many molecular components have been detected in papillae including silicon (Si) callose, cellulose, lignins, araboxylans, reactive oxygen species, phenolics, peroxidases, thionins, and aromatic compounds (Thordal-Christensen et al., 1997; Cai et al., 2008; Voigt, 2014; Guerriero et al., 2018).

In this study, we focus on the form and function of abnormally large or abundant papillae, which are located on the subsidiary cells of stomatal complexes of particular rice cultivars, which we term "mega-papillae." We assess gas exchange, stomatal dynamics and pathogen responses with a view to understanding if mega-papillae could help improve the performance of future rice crops.

MATERIALS AND METHODS

Plant Material and Growth Conditions

The 164 international rice germplasm screened in this study were obtained from either the International Rice Research Institute, Los Banos, Philippines (100 varieties) or the Thai seedbank, Kamphaeng Saen, Thailand (64 varieties) and are listed in **Supplementary Table 1**.

Seedlings were germinated in Petri dishes filled with water and incubated at room temperature (26–27°C) for 4–5 days with 12 h of daylight. Plants were then transferred to trays filled with clay soil (collected from the field) and were subsequently planted into rice paddies at the Kamphaeng Saen Campus, Nakhon Pathom, Thailand. Screening for stomatal properties of flag leaves was conducted on plants grown under field conditions during February to June 2016. The Dharia (Bangladesh) and Kalubala Vee (Sri Lanka) varieties were selected for further study due to their mega-papillae phenotype. The high yielding IR64 rice variety (IRRI, Philippines) was used as a control due to it having an average size and number of SCP. For observations of papillae on different leaves, seedlings were germinated in Petri dishes filled with ∼20 ml of water and cultivated for 7–8 days in a Sanyo growth cabinet set to 12 h 26°C: 12 h 24°C light: dark, with 200 μmol m^{-2} s^{1} photosynthetically active radiation (PAR). Seedlings were then transferred to 13 cm diameter pots (0.88 L) using the soil mixture described by Caine et al. (2019) and propagated in growth cabinets (Conviron Controlled Environments Ltd, Winnipeg, MB, Canada) at 12 h 30°C: 12 h 24°C light: dark cycle, PAR 1,000 μmol m^{-2} s^{-1} and 60% relative humidity. Pots were constantly standing in water, and soil was also supplied with water from above once a week. Plants used for gas exchange and pathogen experiments were grown in 4 liter pots in a greenhouse at Khampaeng Saen Campus with approximately 12 h daily sunlight at ∼348 μmol m^{-2} s^{1} PAR and an average 34°C temperature and 74% humidity, and kept well-watered throughout. Gas exchange experiments were performed on plants which were 75–85 days old, and pathogen experiments were performed on flag leaves of 75 day old plants.

Sample Collection and Imaging

To observe SCP phenotypes in DH, KV and IR across different leaves, epidermal impressions were taken from leaf 5 (20 to 25 days after germination), maximum tillering (45–50 days after germination) and flag leaf stages (75–80 days after germination) from plants grown in growth chambers. Stomatal impressions from mature leaves of *Carica papaya, Cocos nucifera, Echinochloa crus-galli, Musa acuminate, Oryza officinalis, Oryza rufipogon, Oryza nivara, Oryza puntata, Oryza latifolia, Oryza australiansis, Oryza brachyantha, Oryza ridleyi, and Zea Mays* were collected from plants growing around the Kamphaeng Saen campus between December 2018 to February 2019. For *Arabidopsis thaliana*, *Brachypodium distachyon, Hordeum vulgare, Physcomitrium patens, Osmunda regalis,* and *Selaginella kraussiana* stomatal images were collected from mature leaves or sporophytes grown under controlled conditions.

For quantification purposes, 8 biological replicates per genotype per rice leaf stage were collected. Impressions were taken using dental resin (Coltene Whaledent, Switzerland) on the abaxial surface of leaves, 3/4 of the up way from where the leaf emerged from the sheaf. Nail varnish was applied to the set resin to make imprints for microscopy analysis. Imaging of SCP number and size was conducted using a light compound microscope (Leica, DM750-ICC50 HD), with quantification performed using ImageJ (Schindelin et al., 2012). SCP number was counted from five randomly selected stomata per field of view (FOV) and averaged, with all individual papilla areas on each stomate measured using the Polygon plug-in tool. Measured areas were averaged to give an overall value per stomate, and then the 5 stomate values were averaged to give an average papilla area per FOV. We measured 6 FOVs per replicate per developmental stage.

Scanning electron microscopy samples were fixed in 2.5% Glutaraldehyde for 1 h and washed in 0.1 M Sodium-Potassium phosphate buffer solution for 10 min. Samples were then treated in 1% Osmium tetroxide for 1 h at 4°C, followed by a dehydration series in ethanol concentrations of 30, 50, 70, 80, and 90% for 10 min each, and then rinsed three times further with 100% ethanol for 10 min. To completely dry samples, each sample was placed in critical point dryer. Samples were mounted on aluminum stubs, attached with carbon sticky tabs, and coated with approximately 20 nm of gold via an ion coater (Eiko engineering IB-2). Visualization was performed using a Hitachi SU8020 at an accelerating voltage of 10 Kv. For confocal imaging, samples were collected from fully expanded flag leaves, cut into 3–4 mm strips, then fixed and cleared in modified Carnoy's solution (acetic acid 7:1 ethanol). Samples were then stained with propidium iodide (PI, 1:100 of a 1 mg/ml stock) for $\geq$ 5 min and then mounted in chloral hydrate for imaging. For cross-sections, samples were fixed in formaldehyde fixative solution for 2 h and vacuum infiltrated for 1 h. Samples were washed with PEM buffer before dehydration with an ethanol series of 20, 30, 50, 70, 80, 90, 100, and 100% for 30 min each and followed by infiltration with a series of resin in ethanol solutions with resin concentrations of 10, 20, 30, 50, 70, 80, 90, 100, 100, and 100%. The samples were then transferred to gelatin capsules to solidify. Resin capsules were sectioned using a microtome and the sections were stained with 0.25% calcofluor white and washed with 1x PBS

before preparing for imaging. Imaging was performed using a Nikon A1 (Tokyo, Japan).

For elemental analysis of papillae, the samples were collected from fully expanded flag leaves and prepared as described for SEM imaging. Chemical content analysis was performed with a Tescan-Mira3 field emission-scanning electron microscope (Czech Republic), with an energy dispersive X-Ray spectrometer (EDS) installed.

Leaf Gas Exchange

Measurements of A and g_s were conducted on fully expanded flag leaves using a LI-COR LI-6400XT Portable Photosynthesis System (Lincoln, NB, United States). Chamber flow rate was set to 400 μmol s^{-1}, leaf temperature to 32°C, reference [CO_2] to 400 ppm and light intensity to 2,000 μmol m^{-2} s^{-1} PAR. Relative humidity inside the chamber was kept at 65–75% using self-indicating desiccant. For light-dark-light response curves, plants were first acclimatized at saturating light (2,000 μmol m^{-2} s^{-1} PAR) for 15–20 min, measurements were then recorded at steady-state for 10 min, this was then followed by 10 min of complete darkness (0 μmol m^{-2} s^{-1} PAR), and finally, saturating light was re-applied for the final 10 min. At each light intensity, 20 measurements for A and g_s were taken, and intrinsic water use efficiency (iWUE) was calculated as A/g_s.

Infection of Rice Hybrids With *Xanthomonas oryzae* pv. *oryzicola*

For pathogen experiments, mega-papillae bearing Dharia was first crossed with Pathum Thani 1 (PT1), a local rice variety commonly grown in Thailand that has a normal number of SCP. F_1 seeds were left to self-pollinate to produce the F_2 generation, which was then phenotyped and genotyped to confirm the presence or absence of the mega-papillae trait by using the Kompetitive Allele Specific PCR (KASP) marker and these plants were left to self-pollinate. F_2 plants were also PCR genotyped to identify those without the *xa5* resistance allele. In the F_3 generation, 88 seeds from an F_2 homozygous plant (Papillae phenotype without *xa5*) were grown in trays in the greenhouse and irrigated frequently. To prepare the cell suspension, cultures of *Xanthomonas oryzae* pv. *oryzicola* were grown in a peptone sucrose agar medium and incubated for 48–72 h at 28°C. The bacterial cell suspension was prepared, and the concentration was determined and adjusted to an OD of 0.4 at 600 nm (10^8 CFU/ml) using a spectrophotometer. Pathogen inoculation was conducted using a spraying method and inoculated plants were kept in the greenhouse without watering for one night, before watering normally again the following day. Disease symptom evaluations were performed 14 days after inoculation with *Xoc*. Disease scoring standard was adapted from the standard evaluation system of the International Rice Research Institute (IRRI, 2013) which corresponds to 5 index values:

1. Index value 1: A resistant plant that almost no symptoms with leaves that are 0–1% infected.
2. Index value 3: A plant that has good resistance with leaves showing greater than 1% but less than 5% infection.
3. Index value 5: A plant that has moderate resistance, which has leaves that are 6–25% infected.
4. Index value 7: A plant that is susceptible with leaves that are 25–50% infected.
5. Index value 9: A very susceptible plant with more than 50% of the leaf being infected.

Graphs and Statistical Analysis

All graphs were developed, and statistical analysis conducted using Sigmaplot V14 (Systat Software, Inc., San Jose, CA, United States). One-way ANOVAs were performed to determine if there were interactions between samples or treatments for a given parameter measured. *Post hoc* tests (Holm-Sidak) were performed for all graphs on **Figures 1**, **3B,C,F**, **4D,E** to identify significant differences between samples.

RESULTS

Characterization of Papillae on 164 Rice Cultivars

To identify morphological traits that might aid in improving rice abiotic and biotic stress responses, we examined the abaxial flag leaf surfaces of 164 rice cultivars (**Supplementary Table 1**) using light microscopy to inspect leaf impressions. Epidermal pavement cells and stomatal complexes were evident, as were silica cells, trichomes and large numbers of small papillae (**Figure 1A**). For all rice varieties, we found that papillae were not only located on epidermal pavement cells but also on the subsidiary cells of stomatal complexes. There were usually four subsidiary cell papillae (SCP) present on each stomatal complex, with two on each subsidiary cell (see schematic example in **Figure 1A**). However, for two cultivars, Dharia (DH, *Oryza sativa* L. ssp. *Indica*) and Kalubala Vee (KV, *Oryza sativa* L. ssp. *Indica*), we detected striking SCP phenotypes. Compared to the 162 other cultivars examined, including IR64 (IR, a high-yielding representative example), DH had a greater number of SCP (usually 8 SCP per stomatal complex), and KV had much larger SCP (**Figure 1B**). The extended shape and/or spatial positioning of SCP on DH and KV, resulted in papillae extending markedly across the guard cells and into the stomatal pore region (**Figure 1C**). Due to the observed SCP differences, we broadly term the papillae found on DH and KV subsidiary cells as "mega-papillae."

Mega-Papillae Are Present on Leaves at Seedling, Maximum Tillering and Flag Leaf Stages

To assess whether mega-papillae occur on the subsidiary cells of expanded leaves prior to the flag leaf stage, we quantified the SCP number and size in DH and KV, and also in IR (for comparison with a cultivar possessing the normal size and number of SCP) across three different growth stages. These were the seedling (leaf 5, 20–25 days old), maximum tillering (45–50 days old), and flag leaf (75–80 days old) stages. To first confirm our initial screening observations, flag leaf SCP

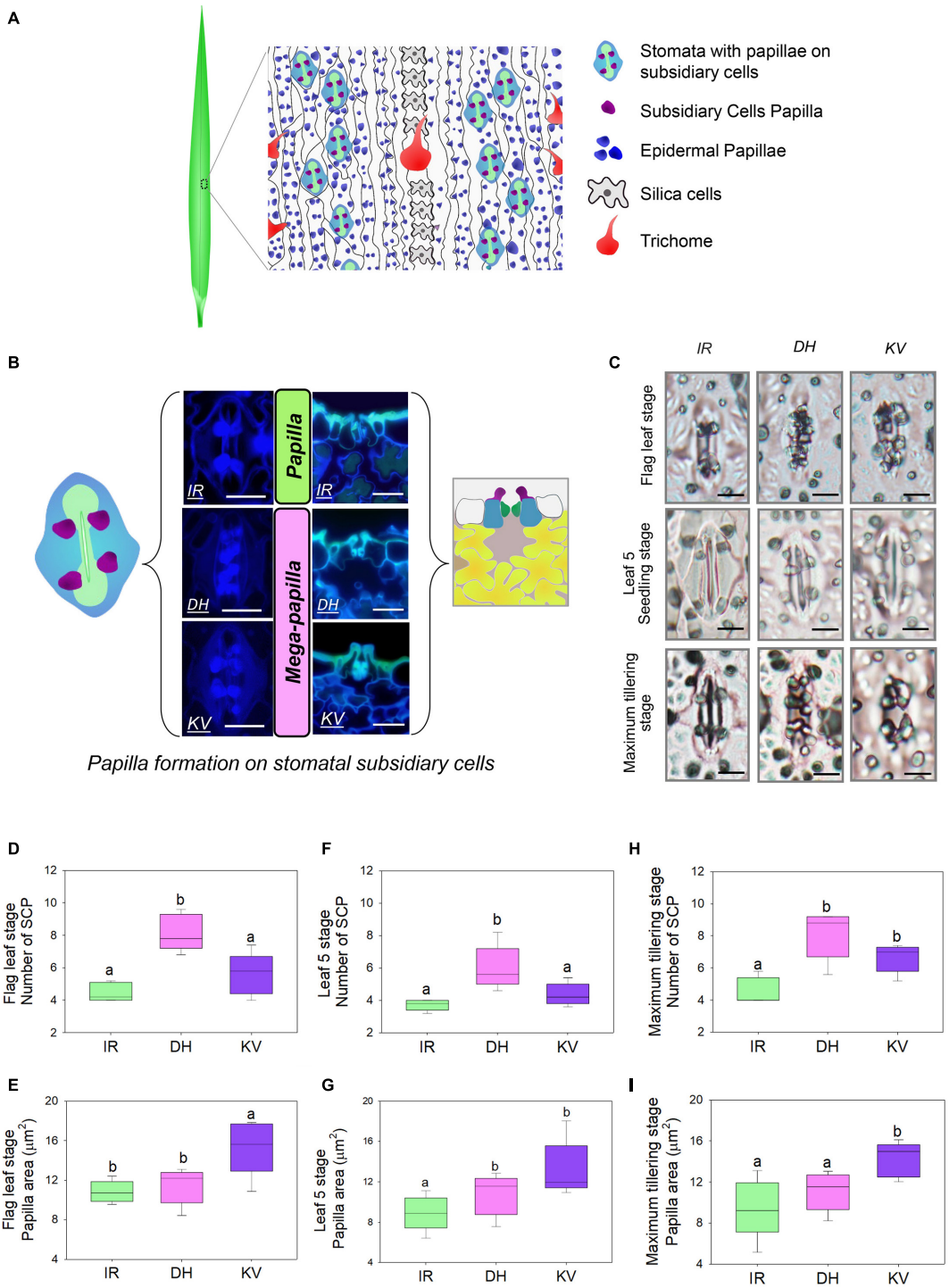

FIGURE 1 | Identification of mega-papillae on the subsidiary cells of stomatal complexes of rice cultivars Dharia (DH) and Kalubala Vee (KV). **(A)** Schematic diagram of flag leaf epidermis illustrating stomatal complexes (guard cells, green; subsidiary cells, light blue) with subsidiary cell papillae (SCP, purple), epidermal cell papillae (dark blue), silica cells (light gray), trichomes and epidermal pavement cells (white with black borders). **(B)** Images of stomatal complexes and SCP from IR64 (IR), Dharia (DH), and Kalubala Vee (KV), taken from above the epidermis via confocal microscopy (left) and taken of the transverse cross sections via fluorescence light microscopy (right) with corresponding schematics. SCP are more numerous for DH, or larger in area for KV, and thus are collectively referred to as mega-papillae. Color scheme as in **(A)**, with underlying mesophyll cells marked in yellow and sub-stomatal cavities in pale pink. **(C)** Light microscopy images of stomatal complexes and SCP of IR, DH, and KV taken from flag leaves (75–80 days), leaf 5 (20–25 days) and at maximum tillering stage (45–50 days). **(D–I)** Number and total area of SCP per stomatal complex of flag leaves **(D,E)**, leaf 5 **(F,G)** and at maximum tillering stage **(H,I)**. For graphs **(D–I)**, horizontal lines within boxes show the median, and boxes the upper (75%) and lower (25%) quartiles. Whiskers indicate the ranges of the minimum and maximum values and different letters indicate values with significantly different means ($P < 0.05$, one-way ANOVA). $n = 6$ plants in **(D–I)**. Scale bar = 10 μm in **(B,C)**.

were quantitatively assessed (**Figures 1D,E**). We found that DH had approximately 82% more SCP than IR and 31% more SCP than KV (DH vs. IR, $P < 0.001$; DH vs. KV, $P < 0.01$; **Figure 1D**), and that KV had approximately 40% larger papillar area compared to IR and DH (IR, $P < 0.05$; DH, $P < 0.05$; **Figure 1E**). At the leaf 5 stage, we also identified mega-papillae, with DH having significantly higher numbers of SCP than IR and KV (IR, $P < 0.05$; KV $P < 0.05$; **Figure 1F**) and KV having significantly larger SCP compared to IR and DH (IR, $P < 0.05$; DH, $P < 0.05$; **Figure 1G**). The same trends were also observed on leaves formed during the maximum tillering stage (**Figures 1H,I**), although a significant difference was not detected for SCP number between DH and KV (**Figure 1H**). Overall, the results consistently show that DH plants had the most numerous SCP, whereas KV had the largest SCP area. The number of SCP in DH (compare **Figures 1D,F,H**), and the size of SCP in KV (compare **Figures 1E,G,I**) both showed trends toward increasing further on later forming leaves. For the SCP of IR, this was not the case, and the number and size of IR SCP remained similar on all leaves examined.

Characterizing the Chemical Components of Rice Papillae

To determine the composition of rice papillae, we assessed the flag leaves of DH (high SCP number) using a scanning electron microscope (SEM) equipped with an energy dispersive X-Ray spectrometer (EDS) (**Figure 2**). The EDS assessment was conducted using two approaches; (1) spot measurements - which focused solely on stomatal complex papillae (**Figures 2A,B**); and (2) line scans - which focused more broadly, assessing stomatal papillae and the surrounding stomatal complex and epidermal pavement cells (**Figures 2C,D**). EDS spot measurements revealed that the DH mega-papillae consisted of four major elements:

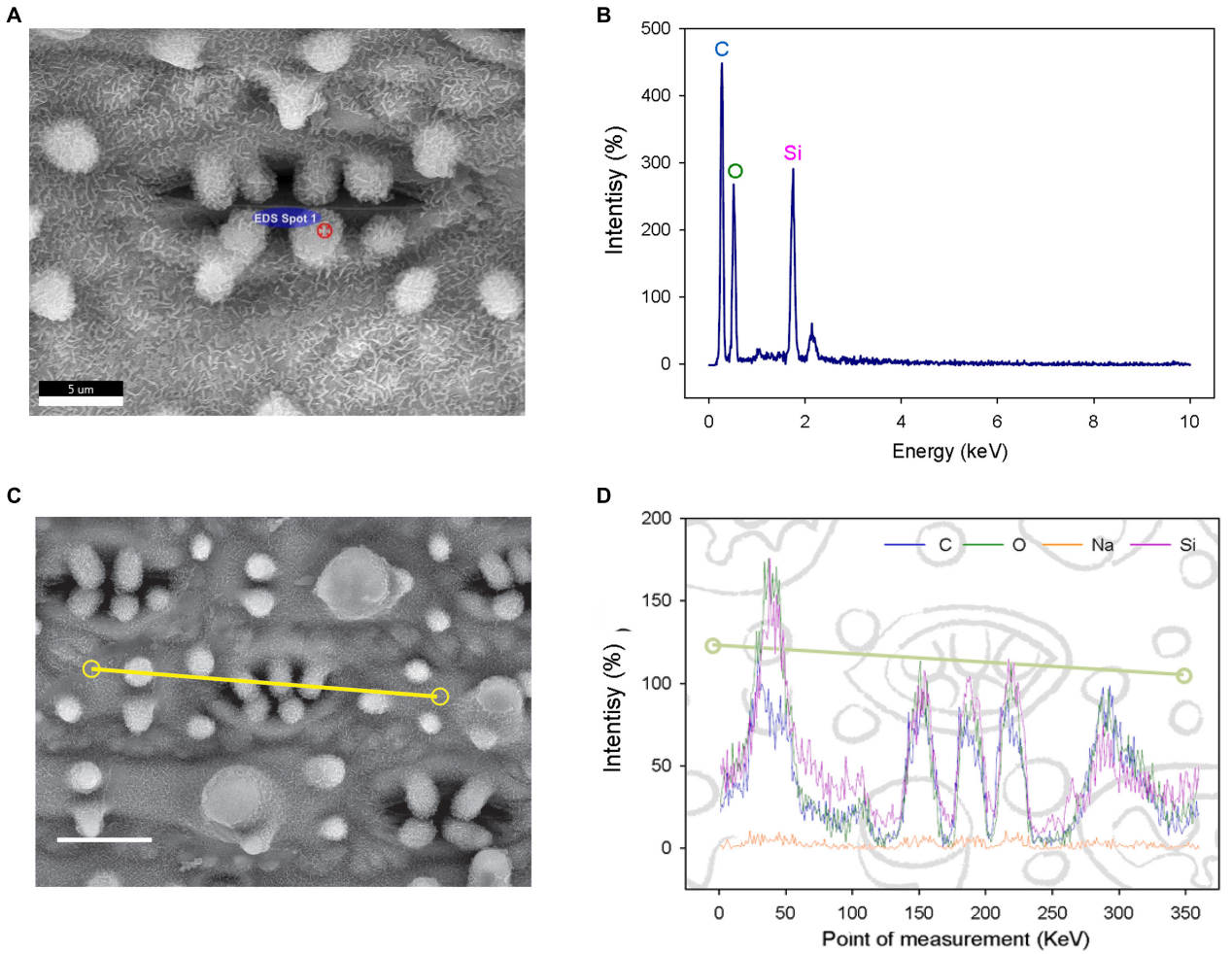

FIGURE 2 | Elemental analysis of subsidiary cell papillae (SCP) and the surrounding epidermal surface on leaves of the Dharia cultivar. **(A)** Scanning electron micrograph (SEM) of a stomatal complex, with a spot measurement of the SCP composition calculated using an energy dispersive X-Ray spectrometer (EDS). **(B)** Element spectrum of an SCP EDS-spot measurement showing all content measured. **(C)** SEM of a stomatal complex illustrating the EDS track path across the epidermal surface (yellow line). **(D)** SEM-EDS spectra of the total of 360 measurement points. Four components were detectable; silicon, oxygen, carbon and a low level of sodium. The peaks represent the concentration of each element at a given point on the line. Scale bars: 5 μm **(A)** and 10 μm **(C)**.

carbon, oxygen, sodium and silicon (Si). After carbon, Si was the next most abundant element, suggesting that Si is a major component of SCP (**Figures 2A,B**). EDS line scans provided similar results, with non-stomatal epidermal papillae exhibiting similar elemental signatures to the mega-papillae found on DH stomatal subsidiary cells, with Si again being an abundant element (**Figures 2C,D**). Several studies implicate Si as being important in pathogen defense (Song et al., 2016; Wang et al., 2017; Mücke et al., 2019), and this could be related to the abundance of silicon in mega-papillae.

Steady-State Gas Exchange of Mega-Papillae Rice Varieties

To assess whether the gas exchange properties of DH or KV were different to IR, we took infrared gas analyzer (IRGA) measurements from greenhouse-grown plants (**Figure 3**). SCP

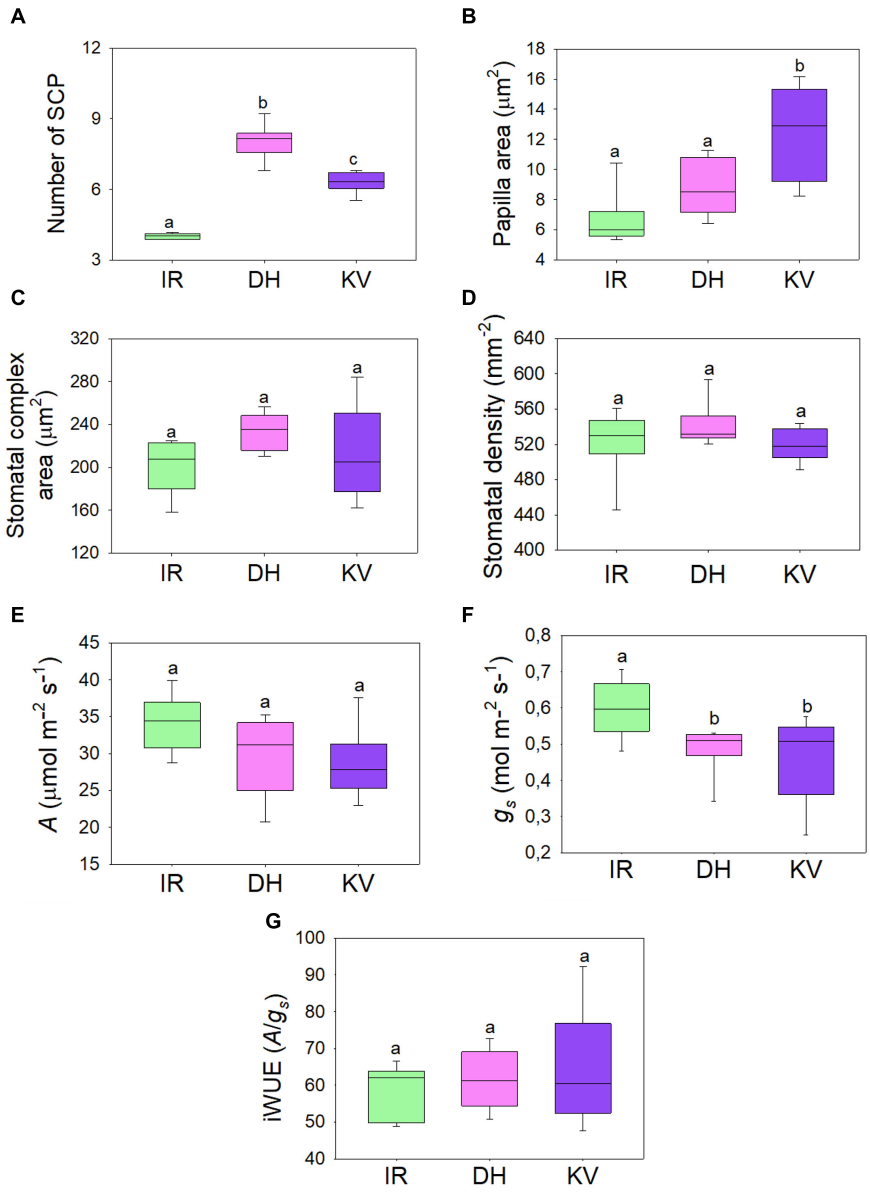

FIGURE 3 | Steady-state gas exchange analysis of mega-papillae cultivars. **(A)** Number and **(B)** total area of subsidiary cell papillae (SCP) per stomatal complex for rice cultivars IR64 (IR), Dharia (DH) and Kalubala Vee (KV). **(C)** Corresponding stomatal complex area and **(D)** stomatal density. **(E–G)** Infra-red gas exchange measurements of **(E)** photosynthetic carbon assimilation rate (A), stomatal conductance and the calculated intrinsic water use efficiency (iWUE; A/g_s). Horizontal lines within boxes show the median and boxes the upper (75%) and lower (25%) quartiles. Whiskers indicate the ranges of the minimum and maximum values and different letters indicate values with a significantly different mean within graph ($P < 0.05$, one-way ANOVA). $n = 8$ plants. Papillae area generated by measuring the outline of each SCP from above view the stomatal complex.

number and size were comparable between these greenhouse-grown plants and the growth chamber-grown plants assessed above (compare **Figures 1D,E** to **Figures 3A,B**). We also assessed the stomatal complex size and stomatal density of IR, DH, and KV (**Figures 3C,D**) and found no differences between the 3 cultivars. Under saturating light (2,000 μmol.m^{-2} s^{-1} PAR), photosynthetic carbon assimilation (A), stomatal conductance and corresponding intrinsic water-use efficiency (iWUE) were measured (**Figures 3E,G**). Both mega-papillae bearing cultivars, DH and KV, had significantly reduced g_s compared to IR ($P < 0.05$). There were no significant differences in A between cultivars (although there appeared to be a trend toward a reduction in A in DH and KV), and despite the approx. 20% reduction in g_s, no significant differences in iWUE were detected (**Figures 3E,G**). The lack of difference in iWUE between cultivars could be explained by a reduced g_s influencing the performance of A, but we cannot also rule out other factors such as slight differences in photochemical properties between cultivars.

Mega-Papillae Cultivars Have Stomata That Are Slower to Close and Re-open

Having ascertained that mega-papillae bearing cultivars have reduced steady-state g_s under saturating light, we next investigated the dynamic stomatal performance of DH, KV and IR (**Figure 4**). To do this, we assessed the light responsiveness of stomata using a light-dark-light illumination treatment. Plants were equilibrated to high light (2,000 μmol.m^{-2} s^{-1} PAR) for 15–20 min and then measured at steady-state for 10 min, the light was then turned off for 10 min, and finally light was re-introduced (2,000 μmol.m^{-2} s^{-1} PAR) for a further 10 min (**Figures 4A–C**). As expected, the 10 min dark treatment caused a rapid drop in A for all three rice cultivars, whereas the g_s responses were slower. When light was re-applied, A was again quicker to respond than g_s in all three cultivars (**Figures 4A–C**). To explore the efficiency of stomatal opening and closing responses, we calculated g_s rate changes over four 5-min periods (two dark segments and two light segments) (**Figures 4D–G**). Our data highlighted clear differences in the rate of stomatal responses between IR and the two mega-papillae cultivars during both darkness-induced stomatal closure and during light-induced stomata re-opening. During two of the four time periods, the initial stomatal closure (**Figure 4D**) and the later stomatal opening (**Figure 4G**), DH and KV had significantly lower rates of change in g_s compared with IR ($P < 0.05$). g_s decreased over 70% faster in IR than in DH or KV during the first 5 min of darkness, and g_s increased over 60% faster in the 5–10 min following the re-exposure to light in IR compared with DH or KV (**Figures 4D,G**). As there were no significant differences in stomatal size or density between cultivars (**Figures 3C,D**), this suggests that the presence of mega-papillae could be associated with the reduced stomatal dynamics observed in DH and KV.

To further assess the dynamic stomatal changes in g_s in **Figure 4**, we also utilized analytical models that predict g_s response to a single step change in PPFD (McAusland et al., 2016; Vialet-Chabrand et al., 2017). However, because DH and KV had slower closure responses and may not have reached steady-state after 10 min dark-induced stomatal closure, we could not confidently extract time constant values (time to reach 63% of the variation in g_s) preventing exact modeled comparisons to be made. Nonetheless, this modeling analysis, shown in **Supplementary Figure 1**, did add further support to the notion that DH and KV mega-papillae prevent stomata from closing efficiently over shorter time periods (compare **Figures 4A,D** with **Figures 4B,C,E,F**), and suggest that further experiments where light fluctuations are altered over a longer duration could be informative in assessing the impact of mega-papillae on stomatal dynamics, g_s and iWUE. Having ascertained that mega-papillae most probably serve as silicon-rich obstacles affecting stomatal dynamics, we next turned our attention to whether mega-papillae can aid in preventing pathogen attack.

Mega-Papillae Hybrid Plants Have Reduced Bacterial Leaf Streak Symptoms

Stomata serve as entry portals for a number of diseases including *Xoc,* which causes rice BLS (Niño-Liu et al., 2006). To examine whether mega-papillae might mitigate *Xoc* infection, we generated an F_3 population from crosses between the Thai cultivar Pathum Thani1 (PT1), which has the normal number of four SCP per stomatal complex, and the mega-papillae DH cultivar, which unusually has eight SCP per stomatal complex (**Figure 5**). We also tried crossing DH and KV with IR, but after multiple attempts, we were unsuccessful. To avoid the bias of *xa5* and other QTLs associated with BLS resistance in rice (Sattayachiti et al., 2020), which are present in DH (Iyer and McCouch, 2004) but not in PT1, we used F_3 individuals segregating for the mega-papillae trait that were derived from F_2 individuals where the *xa5* and other QTLs were absent (**Supplementary Figure 2**). From a pool of 88 F_3 individuals, we selected 26 plants with "normal" SCP and 26 plants with mega-papillae to test for pathogen resistance (**Figures 5A,B**). We sprayed *Xoc* bacterial suspensions directly on to the mature flag leaves of the identified F_3 plants during the reproductive stage (75 days old). BLS symptoms were scored using a standard disease scoring scale, and it was evident that F_3 plants with mega-papillae were approximately 77% less susceptible to *Xoc* than F_3 plants with the normal number of four papillae (**Figures 5C,D**). The results for hybrid plants were similar to those of the parental cultivars where DH had approximately 74% less severe disease symptoms than PT1 at 2 weeks after infection (**Figures 5C,D**).

SCP Prevalence in the Orzyeae Tribe and Beyond

To assess whether papillae form on the stomatal complexes of other plant types, we next surveyed a range of land plant species across evolutionary clades (**Figure 6**). Analysis of earlier diverging land plants (bryophtyes and non-flowering vascular plants) and later diverging plants (extant dicots) provided no evidence of papillae on the stomata of any of the species surveyed (**Figure 6**). We next focused specifically on monocots, first concentrating on some non-grass species *(Cocos nucifera*, coconut and *Musa acuminata*, banana). Despite the presence of

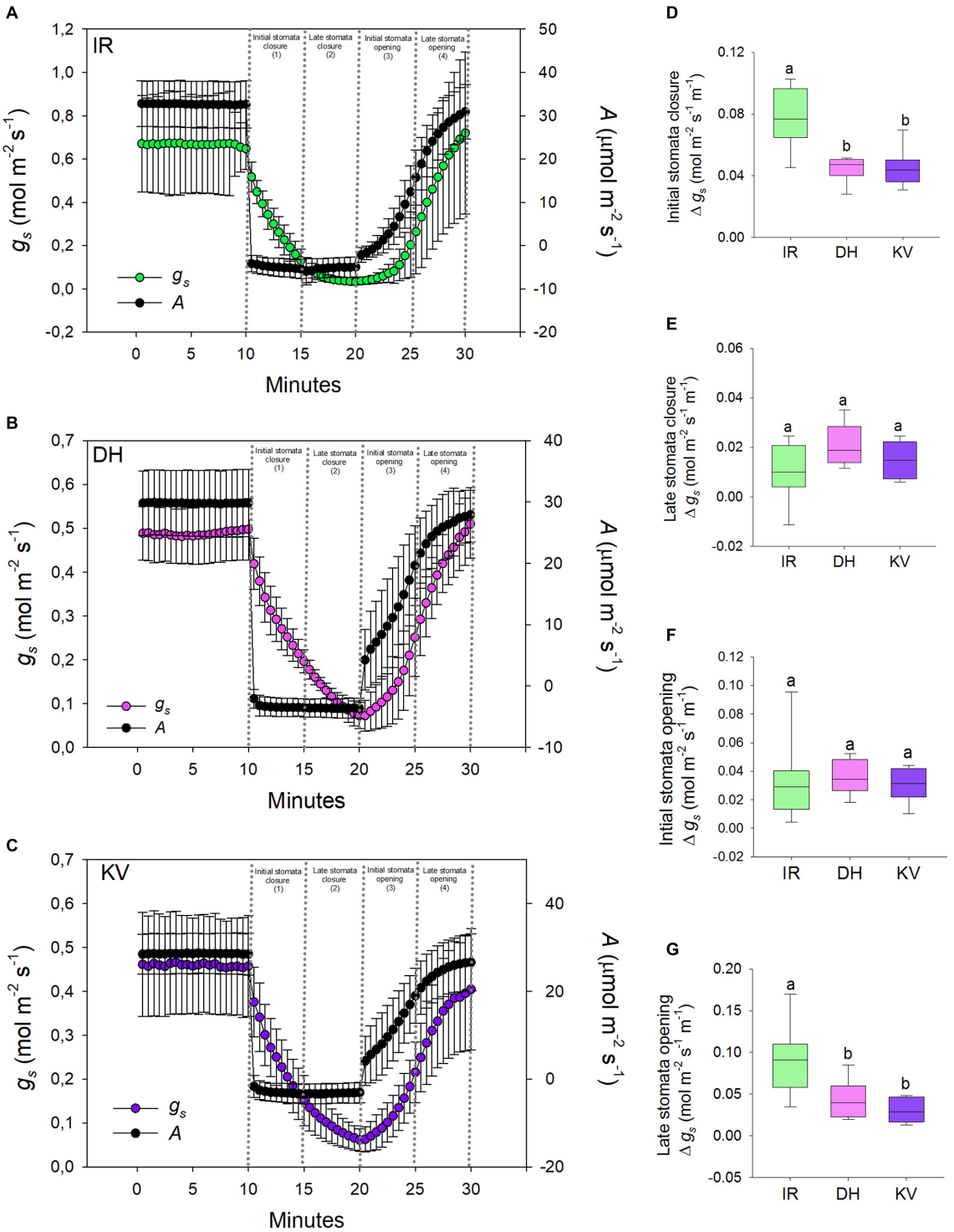

FIGURE 4 | Stomatal responses to dynamic light-dark-light treatments. Flag leaves of **(A)** IR64 (IR), **(B)** Dharia (DH) and **(C)** Kalubala Vee (KV) cultivars treated with 10 min of high light (2,000 µmol.m^{-2} s^{-1} PAR), followed by 10 min darkness (0 µmol.m^{-2} s^{-1} PAR), and subsequently another 10 min of high light. The y-axes of graphs show stomatal conductance on the left and photosynthetic carbon assimilation (*A*) on the right. Analysis of g_s rate change per minute during **(D)** initial stomatal closure, **(E)** late stomatal closure, initial stomatal opening and late stomatal opening. For graphs **(A–C)** error bars = one SD. For **(D–G)**, horizontal lines within boxes show the median, with boxes illustrating the upper (75%) and lower (25%) quartiles. Whiskers indicate the ranges of the minimum and maximum values, and different letters indicate values with a significantly different mean within each graph ($P < 0.05$, one-way ANOVA). $n = 8$ plants for DH and KV, and $n = 7$ plants for IR.

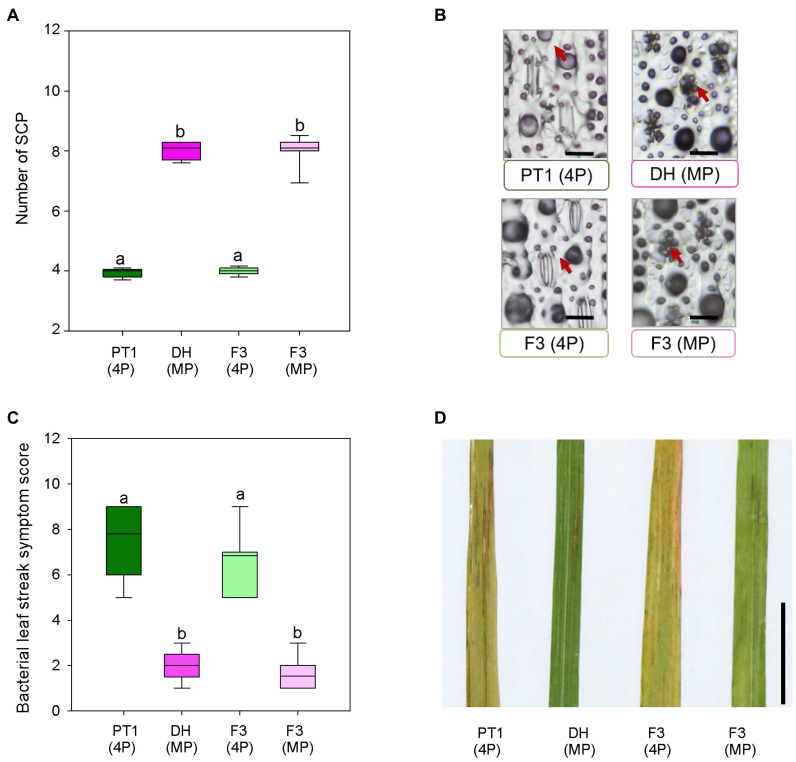

FIGURE 5 | Bacterial leaf streak symptoms of F_3 hybrid plants generated from four papillae (4P) cultivar Pathum Thani 1 (PT1) and the mega-papillae (MP) cultivar Dharia (DH). **(A)** Number of subsidiary cell papillae (SCP) per stomatal complex of PT1, DH, and F_3 (4P) and F_3 hybrid plants. **(B)** Representative images illustrating phenotypes quantified in **(A)**. **(C)** Quantification of bacterial leaf streak symptom scores of plants inoculated 2 weeks prior with *Xanthomonas Oryzae*pv. *oryzicola* (*Xoc*). **(D)** Representative image of leaves assessed to compile the data represented in **(C)**. Scale bars: 50 μm **(B)**, 1 cm **(D)**.

subsidiary cells, we did not detect any papillae on or around the stomata of these monocots. Assessment of the true grass species *Echinochloa crus-Galli* (Cockspur grass), *Brachypodium distachyon* (Brachypodium) and *Zea mays* (maize) led to the detection of papillae on the epidermis, but no SCP were present on stomatal complexes (**Figure 6**). We then looked at other *Oryza* species members to see whether the SCP trait was common in rice species other than *O. sativa*. SCP were present in all the rice species surveyed, including *O. rufipogon, O. officinalis, O. nivara, O. punctata, O. latifolia, O. australiansis, O. brachyantha,* and *O. ridleyi*. Most of these rice species had a similar number and size of SCP to that found in IR. However, two additional SCP traits were identified; in *O. ridleyi,* the SCP appeared to be smaller in size and in *O. brachyantha*, ectopic papillae formed which were not on subsidiary cells. For *O. brachyantha*, papillae arched over the stomatal complex from neighboring epidermal cells. Our results indicate that papillae may well be present, on or adjacent to stomatal complexes, across all rice species but are absent or rare on the stomata of other plant groups.

DISCUSSION

Plant stomata regulate gaseous exchange with the environment, and in some cases prevent pathogens from entering the leaf interior. In the short term, these processes can be regulated via alterations to stomatal pore aperture, and over longer durations, via changes to stomatal size and/or density (Zeiger et al., 1987; Lake and Woodward, 2008; Martin-StPaul et al., 2017; Dutton et al., 2019; Ye et al., 2020). A number of other specialized epidermal adaptions have also evolved that influence airflow and/or pathogen entry in and around stomata, and these include papillae outgrowths (Barthlott et al., 1998; Hückelhoven et al., 1999; Wakte et al., 2007; Mohammadian et al., 2009; Ensikat et al., 2011; Müller et al., 2017). To find beneficial stomatal or other epidermal traits that might lead to improved rice performance, we screened the flag leaves of 164 different rice varieties. We detected two mega-papillae bearing rice varieties; DH from Bangladesh that has more numerous SCP; and KV from Sri Lanka that has larger S. There have been no previous studies looking at how SCP might affect rice gas exchange, but for DH, work has been conducted highlighting the presence of the *xa5* gene which aids in preventing bacterial leaf blight (Iyer and McCouch, 2004). Given that mega-papillae cover significant portions of the stomatal pore area in both DH and KV, we decided to characterize SCP further, and to study phenotypic responses associated with stomatal function.

DH and KV mega-papillae are present on both earlier and later developing leaves (**Figure 1**), implying that mega-papillae

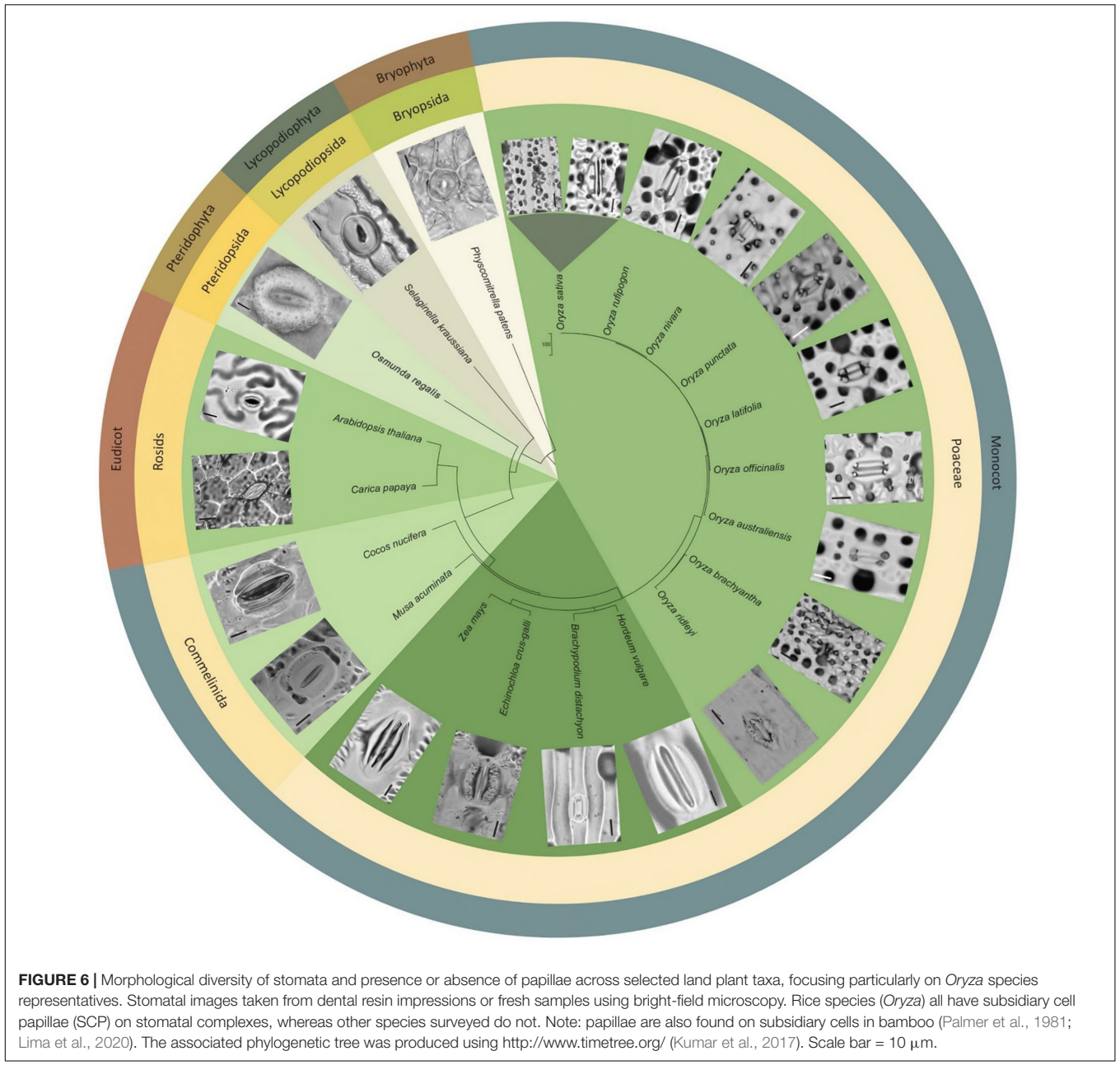

FIGURE 6 | Morphological diversity of stomata and presence or absence of papillae across selected land plant taxa, focusing particularly on *Oryza* species representatives. Stomatal images taken from dental resin impressions or fresh samples using bright-field microscopy. Rice species (*Oryza*) all have subsidiary cell papillae (SCP) on stomatal complexes, whereas other species surveyed do not. Note: papillae are also found on subsidiary cells in bamboo (Palmer et al., 1981; Lima et al., 2020). The associated phylogenetic tree was produced using http://www.timetree.org/ (Kumar et al., 2017). Scale bar = 10 μm.

could be beneficial throughout the majority of both cultivars' life cycles. Whilst we did not specifically study early mega-papillae development to detect when the corresponding SCP first formed, others have shown that rice SCP formation begins very early in stomatal development around the time that guard mother cells have just divided near the leaf base (Yoo et al., 2011; Luo et al., 2012). SCP development occurs slightly after neighboring epidermal pavement cell papillae. For both types of papillae (pavement cell and SCP), development is concluded well before leaves protrude from encircling sheaves (Luo et al., 2012). These findings suggest that it might be beneficial for rice leaves to have developed papillae prior to beginning to interact with the surrounding environment.

Prior research sheds some light on the molecular underpinnings governing rice SCP development (Yoo et al., 2011; Xia et al., 2015; Zhou et al., 2016). Using a map based cloning approach, Yoo et al. (2011), identified a ROP protein guanine exchange factor OsROPGEF10 as integral for the correct development of both pavement cell papillae and SCP formation. Mutant *bright green leaf* (*bgl*) rice plants have smooth epidermises with both pavement cells and stomatal complexes devoid of Papillae. This leads to increased leaf reflectance (Yoo et al., 2011), but how this impacts on plant physiology, particularly gas exchange and pathogen resistance, is not known. Whether *OsROPGEF10* expression is altered in DH and KV to orchestrate mega-papillae formation is unknown, but when

OsROPGEF10 was over-expressed to rescue the *bgl* mutant, papillae did not seem to be increasingly profuse or larger, and so this seems unlikely. Xia et al. (2015) identified *OsWS1,* a member of the membrane-bound O-acyl transferase gene family, involved in wax biosynthesis, to also be involved in papillae formation. Over-expression of *OsWS1* leads to increased amounts of wax throughout the epidermis, including on SCP, whereas a reduction in *OsWS1* levels resulted in fewer pavement cells papillae and SCP forming. When water-loss and drought studies were undertaken, *OsWS1* over-expressers performed better than controls, whereas plants with depleted *OsWS1* performed worse (i.e., required more water). The *LESS PRONOUNCED LOBE EPIDERMAL CELL 2* (*LPL2*) and *LPL3* genes encode PIR/SRA1-like and NAP1-like proteins, respectively, and both contribute to SCP formation (Zhou et al., 2016). These homologous components of the functionally conserved SCAR/WAVE complex play important roles in actin organization throughout the epidermis. In mutant *lpl2* and *lpl3* plants, the development of small epidermal papillae and SCP are perturbed. In both mutants, fewer, larger papillae form which lack definition. The activities of each of these genes remains unknown in DH and KV and warrants further investigation to determine whether they might contribute to the observed mega-papillae phenotypes.

Our SEM-EDS observations showed that DH mega-papillae have high Si content (**Figure 2**), and together with the observations of others, this suggests that all papillae on rice leaves, including SCP, are to a large degree comprised of Si (Cai et al., 2008; Yoo et al., 2011). At the plant level, Si is distributed in multiple organs including within roots and leaves, and it is found in a range of epidermal cells including pavement and subsidiary cells (Kumar et al., 2017). Uptake of Si occurs in the roots of rice via specialized Si transporters, *LowSilicon1* (*OsLsi1)* and *OsLsi2* (Ma et al., 2006, 2007). Following this, Si is translocated to the aboveground tissue, with *OsLsi6* involved in xylem unloading and deposition of Si in the leaf sheaths and leaf blades (Yamaji et al., 2008). Our Si SEM-EDS results correspond with previous studies in bamboo and cucumber where high Si content was also observed, and in these cases, Si improved plant pathogen resistance (Kauss et al., 2003; Motomura et al., 2004). Indeed, Si is increasingly becoming associated with pathogen resistance (Ning et al., 2014; Wang et al., 2017). One recent article found that *Xoo* and *Xoc* encode TALE (transcription activator-like effector) proteins that both downregulate *OsLsi1*, and it is therefore intriguing to speculate that *Xanthomonas* bacteria specifically downregulate silicon uptake to increase the chances of successful pathogen attack (Mücke et al., 2019). Future studies looking at *OsLsi1*, *OsLsi2,* and *OsLsi6* functioning in DH and KV might help to reveal how these varieties (1) produce mega-papillae and (2) ward off infection.

We found that the gas exchange rates and stomatal dynamics of mega-papillae bearing cultivars were different to IR, which has normal SCP (**Figures 3**, **4**). Because smaller stomata have been suggested to be faster (Raven, 2014; Lawson and Vialet-Chabrand, 2019), and because more stomata can achieve a higher g_{smax} (Bertolino et al., 2019; Caine et al., 2019), we compared the stomatal size and density of mega-papillae bearing cultivars with IR, but found no differences for either stomatal trait (**Figures 3C,D**). Steady-state gas exchange revealed that DH and KV have significantly reduced g_s in comparison to IR, but despite displaying a trend toward being reduced, *A* was not significantly different between cultivars and nor was iWUE (**Figures 3E,G**). To test whether mega-papillae hindered dynamic stomatal movements, we next assayed DH, KV and IR using a light-dark-light treatment with the light set at 2,000 $\mu mol.m^{-2}\ s^{-1}$ PAR (**Figure 4**). Our results show that DH and KV both displayed reduced g_s rate changes comparatively to IR during both early stomatal closure (**Figure 4D**) and late stomatal opening (**Figure 4G**). We note, however, that stomatal or non-stomatal factors other than SCP might contribute to our observed differences in both the steady-state gas exchange and stomatal dynamic movements. Current research has highlighted the importance of "speedy" stomata in grasses which accounts for their characteristic high iWUE values (McAusland et al., 2016; Raissig et al., 2016; Lawson and Vialet-Chabrand, 2019). Our results suggest that under dynamic light environments, having mega-papillae may result in a lower iWUE during both stomatal closing and re-opening; however, these inefficiencies might well be offset by lower g_s under steady-state conditions. How such plants will perform under future predicted high CO_2 climates is unclear at this stage, and future experiments, particularly at higher temperature and or under water-deficit conditions are required.

The majority of research relating to papillae functionality is in the area of pathogen defense (Ride and Pearce, 1979; Thordal-Christensen et al., 1997; Murillo et al., 1999; Chowdhury et al., 2014; Maekawa et al., 2014; Ning et al., 2014; Wang et al., 2017). Therefore, we examined the role that mega-papillae might play in rice defense against *Xoc*, a pathogen that enters through stomata and causes BLS disease (Niño-Liu et al., 2006; **Figure 5**). Analysis of F_3 generation progeny of crosses between DH and PT1 (which did not carry the *xa5* gene as well as other QTLs) revealed that mega-papillae could contribute to increased resistance to *Xoc* (**Figures 5C,D**). Whether this result is due to an increased physical barrier around the stomatal pore, and/or because of increased Si presence due to more/larger papillae is unclear. Indeed, both of these factors may contribute toward preventing waterborne bacteria from entering underlying tissues. Such waterproofing could also permit sustained gas exchange when otherwise stomata may typically become filled with water. Further experiments looking at the gas exchange rates and stomatal dynamics of DH, PT1, and hybrid plants treated with XOC would give some indication as to whether such a response occurred in rice with mega-papillae. It would also be useful to look at gene expression in the hybrid plants after pathogen inoculation, either via application directly onto leaves or via infiltration, to reveal if other mechanisms other than papillae presence are also employed to achieve the BLS resistance observed in mega-papillae rice lines.

We observed the stomatal morphology across various taxa including dicots, monocots, non-flowering vascular plants and a bryophyte representative (**Figure 6**) and as expected found a high degree of size and morphological diversity, with earlier diverging land plants and dicots exhibiting kidney-shaped guard cell pairs (except *Physcomitrium patens*: a moss with unusual undivided

single guard cells), and monocots exhibiting dumbbell-shaped guard cell pairs surrounded by subsidiary cells. In our assessment, we did not detect papillae near stomata, except on the subsidiary cells of almost all the rice species we surveyed. On the other grasses surveyed, we did detect epidermal pavement cell papillae, suggesting that this may be an ancestral trait within the Poaceae family. Bamboo representatives (closely related to rice) are also reported to have SCP on stomatal complexes (Lima et al., 2020). Given the relatedness of bamboo and rice species, this suggests that the ancestor of Oryzoideae and Bambusoideae may have had SCP on the stomatal complex. A better understanding of the molecular underpinnings of SCP development might in the future help to reveal whether rice and bamboo SCP could have been evolutionarily conserved, or whether SCP have evolved on multiple occasions.

CONCLUSION

Here we identify mega-papillae: unusually large or numerous subsidiary cell papillae that appear to limit accessibility to rice stomatal pores. We show that mega-papillae contain silicon and that mega-papillae bearing cultivars have reduced g_s rate changes during stomatal closing and re-opening. The presence of mega-papillae co-segregates with an increased resistance to *Xoc* infection in hybrid lines suggesting a role for mega-papillae in presenting disease. Future work is required to assess the viability of using mega-papillae to improve future crop performance.

DATA AVAILABILITY STATEMENT

The original contributions presented in the study are included in the article/**Supplementary Material**, further inquiries can be directed to the corresponding author/s.

AUTHOR CONTRIBUTIONS

MP designed and undertook the first phenotypic screening experiment, conducted the first and second phenotyping of the identified mega-papillae plants, conducted the gas exchange and pathogen experiments, and analyzed the corresponding data. RC helped in designing and conducting the gas exchange experiment, advised in data analysis and helped conceive, and write the manuscript. CH helped in designing and conducting the gas exchange experiments and advised on data analysis and interpretation. EH helped in stomatal imaging and conducting gas exchange experiments. WP contributed to phenotypic measurements and elemental analysis. RB helped in physiological data analysis. SN helped during leaf gas exchange experiments. TT assisted the project and advised on the manuscript concept. SW contributed experimental ideas and helped revise the manuscript. AV, JG, RC, and SA contributed to the original idea of the project and supervised the study and prepared the manuscript. SA conceived the project and provided advice and experimental materials. All authors contributed to the article and approved the submitted version.

FUNDING

This research was funded by grants from the BBSRC Newton Rice Research Initiative BB/N013646/1, National Science and Technology Development Agency (NSTDA) P-16-50286 and the National Research Council of Thailand (NRCT) NRCT5-RSA63002-06 and NRCT-RTA/812/2563. MP was supported in part by a Graduate Program Scholarship from Kasetsart University.

ACKNOWLEDGMENTS

We thank graduate student Shauni McGregor for providing the *B. disatchyon* and *H. vulgare* stomatal images presented in **Figure 6**.

SUPPLEMENTARY MATERIAL

The Supplementary Material for this article can be found online at: https://www.frontiersin.org/articles/10.3389/fpls.2021.677839/full#supplementary-material

REFERENCES

Banks, H. P., and Davis, M. R. (1969). Crenaticaulis, a new genus of devonian plants allied to zosterophyllum, and its bearing on the classification of early land plants. *Am. J. Botany* 56, 436–449. doi: 10.2307/2440821

Barthlott, W., Neinhuis, C., Cutler, D., Ditsch, F., Meusel, I., Theisen, I., et al. (1998). Classification and terminology of plant epicuticular waxes. *Botanical J. Linnean Soc.* 126, 237–260. doi: 10.1111/j.1095-8339.1998.tb02529.x

Beerling, D. J., and Franks, P. J. (2009). Evolution of stomatal function in 'lower' land plants. *New Phytol.* 183, 921–925. doi: 10.1111/j.1469-8137.2009.02973.x

Bertolino, L. T., Caine, R. S., and Gray, J. E. (2019). Impact of stomatal density and morphology on water-use efficiency in a changing world. *Front. Plant Sci.* 10:225. doi: 10.3389/fpls.2019.00225

Bouman, B. A. M. (2009). *How Much Water Does Rice Use? Rice Today*. Philippine: IRRI.

Cai, K., Gao, D., Luo, S., Zeng, R., Yang, J., and Zhu, X. (2008). Physiological and cytological mechanisms of silicon-induced resistance in rice against blast disease. *Physiol. Plantarum* 134, 324–333. doi: 10.1111/j.1399-3054.2008.01140.x

Cai, S., Papanatsiou, M., Blatt, M. R., and Chen, Z. H. (2017). Speedy grass stomata: emerging molecular and evolutionary features. *Mol. Plant* 10, 912–914. doi: 10.1016/j.molp.2017.06.002

Caine, R. S., Yin, X., Sloan, J., Harrison, E. L., Mohammed, U., Fulton, T., et al. (2019). Rice with reduced stomatal density conserves water and has improved drought tolerance under future climate conditions. *New Phytol.* 221, 371–384. doi: 10.1111/nph.15344

Casson, S., and Gray, J. E. (2008). Influence of environmental factors on stomatal development. *New Phytol.* 178, 9–23. doi: 10.1111/j.1469-8137.2007.02351.x

Chatterjee, J., Thakur, V., Nepomuceno, R., Coe, R. A., Dionora, J., Elmido-Mabilangan, A., et al. (2020). Natural diversity in stomatal features of cultivated and wild oryza species. *Rice* 13:58.

Chen, Z.-H., Chen, G., Dai, F., Wang, Y., Hills, A., Ruan, Y.-L., et al. (2017). Molecular evolution of grass stomata. *Trends Plant Sci.* 22, 124–139. doi: 10.1016/j.tplants.2016.09.005

Chowdhury, J., Henderson, M., Schweizer, P., Burton, R. A., Fincher, G. B., and Little, A. (2014). Differential accumulation of callose, arabinoxylan and cellulose in nonpenetrated versus penetrated papillae on leaves of barley infected with blumeria graminis F. Sp. Hordei. *New Phytol.* 204, 650–660. doi: 10.1111/nph.12974

Duarte-Silva, A. G., Carvalho-Silva, M., and Câmara, P. E. A. S. (2013). Morphology and development of leaf papillae in the pilotrichaceae. *Acta Botanica Brasilica* 27, 737–742. doi: 10.1590/s0102-33062013000400013

Dutton, C., Hõrak, H., Hepworth, C., Mitchell, A., Ton, J., Hunt, L., et al. (2019). Bacterial infection systemically suppresses stomatal density. *Plant Cell Environ.* 42, 2411–2421. doi: 10.1111/pce.13570

Ensikat, H. J., Ditsche-Kuru, P., Neinhuis, C., and Barthlott, W. (2011). Superhydrophobicity in perfection: the outstanding properties of the lotus leaf. *Beilstein J. Nanotechnol.* 2, 152–161. doi: 10.3762/bjnano.2.19

Fischer, T. C., Meller, B., Kustatscher, E., and Butzmann, R. (2010). Permian ginkgophyte fossils from the dolomites resemble extant o-ha-tsuki aberrant leaf-like fructifications of ginkgo biloba l. *BMC Evol. Biol.* 10:337. doi: 10.1186/1471-2148-10-337

Flexas, J., and Medrano, H. (2002). Drought-inhibition of photosynthesis in c(3) plants: stomatal and non-stomatal limitations revisited. *Annals Botany* 89, 183–189. doi: 10.1093/aob/mcf027

Gorb, E. V., Dai, Z., and Gorb, S. N. (2017). Micromorphology of stem surface in three species of bambusa (poaceae, bambusoideae) with a focus on its impact on plant-insect interactions. *Flora* 230, 14–25. doi: 10.1016/j.flora.2017.03.004

Guerriero, G., Stokes, I., and Exley, C. (2018). Is callose required for silicification in plants? *Biol. Lett.* 14:20180338. doi: 10.1098/rsbl.2018.0338

Haworth, M., and McElwain, J. (2008). Hot, dry, wet, cold or toxic? Revisiting the ecological significance of leaf and cuticular micromorphology. *Palaeogeography Palaeoclimatol. Palaeoecol.* 262, 79–90. doi: 10.1016/j.palaeo.2008.02.009

Hepworth, C., Caine, R. S., Harrison, E. L., Sloan, J., and Gray, J. E. (2018). Stomatal development: focusing on the grasses. *Curr. Opin. Plant Biol.* 41, 1–7. doi: 10.1016/j.pbi.2017.07.009

Hepworth, C., Doheny-Adams, T., Hunt, L., Cameron, D. D., and Gray, J. E. (2015). Manipulating stomatal density enhances drought tolerance without deleterious effect on nutrient uptake. *New Phytol.* 208, 336–341. doi: 10.1111/nph.13598

Hetherington, A. M., and Woodward, F. I. (2003). The role of stomata in sensing and driving environmental change. *Nature* 424, 901–908. doi: 10.1038/nature01843

Hu, Y., Wu, Q., Peng, Z., Sprague, S. A., Wang, W., Jagadish, K. S. V., et al. (2017). Silencing of osgrxs17 in rice improves drought stress tolerance by modulating ros accumulation and stomatal closure. *Nat. Sci. Rep.* 7:15950.

Huang, X. Y., Chao, D. Y., Gao, J. P., Zhu, M. Z., Shi, M., and Lin, H. X. (2009). A previously unknown zinc finger protein, dst, regulates drought and salt tolerance in rice via stomatal aperture control. *Genes Dev.* 23, 1805–1817. doi: 10.1101/gad.1812409

Hückelhoven, R., Fodor, J., Preis, C., and Kogel, K.-H. (1999). Hypersensitive cell death and papilla formation in barley attacked by the powdery mildew fungus are associated with hydrogen peroxide but not with salicylic acid accumulation. *Plant Physiol.* 119:1251. doi: 10.1104/pp.119.4.1251

Hughes, J., Hepworth, C., Dutton, C., Dunn, J. A., Hunt, L., Stephens, J., et al. (2017). Reducing stomatal density in barley improves drought tolerance without impacting on yield. *Plant Physiol.* 174, 776–787. doi: 10.1104/pp.16.01844

IRRI, (2013). *Ses Standard Evaluation System for Rice*, 5th Edn. Manila: IRRI.

Iyer, A. S., and McCouch, S. R. (2004). The rice bacterial blight resistance gene xa5 encodes a novel form of disease resistance. *Mol. Plant Microbe Interact* 17, 1348–1354. doi: 10.1094/mpmi.2004.17.12.1348

Jagadish, S. V., Murty, M. V., and Quick, W. P. (2015). Rice responses to rising temperatures–challenges, perspectives and future directions. *Plant Cell Environ.* 38, 1686–1698. doi: 10.1111/pce.12430

Jordan, G. J., Dillon, R. A., and Weston, P. H. (2005). Solar radiation as a factor in the evolution of scleromorphic leaf anatomy in proteaceae. *Am. J. Botany* 92, 789–796. doi: 10.3732/ajb.92.5.789

Kang, Y., Jabbour, F., Cao, S., Wang, Y., Guo, J., and Huang, J. (2017). Leaf epidermal features of chinese stephania lour. (menispermaceae) and their systematic significance. *Kew Bull.* 72:26.

Kauss, H., Seehaus, K., Franke, R., Gilbert, S., Dietrich, R. A., and Kröger, N. (2003). Silica deposition by a strongly cationic proline-rich protein from systemically resistant cucumber plants. *Plant J.* 33, 87–95. doi: 10.1046/j.1365-313x.2003.01606.x

Kumar, S., Soukup, M., and Elbaum, R. (2017). Silicification in grasses: variation between different cell types. *Front. Pant Sci.* 8:438. doi: 10.3389/fpls.2017.00438

Lake, J. A., Quick, W. P., Beerling, D. J., and Woodward, F. I. (2001). Plant development - signals from mature to new leaves. *Nature* 411, 154–154. doi: 10.1038/35075660

Lake, J. A., and Woodward, F. I. (2008). Response of stomatal numbers to co2 and humidity: control by transpiration rate and abscisic acid. *New Phytol.* 179, 397–404. doi: 10.1111/j.1469-8137.2008.02485.x

Lawson, T., and Vialet-Chabrand, S. (2019). Speedy stomata, photosynthesis and plant water use efficiency. *New Phytol.* 221, 93–98. doi: 10.1111/nph.15330

Li, J., Li, Y., Yin, Z., Jiang, J., Zhang, M., Guo, X., et al. (2017). Osasr5 enhances drought tolerance through a stomatal closure pathway associated with aba and h2 o2 signalling in rice. *Plant Biotechnol. J.* 15, 183–196. doi: 10.1111/pbi.12601

Lima, J. F., Leite, K. R. B., Clark, L. G., and De Oliveira, R. P. (2020). Leaf micromorphology in poaceae subtribe olyrinae (bambusoideae) and its systematic implications. *Botanical J. Linnean Soc.* 192, 184–207. doi: 10.1093/botlinnean/boz071

Liu, J., Zhang, F., Zhou, J., Chen, F., Wang, B., and Xie, X. (2012). Phytochrome b control of total leaf area and stomatal density affects drought tolerance in rice. *Plant Mol. Biol.* 78, 289–300. doi: 10.1007/s11103-011-9860-3

Liu, T., Ohashi-Ito, K., and Bergmann, D. C. (2009). Orthologs of arabidopsis thaliana stomatal bhlh genes and regulation of stomatal development in grasses. *Development* 136, 2265–2276. doi: 10.1242/dev.032938

Liu, W., Liu, J., Triplett, L., Leach, J. E., and Wang, G.-L. (2014). Novel insights into rice innate immunity against bacterial and fungal pathogens. *Annual Rev. Phytopathol.* 52, 213–241. doi: 10.1146/annurev-phyto-102313-045926

Luo, L., Zhou, W. Q., Liu, P., Li, C. X., and Hou, S. W. (2012). The development of stomata and other epidermal cells on the rice leaves. *Biol. Plantarum* 56, 521–527. doi: 10.1007/s10535-012-0045-y

Ma, J. F., Tamai, K., Yamaji, N., Mitani, N., Konishi, S., Katsuhara, M., et al. (2006). A silicon transporter in rice. *Nature* 440, 688–691.

Ma, J. F., Yamaji, N., Mitani, N., Tamai, K., Konishi, S., Fujiwara, T., et al. (2007). An efflux transporter of silicon in rice. *Nature* 448, 209–212. doi: 10.1038/nature05964

Maekawa, S., Inada, N., Yasuda, S., Fukao, Y., Fujiwara, M., Sato, T., et al. (2014). The carbon/nitrogen regulator arabidopsis toxicos en levadura31 controls papilla formation in response to powdery mildew fungi penetration by interacting with syntaxin of plants121 in arabidopsis. *Plant Physiol.* 164, 879–887. doi: 10.1104/pp.113.230995

Maricle, B. R., Koteyeva, N. K., Voznesenskaya, E. V., Thomasson, J. R., and Edwards, G. E. (2009). Diversity in leaf anatomy, and stomatal distribution and conductance, between salt marsh and freshwater species in the c4 genus spartina (poaceae). *New Phytol.* 184, 216–233. doi: 10.1111/j.1469-8137.2009.02903.x

Martin-StPaul, N., Delzon, S., and Cochard, H. (2017). Plant resistance to drought depends on timely stomatal closure. *Ecol. Lett.* 20, 1437–1447. doi: 10.1111/ele.12851

McAusland, L., Vialet-Chabrand, S., Davey, P., Baker Neil, R., Brendel, O., and Lawson, T. (2016). Effects of kinetics of light-induced stomatal responses on photosynthesis and water-use efficiency. *New Phytol.* 211, 1209–1220. doi: 10.1111/nph.14000

McElwain, J. C., and Steinthorsdottir, M. (2017). Paleoecology, ploidy, paleoatmospheric composition, and developmental biology: a review

of the multiple uses of fossil stomata. *Plant Physiol.* 174, 650–664. doi: 10.1104/pp.17.00204

McKown, K. H., and Bergmann, D. C. (2018). Grass stomata. *Curr. Biol.* 28, R814–R816.

Mohammadian, M. A., Hill, R. S., and Watling, J. R. (2009). Stomatal plugs and their impact on fungal invasion in agathis robusta. *Australian J. Botany* 57, 389–395. doi: 10.1071/bt08175

Motomura, H., Fujii, T., and Suzuki, M. (2004). Silica deposition in relation to ageing of leaf tissues in sasa veitchii (carrière) rehder (poaceae: Bambusoideae). *Annals Botany* 93, 235–248. doi: 10.1093/aob/mch034

Mücke, S., Reschke, M., Erkes, A., Schwietzer, C.-A., Becker, S., Streubel, J., et al. (2019). Transcriptional reprogramming of rice cells by xanthomonas oryzae tales. *Front. Plant Sci.* 10:162. doi: 10.3389/fpls.2019.00162

Müller, H. M., Schäfer, N., Bauer, H., Geiger, D., Lautner, S., Fromm, J., et al. (2017). The desert plant phoenix dactylifera closes stomata via nitrate-regulated slac1 anion channel. *New Phytol.* 216, 150–162. doi: 10.1111/nph.14672

Murillo, I., Cavallarin, L., and Segundo, B. S. (1999). Cytology of infection of maize seedlings by fusarium moniliforme and immunolocalization of the pathogenesis-related prms protein. *Phytopathology* 89, 737–747. doi: 10.1094/phyto.1999.89.9.737

Ning, D., Song, A., Fan, F., Li, Z., and Liang, Y. (2014). Effects of slag-based silicon fertilizer on rice growth and brown-spot resistance. *PLoS One* 9:e102681. doi: 10.1371/journal.pone.0102681

Niño-Liu, D. O., Ronald, P. C., and Bogdanove, A. J. (2006). *Xanthomonas oryzae* pathovars: model pathogens of a model crop. *Mol. Plant Pathol.* 7, 303–324. doi: 10.1111/j.1364-3703.2006.00344.x

Nunes, T. D. G., Zhang, D., and Raissig, M. T. (2020). Form, development and function of grass stomata. *Plant J.* 101, 780–799. doi: 10.1111/tpj.14552

Pachauri, R. K., Allen, M. R., Barros, V. R., Broome, J., Cramer, W., Christ, R., et al. (2014). *Climate change 2014: Synthesis report. Contribution of working groups i, ii and iii to the fifth assessment report of the intergovernmental panel on climate change*. Available online at: https://epic.awi.de/id/eprint/37530/ (accessed 9 December 2015).

Palmer, P. G., Tucker, A. E., and Gerbeth-Jones, S. (1981). *A Scanning Electron Microscope Survey of the Epidermis of East African Grasses*. Washington: Smithsonian Institution Press.

Palmer, P. G., Tucker, A. E., and Smithsonian Institution, P. (1983). *A scanning Electron Microscope Survey of the Epidermis of East African Grasses, ii*. Washington, DC: Smithsonian Institution Press.

Pant, D. D., and Mehra, B. (1964). Epidermal structure and development of stomata in ephedra foliata boiss. *New Phytol.* 63, 91–95. doi: 10.1111/j.1469-8137.1964.tb07362.x

Prasad, V., Stromberg, C. A. E., Leache, D., Samant, B., Patnaik, R., Tang, L., et al. (2011). Late cretaceous origin of the rice tribe provides evidence for early diversification in poaceae. *Nat. Commun.* 2:9.

Proust, H., Honkanen, S., Jones, V. A., Morieri, G., Prescott, H., Kelly, S., et al. (2016). Rsl class i genes controlled the development of epidermal structures in the common ancestor of land plants. *Curr. Biol.* 26, 93–99. doi: 10.1016/j.cub.2015.11.042

Raissig, M. T., Abrash, E., Bettadapur, A., Vogel, J. P., and Bergmann, D. C. (2016). Grasses use an alternatively wired bhlh transcription factor network to establish stomatal identity. *Proc. Natl. Acad. Sci. U S A.* 113, 8326–8331. doi: 10.1073/pnas.1606728113

Raissig, M. T., Matos, J. L., Anleu Gil, M. X., Kornfeld, A., Bettadapur, A., Abrash, E., et al. (2017). Mobile mute specifies subsidiary cells to build physiologically improved grass stomata. *Science* 355, 1215–1218. doi: 10.1126/science.aal3254

Raven, J. A. (2014). Speedy small stomata? *J. Exp. Botany* 65, 1415–1424. doi: 10.1093/jxb/eru032

Redfern, S. K., Azzu, N., and Binamira, J. S. (2012). Rice in southeast asia: Facing risks and vulnerabilities to respond to climate change. *Building resilience for adaptation to climate change in the agriculture sector.* 23:295.

Ride, J. P., and Pearce, R. B. (1979). Lignification and papilla formation at sites of attempted penetration of wheat leaves by non-pathogenic fungi. *Physiol. Plant Pathol.* 15, 79–92. doi: 10.1016/0048-4059(79)90041-9

Rudall, P. J., Chen, E. D., and Cullen, E. (2017). Evolution and development of monocot stomata. *Am. J. Bot.* 104, 1122–1141. doi: 10.3732/ajb.1700086

Sack, L., and Buckley, T. N. (2016). The developmental basis of stomatal density and flux. *Plant Physiol.* 171, 2358–2363. doi: 10.1104/pp.16.00476

Sattayachiti, W., Wanchana, S., Arikit, S., Nubankoh, P., Patarapuwadol, S., Vanavichit, A., et al. (2020). Genome-wide association analysis identifies resistance loci for bacterial leaf streak resistance in rice (oryza sativa l.). *Plants* 9:1673. doi: 10.3390/plants9121673

Schindelin, J., Arganda-Carreras, I., Frise, E., Kaynig, V., Longair, M., Pietzsch, T., et al. (2012). Fiji: an open-source platform for biological-image analysis. *Nat. Methods* 9, 676–682. doi: 10.1038/nmeth.2019

Song, A., Xue, G., Cui, P., Fan, F., Liu, H., Yin, C., et al. (2016). The role of silicon in enhancing resistance to bacterial blight of hydroponic- and soil-cultured rice. *Sci. Rep.* 6:24640.

Stebbins, G. L., and Shah, S. S. (1960). Developmental studies of cell differentiation in the epidermis of monocotyledons: Ii. cytological features of stomatal development in the gramineae. *Dev. Biol.* 2, 477–500. doi: 10.1016/0012-1606(60)90050-6

Taylor, S. H., Franks, P. J., Hulme, S. P., Spriggs, E., Christin, P. A., Edwards, E. J., et al. (2012). Photosynthetic pathway and ecological adaptation explain stomatal trait diversity amongst grasses. *New Phytol.* 193, 387–396. doi: 10.1111/j.1469-8137.2011.03935.x

Thordal-Christensen, H., Zhang, Z., Wei, Y., and Collinge, D. B. (1997). Subcellular localization of h2o2 in plants. H2o2 accumulation in papillae and hypersensitive response during the barley—powdery mildew interaction. *Plant J.* 11, 1187–1194. doi: 10.1046/j.1365-313x.1997.11061187.x

Vialet-Chabrand, S. R. M., Matthews, J. S. A., Mcausland, L., Blatt, M. R., Griffiths, H., and Lawson, T. (2017). Temporal dynamics of stomatal behavior: Modeling and implications for photosynthesis and water use. *Plant Physiol.* 174:603.

Voigt, C. A. (2014). Callose-mediated resistance to pathogenic intruders in plant defense-related papillae. *Front. Plant Sci.* 5:168. doi: 10.3389/fpls.2014.00168

Wakte, K. V., Nadaf, A. B., Krishnan, S., and Thengane, R. J. (2007). Studies on lower epidermal papillae, the site of storage of basmati rice aroma compounds in pandanus amaryllifolius roxb. *Curr. Sci.* 93, 238–242.

Wang, M., Gao, L., Dong, S., Sun, Y., Shen, Q., and Guo, S. (2017). Role of silicon on plant–pathogen interactions. *Front. Plant Sci.* 8:701. doi: 10.3389/fpls.2017.00701

Whitty, C. J. M., Jones, M., Tollervey, A., and Wheeler, T. (2013). Africa and asia need a rational debate on gm crops. *Nature* 497:31. doi: 10.1038/497031a

Wu, X. H., Wang, W., Yin, C. M., Hou, H. J., Xie, K. J., and Xie, X. L. (2017). Water consumption, grain yield, and water productivity in response to field water management in double rice systems in china. *PLoS One* 12:e0189280. doi: 10.1371/journal.pone.0189280

Xia, K., Ou, X., Gao, C., Tang, H., Jia, Y., Deng, R., et al. (2015). Osws1 involved in cuticular wax biosynthesis is regulated by osa-mir1848. *Plant Cell Environ.* 38, 2662–2673. doi: 10.1111/pce.12576

Yamaji, N., Mitatni, N., and Ma, J. F. (2008). A transporter regulating silicon distribution in rice shoots. *Plant Cell* 20:1381. doi: 10.1105/tpc.108.059311

Yang, X., Wang, B., Chen, L., Li, P., and Cao, C. (2019). The different influences of drought stress at the flowering stage on rice physiological traits, grain yield, and quality. *Sci. Rep.* 9:3742.

Ye, W., Munemasa, S., Shinya, T., Wu, W., Ma, T., Lu, J., et al. (2020). Stomatal immunity against fungal invasion comprises not only chitin-induced stomatal closure but also chitosan-induced guard cell death. *Proc. Natl. Acad. Sci. U S A.* 117:20932. doi: 10.1073/pnas.1922319117

Yoo, C. Y., Pence, H. E., Jin, J. B., Miura, K., Gosney, M. J., Hasegawa, P. M., et al. (2010). The arabidopsis gtl1 transcription factor regulates water use efficiency and drought tolerance by modulating stomatal density via transrepression of sdd1. *Plant Cell* 22, 4128–4141. doi: 10.1105/tpc.110.078691

Yoo, J.-H., Park, J.-H., Cho, S.-H., Yoo, S.-C., Li, J., Zhang, H., et al. (2011). The rice bright green leaf (bgl) locus encodes osropgef10, which activates the development of small cuticular papillae on leaf surfaces. *Plant Mol. Biol.* 77, 631–641. doi: 10.1007/s11103-011-9839-0

Young, A. J., Suarez, L. P., Kapralov, M., and Opel, M. R. (2017). Leaf epidermal structure in the dwarf succulent genus conophytum n.E. Br. (aizoaceae). *Bradleya* 2017, 217–237. doi: 10.25223/brad.n35.2017.a25

Zeiger, E., Farquhar, G. D., and Cowan, I. R. (1987). *Stomatal Function*. Stanford, CA: Stanford University Press.

Zhou, Q., Ju, C.-X., Wang, Z.-Q., Zhang, H., Liu, L.-J., Yang, J.-C., et al. (2017). Grain yield and water use efficiency of super rice under soil water deficit and alternate wetting and drying irrigation. *J. Int. Agriculture* 16, 1028–1043. doi: 10.1016/s2095-3119(16)61506-x

Zhou, W., Wang, Y., Wu, Z., Luo, L., Liu, P., Yan, L., et al. (2016). Homologs of scar/wave complex components are required for epidermal cell morphogenesis in rice. *J. Exp. Botany* 67, 4311–4323. doi: 10.1093/jxb/erw214

Conflict of Interest: The authors declare that the research was conducted in the absence of any commercial or financial relationships that could be construed as a potential conflict of interest.

frontiers in Plant Science

PERSPECTIVE
published: 24 June 2021
doi: 10.3389/fpls.2021.678417

The Role of Grass *MUTE* Orthologs in GMC Progression and GC Morphogenesis

*Laura Serna**

Facultad de Ciencias Ambientales y Bioquímica, Universidad de Castilla-La Mancha, Toledo, Spain

Stomata arose about 400 million years ago when plants left their aquatic environment. The last step of stomatal development is shared by all plant groups, and it implies a symmetrical cell division from the guard mother cell (GMC) to produce two guard cells (GCs) flanking a pore. In Arabidopsis, the basic helix-loop-helix transcription factor MUTE controls this step, upregulating cell-cycle regulators of the GMC division, and immediately afterward, repressors of theses regulators like *FAMA* and *FOUR LIPS*. Recently, three grass *MUTE* orthologs (*BdMUTE* from *Brachypodium distachyon*, *OsMUTE* from rice, and *ZmMUTE* from maize) have been identified and characterized. Mutations in these genes disrupt GMC fate, with *bdmute* also blocking GC morphogenesis. However, because these genes also regulate subsidiary cell recruitment, which takes place before GMC division, their functions regulating GMC division and GC morphogenesis could be an indirect consequence of that inducing the recruitment of subsidiary cells. Comprehensive data evaluation indicates that *BdMUTE*, and probably grass *MUTE* orthologs, directly controls GMC fate. Although grass MUTE proteins, whose genes are expressed in the GMC, move between cells, they regulate GMC fate from the cells where they are transcribed. Grass *MUTE* genes also regulate GC morphogenesis. Specifically, OsMUTE controls GC shape by inducing *OsFAMA* expression. In addition, while SCs are not required for GMC fate progression, they are for GC maturation.

Keywords: ***FAMA***, ***FOUR LIPS***, **grasses, guard cells, guard mother cell, morphogenesis,** ***MUTE***, **orthologs**

OPEN ACCESS

Edited by:
Juan Dong,
Rutgers, The State University of New Jersey, United States

Reviewed by:
Jie Le,
Key Laboratory of Plant Molecular Physiology, Institute of Botany (CAS), China
Suiwen Hou,
Lanzhou University, China

***Correspondence:**
Laura Serna
laura.serna@uclm.es

Specialty section:
This article was submitted to Plant Cell Biology, a section of the journal Frontiers in Plant Science

Received: *09 March 2021*
Accepted: *26 April 2021*
Published: *24 June 2021*

Citation:
Serna L (2021) The Role of Grass MUTE Orthologs in GMC Progression and GC Morphogenesis. Front. Plant Sci. 12:678417. doi: 10.3389/fpls.2021.678417

INTRODUCTION

Plants conquered land over 470 million years ago (Edwards et al., 1998; Berry et al., 2010). This event was contemporaneous with a series of innovations, among them, the appearance of a water-repellent cuticle interrupted by tiny stomatal pores (Edwards et al., 1998; Berry et al., 2010). Stomatal pores, flanked by two kidney-shaped guard cells (GCs), allowed gas exchange between the plant and the atmosphere to perform photosynthesis with a minimal water loss. To date, no other structure has managed to replace them, although GC morphogenesis has evolved over time, with grasses developing dumbbell-shaped GCs, instead of kidney-shaped ones (Stebbins and Shah, 1960; Rudall et al., 2017; Hepworth et al., 2018; Nunes et al., 2019).

In all plant species, stomatal development takes place through stereotyped patterns of cell divisions. The differences in these patterns among species give rise to a great diversity in the

structure of the stomatal complexes. In the model plant Arabidopsis, protodermal cells commit to the stomatal lineage adopting, in a basipetal manner, the identity of meristemoid mother cell (MMC; **Figure 1A**; Peterson et al., 2010; Vatén and Bergmann, 2012). These MMCs undergo an asymmetric division to produce a smaller meristemoid (M) and a larger stomatal lineage ground cell (SLGC). Ms usually undergo additional self-renewing asymmetric divisions, in an inward spiral, until they become guard mother cells (GMCs). Then GMCs divide symmetrically to produce a pair of kidney-shaped GCs. SLGCs can differentiate into pavement cells, or they can assume an MMC fate producing secondary stomata. This cell division pattern differs from that taking place in grasses, where epidermal cells are organized in files, and stomatal development, which occurs only in some of them, proceeds along a spatiotemporal gradient with the earliest developmental stages occurring in the leaf base and proceeding as cells expand and differentiate toward the tip of the leaf (Stebbins and Shah, 1960). In this plant group, potential stomatal precursor cells proliferate in particular files and as these cells are pushed further up the leaf blade, some of them divide asymmetrically leading to a smaller GMC and a larger sister cell (Stebbins and Shah, 1960; Serna, 2011; Hepworth et al., 2018; Nunes et al., 2019; **Figure 1B**). Before GMC division, cells from files in either side of newly formed GMC acquire subsidiary mother cell (SMC) identity and divide asymmetrically. The smaller cells resulting from these cell divisions, which are always placed next to the GMC, differentiate as subsidiary cells (SCs). Following SCs recruitment, the GMC divides symmetrically, with the cell division plane being parallel to the main axis of leaf growth. This cell division, followed by a complex process of morphogenesis, yields two elongated, dumbbell-shaped GCs. The recruitment of SCs, together with the differentiation of dumbbell-shaped GCs, only takes place in this plant group.

In Arabidopsis, the transition from GMC to paired GCs is regulated by *MUTE* (Han et al., 2018; **Figures 1A**, **2A** and **Table 1**), which also controls the previous step, that is, the GMC formation from the last M (MacAlister et al., 2007; Pillitteri et al., 2007). The presence of arrested Ms, after an excess of self-renewing cell divisions, instead of stomata in *mute* loss-of-function mutants (MacAlister et al., 2007; Pillitteri et al., 2007), and the conversion of all epidermal cells to stomata in plants overexpressing *MUTE* (MacAlister et al., 2007; Pillitteri et al., 2007), are consistent with the functions attributed to this gene. *MUTE* encodes a basic-helix-loop-helix (bHLH) protein (MacAlister et al., 2007; Pillitteri et al., 2007), and its functions depend on its heterodimerization with the functionally redundantly bHLH proteins ICE1 (also known as SCREAM) and SCREAM2 (Kanaoka et al., 2008). Its expression, which overlaps with the localization of the protein encoded by this gene (Wang et al., 2019), is restricted to Ms and GMCs (MacAlister et al., 2007; Pillitteri et al., 2007). MUTE controls the last cell division of stomatal development directly upregulating cell-cycle regulators, and later transcriptional repressors of these cell-cycle regulators, like *FAMA* and *FOUR LIPS* (*FLP*) (Han et al., 2018 and references therein; **Figure 2A**). *FAMA*, which also encodes a bHLH protein that forms heterodimers with ICE1 and SCREAM2 (Ohashi-Ito and Bergmann, 2006; Kanaoka et al., 2008), not only ensures that GMCs undergo a single cell division, but also guides GC differentiation (Ohashi-Ito and Bergmann, 2006; **Table 1**). This gene is expressed and translated in GMCs and differentiating GCs (Ohashi-Ito and Bergmann, 2006). Independently of *FAMA*, the *MYB* gene *FLP*, which is strongly expressed in GMCs and in young GCs, together with its paralogous *MYB88*, also restricts GMC-division and guides GC differentiation (Lai et al., 2005; **Table 1**).

Three grass *MUTE* orthologs have been recently isolated and characterized (Raissig et al., 2017; Wang et al., 2019; Wu et al., 2019; **Table 1**): *BdMUTE* from *Brachypodium distachyon*, *ZmMUTE* from maize and *OsMUTE* from rice. They also regulate stomatal development but in a very different way to *MUTE* (Raissig et al., 2017; Wang et al., 2019; Wu et al., 2019). OsMUTE and BdMUTE, like MUTE, associate with their orthologs of both SCREAM and SCREAM2 to control stomatal development, although there are differences in the function of these bHLH proteins between the grasses and Arabidopsis, and also within the grasses themselves (Kanaoka et al., 2008; Raissig et al., 2016; Wu et al., 2019). In contrast with *MUTE*, these grass *MUTE* orthologs induce the recruitment of SCs, and the proteins encoded by them move from the GMC, where they are expressed, to the SMCs (Raissig et al., 2017; Wang et al., 2019; Wu et al., 2019). This led to speculation that grass *MUTE* genes function in a non-cell-autonomous way, meaning that they influence adjacent SMC where they are not transcribed (Raissig et al., 2017; Wang et al., 2019; Wu et al., 2019; Serna, 2020). Mutations in grass *MUTE* orthologs, in addition to blocking SCs formation, also disrupt GMC fate (Raissig et al., 2017; Wang et al., 2019; Wu et al., 2019). In Brachypodium, it is known that mutations in *BdMUTE* not only block GMC fate but also GC morphogenesis (Raissig et al., 2017). However, given that the execution of the GMC fate takes place after the recruitment of the SCs, it is not known if the effect of *MUTE* orthologs during GMC division and GC differentiation is direct or, conversely, a consequence of their requirement in the previous step. Here, I delve into the possible function of grass *MUTE* genes in GMC fate progression and GC differentiation. The emerging picture unravels that they control GMC fate in an autonomous manner. They also regulate GC morphogenesis. In addition, in rice, GC morphogenesis takes place through positive regulation of *OsFAMA* by OsMUTE. Moreover, several observations strongly suggest that SCs formation is not required for grass *MUTE* genes to trigger the GMC division, but for GC maturation.

BdMUTE CONTROLS AUTONOMOUSLY GMC FATE

In Arabidopsis, *MUTE* promotes both the transition from the M to the GMC and the symmetric division of the GMC to produce two paired GCs (MacAlister et al., 2007; Pillitteri et al., 2007; Han et al., 2018). Ms appear to be absent in grasses, where a single asymmetric division from the MMC directly produces the immediate stomatal precursor (Nunes et al., 2019; Serna, 2020). This stomatal precursor, the GMC, divides symmetrically to produce the two GCs. Do grass *MUTE* genes regulate the

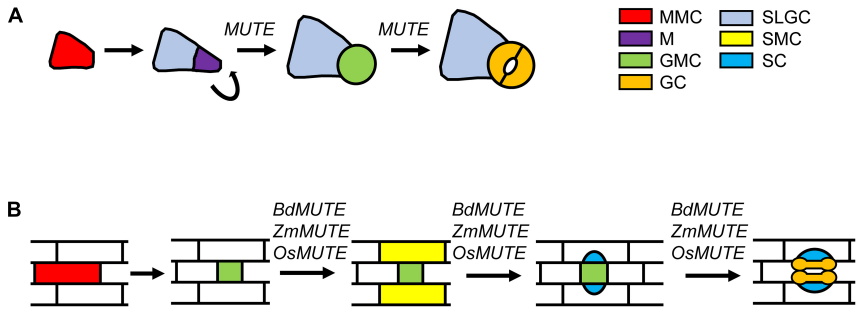

FIGURE 1 | Steps regulated by *MUTE* and *MUTE* orthologs of grasses during stomatal development. **(A)** Stomatal development in Arabidopsis initiates when a protodermal cells acquires MMC identity. The MMC undergoes an asymmetric division that generates a small M and a larger SLGC. Ms usually reiterate their asymmetric divisions in an inward spiral. Ms activity stop when they assume GMC identity. GMCs divide symmetrically to produce the two kidney-shaped GCs. *MUTE* controls the transition from M to GMC, and the GMC division to produce a pair of kidney-shaped cells. **(B)** In grasses, stomatal development starts with an asymmetric division from an MMC that, in contrast with Arabidopsis, directly produces the GMC. Then, cells from files on either side of the GMC adopt SMC identity. SMCs divide asymmetrically to produce the two SCs making contact with the GMC. Once GMC is flanked by the SCs, it undergoes a symmetric division producing the two dumbbell-shaped GCs. Grass *MUTE* genes, in addition to control SMC identity and SCs formation, they also regulate GMC fate and GC morphogenesis. GC, guard cell; GMC, guard mother cell; M, meristemoid; MMC, meristemoid mother cell; SC subsidiary cell; SLGC, stomatal lineage ground cell; SMC, subsidiary mother cell.

transition from GMC to the paired GCs as *MUTE* does in Arabidopsis?

Most GMCs (70%) of *bdmute* divide symmetrically with their division plane orientating like those of wild-type plants, but to produce dicot-like stomata (Raissig et al., 2017). The remaining of GMCs (around 30%) of this mutant do not produce stomata (Raissig et al., 2017). They fail to specify the orientation of the GMC division plane and/or undergo excessive and randomly oriented cell divisions (Raissig et al., 2017). These results indicate that *BdMUTE*, in a redundant manner with other factors, controls GMC fate. Given that *bdmute* is completely devoid of SCs, its ability to develop stomata are telling us that *BdMUTE*, together with unknown factors, regulates autonomously, that is, in the cells in which it is made, GMC fate.

In contrast to *bdmute*, both *bzu2-1* and *c-osmute,* with loss-of-function mutations in *ZmMUTE* and *OsMUTE* respectively, completely lack stomata (Wang et al., 2019; Wu et al., 2019). Instead, these mutants produce GMCs that undergo excessive, randomly oriented and/or asymmetric divisions, which give rise to short columns of elongated cells (Wang et al., 2019; Wu et al., 2019; Buckley et al., 2020; Serna, 2020). While in *c-osmute* these columns consist of two cells, in *bzu2-1* can appear up to four cells. Interestingly, *bzu2-1*, which develops a small percentage (4.61%; $n = 802$) of complexes with one SCs, does not develop GCs (Wang et al., 2019). This observation suggests that, in maize, GMC fate progression does not depend on SCs formation. Then *BdMUTE*, and probably grass *MUTE* orthologs, controls GMC fate in a fully autonomous manner, and not by inducing a signaling from SCs.

But how do grass *MUTE* genes control GMC division? In Arabidopsis, cyclin-dependent kinase complexes consisting of a CYCA2s and CDKB1;1 positively regulate GMC division (Boudolf et al., 2009; Vanneste et al., 2011). CYCD5;1, which interacts with CDKA1;1 (Boruc et al., 2010), also promotes GMC division (Han et al., 2018). The same happens with CYCD7;1 together with CDKB1, which also executes GMC division (Weimer et al., 2018). Upstream of these complexes is

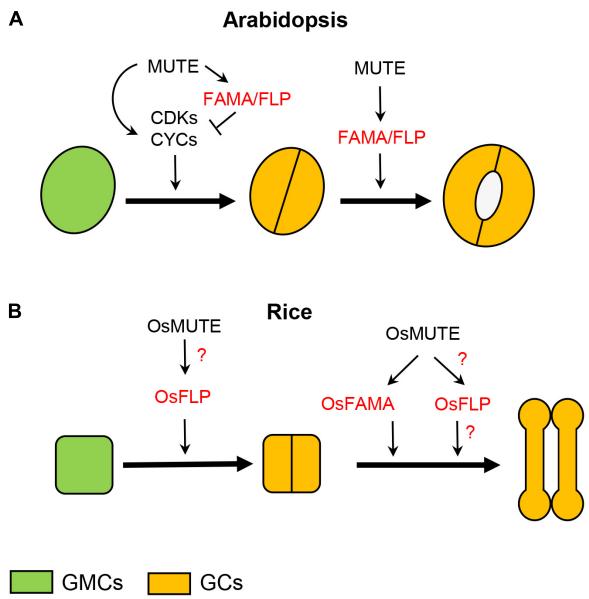

FIGURE 2 | Role of *MUTE*, *FAMA*, *FLP*, and their orthologs in rice during GMC progression and GC morphogenesis. **(A)** In the GMC of Arabidopsis, MUTE positively regulates cell-cycle genes, but also, immediately after, repressors of them, among them *FAMA* and *FLP*. This makes possible that the GMC undergoes a single cell division. MUTE, by promoting *FAMA* and *FLP* expression, in addition to halt proliferative GMC divisions, controls GC differentiation. **(B)** In rice, OsMUTE guides GMC face by correctly orientating its cell division plane, perhaps by positively regulating *OsFLP*. OsMUTE also controls GC morphogenesis by promoting *OsFAMA* expression. OsMUTE may also regulate *OsFLP* to guide GC morphogenesis. It is not known what makes it possible for GMCs to undergo a single cell division. GC, guard cell; GMC, guard mother cell.

MUTE, which directly upregulates the expression of the genes encoding for these cell cycle regulator proteins (Han et al., 2018; Weimer et al., 2018). Later, FLP, whose expression is positively

regulated by MUTE (Han et al., 2018), represses *CDKB1;1* expression, and GMC division, by binding to a *cis*-regulatory region in its promoter (Xie et al., 2010). Like *CDKB1;1*, *CDKA;1* is also a direct target of FLP/MYB88, which bind to its promoter (Yang et al., 2014). FLP/MYB88 also repress *CYCD7;1* expression (Weimer et al., 2018). This makes possible that GMCs undergo a single cell division. *FAMA*, whose expression is also induced by MUTE (Han et al., 2018), may also negatively regulate *CDKB1;1* to halt cell division (Boudolf et al., 2004). FAMA also binds to the *CYCD7;1* promoter to restrict *CYCD7;1* expression (Weimer et al., 2018). In contrast to Arabidopsis, rice has only one ortholog to *CYCA2s*, named *OsCYCA2;1* (La et al., 2006; Qu et al., 2018). OsCYCA2;1 forms a complex with OsCDKB1, which is the ortholog of Arabidopsis CDKB1;1 (Qu et al., 2018). This complex, in contrast to those between CYCA2s and CDBK1;1, does not regulate GMC divisions, but it controls the previous step that generates the GMC (Qu et al., 2018). Although we know the targets of MUTE, and of its downstream components FLP and FAMA, to control GMC fate, the same does not happen for OsMUTE and OsFLP. The only thing we know now is that *OsMUTE* regulates GMC division in a different way than *MUTE* does in Arabidopsis.

OsMUTE INDUCES GC MORPHOGENESIS POSITIVELY REGULATING *OsFAMA* EXPRESSION

BdMUTE not only controls GMC fate but also GC morphogenesis as shows the fact that *bdmute* develops dicot-like stomata. Does this regulation of GC shape extend to the other grass *MUTE* genes? Or, on the contrary, is it exclusive to Brachypodium and perhaps lost with the domestication of grasses?

In the GMC of Arabidopsis, MUTE not only positively regulates cell-cycle genes (Han et al., 2018; Weimer et al., 2018; **Figure 2A**), but also the transcriptional repressors of theses cell-cycle genes (Han et al., 2018; **Figure 2A**). Among these repressors is *FAMA* (Han et al., 2018). Loss-of-function *fama* mutants fail to develop stomata, and instead they produce clusters of small and narrow cells named *fama* tumors (Ohashi-Ito and Bergmann, 2006), and overexpression of this gene converts all epidermal cells to unpaired GC-like cells (Ohashi-Ito and Bergmann, 2006). Thus, *FAMA* in addition to halt proliferative GMC divisions, induces GC morphogenesis (Ohashi-Ito and Bergmann, 2006; **Figure 2A**). This network started by MUTE ensures that GMCs undergo a single division producing the paired kidney-shaped GCs (Han et al., 2018). Analysis of relative expression of *OsFAMA* in *c-osmute* showed that it is significatively smaller than that in wild-type plants, indicating that, like in Arabidopsis (Han et al., 2018), OsMUTE induces *OsFAMA* expression (Wu et al., 2019), more probably in GMC and young GCs. Agree with this, RNA *in situ* hybridization determined the localization of *OsFAMA* transcript in the leaf epidermis of the sheath elongation zone (Liu et al., 2009), where GMC division and GC differentiation take place. However, the function of *FAMA* and *OsFAMA* does not seem identical: while loss-of-function mutations in *FAMA* induce *fama* tumors (Ohashi-Ito and Bergmann, 2006), those in *OsFAMA* usually result in the formation of stomata with box-shaped GCs instead of dumbbell-shaped ones (Liu et al., 2009; Wu et al., 2019). GMCs of *c-osfama* do not undergo extra cell divisions. So that while *FAMA* controls both GMC division and GC morphogenesis, *OsFAMA* only regulates GC differentiation (**Figure 2**). Agree with this, the expression of *ProFAMA:OsFAMA* in the Arabidopsis *fama-1* mutant induces GC differentiation but does not prevent stomatal cluster formation (Liu et al., 2009). In contrast, the expression under the control of *FAMA* promoter of the *Solanum lycopersicum* ortholog of *FAMA* (*SolycFAMA*) in *fama-1* complements the two defects of *fama-1*, preventing stomatal clusters formation and triggering GC differentiation (Ortega et al., 2019). This suggests that *OsFAMA*, and perhaps *FAMA* orthologs from grasses, has lost its ability to regulate GMC fate. The divergence between *FAMA* and *OsFAMA* is also evident when comparing their overexpression phenotypes: while ectopic *FAMA* expression is sufficient to confer GC character (Ohashi-Ito and Bergmann, 2006), ectopic expression of *OsFAMA* is not (Wu et al., 2019). Occasionally, *osfama* develops stomata devoid of one SC, suggesting that *OsFAMA* contributes to the recruitments of SCs (Wu et al., 2019). The presence of SCs in *osfama* is telling

TABLE 1 | Role of *MUTE, FAMA,* and *FLP*, and their orthologs in grasses.

Gene name	Species	Gene function	References
MUTE	*Arabidopsis thaliana* (Eudicot)	Transition from M to GMC, and from GMC to paired GCs	MacAlister et al., 2007; Pillitteri et al., 2007; Han et al., 2018
FAMA	*Arabidopsis thaliana* (Eudicot)	GMC and GCs identities	Ohashi-Ito and Bergmann, 2006; Han et al., 2018
FLP	*Arabidopsis thaliana* (Eudicot)	GMC and GCs identities	Lai et al., 2005; Han et al., 2018
BdMUTE	*Brachypodium distachyon* (Monocot, Poaceae)	Recruitment of SCs. GMC and GCs identities	Raissig et al., 2017
ZmMUTE/BZU2	*Zea mays* (Monocot, Poaceae)	Recruitment of SCs. GMC and GCs identities	Wang et al., 2019
OsMUTE	*Oryza sativa* (Monocot, Poaceae)	Recruitment of SCs. GMC and GCs identities	Wu et al., 2019
OsFAMA	*Oryza sativa* (Monocot, Poaceae)	GC morphogenesis	Liu et al., 2009; Wu et al., 2019
OsFLP	*Oryza sativa* (Monocot, Poaceae)	GMC and GCs identities	Wu et al., 2019

GCs, guard cells; GMC, guard mother cell; M, meristemoid; SCs, subsidiary cells.

us that GC morphogenesis, at least in rice, does not depend on a mechanical force generated by the SCs. Although the functions of *FAMA* and *OsFAMA* are not identical, both MUTE and OsMUTE control GC morphogenesis by regulating *FAMA* and *OsFAMA,* respectively (**Figure 2**). The role of *MUTE* orthologs in GC morphogenesis is not, therefore, exclusive to Brachypodium, but extends, at least to rice, and probably to the remaining grasses.

MUTE also represses GMC division upregulating the expression of the transcriptional repressor of regulatory genes of the cell cycle *FLP* (Han et al., 2018), with loss-of-function mutations in both *FLP* and its paralogous *MYB88* resulting in exaggerated stomatal cluster with undifferentiated stomatal precursor cells (Lai et al., 2005). Previous studies have shown that *FLP* and *MYB88* function independently of *FAMA* (Ohashi-Ito and Bergmann, 2006). Mutations in *OsFLP* disrupt the orientation of the GMC division plane and GC differentiation (Wu et al., 2019), but in contrast to those in *FLP* and *MYB88*, they do not induce extra GMC divisions. Then, OsMUTE may regulate the orientation of the GMC division plane by regulating *OsFLP* expression (**Figure 2B**). Thus, it is not clear how grasses ensure that GMCs undergo a single cell division. We also do not know if the differences between *FAMA*/*FLP* and *OsFAMA*/*OsFLP* extend to the rest of grass *FAMA*/*FLP* orthologs.

SCs ARE REQUIRED FOR GC MORPHOGENESIS

OsMUTE promotes GC morphogenesis producing dumbbell-shaped GCs in rice leaves (Wu et al., 2019). Surprisingly, the stomata placed on rice coleoptiles are like those of Arabidopsis and quite different from those in rice leaves (Guo et al., 2016). What prevents the coleoptile GCs from undergoing the morphogenesis process that gives rise to dumbbell-shaped GCs? The stomatal complexes of rice coleoptiles not only consist of kidney-shaped GC pairs, but they are anomocytic, and therefore devoid of SCs (Guo et al., 2016). Then, one possibility is that SCs, which do not seem to be required for GMC division, are for GC morphogenesis.

In rice leaves, OsMUTE moves from GMC, where its gene is transcribed (Liu et al., 2009; Wang et al., 2019), to epidermal cells of neighboring files, where it is likely to regulate the transcription of genes required for SCs recruitment (Wang et al., 2019; Serna, 2020). MUTE, whose gene is expressed in GMCs (MacAlister et al., 2007; Pillitteri et al., 2007), does not move from GMC to surrounding epidermal cells (Wang et al., 2019). In agreement with this, Arabidopsis does not recruit SCs, or its GCs undergo the morphogenesis process typical of the GCs of grasses. *OsMUTE* is also expressed in coleoptiles of rice (Guo et al., 2016). An attractive hypothesis lies in the inability of movement of OsMUTE from GMC to its adjacent epidermal cells placed on neighboring files, preventing SCs formation, and consequently GC morphogenesis. Alternatively, OsMUTE may move among cells but its function that induces the recruitment of lateral SCs may be blocked in coleoptiles.

The development of dicot-like stomata in coleoptiles of rice suggests that signals emanating from SCs trigger GC morphogenesis in rice leaves. But what is the molecular nature of these signals? The role of *OsFLP* in GC morphogenesis is unclear, but *OsFAMA,* positively regulated by OsMUTE, promotes GC morphogenesis (Wu et al., 2019). OsMUTE may regulate *OsFAMA* from SCs and, consequently, in a non-autonomous way, by inducing the expression of unknown genes. What seems to be clear is that SCs are required for GC morphogenesis. Agree with this view, *MUTEp:OsMUTE* expression partially complements the defects of *mute-1* by inducing the formation of kidney-shaped GCs from some stomatal precursor (Liu et al., 2009), but is not capable of inducing the differentiation of dumbbell-shaped GCs in the absence of SCs. Like *OsMUTE*, *ZmMUTE* driven by the *MUTE* promoter in *mute-1* produces kidney-shaped GCs from some stomatal precursors (Liu et al., 2009), but it is not capable of producing grass stomata or SCs.

MUTE and grass *MUTE* retain the control of GMC division, but they have also diverged, with grass *MUTE* acquiring two new functions: the recruitment of SCs and the production of dumbbell-shaped GCs. It is time to speculate that the grass stomata have evolved from those of plants with kidney-shaped GCs, and through a mechanism that involves the intercellular movement of grass MUTE. At an intermediate point of this evolutionary path is *Flagellaria indica*, which is closely related to grasses, and exhibits intermediate morphologies in its GCs, neither dumbbell nor kidney-shaped ones (Sack, 1994). Because *Flagellaria indica* exhibits SCs like those of grasses, that is, its complexes are paracytic-non-oblique (Sack, 1994; Rudall et al., 2017), it is likely that SCs only trigger the first steps of GC morphogenesis of grasses.

CONCLUDING REMARKS

BdMUTE, in addition to recruit SCs, controls GMC fate in a fully autonomous manner. Although possibly grass *MUTE* orthologs also autonomously control GMC fate, experimental data are necessary to confirm it. Interestingly, the *bdmute* incomplete penetrance unravels that unknown factors trigger stomatal formation in this mutant (Nunes et al., 2019; Serna, 2020). The full disruption of GMC fate in both *osmute* and *bzu2-1* suggests that these unknown genes regulating GMC fate in Brachypodium may have been blocked with the agricultural practices (Ohashi-Ito and Bergmann, 2006; Serna, 2020). The isolation and characterization of additional grass *MUTE* genes from both domesticated and wild plants will be essential to determine whether there is a direct link between *BdMUTE* divergence and the human influence on agriculture.

Grass *MUTE* genes also control GC morphogenesis. In rice, the proteins encoded by these genes do it, like in Arabidopsis, by positively regulating *OsFAMA* expression. Because *OsFLP* controls the orientation of the GMC division plane (Wu et al., 2019), perhaps positively regulated by OsMUTE, its possible role during GC morphogenesis is unclear. Analysis of the morphogenesis of the GCs of *osflp* produced by correctly orientated GMC divisions, will help to deep into the function/s of *OsFLP* and to unravel how much it has diverged from *FLP*.

It is important to note that while *FAMA* and *FLP*, regulated by MUTE, in addition to controlling GC differentiation, also ensure that GMCs undergo a single division (Lai et al., 2005; Ohashi-Ito and Bergmann, 2006; Han et al., 2018), *OsFAMA* and *OsFLP* do not ensure the repression of extra GMCs division. So far, we do not have any information about the function/s of *FAMA* and *FLP* genes in Brachypodium and maize. The analysis of the *FAMA* and *FLP* orthologs function/s in these plant species will let us know if the differences in *FAMA* and *FLP* functions between Arabidopsis and rice extend to the rest of grasses.

Finally, the presence of stomata like those of Arabidopsis in rice coleoptiles questions the role of *OsMUTE*/*OsFAMA* in this embryonic organ and suggests that SCs are required for GC morphogenesis. We could be close to revealing the origin of the peculiar and highly efficient stomata of grasses, which seems to be related to the intercellular movement of grass MUTE. This unique and highly efficient structure is likely to have contributed, 30–45 million years ago, to the successful expansion of this plant group (Kellogg, 2001; Hetherington and Woodward, 2003; Chen et al., 2017).

AUTHOR CONTRIBUTIONS

LS wrote the manuscript and designed the figures.

REFERENCES

Berry, J. A., Beerling, D. J., and Franks, P. J. (2010). Stomata: key players in the earth system, past and present. *Curr. Opin. Plant Biol.* 13, 233–240. doi: 10.1016/j.pbi.2010.04.013

Boruc, J., Inze, D., and Russinova, E. (2010). A high-throughput bimolecular fluorescence complementation protein-protein interaction screen identifies functional *Arabidopsis* CDKA/B-CYCD4/5 complexes. *Plant Signal. Behav.* 5, 1276–1281. doi: 10.4161/psb.5.10.13037

Boudolf, V., Barroco, R., de Almeida Engler, J. A., Verkest, A., Beeckman, T., Naudts, M., et al. (2004). B1-type cyclin-dependent kinases are essential for the formation of stomatal complexes in *Arabidopsis thaliana*. *Plant Cell* 16, 945–955. doi: 10.1105/tpc.021774

Boudolf, V., Lammens, T., Boruc, J., Van Leene, J., Van Den Daele, H., Maes, S., et al. (2009). CDKB1;1 forms a functional complex with CYCA2;3 to suppress endocycle onset. *Plant Physiol.* 150, 1482–1493. doi: 10.1104/pp.109.140269

Buckley, C. R., Caine, R. S., and Gray, J. E. (2020). Pores for thought: can genetic manipulation of stomatal density protect future rice yields? *Front. Plant Sci.* 10:1783. doi: 10.3389/fpls.2019.01783

Chen, Z. H., Chen, G., Dai, F., Wang, Y., Hills, A., Ruan, Y. L., et al. (2017). Molecular evolution of grass stomata. *Trends Plant Sci.* 22, 124–139. doi: 10.1016/j.tplants.2016.09.005

Edwards, D., Kerp, H., and Hass, H. (1998). Stomata in early land plants: an anatomical and ecophysiological approach. *J. Exp. Bot.* 49, 255–278. doi: 10.1093/jxb/49.Special_Issue.255

Guo, F., Han, N., Xie, Y., Fang, K., Yang, Y., Zhu, M., et al. (2016). The miR393a/target module regulates seed germination and seedling establishment under submergence in rice (*Oryza Sativa* L.). *Plant Cell Environ.* 39, 2288–2302. doi: 10.1111/pce.12781

Han, S.-K., Qi, X., Sugihara, K., Dang, J. H., Endo, T. A., Miller, K. L., et al. (2018). MUTE directly orchestrates cell-state switch and the single symmetric division to create stomata. *Dev. Cell* 45, 303.e–315.e. doi: 10.1016/j.devcel.2018.04.010

Hepworth, C., Caine, R. S., Harrison, E. L., Sloan, J., and Gray, J. E. (2018). Stomatal development: focusing on the grasses. *Curr. Opin. Plant Biol.* 41, 1–7. doi: 10.1016/j.pbi.2017.07.009

Hetherington, A. M., and Woodward, F. I. (2003). The role of stomata in sensing and driving environmental change. *Nature* 424, 901–908. doi: 10.1038/nature01843

Kanaoka, M. M., Pillitteri, L. J., Fujii, H., Yoshida, Y., Bogenschutz, N. L., Takabayashi, J., et al. (2008). *SCREAM/ICE1* and *SCREAM2* specify three cell-state transitional steps leading to *Arabidopsis* stomatal differentiation. *Plant Cell* 20, 1775–1785.

Kellogg, E. A. (2001). Evolutionary history of the grasses. *Plant Physiol.* 125, 1198–1205. doi: 10.1104/pp.125.3.1198

La, H., Li, J., Ji, Z., Cheng, Y., Li, X., Jiang, S., et al. (2006). Genome-wide analysis of cyclin family in rice (*Oryza Sativa L.*). *Mol. Genet. Genomics* 275, 374–386. doi: 10.1007/s00438-005-0093-5

Lai, L. B., Nadeau, J. A., Lucas, J., Lee, E. K., Nakagawa, T., Zhao, L., et al. (2005). The Arabidopsis R2R3 MYB proteins FOUR LIPS and MYB88 restrict divisions late in the stomatal cell lineage. *Plant Cell* 17, 2754–2567. doi: 10.1105/tpc.105.034116

Liu, T., Ohashi-Ito, K., and Bergmann, D. C. (2009). Orthologues of Arabidopsis thaliana stomatal bHLH genes and regulation of stomatal development in grasses. *Development* 136, 2265–2276. doi: 10.1242/dev.032938

MacAlister, C. A., Ohashi-Ito, K., and Bergmann, D. C. (2007). Transcription factor control of asymmetric cell divisions that establish the stomatal lineage. *Nature* 445, 537–540. doi: 10.1038/nature05491

Nunes, T. D. G., Zhang, D., and Raissig, M. T. (2019). Form, development and function of grass stomata. *Plant J.* 101, 780–799. doi: 10.1111/tpj.14552

Ohashi-Ito, K., and Bergmann, D. C. (2006). Arabidopsis FAMA controls the final proliferation/differentiation switch during stomatal development. *Plant Cell* 18, 2493–2505. doi: 10.1105/tpc.106.046136

Ortega, A., de Marcos, A., Illescas-Miranda, J., Mena, M., and Fenoll, C. (2019). The tomato genome encodes SPCH, MUTE, and FAMA candidates that can replace the endogenous functions of their *Arabidopsis* orthologs. *Front. Plant Sci.* 10:1300. doi: 10.3389/fpls.2019.01300

Peterson, K. M., Rychel, A. L., and Torii, K. U. (2010). Out of the mouths of plants: the molecular basis of the evolution and diversity of stomatal development. *Plant Cell* 22, 296–306. doi: 10.1105/tpc.109.072777

Pillitteri, L. J., Sloan, D. B., Bogenschutz, N. L., and Torii, K. U. (2007). Termination of asymmetric cell division and differentiation of stomata. *Nature* 445, 501–505. doi: 10.1038/nature05467

Qu, X., Yan, M., Zou, J., Jiang, M., Yang, K., and Le, J. (2018). A2-type cyclin is required for the asymmetric entry division in rice stomatal development. *J. Exp. Bot.* 69, 3587–3599. doi: 10.1093/jxb/ery158

Raissig, M. T., Abrash, E., Bettadapur, A., Vogel, J. P., and Bergmann, D. C. (2016). Grasses use an alternatively wired bHLH transcription factor network to establish stomatal identity. *Proc. Natl. Acad. Sci. U S A.* 113, 8326–8331.

Raissig, M. T., Matos, J. L., Gil, M. X. A., Kornfeld, A., Bettadapur, A., Abrash, E., et al. (2017). Mobile MUTE specifies subsidiary cells to build physiologically improved grass stomata. *Science* 355, 1215–1218. doi: 10.1126/science.aal3254

Rudall, P. J., Chen, E. D., and Cullen, E. (2017). Evolution and development of monocot stomata. *Am. J. Bot.* 104, 1122–1140. doi: 10.3732/ajb.1700086

Sack, F. D. (1994). Structure of the stomatal complex of the monocot *Flagellaria indica*. *Am. J. Bot.* 81, 339–344. doi: 10.1002/j.1537-2197.1994.tb15452.x

Serna, L. (2011). Stomatal development in Arabidopsis and grasses: differences and commonalities. *Int. J. Dev. Biol.* 55, 5–10. doi: 10.1387/ijdb.103094ls

Serna, L. (2020). The role of grass *MUTE* orthologues during stomatal development. *Front. Plant Sci.* 11:55. doi: 10.3389/fpls.2020.00055

Stebbins, G. L., and Shah, S. S. (1960). Developmental studies of cell differentiation in the epidermis of monocotyledons. II. Cytological features of stomatal development in the Gramineae. *Dev. Biol.* 2, 477–500. doi: 10.1016/0012-1606(60)90050-6

Vanneste, S., Coppens, F., Lee, E., Donner, T. J., Xie, Z., Van Isterdael, G., et al. (2011). Developmental regulation of CYCA2s contributes to tissue-specific proliferation in Arabidopsis. *EMBO J.* 30, 3430–3441. doi: 10.1038/emboj.2011.240

Vatén, A., and Bergmann, D. C. (2012). Mechanisms of stomatal development: an evolutionary view. *EvoDevo* 3:11. doi: 10.1186/2041-9139-3-11

Wang, H., Guo, S., Qiao, X., Guo, J., Li, Z., Zhou, Y., et al. (2019). BZU2/ZmMUTE controls symmetrical division of guard mother cell and specifies neighbor cell fate in maize. *PLoS Genet.* 15:e1008377. doi: 10.1371/journal.pgen.1008377

Weimer, A. K., Matos, J. L., Sharma, N., Patell, F., Murray, J. A. H., Dewitte, W., et al. (2018). Lineage- and stage-specific expressed CYCD7;1 coordinates the single symmetric division that creates stomatal guard cells. *Development* 145:dev160671. doi: 10.1242/dev.160671

Wu, Z., Chen, L., Yu, Q., Zhou, W., Gou, X., Li, J., et al. (2019). Multiple transcriptional factors control stomata development in rice. *N. Phytol.* 223, 220–232. doi: 10.1111/nph.15766

Xie, Z., Lee, E., Lucas, J. R., Morohashi, K., Li, D., Murray, J. A. H., et al. (2010). Regulation of cell proliferation in the stomatal lineage by the Arabidopsis MYB FOUR LIPS via direct targeting of core cell cycle genes. *Plant Cell* 22, 2306–2321. doi: 10.1105/tpc.110.074609

Yang, K., Wang, H., Xue, S., Qu, X., Zou, J., and Le, J. (2014). Requirement for A-type cyclin-dependent kinase and cyclins for the terminal division in the stomatal lineage of *Arabidopsis*. *J. Exp. Bot.* 65, 2449–2461. doi: 10.1093/jxb/eru139

Conflict of Interest: The author declares that the research was conducted in the absence of any commercial or financial relationships that could be construed as a potential conflict of interest.

frontiers in Plant Science

METHODS
published: 29 July 2021
doi: 10.3389/fpls.2021.715309

An Affordable Image-Analysis Platform to Accelerate Stomatal Phenotyping During Microscopic Observation

Yosuke Toda[1,2,3]†, Toshiaki Tameshige[4,5]*†, Masakazu Tomiyama[2], Toshinori Kinoshita[3] and Kentaro K. Shimizu[4,6]*

[1] Japan Science and Technology Agency, Saitama, Japan, [2] Phytometrics co., ltd., Shizuoka, Japan, [3] Institute of Transformative Bio-Molecules (WPI-ITbM), Nagoya University, Nagoya, Japan, [4] Kihara Institute for Biological Research, Yokohama City University, Yokohama, Japan, [5] Department of Biology, Faculty of Science, Niigata University, Niigata, Japan, [6] Department of Evolutionary Biology and Environmental Studies, University of Zurich, Zurich, Switzerland

OPEN ACCESS

Edited by:
Naoki Hirotsu,
Toyo University, Japan

Reviewed by:
Alex Wu,
The University of Queensland, Australia
Christoph Sommer,
Institute of Science and Technology Austria (IST Austria), Austria

***Correspondence:**
Yosuke Toda
tyosuke@aquaseerser.com
Toshiaki Tameshige
tame_t@yokohama-cu.ac.jp

† These authors have contributed equally to this work and share first authorship

Specialty section:
This article was submitted to Plant Physiology, a section of the journal Frontiers in Plant Science

Received: 26 May 2021
Accepted: 08 July 2021
Published: 29 July 2021

Citation:
Toda Y, Tameshige T, Tomiyama M, Kinoshita T and Shimizu KK (2021) An Affordable Image-Analysis Platform to Accelerate Stomatal Phenotyping During Microscopic Observation. Front. Plant Sci. 12:715309. doi: 10.3389/fpls.2021.715309

Recent technical advances in the computer-vision domain have facilitated the development of various methods for achieving image-based quantification of stomata-related traits. However, the installation cost of such a system and the difficulties of operating it on-site have been hurdles for experimental biologists. Here, we present a platform that allows real-time stomata detection during microscopic observation. The proposed system consists of a deep neural network model-based stomata detector and an upright microscope connected to a USB camera and a graphics processing unit (GPU)-supported single-board computer. All the hardware components are commercially available at common electronic commerce stores at a reasonable price. Moreover, the machine-learning model is prepared based on freely available cloud services. This approach allows users to set up a phenotyping platform at low cost. As a proof of concept, we trained our model to detect dumbbell-shaped stomata from wheat leaf imprints. Using this platform, we collected a comprehensive range of stomatal phenotypes from wheat leaves. We confirmed notable differences in stomatal density (*SD*) between adaxial and abaxial surfaces and in stomatal size (*SS*) between wheat-related species of different ploidy. Utilizing such a platform is expected to accelerate research that involves all aspects of stomata phenotyping.

Keywords: affordable phenotyping, real-time image analysis, stomatal density, stomatal size, microscopy

INTRODUCTION

Stomata are pores of plant leaves that regulate gas exchange. Plants modulate the degree of stomatal opening (aperture) to adjust CO_2 uptake and water loss in response to environmental conditions such as light intensity, humidity, temperature and CO_2 concentrations. In addition to the regulation of stomatal aperture, stomatal density (*SD*) and stomatal size (*SS*) are also known to influence gas exchange efficiency (Bertolino et al., 2019). From this viewpoint, quantification of such traits

is important to gain insights into the molecular mechanisms that underlie the environmental adaptability of the plant. Genetic approaches such as Quantitative Trait Loci analysis and Genome-Wide Association Studies, in addition to forward chemical genetic screening, have successfully identified factors involved in such traits (Ziadi et al., 2017; Chen et al., 2020). To detect genetic and environmental effects on a quantitative trait, it is crucial to measure the data variation using a large sample (Tsuchimatsu et al., 2020). However, quantification of stomata-related phenotypes has often had to rely on manual methods, limiting the throughput of the research.

Recent technological advances in the computer-vision domain have allowed the development of various algorithms, pipelines or platforms to quantify stomata-related phenotypes through analysis of microscopic images. For example, Jayakody et al. (2017) have built a HOG classifier to detect the stomata of grapevine leaf imprints. Toda et al. (2018) have also utilized HOG in an image-analysis pipeline to detect the stomata of dayflower leaf disks. Meanwhile, Fetter et al. (2019) have utilized a convolutional neural network (CNN), a deep learning architecture, to identify stomata from a variety of microscopic images taken from various plant species. Other deep learning models, e.g., YOLO, SSD, and Mask R-CNN, have been proposed as useful adjuncts in stomata detection and trait measurement (Sakoda et al., 2019; Casado-García et al., 2020; Jayakody et al., 2021). As exemplified by those studies, deep learning has been demonstrated to be efficacious in the quantification of stomatal traits.

However, we faced several issues in implementing the above systems in a laboratory environment. First, to train a deep neural network model, a computer equipped with a high-performance graphics processing unit (GPU) and sufficient random-access memory (RAM) was required. Moreover, to use the trained deep learning model in daily analysis, an additional personal computer (PC), preferably also with a GPU, was ideally needed. This involves a high implementation cost to establish the image-analysis system. Second, we experienced difficulty in implementing real-time analysis that could observe and detect stomata on the fly. Attainment of such systems has been desirable for experimental biologists because they are expected to relieve the labor of injecting the acquired microscopic image into an independent program. However, manufacturers of laboratory-grade CCD/CMOS cameras designed for microscopic image acquisition often do not make drivers, software development kits or application programming interfaces available to users, but use proprietary dedicated software to run the devices. This makes it difficult for a "home-brewed" image-analysis program to access the camera connected to the microscope for on-site analysis.

To resolve such issues, we designed a microscopic system intended to analyze stomatal traits in real time, which can be easily and affordably prepared. The hardware system consists of an upright microscope connected to a USB video device class (UVC)-compatible camera and a Jetson Nano, a GPU-supported single-board computer. We chose each component to be generally available at electronic commerce sites (e.g., Amazon, eBay) at an affordable price, so that the total cost does not exceed USD 1,000. Moreover, the UVC compatibility of the camera allows it to be controlled from open-source computer-vision libraries. Using this system, we built an analysis pipeline to detect the stomata of wheat leaf blade imprints using an SSD, a deep learning architecture designed for object detection (Liu et al., 2015). The train/test dataset annotation and the model training were performed using free cloud services, which also minimized the preparation cost.

Using this platform, we investigated the phenotypic traits of wheat stomata. Here, we demonstrate that our platform can easily quantify wheat *SD* and *SS* in large numbers of samples. By increasing the sample number, we were able to detect the difference in the *SD* between adaxial and abaxial surfaces with high statistical confidence. Notably, a negative correlation between *SD* and *SS* within a single leaf was also detected. As exemplified by the case study, utilizing such a platform is expected to accelerate research involving all aspects of stomata phenotyping in fields such as plant physiology, breeding and agriculture.

MATERIALS AND EQUIPMENT

Required Hardware

Server PC

- NVIDIA Jetson Nano B01 (NVIDIA, United States).
- 5 V/4 A AC/DC power supply for Jetson Nano.
- UHS-I microSD card (preferably larger than 64 GB).
- USB A-MicroB conversion cable.
- LAN cable.
- Internet accessible environment.
- (Optional) USB memory for storing the acquired image.
- An additional PC or an adapter that can read/write a SD card image for the Server PC.

Microscope

- Upright C-mount trinocular microscope with ×4 and ×10 lenses, e.g., SW380T 40–2500X (Swift Optical Instruments, United States). Alternatively, a binocular microscope can be used with an additional eyepiece C-mount adapter.
- UVC-compatible with C/CS mountable camera with a resolution preferably over 8 MP. e.g., WE3170 (GAZO, Japan), ELP-USB13M02-MFV (ELP, China).

Client PC

- Arbitrary PC with USB 2.0 connection available.

Required Software

Server PC

- Configuration provided by NVIDIA[1]. However, for the initial SD card image, we strongly prefer using JetCard,[2] an AI development friendly configuration. This image enables

[1]https://developer.nvidia.com/embedded/learn/get-started-jetson-nano-devkit
[2]https://github.com/NVIDIA-AI-IOT/jetcard

users to skip the time consuming and complex installation of the python-related libraries including ones that are required by our GUI system, as well as Jupyter Notebook (Lab) Server and initial user account setup. Instructions written in the section "Methods" assume that users have used the JetCard image.
- We prepared a simple browser-based GUI that can be run in Jupyter Notebook[3]. This package also contains the stomata detection SSD model weights prepared as described in the Methods section. Alternatively, users can run their custom python code that receives camera input and simultaneously processes data.
- Users may connect the display to the Jetson Nano while setup, however, upon running the analysis program, the display must be disconnected and be controlled by the client PC (headless mode) to ensure sufficient free GPU memory for executing the deep neural network model and image analysis upon real-time analysis.

Client PC

- Any software that can perform an SSH connection to the server PC.
- Web browser.
- 1x USB-A port.
- The present system has been tested in the following PC environments, although most of the commercially available PC environments are expected to work. If the OS does not have an SSH client at default, download any arbitrary SSH client.
  - macOS Catalina 10.15.7 with Google Chrome (91.0.4472.114).
  - Windows 10 Pro version 1909 (OS Build: 18363.1440) with Microsoft Edge (91.0.864.59).

METHODS

Configuration

Microscopy

- Remove the lens unit of the camera if present and mount it on the C-mount trinocular tube of the microscope. The camera can alternatively be mounted to the eyepiece of the microscope using the eyepiece/C-mount adapter.

Server PC

- Create the SD card image of Jetson Nano using the JetCard image at any available PC by downloading and writing the image file available at https://github.com/NVIDIA-AI-IOT/jetcard. Users will need a PC with an adapter to read/write SD card. Detailed instructions of how to prepare are thoroughly described at the website.
- Insert the SD card with its image into the Jetson Nano.
- Power on the Jetson Nano with headless mode (no monitor connected).
- Connect the microscopy camera to the USB A port of Jetson Nano.
- Connect the LAN cable to Jetson Nano.
  - For security reasons, we do not recommend the Jetson Nano to be always connected to the internet. We prefer the LAN cable to be disconnected after the initialization step described below. After setup, the system can be run completely offline.

Client PC

- Initialization.
  - Connect the client PC to the Jetson Nano with the USB A-Micro B cable.
  - Open the terminal and establish SSH connection with the following command.
    - ssh -p jetson jetson@192.168.55.1.
    - Using the Jetson Nano as the server PC through USB connection will automatically assign its IP address to 192.168.55.1, which is the default value configured in NVIDIA Jetson series (e.g., Nano, Xavier, TX2) as of June 2021.
  - Install additional python libraries with the following command in the terminal.
    - pip3 install ipywidgets scikit-image.
- Download the GUI and dependencies with the following command. Ensure the user is in the home directory (e.g. cd $HOME).
  - git clone https://github.com/totti0223/onsite_stomata_platform.git.
  - cd onsite_stomata_platform.
  - git clone https://github.com/tensorflow/models.git.
  - Close the terminal.
  - Disconnect LAN cable from the Jetson NANO.
- GUI execution for stomatal detection.
  - Open the terminal again and establish SSH connection this time with port forwarding.
    - ssh -p jetson -L 8888:localhost:8888 jetson@192.168.55.1.
      - If the JetCard image is used for Jetson Nano, port 8888 is occupied by JupyterLab instead of Jupyter Notebook. Both applications are compatible at the current state.
  - Open a web browser, and type the following url for JupyterLab connection.
    - localhost:8888.

[3]https://github.com/totti0223/onsite_stomata_platform

- Type jetson for password.
- Locate and click the folder "onsite_stomata_platform" to move to its directory.
- Click and open "main_En.ipynb."
- Execute each cell from the top. Execute the cell as described below and the GUI will start inside the notebook.
  - _ = pme.stream(pipeline_func = pipeline_func, output_directory = None, camera_id = 0, videocapture_api_backend = 200, camera_initial_settings = {'format': ['M', 'J', 'P', 'G'], 'height': 768, 'width': 1024, 'fps': 30}).
    - The above code assumes users are using the ELP-USB13M02-MFV camera. If users want to test their Jetson Nano with a USB Web Camera or other input devices, simply delete camera_initial_settings = {...} from above.
    - If the GUI would not start or execute properly due to JupyterLab specific configuration or version incompatibility, shutdown the ipynb notebook and reaccess by Jupyter Notebook. In brief, change the "/lab" to "/tree" in the URL. See https://jupyterlab.readthedocs.io/en/stable/getting_started/starting.html for details.

- GUI execution for custom image analysis interface.
  - If users want to use their own stomata detection model in their GUI, the most simple way is to rename the existing "saved_model" folder to "_saved_model" and copy their own "saved_model" folder into the directory. Depending on their training condition and *SS*, users may have to change their input image size from the camera (from the GUI pulldown menu) to obtain optimal results. Notably, if users would like to prepare an image analysis module other than bounding box detection (e.g., instance segmentation), the user will need to prepare a custom pipeline func. In any case, the module can be modified in the notebook cell, in which the existing codes are self explanatory for users who have sufficient skills to prepare their own custom pipeline.

- Access https://github.com/totti0223/onsite_stomata_platform for further details online and future updates.

Generation of Stomata Detection Model

For annotating images used for machine-learning model training, we used Labelbox[4], a cloud labeling service that is currently free for academic usage. We uploaded and labeled 697 wheat leaf imprint images so that each stoma for the training set was annotated with a circumscribed bounding box. Each image had a resolution of 2048 × 3072 (height × width) pixels that were acquired as described in the following section "Plant Materials, Growth Condition, and Sample Preparation." Annotated dataset was then exported from Labelbox to the local environment in JSON format. Next, labeled images were resized to 1024 × 1536, padded with black pixels to the size of 1024 × 2048, and were split into two sized 1024 × 1024. The image transformation and the converting bounding-box coordinates were performed using Albumentations (Buslaev et al., 2020), an image augmentation library. Sets of images and annotations were then converted to COCO json format, then finally to TFRecord format.

The training of the stomata detection model was performed by following the steps of the section "Training and Evaluation with TensorFlow 2" of the Tensorflow Model Garden repository[5]. The training process was run in Google Colaboratory[6], a freely available cloud programming service with GPU accessibility. Detailed codes and instructions to reproduce the regarding system as well as the stomata detection model is described in Google Colaboratory executable notebook[7] hosted at https://github.com/totti0223/onsite_stomata_platform. Briefly, the default config parameters provided in the repository were used for training. We used an SSD (Liu et al., 2015) with MobileNetV2 backbone, pretrained with COCO dataset, with an input size of 640 × 640 (Refer to ssd_mobilenet_v2_fpnlite_640 × 640_coco17_tpu-8 at Tensorflow Model Garden). As a result, we obtained a model that detects stomata with a mean Average Precision (mAP) of 0.825 and 0.636 with the intersection-over-union (IoU) threshold of 0.3 and 0.5 against the test dataset, respectively. The trained model was downloaded from Google Colaboratory to the local environment as a SavedModel format, and used for the GUI. Notably, the test dataset was created by acquiring 50 images using the microscopy proposed in this research with a resolution of 768 × 1024.

Plant Materials, Growth Condition and Sample Preparation

Training Data

A series of 25 bread wheat accessions with serial numbers from LPGKU2305 to LPGKU2329 (National BioResource Project–Wheat, Japan) and a Swiss winter wheat cultivar "ArinaLrFor" (Singla et al., 2017) were used as training data. The first leaves of young plants and the flag leaves after heading were collected from those wheat accessions in the greenhouse. The epidermal thin imprints were prepared by pasting and drying clear nail polish on the leaves. In some cases, first imprints were taken from the leaves using dental impression material (Dent Silicone AQUA, Shofu Inc., Kyoto, Japan) and used as the templates for the nail-polish imprints. The nail-polish imprints were put on glass slides and observed directly or after mounting with glycerol. Of note, samples were placed on the microscopic stage so that stomata were aligned as horizontally as possible. The microscope was a normal bright-field microscope, Olympus BX61 (Tokyo, Japan), equipped with a normal lens UPlanFLN. The camera was an RGB camera of 6.3 MP CMOS, a WRAYCAM-NOA

[4]https://labelbox.com

[5]https://github.com/tensorflow/models/blob/master/research/object_detection/g3doc/tf2_training_and_evaluation.md

[6]https://colab.research.google.com

[7]https://colab.research.google.com/github/totti0223/onsite_stomata_platform/blob/main/StomataDetectorModelTraining.ipynb

630 (Wraymer Inc. Osaka, Japan). These images were used for initial training for the detection model described in the prior "Generation of Stomata Detection Model" section. Other bread wheats, a cultivar Yumechikara and a synthetic hexaploid wheat, were used to acquire datasets for validation. These samples were observed using the same method as the samples used for the measurements below.

SD and *SS* Measurements

A hexaploid bread wheat *Triticum aestivum* (cultivar: Chinese Spring), a tetraploid wheat *Triticum turgidum* (extracted tetraploid wheat harboring AABB subgenomes of Chinese Spring) (Yang et al., 1999), diploid wheat-relative grasses *Triticum urartu* (accession: KU-199-01) and *Aegilops tauschii* (accession: KU-2076), and a model grass *Brachypodium distachyon* (accession: Bd21) were used in this study. The seeds were germinated on moist filter papers in the dark at 4°C, then the seedlings were grown in plant pots under continuous white LED light in an air-conditioned room maintained at 22°C. The first leaves of four-leaf-stage plants were used for observation. Microscopic images were taken from three plants of each species. The slides were prepared using the same method as for preparing the training data described above. The microscope, camera and image processing devices were as described above.

To sample images from a wide range of leaf areas in an unbiased manner, images were acquired according to the following protocol. At first, we decided a whole target area to be acquired and prepared the imprint. Approximately a middle third of total leaf length was selected as the target because the middle parts of wheat leaves show smaller variation in *SD* among subsamples than subsamples from the distal and proximal parts of the leaves (Teare et al., 1971). Second, the angles of the imprint and camera were adjusted to align cell files along the left-right axis in the image. Third, start acquiring a series of images from the top left and scanned across the target area to the bottom right. Each horizontal scan-lines is distant from the next ones with approximately the image size. When the current frame displayed is not good due to distortion, breaking, bubbles or shallowness of the imprint, we ignored that frame and went further to a better frame. During such a data quality evaluation, the real-time feedback was helpful to know whether or not the image quality was in a permissible range.

Data Analysis and Visualization of *SD* and *SS*

To calculate the *SD*, the total number of automatically detected stomata was divided by the microscopic field area (0.984 mm^2 in our hardware setting). To measure the *SS*, the *x*- and *y*-lengths of each bounding-box were used as stomatal length and width, respectively, after scaling the values from units of pixels to micrometers (1.116 μm/pixel for ×4 lens, and 0.445 μm/pixel for ×10 lens). The bounding-box size of the stomata may be incorrect when the box coordinates contain a lower limit (0) or upper limit (1024 for the *x*-axis and 768 for the *y*-axis) because some part of the stomata protrudes from the image. Therefore, these marginal stomata were ignored in the *SS* calculation. The ground truth of stomatal length and width were manually measured on imageJ[8] with Rectangle selection tool. Data visualization by scatter, density, box and jitter plots was performed using the *ggplot2* package (Wickham, 2016) in the R language[9]. Statistical tests including *t* test and correlation tests were performed using the *stats* package in the R language.

RESULTS

Platform Appearance

The appearance of the platform and the schematic diagram of the dataflow prepared by following the Methods section are shown in **Figures 1A,B**. The camera input image was processed in the server PC (Jetson Nano), while the client PC was connected to the server PC by a web browser through a USB connection. Therefore, the latter does not require a specific operating system or hardware specification, which allows multiple users to connect their PCs to the platform without installing any specific programs (Supplementary Movie)[10].

The executed GUI is embedded inside the Jupyter Notebook (**Figure 1C** and **Supplementary Figure 1**). Moreover, the raw program code of the image-analysis module is written directly inside the cell of the Notebook. This allows easy program development and debugging for any users upon customization. In our configuration, the camera image sequence is processed through an SSD to obtain the coordinates of the detected stomata and then displayed as an annotated output. The processing speed of the platform depends on the camera input image size and the content of the image-analysis program, as well as the presence or absence of a display of the annotated image. In our configuration, it was about 1.4 frames per second.

Stomatal Density Measurement

To test the performance of stomata counting, we compared stomatal numbers per unit area (*SD*) from different types of tissues. In general, *SD*s differ between adaxial and abaxial leaf surfaces. In the case of Triticeae, the adaxial surface has a higher *SD* than the abaxial (Rajendra et al., 1978; Wang and Clarke, 1993). We measured *SD*s from adaxial and abaxial imprints of bread wheat leaves. More than 150 images, each of a 0.984 mm^2 microscopic field, were analyzed. The mean *SD*s were 23.2 and 16.8 stomata/mm^2 for adaxial and abaxial surfaces, respectively (**Figure 2A**). The true *SD*s, that is, the manually counted data, were 22.5 and 16.2 stomata/mm^2, indicating error rates of only 2.84 and 3.70% for *SD* estimation.

Despite the obvious difference in *SD* between adaxial and abaxial surfaces as shown in **Figure 2A**, the stomatal counts of single images varied, and the distributions of adaxial and abaxial surfaces largely overlap. This means that no significant difference between the surfaces can be detected in some cases of small samples. When four images were randomly sampled from our dataset and Welch's *t* tests were performed, 3,652 of 10,000 (∼37%) simulations resulted in no significant difference

[8]https://imagej.nih.gov/ij/

[9]https://www.r-project.org/

[10]https://youtu.be/CHk6Mw3kabc

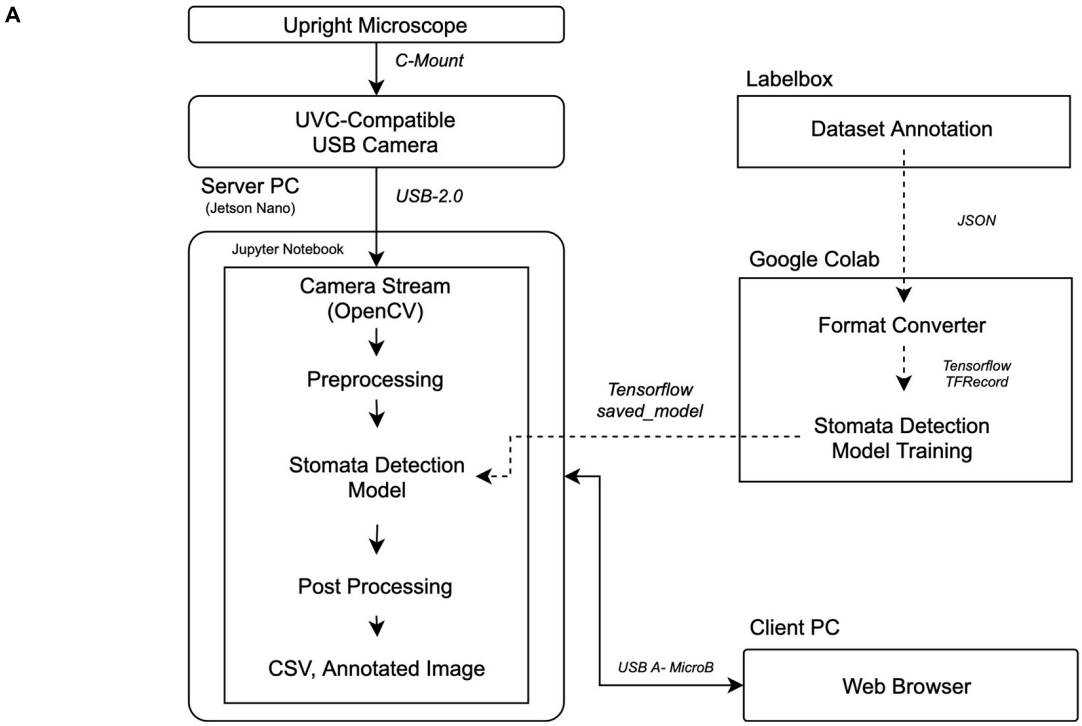

FIGURE 1 | Stomatal detection platform. **(A)** Schematic diagram of the workflow. **(B)** Appearance of the platform. Numbers in insets describe the individual components. 1, UVC-compatible camera (ELP-USB13M02-MFV); 2, upright trinocular microscope (SW380T); 3, server PC (Jetson Nano B01); 4, client PC (Macbook Pro 13-inch, 2017). **(C)** Screenshot of the GUI run in the client PC through the Google Chrome web browser.

($p > 0.05$). In the case of 10-each random samples, only 33 of 10,000 (0.33%) simulations resulted in no significant difference, confirming the importance of sample size in statistical tests. While these simulations were performed from data for manually counted *SD*, the same random sampling with our automatically estimated *SD*s that included some errors resulted in no significant difference in 4,907 (∼49%) and 81 (0.81%), respectively, of 10,000 simulations of 4- and 10-each random samples. These simulations suggest that increasing sample size has a higher impact than increasing accuracy in *SD* estimation and statistical power, given that the error rate is sufficiently low.

In addition, we asked whether our phenotyping system can also be used to quantify the stomatal patterning parameter. Our image acquisition protocol provides the images in which cell files are aligned horizontally, thus the y-coordinates of stomata are limited to the position of stomatal files. This property allows us to automatically collect the interval lengths between stomatal files along the *y*-axis of the image (**Supplementary Figure 2A**). Such

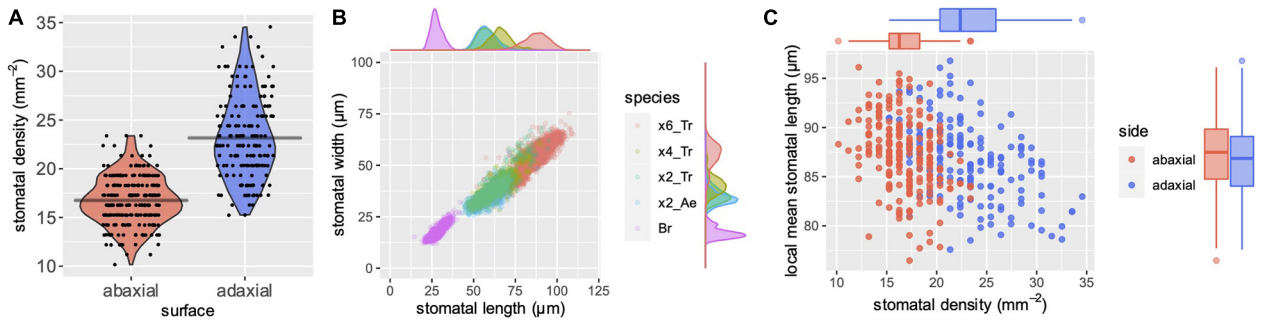

FIGURE 2 | A case study of *SD* and *SS*. **(A)** Automatically measured *SD* of abaxial (red) and adaxial (blue) surfaces. The first leaves from bread wheat (*Triticum aestivum*) were observed at the four-leaf stage of seedlings. Gray horizontal bars indicate mean values. **(B)** Automatically measured *SS* of different species with a series of genome sizes. Besides a scatter plot of length (*x*-axis) and width (*y*-axis), the density plots along each axis are shown. "x6_Tr," "x4_Tr," "x2_Tr," "x2_Ae," and "Br" indicate hexaploid *T. aestivum*, tetraploid *Triticum turgidum*, diploid *Triticum urartu*, diploid *Aegilops tauschii* and diploid *Brachypodium distachyon*, respectively. More than a thousand stomata were measured for each species. Abaxial stomata from the former four species and adaxial stomata of *Brachypodium* were measured because the *Brachypodium* has rich abaxial prickle hairs that hinder automatic measurements. **(C)** Local *SD* and local mean stomatal length of bread wheat (*T. aestivum*). Data were collected by automatic measurements. Each point represents a single microscopic image with a size of 0.984 mm^2. Besides a scatter plot of *SD* (*x*-axis) and length (*y*-axis), the box plots along each axis are shown.

analyses for the interval lengths were performed for our adaxial and abaxial datasets of the bread wheat. The results indicate that there are two types of intervals, namely around 130 and 230 μm, in the abaxial surface (**Supplementary Figure 2B**). On the other hand, the adaxial data show continuously varying interval lengths from 140 to 240 μm (**Supplementary Figure 2C**). As exemplified by those results, the stomatal position data obtained from the present system can be used to quantify some aspects of the stomatal pattern.

Stomatal Size Measurement

Our analysis system detects each stoma as a bounding box and records each box size as representing the individual *SS*. Thus, the x-length and y-length indicate the stomatal length (guard cell length) and stomatal width (sum of guard cell widths, subsidiary cell widths and pore width), respectively, when the leaf distal–proximal axis corresponds to the left–right axis of the microscopic field (**Supplementary Figure 3A**). Comparison between the predicted and hand-measured *SS* of wheat-related species with different *SS* below resulted in Pearson's correlation coefficients of $r = 0.92$ and $r = 0.73$ for stomatal length and width, respectively (**Supplementary Figures 3B,C**).

The mean *SS*, or the range of *SS*, is a species-specific trait, and useful for taxonomic classification in a case where no macroscopic trait is available to classify the different species clearly (Aryavand et al., 2003; Boza Espinoza et al., 2020). It is known that *SS*s correlate well with genome size in Triticum and other plants (Masterson, 1994; Beaulieu et al., 2008). Hexaploid bread wheat (*T. aestivum*) has a large genome consisting of A, B and D subgenomes (∼17 Gb) (International Wheat Genome Sequencing Consortium (IWGSC) et al., 2018). Tetraploid wheat with A and B subgenomes has approximately two-thirds of the hexaploid genome size. The diploid wild species, *A. tauschii* and *T. urartu*, which are the progenitors of bread wheat D and A subgenomes, respectively, have approximately a third of the genome size (Luo et al., 2017; Ling et al., 2018). We measured the *SS* of these plants using our bounding-box measurement system. The mean *SS*s were 87.2 μm × 54.4 μm, 66.3 μm × 40.7 μm, 59.0 μm × 36.4 μm, and 57.4 μm × 33.9 μm (length × width) for the AABBDD hexaploid, AABB tetraploid, AA diploid and DD diploid species, respectively, showing a clear correlation with the genome sizes (**Figure 2B**). This result shows that our automatic measurement performs well for a particular variation in *SS*, and is thus useful to describe this species-specific stomatal trait. Interestingly, the *SS* distributions partly overlapped between plants of different genome sizes, as shown by the scatter and the density plots (**Figure 2B**). In addition to determining the mean values, revealing such variations in a large sample number is important to identify the presence or absence of significant differences among species.

Brachypodium distachyon, a model grass, has a small genome (0.27 Gb) (The International Brachypodium Initiative, 2010). The molecular mechanism of formation of the dumbbell-shaped stomata of grass has been demonstrated in genetic studies using this species (Raissig et al., 2017). Its stomata are so small that only a portion of the stomata were detected when the low magnification (×4) lens was used, as was the case for wheat stomata in the present study (**Supplementary Figure 4**). This was because our model was trained with images of large wheat stomata. However, they were successfully detected with a lens of greater magnification (×10) (**Supplementary Figure 4**). The *Brachypodium* stomatal length and width were 27.9 ± 3.5 and 17.3 ± 2.8 μm (mean ± standard deviation), respectively (**Figure 2B**). Most cereal crops and wild grass species have genome sizes intermediate between those of *B. distachyon* and *T. aestivum*, thus their stomata can be expected to be detected if the image is acquired with an appropriate lens and resolution.

Correlation Between *SD* and *SS*

Previous studies have demonstrated that the variation in *SS* within a species is negatively correlated with the *SD* of the tissues

observed (Rajendra et al., 1978). Such a negative correlation has been reported between different genotypes and between different leaf positions in a shoot. However, our knowledge is very limited (Smith et al., 1989) about whether the same relationship exists between small microscopic fields within leaves of the same genotype, leaf position and growth condition. We found that this negative correlation was observed in our dataset that consisted only of the first leaves from a single cultivar (**Figure 2C**). The adaxial and abaxial datasets showed significant negative correlations (p = 6.26e–08 and 1.55e–07, respectively, in Pearson's correlation test) between mean stomatal lengths and *SD*s of different microscopic fields. Interestingly, the mean stomatal lengths were almost the same for adaxial and abaxial surfaces (86.7 $\pm$ 3.9 and 87.2 $\pm$ 3.7 μm, respectively), although the *SD*s were different (**Figure 2C**). This may suggest that the size of each stoma is determined according to the local *SD* of only a small surrounding region, but the response to the local *SD* differs between adaxial and abaxial stomata. Our system and others that support high-throughput phenotyping can contribute to obtaining greater insight into such unknown developmental mechanisms.

DISCUSSION

In this study, we proposed a platform that enables real-time stomata detection using microscopic observation. The setup cost of the hardware does not exceed USD 1,000, and the stomata detection model and the training data labeling can be prepared based on freely available services. Using the platform, we demonstrated *SD*s and their variation in adaxial and abaxial leaf surfaces, and characterized the *SS* distribution in several wheat-related species of different genome sizes. In addition, we could show that the adaxial and abaxial stomata in a bread wheat exhibit the same mean size even though they show different densities, and *SD* and *SS* of each surface correlate negatively. Our results indicate that experimental biologists can benefit from these cutting-edge technologies in image processing, not only by developing the algorithm but also by using free cloud services and reasonably inexpensive hardware, implementing real-time image processing and a user-friendly user interface. We discuss below some possible options, applications and future challenges of the present system.

In recent years, many companies have released inexpensive single-board computers. Of these, we used the Jetson Nano for the system because at present it is one of the most affordable GPU-harboring PCs (approx. USD 60). However, the GPU memory of the Jetson Nano is limited to 2 GB, which restricts the deep learning architecture that can be loaded into the pipeline. Superior NVIDIA Jetson models such as XAVIER and the TX2 series possess larger GPU memory, thus providing more choices of system configuration.

For stomata detection, we utilized a deep learning-based object detection algorithm to infer the bounding-box coordinates of the stomata. Because the stomata are always oriented horizontally both in our dataset and under observation conditions (**Figure 1C**), the bounding-box coordinates obtained can be used to estimate the width and length of the stomata. Although further refinement of the model is potentially needed to improve accuracy, the current parameters were adequate to highlight the differences in *SS* between species (**Figure 2B**). Application of alternative deep learning architecture intended for segmentation, such as Mask R-CNN (He et al., 2017), is expected to achieve a more precise measurement of the morphology of the stomata (Jayakody et al., 2021).

We focused on the detection of stomata from wheat-related species, which have the dumbbell-shaped stomata typical of grass plants. Similarly, to the increasing reports of stomata detection of kidney shaped stomata of dicots, detection of dumbbell shaped stomata of grass are also starting to be established, exemplified by that of wheat (Sun et al., 2021). In the present study, the training dataset was prepared from only hexaploid wheat cultivars with some augmentation, thus the variations in *SS* and morphology of diploid and tetraploid species were not included. Despite this limitation, the trained model detected most of the stomata from diploid and tetraploid species. This possibly reflects the morphological similarity of dumbbell-shaped stomata in imprint images. Enhancing the generalization of performance to detect the stomata of various grass species might be accomplished with little effort.

Image processing methods may not perform well because of difficulties that are common in biological images (Uchida, 2013). Raw microscopic images acquired on-site often include low-quality data unsuitable for analysis (Koho et al., 2016), such as out-of-focus images, nonuniform lighting or physical damage of the sample. These are often not taken into consideration during the development of analysis algorithms, and can be a potential difficulty in operation. An advantage of real-time analysis is that we can prevent the acquisition of such low-quality images because we can judge the quality of image-analysis results during observation. In the case of stomatal detection using imprint images, causes for these may include contamination by dust or distortion or a shallow imprint. It is costly to use manual analysis or to develop another program to complement the data. Thus, real-time image analysis during observation enables quality assurance of the analyzed data by the operator. In addition, high-speed image analysis enables a time-course analysis, which reveals the dynamics of stomatal aperture when living cells are observed (Sun et al., 2021). There is another potential benefit of real-time image processing for the development of further automatic high-throughput phenotyping systems. Just as an automatic car-driving system regulates the speed in response to the real-time detection of pedestrians and road signs in the camera images, it is possible to move the stage automatically and acquire multiple images using a program that links the microscope camera and a motorized stage. The functionality of an imaging system with an automated motorized stage has been proposed for high-throughput stomatal phenotyping (Millstead et al., 2020). There are motorized stages that are commercially available at a low price and that are controllable from a PC. Real-time image processing systems can expand the possibilities of cooperation between computer and robot as well as cooperation between computer and human.

While there are some potential challenges for further generalization of performance and higher throughput, our present approach will provide the possibility for many experimental biologists to introduce a cost-effective high-throughput system that will accelerate a range of studies involving stomata-related trait analysis.

DATA AVAILABILITY STATEMENT

The raw data supporting the conclusions of this article will be made available by the authors, without undue reservation.

AUTHOR CONTRIBUTIONS

YT and TT directed and designed the study. YT wrote the program codes and assembled the analysis platform. TT conducted the biological experiments, collected the wheat images, and involved in the conceptualization of this research. YT and MT annotated and verified the image dataset. KKS and TK provided advice to assure the scientific validity of the project. All of the coauthors were involved in the writing and verification of the manuscript.

FUNDING

This work was supported by Japan Science and Technology Agency (JST) PRESTO [Grant No. JPMJPR17O5 (YT)], JST CREST [Grant No. JPMJCR16O3 (KKS)], Japan Society for the Promotion of Science (JSPS) KAKENHI [Grant No. 16H06469 (KKS), 18H04785(KKS), 20H05687 (TK), 20H05910 (TK), and 20K15807 (TT)], Swiss National Science Foundation [Grant No. 31003A_182318 (KKS)], and the University Research Priority Program of Evolution in Action of the University of Zurich (KKS).

ACKNOWLEDGMENTS

We thank Labelbox for providing access to the academic usage of dataset labeling. We thank Yoko Tomita at Nagoya University for assistance in annotation to generate a baseline test dataset of stomata imprint images. Yoko Kamiya and Aya Iso (KIBR, Yokohama City University, Japan) provided generous support for wheat cultivation and image acquisition. We also thank the following people for providing the material used in this research. The seeds of *Triticum aestivum* (25 accessions from LPGKU2305 to LPGKU2329), *Aegilops tauschii* (KU-2076) and *Triticum urartu* (KU-199-01) were provided by the National BioResource Project–Wheat, Japan. The bread wheat cv. ArinaLrFor was supplied by Beat Keller (University of Zurich, Switzerland). The bread wheat cv. Yumechikara was supplied by Koichi Hatta (NARO, Japan). The tetraploid wheat (tetra-Chinese Spring) seeds were supplied by Hisashi Tsujimoto (Tottori University, Japan). *Brachypodium distachyon* (accession Bd21) seeds were supplied by Yusuke Kouzai and Keiichi Mochida (RIKEN Center for Sustainable Resource Science, Japan). Synthetic hexaploid wheat generated from a cross between a tetraploid wheat cv. Langdon and a diploid *Aegilops tauschii* (KU-2076) was supplied by Shigeo Takumi and Yoshihiro Matsuoka (Kobe University, Japan).

SUPPLEMENTARY MATERIAL

The Supplementary Material for this article can be found online at: https://www.frontiersin.org/articles/10.3389/fpls.2021.715309/full#supplementary-material

REFERENCES

Aryavand, A., Ehdaie, B., Tran, B., and Waines, J. G. (2003). Stomatal frequency and size differentiate ploidy levels in *Aegilops neglecta*. *Genet. Resour. Crop Evol.* 50, 175–182. doi: 10.1023/a:1022941532372

Beaulieu, J. M., Leitch, I. J., Patel, S., Pendharkar, A., and Knight, C. A. (2008). Genome size is a strong predictor of cell size and stomatal density in angiosperms. *New Phytol.* 179, 975–986. doi: 10.1111/j.1469-8137.2008.02528.x

Bertolino, L. T., Caine, R. S., and Gray, J. E. (2019). Impact of stomatal density and morphology on water-use efficiency in a changing world. *Front. Plant Sci.* 10:225. doi: 10.3389/fpls.2019.00225

Boza Espinoza, T. E., Popp, V., and Kessler, M. (2020). Guard cell sizes and ploidy levels in *Polylepis* (Rosaceae). *Neotrop. Biodivers.* 6, 178–192. doi: 10.1080/23766808.2020.1844992

Buslaev, A., Iglovikov, V. I., Khvedchenya, E., Parinov, A., Druzhinin, M., and Kalinin, A. A. (2020). Albumentations: fast and flexible image augmentations. *Information* 11:125. doi: 10.3390/info11020125

Casado-García, A., del-Canto, A., Sanz-Saez, A., Pérez-López, U., Bilbao-Kareaga, A., Fritschi, F. B., et al. (2020). LabelStoma: a tool for stomata detection based on the YOLO algorithm. *Comput. Electron. Agric.* 178:105751. doi: 10.1016/j.compag.2020.105751

Chen, H., Zhao, X., Zhai, L., Shao, K., Jiang, K., Shen, C., et al. (2020). Genetic bases of the stomata-related traits revealed by a genome-wide association analysis in rice (*Oryza sativa* L.). *Front. Genet.* 11:611. doi: 10.3389/fgene.2020.00611

Fetter, K. C., Eberhardt, S., Barclay, R. S., Wing, S., and Keller, S. R. (2019). StomataCounter: a neural network for automatic stomata identification and counting. *New Phytol.* 223, 1671–1681. doi: 10.1111/nph.15892

He, K., Gkioxari, G., Dollár, P., and Girshick, R. (2017). *Mask R-CNN*. Available online at: http://arxiv.org/abs/1703.06870 (accessed April 6, 2021).

International Wheat Genome Sequencing Consortium (IWGSC), IWGSC RefSeq principal investigators, Appels, R., Eversole, K., Feuillet, C., Keller, B., et al. (2018). Shifting the limits in wheat research and breeding using a fully annotated reference genome. *Science* 361:eaar7191. doi: 10.1126/science.aar7191

Jayakody, H., Liu, S., Whitty, M., and Petrie, P. (2017). Microscope image based fully automated stomata detection and pore measurement method for grapevines. *Plant Methods* 13:94. doi: 10.1186/s13007-017-0244-9

Jayakody, H., Petrie, P., de Boer, H. J., and Whitty, M. (2021). A generalised approach for high-throughput instance segmentation of stomata in microscope images. *Plant Methods* 17:27. doi: 10.1186/s13007-021-00727-4

Koho, S., Fazeli, E., Eriksson, J. E., and Hänninen, P. E. (2016). Image quality ranking method for microscopy. *Sci. Rep.* 6:28962. doi: 10.1038/srep28962

Ling, H.-Q., Ma, B., Shi, X., Liu, H., Dong, L., Sun, H., et al. (2018). Genome sequence of the progenitor of wheat A subgenome *Triticum urartu*. *Nature* 557, 424–428. doi: 10.1038/s41586-018-0108-0

Liu, W., Anguelov, D., Erhan, D., Szegedy, C., Reed, S., Fu, C.-Y., et al. (2015). SSD: single-shot multiBox detector. *ECCV* 2016, 21–37. doi: 10.1007/978-3-319-46448-0_2

Luo, M.-C., Gu, Y. Q., Puiu, D., Wang, H., Twardziok, S. O., Deal, K. R., et al. (2017). Genome sequence of the progenitor of the wheat D genome *Aegilops tauschii*. *Nature* 551, 498–502. doi: 10.1038/nature24486

Masterson, J. (1994). Stomatal size in fossil plants: evidence for polyploidy in majority of angiosperms. *Science* 264, 421–424. doi: 10.1126/science.264.5157.421

Millstead, L., Jayakody, H., Patel, H., Kaura, V., Petrie, P. R., Tomasetig, F., et al. (2020). Accelerating automated stomata analysis through simplified sample collection and imaging techniques. *Front. Plant Sci.* 11:580389. doi: 10.3389/fpls.2020.580389

Raissig, M. T., Matos, J. L., Anleu Gil, M. X., Kornfeld, A., Bettadapur, A., Abrash, E., et al. (2017). Mobile MUTE specifies subsidiary cells to build physiologically improved grass stomata. *Science* 355, 1215–1218. doi: 10.1126/science.aal3254

Rajendra, B. R., Mujeeb, K. A., and Bates, L. S. (1978). Relationships between 2*X hordeum* sp., 2*X Secale* sp. and 2*X*, 4*X*, 6*X triticum* spp. for stomatal frequency, size and distribution. *Environ. Exp. Bot.* 18, 33–37. doi: 10.1016/0098-8472(78)90018-7

Sakoda, K., Watanabe, T., Sukemura, S., Kobayashi, S., Nagasaki, Y., Tanaka, Y., et al. (2019). Genetic diversity in stomatal density among soybeans elucidated using high-throughput technique based on an algorithm for object detection. *Sci. Rep.* 9:7610. doi: 10.1038/s41598-019-44127-0

Singla, J., Luthi, L., Wicker, T., Bansal, U., Krattinger, S. G., and Keller, B. (2017). Characterization of Lr75: a partial, broad-spectrum leaf rust resistance gene in wheat. *Theor. Appl. Genet.* 130, 1–12. doi: 10.1007/s00122-016-2784-1

Smith, S., Weyers, J. D. B., and Berry, W. G. (1989). Variation in stomatal characteristics over the lower surface of *Commelina communis* leaves. *Plant Cell Environ.* 12, 653–659. doi: 10.1111/j.1365-3040.1989.tb01234.x

Sun, Z., Song, Y., Li, Q., Cai, J., Wang, X., Zhou, Q., et al. (2021). An integrated method for tracking and monitoring stomata dynamics from microscope videos. *Plant Phenomics* 2021:9835961. doi: 10.34133/2021/9835961

Teare, I. D., Peterson, C. J., and Law, A. G. (1971). Size and frequency of leaf stomata in cultivars of *Triticum aestivum* and other *Triticum* species. *Crop Sci.* 11, 496–498. doi: 10.2135/cropsci1971.0011183X001100040010x

The International Brachypodium Initiative (2010). Genome sequencing and analysis of the model grass *Brachypodium distachyon*. *Nature* 463, 763–768. doi: 10.1038/nature08747

Toda, Y., Toh, S., Bourdais, G., Robatzek, S., and Maclean, D. (2018). DeepStomata: facial recognition technology for automated stomatal aperture measurement. *bioRxiv* [Preprint]. doi: 10.1101/365098

Tsuchimatsu, T., Kakui, H., Yamazaki, M., Marona, C., Tsutsui, H., Hedhly, A., et al. (2020). Adaptive reduction of male gamete number in the selfing plant *Arabidopsis thaliana*. *Nat. Commun.* 11:2885. doi: 10.1038/s41467-020-16679-7

Uchida, S. (2013). Image processing and recognition for biological images. *Dev. Growth Differ.* 55, 523–549. doi: 10.1111/dgd.12054

Wang, H., and Clarke, J. M. (1993). Genotypic, intraplant, and environmental variation in stomatal frequency and size in wheat. *Can. J. Plant Sci.* 73, 671–678. doi: 10.4141/cjps93-088

Wickham, H. (2016). *ggplot2: Elegant Graphics for Data Analysis*. New York, NY: Springer-Verlag New York.

Yang, Y. F., Furuta, Y., Nagata, S.-I., and Watanabe, N. (1999). Tetra Chinese Spring with AABB genomes extracted from the hexaploid common wheat, Chinese Spring. *Genes Genet. Syst.* 74, 67–70. doi: 10.1266/ggs.74.67

Ziadi, A., Uchida, N., Kato, H., Hisamatsu, R., Sato, A., Hagihara, S., et al. (2017). Discovery of synthetic small molecules that enhance the number of stomata: C–H functionalization chemistry for plant biology. *Chem. Commun.* 53, 9632–9635. doi: 10.1039/C7CC04526C

Conflict of Interest: YT and MT were employed in phytometrics, co., ltd.

The remaining authors declare that the research was conducted in the absence of any commercial or financial relationships that could be construed as a potential conflict of interest.

Publisher's Note: All claims expressed in this article are solely those of the authors and do not necessarily represent those of their affiliated organizations, or those of the publisher, the editors and the reviewers. Any product that may be evaluated in this article, or claim that may be made by its manufacturer, is not guaranteed or endorsed by the publisher.

frontiers in Plant Science

ORIGINAL RESEARCH
published: 03 September 2021
doi: 10.3389/fpls.2021.716784

A Deep Learning-Based Method for Automatic Assessment of Stomatal Index in Wheat Microscopic Images of Leaf Epidermis

Chuancheng Zhu[1], Yusong Hu[1], Hude Mao[2], Shumin Li[2], Fangfang Li[2], Congyuan Zhao[1], Lin Luo[1], Weizhen Liu[1,3] and Xiaohui Yuan[1,4,5]**

[1] School of Computer and Artificial Intelligence, Wuhan University of Technology, Wuhan, China, [2] State Key Laboratory of Crop Stress Biology for Arid Areas, College of Plant Protection, Northwest A&F University, Shaanxi, China, [3] Chongqing Research Institute, Wuhan University of Technology, Chongqing, China, [4] Engineering Research Centre of Chinese Ministry of Education for Edible and Medicinal Fungi, Jilin Agricultural University, Changchun, China, [5] Jiaxing Key Laboratory for New Germplasm Breeding of Economic Mycology, Jiaxing, China

The stomatal index of the leaf is the ratio of the number of stomata to the total number of stomata and epidermal cells. Comparing with the stomatal density, the stomatal index is relatively constant in environmental conditions and the age of the leaf and, therefore, of diagnostic characteristics for a given genotype or species. Traditional assessment methods involve manual counting of the number of stomata and epidermal cells in microphotographs, which is labor-intensive and time-consuming. Although several automatic measurement algorithms of stomatal density have been proposed, no stomatal index pipelines are currently available. The main aim of this research is to develop an automated stomatal index measurement pipeline. The proposed method employed Faster regions with convolutional neural networks (R-CNN) and U-Net and image-processing techniques to count stomata and epidermal cells, and subsequently calculate the stomatal index. To improve the labeling speed, a semi-automatic strategy was employed for epidermal cell annotation in each micrograph. Benchmarking the pipeline on 1,000 microscopic images of leaf epidermis in the wheat dataset (*Triticum aestivum* L.), the average counting accuracies of 98.03 and 95.03% for stomata and epidermal cells, respectively, and the final measurement accuracy of the stomatal index of 95.35% was achieved. R^2 values between automatic and manual measurement of stomata, epidermal cells, and stomatal index were 0.995, 0.983, and 0.895, respectively. The average running time (ART) for the entire pipeline could be as short as 0.32 s per microphotograph. The proposed pipeline also achieved a good transferability on the other families of the plant using transfer learning, with the mean counting accuracies of 94.36 and 91.13% for stomata and epidermal cells and the stomatal index accuracy of 89.38% in seven families of the plant. The pipeline is an automatic, rapid, and accurate tool for the stomatal index measurement, enabling high-throughput phenotyping, and facilitating further understanding of the stomatal and epidermal development for the plant physiology community. To the best of our knowledge, this is the first deep learning-based microphotograph analysis pipeline for stomatal index assessment.

Keywords: stomatal index, cell counting, stomata detection, convolutional network, transfer learning

OPEN ACCESS

Edited by:
Wenxiu Ye,
Shanghai Jiao Tong University, China

Reviewed by:
Francis Wyffels,
Ghent University, Belgium
Toshiaki Tameshige,
Yokohama City University, Japan

***Correspondence:**
Weizhen Liu
liuweizhen@whut.edu.cn
Xiaohui Yuan
yuanxiaohui@whut.edu.cn

Specialty section:
This article was submitted to Plant Physiology, a section of the journal Frontiers in Plant Science

Received: *29 May 2021*
Accepted: *10 August 2021*
Published: *03 September 2021*

Citation:
Zhu C, Hu Y, Mao H, Li S, Li F, Zhao C, Luo L, Liu W and Yuan X (2021) A Deep Learning-Based Method for Automatic Assessment of Stomatal Index in Wheat Microscopic Images of Leaf Epidermis. Front. Plant Sci. 12:716784. doi: 10.3389/fpls.2021.716784

INTRODUCTION

Stomata are formed by pairs of specialized epidermal guard cells, which are the main pathways for gas exchange in the essential physiological processes of leaf plants, such as carbon assimilation, respiration, and transpiration (Kim et al., 2010). The counting and measuring of stomata in microscopic images of leaf epidermis have been one of the most typical plant biological activities (Willmer and Fricker, 1996). The stomatal density and size are good indicators that reflect the response of plants to abiotic stresses in the environment and permit quantitative estimation of the stomatal gas exchange parameters (Sack and Buckley, 2016). However, these traits will alter with the growth of plants or the environment that cannot be used to reveal the stomata initiation and epidermal development across plant genotypes or species. The stomatal index, estimated as the number of stomata per number of epidermal cells plus stomata, is relatively constant during plant growth (Salisbury, 1928). It is of greater significance in studying the epidermal development process in plant physiology and their genetic basis in plant breeding for productivity (Royer, 2001; Sack and Buckley, 2016).

The microscopic images of plant leaf epidermis contain two types of cells, namely, the tightly arranged epidermal cells and the guard cells. Stomata in the leaf epidermis are bounded by the bean- or dumbbell-shaped guard cells with fixed shapes, and in some species but not all, they are surrounded by one-to-many subsidiary cells (Boetsch et al., 1996). At present, various image analysis tools have been developed for detecting, counting (Aono et al., 2019; Fetter et al., 2019), and measuring stomatal aperture (Omasa and Onoe, 1984; Li et al., 2019) as well as assessing stomatal density (Vialet-Chabrand and Brendel, 2014). However, to the best of our knowledge, there is no pipeline designed for the stomatal index measurement, possibly due to the difficulty in epidermal cell detection. For that reason, this study aims to develop a pipeline for automatically measuring stomatal index by simultaneously counting epidermal cells and stomata from microscopic images of plant epidermis.

So far, many image processing-based stomata analysis tools have been proposed for a diversity of plant species. For tomato, Sanyal et al. (2008) isolated the stomata using a watershed algorithm, eliminated noise using morphological operations, and extracted the stomatal edges using the Sobel operator to measure the morphological features of the stomata (e.g., area, center of gravity, and compactness). As an edge-based method, its performance is insufficient when the edge of the stoma is discontinuous or has considerable noise. Laga et al. (2014) proposed a fully automatic tool for phenotyping the length and width of stomata openings and the size of guard cells in wheat. But this tool relied on a template-matching technique to detect stomata, which reduced its versatility in the presence of considerable variability in the stomata shapes. Another automatic method for stomata detection and counting used morphological operations (Da Silva Oliveira et al., 2014). This method required relatively high image quality and was not robust to images containing impurities. These disadvantages of image processing-based methods have led to the adoption of more advanced computer vision techniques. Recently, deep learning techniques, especially convolutional neural networks (CNNs), have emerged as powerful methods for automatically training the feature detector with the classifier. They made remarkable achievements in a range of object detection tasks. Stomata recognition is not an exception. General one-stage object detection algorithms, single shot multiBox detector (SSD, Sakoda et al., 2019) and you only look once (YOLO, Casado-García et al., 2020), and two-stage object detection algorithm, real-time object detection with Faster R-CNN (Li et al., 2019) and mask region-based CNN (Mask R-CNN, Bheemanahalli et al., 2021) built accurate stomata detection models for many plant species such as rice, soybean, wheat, barley, or sorghum. This study selected the Faster R-CNN for detecting and counting stomata by considering the speed-accuracy trade-off of the model.

Identifying and counting epidermal cells in leaf images are vital for developing the stomatal index measurement algorithm. Unlike stomata with fixed shapes and distinct morphological features, epidermal cells exhibit great diversities in size, shape, and clustering in different plant species. The epidermal cells of the wheat leaf are long, thin, transparent, and tightly touching with one another. Although we attempted multiple generic object detection algorithms, none of them achieved satisfying performance in recognizing epidermal cells. U-Net, a deep-learning model designed for frequently occurring quantification tasks such as cell detection and semantic segmentation in biomedical image data (Ronneberger et al., 2015), may be a suitable solution. Modified and extended from a fully convolutional network (FCN), U-Net used excessive elastic deformations for data augmentation and trained on a diverse set of data, allowing adaption to new tasks with a small number of annotated images. Recently, some animal cell segmentation studies, such as bladder cancer cell segmentation in phase-contrast microscopy images (Hu et al., 2019) and nuclei segmentation (Zeng et al., 2019) were based on the U-Net structure. Some studies of smart farming showed promising performance using U-Net, such as segmentation of cucumber leaf disease (Lin et al., 2019) and field study of wheat yellow rust monitoring (Su et al., 2020). A weight loss in U-Net was designed for isolating background labels between touching cells, which is suitable for the detection task of epidermal cells. Unfortunately, there is currently no example of applying U-Net to plant cell segmentation to the best of our knowledge.

In this study, we developed an automatic image analysis pipeline to assess the stomatal index from microscopic images of the leaf epidermis. Faster R-CNN was deployed to count the stomata number. U-Net was utilized to extract the epidermal cell network. After a series of morphological image post-processing, the number of epidermal cells was calculated by counting the number of connected domains from the epidermal cell network. Finally, the stomatal index of the current microscopic image was calculated by dividing the stomata number by the total number of stomata and epidermal cells.

MATERIALS AND METHODS

Image Acquisition

Wheat Dataset

A total of 1,000 microscopic images was collected from the leaf abaxial epidermis of fully expanded leaves derived from 100 wheat varieties (*Triticum aestivum* L., **Supplementary Table 1**). Seedlings were grown in a growth chamber at 14°C with 16 h of light and 8 h of darkness. At the two-leaf stage, the fully expanded second leaves were cut from the plants. We stuck the abaxial surface of the collected wheat leaves on tapes and scraped off the epidermis and mesophyll cells at the adaxial surface of the leaves with a sharp scalpel, leaving only the colorless and transparent abaxial epidermal cells attached to the tape. The tape with intact and clean abaxial epidermal cells and stomata was stuck onto a clean slide and then imaged the leaf areas on either side of the primary veins at ×10 magnification using the Olympus DP72 microscope camera (**Figure 1A**). Five micrographs were taken for each specimen, and a total of 15 micrographs were collected for three specimens of each variety. They were stored in JPEG format with a resolution of 1,360 × 1,024 (**Figure 1B**). A total of 500 images, were randomly selected and cropped to 680 × 512 and reshaped to 1,360 × 1,024 using cubic interpolation to obtain 500 images at × 20 magnification. In the end, 500 images at × 20 magnification and the remaining 500 images at × 10 magnification were combined as the wheat dataset for this study.

Cuticle Dataset

To verify whether the pipeline can be applied to other species, 156 microscopic images of plant cuticles derived from 31 plant families (**Supplementary Table 2**) were downloaded from the cuticle database (https://cuticledb.eesi.psu.edu/, Barclay et al., 2007). As shown in **Supplementary Figure 1**, the morphologies of stomata and epidermal cells of these 31 plant families are pretty diverse. These micrographs were obtained *via* imaging the specimens of stained leaf tissues (Barclay et al., 2007; Fetter et al., 2019).

Automatic Pipeline for Stomatal Index Measurement

We developed a fully automatic solution for stomatal index measurement that mainly consisted of two parts, namely, stomata and epidermal cell counting (**Figure 2**). The details are described as follows: At first, the microscopic images of crop leaves were annotated and augmented to build the dataset. The Faster R-CNN was used to identify the stomata and counting in a given microscopic image. The U-Net was employed to segment the epidermal cells as connected domains. Several image-processing techniques were applied to refine the segmentation results of U-Net based on cell morphological features of epidermal cells. The number of epidermal cells in a given microscopic image was measured by counting the number of high-quality connected domains. Subsidiary cells associated with the guard cells were present in wheat and many (but not all) plant families of the cuticle dataset (**Figure 1B** and **Supplementary Figure 1**). It should be noted that they were not counted as epidermal cells in the study. Finally, the stomatal index was calculated by the following formula.

$$stomatal\ index = \frac{stomata\ number}{(stomata\ number\ +\ epidermal\ cell\ number)} \times 100\% \quad (1)$$

Image Annotation

Stomata in the 1,000 microscopic images were manually annotated by three experts using the Colabeler (AI labeling tool, http://www.colabeler.com). For each annotated image, an additional extensible markup language (XML) file with the same name as the original image file was exported in Pascal VOC format of object detection (Everingham et al., 2010). Each stoma was marked by the smallest circumscribed rectangle $\{x_{min}, y_{min}, x_{max}, y_{max}\}$ to determine its relative position on the image. All the complete stomata or stomata with more than half of the length at the edge of the image were marked. For epidermal cell annotation, we utilized the semi-automatic strategy considering a large number of epidermal cells in each microscopic image. There were two types of annotations for each epidermal cell segmentation experiment: black and white. We used black (RGB: 0, 0, 0) to label the cell wall or leaf vein and white (RGB: 255, 255, 255) to label the intracellular regions. In addition, we ignored trichomes by marking them as white to eliminate their interferences for epidermal cell segmentation. Subsidiary cells were labeled in black since they were not counted as epidermal cells (**Figure 3A**). Usually, it is very time-consuming and laborious to obtain the ground truth of the semantic segmentation task. A semiautomatic annotation method was used to improve the efficiency of cellular annotation. The whole annotation process was shown in **Figure 3B**. In brief, 210 images were grayscaled, binarized, and manually annotated using Microsoft Paint 3D for Windows. These annotated images trained the U-Net with image augmentation for 200 epochs to obtain an initial segmentation model (Model_1). The remaining 790 images in the dataset were fitted into Model_1 to generate corresponding pseudo labels. After manual modification to the ground truths, all the 1,000 microscopic images were annotated. The proposed semiautomatic annotation method was much more efficient than the manual method. It took about 10 min to generate an annotation with manual correction, while fully manual annotation cost about 1 h per image.

Deep Learning-Based Algorithms

Stomata Detection by Faster R-CNN

ResNet101 (He et al., 2016) was implemented as the backbone of Faster R-CNN to extract feature maps. In this network, the region proposal network (RPN) was used to scan the backbone feature map, which effectively reused the extracted features and avoided repeated calculation of region of interest (ROI). The region proposal generated by RPN was combined with the feature map obtained in the last layer of Resnet101 to generate a fixed size proposal feature map using ROIPooling, and prepare for

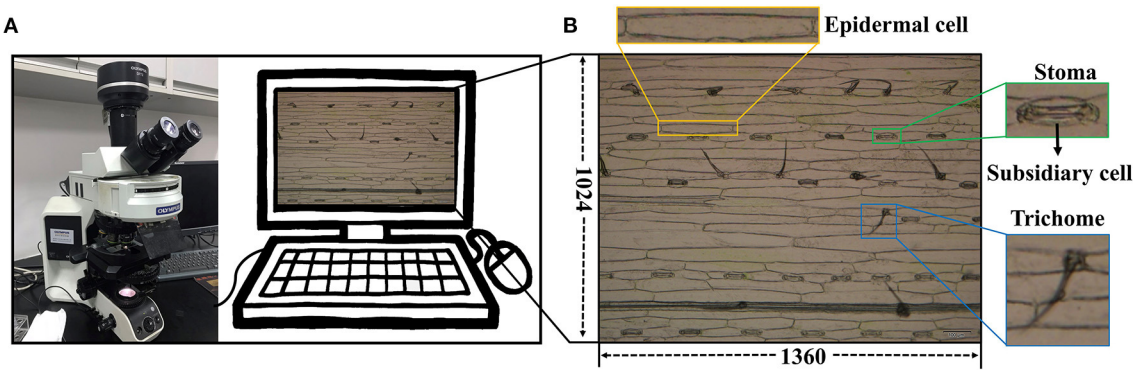

FIGURE 1 | Data collection platform. **(A)** Olympus DP72 industrial microscope. **(B)** Microscope image of wheat leaf epidermis.

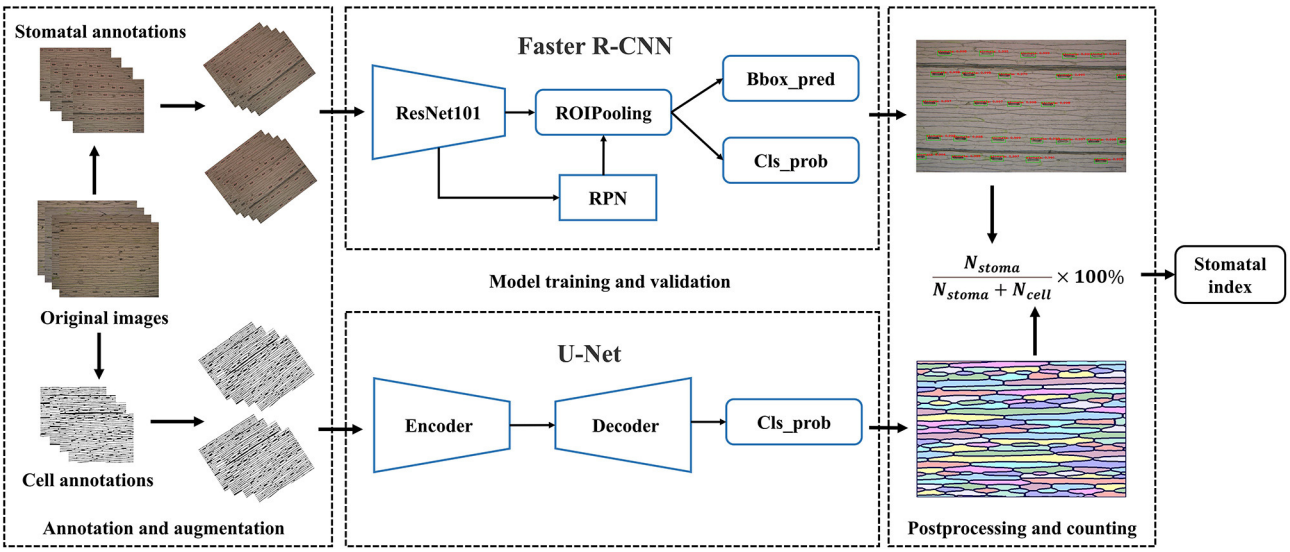

FIGURE 2 | A flow chart of the proposed pipeline of the stomatal index measurement.

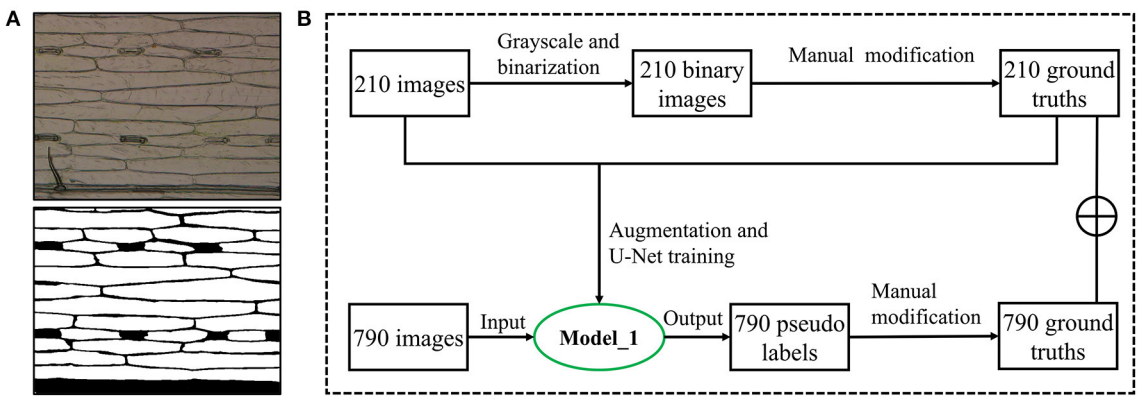

FIGURE 3 | Epidermal cell annotation. **(A)** Original image of wheat leaf epidermis microscope (upper) and its annotation image (lower). **(B)** Semiautomatic annotation process using an initial segmentation model (Model_1).

the following full connection operation target classification and location regression. After that, softmax was used for object classification. In addition, the smooth L1 loss was adopted to complete the bounding box (bbox) regression operation and obtain the exact position of the object. The loss function is as follows:

$$L\left(\{p_i\},\{t_i\}\right)=\frac{1}{N_{cls}}\sum_i L_{cls}\left(p_i,p_i^*\right)+\lambda\frac{1}{N_{reg}}\sum_i p_i^* L_{reg}\left(t_i,t_i^*\right) \quad (2)$$

$$smooth_{L1}(x)=\begin{cases}0.5x^2 & if\ |x|<1\\ |x|-0.5 & otherwise\end{cases} \quad (3)$$

where L_{cls} is the Softmax Loss, $L_{reg}\left(t_i,t_i^*\right)=smooth_{L1}(t_i-t_i^*)$ defined in Formula (3) and λ =10.

We trained the Faster R-CNN model with a specific configuration. The general idea is to use mini-batch gradient descent. The batch size was set to 16, and the input image size was adjusted to 800 × 600, considering the limited graphics processing unit (GPU) memory. The initial learning rate was 0.0005 and attenuated to 0.00005 during 20 epochs using the cosine annealing algorithm (Loshchilov and Hutter, 2016). Considering the relatively small proportion of stomata in the image, we set the anchor scale to 4, 8, 16, and anchor ratios to 0.5, 1, and 2. The loss weight of the RPN class, RPN bbox, Faster R-CNN class, and Faster R-CNN bbox were the same. Details of other parameters can be obtained from the literature (Ren et al., 2015). The backbone of the Faster R-CNN was initialized by the ResNet101 pretrained model of ImageNet (Deng et al., 2009), and the other parts were initialized randomly by a normal distribution.

Epidermal Cell Segmentation by U-Net

We applied the U-Net, a semantic segmentation network specially designed for biomedical images (Ronneberger et al., 2015), for segmenting leaf epidermal cells. Since semantic segmentation belongs to the classification of each pixel, it is very sensitive to light. To better extract, the cellular network, each channel of the training image was standardized before training using formula (4). The resolution of the image was adjusted to 512 × 512 for training the U-Net model, which is a compromise between obtaining as many image details as possible and GPU memory limit.

$$\hat{I}=\frac{I-\mu}{adjusted\_stddev},\ adjusted\_stddev=max(\sigma,\frac{1.0}{\sqrt{N}}) \quad (4)$$

where μ is the mean value of all image pixels in the dataset, I is an image matrix, σ is the SD of all image pixels in the dataset, and N is the number of pixels in I, $\hat{I}$ is the standardized image matrix.

Parameters for the training model were as follows: the initial learning rate was 0.0001 (Smith, 2017); it was decayed to 0.00001 by the cosine annealing algorithm (Loshchilov and Hutter, 2016) during 200 epochs; the batch size was set as 8. Kaiming initialization method (He et al., 2015) was used for the initialization of the weights. The loss function was binary cross-entropy, as shown in Formula (5).

$$H_p\left(q\right)=-\frac{1}{N}\sum_{i=1}^{N} y_i\cdot\log(p\left(y_i\right))+(1-y_i)\cdot\log(1-p(y_i)) \quad (5)$$

Stomatal Index Measurement

Both the Faster R-CNN-based stomata detection algorithm and U-Net-based epidermal cell segmentation algorithm did not export the number of stomata and epidermal cells. Before measuring the stomatal index in each microscopic image, we need to count stomata and epidermal cells. The stomata detection model returned a series of five-dimensional vectors for each microscope image, given by {score,xmin,ymin,xmax,ymax}. The score in the vector represents the confidence of each bbox, and the following four parameters represent the position of the bbox on the image. To avoid counting low-probability stomata within the noise, the bbox with a score >0.9 was counted as a stoma.

Epidermal cell segmentation by U-Net generated a corresponding cell network image for each leaf microscopic image. We regarded each connected domain as an epidermal cell and counted the number of connected domains in each image as the epidermal cell number. Before counting, bilateral filtering (Tomasi and Manduchi, 1998) was used to remove noise from the prediction, binarization, and morphological opening operations (first erosion and then dilation) were performed to connect breaks of some cell walls. The incomplete connected domains were filtered out if their pixel numbers were <1/10 of the average pixel number of all connected domains in the image. In the end, the stomatal index of each microscopic image was calculated as the ratio of stomata number to the total number of stomata and epidermal cells, as shown in the Formula (1).

Performance Evaluations

We evaluated the performance of the stomata detection algorithm using average precision (AP), which is defined as the area under an interpolated precision-recall curve. The AP was computed as follows:

$$AP=\int_0^1 P(R)dR \quad (6)$$

where precision is $P=\frac{N_{TP}}{N_{TP}+N_{FP}}$ and recall is $R=\frac{N_{TP}}{N_{TP}+N_{FN}}$. N_{TP} is the true positive, N_{TN} is the true negative, N_{FP} is the false positive, and N_{FN} is the false negative.

The performance of the epidermal cell segmentation algorithm was assessed using the Dice Coefficient (DC) (Formula 7), which compares the overlap rate of segmentation results of the models with the manual annotation.

$$Dice\ coefficient=\frac{2N_{TP}}{2N_{TP}+N_{FP}+N_{FN}} \quad (7)$$

where N_{TP}, N_{FP}, and N_{FN} represent the true positives, false positives, and false negatives of pixel numbers, respectively.

As shown in Formula 8, counting accuracy was defined to evaluate the stomata and epidermal cell counting pipeline performance. We assumed the manual counts by experts containing true positives and the automatic counts by the image analysis pipeline containing true positives and false positives. Therefore, counting error could be obtained by subtracting the automatic results from the manual results, and the counting accuracies for stomata and epidermal cells were defined as:

$$Counting\ accurary = 1 - \frac{abs(Automatic\ Count - Manual\ Count)}{Manual\ Count} \quad (8)$$

To detect the overcounting and undercounting errors, we defined counting precision as:

$$Counting\ precision = log(\frac{Manual\ Count}{Automatic\ Count}) \quad (9)$$

The negative values of counting precision indicated the overcounting errors, and the positive values indicated undercounting errors. The counting precision was undefined when the manual count or the automatic count is zero. Simple linear regression was also applied to explore the relationship between manual and automated counting of stomata and epidermal cells.

To explore the accuracy and precision of stomatal index measurement, we calculated the stomatal index using the manual results of stomata and epidermal cells and their automatic results. Equations were defined as:

$$Stomatal\ index\ accuracy\ = \quad (10)$$
$$1 - \frac{abs(Automatic\ result - Manual\ result)}{Manual\ result}$$

$$Stomatal\ index\ precision = log(\frac{Manual\ result}{Automatic\ result}) \quad (11)$$

We assessed the measurement speed of the stomatal index on the central processing unit (CPU) and GPU (1080Ti) by calculating the average running time (ART) for each image. The measurement time of the stomatal index is equal to the sum of stomata counting time and cell counting time.

$$ART = \frac{T_{N\_stoma} + T_{N\_cell} + T_{N\_SI}}{N} \quad (12)$$

where N represents the number of images, T_{N_stoma}, T_{N_cell}, and T_{N_SI} represent the total running time for counting stomata and cells and stomatal index formula calculation for N images, respectively.

Statistical Analysis

R version 3.6 (R Core Team, 2020) was used to perform simple linear regressions ($y = x$) for assessing the linear relationship between manual counting by experts and automatic counting by the proposed pipeline. The equations of coefficient of determination (R^2) and root mean square error (RMSE) for the simple linear regression are as follows:

$$R^2 = 1 - \frac{\sum_i (x_i - y_i)^2}{\sum_i (x_i - \bar{y})^2} \quad (13)$$

$$RMSE = \sqrt{\frac{\sum_i (x_i - y_i)^2}{N}} \quad (14)$$

where N represents the total number of measurements; x_i is the manual counting; y_i is the automatic counting, and $\bar{y}$ is the mean.

Code and Data Availability

The detection and segmentation models were all developed using the PyTorch software library (Facebook Artificial Intelligence Research Institute, FAIR), which is an open-source Python deep learning library. The code is fully open-source for academic usage and can be downloaded at https://github.com/WeizhenLiuBioinform/stomatal_index. The wheat dataset is available for downloading at https://github.com/WeizhenLiuBioinform/stomatal_index/releases/download/wheat1.0/wheat_dataset.zip.

RESULTS AND DISCUSSION

The hardware for training the proposed stomatal index measurement pipeline is a GPU server equipped with an Intel Xeon(R) E5-2650 CPU and four GeForce GTX 1080Ti GPUs with 11G memory, but only two of the four GPUs were used. The pipeline was implemented using the PyTorch framework running on the CentOS 7.7 operating system.

Stomata Detection

The Faster R-CNN-based stomata detection model was set up with the initial learning rate of 0.0005 and the batch size of 16. It was trained over 20 epochs. To evaluate the stability and reliability of the model, we conducted five-fold cross-validation that shifted the training and test sets for each fold. The 1,000 microscopic images of leaf epidermis were randomly divided into five mutually exclusive subsets. One subset was used as the validation set (200 images), and the other four were used as the training set (800 images). Offline data augmentation was performed to expand each subset by applying rotations of 45, 90, and 135°, respectively, to each image and keeping the original images. By these geometric transformations, 4,000 images were obtained that can be used to enhance the robustness of the model to different stomata angles.

The stomata detection results of the proposed model were quite satisfactory, which achieved a mean validation AP of 0.997 across the five-fold cross-validation with an SD = 0.000521. The evolutionary curves of the AP and loss over 20 epochs are shown in **Figure 4**. An "epoch" was defined as the process of training the model once using all of the images in the training set. In this study, we took the prediction bbox with the intersection over union (IoU) of ground truth >0.6 as the true positive. The curves showed a good learning ability since the loss of

training sets decreased rapidly in the first two epochs and reached a small value of 0.12 after five epochs. The AP of validation sets rose rapidly that reached 0.975 after the first epoch. It had satisfactory convergence after 10 epochs until finally reaching its optimal prediction performance. The fast convergence is also due to adopting the ResNet101 pretraining weight on ImageNet to initialize the feature extraction network. All the AP curves of the five-fold cross-validation were close to each other with small fluctuations before the first 10 epochs, illustrating the high stability and reliability of the model for stomata detection.

An example of the stomata detection result conducted was present in **Figure 5**. The Faster R-CNN-based model generated 112 proposal bboxes (**Figure 5A**). After applying the filtration with a confidence threshold value of 0.9, all 32 stomata on the leaf epidermal image were accurately detected (**Figure 5B**).

Epidermal Cell Segmentation

The UNet-based epidermal cell segmentation model was set up with a batch size of 8 and an initial learning rate of 0.0001. Unlike the Faster R-CNN-based stomata detection model, it was trained over 200 epochs, since it decayed to 0.00001 by the cosine annealing algorithm until 200 epochs. We also performed the five-fold cross-validation using the same 1,000 microscopic images as stomata detection. Online augmentation was used to enlarge the image dataset. This augmentation focuses on "batches," which refers to various transformations of images during training to increase the diversity of image samples. The number of iterations can be increased to ensure that the number of images for training increases. In this study, in each batch, before the data being fed into U-Net, online data augmentation was performed to transform images and the corresponding ground truths by applying affine transformation with a probability of 0.2 and rotating 90° with a probability of 0.5.

The epidermal cell segmentation of the proposed model achieved the mean DC of 0.978 with SD = 0.00121 across the five-fold cross-validation that demonstrates segmentation performances of the models which are reliable and stable. As shown in **Figure 6**, the U-Net model started to converge after 100 epochs. Although the loss of the training sets fluctuated, the DC stabilized above 0.97 after 150 epochs and finally reached its optimal performance over 200 epochs. During the whole convergence, the DC fluctuated upward, while the loss continued in a fluctuational decline, indicating that the models were continuously learning rather than being trapped in a local optimal.

For epidermal cell segmentation, the U-Net-based model predicted the epidermal cell network (**Figure 7**). Comparing to the ground truth (**Figure 7A**), the predicted cell network (**Figure 7B**) had several breakpoints in some cell walls, which affected the cell counting accuracy because the connected domain method was used for counting. To connect these breakpoints, a series of image-processing techniques were utilized, including bilateral filtering, binarization, and morphological opening operation (**Figures 7C,D**). Considering the incomplete cells present in the image, before cell counting, the small connected domains were filtered out whose areas were <1/10 of the mean area of connected domains. In **Figures 7E,F**, after this area filtering, 39 connected domains remained as the epidermal cells, while six small connected domains at the edge (filled with red) were not counted.

Performance Evaluations of Stomatal Index Measurement

Accuracy and Precision

We counted the number of stomata and epidermal cells for all the microscopic images over the five-fold cross-validation using the proposed Faster-RCNN and U-Net-based models, respectively. For each fold, their counting accuracies were estimated and summarized in **Table 1**. Both models had good counting accuracy, ranging from 97.577 to 98.451% for stomata and 94.584 to 95.330% for epidermal cells. The epidermal cell model had slightly lower counting accuracy than the stomata model. This result was easily understood because morphological features of epidermal cells were less distinct from the background than stomata, making accurately count the numbers of epidermal cells more challenging. Since the high-counting accuracies and precisions of stomata and epidermal cells, as expected, the stomatal index, which is the ratio of stomata number over the total numbers of stomata and epidermal cells, also achieved a high accuracy of 95.35%.

To further evaluate the differences between results of automatic counting by the proposed pipeline and ground truths, the numbers of stomata and epidermal cells were counted manually for all the 1,000 microscopic images in the dataset. Regression analysis was performed between the manual and automatic counting (**Figure 8**). R^2 for stomata, epidermal cells, and stomatal indices were 0.995, 0.983, and 0.895, respectively, and the RMSE values were 0.821, 6.460, and 1.099, respectively. These results verified strong correlations between manual and automatic counting results. Counting and measurement precisions were also estimated to detect the overcounting (negative values) and undercounting (positive values) errors. As the distributions shown in **Table 2**, the means of counting precisions for stomata and epidermal cells, and stomatal index were very close to 0 (−0.009, 0.019, and −0.016, respectively) with SD = 0.024, 0.027, and 0.023, respectively. Overall, automatic counting results in most of the microscopic images were identical to manual counting results, illustrating the high precision of the proposed pipeline. To be more specific, the Faster R-CNN-based stomata counting algorithm was a little bit more likely to overcounting, while the U-Net-based epidermal cell counting algorithm was more likely to undercounting. The stomatal index using the proposed pipeline was prone to be slightly overestimated.

Average Running Time

We estimated the speed of the proposed automatic analysis pipeline for stomatal index measurement using the 1,080 Ti GPU and CPU. The ART of the pipeline mainly came from the counting time for stomata and epidermal cells and the calculation time of the stomatal index (Formula 1). From inputting the microscopic image to outputting the stomatal index value, the ART per image was only 0.32 s using the GPU *via* the matrix acceleration calculation but 7.49 s on the CPU. Specifically, the

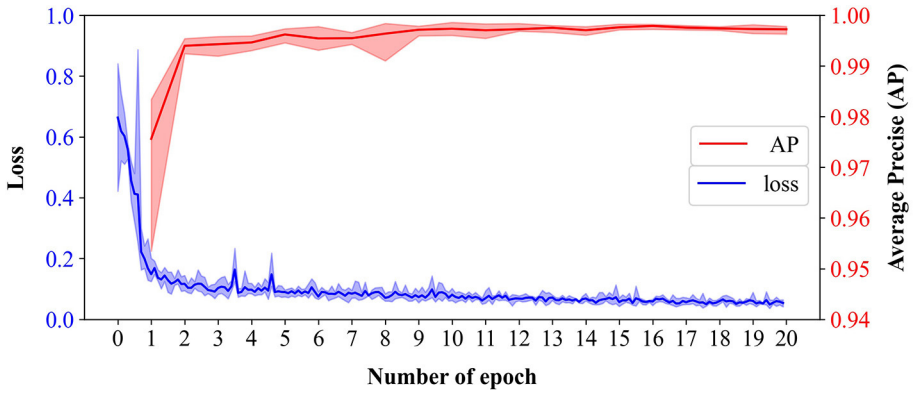

FIGURE 4 | The evolutionary curves of loss of training sets and average precision (AP) of validation sets of the Faster R-CNN-based model across 20 epochs from five-fold cross-validation. Bold lines represent the mean of loss (blue) and AP (red), and the translucent bands represent the range of loss and AP across five-fold.

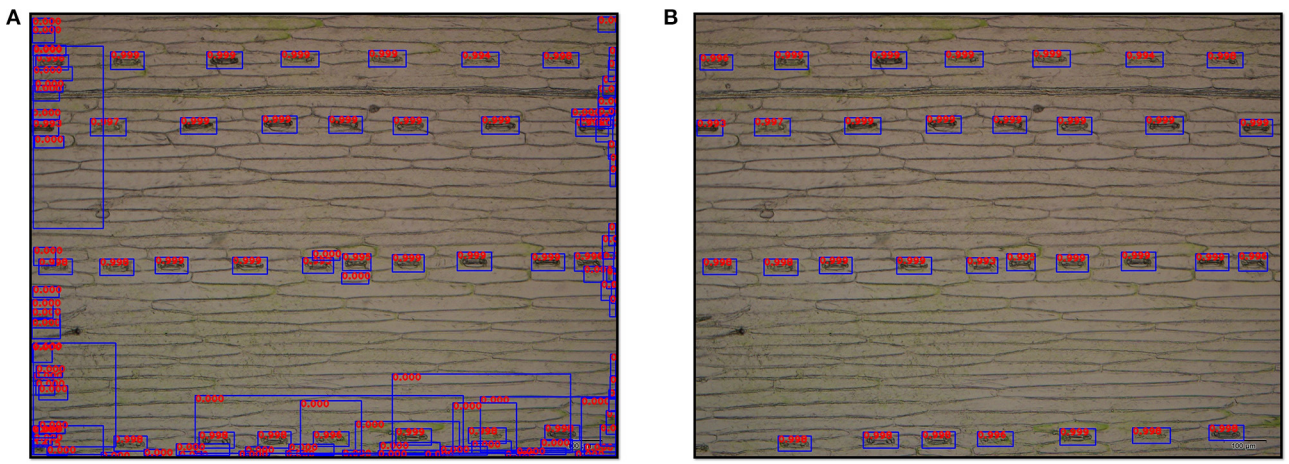

FIGURE 5 | Output images of stomata detection results by the Faster R-CNN-based model at ×10 magnification. **(A)** Original detection result with all proposal bboxes (112 bboxes), and the number on the bbox represents its detection score. **(B)** Detection result after filtering (32 stomata).

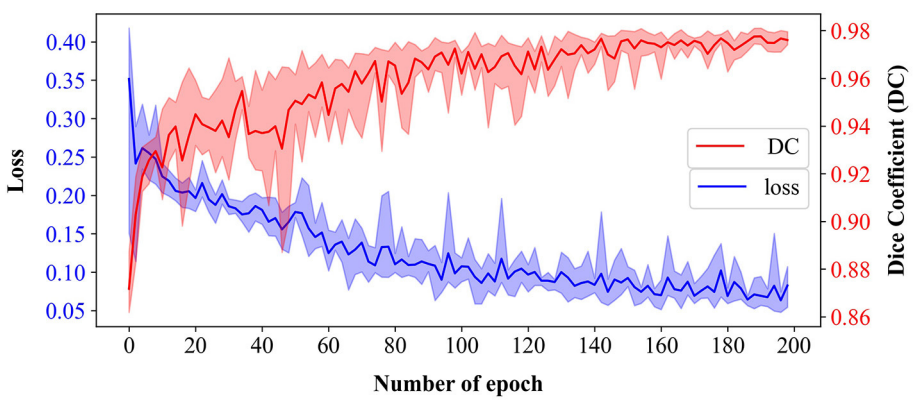

FIGURE 6 | Training loss and validation dice coefficient (DC) of U-Net-based model over 200 epochs from five-fold cross-validation. Bold lines represent the mean of loss (blue) and DC (red), and the translucent bands represent the range of loss and DC across five-fold.

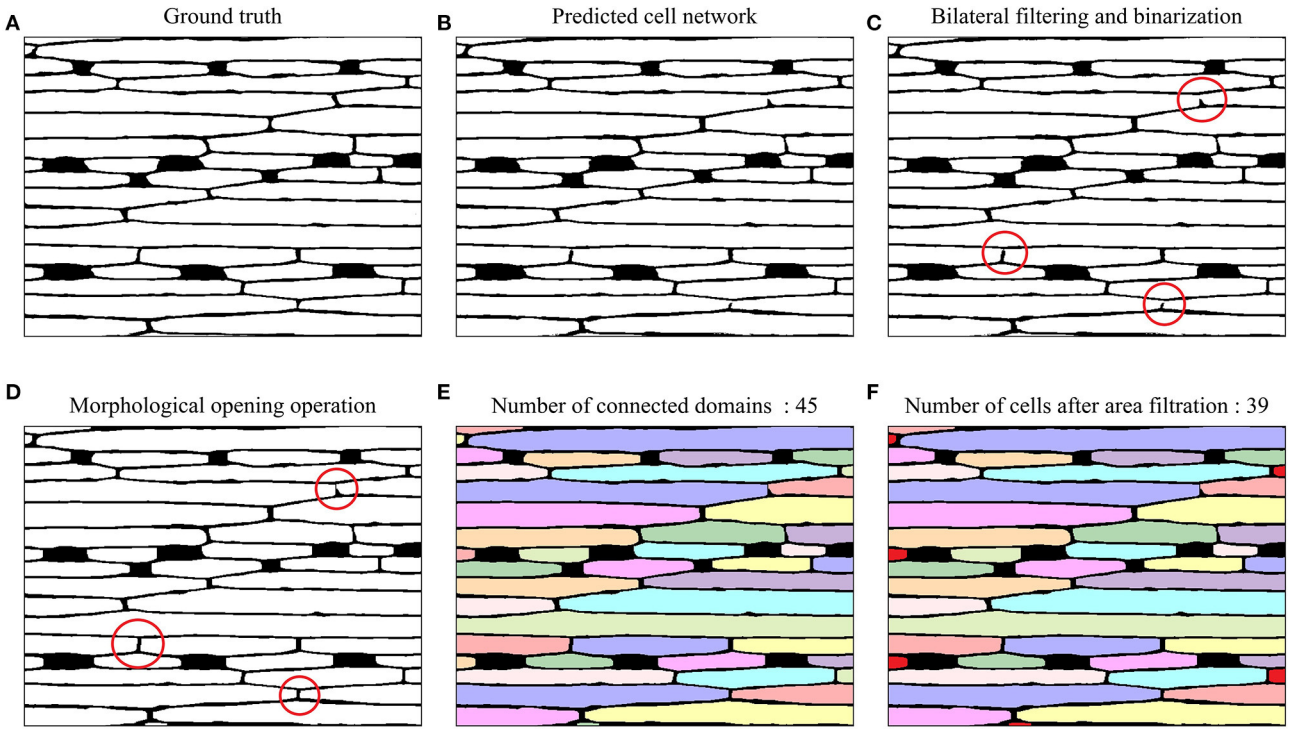

FIGURE 7 | Example images of epidermal cell segmentation by the U-Net-based model and morphological post-processing on a 20× magnified microscope image of the wheat leaf. **(A)** Ground truth. **(B)** Epidermal cell network predicted by U-Net. **(C)** Bilateral filtering and binarization; Red circles highlighted the breakpoints in the cell network. **(D)** Morphological opening operation; red circles highlighted connected breakpoints in the cell network after the morphological opening operation. **(E)** Connected domains with different colors (45 connected domains). **(F)** Epidermal cell counting after area filtering (39 epidermal cells). The six small connected domains that were filtered out were marked with red color.

TABLE 1 | The counting accuracies of stomata and epidermal cells over 5-fold cross-validation.

Trait	Accuracy (%)					
	Fold_1	Fold_2	Fold_3	Fold_4	Fold_5	Mean
Stomata	97.675	98.058	97.577	98.451	98.397	98.031
Epidermal cell	94.584	95.106	95.33	94.977	95.168	95.033

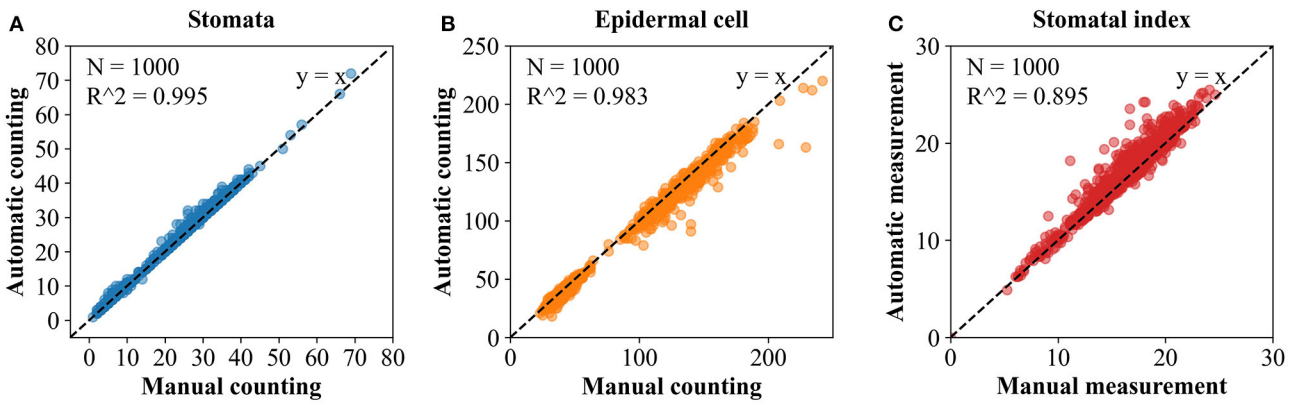

FIGURE 8 | Simple linear regression between the manual and automatic measurement. **(A)** Stomata. **(B)** Epidermal cell. **(C)** Stomatal index.

TABLE 2 | The precisions of stomata and epidermal cell counting and stomatal index measurement in 1,000 microscopical images of the wheat dataset.

Trait	Precision			
	Min	Max	Mean	SD
Stomata	−0.204	0.067	−0.009	0.024
Epidermal cell	−0.056	0.250	0.019	0.027
Stomatal index	−0.214	0.097	−0.016	0.023

ART for the stomata counting was 0.15 and 5.96 s using GPU and CPU, respectively. As the ART for the stomata counting part was comprised by the time of inference of Faster R-CNN-based stomata detection model and non-maximum suppression (NMS) of bboxes, the large difference of ART using GPU and CPU came mainly from the NMS process. For the epidermal cell counting, the ART, including the time of inference of the cell segmentation model and the morphological postprocessing time, was 0.17 and 1.53 s using the GPU and CPU, respectively. The speed difference came from the inference of the U-Net-based-segmentation model running on the different hardware because the post-processing procedures could only be run on the CPU. Overall, the proposed automatic pipeline for stomatal index measurement had an excellent running efficiency.

Stomatal Index Values at Different Magnifications

Using the proposed pipeline, we explored the measurement results of stomata number, epidermal cell number, and stomatal index of wheat leaf epidermal at × 10 and × 20 magnifications (**Table 3**). A total of 50 brand new images that were not used to train the pipeline at ×10 magnification were selected and used to generate 50 images at × 20 magnification by cropping and reshaping. The mean numbers of stomata and epidermal cells at × 10 magnification were 27.16 and 133.82, which were more than four times compared with those at × 20 magnification. More importantly, the means of the stomatal indices at × 10 and × 20 magnifications were 16.76 and 13.70, which were significantly different from each other (pairwise T-test: $t = 5.752$, $df = 49$, and $P = 5.623\text{E-}7$). The same trend was also observed in the 1,000 images (500 images at × 10 and × 20 magnifications, respectively) previously used for training the pipeline (**Supplementary Table 3**). This systematic difference hints that the larger field of view, the higher the stomatal index value from the same leaf. When comparing values of the stomatal index among different samples or genotypes, we should make sure they are at the same magnification.

Comparison Between Stomatal Index and Stomatal Density

The stomatal index and stomatal density of two wheat varieties were assessed (Gharflor-1611 and Ningmai9) using the proposed pipeline. Stomatal density was defined as the number of stomata divided by the area of the field of view. Five micrographics at ×10 magnification were sampled for each variety, and the field of view of each image is 1.428 mm^2. As expected, a smaller coefficient of variation was obtained for the stomatal index than the stomatal density in two wheat cultivars (**Table 4**). It illustrates that the stomatal indices were more constant than stomatal densities within a cultivar. Moreover, Pearson's correlation coefficients between stomatal density and stomatal index were high, which are 0.878 and 0.926 for Gharflor-1611 and Ningmai9, respectively.

Applications on Other Plant Families

How well the proposed pipeline can be applied to other plant families is an interesting point worth studying. The cuticle dataset with 156 micrographs collected from 31 plant families (**Supplementary Table 2**) was used. Considering the morphological differences of stomata and epidermal cells between the wheat (**Figure 1**) and the cuticle dataset (**Supplementary Figure 1**), transfer learning was employed that the Faster RCNN and U-Net were initialized using the model parameters in the wheat dataset and all parts of the models were then finetuned by the training set of the cuticle dataset. In this way, an excellent model can be trained using a small amount of data (Zhuang et al., 2020). To avoid the possible overfitting of the model parameters to the wheat dataset, the intermediate checkpoints were selected (the 10th epoch of Faster RCNN and the 100th epoch of U-Net) in the training process of the wheat dataset as the pretraining model and finetuned the model with a smaller initial learning rate (0.0001 for Faster RCNN and 0.00005 for U-Net). A total of 105 images in the cuticle dataset were used as the training set and 51 images as the testing set (**Supplementary Table 2**). After 20 epochs for Faster RCNN and 100 epochs for U-Net, the models reached convergences.

The finetuned pipeline achieved good counting accuracies and precisions for stomata and epidermal cells on the testing set derived from seven plant families (**Table 5** and **Figure 9**). The average counting accuracies of all families were 94.355% for stomata and 91.127% for epidermal cells, and the stomatal index accuracy reached 89.384%. The counting precisions for stomata, epidermal cells, and stomatal index were very close to 0 (0.006, −0.02, and 0.023, respectively). In five of seven families, the Faster RCNN-based stomata counting model achieved better performance than the U-Net-based epidermal cell counting model. The same situation was observed in the wheat dataset. In the Araceae family, all the stomata were accurately predicted, and the counting accuracy of epidermal cells reached 93.895%. Therefore, the stomatal index accuracy (94.63%) was the highest in all the families. The Euphorbiaceae family obtained the lowest counting accuracy of the stomatal index (82.68%) due to the relatively low-counting accuracy of epidermal cells.

Regression analysis on the cuticle test set was performed between the manual and automatic counting

TABLE 3 | Summary of average numbers of stomata and epidermal cells and the stomatal index trait in 50 epidermis images at × 10 and × 20 magnifications, respectively.

Magnification	Stomata			Epidermal cell			Stomatal index (%)		
	Min	Max	Mean	Min	Max	Mean	Min	Max	Mean
10x	14	53	27.16	83	209	133.82	10.83	20.99	16.76
20x	0	17	6.44	24	60	38.66	0	24.29	13.70

TABLE 4 | Summary of the stomatal index and stomatal density characters of two wheat varieties.

Cultivar	Stomatal density (pores|mm^2)			Stomatal index (%)			Correlation coefficient
	Range	Mean	CV	Range	Mean	CV	
Gharflor-1611	17.503–26.605	21.704	0.134	16.779–19.388	17.922	0.051	0.878
Ningmai9	2.800–9.802	7.000	0.329	3.810–9.910	8.066	0.271	0.926

CV, coefficient of variation; correlation coefficient of each cultivar was calculated using stomatal density values and stomatal index values of five micrographs.

TABLE 5 | Summary of performance evaluations of the proposed pipeline on the cuticle dataset.

Plant family	N_{image}	Stomata				Epidermal cell				Stomatal index			
		CA (%)	CP	R^2	RMSE	CA (%)	CP	R^2	RMSE	SIA(%)	SIP	R^2	RMSE
Annonaceae	6	92.59	0.034	0.89	2.68	94.58	0.02	0.97	10.71	90.11	0.046	0.71	1.9
Apocynaceae	7	92.49	−0.001	0.96	1.41	90.65	−0.001	0.94	12.83	85.55	−0.0002	0.65	2.56
Araceae	5	100	0	1	0	93.9	−0.02	0.96	9.45	94.63	0.019	0.95	0.43
Euphorbiaceae	7	93.36	0.032	0.98	1	82.35	−0.064	0.58	18.81	82.68	0.084	0.43	2.61
Fabaceae	7	91.19	−0.017	0.88	1.46	95.18	0.002	0.98	5.2	89.22	−0.067	0.96	1.12
Lauraceae	13	94.85	−0.0003	0.98	1.98	91.46	−0.001	0.97	19.72	92.19	0.008	0.91	0.92
Sapindaceae	6	97.37	0.012	0.98	0.91	90.72	−0.027	0.71	16.98	90.68	0.034	0.67	1.42
All	51	94.36	0.006	0.98	1.63	91.13	−0.02	0.97	15.17	89.38	0.023	0.84	1.7

N_{image}, the number of microscopic images used for individual plant family; CA, counting accuracy; CP, counting precision; SIA, stomatal index accuracy; SIP, stomatal index precision; R^2 and RMSE were obtained from the simple linear regression ($y = x$) between manual counting by experts and automatic counting.

(**Table 5** and **Supplementary Figure 2**). R^2 for stomata, epidermal cells, and the stomatal index was 0.976, 0.967, and 0.841, respectively, and the RMSE values were 1.627, 15.17, and 1.704, respectively, indicating that the proposed pipeline also showed excellent performances in many other species besides wheat.

CONCLUSIONS AND FUTURE WORK

In this study, an automatic deep learning-based method was proposed for measuring stomatal index, taking microscope images of wheat leaves as the input. The proposed method consisted of three parts that were the Faster R-CNN target detection algorithm for detecting and counting the stomata; the U-Net semantic segmentation network for extracting the epidermal cell network and measuring the number of connected domains as the number of epidermal cells; and subsequently calculated stomatal index of each image using the previous counting results. Satisfactory accuracies were obtained for stomata detection and counting, cell segmentation and counting, and stomatal index measurements. High correlations were observed between manual and automatic methods. In addition, the proposed image analysis pipeline was quite fast. Using the GPU (1080Ti), it took only 0.32 s to estimate the stomatal index of an image. It should be noticed that a possible difference in the stomatal index could be identified from the same leaf at different magnifications. If using this trait as a diagnostic characteristic for a given genotype or species, magnification of the microscopic images should be taken into consideration. The wheat stomatal index assessment model also exhibited a promising transferability on the other plant species. Using a small number of images to finetune the model, it achieved good accuracies and precisions on seven plant families.

The proposed pipeline regarded stomata and epidermal cell counting as two independent tasks and trained their neural networks separately. In reality, they are related to each other. Multitask deep neural network, as a subfield of machine learning, solves multiple tasks simultaneously by taking advantage of the sharing representations between related tasks. It was utilized successfully across many applications in computer vision (Zhang et al., 2014; Li et al., 2016). In the future, we can attempt the multitask deep neural network to improve the performance of the proposed stomatal index measurement pipeline. The hidden

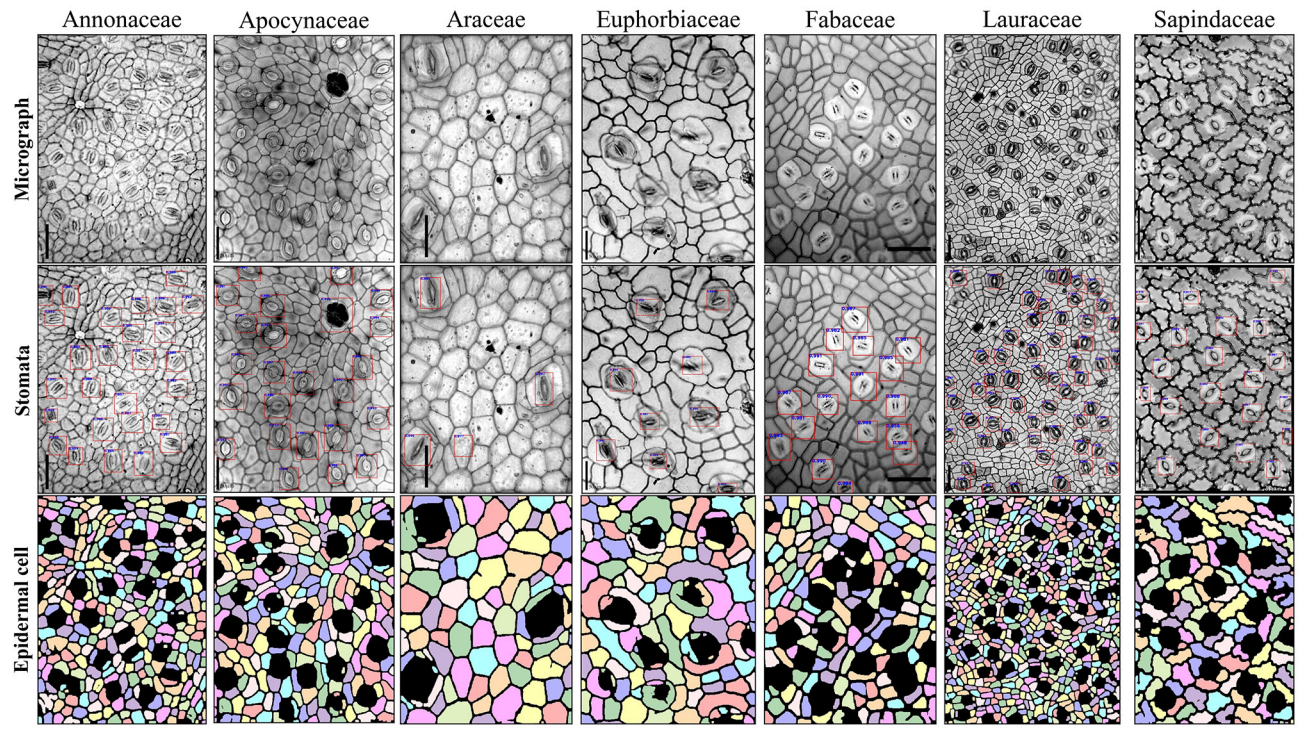

FIGURE 9 | Example images of seven plant families in the testing set of cuticle dataset using stomata detection and epidermal cell segmentation algorithms.

layers of the stomatal detection and epidermal cell segmentation networks can be soft- or hard-shared to obtain an end-to-end model for stomatal index estimation, possibly achieving a better generalization ability and a faster analysis speed.

DATA AVAILABILITY STATEMENT

The datasets presented in this study can be found in online repositories. The names of the repository/repositories and accession number(s) can be found in the article/**Supplementary Material**.

AUTHOR CONTRIBUTIONS

WL, XY, and CZhu conceived the study. WL and CZhu wrote the manuscript. HM, SL, and FL collected the microscopic images of the leaf epidermis. CZhu, YH, CZha, and LL annotated the datasets. CZhu, YH, WL, and XY designed the stomatal index measurement pipeline. CZhu wrote PYTHON scripts. All authors edited and approved the manuscript.

FUNDING

This study was supported by the Major Program of the National Natural Science Foundation of China (Grant No. 32090061), Sanya Science and Education Innovation Park of the Wuhan University of Technology of China (Grant No. 2020KF0053), and the start-up grant from the Wuhan University of Technology (Grant No. 104-40120526).

ACKNOWLEDGMENTS

We thank Chang Liu and Pinfan Wang at the Wuhan University of Technology for assisting in data annotation.

SUPPLEMENTARY MATERIAL

The Supplementary Material for this article can be found online at: https://www.frontiersin.org/articles/10.3389/fpls.2021.716784/full#supplementary-material

Supplementary Figure 1 | Microscopic images of the cuticle dataset. **(A)** Training set. **(B)** Testing set.

Supplementary Figure 2 | Simple linear regression between the manual and automatic measurement in the cuticle dataset. **(A)** Stomata. **(B)** Epidermal cell. **(C)** Stomatal index.

Supplementary Table 1 | Variety information of wheat (*Triticum aestivum* L.) dataset.

Supplementary Table 2 | Description of the cuticle dataset used for training and testing the stomatal index measurement model.

Supplementary Table 3 | Summary of average numbers of stomata and epidermal cells and the stomatal index trait in 500 epidermis images at × 10 and × 20 magnifications, respectively, in the wheat dataset.

REFERENCES

Aono, A. H., Nagai, J. S., Da Sm Dickel, G., Marinho, R. C., De Oliveira, P. E., and Faria, F. A. (2019). A stomata classification and detection system in microscope images of maize cultivars. *bioRxiv [Preprint]*. 538165. doi: 10.1101/538165

Barclay, R., Mcelwain, J., Dilcher, D., and Sageman, B. (2007). The cuticle database: developing an interactive tool for taxonomic and paleoenvironmental study of the fossil cuticle record. *Courier-Forschungsinst. Sencken*. 258, 39–55.

Bheemanahalli, R., Wang, C., Bashir, E., Chiluwal, A., Pokharel, M., Perumal, R., et al. (2021). Classical phenotyping and deep learning concur on genetic control of stomatal density and area in sorghum. *Plant Physiol.* 186, 1562–1579. doi: 10.1093/plphys/kiab174

Boetsch, J., Chin, J., Ling, M., and Croxdale, J. (1996). Elevated carbon dioxide affects the patterning of subsidiary cells in Tradescantia stomatal complexes. *J. Exp. Bot.* 47, 925–931. doi: 10.1093/jxb/47.7.925

Casado-García, A., Del-Canto, A., Sanz-Saez, A., Pérez-López, U., Bilbao-Kareaga, A., Fritschi, F. B., et al. (2020). LabelStoma: a tool for stomata detection based on the YOLO algorithm. *Comput.Electron. Agric.* 178:105751. doi: 10.1016/j.compag.2020.105751

Da Silva Oliveira, M. W., Da Silva, N. R., Casanova, D., Pinheiro, L. F. S., Kolb, R. M., and Bruno, O. M. (2014). "Automatic counting of stomata in epidermis microscopic images," in *X Workshop de Vis Ì83ao Computacional-WVC 2014* (Uberlândia).

Deng, J., Dong, W., Socher, R., Li, L.-J., Li, K., and Fei-Fei, L. (2009). "Imagenet: a large-scale hierarchical image database," in *2009 IEEE Conference on Computer Vision and Pattern Recognition* (Miami, FL: IEEE).

Everingham, M., Van Gool, L., Williams, C. K., Winn, J., and Zisserman, A. (2010). The pascal visual object classes (voc) challenge. *Int. J. Comput. Vis.* 88, 303–338. doi: 10.1007/s11263-009-0275-4

Fetter, K. C., Eberhardt, S., Barclay, R. S., Wing, S., and Keller, S. R. (2019). StomataCounter: a neural network for automatic stomata identification and counting. *New Phytol.* 223, 1671–1681. doi: 10.1111/nph.15892

He, K., Zhang, X., Ren, S., and Sun, J. (2015). "Delving deep into rectifiers: Surpassing human-level performance on imagenet classification," in *Paper Presented at the Proceedings of the IEEE International Conference on Computer Vision* (Santiago).

He, K., Zhang, X., Ren, S., and Sun, J. (2016). "Deep residual learning for image recognition," in *Proceedings of the IEEE Conference on Computer Vision and Pattern Recognition* (Las Vegas, NV).

Hu, H., Zheng, Y., Zhou, Q., Xiao, J., Chen, S., and Guan, Q. (2019). "MC-Unet: multi-scale convolution unet for bladder cancer cell segmentation in phase-contrast microscopy images," in *2019 IEEE International Conference on Bioinformatics and Biomedicine (BIBM)* (Las Vegas, NV: IEEE).

Kim, T.-H., Böhmer, M., Hu, H., Nishimura, N., and Schroeder, J. I. (2010). Guard cell signal transduction network: advances in understanding abscisic acid, CO2, and Ca2+ signaling. *Annu. Rev. Plant Biol.* 61, 561–591. doi: 10.1146/annurev-arplant-042809-112226

Laga, H., Shahinnia, F., and Fleury, D. (2014). "Image-based plant stomata phenotyping," in *2014 13th International Conference on Control Automation Robotics and Vision (ICARCV)* (Singapore: IEEE).

Li, K., Huang, J., Song, W., Wang, J., Lv, S., and Wang, X. (2019). Automatic segmentation and measurement methods of living stomata of plants based on the CV model. *Plant Methods* 15, 1–12. doi: 10.1186/s13007-019-0453-5

Li, X., Zhao, L., Wei, L., Yang, M.-H., Wu, F., Zhuang, Y., et al. (2016). "Deepsaliency: multi-task deep neural network model for salient object detection," in *2016 IEEE Transactions on Image Processing 25* (Phoenix, AZ).

Lin, K., Gong, L., Huang, Y., Liu, C., and Pan, J. (2019). Deep learning-based segmentation and quantification of cucumber powdery mildew using convolutional neural network. *Front. Plant Sci.* 10:155. doi: 10.3389/fpls.2019.00155

Loshchilov, I., and Hutter, F. (2016). SGDR: Stochastic gradient descent with warm restarts. *arXiv [Preprint] arXiv:1608.03983*.

Omasa, K., and Onoe, M. (1984). Measurement of stomatal aperture by digital image processing. *Plant. Cell. Physiol.* 25, 1379–1388. doi: 10.1093/oxfordjournals.pcp.a076848

R Core Team (2020). *R: A Language and Environment for Statistical Computing*. Vienna: R Foundation for Statistical Computing. Available online at: https://www.R-project.org/

Ren, S., He, K., Girshick, R., and Sun, J. (2015). Faster r-cnn: towards real-time object detection with region proposal networks. *Adv. Neural Inform. Process. Syst.* 28, 91–99. doi: 10.1109/tpami.2016.2577031

Ronneberger, O., Fischer, P., and Brox, T. (2015). "U-net: convolutional networks for biomedical image segmentation," in *International Conference on Medical Image Computing and Computer-Assisted Intervention* (Munich: Springer).

Royer, D. (2001). Stomatal density and stomatal index as indicators of paleoatmospheric CO_2 concentration. *Rev. Palaeobot. Palynol.* 114, 1–28. doi: 10.1016/s0034-6667(00)00074-9

Sack, L., and Buckley, T. N. (2016). The developmental basis of stomatal density and flux. *Plant Physiol.* 171, 2358–2363. doi: 10.1104/pp.16.00476

Sakoda, K., Watanabe, T., Sukemura, S., Kobayashi, S., Nagasaki, Y., Tanaka, Y., et al. (2019). Genetic diversity in stomatal density among soybeans elucidated using high-throughput technique based on an algorithm for object detection. *Sci. Rep.* 9, 1–9. doi: 10.1038/s41598-019-44127-0

Salisbury, E. J. (1928). I. On the causes and ecological significance of stomatal frequency, with special reference to the woodland flora. *Philos. Trans. R. Soc. Lond. Ser. B* 216, 1–65. doi: 10.1098/rstb.1928.0001

Sanyal, P., Bhattacharya, U., and Bandyopadhyay, S. K. (2008). "Analysis of SEM images of stomata of different tomato cultivars based on morphological features," in *2008 Second Asia International Conference on Modelling and Simulation (AMS)* (Washington, DC: IEEE).

Smith, L. N. (2017). "Cyclical learning rates for training neural networks," in *2017 IEEE Winter Conference on Applications of Computer Vision (WACV)* (Santa Rosa, CA).

Su, J., Yi, D., Su, B., Mi, Z., Liu, C., Hu, X., et al. (2020). Aerial visual perception in smart farming: field study of wheat yellow rust monitoring. *IEEE Trans. Indus. Inform.* 17, 2242–2249. doi: 10.1109/TII.2020.2979237

Tomasi, C., and Manduchi, R. (1998). "Bilateral filtering for gray and color images," in *Sixth International Conference on Computer Vision (IEEE Cat. No. 98CH36271): IEEE)*, (Bombay) 839–846.

Vialet-Chabrand, S., and Brendel, O. (2014). Automatic measurement of stomatal density from microphotographs. *Trees* 28, 1859–1865. doi: 10.1007/s00468-014-1063-5

Willmer, C., and Fricker, M. (1996). "The distribution of stomata," in *Stomata*. eds M. Black, and B. Charlwood (Berlin: Springer), 12–35. doi: 10.1007/978-94-011-0579-8_2

Zeng, Z., Xie, W., Zhang, Y., and Lu, Y. (2019). RIC-Unet: an improved neural network based on Unet for nuclei segmentation in histology images. *IEEE Access* 7, 21420–21428. doi: 10.1109/ACCESS.2019.2896920

Zhang, Z., Luo, P., Loy, C. C., and Tang, X. (2014). "Facial landmark detection by deep multi-task learning," in *European Conference on Computer Vision* (Zurich: Springer).

Zhuang, F., Qi, Z., Duan, K., Xi, D., Zhu, Y., Zhu, H., et al. (2020). A comprehensive survey on transfer learning. *Proc. IEEE* 109, 43–76. doi: 10.1109/JPROC.2020.3004555

Conflict of Interest: The authors declare that the research was conducted in the absence of any commercial or financial relationships that could be construed as a potential conflict of interest.

frontiers in Plant Science

ORIGINAL RESEARCH
published: 10 September 2021
doi: 10.3389/fpls.2021.735328

Protease Inhibitor-Dependent Inhibition of Light-Induced Stomatal Opening

*Tenghua Wang[1,2], Wenxiu Ye[3,4], Yin Wang[3,5], Maoxing Zhang[3,6], Yusuke Aihara[3] and Toshinori Kinoshita[1,3]**

[1] Graduate School of Science, Nagoya University, Nagoya, Japan, [2] Graduate School of Science, Kyoto University, Kyoto, Japan, [3] Institute of Transformative Bio-Molecules (WPI-ITbM), Nagoya University, Nagoya, Japan, [4] School of Agriculture and Biology, Shanghai Jiao Tong University, Shanghai, China, [5] College of Urban and Environmental Sciences and Key Laboratory for Earth Surface Processes of Ministry of Education, Institute of Ecology, Peking University, Beijing, China, [6] Department of Horticulture, International Research Centre for Environmental Membrane Biology, Foshan University, Foshan, China

OPEN ACCESS

Edited by:
Mamoru Okamoto,
University of Adelaide, Australia

Reviewed by:
Agepati S. Raghavendra,
University of Hyderabad, India
Qingfeng Song,
Center for Excellence in Molecular Plant Sciences, Chinese Academy of Sciences (CAS), China

***Correspondence:**
Toshinori Kinoshita
kinoshita@bio.nagoya-u.ac.jp

Specialty section:
This article was submitted to Plant Physiology, a section of the journal Frontiers in Plant Science

Received: 02 July 2021
Accepted: 16 August 2021
Published: 10 September 2021

Citation:
Wang T, Ye W, Wang Y, Zhang M, Aihara Y and Kinoshita T (2021) Protease Inhibitor-Dependent Inhibition of Light-Induced Stomatal Opening. Front. Plant Sci. 12:735328. doi: 10.3389/fpls.2021.735328

Stomata in the epidermis of plants play essential roles in the regulation of photosynthesis and transpiration. Stomata open in response to blue light (BL) by phosphorylation-dependent activation of the plasma membrane (PM) H^+-ATPase in guard cells. Under water stress, the plant hormone abscisic acid (ABA) promotes stomatal closure *via* the ABA-signaling pathway to reduce water loss. We established a chemical screening method to identify compounds that affect stomatal movements in *Commelina benghalensis*. We performed chemical screening using a protease inhibitor (PI) library of 130 inhibitors to identify inhibitors of stomatal movement. We discovered 17 PIs that inhibited light-induced stomatal opening by more than 50%. Further analysis of the top three inhibitors (PI1, PI2, and PI3; inhibitors of ubiquitin-specific protease 1, membrane type-1 matrix metalloproteinase, and matrix metalloproteinase-2, respectively) revealed that these inhibitors suppressed BL-induced phosphorylation of the PM H^+-ATPase but had no effect on the activity of phototropins or ABA-dependent responses. The results suggest that these PIs suppress BL-induced stomatal opening at least in part by inhibiting PM H^+-ATPase activity but not the ABA-signaling pathway. The targets of PI1, PI2, and PI3 were predicted by bioinformatics analyses, which provided insight into factors involved in BL-induced stomatal opening.

Keywords: stomata, chemical biology, protease inhibitor, *Commelina*, Arabidopsis

INTRODUCTION

Stomata, each surrounded by a pair of guard cells, are specialized pores on the surface of leaves. Stomatal pores enable plants to regulate CO_2 uptake and water loss for photosynthesis and transpiration, respectively (Shimazaki et al., 2007). Stomata are also important routes of infection for plant pathogens (Ye and Murata, 2016; Melotto et al., 2017). Stomatal movements

are controlled by diverse stimuli, such as blue light (BL), red light (RL), the phytotoxin fusicoccin (FC), CO_2, the plant hormone abscisic acid (ABA), and microbial elicitors (Munemasa et al., 2015; Inoue and Kinoshita, 2017; Ye et al., 2020). BL receptor phototropins activate PM H^+-ATPase by phosphorylating the C-terminal Thr (Kinoshita and Shimazaki, 1999; Kinoshita et al., 2001). Activated PM H^+-ATPase generates a transmembrane electrochemical gradient and establishes an inside-negative electrical potential that drives the influx of K^+ into guard cells through inward-rectifying voltage-gated K^+ channels (Schroeder et al., 1987). The accumulation of K^+ leads to turgor elevation and stomatal opening (Schroeder et al., 2001; Shimazaki et al., 2007). Several signaling mediators are reported to be involved in the signaling pathway of BL-induced stomatal opening. Protein kinase BLUE LIGHT SIGNALING1 (BLUS1) is phosphorylated by phot1 directly as the primary step in phototropin signaling (Takemiya et al., 2013). The Raf-like protein kinase BLUE LIGHT-DEPENDENT H^+-ATPASE PHOSPHORYLATION (BHP) binds to BLUS1 and regulates BL-dependent phosphorylation of PM H^+-ATPase (Hayashi et al., 2017). Type 1 protein phosphatase (PP1) positively mediates BL signaling between phototropin and PM H^+-ATPase (Takemiya et al., 2006). However, the molecular mechanism of signal transduction for BL-induced stomatal opening is incompletely understood (Inoue and Kinoshita, 2017).

The phytohormone ABA is synthesized under drought-stress conditions and reduces stomatal aperture by two mechanisms. ABA promotes stomatal closure by activating outward-rectifying K^+ channels and anion channels (Kim et al., 2010; Inoue and Kinoshita, 2017; Saito and Uozumi, 2019). In parallel, ABA inhibits light-induced stomatal opening by inhibiting PM H^+-ATPase and inward-rectifying K^+ channels in the PM of guard cells. The ABA receptors, PYR/PYL/RCARs, negatively regulate type-2C protein phosphatases (PP2Cs), which inactivate members of the SRK2/SnRK2 family, including open stomata 1 (OST1) (Ma et al., 2009; Park et al., 2009; Santiago et al., 2009; Cutler et al., 2010). Activation of K^+_{out} channels requires depolarization of the PM by activation of anion channels meditated by the PYR/PYL/RCAR-PP2Cs-SnRK2s pathway (Negi et al., 2008; Vahisalu et al., 2008; Kim et al., 2010; Joshi-Saha et al., 2011). SnRK2s suppress BL-induced phosphorylation of PM H^+-ATPase and the activity of inward-rectifying K^+ channels, inhibiting stomatal opening (Sato et al., 2009; Hayashi et al., 2011; Acharya et al., 2013).

Chemical genetics can provide insight into biological systems at the molecular level. It can overcome the problems of traditional genetic approaches, such as gene essentiality and redundancy in gene families (Dejonghe and Russinova, 2017). Chemical screenings related to stomatal movements and development revealed several aspects of stomatal function and development (Kinoshita et al., 2021). Toh et al. (2018) established a comprehensive chemical screening method using *Commelina benghalensis* as a model plant and identified nine stomatal closing compounds (SCL1–SCL9) that suppress light-induced stomatal opening by >50%, and two compounds (temsirolimus and CP-100356) that induce stomatal opening in the dark. This indicates the feasibility of chemical approaches for analyzing stomatal movements. Notably, BHP, a factor involved in BL-induced stomatal opening, was identified by a combination of chemical screening focused on BL-induced phosphorylation of PM H^+-ATPase in guard cells and reverse genetics in *Arabidopsis thaliana* (Hayashi et al., 2017). In this study, we performed chemical genetics screening of a protease inhibitor (PI) library and identified three inhibitors of light-induced stomatal opening and BL-induced phosphorylation of PM H^+-ATPase in guard cells. Interestingly, spraying leaves onto monocot and dicot plants with PI1 suppressed wilting of leaves, indicating that inhibition of stomatal opening by PI1 decreases water loss in plants. To our knowledge, screening of PIs that affect stomatal movements has not been reported. We also investigated the molecular mechanisms of these inhibitors and laid the foundation for the identification of novel factors in the BL-signaling pathway.

MATERIALS AND METHODS

Plant Materials and Growth Conditions

Plants of *Commelina benghalensis* ssp. were cultured in soil at 25 ± 3°C in a greenhouse for 4 weeks. *Arabidopsis thaliana* (ecotype Col-0) plants were grown in soil for 4–6 weeks under controlled conditions (20–24°C, 55–70% humidity, 16 h light/8 h dark) in growth chambers. Seeds were vernalized at 4°C in the dark for 2 days before being transferred to soil. Oat (*Avena sativa*) seedlings were grown in growth chambers with same conditions of Arabidopsis for 10 days.

Chemicals

A protease inhibitor (PI) library (130 PIs dissolved in DMSO at 10 mM) was purchased from APExBIO Company. Repurchased chemicals were SJB3-019A (CAS No. 2070015-29-9, >99.00% purity, Medchem Express), NSC 405020 (CAS No. 7497-07-6, >99.07% purity, Sellek Chemicals), SB-3CT (CAS No. 292605-14-2, >98.00% purity, TCI). All chemicals were stored at −20°C.

Chemical Screening

Screening of chemicals was performed as described previously (Toh et al., 2018) with some modifications. Four-week-old *C. benghalensis* plants were transferred from a greenhouse to a dark room for incubation overnight to ensure complete stomatal closure on day 2. Leaf discs of 4 mm diameter were excised from dark-adapted *C. benghalensis* using a hole punch under dim light. The leaf discs were floated on basal reaction buffer [5 mM MES-BTP (Bis-trispropane), pH 6.5, 50 mM KCl and 0.1 mM $CaCl_2$] with chemical compounds and incubated in light (150 μmol m^{-2} s^{-1} red light and 50 μmol m^{-2} s^{-1} BL) or in the dark for 3 h. Leaf discs were incubated with compounds for 30 min before light exposure. Stomatal apertures of the abaxial epidermis were measured as described previously (Toda et al., 2018). Inhibition by PI1, PI2, and PI3 of stomatal opening was identified. To assay viability, abaxial epidermis was removed from leaf discs using forceps after chemical and light treatments and incubated in fresh basal reaction buffer

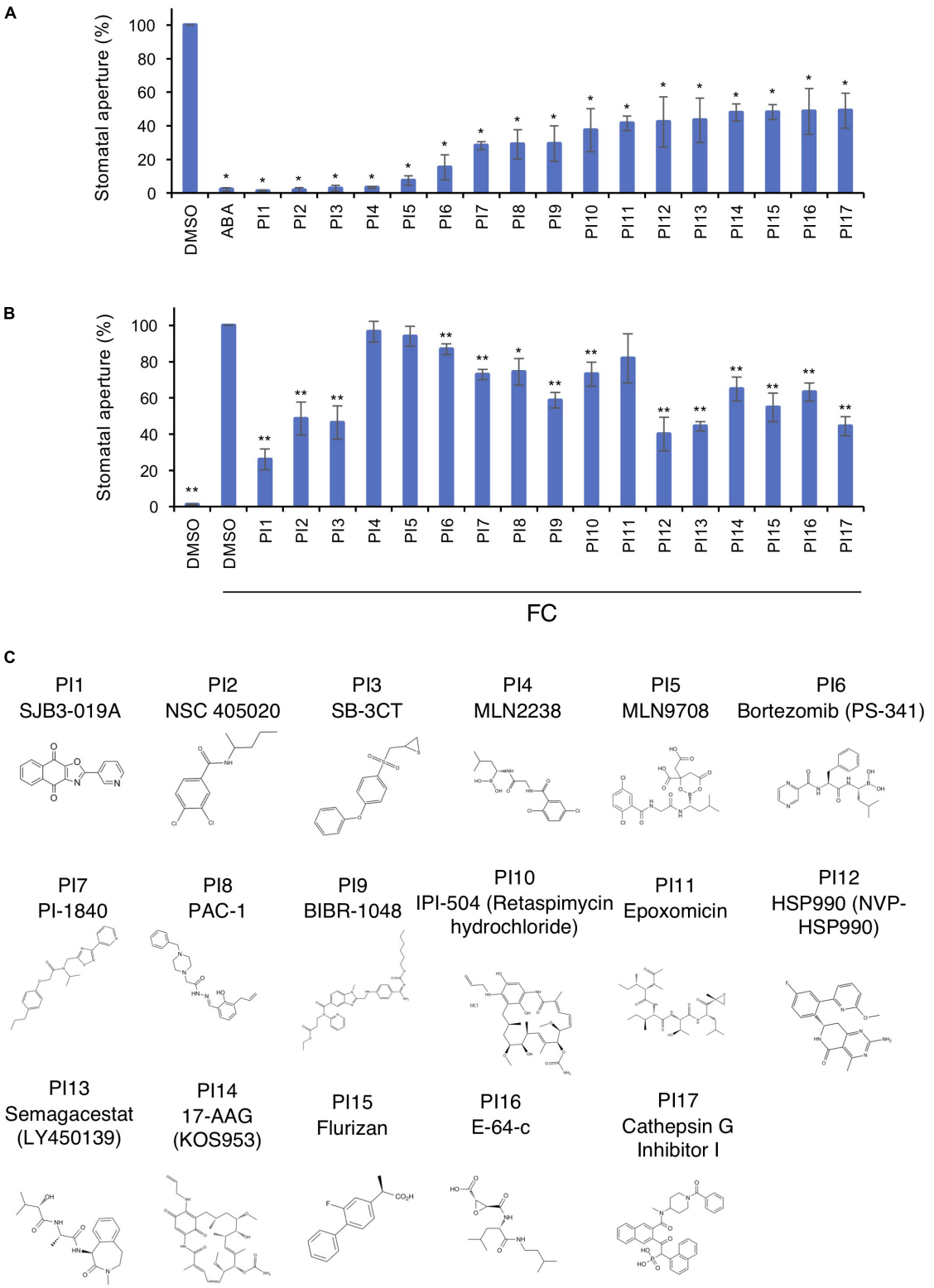

FIGURE 1 | Inhibition of light- and FC-induced stomatal opening by proteinase inhibitors (PIs). **(A)** Inhibition by PIs of light-induced stomatal opening. Leaf discs were pre-treated with compounds for 30 min in the dark and illuminated with light (150 μmol m^{-2} s^{-1} red light and 50 μmol m^{-2} s^{-1} BL) for 3 h. ABA, 10 μM; PIs, 100 μM. Means ± SE (n = 5, 30 stomata per 2 leaf discs per repeat). Student's t-test, $^{*}P < 0.01$. **(B)** Suppression by PIs of FC-induced stomatal opening. Leaf discs were incubated with PIs in basal buffer for 30 min, FC was added, and incubated for 3 h in the dark. PIs, 100 μM; FC, 10 μM. Means ± SE (n = 4, >50 stomata from 3 leaf discs per repeat). Student's t-test, $^{*}P < 0.05$, $^{**}P < 0.01$. **(C)** Chemical structures of PIs.

containing 1 μg/mL fluorescein diacetate (FDA) for 30 min in the dark. Epidermis was washed three times with Milli-Q water to remove FDA. Fluorescence microscopy was used to detect fluorescence.

Immunohistochemical Analysis

Phosphorylation of PM H^+-ATPase was determined by immunohistochemical analysis following previous methods using ImageJ (Hayashi et al., 2011; Ando and Kinoshita, 2018).

Detection of Phototropin Autophosphorylation

Leaf discs excised from dark-adapted 5-week-old Arabidopsis were incubated in basal reaction buffer with PIs (100 μM) or an equal volume of DMSO in the dark for 1 h in advance. Leaf discs were irradiated with BL (50 μmol m^{-2} s^{-1}) or kept in the dark for 1 h. Immunoblot analysis was performed as described previously (Kinoshita et al., 2003; Inoue et al., 2008). Proteins were separated by 7.5% sodium dodecyl sulfate-polyacrylamide gel electrophoresis (SDS-PAGE) and transferred to nitrocellulose membranes. The primary and secondary antibodies were anti-phot1 (Emi et al., 2005; Inoue et al., 2008) and anti-rabbit IgG HRP (Bio-Rad, CA) respectively.

Quantification of ABA-Dependent Gene Expression and Germination Assay

We determined the expression of the ABA-maker genes *RAB18* (At5g66400) and *RD29B* (At5g52300) by quantitative RT-PCR in Arabidopsis (Tomiyama et al., 2014). Two-week-old seedlings cultured in solid 1/2 MS medium were transferred to liquid 1/2 MS medium containing 50 μM ABA or 100 μM PIs or an equal volume of DMSO and irradiated with white fluorescent light for 3 h at 24°C. Total RNA was isolated from seedlings and first-strand cDNA was synthesized using the Prime Script II First Strand cDNA Synthesis Kits (TaKaRa, Tokyo, Japan). Quantitative RT-PCR was performed using Power SYBR Green PCR Master Mix and the Step One Real-Time PCR System (Applied Biosystems, Foster City, CA). *RAB18*, *RD29B*, and *TUB2* cDNAs were amplified using specific primers (**Supplementary Table 1**).

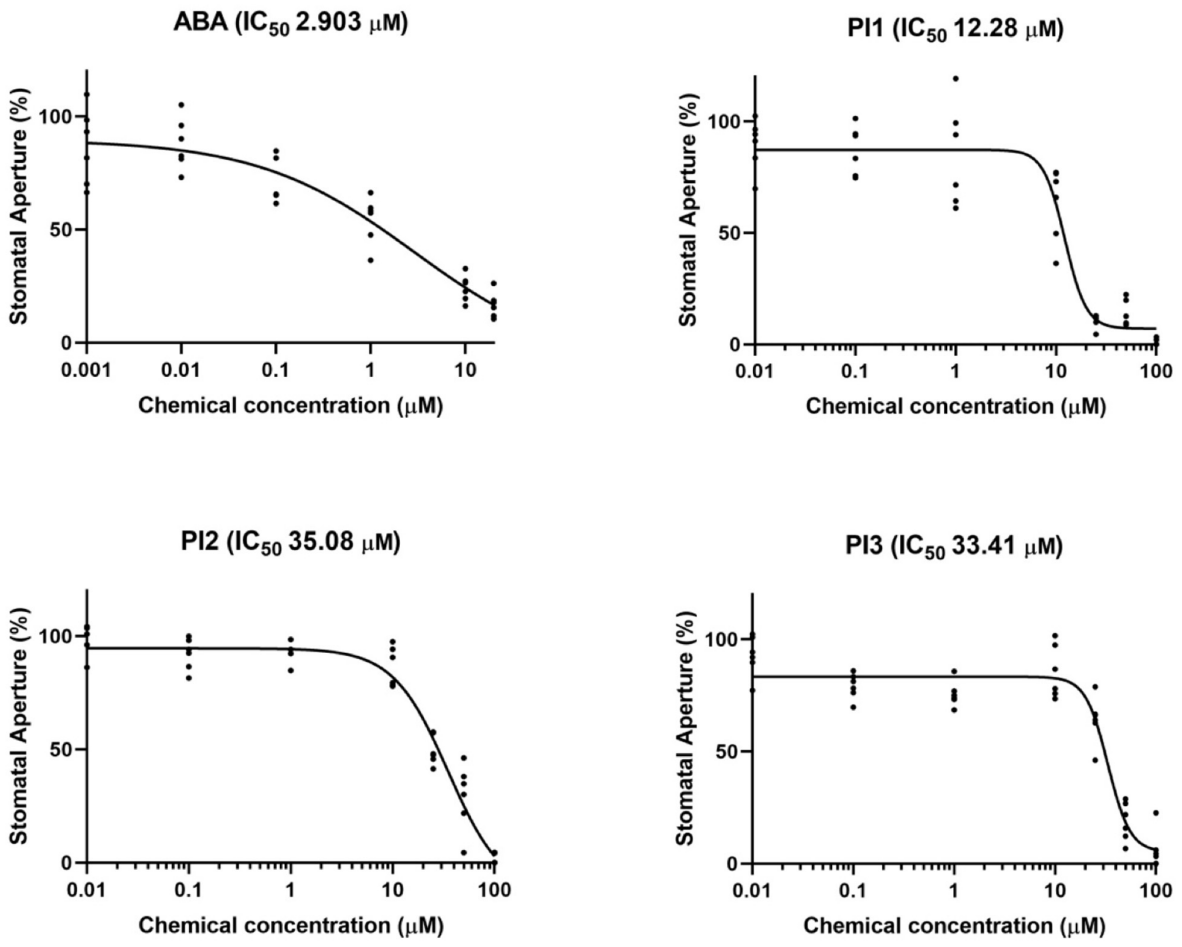

FIGURE 2 | IC_{50} curves of ABA, PI1, PI2, and PI3 for light-induced stomatal opening. The concentrations used to obtain IC_{50} curves were 0.001, 0.01, 0.1, 1, 10, and 20 μM for ABA and 0.01, 0.1, 1, 10, 25, 50, and 100 μM for PIs. IC_{50} values were computed by GraphPad Prism (n = 6, 30 stomata from 3 leaf discs per concentration).

Arabidopsis seeds were incubated in MQ water containing 50 μM ABA or 100 μM PIs or an equal volume of DMSO in 96-well plates sealed with surgical tapes. The space between wells was filled with water. The plates were kept at 4°C in darkness for 2 days and transferred to an illumination incubator at 24°C with a 16 h light/8 h dark cycle for 7 days.

Chemical Spraying for Drought Tolerance Assay

Drought tolerance assays were performed as described previously (Toh et al., 2018) with slight modifications. Rose bouquets purchased from a local shop were cultured in a light incubator for 2 days for environmental adaption. Rose leaves and 10-day-old oat seedlings were sprayed with 100 μM PIs or an equal volume of DMSO in 0.05% Approach BI (Maruwa Biochemical) and 0.02% Silwet L77 (Biomedical Science) under white light (50 μmol m^{-2} s^{-1}) and 70% humidity for 3 h at 24°C. Rose and oat leaves were removed and illuminated with 50 μmol m^{-2} s^{-1} white light for 8 h and 30 min, respectively, at 27°C with 40% humidity.

RESULTS

Chemical Screening for Stomatal Movement

We evaluated the ability of 130 PIs on stomatal movements (**Supplementary Figure 1**). *C. benghalensis* is useful for determination of stomatal aperture due to its larger stomata compared to *A. thaliana*. Seventeen inhibitors suppressed light-induced stomatal opening by >50% compared to the control (**Supplementary Figure 2**). No PI induced stomatal opening in the dark (**Supplementary Figure 3**). Staining with the fluorescent dye FDA showed that none of the PIs affected cell viability (**Supplementary Figure 4**).

Figure 1A shows inhibition of light-induced stomatal opening by 17 chemicals selected through screenings. These inhibitors were designated PI1–PI17 and their structures are shown in **Figure 1C**. The targets of PIs in mammals are shown in **Supplementary Table 2**. The fungal phytotoxin FC leads to irreversible stomatal opening in the dark by binding of 14-3-3 protein to phosphorylated PM H^+-ATPase, preventing dephosphorylation of PM H^+-ATPase (Kinoshita and Shimazaki, 2001). To investigate whether the 17 PIs function upstream or downstream of PM H^+-ATPase activation, we examined their effects on FC-induced stomatal opening (**Figure 1B**). PI4, PI5 and PI11 did not inhibit FC-induced stomatal opening, indicating that they may have effects upstream of PM H^+-ATPase. The other PIs significantly inhibited stomatal opening induced by FC to varying degrees, suggesting that they regulate downstream of PM H^+-ATPase, but not the BHP or PP1, or inhibit PM H^+-ATPase phosphorylation.

Next, we examined the concentration-dependency of the top three inhibitors (PI1, an inhibitor of ubiquitin-specific protease 1; PI2 and PI3, inhibitors of membrane type-1 matrix metalloproteinase and matrix metalloproteinase-2, respectively) for light-induced stomatal opening (**Figure 2**). Leaf discs were treated with the indicated compounds and exposed to light for 3 h. The 50% inhibitory concentration (IC_{50}) values of PI1, PI2, and PI3 were 12.28, 35.08, and 33.41 μM, respectively, indicating that PI1 inhibited light-induced stomatal opening more efficiently than PI2 and PI3 at low concentrations. The IC_{50} value of ABA was 2.903 μM.

Effects of PI1, PI2, and PI3 on Phosphorylation of PM H^+-ATPase and Phototropin

To investigate whether PI1, PI2, and PI3 influence BL-dependent phosphorylation of PM H^+-ATPase, we performed immunohistochemical analysis of guard cells using epidermis

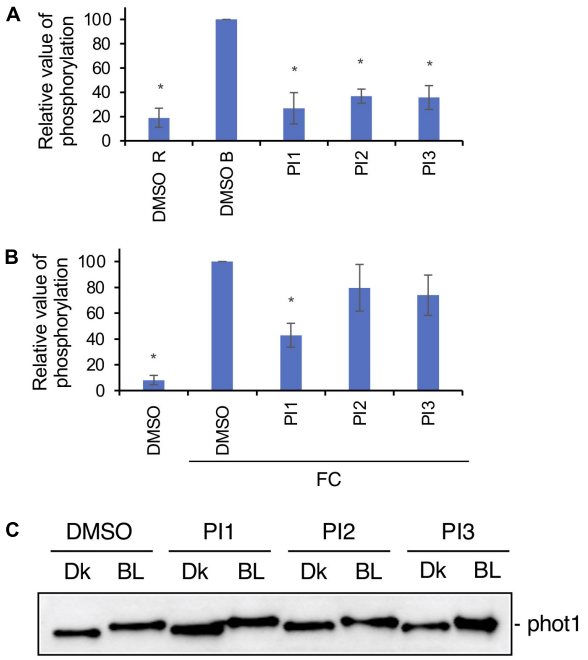

FIGURE 3 | Effects of PIs on phosphorylation of PM H^+-ATPase in guard cells and phototropin. **(A)** Inhibition by PIs of BL-dependent H^+-ATPase phosphorylation in guard cells of Arabidopsis. Leaf epidermis was pre-treated with compounds for 20 min in the dark and illuminated with 50 μmol m^{-2} s^{-1} red light for 20 min (DMSO R), after which 10 μmol m^{-2} s^{-1} BL was superimposed on the red light for 2.5 min (DMSO B, PI1, PI2, PI3). PIs, 100 μM. Means ± SE (n = 3). Student's t-test, $^*P < 0.01$. **(B)** Suppression by PIs of FC-induced phosphorylation of PM H^+-ATPase. Leaf epidermis from Arabidopsis was incubated with DMSO or PIs in basal buffer for 30 min in the dark, FC was added, and incubated for 30 min under red light (50 μmol m^{-2} s^{-1}). PIs, 100 μM; FC, 10 μM. Means ± SE (n = 3). Student's t-test, $^*P < 0.01$. Phosphorylation of PM H^+-ATPase was detected using an anti-pThr (phosphorylated threonine, the penultimate residue of the PM H^+-ATPase) primary antibody and Alexa 488 conjugated anti-rabbit IgG secondary antibody in panels **(A,B)**. **(C)** Effects of PI1, PI2, and PI3 on BL-induced phot1 autophosphorylation in Arabidopsis detected by mobility shift assay. Dk, leaf discs from Arabidopsis treated with DMSO or PIs and incubated in the dark for 2 h. BL, leaf discs treated with DMSO or PIs, incubated in the dark for 1 h and transferred to BL (50 μmol m^{-2} s^{-1}) for 1 h. PIs, 100 μM. Phot1 protein was detected using an anti-phot1 antibody. Experiments were repeated on three different occasions with similar results.

isolated from *Arabidopsis thaliana* (Hayashi et al., 2011). BL-induced phosphorylation was suppressed completely by these three PIs (**Figure 3A**). We next determined the inhibitory effects of PI1, PI2, and PI3 on FC-induced phosphorylation of the PM H^+-ATPase. FC-induced phosphorylation was significantly inhibited by PI1, and partially by PI2 and PI3 (**Figure 3B**). The different inhibitory effects of these inhibitors are consistent with their IC_{50} values for light-induced stomatal opening (**Figure 2**).

Next, we determined whether PI1, PI2, and PI3 inhibit the kinase activity of phototropin. Autophosphorylation of phot1 induced by BL in leaves was detected by mobility shift assay using an antibody against phot1 in Western blotting (Emi et al., 2005; Inoue et al., 2008). PI1, PI2, and PI3 did not affect the BL-induced mobility shift of phot1 (**Figure 3C**), suggesting that PI1, PI2, and PI3 inhibit light-induced stomatal opening without affecting phototropin activity.

Effects of PIs on ABA-Responsive Genes and Germination

To investigate whether PI1, PI2, and PI3 inhibit BL-induced stomatal opening in a manner similar to ABA, we analyzed the expression levels of the ABA-responsive genes, *RAB18* and *RD29B*, by quantitative RT-PCR in Arabidopsis seedlings and germination of Arabidopsis seeds (Toh et al., 2018). Incubation of seedlings with 50 μM ABA for 3 h induced expression of *RAB18* and *RD29B* (**Figure 4A**). By contrast, PI1, PI2, and PI3 did not induce the expression of ABA-responsive genes (**Figure 4A**). Moreover, ABA at 50 μM inhibited germination of Arabidopsis seeds (**Figure 4B**). However, PI1, PI2, and PI3 had no effect on germination (**Figure 4B**). The results suggest that the mechanisms underlying the inhibitory effects of the PIs and ABA on light-induced stomatal opening are different and that the PIs have more specific roles in regulating stomatal movement.

PI1 Reduces Water Loss in Plants

SCL1, which reportedly induces stomatal closure, prevents wilting of detached oat and rose leaves, which is likely to be by inhibiting light-induced stomatal opening (Toh et al., 2018). We investigated the effect of PI1 on drought resistance using the same method with slight modifications. Oat and rose leaves were sprayed with PI1 at 100 μM and incubated for 3 h, and the leaves were detached. PI1 inhibited leaf withering in oat plants compared with the control (**Figure 5A**). Rose leaves treated with PI1 wilted slower than that of control (**Figure 5B**). Therefore, PI1 improves drought resistance in dicot and monocot plants.

DISCUSSION

Effect of PI1 on Light-Induced Stomatal Opening

We screened for compounds that affect light-induced stomatal opening using a commercially available PI library (APExBIO) and identified 17 PIs that significantly suppressed light-induced stomatal opening by >50% (**Figure 1A**). PI1, which had the greatest inhibitory effect on stomatal opening, inhibited both light- and FC-induced stomatal opening (**Figures 1A,B**) and both BL- and FC-induced phosphorylation of PM H^+-ATPase in guard cells (**Figures 3A,B**). By contrast, PI1 had no effect on phototropin activity (**Figure 3C**) and did not induce ABA-dependent responses, such as inhibition of seed germination and expression of ABA-responsive genes (**Figure 4**). These results suggest that PI1-sensitive proteases mediate phosphorylation of PM H^+-ATPase (**Figure 6**) by positively regulating unidentified kinases that directly phosphorylate PM H^+-ATPase or down-regulating protein phosphatases that directly dephosphorylate PM H^+-ATPase (Inoue and Kinoshita, 2017). PI2 and PI3 markedly suppressed light-induced stomatal opening (**Figure 1A**), and partially inhibited FC-induced stomatal opening (**Figure 1B**) and FC-induced phosphorylation of PM H^+-ATPase in guard cells (**Figure 3B**). Therefore, the targets of PI2 and PI3 are likely to include PM H^+-ATPase and downstream components of light-induced stomatal opening (**Figure 6**).

It is worth noting that PI4, PI5 and PI11 suppressed light-induced stomatal opening and didn't inhibit FC-induced

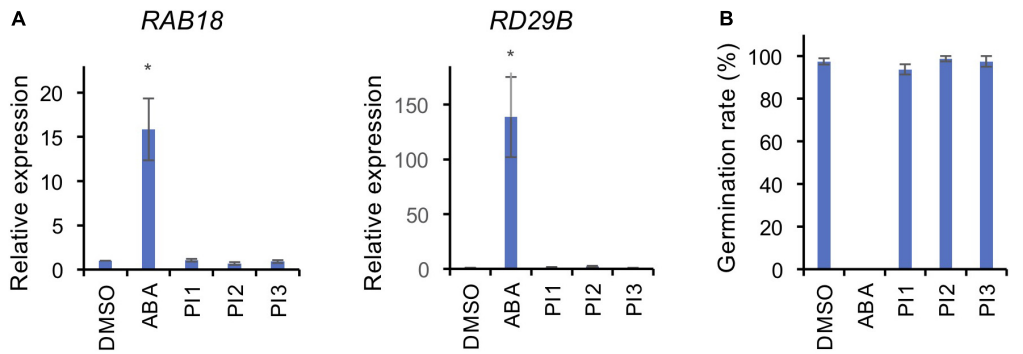

FIGURE 4 | Effects of PIs on ABA-induced gene expression and seed germination. **(A)** Expression levels of ABA-responsive genes, *RAB18* and *RD29B*, were determined by qRT-PCR in response to ABA and PIs in Arabidopsis seedlings. *TUB2* was used as the internal standard. Two-week-old seedlings were treated with 50 μM ABA or 100 μM PIs or an equal volume of DMSO under white light for 3 h at 24°C. Means ± SE (n = 3; 3 whole seedlings per replicate). Student's t-test, $^*P < 0.05$. **(B)** Effects of PIs on Arabidopsis seed germination. Seeds were immersed in water with 50 μM ABA or 100 μM PIs or an equal volume of DMSO in the dark for 2 days for vernalization, and 7 days for germination under light. Means ± SE (n = 4; 20 seeds per replicate).

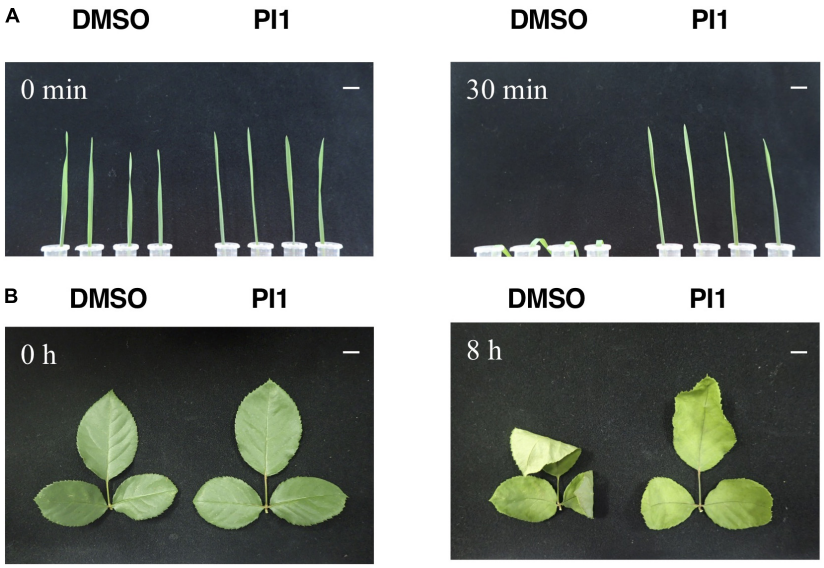

FIGURE 5 | Effect of PI1 on leaf wilting. Oat leaves **(A)** and rose leaves **(B)**. Ten-day-old oat seedlings grown in soil **(A)** and rose leaves in bouquets **(B)** were sprayed with 100 μM PI1 or an equal volume of DMSO in 0.05% Approach BI and 0.02% Silwet L77 and incubated under white light (50 μmol m^{-2} s^{-1}) and 70% relative humidity at 24°C for 3 h. Next, leaves were excised and incubated for 30 min (oat) and 8 h (rose) at 27°C under 50 μmol m^{-2} s^{-1} at ∼40% relative humidity. Scale bars = 1 cm. Experiments were repeated on three different occasions with similar results.

stomatal opening significantly (**Figures 1A, B**), suggesting that the targets of these inhibitors are components upstream of BL-signaling pathway, such as phototropins, BLUS1, BHP, and PP1.

Candidate Targets of PI1 in Arabidopsis

In mammalian cells, PI1 is a specific inhibitor of ubiquitin-specific protease 1 (USP1) (Mistry et al., 2013; Das et al., 2017). To predict the target of PI1 in Arabidopsis, we performed a BLAST search (The National Center for Biotechnology Information)[1] using the amino acid sequence of USP1 from *Homo sapiens* and found two ubiquitin specific processing proteases (UBP3 and UBP4) with relatively high identity (around 33%) to USP1 (**Supplementary Table 3**). The UBP family in Arabidopsis has a similar sequence to human USPs and plays a critical role in de-ubiquitination of proteins (March and Farrona, 2018). In Arabidopsis, the UBP family has 27 members (**Supplementary Figure 5A**), which are divided into 14 subfamilies based on their domains (Yan et al., 2000; Liu et al., 2008; Zhou et al., 2017). All Arabidopsis UBPs contain a UBP domain, and each subfamily shares other conserved domains that are likely to mediate protein-protein interactions (Liu et al., 2008; Komander et al., 2009; March and Farrona, 2018). To our knowledge, the binding site of USP1 with PI1 is unknown.

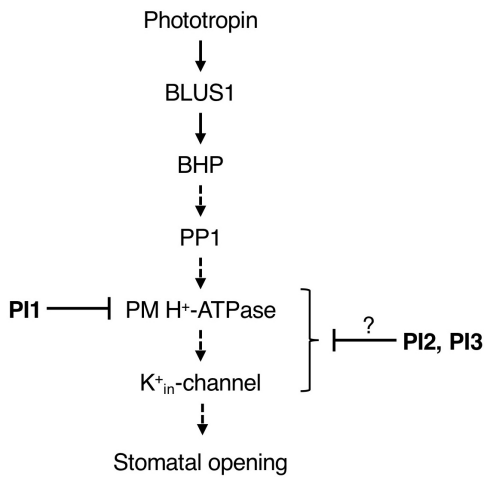

FIGURE 6 | Proposed model of the inhibitory effects of PI1, PI2, and PI3 on the signaling pathway of BL-dependent stomatal opening. The pathway starts from phototropin, followed by BLUS1, BHP, PP1, a key enzyme PM H^+-ATPase and K^+_{in}-channel. PI1, PI2, and PI3 inhibited BL-induced phosphorylation of PM H^+-ATPase. Arrows indicate positive regulation. Blunt arrows indicate repression.

We hypothesized that some of the 27 UBPs participate in the stomatal-opening pathway in response to BL. These UBPs may function separately or redundantly and up-regulate the unidentified kinases that directly phosphorylate or down-regulate phosphatases that dephosphorylate the PM H^+-ATPase. We also investigated their expression levels in guard cells using Arabidopsis eFP Browser[2] (**Supplementary Figure 5B**). *UBP6* and *UBP13* exhibited the highest expression levels. Stomatal closure in the mutant of *ubp24* was less sensitive to ABA than the WT and the stomata of complemented transgenic plants showed sensitivity to ABA similar to the WT, indicating that UBP24 is involved in ABA-mediated stomatal closure (Zhao et al., 2016). However, PI1 is less likely to modulate the

[1]https://www.ncbi.nlm.nih.gov/

[2]http://bar.utoronto.ca/efp/cgi-bin/efpWeb.cgi?dataSource=Guard_Cell

factors in the ABA signaling pathway (**Figure 4**), so UBP24 may not be the target of PI1.

Presumption of PI2 and PI3 Targets in Arabidopsis

In mammals, the targets of PI2 and PI3 are membrane type-1 matrix metalloproteinase (MT1-MMP/MMP-14) and matrix metalloproteinase-2 (MMP-2), respectively (Kleifeld et al., 2001; Remacle et al., 2012). MMPs are a large family of zinc- and calcium-dependent endopeptidases (Rawlings et al., 2006). In human, MT1-MMP and MMP-2 have a common domain structure that includes a signal peptide, a propeptide, a catalytic domain with the active zinc binding site, a hinge region, and a hemopexin-like domain. MT1-MMP has two domains absent in MMP-2—membrane linker and cytoplasmic domains (Overall and López-Otín, 2002). PI2 directly targets the hemopexin-like domain of MT1-MMP (Remacle et al., 2012). PI3 is an MMP-2 inhibitor that specifically binds the catalytic zinc ion (Kleifeld et al., 2001). In Arabidopsis, five genes named *At1-MMP* to *At5-MMP* encode MMPs with common structural features with mammalian MMPs but lacking a hemopexin-like domain (Maidment et al., 1999; Marino and Funk, 2012; **Supplementary Figures 6A,B**). We evaluated the expression levels of five MMPs in Arabidopsis guard cells using an eFP Browser; the expression of *AT5-MMP* was highest (**Supplementary Figure 6C**). The identities of At-MMPs aligned with human MMP-2 are shown in **Supplementary Table 3**. In soybean, glycine max1-matrix metalloproteinase (GM1-MMP) and glycine max2-matrix metalloproteinase (GM2-MMP) are PM proteins, and the stomatal aperture of transgenic Arabidopsis plants overexpressing *GM1-MMP* and *GM2-MMP* was significantly larger than the WT (Liu et al., 2017, 2018), suggesting that *GM1-MMP* and *GM2-MMP* regulate stomatal opening. Therefore, *AtMMPs* are candidate targets of PI3 in Arabidopsis.

CONCLUSION

In conclusion, we identified seventeen PIs that suppress stomatal opening under light and found that among them, PI1, PI2, and PI3 inhibit phosphorylation of penultimate residue, threonine, in guard-cell PM H^+-ATPase, which is important for stomatal opening. Our findings will facilitate identification of novel regulators and provide insight into the molecular mechanisms of light-induced stomatal opening. Further investigations of these inhibitors are expected to shed light on the BL- signaling pathway and future development of agrochemicals that control drought tolerance and plant growth. In particular, drought stress severely affects quality and yield of crops. If agrochemicals confer drought tolerance like the compounds identified in this study, it is possible not only to improve the yield of crops but also to cultivate crops in non-farming areas due to a shortage of rainfall.

DATA AVAILABILITY STATEMENT

The raw data supporting the conclusions of this article will be made available by the authors, without undue reservation.

AUTHOR CONTRIBUTIONS

TW, WY, and TK designed the experiments and wrote the manuscript. TW, WY, YW, MZ, YA, and TK performed the experiments. All authors reviewed the manuscript.

FUNDING

This research was supported by Grants-in-Aid for Scientific Research from MEXT (15H05956, 20H05687, and 20H05910 to TK).

SUPPLEMENTARY MATERIAL

The Supplementary Material for this article can be found online at: https://www.frontiersin.org/articles/10.3389/fpls.2021.735328/full#supplementary-material

REFERENCES

Acharya, B. R., Jeon, B. W., Zhang, W., and Assmann, S. M. (2013). Open Stomata 1 (OST1) is limiting in abscisic acid responses of *Arabidopsis* guard cells. *New Phytol.* 200, 1049–1063. doi: 10.1111/nph.12469

Ando, E., and Kinoshita, T. (2018). Red light-induced phosphorylation of plasma membrane H^+-ATPase in stomatal guard cells. *Plant Physiol.* 178, 838–849. doi: 10.1104/pp.18.00544

Cutler, S. R., Rodriguez, P. L., Finkelstein, R. R., and Abrams, S. R. (2010). Abscisic acid: emergence of a core signaling network. *Annu. Rev. Plant Biol.* 61, 651–679. doi: 10.1146/annurev-arplant-042809-112122

Das, D. S., Das, A., Ray, A., Song, Y., Samur, M. K., Munshi, N. C., et al. (2017). Blockade of deubiquitylating enzyme USP1 inhibits DNA repair and triggers apoptosis in multiple myeloma cells. *Clin. Cancer Res.* 23, 4280–4289. doi: 10.1158/1078-0432.CCR-16-2692

Dejonghe, W., and Russinova, E. (2017). Plant chemical genetics: from phenotype-based screens to synthetic biology. *Plant Physiol.* 174, 5–20. doi: 10.1104/pp.16.01805

Emi, T., Knoshita, T., Sakamoto, K., Mineyuki, Y., and Shimazaki, K.-I. (2005). Isolation of a protein interacting with Vfphot1a in guard cells of *Vicia faba*. *Plant Physiol.* 138, 1615–1626. doi: 10.1104/pp.104.052639

Hayashi, M., Inoue, S., Takahashi, K., and Kinoshita, T. (2011). Immunohistochemical detection of blue light-induced phosphorylation of the plasma membrane H^+-ATPase in stomatal guard cells. *Plant Cell Physiol.* 52, 1238–1248. doi: 10.1093/pcp/pcr072

Hayashi, M., Inoue, S., Ueno, Y., and Kinoshita, T. (2017). A Raf-like protein kinase BHP mediates blue light-dependent stomatal opening. *Sci. Rep.* 7:45586. doi: 10.1038/srep45586

Inoue, S., and Kinoshita, T. (2017). Blue light regulation of stomatal opening and the plasma membrane H^+-ATPase. *Plant Physiol.* 174, 531–538. doi: 10.1104/pp.17.00166

Inoue, S., Kinoshita, T., Matsumoto, M., Nakayama, K. I., Doi, M., and Shimazaki, K. (2008). Blue light-induced autophosphorylation of phototropin is a primary step for signaling. *Proc. Natl. Acad. Sci. U.S.A.* 105, 5626–5631. doi: 10.1073/pnas.0709189105

Joshi-Saha, A., Valon, C., and Leung, J. (2011). Abscisic acid signal off the STARting block. *Mol. Plant* 4, 562–580. doi: 10.1093/mp/ssr055

Kim, T. H., Bohmer, M., Hu, H., Nishimura, N., and Schroeder, J. I. (2010). Guard cell signal transduction network: advances in understanding abscisic acid, CO_2, and Ca^{2+} signaling. *Annu. Rev. Plant Biol.* 61, 561–591. doi: 10.1146/annurev-arplant-042809-112226

Kinoshita, T., Doi, M., Suetsugu, N., Kagawa, T., Wada, M., Shimazaki, K. (2001). phot1 and phot2 mediate blue light regulation of stomatal opening. *Nature* 414, 656–660. doi: 10.1038/414656a

Kinoshita, T., Emi, T., Tominaga, M., Sakamoto, K., Shigenaga, A., Doi, M., et al. (2003). Blue light- and phosphorylation-dependent binding of a 14-3-3 protein to phototropins in stomatal guard cells of broad bean. *Plant Physiol.* 133, 1453–1463. doi: 10.1104/pp.103.029629

Kinoshita, T., and Shimazaki, K. I. (1999). Blue light activates the plasma membrane H^+-ATPase by phosphorylation of the C-terminus in stomatal guard cells. *EMBO J.* 18, 5548–5558. doi: 10.1093/emboj/18.20.5548

Kinoshita, T., and Shimazaki, K. I. (2001). Analysis of the phosphorylation level in guard-cell plasma membrane H^+-ATPase in response to fusicoccin. *Plant Cell Physiol.* 42, 424–432. doi: 10.1093/pcp/pce055

Kinoshita, T., Toh, S., and Torii, K. U. (2021). Chemical control of stomatal function and development. *Curr. Opin. Plant Biol.* 60:102010. doi: 10.1016/j.pbi.2021.102010

Kleifeld, O., Kotra, L. P., Gervasi, D. C., Brown, S., Bernardo, M. M., Fridman, R., et al. (2001). X-ray absorption studies of human matrix metalloproteinase-2 (MMP-2) bound to a highly selective mechanism-based inhibitor. Comparison with the latent and active forms of the enzyme. *J. Biol. Chem.* 276, 17125–17131. doi: 10.1074/jbc.M011604200

Komander, D., Clague, M. J., and Urbé, S. (2009). Breaking the chains: structure and function of the deubiquitinases. *Nat. Rev. Mol. Cell Biol.* 10, 550–563. doi: 10.1038/nrm2731

Liu, S., Jia, Y., Zhu, Y., Zhou, Y., Shen, Y., Wei, J., et al. (2018). Soybean matrix metalloproteinase *Gm2-MMP* relates to growth and development and confers enhanced tolerance to high temperature and humidity stress in transgenic *Arabidopsis*. *Plant Mol. Biol. Rep.* 36, 94–106. doi: 10.1007/s11105-017-1065-8

Liu, S., Liu, Y., Jia, Y., Wei, J., Wang, S., Liu, X., et al. (2017). Gm1-*MMP* is involved in growth and development of leaf and seed, and enhances tolerance to high temperature and humidity stress in transgenic *Arabidopsis*. *Plant Sci.* 259, 48–61. doi: 10.1016/j.plantsci.2017.03.005

Liu, Y., Wang, F., Zhang, H., He, H., Ma, L., and Deng, X. W. (2008). Functional characterization of the *Arabidopsis ubiquitin-specific protease* gene family reveals specific role and redundancy of individual members in development. *Plant J.* 55, 844–856. doi: 10.1111/j.1365-313X.2008.03557.x

Ma, Y., Szostkiewicz, I., Korte, A., Moes, D., Yang, Y., Christmann, A., et al. (2009). Regulators of PP2C phosphatase activity function as abscisic acid sensors. *Science* 324, 1064–1068. doi: 10.1126/science.1172408

Maidment, J. M., Moore, D., Murphy, G. P., Murphy, G., and Clark, I. M. (1999). Matrix metalloproteinase homologues from *Arabidopsis thaliana*. Expression and activity. *J. Biol. Chem.* 274, 34706–34710. doi: 10.1074/jbc.274.49.34706

March, E., and Farrona, S. (2018). Plant deubiquitinases and their role in the control of gene expression through modification of histones. *Front. Plant Sci.* 8:2274. doi: 10.3389/fpls.2017.02274

Marino, G., and Funk, C. (2012). Matrix metalloproteinases in plants: a brief overview. *Physiol. Plant.* 145, 196–202. doi: 10.1111/j.1399-3054.2011.01544.x

Melotto, M., Zhang, L., Oblessuc, P. R., and He, S. Y. (2017). Stomatal defense a decade later. *Plant Physiol.* 174, 561–571. doi: 10.1104/pp.16.01853

Mistry, H., Hsieh, G., Buhrlage, S. J., Huang, M., Park, E., Cuny, G. D., et al. (2013). Small-molecule inhibitors of USP1 target ID1 degradation in leukemic cells. *Mol. Cancer Ther.* 12, 2651–2662. doi: 10.1158/1535-7163.MCT-13-0103-T

Munemasa, S., Hauser, F., Park, J., Waadt, R., Brandt, B., and Schroeder, J. I. (2015). Mechanisms of abscisic acid-mediated control of stomatal aperture. *Curr. Opin. Plant Biol.* 28, 154–162. doi: 10.1016/j.pbi.2015.10.010

Negi, J., Matsuda, O., Nagasawa, T., Oba, Y., Takahashi, H., Kawai-Yamada, M., et al. (2008). CO_2 regulator SLAC1 and its homologues are essential for anion homeostasis in plant cells. *Nature* 452, 483–486. doi: 10.1038/nature06720

Overall, C. M., and López-Otín, C. (2002). Strategies for MMP inhibition in cancer: innovations for the post-trial era. *Nature Rev. Cancer* 2, 657–672. doi: 10.1038/nrc884

Park, S. Y., Fung, P., Nishimura, N., Jensen, D. R., Fujii, H., Zhao, Y., et al. (2009). Abscisic acid inhibits type 2C protein phosphatases via the PYR/PYL family of START proteins. *Science* 324, 1068–1071. doi: 10.1126/science.1173041

Rawlings, N. D., Morton, F. R., and Barrett, A. J. (2006). MEROPS: the peptidase database. *Nucleic Acids Res.* 34, D270–D272. doi: 10.1093/nar/gkp971

Remacle, A. G., Golubkov, V. S., Shiryaev, S. A., Dahl, R., Stebbins, J. L., Chernov, A. V., et al. (2012). Novel MT1-MMP small-molecule inhibitors based on insights into hemopexin domain function in tumor growth. *Cancer Res.* 72, 2339–2349. doi: 10.1158/0008-5472.CAN-11-4149

Saito, S., and Uozumi, N. (2019). Guard cell membrane anion transport systems and their regulatory components: an elaborate mechanism controlling stress induced stomatal closure. *Plants* 8:9. doi: 10.3390/plants8010009

Santiago, J., Rodrigues, A., Saez, A., Rubio, S., Antoni, R., Dupeux, F., et al. (2009). Modulation of drought resistance by the abscisic acid receptor PYL5 through inhibition of clade A PP2Cs. *Plant J.* 60, 575–588. doi: 10.1111/j.1365-313X.2009.03981.x

Sato, A., Sato, Y., Fukao, Y., Fujiwara, M., Umezawa, T., Shinozaki, K., et al. (2009). Threonine at position 306 of the KAT1 potassium channel is essential for channel activity and is a target site for ABA-activated SnRK2/OST1/SnRK2.6 protein kinase. *Biochem. J.* 424, 439–448. doi: 10.1042/BJ20091221

Schroeder, J. I., Allen, G. J., Hugouvieux, V., Kwak, J. M., and Waner, D. (2001). Guard cell signal transduction. *Annu. Rev. Plant Physiol. Plant Mol. Biol.* 52, 627–658.

Schroeder, J. I., Raschke, K., and Neher, E. (1987). Voltage dependence of K^+ channels in guard-cell protoplasts. *Proc. Natl. Acad. Sci. U.S.A.* 84, 4108–4112. doi: 10.1073/pnas.84.12.4108

Shimazaki, K. I., Doi, M., Assmann, S. M., and Kinoshita, T. (2007). Light regulation of stomatal movement. *Annu. Rev. Plant Biol.* 58, 219–247. doi: 10.1146/annurev.arplant.57.032905.105434

Takemiya, A., Kinoshita, T., Asanuma, M., and Shimazaki, K. (2006). Protein phosphatase 1 positively regulates stomatal opening in response to blue light in *Vicia faba*. *Proc. Natl. Acad. Sci. U.S.A.* 103, 13549–13554. doi: 10.1073/pnas.0602503103

Takemiya, A., Sugiyama, N., Fujimoto, H., Tsutsumi, T., Yamauchi, S., Hiyama, A., et al. (2013). Phosphorylation of BLUS1 kinase by phototropins is a primary step in stomatal opening. *Nat. Commun.* 4:2094. doi: 10.1038/ncomms3094

Toda, Y., Toh, S., Bourdais, G., Robatzek, S., Maclean, D., and Kinoshita, T. (2018). DeepStomata: Facial recognition technology for automated stomatal aperture measurement. *BioRxiv* [preprint]. doi: 10.1101/365098

Toh, S., Inoue, S., Toda, Y., Yuki, T., Suzuki, K., Hamamoto, S., et al. (2018). Identification and characterization of compounds that affect stomatal movements. *Plant Cell Physiol.* 59, 1568–1580. doi: 10.1093/pcp/pcy061

Tomiyama, M., Inoue, S., Tsuzuki, T., Soda, M., Morimoto, S., Okigaki, Y., et al. (2014). Mg-chelatase I subunit 1 and Mg-Protoporphyrin IX methyltransferase affect the stomatal aperture in *Arabidopsis thaliana*. *J. Plant Res.* 127, 553–563. doi: 10.1007/s10265-014-0636-0

Vahisalu, T., Kollist, H., Wang, Y. F., Nishimura, N., Chan, W. Y., Valerio, G., et al. (2008). SLAC1 is required for plant guard cell S-type anion channel function in stomatal signalling. *Nature* 452, 487–491. doi: 10.1038/nature06608

Yan, N., Doelling, J. H., Falbel, T. G., Durski, A. M., and Vierstra, R. D. (2000). The ubiquitin-specific protease family from *Arabidopsis*. *At*UBP1 and 2 are

required for the resistance to the amino acid analog canavanine. *Plant Physiol.* 124, 1828–1843. doi: 10.1104/pp.124.4.1828

Ye, W., Munemasa, S., Shinya, T., Wu, W., Ma, T., Lu, J., et al. (2020). Stomatal immunity against fungal invasion comprises not only chitin-induced stomatal closure but also chitosan-induced guard cell death. *Proc. Natl. Acad. Sci. U.S.A.* 117, 20932–20942. doi: 10.1073/pnas.1922319117

Ye, W., and Murata, Y. (2016). Microbe associated molecular pattern signaling in guard cells. *Front. Plant Sci.* 7:583. doi: 10.3389/fpls.2016.00583

Zhao, J., Zhou, H., Zhang, M., Gao, Y., Li, L., Gao, Y., et al. (2016). Ubiquitin-specific protease 24 negatively regulates abscisic acid signalling in *Arabidopsis thaliana*. *Plant Cell Environ.* 39, 427–440. doi: 10.1111/pce.12628

Zhou, H., Zhao, J., Cai, J., and Patil, S. B. (2017). UBIQUITIN-SPECIFIC PROTEASES function in plant development and stress responses. *Plant Mol. Biol.* 94, 565–576. doi: 10.1007/s11103-017-0633-5

Conflict of Interest: The authors declare that the research was conducted in the absence of any commercial or financial relationships that could be construed as a potential conflict of interest.

Publisher's Note: All claims expressed in this article are solely those of the authors and do not necessarily represent those of their affiliated organizations, or those of the publisher, the editors and the reviewers. Any product that may be evaluated in this article, or claim that may be made by its manufacturer, is not guaranteed or endorsed by the publisher.

frontiers in Plant Science

ORIGINAL RESEARCH
published: 21 September 2021
doi: 10.3389/fpls.2021.748543

Expression Pattern and Functional Analyses of *Arabidopsis* Guard Cell-Enriched GDSL Lipases

*Chuanlei Xiao[1], Huimin Guo[1], Jing Tang[1], Jiaying Li[1], Xuan Yao[2] and Honghong Hu[1]**

[1]National Key Laboratory of Crop Genetic Improvement, College of Life Science and Technology, Huazhong Agricultural University, Wuhan, China, [2]College of Plant Science and Technology, Huazhong Agricultural University, Wuhan, China

There are more than 100 GDSL lipases in *Arabidopsis*, but only a few members have been functionally investigated. Moreover, no reports have ever given a comprehensive analysis of GDSLs in stomatal biology. Here, we systematically investigated the expression patterns of 19 putative *Guard-cell-enriched GDSL Lipases* (*GGLs*) at various developmental stages and in response to hormone and abiotic stress treatments. Gene expression analyses showed that these *GGLs* had diverse expression patterns. Fifteen *GGLs* were highly expressed in guard cells, with seven preferentially in guard cells. Most GGLs were localized in endoplasmic reticulum, and some were also localized in lipid droplets and nucleus. Some closely homologous *GGLs* exhibited similar expression patterns at various tissues and in response to hormone and abiotic stresses, or similar subcellular localization, suggesting the correlation of expression pattern and biological function, and the functional redundancy of *GGLs* in plant development and environmental adaptations. Further phenotypic identification of *ggl* mutants revealed that *GGL7*, *GGL14*, *GGL22*, and *GGL26* played unique and redundant roles in stomatal dynamics, stomatal density and morphology, and plant water relation. The present study provides unique resources for functional insights into these GGLs to control stomatal dynamics and development, plant growth, and adaptation to the environment.

Keywords: Arabidopsis, drought tolerance, expression pattern, guard cells, GDSL lipases, stomatal density, stomatal dynamics, subcellular localization

OPEN ACCESS

Edited by:
Juan Dong,
Rutgers, The State University of New Jersey, United States

Reviewed by:
Yintong Chen,
The Pennsylvania State University (PSU), United States
Xiaoyu Guo,
Rutgers, The State University of New Jersey - Busch Campus, United States

****Correspondence:***
Honghong Hu
huhh@mail.hzau.edu.cn

Specialty section:
This article was submitted to Plant Physiology, a section of the journal Plant Science

Received: *28 July 2021*
Accepted: *18 August 2021*
Published: *21 September 2021*

Citation:
Xiao C, Guo H, Tang J, Li J, Yao X and Hu H (2021) Expression Pattern and Functional Analyses of Arabidopsis Guard Cell-Enriched GDSL Lipases. Front. Plant Sci. 12:748543. doi: 10.3389/fpls.2021.748543

INTRODUCTION

GDSL lipases or esterases (EC 3.1.1.3) are lipid hydrolases with a GDSL motif at the N-terminus. GDSLs have four invariant important catalytic residues: Ser, Gly, Asn, and His in blocks I, II, III, and V, respectively (Akoh et al., 2004). GDSLs widely exist in prokaryotes and eukaryotes. In plants, it exists as a big family with many members, more than 100 members in *Arabidopsis* (Ling, 2008; Dong et al., 2016; Lai et al., 2017; Su et al., 2020), 114 members in rice (Chepyshko et al., 2012), 121 in *Brassica rapa* (Dong et al., 2016), and 194 in soybean (Su et al., 2020). However, only a few members have been identified in each plant species with their broad biological functions and substrates.

GDSLs play roles in plant growth and organ development. *Arabidopsis* EXL4 (EXTRACELLULAR LIPASE 4) is required for pollen on stigma to hydrate efficiently. Loss function of *EXL4* led

to the delayed and reduced rate of pollen hydration (Mayfield et al., 2001; Updegraff et al., 2009). CDEF1 (CUTICLE DESTRUCTING FACTOR 1) acts as a cutinase, which directly degrades the polyester in the cuticle of stigma and mediates pollen tube penetration into the stigma (Takahashi et al., 2010). Tomato GDSL1 plays a specific role in cutin polyester deposition in the tomato fruit cuticle (Girard et al., 2012), and CD1 is required for cutin accumulation by catalyzing 2-MHG *in vivo* and catalyzes the formation of primarily linear cutin oligomers *in vitro* (Yeats et al., 2012, 2014). Two rice GDSLs, BS1 (Brittle Leaf Sheath 1) and DARX1 (DEACETYLASE ON ARABINOSYL SIDECHAIN OF XYLAN 1), are identified as deacetylases that are crucial for secondary wall formation and patterning. BS1 cleaves acetyl moieties from xylopyranosyl residues (Zhang et al., 2017a), and DARX1 specifically deacetylates the side chain of the major rice hemicellulose, arabinoxylan (Zhang et al., 2019). *ZmMs30*, a maize genic male sterility gene, regulates male fertility by modulating cuticle deposition on anthers (An et al., 2019). OsGELP34, OsGELP110, and OsGELP115 control male fertility by regulating exine formation (Zhang et al., 2020). BnSCE3 serves as a sinapine esterase that controls seed weight, size, and water content (Ling et al., 2006; Clauss et al., 2008, 2011).

GDSLs regulate plant adaptation to biotic and abiotic stresses. *Arabidopsis* GDSL LIPASE1 (GLIP1) is a critical component in plant resistance to several bacterial and fungal pathogens, directly disrupting fungal spore integrity and inhibiting its germination (Oh et al., 2005; Kwon et al., 2009). Pepper GLIP1 plays as a negative regulator in resistance to *Xanthomonas campestris pv. vesicatoria* (Xcv) (Hong et al., 2008). Rice GLIP1 and GLIP2 act as negative regulators of disease resistance to bacterial and fungal pathogens by changing the levels of DGDG and MGDG (Gao et al., 2017). *Arabidopsis* Li-tolerant lipase 1 (AtLTL1) increases salt tolerance of *Arabidopsis* and LiCl tolerance of yeast (Naranjo et al., 2006). Rice WDL1 (Wilted Dwarf and Lethal 1) mediates water loss by regulating wax synthesis (Park et al., 2010). Our recent research has shown that *Arabidopsis* OSP1 (Occlusion of Stomatal Pore 1) confers drought tolerance through the control of wax biosynthesis, stomatal outer cuticular ledge formation, and stomatal density (Tang et al., 2020). However, the functions of most GDSLs are unexplored.

GDSL lipase has a flexible active site (Akoh et al., 2004), which leads to catalytic activity on different substrates by changing conformations. Due to this changeable structure feature, isolation and characterization of GDSL substrates is a big challenge. For example, a bread wheat (*Triticum aestivum*) xanthophyll acyltransferase (XAT) has broad substrate specificity. XAT can esterify lutein, β-cryptoxanthin, and zeaxanthin (Watkins et al., 2019). Tremendously functional redundancy and tandem duplications in chromosomes could be other challenges to identify the biological functions of GDSLs (Lai et al., 2017). Their functions may only be determined when higher-order mutants are generated by crossing, CRISPR/Cas9 gene editing, or artificial microRNA technologies (Feng et al., 2013; Hauser et al., 2013; Miao et al., 2013). Therefore, detailed expression patterns are critical for characterizing the functions of GDSL lipases in plant development, plant growth, and adaptation to the environment.

Stomata are pores formed by pairs of guard cells in the surface of aerial parts of most higher plants, which respond quickly to the environmental changes by opening or closing the pores. It has been suggested that manipulation of stomatal development and behavior is a good strategy for improving plant abiotic and biotic tolerance (Hughes et al., 2017; Dunn et al., 2019; Papanatsiou et al., 2019; Huang et al., 2021). GDSLs exist as a big family, but only OSP1 has been identified with essential roles in stomata (Tang et al., 2020). Therefore, it is very important to identify GDSLs that function in stomata. In this study, we identified 29 predicted *GGLs* (*Guard-cell-enriched GDSL Lipases*) from microarray data and determined the temporal–spatial expression patterns of 19 *GGLs* by driving the *GUS* reporter gene in *Arabidopsis*. We also explored their cellular localizations by transient expression of GFP or YFP fused GGLs in *Nicotiana benthamiana*. Furthermore, we investigated the roles of six guard cell preferentially expressed *GGLs* in stomatal biology and plant water maintenance. Our data provide unique resources for the future investigation of the roles of *GGLs* in controlling stomatal dynamics and stomatal development, plant growth, and adaptation to the environment.

MATERIALS AND METHODS

Plant Materials and Growth Conditions

Arabidopsis (*Arabidopsis thaliana*) accession Col-0 and *N. benthamiana* plants were used in this study. The single T-DNA insertion mutants, *ggl7* (CS393512), *ggl12* (SALK_024323C), *ggl14* (SALK_106116C), *ggl22* (SALK_062226C), *ggl23* (CS874407), *ggl26* (SALK_116756), and *ggl27* (CS857064), were obtained from the Arabidopsis Biological Resource Center (ABRC). The *Arabidopsis* plants and *N. benthamiana* were grown in a well-controlled growth chamber or a greenhouse at 22°C with a 16 h light/8 h dark regime.

Plasmid Construction

To generate the promoter::*GUS* expression vectors, we cloned 1.5–2 kb promoter regions (DNA fragment upstream of the ATG start codon) into the expression vector *pLP100* or *pMDC163* (Szabados et al., 1995; Charrier et al., 1996; Curtis and Grossniklaus, 2003). All promoter sequences were confirmed by DNA sequencing, and the primers used are listed in **Supplementary Table S2**.

To investigate the subcellular localization of the predicted GGLs, we amplified the open reading frames of GGLs from cDNA of Col-0 seedlings using gene-specific primers (**Supplementary Table S2**). PCR products were cloned into the Gateway-compatible donor vector *pDONR207* by BP recombination reactions to generate entry clones and confirmed by DNA sequencing. Subsequently, the positive entry clones were further cloned into the destination vector *pGWB541* or *BarII-pUBQ10-GWB-GFP* (Walter et al., 2004; Nakagawa et al., 2007) by LR recombination reactions.

Generation of Transgenic Plants and GUS Staining

The generated *GGL*pro::*GUS* constructs were transformed into Col-0 plants by flower dipping method (Zhang et al., 2006). Transgenic plants were screened by Kanamycin or Hygromycin B. Positive transgenic plants were further confirmed by detecting the existence of the *GUS* reporter gene. The transgenic seedlings of 1.5 days after germination (DAG), 6 DAG, and 14 DAG growing on 1/2 Murashige and Skoog medium supplemented with 1% sucrose and 0.3% phytagel were used for GUS staining. The representative lines showing consistent GUS staining were further analyzed for GUS staining at the reproductive stage (34 DAG). At least three independent transgenic lines were analyzed in parallel.

The seedlings or tissues were immersed in GUS solution buffer [1 mg/ml X-Gluc, 5 mM $K_3Fe(CN)_6$, 5 mM $K_4Fe(CN)_6{\cdot}3H_2O$, 0.042 M $NaH_2PO_4{\cdot}2H_2O$, 0.058 M $Na_2HPO_4{\cdot}12H_2O$, 0.1 mM Na_2EDTA (pH = 8.0), and 1% (v/v) Triton X-100], and incubated overnight at 37°C. After staining, the seedlings and tissues were de-stained in 75% ethanol several times for GUS observation under a microscope.

Subcellular Localization

The constructs of *UBQ10-GGL-GFP* or *35S-GGL-YFP* were transformed into the *Agrobacterium* strain GV3101, and the strains were infiltrated into *N. benthamiana* leaf epidermis. Protoplasts of infiltrated tobacco leaves were prepared as described previously (Walter et al., 2004). Images were obtained by a confocal microscope (TCS-SP8; Leica, Weztlar, Germany) with a 40× water-immersion objective in the sequential scan, between frames mode. For localization in ER, an ER-marker HDEL-OFP (orange fluorescent protein; excitation at 561 nm, emission range is 580 nm to 630 nm) was coexpressed for co-localization. Nile Red staining was performed for localization in lipid droplets, as described in our previous publication (Tang et al., 2020).

To confirm the subcellular localization of GGL13, GGL17, and GGL27 in *Arabidopsis*, GGL13-GFP, GGL17-GFP, or GGL27-GFP was transformed into *Arabidopsis* mesophyll protoplasts with HDEL-OFP (Yoo et al., 2007), respectively. The GFP and OFP signals of protoplasts were recorded 10–12 h after transformation under a confocal microscope (TCS-SP8; Leica, Weztlar, Germany).

Transpiration Rate, Water Use Efficiency, and Stomatal Conductance Analyses

Transpiration rate was determined on rosette leaves of 4-week-old plants using a portable photosynthesis system (LI-6400XT; Li-Cor). The measurement conditions were 150 μmol m^{-2} s^{-1} light intensity, 50–60% relative humidity, and 450 ppm CO_2. Measurements were recorded every 30 s and lasted for 20 min. Data presented are the average value of 10 min for individual plants (at least four plants per genotype) for each experiment. Instantaneous water use efficiency (WUE) was defined as the ratio of CO_2 assimilated to water loss during transpiration (μmol CO_2 mmol H_2O^{-1}). WUE was calculated using the data collected during transpiration rate measurement. The corresponding time points (10 min) were chosen for each plant. Experiments were repeated at least three times.

For stomatal conductance in response to dark-to-light (150 μmol m^{-2} s^{-1} with 10% blue light) transitions, intact leaves of 4 to 5-week-old well-growing plants were measured by a portable gas exchange analyzer (LI-6400XT; Li-Cor). According to the previous publication (Hu et al., 2010), the initial rate of stomatal conductance changes in response to dark-to-light transitions was calculated.

Stomatal Density and Stomatal Morphology Analyses

The seventh or eighth (including cotyledons) rosette leaves of 4-week-old plants were analyzed for stomatal density and index, stomatal pore width and pore ratio (width: length), and stomatal complex length and width. All plants were grown in a well-controlled growth room at 22°C, with 56% humidity and a 16 h light/8 h dark photoperiod regime with 80 μmol m^{-2} s^{-1} light intensity. The central areas derived from the leaf abaxial epidermal layer were imaged using a light microscope (TS100, Nikon, Japan). Stomata and pavement cell numbers were counted with ImageJ software. Stomatal pore width and length, and stomatal complex length and width were measured with ImageJ software. Experiments were repeated three times.

Stress Treatment, RT-PCR, and Real-Time Quantitative PCR Analyses

For different hormone treatments, 7-day-old seedlings growing on 1/2 MS plates were treated with different phytohormones, including 10 μM ABA (abscisic acid), 10 nM BL (brassinolide), 1 μM GA (gibberellin), 1 μM IAA (indoleacetic acid), and solvent (as control). The seedlings were harvested at 0, 0.5, 1, and 3 h after treatments, respectively. For salt stress, 4-week-old plants were treated (watered) with 150 mM NaCl, and the leaf samples were harvested at the time points of 0, 0.5, 1, 3, 6, 12, and 24 h. For dehydration treatment, rosette leaves were detached from 4-week-old plants and dehydrated under the laboratory conditions. The samples were harvested at the time points of 0, 0.25, 0.5, 1, 3, 6, and 12 h after leaf detachments. Total RNA was extracted from 50 to 100 mg of sample tissues using TRIZOL Reagent (Invitrogen). After DNase treatment, the first-strand cDNA was synthesized from 2 μg of RNA using oligo (dT) primers with M-MLV reverse transcriptase (Promega). For RT-PCR analyses, 100 ng cDNA was used as templates for amplification of *Actin7* and *GGLs*. 30–32 cycles were amplified. Primers used for RT-PCR are listed in **Supplementary Table S2**.

Real-time quantitative PCR was performed with the Bio-Rad CFX96™ Real-Time System using SYBR (Vazyme) to monitor double-stranded DNA products. *EFα* was used as an internal control. The relative gene expression during different treatments was calculated by comparison with that of the samples at 0 h, which was defined as 1. Bio-Rad CFX manager software was used for analysis. Primers used for real-time quantitative PCR are listed in **Supplementary Table S2**.

Drought Stress Assay

Plants (each pot containing 25 plants with the same weight of soil and the same water content) were grown in well-watered conditions for 3 weeks. Then, water was withdrawn for 8–10 days until significant differences in the wilted leaves were observed and re-supplied for 2 days. Photographs of the plants at these three time points were taken.

RESULTS

Identification of *GDSLs* Enriched in *Arabidopsis* Guard Cells

To gain insights into the GDSLs that function in stomatal biology, we focused on the guard cell highly expressed *GDSLs* in the *Arabidopsis* genome. Firstly, we extracted the expression data of all putative *GDSL* genes from the microarray data of guard cell and mesophyll cell protoplasts with or without ABA treatment published by Leonhardt et al. (2004) and drew a heat map with TBtools (Chen et al., 2020). The results showed that 29 *GDSLs* belonging to a large clade (L) and a small one (S) had relatively higher expression levels in guard cell protoplasts (**Figure 1**). We then named these *GDSLs* as *GGLs* (*Guard-cell-enriched GDSL Lipases*). Among these 29 *GGLs*, the expression levels of *GGL2* (AT1G28600), *GGL3* (AT1G28610), *GGL15* (AT2G24560), and *GGL28* (AT5G45950) in guard cell protoplasts were upregulated by ABA treatment, while those of another four *GGLs*, *GGL4* (AT1G28660), *GGL10* (AT1G54030), *GGL11* (AT1G67830), and *GGL18* (AT3G14220), were slightly repressed by ABA treatment (**Figure 1**). The remaining *GGLs* were not affected by ABA treatment in guard cell protoplasts (**Figure 1**). Moreover, the expression levels of *GGLs* in L clade were generally higher than those in S clade, and 19 *GGLs* from the L clade were preferentially expressed in guard cells than those in mesophyll cells (**Figure 1**).

We then analyzed the distribution of these *GGLs* on chromosomes by Chromosome Map Tool.[1] These *GGLs* were distributed on all chromosomes. Thirteen *GGLs* were located on chromosome 1, 6 on chromosome 3, 3 on chromosome 4, and 5 on chromosome 5, whereas only two were located on chromosome 2 (**Supplementary Figure S1**). Furthermore, there were cases of two or more *GGLs* arranged in tandem, on the middle and bottom of chromosome 1 (**Supplementary Figure S1**). For example, *GGL1*, *GGL2*, and *GGL3* were tandem duplicated (**Supplementary Figure S1**). Given that tandem repeated genes often show functional redundancy (Tantikanjana et al., 2004; Su et al., 2013), we speculate that tandem repeated *GGLs* might have functional redundancy.

Tissue-Specific Expression Patterns of *GGLs* at the Seedling Stage

To confirm that these predicted *GGLs* in L clade are highly expressed in guard cells, we cloned the regions of 1.5–2.0 kb of DNA fragments upstream of the start codon (ATG) for these 19 *GGLs* (marked in blue fonts in **Figure 1**) as native promoters into the expression vector *pLP100* or *pMDC163* to drive the expression of *GUS* reporter gene (**Figure 2A**). These 1.5–2.0 kb regions should have contained enough regulatory elements to drive the expression of most *Arabidopsis* genes (Korkuæ et al., 2014; Wu et al., 2016). All these constructs were transformed into the wild-type *Arabidopsis* Col-0 accession.

We performed GUS staining of transgenic plants expressing *GGL*pro::*GUS* in different tissues at different developmental stages. At least three independent transgenic lines were used for analyses, and only those lines showing the most consistent patterns were photographed. At 1.5 DAG (Days After Germination), 16 *GGLs* were highly expressed in the emerged cotyledons or hypocotyls, whereas *GGL12*, *GGL20*, and *GGL25* had very weak expressions (**Figure 2B**). Seventeen from 19 *GGLs*, except *GGL20* and *GGL21*, were expressed in the 6-DAG seedlings (**Figure 2B**). Ten members (*GGL6*, *GGL8*, *GGL9*, *GGL13*, *GGL16*, *GGL19*, *GGL22*, *GGL23*, *GGL26*, and *GGL29*) were highly expressed in cotyledons, and nine members (*GGL6*, *GGL8*, *GGL9*, *GGL13*, *GGL16*, *GGL19*, *GGL22*, *GGL23*, and *GGL27*) showed evident expressions in roots (**Figure 2B**). Interestingly, 7 *GGLs* (*GGL7*, *GGL12*, *GGL14*, *GGL17*, *GGL23*, *GGL26*, and *GGL27*) were preferentially expressed in guard cells (**Figure 2B**), indicating that they may function in stomata. Eight *GGLs* (*GGL6*, *GGL8*, *GGL9*, *GGL13*, *GGL16*, *GGL19*, *GGL22*, and *GGL29*) were expressed not only in cotyledon guard cells but also in pavement or mesophyll cells (**Figure 2B**), suggesting their potential roles in other physiological processes in addition to stomatal biology.

To confirm that these *GGLs* are expressed in the guard cells of true leaves, we further determined their expression patterns in the true leaves of 14-DAG seedlings. Consistent with their expression patterns in cotyledons (**Figure 2B**), the same 15 *GGLs* were expressed in the guard cells of true leaves (**Figure 3**). Seven *GGLs* (*GGL7*, *GGL12*, *GGL14*, *GGL17*, *GGL23*, *GGL26*, and *GGL27*) were preferentially expressed in the true leaf guard cells, and eight members (*GGL6*, *GGL8*, *GGL9*, *GGL13*, *GGL16*, *GGL19*, *GGL22*, and *GGL29*) also showed evident expressions in pavement or mesophyll cells in addition to guard cells (**Figure 3**). Moreover, five *GGLs* (*GGL5*, *GGL14*, *GGL17*, *GGL19*, and *GGL23*) were also expressed in trichomes (**Figure 3** and **Supplementary Figure S2**), and seven *GGLs* (*GGL6*, *GGL8*, *GGL9*, *GGL13*, *GGL16*, *GGL22*, and *GGL29*) were expressed in the vascular tissues (**Figure 3**), indicating that these GGLs may also be involved in trichome and vascular tissue development.

Tissue-Specific Expression Patterns of *GGLs* at the Reproductive Tissues

We next determined the expression patterns of these *GGLs* at the reproductive stage. Among 19 *GGLs*, 18 (except *GGL20*) were expressed in the inflorescence of 34-DAG *Arabidopsis* plants (**Figure 4**). *GGL7*, *GGL26*, and *GGL27* were preferentially expressed in guard cells on sepals (**Figure 4**). *GGL6*, *GGL8*, *GGL9*, *GGL13*, *GGL14*, *GGL22*, and *GGL29* showed very similar expression patterns, with strong expressions in filaments, sepals,

[1]https://www.arabidopsis.org/jsp/ChromosomeMap/tool.jsp

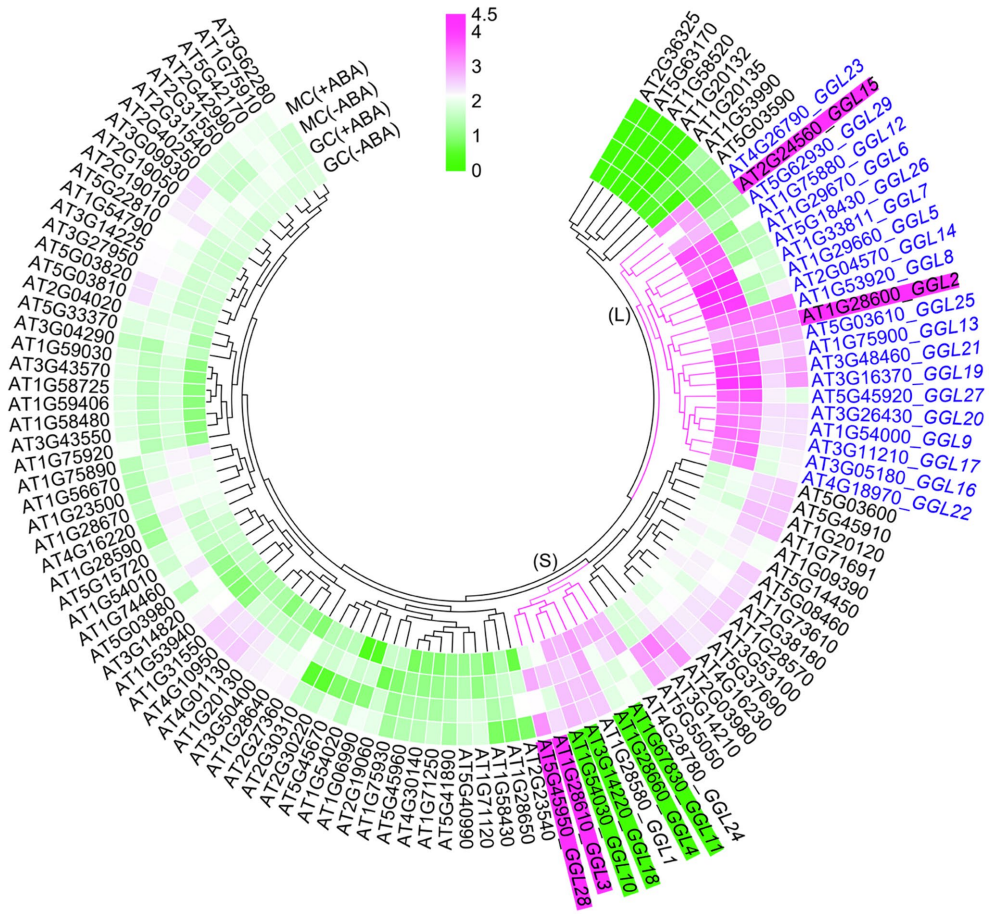

FIGURE 1 | Identification of *GGLs* in *Arabidopsis*. Expression levels of *Arabidopsis GDSLs* in guard cell and mesophyll cell protoplasts in response to ABA or not. ATH1 microarray data of all *Arabidopsis GDSLs* in guard cell (GC) and mesophyll cell (MC) protoplasts treated with ABA or not were obtained from Leonhardt et al. (2004) and Yang et al. (2008). Putative *GDSLs* were merged from Dong et al. (2016) and Lai et al. (2017). The heat map was constructed by TBtools (Chen et al., 2020), and the color code of signal intensities corresponds to the abundance of transcripts, from low (green) to high (magenta) expression. *GGL* means *Guard-cell-enriched GDSL Lipase*. (L) and (S) indicate the large and small clades, respectively. Nineteen *GGLs* in L clade were shown in blue fonts. The *GGLs* highlighted in magenta or green indicated the *GGLs* in guard cell protoplasts induced or repressed by ABA treatment, respectively.

and apex of stigma (**Figure 4**), suggesting that these GGLs may be involved in flower development or fertility. The remaining *GGLs* had relatively narrow expression patterns. *GGL5* was expressed in the apex and base of stigma, *GGL16* and *GGL17* were expressed in sepals and apex of stigma, and *GGL19* was expressed in filaments and sepals (**Figure 4**). Moreover, *GGL14* and *GGL16* were also expressed in anthers. We also found that seven *GGLs* (*GGL12*, *GGL16*, *GGL17*, *GGL19*, *GGL23*, *GGL26*, and *GGL27*) were expressed in the whole siliques, and eight *GGLs* (*GGL5*, *GGL6*, *GGL8*, *GGL9*, *GGL13*, *GGL14*, *GGL22*, and *GGL29*) were expressed only in both ends of siliques (**Figure 4**).

Subcellular Localization Analyses of *GGLs* in *N. benthamiana*

Several GDSLs have been reported to be secreted into the intercellular space; signal peptide prediction using SignalP 4.1 Server[2] revealed that 14 of 19 GGLs possessed a signal peptide at N-terminus (**Supplementary Table S1**). To gain insights into which organelles GGLs are localized in plant cells, we investigated the subcellular localization of 13 GGLs tagged by GFP or YFP under the control of the cauliflower mosaic virus (*CaMV*) *35S* promoter by transient expression in *N. benthamiana* leaf epidermis, a convenient system to study protein intracellular localization (Deeks et al., 2012). Our results showed that most C-terminal GFP- or YFP-tagged GGL proteins were co-localized, at least partially, with the endoplasmic reticulum (ER) marker HDEL-OFP (**Supplementary Figure S3A**). To further confirm that these GGLs are localized in ER, we observed their localizations in the isolated protoplasts. Nine of thirteen GGLs (GGL5, GGL8, GGL13, GGL14, GGL16, GGL17, GGL20, GGL27, and GGL29) were well overlapped

[2]http://www.cbs.dtu.dk/services/SignalP/

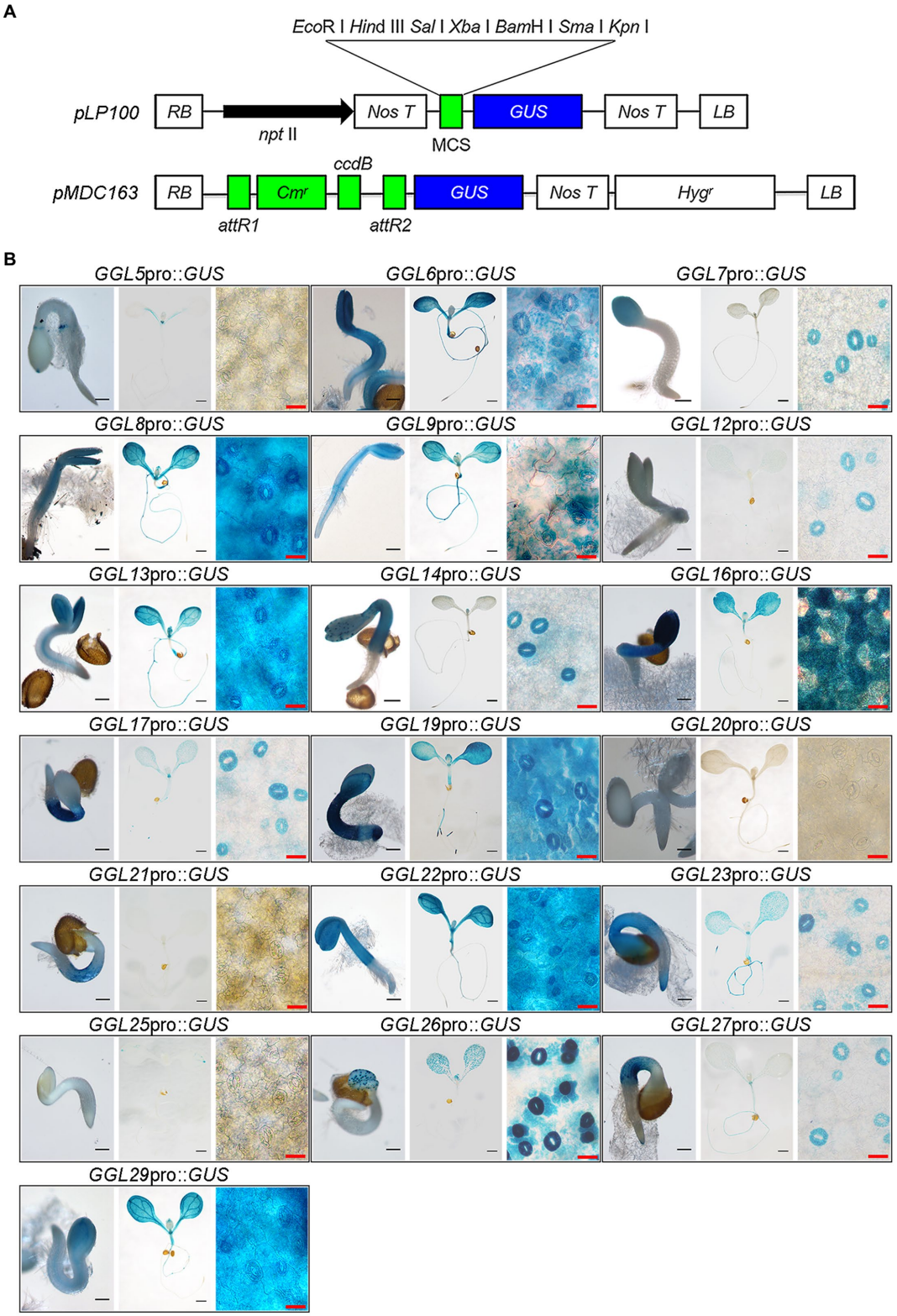

FIGURE 2 | Expression patterns of 19 *GGLs* at the early seedling stage. **(A)** Schematic charts of two destination vectors (*pLP100* and *pMDC163*) used for *GUS* expression driven by *GGL* native promoters. **(B)** Expression profile analyses of 19 *GGLs* at the early seedling stage. *GGL*pro::*GUS* expressing transgenic seedlings that grown in a growth chamber were stained with X-Gluc. For each gene, the images from left to right represent a seedling of 1.5 days after germination (DAG; scale bar = 200 μm), a seedling of 6 DAG (scale bar = 1 mm), and an enlarged part of the cotyledon from the 6-DAG seedling (scale bar = 25 μm), respectively.

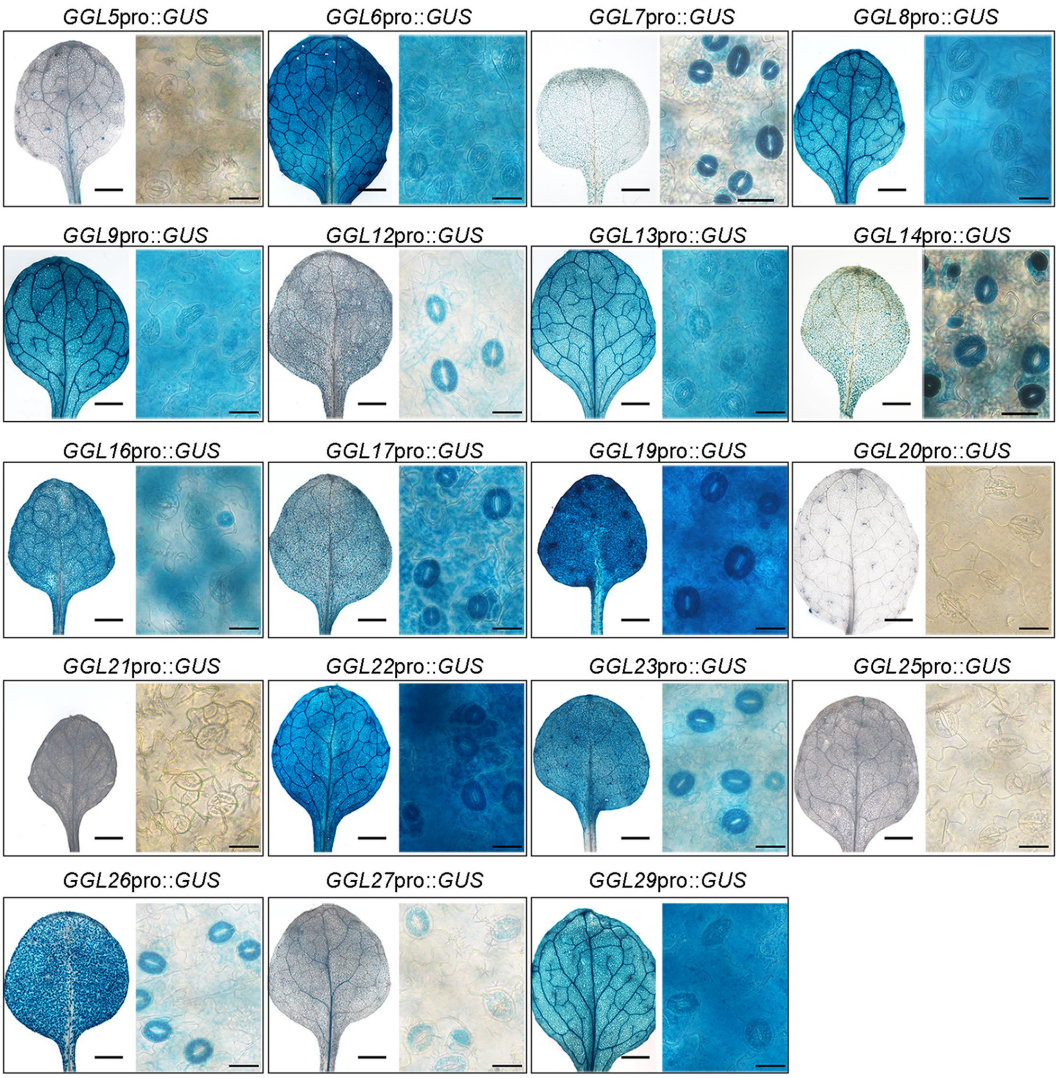

FIGURE 3 | Expression profiles of 19 *GGLs* in 14-DAG true leaves. The true leaves of 14-DAG *GGL*pro::*GUS* expressing seedlings were stained with X-Gluc. For each gene, the images from left to right represent a true leaf from a 14-DAG seedling (scale bar = 1 mm) and an enlarged part of it (scale bar = 25 μm).

with HDEL-OFP (**Figure 5A**), demonstrating that these GGLs are localized in ER. Among nine ER-localized GGLs, three GGLs (GGL5, GGL13, and GGL14) also appeared as punctate localization in the cytoplasm (**Figure 5A**). We speculated that these vesicle structures were lipid droplets, and GGL5 and GGL13 could be dual localization proteins in both ER and lipid droplets as GGL14 (also named OSP1) did (Tang et al., 2020). Therefore, we performed co-localization of GGL5, GGL13, or GGL14 with OsGLIP1-CFP, a protein reported to localize in lipid droplets and ER (Gao et al., 2017), respectively. GGL5, GGL13, and GGL14 overlapped with OsGLIP1-CFP in the vesicle structures and ER networks (**Figure 5B**), suggesting that GGL5, GGL13, and GGL14 may also play roles in lipid homeostasis. GGL6 and GGL9 appeared in the vesicle structures in tobacco epidermal cells (**Supplementary Figure S3B**), and lipophilic Nile Red staining showed that these vesicle structures were lipid droplets (**Figure 5C**). Moreover, GGL9, GGL17, GGL27, and GGL29 were also localized in nucleus (**Figures 5A,C** and **Supplementary Figure S3**). We further validated the subcellular localization of three GGLs in *Arabidopsis* mesophyll protoplasts. The results showed that GGL13, GGL17, and GGL27 overlapped well with HDEL-OFP (**Supplementary Figure S3C**), consistent with their localizations in *N. benthamiana* leaf epidermis (**Figure 5A**). These results suggest that subcellular localization of these *Arabidopsis* GGLs in *N. benthamiana* leaf epidermis by our system is suitable and reliable.

Phylogenetic Relationship and Exon-Intron Structures of *GGLs* in *Arabidopsis*

To investigate the evolutionary relationship between these 19 GGL proteins, we constructed a maximum likelihood

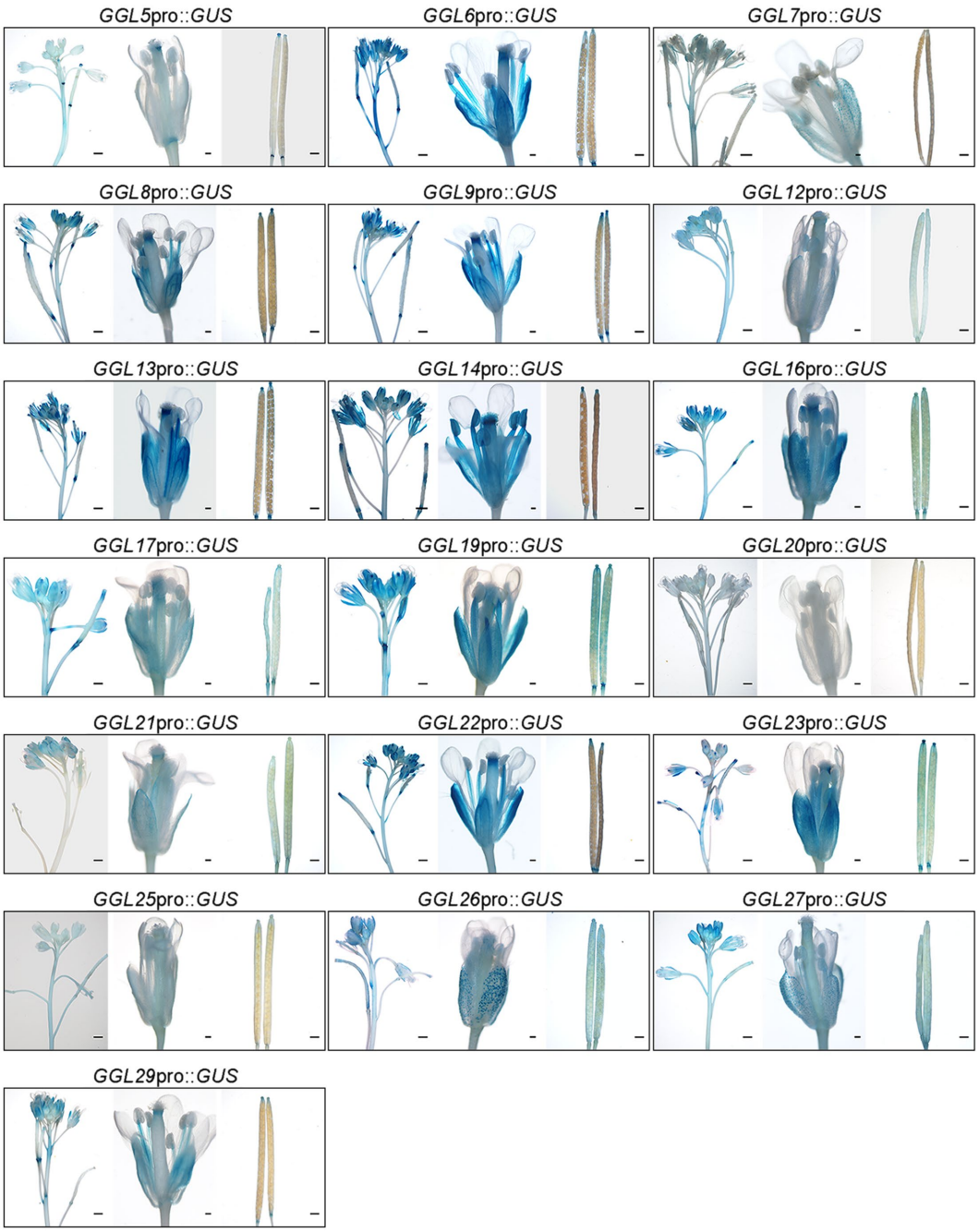

FIGURE 4 | Expression patterns of 19 *GGLs* at reproductive stage. The tissues from 34-DAG *GGL*pro::*GUS* expressing plants were stained with X-Gluc. For each gene, the images from left to right represent an inflorescence from a 34-DAG plant (scale bar = 100 μm), a mature flower from a 34-DAG plant (scale bar = 1 mm), and mature siliques from a 34-DAG plant (scale bar = 100 μm), respectively.

tree using GGL protein sequences (**Supplementary Figure S4**). GGL5 showed a close relationship with GGL6, GGL7, and GGL22 (**Supplementary Figure S4**). GGL14 and GGL23, GGL12 and GGL13, and GGL16 and GGL20 were highly homologous proteins, respectively (**Supplementary Figure S4**). GGL17 exhibited a close relationship with GGL27 and GGL29 (**Supplementary Figure S4**). Some closely homologous GGLs, such as GGL5 and GGL6, and GGL12 and GGL13, were found to be arranged in tandem on chromosomes (**Supplementary Figure S1**). These closely related GGLs are mostly expressed in guard cells, indicating that they may function redundantly in stomatal biology.

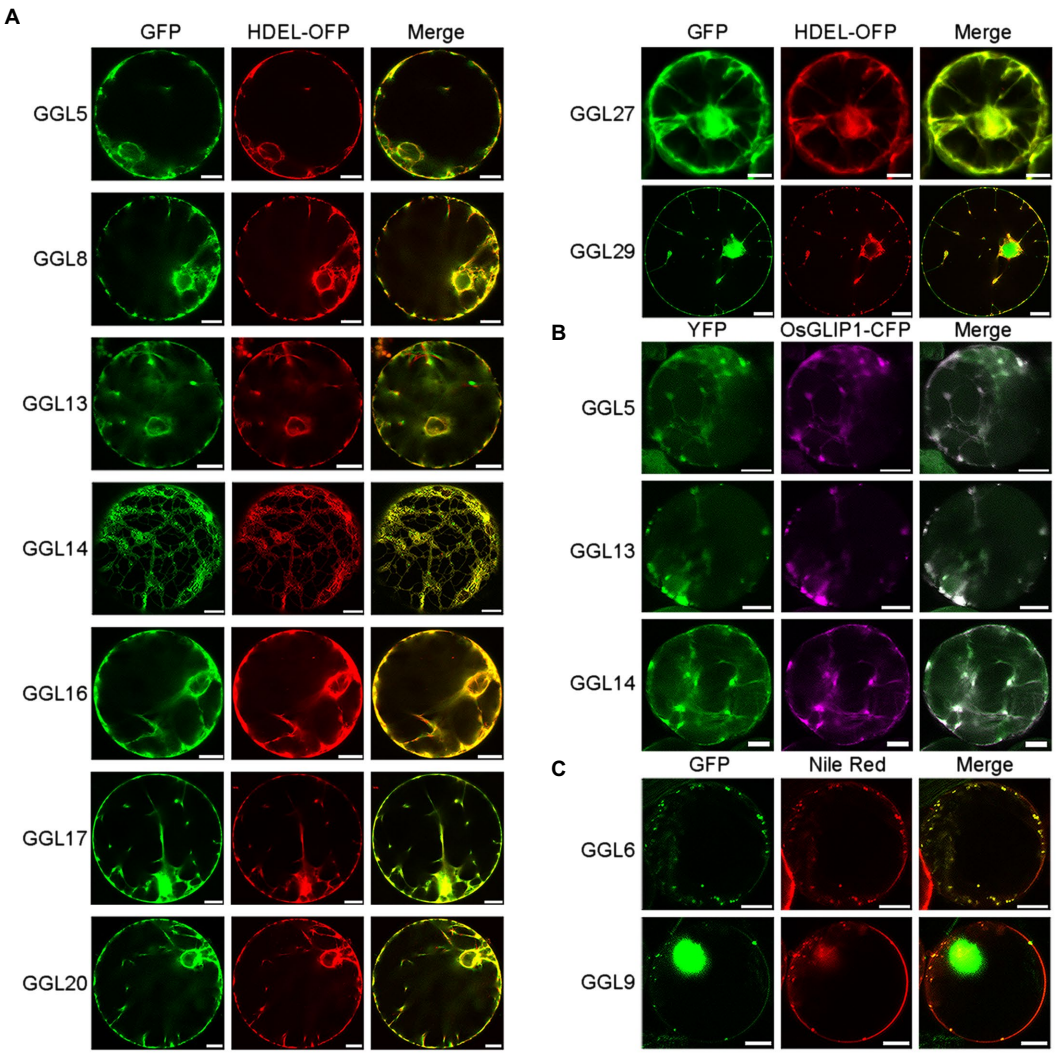

FIGURE 5 | Subcellular localization of GGLs in protoplasts of *Nicotiana benthamiana* leaves. Subcellular localization of C-terminal GFP or YFP fused GGL proteins in *N. benthamiana* protoplasts **(A-C)**. C-terminal GFP or YFP fused GGL proteins under the control of the *CaMV 35S* promoter were transiently expressed in *N. benthamiana* leaf epidermal cells. GFP or YFP signals in the isolated protoplasts were imaged by a confocal microscope. HDEL-OFP was coexpressed with GGLs to indicate endoplasmic reticulum localization **(A)**. Lipid droplet localization of GGLs was confirmed by co-localization with OsGLIP1-CFP (Gao et al., 2017) **(B)** or Nile Red staining **(C)**. Scale bar = 10 μm.

We next analyzed the exon and intron structures of these 19 *GGLs* based on exon assignment information from the TAIR Web site.[3] Among these *GGLs*, only *GGL12*, *GGL22*, and *GGL23* have two transcripts, and the others all have only one transcript (**Supplementary Figure S4**). Most *GGLs* contain five exons. *GGL14*, *GGL21*, and *GGL23* have three exons, and *GGL9* has four exons, whereas *GGL7*, *GGL17*, and *GGL22.2* have six exons (**Supplementary Figure S4**). We surprisingly found that *GGL20* was a unique one, which possessed a long 5′ untranslated region of about 2.5 kb (**Supplementary Figure S4**), which may have a regulatory effect on its expression (Broad et al., 2019; Nitschke et al., 2020).

[3]www.arabidopsis.org

Some *GGLs* Play Roles in Water Transpiration and Light-Induced Stomatal Opening

To explore the function of *GGLs* in stomatal biology, we ordered T-DNA insertion mutants of seven guard cell preferentially expressed *GGLs* (**Figures 2B, 3**) from ABRC stock, which were speculated to have specific roles in stomata. Genotyping and RT-PCR analyses showed that *ggl12*, *ggl14*, *ggl22*, and *ggl27* were knockout mutants, and *ggl7* and *ggl26* were knockdown mutants (**Supplementary Figure S5B**). However, the expression level of *GGL23* was not changed in the *ggl23* mutant (**Supplementary Figure S5B**). Therefore, the *ggl23* mutant was not used for further analyses in this study. We firstly

used thermal imaging to detect the leaf temperature of these six single mutants, which reflects the transpiration efficiency through the stomatal pores and epidermis. Thermal imaging analyses revealed that *ggl14* mutant (*osp1-1*) exhibited higher leaf temperature, consistent with our previous study (Tang et al., 2020), and *ggl22* mutant exhibited lower leaf temperature than Col-0, whereas the remaining four mutants showed comparable leaf temperatures as Col-0 (**Figures 6A,B**). To determine whether there is functional redundancy between *GGL14* with the other guard cell preferentially expressed *GGLs*, *ggl14* was crossed with *ggl7* and *ggl26* to generate double and triple mutants since these three genes are relatively higher and specifically expressed in guard cells than other *GGLs*, and are coexpressed with known components that function in stomata by coexpression analyses (Obayashi et al., 2009). *ggl7ggl14* and *ggl14ggl26* showed similar leaf temperatures as *ggl14*, and *ggl7ggl26* behaved WT-like leaf temperature (**Figures 6C,D**). However, the *ggl7ggl14ggl26* triple mutant showed significantly higher leaf temperature than *ggl14* and double mutants (**Figures 6C,D**), suggesting that GGL7, GGL14, and GGL26 have functional redundancy in transpiration, and GGL14 is a major contributor in this process. We next measured the transpiration rate and WUE of these single, double, and triple mutant plants. *ggl14* mutant exhibited a reduced transpiration rate and increased WUE than Col-0, while *ggl22* had an increased transpiration rate than Col-0 (**Figures 6E,F**), in accordance with their leaf temperatures (**Figures 6A,B**). Consistently, the transpiration rate of *ggl7ggl14ggl26* triple mutant was further reduced, and the increase of WUE in *ggl7ggl14ggl26* was aggravated compared to *ggl14* (**Figures 6G,H**), further supporting the functional redundancy among GGL7, GGL14, and GGL26.

We then detected their stomatal dynamics to dark-to-light transitions to determine whether these six *GGLs* are involved in stomatal dynamics when responses to environmental changes. *ggl14* exhibited impaired light-induced stomatal opening (**Figures 7A-C**), in agreement with our previous study (Tang et al., 2020), and the other single mutants retained intact stomatal response (**Figures 7A–C**). However, *ggl22* and *ggl26* single mutants exhibited relatively larger stomatal conductance when the stomatal aperture reached maximum value (**Figure 7B**), indicating that mutation of *GGL22* or *GGL26* increased stomatal movement capacity but not the stomatal sensitivity (Hu et al., 2015). To explore whether other GGLs have functional redundancy with GGL14 in stomatal dynamics to dark-to-light transitions, we also investigated the stomatal response of double and triple mutant plants to dark-to-light transitions. Similar to transpiration rate and WUE (**Figure 6**), *ggl7ggl14* and *ggl14ggl26* had similar stomatal dynamics as *ggl14*, which was greatly impaired compared to Col-0 (**Figures 7D–F**). However, the impairment in the light-induced stomatal opening was aggravated in *ggl7ggl14ggl26* triple mutant compared to *ggl14* (**Figures 7D–F**). These results suggest that GGL7, GGL14, and GGL26 are redundant in stomatal responses, at least to dark-to-light transitions and water maintenance.

Mutation of *GGLs* Affects Stomatal Density and Stomatal Morphology

We were also interested in whether these *GGLs* played roles in stomatal density and stomatal morphology. The stomatal density and index of *ggl22* were significantly increased than those in Col-0, and *ggl14* showed reduced stomatal density and index than Col-0 (**Figures 8A**,**B**). These results suggest that GGL22 is a negative regulator and GGL14 is a positive one to mediate stomatal density. Moreover, the stomatal density and index of *ggl7ggl14ggl26* triple mutant were not different from those in *ggl14* (**Supplementary Figures S6A,B**), suggesting that GGL7 and GGL26 are not involved in stomatal density. It has been reported that some guard cell-expressed genes affect stomatal patterning and shape (Lee et al., 2013; Negi et al., 2013; Castorina et al., 2016; Rui et al., 2017). We found that the one-spacing rule in these single, double, and triple mutants was not disrupted (data not shown), suggesting that these GGLs are not involved in this stomatal developmental process.

Furthermore, stomatal pore width, length, and stomatal complex size were measured in these mutants at normal growth conditions. The stomatal pore width and the width to length ratio (pore ratio) of *ggl14* were significantly smaller than Col-0 (**Figures 8C,D**), partially explaining the higher leaf temperature of *ggl14* mutant (**Figures 6A,B**). Although the stomatal pore width of *ggl26* was not obviously different from that in Col-0, its pore ratio was greater than Col-0 (**Figures 8C,D**). Measurement of stomatal complex length and width revealed that *ggl22* had a smaller stomatal complex size than Col-0, while the other five *ggl* single mutants showed a comparable stomatal complex size as Col-0 (**Figures 8E,F**). These results suggest that GGL26 and GGL22 influence stomatal pore dimension and stomatal complex size, respectively. *ggl7ggl14ggl26* phenocopied *ggl14* with respect to stomatal pore width and pore ratio (**Supplementary Figures S6C,D**), indicating GGL7 and GGL26 do not show functional redundancy with GGL14 in this developmental process. We interestingly found that *ggl7ggl14ggl26* had a larger stomatal complex length, whereas their corresponding single mutants showed a similar length as Col-0 (**Figure 8E** and **Supplementary Figure S6E**). These results suggest that GGL7, GGL14, and GGL26 are required and show redundancy in keeping stomatal complex at suitable size during development.

Mutation of *GGLs* Affects Plant Drought Performance

Environmental changes affect stomatal status and stomatal development. The public database (AtGenExpress Visualization Tool) showed that some *GGLs* were hormone or abiotic stress-inducible (Kilian et al., 2007). To further determine their expression profiles, we determined the expression patterns of these 19 *GGLs* during hormone or stress treatments by RT-PCR (**Supplementary Figures S7, S8**). The results revealed that *GGL13*, *GGL21*, and *GGL23* were upregulated by ABA treatment (**Supplementary Figure S7**). *GGL13* showed dynamic responses to IAA treatment, and IAA treatment inhibited *GGL21* expression

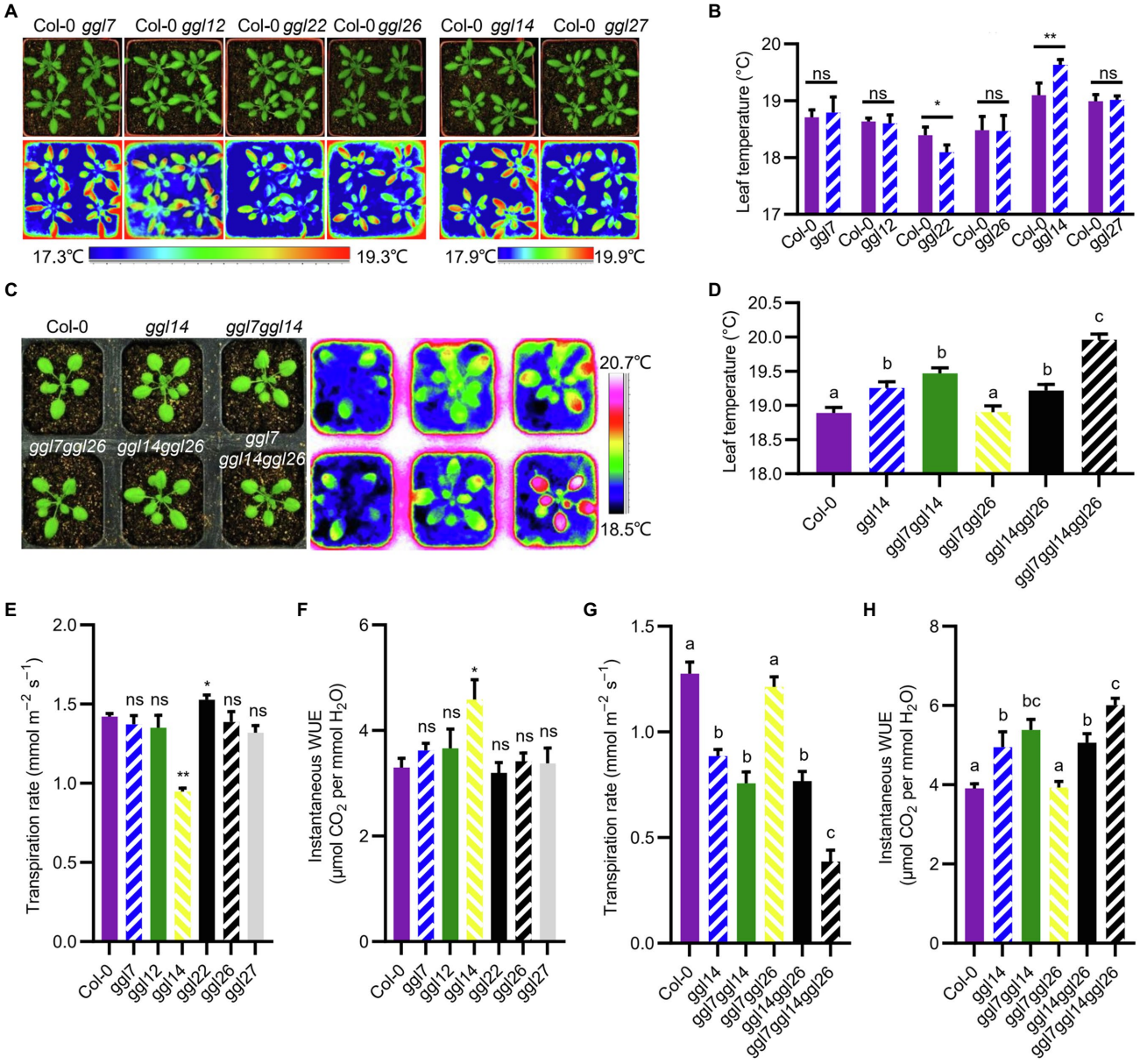

FIGURE 6 | Leaf temperature, transpiration rate, and instantaneous water use efficiency (WUE) of *ggl* mutants. **(A)** Photograph (up) and infrared thermal imaging (down) of Col-0 and *ggl* single mutants. **(B)** Quantification and statistical analyses of leaf temperature of Col-0 and *ggl* single mutant plants in **(A)**. Values are means ± SE (n = three independent experiments, each with four plants per genotype). *$p < 0.05$; **$p < 0.01$; ns, no significant difference; Student's t-test. **(C)** Photograph (left) and infrared thermal imaging (right) of Col-0, *ggl14*, the corresponding double mutant, and triple mutant plants. **(D)** Quantification and statistical analyses of leaf temperature of Col-0, *ggl14*, the corresponding double mutant, and triple mutant plants in **(C)**. Values are means ± SE (n = three independent experiments, each with six plants per genotype). Different letters indicate statistically significant differences ($p < 0.05$) by one-way ANOVA and Tukey's test analyses. **(E–H)** The transpiration rate and WUE of *ggl* mutants were measured using a portable gas exchange system (LI-6400XT). Values are means ± SE (n = three independent experiments, each with six plants per genotype). *$p < 0.05$; **$p < 0.01$; ns, no significant difference; Student's t-test **(E, F)**, and different letters indicate statistically significant differences ($p < 0.05$) by one-way ANOVA and Tukey's test analyses **(G, H)**. Quantification of leaf temperature by the software ThermaCAM Researcher Professional 2.10 **(B, D)**.

(**Supplementary Figure S7**). *GGL27* was repressed by BL treatment and accumulated by GA treatment (**Supplementary Figure S7**). GA treatment inhibited the expression of *GGL8*, *GGL12*, and *GGL26* (**Supplementary Figure S7**). *GGL5* and *GGL22* were prominently downregulated, and *GGL7* was activated during the process of salt treatment (**Supplementary Figure S8A**), whereas *GGL6*, *GGL8*, *GGL12*, *GGL13*, *GGL14*, *GGL16*, *GGL17*, and *GGL26* showed dynamic changes during salt treatment (**Supplementary Figure S8A**). Under dehydration stresses, the expression levels of *GGL5*, *GGL6*, *GGL16*, *GGL19*, *GGL22*, *GGL23*,

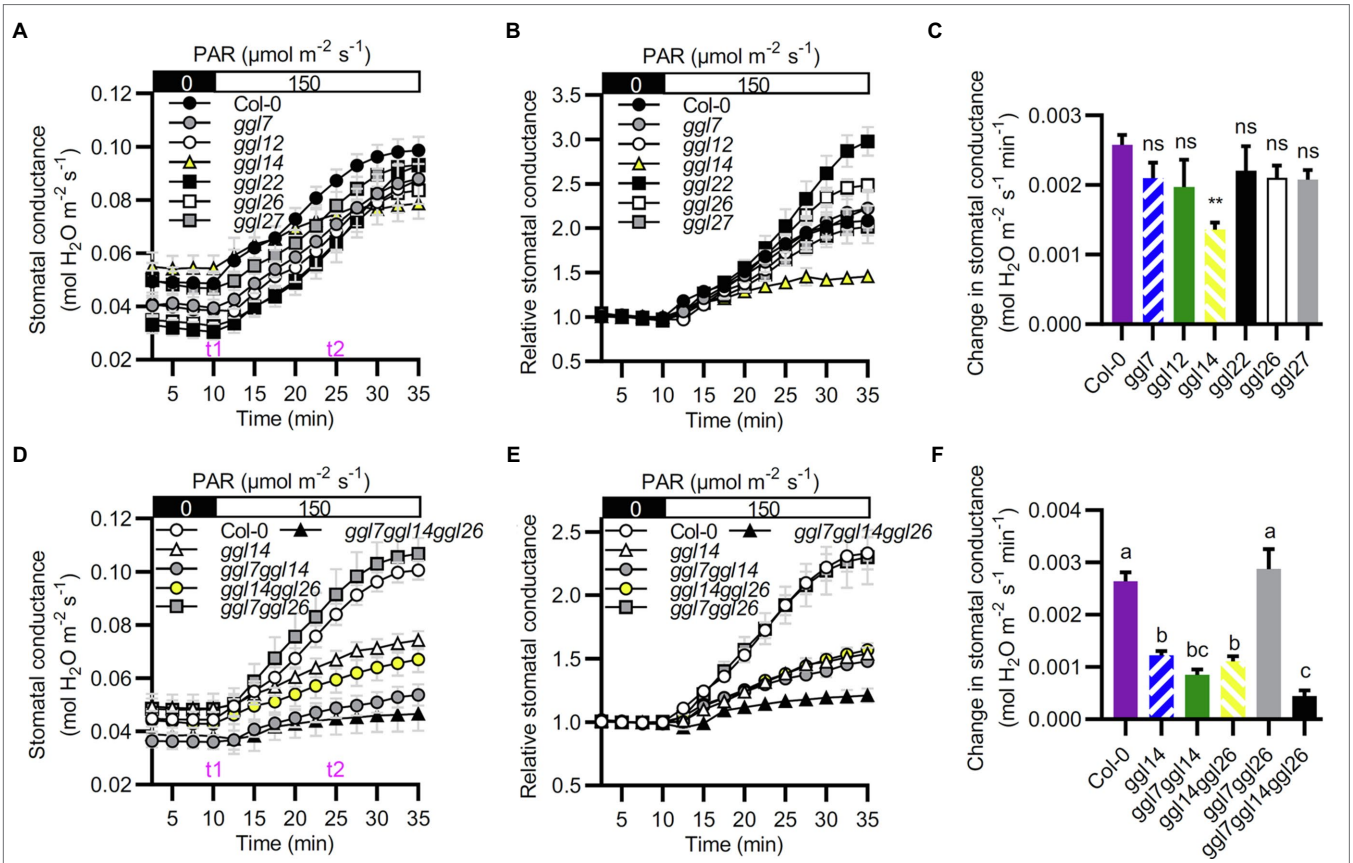

FIGURE 7 | *GGL7*, *GGL14*, and *GGL26* show functional redundancy in stomatal dynamics during the dark-to-light transition. **(A–C)** Time-resolved stomatal conductance responses to dark to light transitions in Col-0 and *ggl* single mutant plants. **(B)** Relative stomatal conductance. Normalized stomatal conductance of **(A)**. **(C)** The initial rates of stomatal conductance changes in the period of t1 to t2 in **(A)**, presented as mol H_2O m^{-2} s^{-1} min^{-1}. Values are means ± SE ($n = 3$ independent experiments, each with at least four leaves per genotype). $^{**}p < 0.01$; ns, no significant difference; Student's *t*-test. **(D–F)** Time-resolved stomatal conductance responses to dark to light transitions in Col-0, *ggl14*, *ggl7ggl14*, *ggl14ggl26*, *ggl7ggl26*, and *ggl7ggl14ggl26* mutant plants. **(E)** Relative stomatal conductance. Normalized stomatal conductance of **(D)**. **(F)** The initial rates of stomatal conductance changes in the time of t1 to t2 in **(D)**, presented as mol H_2O m^{-2} s^{-1} min^{-1}. Values are means ± SE ($n = 3$ independent experiments, each with at least four leaves per genotype). Different letters indicate statistically significant differences ($p < 0.05$) by one-way ANOVA and Tukey's test analyses. PAR: photosynthetically active radiation.

and *GGL29* were downregulated (**Supplementary Figure S8B**), whereas another four *GGLs* (*GGL8*, *GGL13*, *GGL14*, and *GGL17*) were significantly upregulated at different time points under dehydration stresses (**Supplementary Figure S8B**). Furthermore, the expression of six *GGLs* (*GGL7*, *GGL9*, *GGL12*, *GGL21*, *GGL26*, and *GGL27*) increased first and then decreased during dehydration treatment (**Supplementary Figure S8B**). To further confirm these results, we determined expression patterns of several hormone or stress-inducible *GGLs* (**Supplementary Figures S7, S8**) by real-time quantitative PCR. Our qPCR analyses showed that the expression patterns of these selected *GGLs* in response to hormones, salt, or dehydration stresses were generally consistent with RT-PCR results (**Supplementary Figure S9**). These results indicate that *GGLs* are more inducible to drought stresses and that hormone or stress-inducible *GGLs* might be involved in plant development and adaptation to stresses.

To test the effects of *GGLs* on drought performance, we subjected six *ggl* single mutants and the double and triple mutant plants to drought stresses. Under moderate drought stresses, *ggl14* showed greatly enhanced drought tolerance (**Figure 9B**), consistent with WUE (**Figure 6F**) and our previous report (Tang et al., 2020). *ggl22* showed slightly increased drought recovery capacity (**Figure 9A**). The rest four *ggl* single mutants performed the same drought performance as Col-0 (**Figure 9A**). *ggl7ggl14* and *ggl14ggl26* double mutants behaved similar drought performance as *ggl14* (**Figure 9B**). Under severe drought stresses, *ggl14ggl26* showed enhanced drought tolerance than *ggl14* mutant plants, and the drought tolerance in *ggl7ggl14ggl26* triple mutant was much stronger than *ggl14ggl26* (**Figure 9C**), suggesting GGL7, GGL14, and GGL26 have redundancy in water maintenance.

DISCUSSION

Plants encounter many environmental changes and have to deal with these badly living conditions for survival by triggering

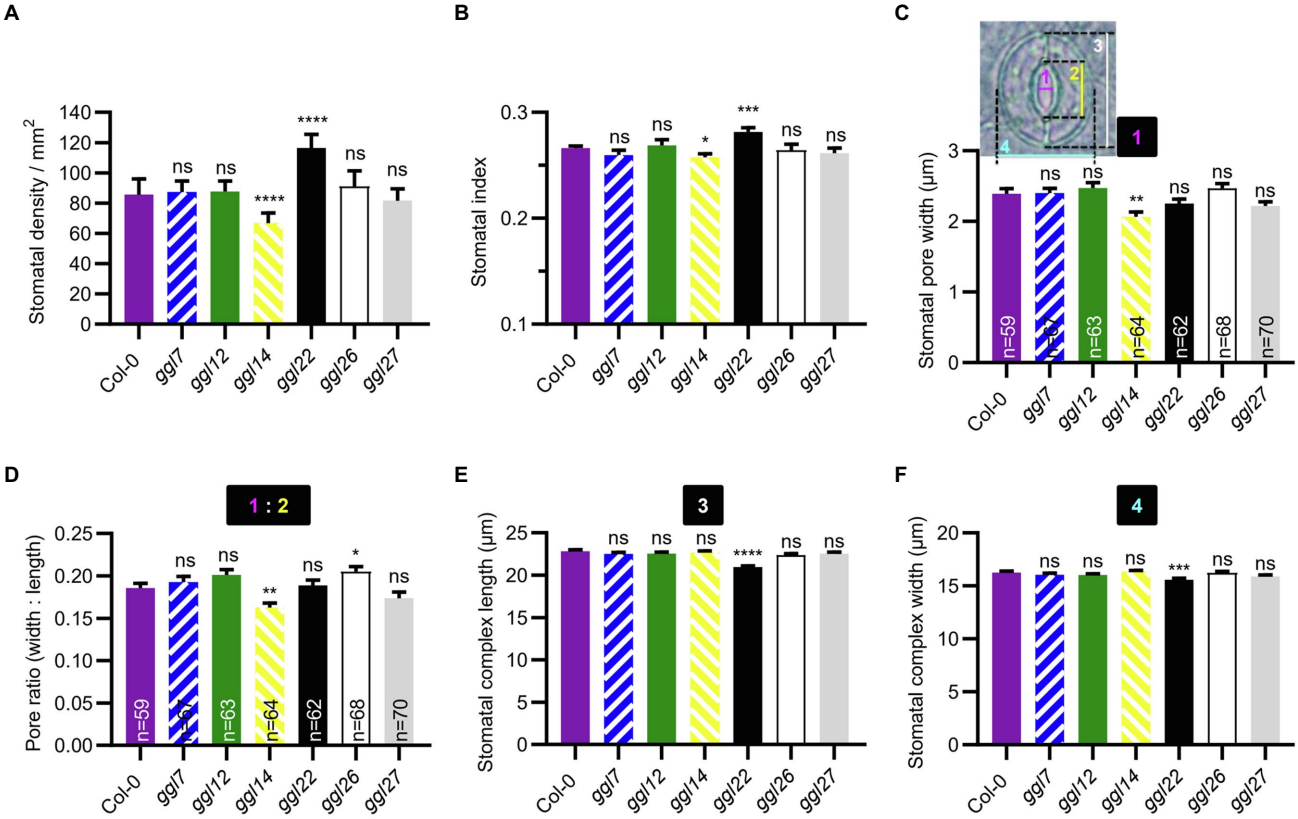

FIGURE 8 | Stomatal density and stomatal morphology of *ggl* single mutants. **(A, B)** Stomatal density **(A)** and stomatal index **(B)** in the abaxial leaves of Col-0 and *ggl* single mutants. Values are means ± SE ($n = 3$ independent experiments, each with at least 8 leaves per genotype). *$p < 0.05$; ***$p < 0.001$; ****$p < 0.0001$; ns, no significant difference; Student's *t*-test. **(C–F)** Stomatal pore width **(C)**, pore ratio (width: length) **(D)**, stomatal complex length **(E)**, and width **(F)** of Col-0 and *ggl* single mutants. Number 1 represents stomatal pore width, 2 represents stomatal pore length, 3 represents stomatal complex length, and 4 represents stomatal complex width. Pore ratio (1:2) is the ratio of pore width to pore length. Data are means ± SE, $n = 60$ stomata from at least six leaves per genotype **(E)** and **(F)**. *$p < 0.05$; **$p < 0.01$; ***$p < 0.001$; ****$p < 0.0001$; ns, no significant difference; Student's *t*-test. The measurement of stomatal pore width and length, and stomatal complex length and width was indicated in **(C)**.

different cellular responses. Stomata respond quickly to these environmental changes. GDSL lipases exist as a big family in most plant species, and more than 100 members have been identified in different plant species (Ling, 2008; Chepyshko et al., 2012; Dong et al., 2016; Lai et al., 2017; Su et al., 2020). However, only a few members have been studied for their biological and biochemical functions, especially in stomatal biology, though GDSL lipases/esterases that identified play essential roles in many aspects, such as regulation of plant growth, development, and stress adaptations (Naranjo et al., 2006; Hong et al., 2008; Takahashi et al., 2010; Girard et al., 2012; Gao et al., 2017; An et al., 2019).

It has been suggested that gene function is highly correlated with its expression pattern (Wu et al., 2016). For instance, two flower-expressed *GDSLs* (*EXL4* and *CDEF1*) promoted pollen hydration on the stigma and facilitated pollen tube penetration into the stigma, respectively (Updegraff et al., 2009; Takahashi et al., 2010). In the present study, we firstly isolated 29 putative guard cell highly expressed *GDSLs* (here named *GGLs*) through the published microarray data (Leonhardt et al., 2004; Yang et al., 2008) and confirmed the expression patterns of 19 *GGLs* in L clade by *GGL*pro::*GUS* analyses (**Figure 1**). *GGL6* (*GELP16*/*GLIP9*/*AtGDSL1*) and *GGL22* (*GELP80*/*SFAR5*) were highly expressed in the seed germination stage (**Figure 2B** and **Table 1**), consistent with previous studies (Chen et al., 2012; Ding et al., 2019), suggesting our system works well. Nineteen *GGLs* showed diverse expression patterns during the whole plant growth stages. Fifteen of them were confirmed to express in leaf guard cells, and seven (*GGL7*, *GGL12*, *GGL14*, *GGL17*, *GGL23*, *GGL26*, and *GGL27*) were preferentially expressed in leaf guard cells (**Figures 2B, 3**). These results indicate the potential roles of these GGLs in stomatal biology and the possibility of functional redundancy among them.

The roles of GGLs in stomata were further confirmed by phenotypic identification of T-DNA insertion mutants of six guard cell preferentially expressed *GGLs*. Our previous study has shown that *OSP1*/*GGL14* plays an essential role in stomata (Tang et al., 2020). Here, we identified the functional redundancy of GGL7 and GGL26 with GGL14 in modulating transpiration, WUE, and stomatal dynamics (**Figures 6, 7, 9**), but not in stomatal density

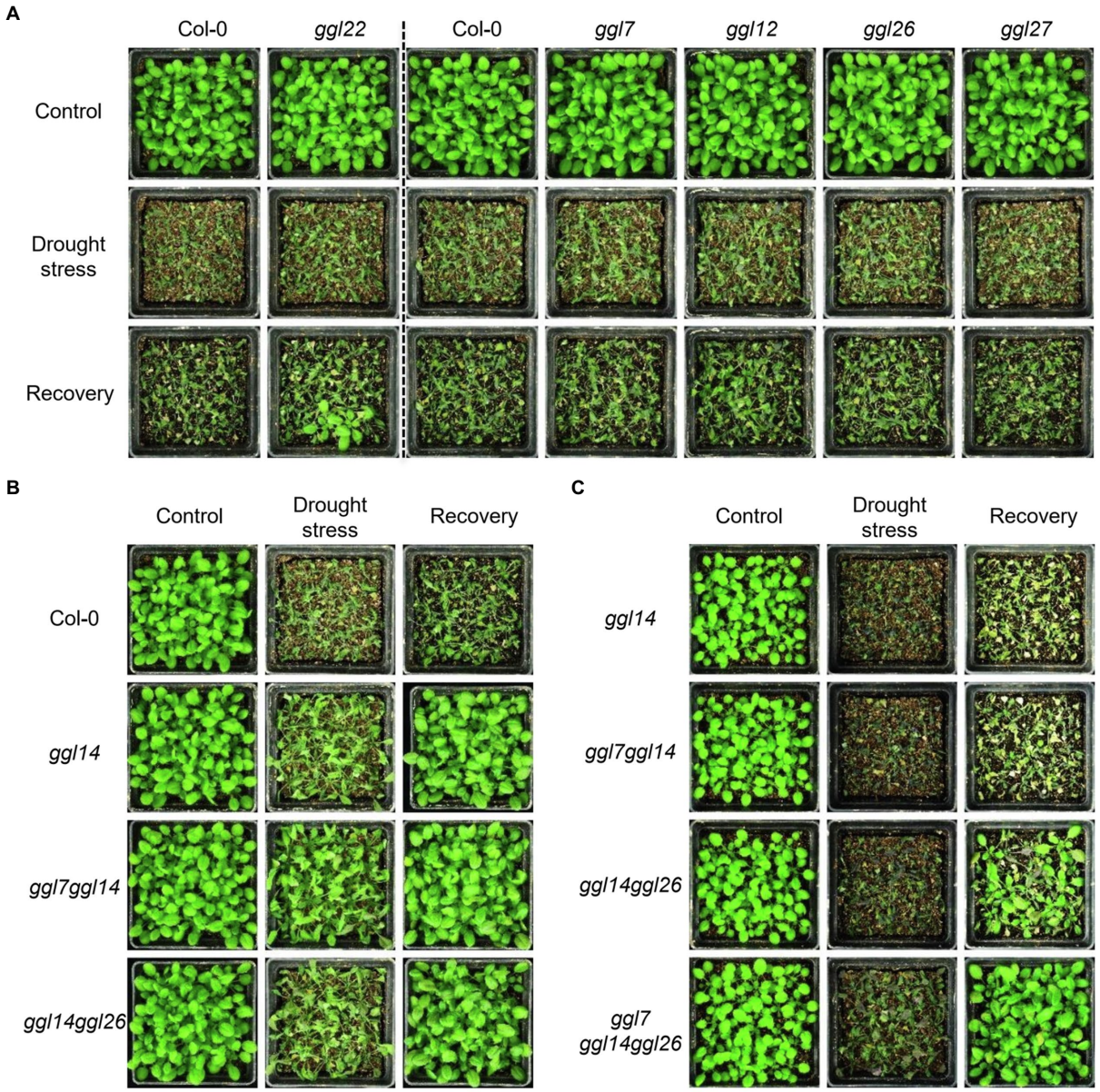

FIGURE 9 | *GGL7*, *GGL14*, and *GGL26* show functional redundancy in plant drought performance. **(A)** Drought performance of *ggl7*, *ggl12*, *ggl22*, *ggl26*, and *ggl27* single mutants under moderate drought stresses. **(B)** Drought performance of *ggl14*, *ggl7ggl14*, and *ggl14ggl26* mutant plants under moderate drought stresses. **(C)** Drought performance of *ggl14*, *ggl7ggl14*, *ggl14ggl26*, and *ggl7ggl14ggl26* under severe drought stresses. Twenty-five plants per genotype were grown in the pots containing the same weight of soil and water content. For moderate drought stresses, plants were rewatered when *ggl14* and WT plants showed significantly different wilting phenotypes. For severe drought stresses, plants were rewatered when significantly different wilting phenotypes were observed in *ggl14* and *ggl7ggl14ggl26* plants. The experiment was repeated two times with similar results.

and stomatal pore dimension (**Supplementary Figures S6A–D**). Our study shows that GGL14 and GGL26 play essential roles in regulating the pore dimension. Mutation of *GGL14* or *GGL26* influenced the size of stomatal pores with opposite effects (**Figures 8C,D**). However, *ggl7ggl14ggl26* and *ggl14* had similar pore width and pore ratio (**Supplementary Figures S6C,D**), which may be due to the major role of GGL14 in this aspect. In addition, GGL7, GGL14, and GGL26 also have a role in controlling stomatal complex length with redundancy (**Figure 8E** and **Supplementary Figure S6E**). These results suggest that GGLs have functional similarity but also specificity in stomatal development and stomatal behavior.

Our study also suggests that GGL22 is a component involved in stomatal biology. *GGL22* mutation increased stomatal density and stomatal index (**Figures 8A,B**), partially explaining the increased transpiration rate and reduced leaf temperature than Col-0 at normal growth conditions (**Figures 6A,B,E**). However, *ggl22* exhibited increased stomatal movement capacity and

TABLE 1 | Gene name and AGI gene code comparison.

Gene name	AGI Gene Code	Gene name	Reference
GGL5	AT1G29660	*AtGELP15 (AED4)*	Breitenbach et al. (2014) and Lai et al. (2017)
GGL6	AT1G29670	*AtGELP16 (GLIP9/ AtGDSL1)*	Lai et al. (2017) and Ding et al. (2019)
GGL7	AT1G33811	*AtGELP18*	Lai et al. (2017)
GGL8	AT1G53920	*AtGELP19 (GLIP5)*	Lai et al. (2017)
GGL9	AT1G54000	*AtGELP22 (GLL22)*	Lai et al. (2017)
GGL12	AT1G75880	*AtGELP39 (EXL1)*	Lai et al. (2017)
GGL13	AT1G75900	*AtGELP41 (EXL3)*	Lai et al. (2017)
GGL14	AT2G04570	*AtGELP47 (OSP1)*	Lai et al. (2017) and Tang et al. (2020)
GGL16	AT3G05180	*AtGELP61 (AED5)*	Breitenbach et al. (2014) and Lai et al. (2017)
GGL17	AT3G11210	GELP pseudoenzyme	Dong et al. (2016)
GGL19	AT3G16370	*AtGELP67*	Lai et al. (2017)
GGL20	AT3G26430	*AtGELP68*	Lai et al. (2017)
GGL21	AT3G48460	*AtGELP72 (SFAR4)*	Lai et al. (2017)
GGL22	AT4G18970	*AtGELP80 (SFAR5)*	Lai et al. (2017)
GGL23	AT4G26790	*AtGELP81*	Lai et al. (2017)
GGL25	AT5G03610	*AtGELP86*	Lai et al. (2017)
GGL26	AT5G18430	*AtGELP93*	Lai et al. (2017)
GGL27	AT5G45920	GELP pseudoenzyme	Dong et al. (2016)
GGL29	AT5G62930	GELP pseudoenzyme	Dong et al. (2016)

reduced stomatal complex size (**Figures 7B, 8E,F**), which may account for the slightly increased drought tolerance compared to Col-0 (**Figure 9A**). Given that mutation of *GGLs* affects stomatal density, stomatal pore dimension, and stomatal complex size, whether these *GGLs* control stomatal development and the underlying mechanism need to be further investigated in the future. Moreover, in these guard cell preferentially expressed *GGLs*, others may also be involved in stomatal biology if more double or triple mutants are generated and investigated according to our expression pattern data. Our present investigations further support the correlation between the expression pattern and biological function, and also suggest that investigation of expression patterns of genes gives valuable and vital information for determining their functions.

Five *GGLs* (*GGL5*, *GGL14*, *GGL17*, *GGL19*, and *GGL23*) showed expressions in trichomes (**Figure 3** and **Supplementary Figure S2**), and seven *GGLs* (*GGL6*, *GGL8*, *GGL9*, *GGL13*, *GGL16*, *GGL22*, and *GGL29*) were also expressed in the vascular tissues of true leaves (**Figure 3**). These results imply that these *GGLs* may play vital roles in trichome or vascular tissue development. Moreover, most of these 19 *GGLs* were expressed in the floral organ of 34-DAG plants (**Figure 4**), indicating these *GGLs* may also be involved in regulating floral organ development or fertility, possibly with redundancy. The deficiency in early siliques fertility and trichome development in the *osp1* mutants (Tang et al., 2020) and an increasing number of reports showing that GDSLs play important roles in regulating plants fertility (Huo et al., 2020; Zhao et al., 2020; Zhu et al., 2020) support our conclusions. During the whole plant growth process, the GUS signal of *GGL20*pro::*GUS* expressing plants was not detected (**Figures 2B, 3, 4**). It may be due that *GGL20* contains a long 5′ UTR (**Supplementary Figure S4**), which regulates its basal expression (Broad et al., 2019; Nitschke et al., 2020), or the upstream sequence of ATG we obtained may not include the intact promoter of *GGL20*. Our expression profile analyses revealed that some *GGLs* were inducible by hormones (**Supplementary Figure S7**), and most of them were influenced by dehydration (**Supplementary Figure S8B**), suggesting that they may have essential roles in plant development, adaptation to environmental changes, and hormone treatment. During dehydration, *GGL22* was downregulated, and *GGL14* was activated, whereas *GGL7* and *GGL26* showed dynamic responses (**Supplementary Figure S8B**). The functions of these four GGLs in stomatal biology and plant drought performance were validated in this study (**Figures 7–9**) and our previous report (Tang et al., 2020). These results further support the correlation of expression patterns and biological functions. The roles of other GGLs in abiotic stresses and hormone pathways need to be further investigated.

Proteins are distributed in different cell compartments to fulfill their diverse biological functions. In the present study, we found that GGL5, GGL8, GGL13, GGL14, GGL16, GGL17, GGL20, GGL27, and GGL29 were localized in ER (**Figure 5A**). A previous study has shown that GGL5 is not located in ER (Barbaglia et al., 2016). The difference in its location between the two labs may be due to the fact that only a tiny amount of GGL5 in ER can only be monitored by a high-resolution confocal microscope, or GGL5-YFP controlled by a *35S* promoter leads to an artifact in *N. benthamiana* leaf epidermis. Together with that some GGLs were located in lipid droplets (**Figure 5** and **Supplementary Figure S3**), these results imply that GGLs may function in stomata through regulating lipid biosynthesis and homeostasis. The previous studies revealed that the eukaryotic lipid metabolic pathway and the breakdown of stored triacylglycerols (TAGs) are essential for stomatal response to light intensity changes in *Arabidopsis* guard cells (McLachlan et al., 2016; Negi et al., 2018). Recently, more and more reports have shown that biochemical enzymes have other functions. For example, rice aldehyde dehydrogenase ALDH2B1 and rice glyceraldehyde-3-phosphatedehydrogenase (GAPDH) also act as transcriptional regulators to regulate gene expression (Zhang et al., 2017b; Ke et al., 2020). We found that four GGLs were localized in nucleus (**Figures 5A,C** and **Supplementary Figure S3**), suggesting that GGLs may have some special roles in nucleus. The diverse expression patterns and subcellular localization suggest that these GGLs may have diverse functions in plant development and environmental adaptations.

The previous phylogenetic analysis classified the *Arabidopsis* GDSLs into four clades (Lai et al., 2017). Our phylogenetic analyses of these 19 GGLs suggest that members of GGLs with high homology show similar tissue or subcellular expression patterns. GGL6 and GGL22, and GGL14 and GGL23 had mostly closed homologies, respectively, and showed similar expression patterns in most plant tissues (**Figures 2B, 3, 4** and **Supplementary Figure S2**). GGL14 and GGL22 are involved

in stomatal biology (**Figures 7, 8**). GGL6 and GGL23 may also have some roles in stomata, which need to be further determined. GGL17, GGL27, and GGL29 showed high homology and displayed the same subcellular localization (**Figure 5A** and **Supplementary Figures S3A,C**), indicating the similarity of functions among them.

In conclusion, we systematically investigated the expression patterns of 19 *GGLs* in *Arabidopsis*. Our results showed that most of these *GGLs* exhibited consistent expression patterns under normal growth conditions. At the cellular level, seven *GGLs* were preferentially, and eight were highly expressed in leaf guard cells. Expression pattern analyses under dehydration and phenotypic identification of mutants revealed a high correlation between expression pattern and biological function, and functional redundancy among the genes with similar expression patterns. Our findings also showed that protein sequence similarity had some degree of correlation with tissue or subcellular expression patterns. These findings provide valuable resources for future functional analyses of these GGLs in stomatal biology and developmental processes.

DATA AVAILABILITY STATEMENT

The original contributions presented in the study are included in the article/**Supplementary Material**; further inquiries can be directed to the corresponding author.

AUTHOR CONTRIBUTIONS

HH and CX conceived and designed the research, analyzed the data, and wrote the paper. CX, HG, JT, and JL performed the experiments. XY discussed the data. All authors contributed to the article and approved the submitted version.

FUNDING

This work was supported by grants from the National Science Foundation of China (31970730 and 31771552) and the National Key Research and Development Program (2016YFD0100604).

ACKNOWLEDGMENTS

We thank Dr. Shunping Yan (College of Life Science and Technology, Huazhong Agricultural University) for providing the *pMDC163* vector.

SUPPLEMENTARY MATERIAL

The Supplementary Material for this article can be found online at: https://www.frontiersin.org/articles/10.3389/fpls.2021.748543/full#supplementary-material

REFERENCES

Akoh, C. C., Lee, G. C., Liaw, Y. C., Huang, T. H., and Shaw, J. F. (2004). GDSL family of serine esterases/lipases. *Prog. Lipid Res.* 43, 534–552. doi: 10.1016/j.plipres.2004.09.002

An, X., Dong, Z., Tian, Y., Xie, K., Wu, S., Zhu, T., et al. (2019). ZmMs30 encoding a novel GDSL lipase is essential for male fertility and valuable for hybrid breeding in maize. *Mol. Plant* 12, 343–359. doi: 10.1016/j.molp.2019.01.011

Barbaglia, A. M., Tamot, B., Greve, V., and Hoffmann-Benning, S. (2016). Phloem proteomics reveals new lipid-binding proteins with a putative role in lipid-mediated signaling. *Front. Plant Sci.* 7:563. doi: 10.3389/fpls.2016.00563

Breitenbach, H. H., Wenig, M., Wittek, F., Jordá, L., Maldonado-Alconada, A. M., Sarioglu, H., et al. (2014). Contrasting Roles of the Apoplastic Aspartyl Protease APOPLASTIC, ENHANCED DISEASE SUSCEPTIBILITY1-DEPENDENT1 and LEGUME LECTIN-LIKE PROTEIN1 in Arabidopsis Systemic Acquired Resistance. *Plant Physiol.* 165, 791–809. doi: 10.1104/pp.114.239665

Broad, R. C., Bonneau, J. P., Beasley, J. T., Roden, S., Philips, J. G., Baumann, U., et al. (2019). Genome-wide identification and characterization of the GDP-L-galactose phosphorylase gene family in bread wheat. *BMC Plant Biol.* 19:515. doi: 10.1186/s12870-019-2123-1

Castorina, G., Fox, S., Tonelli, C., Galbiati, M., and Conti, L. (2016). A novel role for STOMATAL CARPENTER 1 in stomata patterning. *BMC Plant Biol.* 16:172. doi: 10.1186/s12870-016-0851-z

Charrier, B., Leroux, C., Kondorosi, A., and Ratet, P. (1996). The expression pattern of alfalfa flavanone 3-hydroxylase promoter-gus fusion in *Nicotiana benthamiana* correlates with the presence of flavonoids detected in situ. *Plant Mol. Biol.* 30, 1153–1168. doi: 10.1007/BF00019549

Chen, C., Chen, H., Zhang, Y., Thomas, H. R., Frank, M. H., He, Y., et al. (2020). TBtools: An integrative toolkit developed for interactive analyses of big biological data. *Mol. Plant* 13, 1194–1202. doi: 10.1016/j.molp.2020.06.009

Chen, M., Du, X., Zhu, Y., Wang, Z., Hua, S., Li, Z., et al. (2012). Seed fatty acid reducer acts downstream of gibberellin signalling pathway to lower seed fatty acid storage in Arabidopsis. *Plant Cell Environ.* 35, 2155–2169. doi: 10.1111/j.1365-3040.2012.02546.x

Chepyshko, H., Lai, C. P., Huang, L. M., Liu, J. H., and Shaw, J. F. (2012). Multifunctionality and diversity of GDSL esterase/lipase gene family in rice (Oryza sativa L. japonica) genome: new insights from bioinformatics analysis. *BMC Genomics* 13:309. doi: 10.1186/1471-2164-13-309

Clauss, K., Baumert, A., Nimtz, M., Milkowski, C., and Strack, D. (2008). Role of a GDSL lipase-like protein as sinapine esterase in Brassicaceae. *Plant J.* 53, 802–813. doi: 10.1111/j.1365-313X.2007.03374.x

Clauss, K., von Roepenack-Lahaye, E., Bottcher, C., Roth, M. R., Welti, R., Erban, A., et al. (2011). Overexpression of sinapine esterase BnSCE3 in oilseed rape seeds triggers global changes in seed metabolism. *Plant Physiol.* 155, 1127–1145. doi: 10.1104/pp.110.169821

Curtis, M. D., and Grossniklaus, U. (2003). A gateway cloning vector set for high-throughput functional analysis of genes in planta. *Plant Physiol.* 133, 462–469. doi: 10.1104/pp.103.027979

Deeks, M. J., Calcutt, J. R., Ingle, E. K., Hawkins, T. J., Chapman, S., Richardson, A. C., et al. (2012). A superfamily of actin-binding proteins at the actin-membrane nexus of higher plants. *Curr. Biol.* 22, 1595–1600. doi: 10.1016/j.cub.2012.06.041

Ding, L. N., Guo, X. J., Li, M., Fu, Z. L., Yan, S. Z., Zhu, K. M., et al. (2019). Improving seed germination and oil contents by regulating the GDSL transcriptional level in Brassica napus. *Plant Cell Rep.* 38, 243–253. doi: 10.1007/s00299-018-2365-7

Dong, X., Yi, H., Han, C. T., Nou, I. S., and Hur, Y. (2016). GDSL esterase/lipase genes in Brassica rapa L.: genome-wide identification and expression analysis. *Mol. Gen. Genomics.* 291, 531–542. doi: 10.1007/s00438-015-1123-6

Dunn, J., Hunt, L., Afsharinafar, M., Meselmani, M. A., Mitchell, A., Howells, R., et al. (2019). Reduced stomatal density in bread wheat leads to increased water-use efficiency. *J. Exp. Bot.* 70, 4737–4748. doi: 10.1093/jxb/erz248

Feng, Z., Zhang, B., Ding, W., Liu, X., Yang, D. L., Wei, P., et al. (2013). Efficient genome editing in plants using a CRISPR/Cas system. *Cell Res.* 23, 1229–1232. doi: 10.1038/cr.2013.114

Gao, M., Yin, X., Yang, W., Lam, S. M., Tong, X., Liu, J., et al. (2017). GDSL lipases modulate immunity through lipid homeostasis in rice. *PLoS Pathog.* 13:e1006724. doi: 10.1371/journal.ppat.1006724

Girard, A. L., Mounet, F., Lemaire-Chamley, M., Gaillard, C., Elmorjani, K., Vivancos, J., et al. (2012). Tomato GDSL1 is required for cutin deposition in the fruit cuticle. *Plant Cell* 24, 3119–3134. doi: 10.1105/tpc.112.101055

Hauser, F., Chen, W., Deinlein, U., Chang, K., Ossowski, S., Fitz, J., et al. (2013). A genomic-scale artificial microRNA library as a tool to investigate the functionally redundant gene space in Arabidopsis. *Plant Cell* 25, 2848–2863. doi: 10.1105/tpc.113.112805

Hong, J. K., Choi, H. W., Hwang, I. S., Kim, D. S., Kim, N. H., Choi, D. S., et al. (2008). Function of a novel GDSL-type pepper lipase gene, CaGLIP1, in disease susceptibility and abiotic stress tolerance. *Planta* 227, 539–558. doi: 10.1007/s00425-007-0637-5

Hu, H., Boisson-Dernier, A., Israelsson-Nordstrom, M., Bohmer, M., Xue, S., Ries, A., et al. (2010). Carbonic anhydrases are upstream regulators of CO_2-controlled stomatal movements in guard cells. *Nat. Cell Biol.* 12, 87–93. doi: 10.1038/ncb2009

Hu, H., Rappel, W. J., Occhipinti, R., Ries, A., Bohmer, M., You, L., et al. (2015). Distinct cellular locations of carbonic anhydrases mediate carbon dioxide control of stomatal movements. *Plant Physiol.* 169, 1168–1178. doi: 10.1104/pp.15.00646

Huang, S., Ding, M., Roelfsema, M. R. G., Dreyer, I., Scherzer, S., Al-Rasheid, K. A. S., et al. (2021). Optogenetic control of the guard cell membrane potential and stomatal movement by the light-gated anion channel GtACR1. *Sci. Adv.* 7:eabg4619. doi: 10.1126/sciadv.abg4619

Hughes, J., Hepworth, C., Dutton, C., Dunn, J. A., Hunt, L., Stephens, J., et al. (2017). Reducing stomatal density in barley improves drought tolerance without impacting on yield. *Plant Physiol.* 174, 776–787. doi: 10.1104/pp.16.01844

Huo, Y., Pei, Y., Tian, Y., Zhang, Z., Li, K., Liu, J., et al. (2020). IRREGULAR POLLEN EXINE2 encodes a GDSL lipase essential for male fertility in maize. *Plant Physiol.* 184, 1438–1454. doi: 10.1104/pp.20.00105

Ke, Y., Yuan, M., Liu, H., Hui, S., Qin, X., Chen, J., et al. (2020). The versatile functions of OsALDH2B1 provide a genic basis for growth-defense trade-offs in rice. *Proc. Natl. Acad. Sci. U. S. A.* 117, 3867–3873. doi: 10.1073/pnas.1918994117

Kilian, J., Whitehead, D., Horak, J., Wanke, D., Weinl, S., Batistic, O., et al. (2007). The AtGenExpress global stress expression data set: protocols, evaluation and model data analysis of UV-B light, drought and cold stress responses. *Plant J.* 50, 347–363. doi: 10.1111/j.1365-313X.2007.03052.x

Korkuæ, P., Schippers, J. H., and Walther, D. (2014). Characterization and identification of cis-regulatory elements in Arabidopsis based on single-nucleotide polymorphism information. *Plant Physiol.* 164, 181–200. doi: 10.1104/pp.113.229716

Kwon, S. J., Jin, H. C., Lee, S., Nam, M. H., Chung, J. H., Kwon, S. I., et al. (2009). GDSL lipase-like 1 regulates systemic resistance associated with ethylene signaling in Arabidopsis. *Plant J.* 58, 235–245. doi: 10.1111/j.1365-313X.2008.03772.x

Lai, C. P., Huang, L. M., Chen, L. O., Chan, M. T., and Shaw, J. F. (2017). Genome-wide analysis of GDSL-type esterases/lipases in Arabidopsis. *Plant Mol. Biol.* 95, 181–197. doi: 10.1007/s11103-017-0648-y

Lee, E., Liu, X., Eglit, Y., and Sack, F. (2013). FOUR LIPS and MYB88 conditionally restrict the G1/S transition during stomatal formation. *J. Exp. Bot.* 64, 5207–5219. doi: 10.1093/jxb/ert313

Leonhardt, N., Kwak, J. M., Robert, N., Waner, D., Leonhardt, G., and Schroeder, J. I. (2004). Microarray expression analyses of Arabidopsis guard cells and isolation of a recessive abscisic acid hypersensitive protein phosphatase 2C mutant. *Plant Cell* 16, 596–615. doi: 10.1105/tpc.019000

Ling, H. (2008). Sequence analysis of GDSL lipase gene family in Arabidopsis thaliana. *Pak. J. Biol. Sci.* 11, 763–767. doi: 10.3923/pjbs.2008.763.767

Ling, H., Zhao, J., Zuo, K., Qiu, C., Yao, H., Qin, J., et al. (2006). Isolation and expression analysis of a GDSL-like lipase gene from Brassica napus L. *J. Biochem. Mol. Biol.* 39, 297–303. doi: 10.5483/bmbrep.2006.39.3.297

Mayfield, J. A., Fiebig, A., Johnstone, S. E., and Preuss, D. (2001). Gene families from the Arabidopsis thaliana pollen coat proteome. *Science* 292, 2482–2485. doi: 10.1126/science.1060972

McLachlan, D. H., Lan, J., Geilfus, C. M., Dodd, A. N., Larson, T., Baker, A., et al. (2016). The breakdown of stored triacylglycerols is required during light-induced stomatal opening. *Curr. Biol.* 26, 707–712. doi: 10.1016/j.cub.2016.01.019

Miao, J., Guo, D., Zhang, J., Huang, Q., Qin, G., Zhang, X., et al. (2013). Targeted mutagenesis in rice using CRISPR-Cas system. *Cell Res.* 23, 1233–1236. doi: 10.1038/cr.2013.123

Nakagawa, T., Suzuki, T., Murata, S., Nakamura, S., Hino, T., Maeo, K., et al. (2007). Improved gateway binary vectors: high-performance vectors for creation of fusion constructs in transgenic analysis of plants. *Biosci. Biotechnol. Biochem.* 71, 2095–2100. doi: 10.1271/bbb.70216

Naranjo, M. A., Forment, J., Roldan, M., Serrano, R., and Vicente, O. (2006). Overexpression of Arabidopsis thaliana LTL1, a salt-induced gene encoding a GDSL-motif lipase, increases salt tolerance in yeast and transgenic plants. *Plant Cell Environ.* 29, 1890–1900. doi: 10.1111/j.1365-3040.2006.01565.x

Negi, J., Moriwaki, K., Konishi, M., Yokoyama, R., Nakano, T., Kusumi, K., et al. (2013). A Dof transcription factor, SCAP1, is essential for the development of functional stomata in Arabidopsis. *Curr. Biol.* 23, 479–484. doi: 10.1016/j.cub.2013.02.001

Negi, J., Munemasa, S., Song, B., Tadakuma, R., Fujita, M., Azoulay-Shemer, T., et al. (2018). Eukaryotic lipid metabolic pathway is essential for functional chloroplasts and CO_2 and light responses in Arabidopsis guard cells. *Proc. Natl. Acad. Sci. U. S. A.* 115, 9038–9043. doi: 10.1073/pnas.1810458115

Nitschke, L., Tewari, A., Coffin, S. L., Xhako, E., Pang, K., Gennarino, V. A., et al. (2020). miR760 regulates ATXN1 levels via interaction with its 5′ untranslated region. *Genes Dev.* 34, 1147–1160. doi: 10.1101/gad.339317.120

Obayashi, T., Hayashi, S., Saeki, M., Ohta, H., and Kinoshita, K. (2009). ATTED-II provides coexpressed gene networks for Arabidopsis. *Nucleic Acids Res.* 37, D987–D991. doi: 10.1093/nar/gkn807

Oh, I. S., Park, A. R., Bae, M. S., Kwon, S. J., Kim, Y. S., Lee, J. E., et al. (2005). Secretome analysis reveals an Arabidopsis lipase involved in defense against Alternaria brassicicola. *Plant Cell* 17, 2832–2847. doi: 10.1105/tpc.105.034819

Papanatsiou, M., Petersen, J., Henderson, L., Wang, Y., Christie, J. M., and Blatt, M. R. (2019). Optogenetic manipulation of stomatal kinetics improves carbon assimilation, water use, and growth. *Science* 363, 1456–1459. doi: 10.1126/science.aaw0046

Park, J. J., Jin, P., Yoon, J., Yang, J. I., Jeong, H. J., Ranathunge, K., et al. (2010). Mutation in wilted dwarf and lethal 1 (WDL1) causes abnormal cuticle formation and rapid water loss in rice. *Plant Mol. Biol.* 74, 91–103. doi: 10.1007/s11103-010-9656-x

Rui, Y., Xiao, C., Yi, H., Kandemir, B., Wang, J. Z., Puri, V. M., et al. (2017). POLYGALACTURONASE INVOLVED IN EXPANSION3 functions in seedling development, rosette growth, and stomatal dynamics in Arabidopsis thaliana. *Plant Cell* 29, 2413–2432. doi: 10.1105/tpc.17.00568

Su, S. H., Bush, S. M., Zaman, N., Stecker, K., Sussman, M. R., and Krysan, P. (2013). Deletion of a tandem gene family in Arabidopsis: increased MEKK2 abundance triggers autoimmunity when the MEKK1-MKK1/2-MPK4 signaling cascade is disrupted. *Plant Cell* 25, 1895–1910. doi: 10.1105/tpc.113.112102

Su, H. G., Zhang, X. H., Wang, T. T., Wei, W. L., Wang, Y. X., Chen, J., et al. (2020). Genome-wide identification, evolution, and expression of GDSL-type esterase/lipase gene family in soybean. *Front. Plant Sci.* 11:726. doi: 10.3389/fpls.2020.00726

Szabados, L., Charrier, B., Kondorosi, A., Debruijn, F. J., and Ratet, P. (1995). New plant promoter and enhancer testing vectors. *Mol. Breed.* 1, 419–423. doi: 10.1007/BF01248419

Takahashi, K., Shimada, T., Kondo, M., Tamai, A., Mori, M., Nishimura, M., et al. (2010). Ectopic expression of an esterase, which is a candidate for the unidentified plant cutinase, causes cuticular defects in Arabidopsis thaliana. *Plant Cell Physiol.* 51, 123–131. doi: 10.1093/pcp/pcp173

Tang, J., Yang, X., Xiao, C., Li, J., Chen, Y., Li, R., et al. (2020). GDSL lipase occluded stomatal pore 1 is required for wax biosynthesis and stomatal cuticular ledge formation. *New Phytol.* 228, 1880–1896. doi: 10.1111/nph.16741

Tantikanjana, T., Mikkelsen, M. D., Hussain, M., Halkier, B. A., and Sundaresan, V. (2004). Functional analysis of the tandem-duplicated P450 genes SPS/BUS/CYP79F1 and CYP79F2 in glucosinolate biosynthesis and plant development

by Ds transposition-generated double mutants. *Plant Physiol.* 135, 840–848. doi: 10.1104/pp.104.040113

Updegraff, E. P., Zhao, F., and Preuss, D. (2009). The extracellular lipase EXL4 is required for efficient hydration of Arabidopsis pollen. *Sex. Plant Reprod.* 22, 197–204. doi: 10.1007/s00497-009-0104-5

Walter, M., Chaban, C., Schutze, K., Batistic, O., Weckermann, K., Nake, C., et al. (2004). Visualization of protein interactions in living plant cells using bimolecular fluorescence complementation. *Plant J.* 40, 428–438. doi: 10.1111/j.1365-313X.2004.02219.x

Watkins, J. L., Li, M., McQuinn, R. P., Chan, K. X., McFarlane, H. E., Ermakova, M., et al. (2019). A GDSL esterase/lipase catalyzes the esterification of lutein in bread wheat. *Plant Cell* 31, 3092–3112. doi: 10.1105/tpc.19.00272

Wu, Y., Xun, Q., Guo, Y., Zhang, J., Cheng, K., Shi, T., et al. (2016). Genome-wide expression pattern analyses of the Arabidopsis leucine-rich repeat receptor-Like kinases. *Mol. Plant* 9, 289–300. doi: 10.1016/j.molp.2015.12.011

Yang, Y., Costa, A., Leonhardt, N., Siegel, R. S., and Schroeder, J. I. (2008). Isolation of a strong Arabidopsis guard cell promoter and its potential as a research tool. *Plant Methods* 4:6. doi: 10.1186/1746-4811-4-6

Yeats, T. H., Huang, W., Chatterjee, S., Viart, H. M., Clausen, M. H., Stark, R. E., et al. (2014). Tomato cutin deficient 1 (CD1) and putative orthologs comprise an ancient family of cutin synthase-like (CUS) proteins that are conserved among land plants. *Plant J.* 77, 667–675. doi: 10.1111/tpj.12422

Yeats, T. H., Martin, L. B., Viart, H. M., Isaacson, T., He, Y., Zhao, L., et al. (2012). The identification of cutin synthase: formation of the plant polyester cutin. *Nat. Chem. Biol.* 8, 609–611. doi: 10.1038/nchembio.960

Yoo, S. D., Cho, Y. H., and Sheen, J. (2007). Arabidopsis mesophyll protoplasts: a versatile cell system for transient gene expression analysis. *Nat. Protoc.* 2, 1565–1572. doi: 10.1038/nprot.2007.199

Zhang, L., Gao, C., Mentink-Vigier, F., Tang, L., Zhang, D., Wang, S., et al. (2019). Arabinosyl deacetylase modulates the Arabinoxylan acetylation profile and secondary wall formation. *Plant Cell* 31, 1113–1126. doi: 10.1105/tpc.18.00894

Zhang, X., Henriques, R., Lin, S. S., Niu, Q. W., and Chua, N. H. (2006). Agrobacterium-mediated transformation of Arabidopsis thaliana using the floral dip method. *Nat. Protoc.* 1, 641–646. doi: 10.1038/nprot.2006.97

Zhang, H., Wang, M., Li, Y., Yan, W., Chang, Z., Ni, H., et al. (2020). GDSL esterase/lipases OsGELP34 and OsGELP110/OsGELP115 are essential for rice pollen development. *J. Integr. Plant Biol.* 62, 1574–1593. doi: 10.1111/jipb.12919

Zhang, B., Zhang, L., Li, F., Zhang, D., Liu, X., Wang, H., et al. (2017a). Control of secondary cell wall patterning involves xylan deacetylation by a GDSL esterase. *Nat. Plants* 3:17017. doi: 10.1038/nplants.2017.17

Zhang, H., Zhao, Y., and Zhou, D. X. (2017b). Rice NAD^+-dependent histone deacetylase OsSRT1 represses glycolysis and regulates the moonlighting function of GAPDH as a transcriptional activator of glycolytic genes. *Nucleic Acids Res.* 45, 12241–12255. doi: 10.1093/nar/gkx825

Zhao, J., Long, T., Wang, Y., Tong, X., Tang, J., Li, J., et al. (2020). RMS2 encoding a GDSL lipase mediates lipid homeostasis in anthers to determine Rice male fertility. *Plant Physiol.* 182, 2047–2064. doi: 10.1104/pp.19.01487

Zhu, J., Lou, Y., Shi, Q. S., Zhang, S., Zhou, W. T., Yang, J., et al. (2020). Slowing development restores the fertility of thermo-sensitive male-sterile plant lines. *Nat. Plants* 6, 360–367. doi: 10.1038/s41477-020-0622-6

Conflict of Interest: The authors declare that the research was conducted in the absence of any commercial or financial relationships that could be construed as a potential conflict of interest.

Publisher's Note: All claims expressed in this article are solely those of the authors and do not necessarily represent those of their affiliated organizations, or those of the publisher, the editors and the reviewers. Any product that may be evaluated in this article, or claim that may be made by its manufacturer, is not guaranteed or endorsed by the publisher.

frontiers in Plant Science

OPINION
published: 27 September 2021
doi: 10.3389/fpls.2021.761952

Stomatal Closure Sets in Motion Long-Term Strategies of Plant Defense Against Microbial Pathogens

*Shashibhushan Gahir†, Pulimamidi Bharath† and Agepati S. Raghavendra**

Department of Plant Sciences, School of Life Sciences, University of Hyderabad, Hyderabad, India

Keywords: guard cells, innate immunity, peroxisomes, photorespiration, secondary messengers, transpiration

OPEN ACCESS

Edited by:
Juan Dong,
The State University of New Jersey, United States

Reviewed by:
Mohammad Saidur Rhaman,
Bangladesh Agricultural University, Bangladesh

****Correspondence:***
Agepati S. Raghavendra
as_raghavendra@yahoo.com;
asrsl@uohyd.ernet.in

†These authors have contributed equally to this work

Specialty section:
This article was submitted to Plant Cell Biology, a section of the journal Frontiers in Plant Science

Received: *20 August 2021*
Accepted: *01 September 2021*
Published: *27 September 2021*

Citation:
Gahir S, Bharath P and Raghavendra AS (2021) Stomatal Closure Sets in Motion Long-Term Strategies of Plant Defense Against Microbial Pathogens. Front. Plant Sci. 12:761952. doi: 10.3389/fpls.2021.761952

INTRODUCTION

Stomata are the main gateways for the entry of microbial pathogens into leaves (Melotto et al., 2008). However, some try to use hydathodes (Hugouvieux et al., 1998) or breach the cuticle (Grimmer et al., 2012). Stomatal closure, therefore, is an effective measure to restrict pathogen entry and provide the plants an innate immunity (Melotto et al., 2008, 2017; Sawinski et al., 2013; Bharath et al., 2021). Stomata open when the guard cells are turgid and close when guard cells are flaccid (Willmer and Fricker, 1996). Whenever plants are exposed to stress, the guard cells sense and respond by a series of steps that include the production of ROS and NO followed by a rise in Ca^{2+} and the modulation of ion channels. These events promote the efflux of cations and anions from guard cells. As a result, guard cells lose turgor leading to stomatal closure (Arnaud and Hwang, 2015; Agurla et al., 2018; Saito and Uozumi, 2019; Hsu et al., 2021).

The reopening of stomata is usually slower than the closure, ensuring that the leaves conserve water for an extended period. For example, abscisic acid (ABA)-induced stomatal closure in the epidermis took about 30 min (and in leaf 3 h). In contrast, recovery took 1–6 days, implying short-term and long-term effects on stomata (Liang and Zhang, 1999). Recently, we pointed out that the stomatal closure by ABA was an essential component of plant adaptation to stress factors (Bharath et al., 2021). This article proposes that the initial stomatal closure response triggers many defensive strategies to fight the pathogens. We describe the follow-up of events limiting pathogen spread and emphasize stomata's role in ensuring plants' long-term adaptation against microbes.

Stomatal Closure: An Immediate Barrier of Microbial Entry

Stomatal closure was a typical response against microbial attack (Arnaud and Hwang, 2015; Melotto et al., 2017; Agurla et al., 2018). The process of stomatal closure is initiated by sensing the abiotic (e.g., drought, chilling, and UV-B) or biotic stress (pathogens and insects) components (Agurla et al., 2018). Most microbial pathogens produce pathogen-or microbe-or damage-associated molecular patterns (PAMPs/MAMPs/DAMPs), perceived by pattern recognition receptors (PRRs) present on the plant plasma membrane. Upon perception, plants activate a defense response called pattern-triggered immunity (PTI). When pathogens attempt to overcome PTI, plants trigger effector-triggered immunity (Cui et al., 2015; Nguyen et al., 2021). Bacterial elicitors that trigger stomatal closure include flagellin22 (flg22), lipopolysaccharide, and other elicitor peptides, such as, elf26 (Melotto et al., 2008, 2017; Arnaud and Hwang, 2015). Fungal elicitors, such as, chitin oligosaccharide and chitosan, also induced defense responses in plants (Ye et al., 2020).

Guard cells perceive hormones (e.g., ABA) or elicitors (flg22) by their respective receptors. Upon binding to ABA or flg22, the receptor kinases (e.g., *open stomata 1* or *botrytis-induced kinase 1*) activate RbohD/F and stimulate reactive oxygen species (ROS) production during stomatal closure. However, the role of RBOHD in resistance against pathogens, particularly during pre-invasive stage is not clear. The elevated ROS, in turn, trigger a rise in nitric oxide (NO) and Ca^{2+}. The interaction

of these secondary messengers (ROS/NO/Ca^{2+}) regulates the downstream components in guard cells. Both NO and Ca^{2+} (via Ca^{2+}-dependent protein kinases) promote the ion efflux by activating K^+ out, SLAC1, and SLAH3 channels and at the same time inhibit the K-influx channel (Arnaud and Hwang, 2015; Agurla et al., 2018; Kohli et al., 2019; Sun et al., 2019). Similarly, ROS and Ca^{2+} activate Ca^{2+} influx and increase cytosolic Ca^{2+} levels (Klüsener et al., 2002). The elevated ROS, NO, Ca^{2+} and H_2S provide an extended pathogen resistance (Gahir et al., 2020; Liu and Xue, 2021). Cytosolic pH is another secondary messenger that preceded the production of ROS and NO in guard cells, but the exact mechanism is ambiguous (Gonugunta et al., 2009; Bharath et al., 2021). It is necessary to study if such changes in pHcyt can modulate the pathogen resistance as well.

Stomatal Closure Associated With the Modulation of Plant Hormones

Stomatal closure during drought or microbial infection was associated with an increase in plant hormones. Salicylic acid (SA), ABA, methyl jasmonate (MJ), and ethylene (ET) accumulate when microbes attack plants. The concerted action of these hormones causes stomatal closure and induces systemic resistance (Gimenez-Ibanez et al., 2016; van Butselaar and Van den Ackerveken, 2020; Bharath et al., 2021). The modulated hormonal status provides long-term protection to plants against biotic and abiotic stress (Described below).

DISCUSSION

Closure Triggers a Network of Long-Term Events to Ensure the Protection

Stomatal closure in response to microbial infection is an immediate physical measure to prevent microbial entry. However, such closure has long-term effects, such as, a marked decrease in the intercellular CO_2 of leaves, a reduction in photosynthetic carbon assimilation, and an elevation in photo respiratory activity. The reduction in transpiration can cause mineral deficiency in leaves. We describe below the consequences of these events and a few associated components.

Decrease in Photosynthesis and Increase in Photorespiration and Peroxisomal Population

When stomata close, the intercellular CO_2 is lowered, and transpiration decreased, raising the leaf temperature. Both these factors enhance photorespiration. The increase in photorespiration occurred under conditions of biotic (microbial infection) or abiotic stress (drought) (Lal et al., 1996; Pascual et al., 2010; Voss et al., 2013; Vo et al., 2021). Even fluctuations in transpiration triggered an increase in photorespiration (Furutani et al., 2020). The enhanced photorespiration and the associated rise in H_2O_2 could confer disease resistance (Taler et al., 2004; Kubo, 2013; Sørhagen et al., 2013). Further, glycolate, glyoxylate, and glycine, being pathway intermediates, accumulate. Glycolate and glyoxylate are toxic to living cells and can double up as antimicrobial compounds. Glycine is the precursor of glutathione, an essential anti-oxidant in plant cells. Photo respiratory enzymes/metabolites mediated the plant defense during tomato-*Pseudomonas syringae* interactions (Ahammed et al., 2018). Thus, photo respiratory metabolism could help to resist pathogens.

The enhanced photorespiration was often associated with an increase in the peroxisomal population in leaf cells (Chen et al., 2016). Peroxisomal ROS could protect against plant pathogens (Sørhagen et al., 2013). Besides ROS, other components of peroxisomes, namely NO, Ca^{2+}, and polyamines (PA), upregulated the genes involved in SA signaling and PA catabolism, reinforcing plant defense responses (Chen et al., 2016; Wang et al., 2019).

Stomatal Closure Lowers Leaf Sugars

Stomatal closure, whether due to pathogen attack or drought, causes reduced CO_2 assimilation and decreased carbon partitioning into sucrose and starch (Wang et al., 2016; Haider et al., 2017). The pathogens required sugars for growth and infection (Solomon et al., 2003; Scharte et al., 2005; Chang et al., 2017). If sufficient sucrose is not available, the extent of proliferation would be restricted (Huai et al., 2020). Therefore, the deficiency in sugar availability lead to decreased fungal growth (Bezrutczyk et al., 2018).

Reduced Transpiration Creates Mineral Deficiency

Transpiration is a prerequisite for long-distance transport of minerals (Ruiz and Romero, 2002). A deficiency of minerals would occur when stomata are closed. There was a positive relationship between the transpiration rate and mineral content of sunflower (*Helianthus annuus*) and maize leaves (Tanner and Beevers, 2001; Shrestha et al., 2021). Since microbial spread and multiplication within leaves depend on macronutrients/micronutrients, the mineral deficiency could affect microbial growth and enhance pathogen tolerance (Fernández-Escobar, 2019). The N-status of leaves modulated defense-related hormones, NO content, and then genes (Sun et al., 2020). The deficiency of N increased the levels of phenolics and restricted the spread of powdery mildew (Bavaresco and Eibach, 1987). A similar situation under K^+-deficiency was reported with leaf spot, caused by *Helminthosporium cynodontis* (Richardson and Croughan, 1989). Other examples of mineral deficiency that favor pathogen resistance were zinc (Cabot et al., 2019) and iron (Trapet et al., 2021). Readers can find a detailed description of the dual role of the macro-and micronutrients for the infection by bacterial and fungal pathogens elsewhere (Huber et al., 2012).

Continuing Effects of Secondary Messengers, Plant Hormones, and Secondary Metabolites

The secondary messengers produced during stomatal closure can continue to protect plants. For example, the combination of ROS/NO/Ca^{2+} was quite effective in limiting the spread and multiplication of microbes within the leaf. These secondary messengers trigger hypersensitive response (HR), synthesis of pathogenesis-related (PR) proteins, and programmed cell death (PCD) (Serrano et al., 2015; Marcec et al., 2019). Besides NO, H_2S produced during stomatal closure could confer pathogen resistance (Vojtovič et al., 2020). It is possible that these

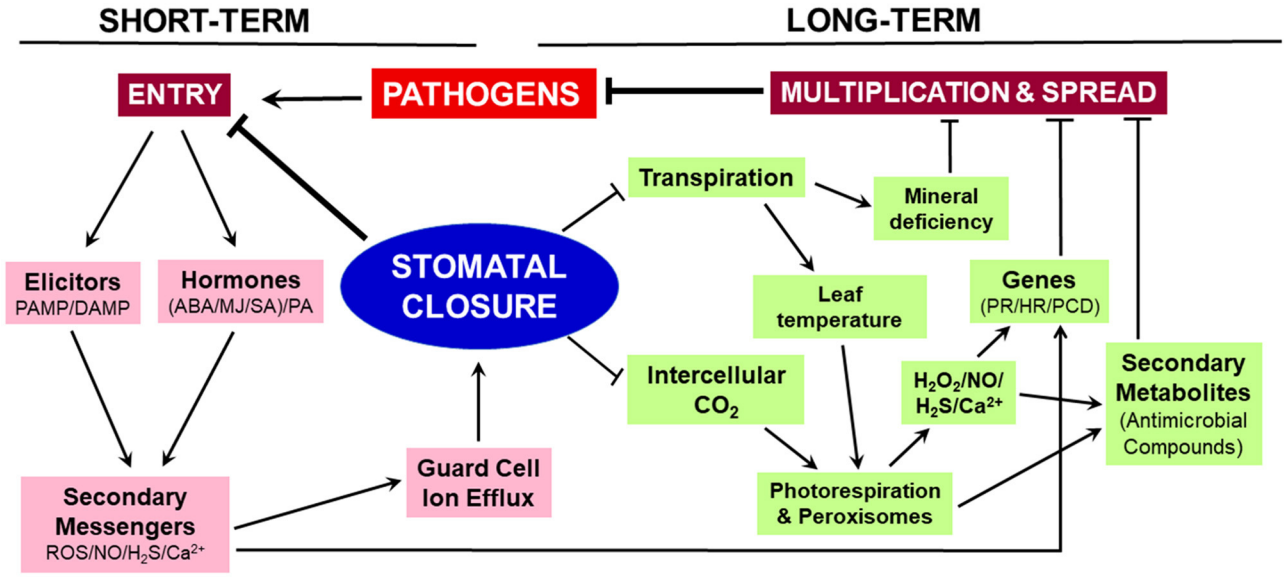

FIGURE 1 | Schematic representation of events associated with stomatal closure. The closure restricts microbial entry during the short term, while the events initiated during closure contribute to long-term adaptation against microbes. On sensing the microbial elicitor molecules, the guard cells trigger a rise in ROS, NO, Ca^{2+}, and H_2S. These secondary messengers cause ion-efflux from guard cells and stomatal closure. As a consequence of closure, the entry of CO_2 and transpirational H_2O loss are restricted, leading to increased photorespiration, decreased leaf sugars, and mineral deficiency. All these events help in restricting microbial multiplication, spread, and growth. The disturbed hormonal status and reactive molecules ensure continued protection by upregulating PR/HR/PCD genes and promoting the levels of antimicrobial secondary metabolites. Arrow represents an increase and ⊣ indicates a decrease.

components ROS/NO/Ca^{2+} can also induce priming effect individually or in combination.

When plants were infected by pathogens, the leaves responded by modulating the hormones, which interacted with each other to impart a long-lasting response. Plant hormones (e.g., SA, methyl salicylate, MJ) and even PAs could induce systemic resistance (Bürger and Chory, 2019; Chen et al., 2019; Seifi et al., 2019; Yuan et al., 2019). These hormones (ABA/MJ/SA) primed the plant tissue to stand against pathogens (Agostini et al., 2019; Feng et al., 2020). These observations open up several exciting lines of work for further research.

Several secondary metabolites produced by the plants are prominently associated with protection against bacterial, fungal, and viral attacks. The elevated levels of H_2O_2, NO, and Ca^{2+} induced accumulation of secondary metabolites like wax, callose, alkaloids, flavonoids, phenols, and PAs, reinforcing the protection against infection (Walters, 2003; Luna et al., 2011; Zaynab et al., 2018; Lewandowska et al., 2020). The PAs also prime the plants against *Botrytis* (Janse van Rensburg et al., 2021). Similarly, allyl isothiocyanate (AITC) keeps microbes like *P. syringae* out by inducing stomatal closure (Bednarek, 2012).

CONCLUSION AND FUTURE PERSPECTIVE

Stomatal closure erects a physical barrier providing immediate relief against the entry of microbial pathogens into leaves while decreasing the rates of photosynthesis and transpiration. The closure has long-term consequences (**Figure 1**). The restricted CO_2 supply to the mesophyll cells lowers the rate of photosynthesis, stimulates photorespiration and associated H_2O_2 production. The elevated levels of H_2O_2, along with NO, H_2S, and Ca^{2+}, can upregulate genes involved in HR, PR, and PCD to prevent the spread of pathogens within the leaf. These reactive molecules also promote the accumulation of antimicrobial secondary metabolites. Parallelly, reduced transpiration creates mineral deficiency and limits microbial growth. We suggest that stomatal closure is a trigger to set off long-term events involved in prolonged plant disease resistance.

We know that stomatal closure may not be a universal mechanism to fight the microbial attack, e.g., root or stem pathogens. But several pathogens are air-borne and land on leaves (Melotto et al., 2008; Zeng et al., 2010). Plant-microbe interactions are not unilateral since the pathogens try to reopen stomata using compounds, such as, coronatine (Arnaud and Hwang, 2015). Further work is needed to understand the implications of stomatal closure on the antagonizing responses by the pathogens. Peroxisomal H_2O_2 limits microbial growth, but there are instances when microbes use peroxisomes to their advantage (Kubo, 2013). An improved understanding of peroxisomes and manipulation through biotechnological techniques could open up possibilities of designing plants for long-term adaptation to stress conditions. We believe that stomatal guard cells are ideal for studying plants' short-and long-term responses to challenging stress situations. Stomatal closure can be exploited to improve crop growth and grain yield under environmental stress conditions. In crops such as, wheat and

rice, reduced water requirement due to stomatal closure was used as one of the physiological traits in crop breeding (Park et al., 2020; Paul et al., 2020). Further studies on the long-term effects of stomatal closure can be translated into additional field applications.

AUTHOR CONTRIBUTIONS

AR conceptualized the idea, prepared the outline, and edited the final version. SG, PB, and AR pooled relevant literature, wrote the manuscript, and approved the final manuscript. All authors contributed to the article and approved the submitted version.

FUNDING

The stomatal work in our laboratory was supported by a grant (to AR) of the Council of Scientific and Industrial Research [No. 38 (1404)/15/EMR-II]. SG was supported by a Senior Research Fellowship from University Grant Commission, New Delhi. PB was supported partially by a University of Hyderabad BBL fellowship.

REFERENCES

Agostini, R. B., Postigo, A., Rius, S. P., Rech, G. E., Campos-Bermudez, V. A., and Vargas, W. A. (2019). Long-lasting primed state in maize plants: salicylic acid and steroid signaling pathways as key players in the early activation of immune responses in silks. *Mol. Plant Microbe Interact.* 32, 95–106. doi: 10.1094/MPMI-07-18-0208-R

Agurla, S., Gahir, S., Munemasa, S., Murata, Y., and Raghavendra, A. S. (2018). Mechanism of stomatal closure in plants exposed to drought and cold stress. *Adv. Exp. Med. Biol.* 1081, 215–232. doi: 10.1007/978-981-13-1244-1_12

Ahammed, G. J., Li, X., Zhang, G., Zhang, H., Shi, J., Pan, C., et al. (2018). Tomato photorespiratory glycolate-oxidase-derived H_2O_2 production contributes to basal defence against *Pseudomonas syringae*. *Plant Cell Environ.* 41, 1126–1138. doi: 10.1111/pce.12932

Arnaud, D., and Hwang, I. (2015). A sophisticated network of signaling pathways regulates stomatal defenses to bacterial pathogens. *Mol. Plant* 8, 566–581. doi: 10.1016/j.molp.2014.10.012

Bavaresco, L., and Eibach, R. (1987). Investigations on the influence of N fertilizer on resistance to powdery mildew (*Oidium tuckeri*) downy mildew (*Plasmopara viticola*) and on phytoalexin synthesis in different grapevine varieties. *Vitis* 26, 192–200.

Bednarek, P. (2012). Chemical warfare or modulators of defence responses—the function of secondary metabolites in plant immunity. *Curr. Opin. Plant Biol.* 15, 407–414. doi: 10.1016/j.pbi.2012.03.002

Bezrutczyk, M., Yang, J., Eom, J. S., Prior, M., Sosso, D., Hartwig, T., et al. (2018). Sugar flux and signaling in plant-microbe interactions. *Plant J.* 93, 675–685. doi: 10.1111/tpj.13775

Bharath, P., Gahir, S., and Raghavendra, A. S. (2021). Abscisic acid-induced stomatal closure: an important component of plant defense against abiotic and biotic stress. *Front. Plant Sci.* 12:615114. doi: 10.3389/fpls.2021.615114

Bürger, M., and Chory, J. (2019). Stressed out about hormones: how plants orchestrate immunity. *Cell Host Microbe.* 26, 163–172. doi: 10.1016/j.chom.2019.07.006

Cabot, C., Martos, S., Llugany, M., Gallego, B., Tolrà, R., and Poschenrieder, C. (2019). A role for zinc in plant defense against pathogens and herbivores. *Front. Plant Sci.* 10:1171. doi: 10.3389/fpls.2019.01171

Chang, Q., Liu, J., Lin, X., Hu, S., Yang, Y., Li, D., et al. (2017). A unique invertase is important for sugar absorption of an obligate biotrophic pathogen during infection. *New Phytol.* 215, 1548–1561. doi: 10.1111/nph.14666

Chen, L., Wang, W. S., Wang, T., Meng, X. F., Chen, T. T., Huang, X. X., et al. (2019). Methyl salicylate glucosylation regulates plant defense signaling and systemic acquired resistance. *Plant Physiol.* 180, 2167–2181. doi: 10.1104/pp.19.00091

Chen, X. L., Wang, Z., and Liu, C. (2016). Roles of peroxisomes in the rice blast fungus. *Biomed Res. Int.* 2016:9343417. doi: 10.1155/2016/9343417

Cui, H., Tsuda, K., and Parker, J. E. (2015). Effector-triggered immunity: from pathogen perception to robust defense. *Ann. Rev. Plant Biol.* 66, 487–511. doi: 10.1146/annurev-arplant-050213-040012

Feng, J., Zhang, M., Yang, K. N., and Zheng, C. X. (2020). Salicylic acid-primed defence response in octoploid strawberry "Benihoppe" leaves induces resistance against *Podosphaera aphanis* through enhanced accumulation of proanthocyanidins and upregulation of pathogenesis-related genes. *BMC Plant Biol.* 20:149. doi: 10.1186/s12870-020-02353-z

Fernández-Escobar, R. (2019). Olive nutritional status and tolerance to biotic and abiotic stresses. *Front. Plant Sci.* 10:1151. doi: 10.3389/fpls.2019.01151

Furutani, R., Makino, A., Suzuki, Y., Wada, S., Shimakawa, G., and Miyake, C. (2020). Intrinsic fluctuations in transpiration induce photorespiration to oxidize P700 in photosystem I. *Plants* 9:1761. doi: 10.3390/plants9121761

Gahir, S., Bharath, P., and Raghavendra, A. S. (2020). The role of gasotransmitters in movement of stomata: mechanisms of action and importance for plant immunity. *Biol. Plant.* 64, 623–632. doi: 10.32615/bp.2020.071

Gimenez-Ibanez, S., Chini, A., and Solano, R. (2016). How microbes twist jasmonate signaling around their little fingers. *Plants* 5:9. doi: 10.3390/plants5010009

Gonugunta, V. K., Srivastava, N., and Raghavendra, A. S. (2009). Cytosolic alkalinization is a common and early messenger preceding the production of ROS and NO during stomatal closure by variable signals, including abscisic acid, methyl jasmonate and chitosan. *Plant Signal. Behav.* 4, 561–564. doi: 10.4161/psb.4.6.8847

Grimmer, M. K., John Foulkes, M., and Paveley, N. D. (2012). Foliar pathogenesis and plant water relations: a review. *J. Exp. Bot.* 63, 4321–4331. doi: 10.1093/jxb/ers143

Haider, M. S., Kurjogi, M. M., Khalil-Ur-Rehman, M., Fiaz, M., Pervaiz, T., Jiu, S., et al. (2017). Grapevine immune signaling network in response to drought stress as revealed by transcriptomic analysis. *Plant Physiol. Biochem.* 121, 187–195. doi: 10.1016/j.plaphy.2017.10.026

Hsu, P. K., Dubeaux, G., Takahashi, Y., and Schroeder, J. I. (2021). Signaling mechanisms in abscisic acid-mediated stomatal closure. *Plant J.* 105, 307–321. doi: 10.1111/tpj.15067

Huai, B., Yang, Q., Wei, X., Pan, Q., Kang, Z., and Liu, J. (2020). TaSTP13 contributes to wheat susceptibility to stripe rust possibly by increasing cytoplasmic hexose concentration. *BMC Plant Biol.* 20:49. doi: 10.1186/s12870-020-2248-2

Huber, D., Römheld, V., and Weinmann, M. (2012). "Relationship between nutrition, plant diseases and pests," in *Mineral Nutrition of Higher Plants, 3rd Edn*, eds P. Marschner (Cambridge, MA: Academic press), 283–298. doi: 10.1016/B978-0-12-384905-2.00010-8

Hugouvieux, V., Barber, C. E., and Daniels, M. J. (1998). Entry of *Xanthomonas campestris* pv. campestris into hydathodes of Arabidopsis thaliana leaves: a system for studying early infection events in bacterial pathogenesis. *Mol. Plant-Microbe Interact.* 11, 537–543. doi: 10.1094/MPMI.1998.11.6.537

Janse van Rensburg, H. C., Limami, A. M., and Van den Ende, W. (2021). Spermine and spermidine priming against *Botrytis cinerea* modulates ROS dynamics and metabolism in Arabidopsis. *Biomolecules* 11:223. doi: 10.3390/biom11020223

Klüsener, B., Young, J. J., Murata, Y., Allen, G. J., Mori, I. C., Hugouvieux, V., et al. (2002). Convergence of calcium signaling pathways of pathogenic elicitors and abscisic acid in Arabidopsis guard cells. *Plant Physiol.* 130, 2152–2163. doi: 10.1104/pp.012187

Kohli, S. K., Khanna, K., Bhardwaj, R., Abd Allah, E. F., Ahmad, P., and Corpas, F. J. (2019). Assessment of subcellular ROS and NO metabolism in higher plants: multifunctional signaling molecules. *Anti-oxidants* 8:641. doi: 10.3390/antiox8120641

Kubo, Y. (2013). Function of peroxisomes in plant-pathogen interactions. *Subcell. Biochem.* 69, 329–345. doi: 10.1007/978-94-007-6889-5_18

Lal, A., Ku, M. S., and Edwards, G. E. (1996). Analysis of inhibition of photosynthesis due to water stress in the C3 species *Hordeum vulgare* and *Vicia faba*: electron transport, CO_2 fixation and carboxylation capacity. *Photosyn. Res.* 49, 57–69. doi: 10.1007/BF00029428

Lewandowska, M., Keyl, A., and Feussner, I. (2020). Wax biosynthesis in response to danger: its regulation upon abiotic and biotic stress. *New Phytol.* 227, 698–713. doi: 10.1111/nph.16571

Liang, J. S., and Zhang, J. H. (1999). The relations of stomatal closure and reopening to xylem ABA concentration and leaf water potential during soil drying and rewatering. *Plant Growth Regul.* 29, 77–86. doi: 10.1023/A:1006207900619

Liu, H., and Xue, S. (2021). Interplay between hydrogen sulfide and other signaling molecules in the regulation of guard cell signaling and abiotic/biotic stress response. *Plant Commun.* 2:100179. doi: 10.1016/j.xplc.2021.100179

Luna, E., Pastor, V., Robert, J., Flors, V., Mauch-Mani, B., and Ton, J. (2011). Callose deposition: a multifaceted plant defense response. *Mol. Plant-Microbe Interact.* 24, 183–193. doi: 10.1094/MPMI-07-10-0149

Marcec, M. J., Gilroy, S., Poovaiah, B. W., and Tanaka, K. (2019). Mutual interplay of Ca^{2+} and ROS signaling in plant immune response. *Plant Sci.* 283, 343–354. doi: 10.1016/j.plantsci.2019.03.004

Melotto, M., Underwood, W., and He, S. Y. (2008). Role of stomata in plant innate immunity and foliar bacterial diseases. *Annu. Rev. Phytopathol.* 46, 101–122. doi: 10.1146/annurev.phyto.121107.104959

Melotto, M., Zhang, L., Oblessuc, P. R., and He, S. Y. (2017). Stomatal defense a decade later. *Plant Physiol.* 174, 561–571. doi: 10.1104/pp.16.01853

Nguyen, Q. M., Iswanto, A., Son, G. H., and Kim, S. H. (2021). Recent advances in effector-triggered immunity in plants: new pieces in the puzzle create a different paradigm. *Int. J. Mol. Sci.* 22:4709. doi 10.3390/ijms22094709

Park, S. I., Kim, J. J., Shin, S. Y., Kim, Y. S., and Yoon, H. S. (2020). ASR enhances environmental stress tolerance and improves grain yield by modulating stomatal closure in rice. *Front. Plant Sci.* 10:1752. doi: 10.3389/fpls.2019.01752

Pascual, I., Azcona, I., Morales, F., Aguirreolea, J., and Sánchez-Díaz, M. (2010). Photosynthetic response of pepper plants to wilt induced by *Verticillium dahliae* and soil water deficit. *J. Plant Physiol.* 167, 701–708. doi: 10.1016/j.jplph.2009.12.012

Paul, J. M., Watson, A., and Griffiths, C. A. (2020). Linking fundamental science to crop improvement through understanding source and sink traits and their integration for yield enhancement. *J. Exp. Bot.* 71, 2270–2280. doi: 10.1093/jxb/erz480

Richardson, M. D., and Croughan, S. S. (1989). Potassium influence on susceptibility of bermudagrass to *Helminthosporium cynodontis* toxin. *Crop Sci.* 29, 1280–1282. doi: 10.2135/cropsci1989.0011183X002900050038x

Ruiz, J. M., and Romero, L. (2002). Renewed debate over transpiration and long-distance transport of minerals in plants. *Trends Plant Sci.* 7:56. doi: 10.1016/S1360-1385(02)02237-9

Saito, S., and Uozumi, N. (2019). Guard cell membrane anion transport systems and their regulatory components: an elaborate mechanism controlling stress-induced stomatal closure. *Plants* 8:9. doi: 10.3390/plants8010009

Sawinski, K., Mersmann, S., Robatzek, S., and Böhmer, M. (2013). Guarding the green: pathways to stomatal immunity. *Mol. Plant-Microbe Interact.* 26, 626–632. doi: 10.1094/MPMI-12-12-0288-CR

Scharte, J., Schön, H., and Weis, E. (2005). Photosynthesis and carbohydrate metabolism in tobacco leaves during an incompatible interaction with *Phytophthora nicotianae*. *Plant Cell Environ.* 28, 1421–1435. doi: 10.1111/j.1365-3040.2005.01380.x

Seifi, H. S., Zarei, A., Hsiang, T., and Shelp, B. J. (2019). Spermine is a potent plant defense activator against gray mold disease on *Solanum lycopersicum*, *Phaseolus vulgaris*, and *Arabidopsis thaliana*. *Phytopathology* 109, 1367–1377. doi: 10.1094/PHYTO-12-18-0470-R

Serrano, I., Romero-Puertas, M. C., Sandalio, L. M., and Olmedilla, A. (2015). The role of reactive oxygen species and nitric oxide in programmed cell death associated with self-incompatibility. *J. Exp. Bot.* 66, 2869–2876. doi: 10.1093/jxb/erv083

Shrestha, R. K., Lei, P., Shi, D., Hashimi, M. H., Wang, S., Xie, D., et al. (2021). Response of maize (*Zea mays* L.) towards vapor pressure deficit. *Environ. Exp. Bot.* 181:104293. doi: 10.1016/j.envexpbot.2020.104293

Solomon, P. S., Tan, K. C., and Oliver, R. P. (2003). The nutrient supply of pathogenic fungi; a fertile field for study. *Mol. Plant Pathol.* 4, 203–210. doi: 10.1046/j.1364-3703.2003.00161.x

Sørhagen, K., Laxa, M., Peterhänsel, C., and Reumann, S. (2013). The emerging role of photorespiration and non-photorespiratory peroxisomal metabolism in pathogen defence. *Plant Biol.* 15, 723–736. doi: 10.1111/j.1438-8677.2012.00723.x

Sun, L. R., Yue, C. M., and Hao, F. S. (2019). Update on roles of nitric oxide in regulating stomatal closure. *Plant Signal. Behav.* 14:e1649569. doi: 10.1080/15592324.2019.1649569

Sun, Y., Wang, M., Mur, L., Shen, Q., and Guo, S. (2020). Unravelling the roles of nitrogen nutrition in plant disease defences. *Int. J. Mol. Sci.* 21:572. doi: 10.3390/ijms21020572

Taler, D., Galperin, M., Benjamin, I., Cohen, Y., and Kenigsbuch, D. (2004). Plant eR genes that encode photorespiratory enzymes confer resistance against disease. *Plant Cell* 16, 172–184. doi: 10.1105/tpc.016352

Tanner, W., and Beevers, H. (2001). Transpiration, a prerequisite for long-distance transport of minerals in plants? *Proc. Natl. Acad. Sci. U.S.A.* 98, 9443–9447. doi: 10.1073/pnas.161279898

Trapet, P. L., Verbon, E. H., Bosma, R. R., Voordendag, K., Van Pelt, J. A., and Pieterse, C. (2021). Mechanisms underlying iron deficiency-induced resistance against pathogens with different lifestyles. *J. Exp. Bot.* 72, 2231–2241. doi: 10.1093/jxb/eraa535

van Butselaar, T., and Van den Ackerveken, G. (2020). Salicylic acid steers the growth-immunity tradeoff. *Trends Plant Sci.* 25, 566–576. doi: 10.1016/j.tplants.2020.02.002

Vo, K., Rahman, M. M., Rahman, M. M., Trinh, K., Kim, S. T., and Jeon, J. S. (2021). Proteomics and metabolomics studies on the biotic stress responses of rice: an update. *Rice* 14:30. doi: 10.1186/s12284-021-00461-4

Vojtovič, D., Luhová, L., and Petrivalský, M. (2020). Something smells bad to plant pathogens: production of hydrogen sulfide in plants and its role in plant defence responses. *J. Adv. Res.* 27, 199–209. doi: 10.1016/j.jare.2020.09.005

Voss, I., Sunil, B., Scheibe, R., and Raghavendra, A. S. (2013). Emerging concept for the role of photorespiration as an important part of abiotic stress response. *Plant Biol.* 15, 713–722. doi: 10.1111/j.1438-8677.2012.00710.x

Walters, D. (2003). Resistance to plant pathogens: possible roles for free polyamines and polyamine catabolism. *New Phytol.* 159, 109–115. doi: 10.1046/j.1469-8137.2003.00802.x

Wang, W., Paschalidis, K., Feng, J. C., Song, J., and Liu, J. H. (2019). Polyamine catabolism in plants: a universal process with diverse functions. *Front. Plant Sci.* 10:561. doi: 10.3389/fpls.2019.00561

Wang, X., Cai, X., Xu, C., Wang, Q., and Dai, S. (2016). Drought-responsive mechanisms in plant leaves revealed by proteomics. *Int. J. Mol. Sci.* 17:1706. doi: 10.3390/ijms17101706

Willmer, C. M., and Fricker, M. (1996). *Stomata*. London: Chapman and Hall. doi: 10.1007/978-94-011-0579-8

Ye, W., Munemasa, S., Shinya, T., Wu, W., Ma, T., Lu, J., et al. (2020). Stomatal immunity against fungal invasion comprises not only chitin-induced stomatal closure but also chitosan-induced guard cell death. *Proc. Natl. Acad. Sci. U.S.A.* 117, 20932–20942. doi: 10.1073/pnas.1922319117

Yuan, M., Huang, Y., Ge, W., Jia, Z., Song, S., Zhang, L., et al. (2019). Involvement of jasmonic acid, ethylene and salicylic acid signaling pathways behind the systemic resistance induced by *Trichoderma longibrachiatum* H9 in cucumber. *BMC Genom.* 20, 1–13. doi: 10.1186/s12864-019-5513-8

Zaynab, M., Fatima, M., Abbas, S., Sharif, Y., Umair, M., Zafar, M. H., et al. (2018). Role of secondary metabolites in plant defense against pathogens. *Microb. Pathog.* 124, 198–202. doi: 10.1016/j.micpath.2018.08.034

Zeng, W., Melotto, M., and He, S. Y. (2010). Plant stomata: a checkpoint of host immunity and pathogen virulence. *Curr. Opin. Biotechnol.* 21, 599–603. doi: 10.1016/j.copbio.2010.05.006

Conflict of Interest: The authors declare that the research was conducted in the absence of any commercial or financial relationships that could be construed as a potential conflict of interest.

frontiers in Plant Science

ORIGINAL RESEARCH
published: 08 October 2021
doi: 10.3389/fpls.2021.744991

Identification of Genes Preferentially Expressed in Stomatal Guard Cells of *Arabidopsis thaliana* and Involvement of the Aluminum-Activated Malate Transporter 6 Vacuolar Malate Channel in Stomatal Opening

Wenxiu Ye[1,2†], Shota Koya[3†], Yuki Hayashi[3], Huimin Jiang[1], Takaya Oishi[3], Kyohei Kato[3], Kohei Fukatsu[3] and Toshinori Kinoshita[2,3]*

[1] School of Agriculture and Biology, Shanghai Jiao Tong University, Shanghai, China, [2] Institute of Transformative Bio-Molecule, Nagoya University, Nagoya, Japan, [3] Graduate School of Science, Nagoya University, Nagoya, Japan

Stomatal guard cells (GCs) are highly specialized cells that respond to various stimuli, such as blue light (BL) and abscisic acid, for the regulation of stomatal aperture. Many signaling components that are involved in the stomatal movement are preferentially expressed in GCs. In this study, we identified four new such genes in addition to an aluminum-activated malate transporter, *ALMT6*, and GDSL lipase, *Occlusion of Stomatal Pore 1* (*OSP1*), based on the expression analysis using public resources, reverse transcription PCR, and promoter-driven β-glucuronidase assays. Some null mutants of GC-specific genes evidenced altered stomatal movement. We further investigated the role played by ALMT6, a vacuolar malate channel, in stomatal opening. Epidermal strips from an *ALMT6*-null mutant exhibited defective stomatal opening induced by BL and fusicoccin, a strong plasma membrane H^+-ATPase activator. The deficiency was enhanced when the assay buffer [Cl^-] was low, suggesting that malate and/or Cl^- facilitate efficient opening. The results indicate that the GC-specific genes are frequently involved in stomatal movement. Further detailed analyses of the hitherto uncharacterized GC-specific genes will provide new insights into stomatal regulation.

Keywords: ***ALMT6***, ***Arabidopsis***, **blue light, malate, proton pump, stomatal opening**

OPEN ACCESS

Edited by:
Tatsuru Masuda,
The University of Tokyo, Japan

Reviewed by:
June M. Kwak,
Daegu Gyeongbuk Institute of Science and Technology (DGIST), South Korea
Takayuki Shimizu,
The University of Tokyo, Japan

***Correspondence:**
Toshinori Kinoshita
kinoshita@bio.nagoya-u.ac.jp

† These authors have contributed equally to this work

Specialty section:
This article was submitted to Plant Physiology, a section of the journal Frontiers in Plant Science

Received: *21 July 2021*
Accepted: *13 September 2021*
Published: *08 October 2021*

Citation:
Ye W, Koya S, Hayashi Y, Jiang H, Oishi T, Kato K, Fukatsu K and Kinoshita T (2021) Identification of Genes Preferentially Expressed in Stomatal Guard Cells of Arabidopsis thaliana and Involvement of the Aluminum-Activated Malate Transporter 6 Vacuolar Malate Channel in Stomatal Opening. Front. Plant Sci. 12:744991. doi: 10.3389/fpls.2021.744991

INTRODUCTION

Stomata that are formed by pairs of guard cells (GCs) in the shoot epidermis of plants are key regulators of gas exchange, such as CO_2 uptake for photosynthesis and water loss during transpiration (Shimazaki et al., 2007; Munemasa et al., 2015). GCs respond to internal and external signals, such as light, CO_2, phytohormones, and microbial elicitors, where the stomata remain either open or close (Murata et al., 2015; Inoue and Kinoshita, 2017). Many critical signaling components that are involved in GC signaling are preferentially expressed in GCs, such as

Open Stomata 1 (OST1) (Mustilli et al., 2002), slow anion channel-associated 1 (SLAC1) (Negi et al., 2008; Vahisalu et al., 2008), high leaf temperature 1 (HT1) (Hashimoto et al., 2006), and aluminum-activated malate transporter 12 (ALMT12) (Meyer et al., 2010; Sasaki et al., 2010), suggesting that GC-specific genes are important candidates in hunting for new GC signaling components.

Blue light (BL) and red light (RL) are major cues for stomatal opening (Shimazaki et al., 2007; Inoue and Kinoshita, 2017). On BL perception, phototropins undergo autophosphorylation, which triggers signaling by BLUS1, BHP1, type 1 protein phosphatase (PP1), and its regulatory subunit PRSL1, in turn leading to phosphorylation of the penultimate threonine (penThr) residues of the plasma membrane (PM) H^+-ATPases, and the subsequent binding of 14-3-3 proteins activates the H^+-ATPases. More recently, RL was shown to induce the activation of GC PM H^+-ATPases by phosphorylation (Ando and Kinoshita, 2018). PM H^+-ATPases are important in terms of stomatal movement; the activation induces PM hyperpolarization, triggering a K^+ influx through inward-rectifying K^+ channels (Shimazaki et al., 2007; Inoue and Kinoshita, 2017). Together with the accumulation of K^+, the increase of counter anions, such as malate, biosynthesized in GCs and/or apoplast and Cl^- from apoplast, and other osmolytes, such as sucrose, lower the water potential in GCs, leading to an inflow of water, the swelling of GCs, and eventually the stomatal opening (Shimazaki et al., 2007; Santelia and Lawson, 2016). Recently, it has been shown that the activation of PM H^+-ATPases occurs upstream of starch degradation associated with BL-induced stomatal opening; this, combined with CO_2 fixation in GC chloroplasts, yields the carbon skeletons required for malate synthesis (Horrer et al., 2016). Vacuoles accumulate most of the ions and water that control stomatal movement (Barbier-Brygoo et al., 2011). The electrophysiological experiments revealed that the ALMT6 and ALMT9 vacuole channels facilitated malate and Cl^- import (Meyer et al., 2011); ALMT9 played a critical role in the light-induced stomatal opening (De Angeli et al., 2013).

To identify new signaling components involved in the light-induced stomatal opening, we reasoned that GC preferentially expressed genes are good candidates and identified four new such genes by the analyses of public resources, reverse transcription PCR (RT-PCR), and promoter GUS assay in *Arabidopsis thaliana*. Functional analysis revealed that some of the GC-specific genes in addition to ALMT6 are critical in the light-induced stomatal opening.

MATERIALS AND METHODS

Plant Materials and Growth Conditions

All *A. thaliana* strains were grown in soil under a photon flux density of 50 μmol m^{-2} s^{-1} and a 16-h-light/8-h-dark regime. The temperature and the relative humidity were 23 $\pm$ 2°C and 55–70%, respectively. All mutants [*at5g18430* (SALK_116756), *almt6-1* (GABI_259D05; Meyer et al., 2011), *at1g33811* (GABI_492D11), *osp1-1* (SALK _106116; Tang et al., 2020), and *at3g23840* (GABI_180G04)] are in the Columbia ecotype background (Col-0).

Isolation of Guard Cell Protoplasts and Mesophyll Cell Protoplasts

Guard cell protoplasts (GCPs) and mesophyll cell protoplasts (MCPs) were isolated from *glabra1-1* (*gl1*) as described previously (Okumura et al., 2016).

Reverse Transcription PCR

RNAs from *gl1* GCPs, MCPs, rosette leaves, roots, petioles, stems, flowers, and etiolated seedlings were extracted using the RNeasy Plant Mini Kit (QIAGEN) according to the protocol of the manufacturer. Complementary DNA was synthesized using the PrimeScript II 1st strand cDNA Synthesis Kit (Takara). The PCR primers are listed in **Supplementary Table 1**.

Promoter GUS Assay

The promoter regions (3-kb upstream of the start codons) of *AT5G18430*, *ALMT6*, *AT1G33811*, *OSP1*, *AT3G23840*, and *AT3G17070* were amplified in two PCR steps using the primers listed in **Supplementary Table 2** and cloned into pCR8/GW/TOPO followed by subcloning into pGWB433 binary vector. The vectors were transformed into *Agrobacterium* GV3101, which were then used to transform Col-0 by floral dip. Transformants were selected using kanamycin and carbenicillin and subjected to GUS staining at various developmental stages.

Stomatal Aperture Measurement

The stomatal aperture measurement was performed as described previously (Tomiyama et al., 2014; Toh et al., 2018). Epidermal tissues and leaf disks were prepared from dark-adapted plants and subjected to light illumination and fusicoccin (FC) treatment. The apertures were measured under a microscope (Olympus).

Immunohistochemical Staining of Plasma Membrane H^+-ATPase in Guard Cells

The immunohistochemical staining was performed as described previously (Hayashi et al., 2011). Epidermal tissues were prepared from dark-adapted plants and subjected to light illumination and FC treatment. RL (50 μmol m^{-2} s^{-1}) was illuminated for 20 min (Red), and BL (10 μmol m^{-2} s^{-1}) was illuminated with superimposed on RL for 2.5 min (Red + Blue). FC at 10 μM was applied to the epidermal tissue for 5 min in the dark (FC). PM H^+-ATPases and the phosphorylation level of the penThr were detected using specific antibodies against the catalytic domain of AHA2 (anti-PM H^+-ATPase antibody) and phosphorylated Thr-947 in AHA2 (anti-pThr) (Hayashi et al., 2010).

Accession Numbers

Sequence data can be found in the Arabidopsis genome database TAIR10 under the following accession numbers: ALMT6 (AT2G17470), OSP1 (AT2G04570), ALMT9 (AT3G18440), AT1G02980, AT1G12030, AT1G33811, AT2G32830, AT3G17070, AT3G23840, and AT5G18430.

RESULTS

Genes Preferentially Expressed in *Arabidopsis* Guard Cells

We analyzed publicly available microarray data on GCPs and MCPs (Yang et al., 2008), and those of the *Arabidopsis* eFP browsers[1]. The inclusion criteria were as follows: (1) a microarray GCP signal unique to GCPs or at least fourfold higher than the MCP signal and (2) the "Tissue-Specific" criteria of the *Arabidopsis* eFP browsers indicated GC-specific expression. We retrieved 124 candidate genes and checked their expression levels by RT-PCR in various cells, tissues, and organs of *A. thaliana* (**Figure 1A**). A total of 10 genes were strongly expressed in GCPs but not in MCPs and roots; these included *SLAC1*, the cation/H^+ exchanger-encoding *AtCHX20*, and genes encoding the GDSL lipases *OSP1* and *ALMT6* (which are preferentially expressed in GCs; Padmanaban et al., 2007; Negi et al., 2008; Vahisalu et al., 2008; Tang et al., 2020) and six functionally uncharacterized genes. The RT-PCR data for *OSP1*, *ALMT6*, and the uncharacterized genes are shown in **Figure 1B**.

To further confirm preferential GC expression in intact plants, we constructed transgenic plants expressing the reporter β-GUS-encoding gene driven by promoter regions ranging to about 3-kb upstream of the start codons. *pALMT6*:*GUS* and *pOSP1*:*GUS* exhibited the high-level GUS activity in GCs (in particular) (**Figure 1C**), consistent with previous findings (Meyer et al., 2011; Tang et al., 2020). Also, the *AT1G33811*, *AT3G23840*, *AT3G17070*, and *AT5G18430* promoters drove GC-preferential GUS expression (**Figures 1C**, **2A**). The *ALMT6*, *AT1G33811*, *OSP1*, *AT3G17070,* and *AT3G23840* promoters drove GUS expression in stipules, lateral roots, and trichomes (**Figure 3A**); however, the *AT5G18430* promoter was active in GCs only (**Figure 2A**). The *AT1G12030* and *AT2G32830* promoters never drove GUS expression, rendering the analyses difficult. This is

[1]https://bar.utoronto.ca/efp/cgi-bin/efpWeb.cgi

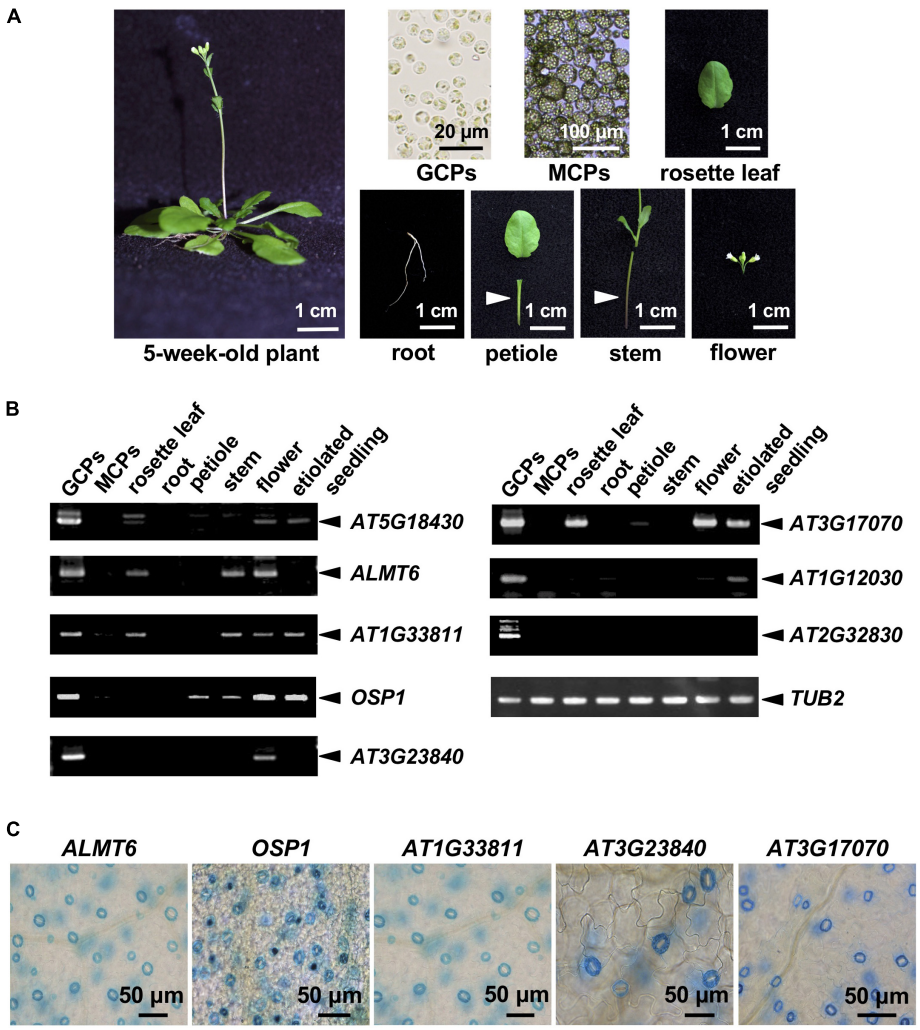

FIGURE 1 | Guard cell (GC)-preferentially expressed genes. **(A)** The plant organs, tissues, and cells used in the analysis. **(B)** GC-preferentially expressed genes as revealed by RT-PCR using the materials shown in panel **(A)**. **(C)** GC-preferentially expressed genes in GUS-reporter-bearing plants.

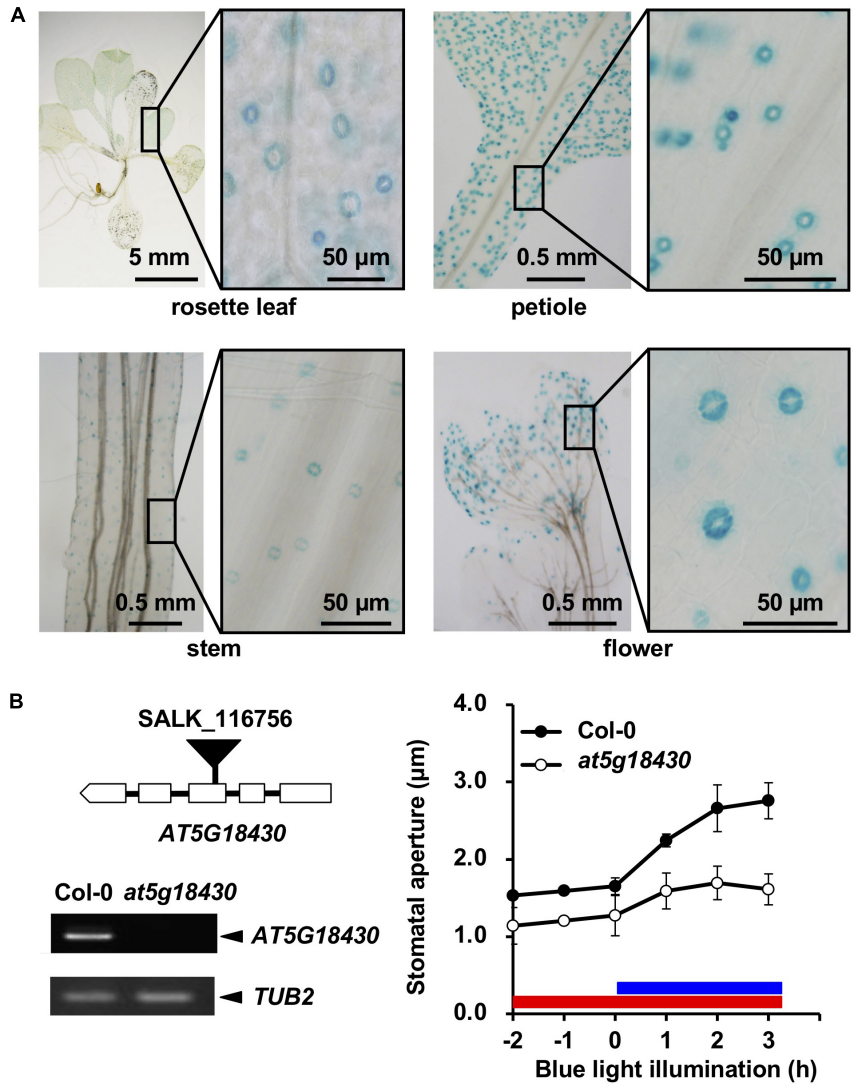

FIGURE 2 | Expression of *At5g18430* and the stomatal phenotype of the *at5g18430* mutant. **(A)** Expression pattern of *At5g18430* in GUS-reporter-bearing plants. **(B)** The stomatal phenotype of the *at5g18430* mutant. Left: A schematic of the T-DNA insertion site in *at5g18430* and the transcript levels in leaves. Right: blue light (BL)-induced stomatal opening in Col-0 and *at5g18430* epidermal tissues. The red bar indicates the red light (RL) illumination period (50 µmol m^{-2} s^{-1}). The blue bar indicates the BL illumination period (10 µmol m^{-2} s^{-1}). Epidermal tissues were incubated in 50 mM KCl, 0.1 mM $CaCl_2$, and 10 mM Mes-BTP (pH 6.5). Averages from three independent experiments are shown. Error bars: SDs (n = 3).

probably due to the lack of or weak activity of the 3-kb upstream promoter regions of these two genes.

Stomatal Phenotypes of Null Mutants of Genes Preferentially Expressed in Guard Cells

We prepared null mutants of *OSP1*, *AT1G33811*, *AT3G23840*, *AT3G17070*, and *AT5G18430*. Although we failed to obtain the knockout mutants of *at3g17070* (SALK_121694), the null mutants of *at5g18430* (SALK_116756) and *at3g23840* (GABI_180G04) were impaired in BL-induced stomatal opening (**Figure 2B**) and light-induced stomatal opening (**Figure 3B**), respectively. Interestingly, the stomata of *at1g33811* (GABI_492D11) null mutant were open even in the dark (**Figure 3B**). The null mutant of *OSP1*, i.e., *osp1-1*, exhibited a normal stable-status stomatal opening in the light (**Figure 3B** and **Supplementary Figure 1**), which is consistent with a previous report (Tang et al., 2020). Thus, the previously uncharacterized GC-specific genes *AT1G33811*, *AT3G23840*, and *AT5G18430* may be involved in stomatal movement.

Characterization of the *ALMT6*-Null Mutant in Terms of Blue Light-Induced Stomatal Opening

The ALMT6 is a vacuolar malate channel (Meyer et al., 2011). We explored the stomatal movements of the *almt6-1* mutant in

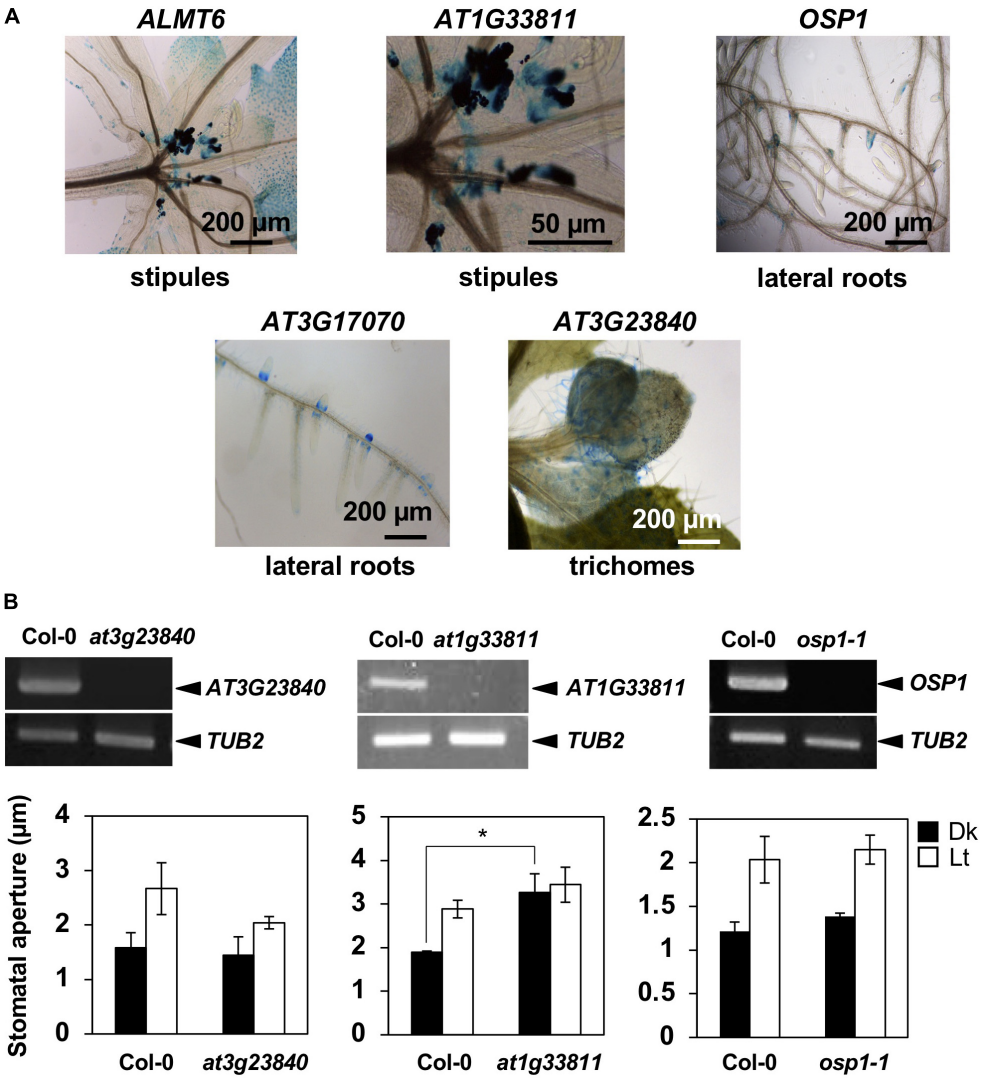

FIGURE 3 | Expression patterns of GC-preferentially expressed genes and the stomatal phenotypes of knockout mutants. **(A)** Gene expression in tissues other than stomata as revealed by the GUS-reporter assay. **(B)** Upper panels show the RT-PCR of target genes. Lower graphs show BL-induced stomatal opening in *at3g23840*, *at1g33811*, and *osp1-1* null mutants. Epidermal tissues (*at3g23840* and *at1g33811* mutants) or leaf disks (*osp1-1* mutant) were incubated in 50 mM KCl, 0.1 mM $CaCl_2$, and 10 mM Mes-BTP (pH 6.5). Dark bars, dark treatment for 3 h (Dk); white bars, light treatment for 3 h (RL, 50 μmol m^{-2} s^{-1}; BL, 10 μmol m^{-2} s^{-1}) (Lt). Average values from three independent experiments are shown. Error bars: SDs (n = 3).

detail. The expression of *ALMT9* in GCs is not altered in *almt6-1* (**Supplementary Figure 2**). As shown in **Figure 4A**, the stomata of *almt6-1* were slightly narrower than wild type under the dark and RL condition, as well as opened but less efficiently to a similar size of those of wild type on BL illumination. Less efficiency of *almt6-1* stomatal opening in response to 10 μM FC, an activator of PM H^+-ATPase, was more prominent compared with the case of BL-induced stomatal opening (**Figure 4B**). Stomatal apertures in the *almt6-1* mutant were comparable to those in wild type when epidermal peels were treated with light or FC for more than 3 or 4 h, respectively (**Figures 4A,B**). Thus, ALMT6 may be required for stomatal opening induced by BL and FC. It is worthy of note that usually BL-insensitive mutants, such as *phot1 phot2* double mutant, show completely insensitive phenotype to BL but open normally in response to FC (Kinoshita et al., 2001). The less efficient phenotype of stomatal opening in *almt6-1* is very similar to a *kincless* mutant (Lebaudy et al., 2008) and *aks1 aks2* mutant (Takahashi et al., 2013), which shows the low activity of PM inward K^+ channels in GCs, suggesting that the deficient of ion transport for stomatal opening leads to less efficiency of stomatal opening.

The ALMT6 transports (principally) malate and fumarate but Cl^- to a lesser extent (Meyer et al., 2011); we thus explored how Cl^- affected BL-induced stomatal opening. The usual stomatal assay buffer contains 50 mM KCl, 0.1 mM $CaCl_2$, and 10 mM Mes-BTP (pH 6.5). To exclude exogenous Cl^-, we evaluated stomatal opening in a buffer with 50 mM potassium gluconate, 0.1 mM $CaCl_2$, and 10 mM Mes-BTP (pH 6.5). Gluconate does

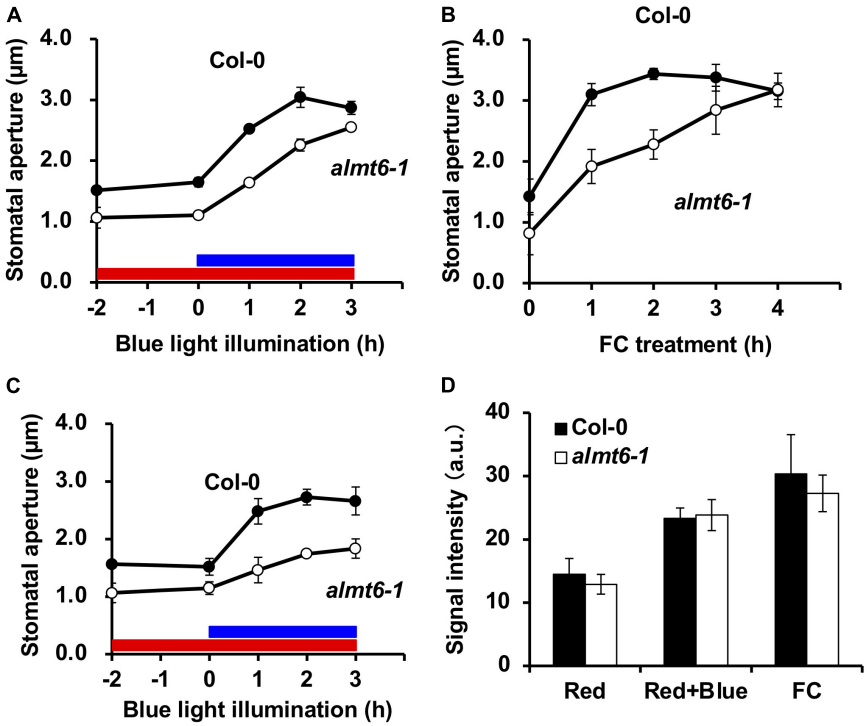

FIGURE 4 | Stomatal phenotypes in wild-type Col-0 and *almt6-1* mutant. **(A)** BL-induced stomatal opening in wild-type Col-0 and *almt6-1* mutant epidermal tissues. Red bar: RL illumination period (50 μmol m^{-2} s^{-1}). Blue bar: BL illumination period (10 μmol m^{-2} s^{-1}). **(B)** Fusicoccin (FC)-induced stomatal opening in Col-0 and *almt6-1* epidermal tissues. In panels **(A,B)**, epidermal tissues were incubated in 50 mM KCl, 0.1 mM $CaCl_2$, and 10 mM Mes-BTP (pH 6.5) and then subjected to light and 10 μM FC treatments. **(C)** BL-induced stomatal opening in low Cl^- (0.2 mM) buffer of Col-0 and *almt6-1* epidermal tissues. Epidermal tissues were incubated in 50 mM potassium gluconate, 0.1 mM $CaCl_2$, and 10 mM Mes-BTP (pH 6.5). Averages from three independent experiments are shown. Error bars: SDs (n = 3). The other conditions are those in panel **(A)**. **(D)** Immunohistochemical detection of BL- and 10 μM FC-induced phosphorylation of PM H^+-ATPase in Col-0 and *almt6-1* GCs. GC fluorescence was quantified using an anti-pThr antibody and Alexa Fluor 488-conjugated secondary antibody as described in section "Materials and Methods." Bars: Averages from three independent experiments. Error bars: SDs (n = 3). a.u., arbitrary units.

not readily cross the PM. **Figure 4C** shows that the 3-h BL-induced stomatal opening at a low [Cl^-] was impaired in the *almt6-1* mutant in terms of both speed and amplitude.

Blue Light- and FC-Induced Phosphorylation of Plasma Membrane H^+-ATPase in the *almt6-1* Mutant

Both BL and FC induce the phosphorylation of the penThr of PM H^+-ATPases, in GCs, which provides a driving force for stomatal opening (Inoue and Kinoshita, 2017). Thus, we immunohistochemically investigated the effects of BL and FC on the phosphorylation status of GC PM H^+-ATPase; such phosphorylation was not impaired in the *almt6-1* mutant (**Figure 4D**). The amount of PM H^+-ATPase in *almt6-1* under BL and FC was comparative to that in wild type (**Supplementary Figure 3**). The *almt6* mutation did not affect PM H^+-ATPase phosphorylation and amount in response to BL and FC.

DISCUSSION

In this study, we identified 10 genes including *SLAC1*, Cation/H^+ Exchanger *AtCHX20*, GDSL lipases *OSP1* and *ALMT6*, preferentially expressed in GCs based on the analyses of public resources, RT-PCR, and promoter GUS assay (**Figures 1–3**). Of these, *AT1G33811*, *AT3G17070*, *AT3G23840*, and *AT5G18430* have not been functionally characterized in stomata. Among these four genes, three genes, namely, *AT1G33811*, *AT3G23840*, and *AT5G18430*, were found involved in the stomatal movement (**Figures 2**, **3**). Remarkably, two of them, *AT1G33811* and *AT5G18430*, are members of the GDSL family of serine esterases/lipases (Akoh et al., 2004), indicating the importance of this family in regulating stomatal movement. Tang et al. (2020) found that a GDSL lipase, i.e., OSP1, is preferentially expressed in GCs, and *osp1* mutants showed low stomatal conductance and high leaf temperature due to a high percentage of occluded stomata. Detail biological and/or biochemical analyses revealed that OSP1 is required for wax biosynthesis and proper formation of the stomatal outer cuticular ledge (Tang et al., 2020). Interestingly, *osp1* mutants were also impaired in abscisic acid (ABA)-induced stomatal closure, indicating a potential role of OSP1 in stomatal movement (Tang et al., 2020). It would be very interesting to investigate whether AT1G33811 and AT5G18430 have similar functions as OSP1. *AT3G23840*, previously named as *CER26-like*, is probably related to very long-chain fatty acid metabolism

(Pascal et al., 2013), and a knockout mutant, *at3g23840*, showed reduced light-induced stomatal opening (**Figure 3B**). Future study is needed to provide a detailed mechanism mediated by those genes in stomatal movement.

The detailed analyses of expression pattern by GUS-reporter assay of *ALMT6*, *OSP1*, *AT1G33811*, *AT3G17070*, *AT3G23840*, and *AT5G18430* revealed that promoter regions, i.e., 3-kb upstream of the start codon, drive GC-preferential gene expression with *AT5G18430* promoter showing the most GC-selective property (**Figures 1–3**). The 1-kb upstream region of the *AT3G23840* start codon was promoter-active in flowers (Pascal et al., 2013). The 3-kb promoter region of *AT3G23840* studied here showed strong GC signals in addition to flower (**Figure 1B**). The 3-kb promoter region of *ALMT6* studied here was more GC-specific than a 1.8-kb region used previously, which exhibited strong activities in floral tissues, such as sepals, petals, and anthers (i.e., not only GCs; Meyer et al., 2011) (**Figures 1C**, **3A**). These results suggest that specific elements and their patterns determine the GC-specific activity of promoters. So far, several GC-preferentially expressed genes, such as *GC1* (Yang et al., 2008) and *MYB60* (Cominelli et al., 2005), were reported. However, these genes were out of our strict criteria, indicating that the genes reported in this study are more specific in GCs (**Supplementary Figure 4**). Cell type-specific promoters are important tools to study gene function and of great application potential (Imlau et al., 1999; Yang et al., 2008; Wang et al., 2014). The promoters identified in this study thus add the options for promoter engineering for GC-specific gene regulation.

Both ALMT6 and ALMT9 were initially identified as channels mediating malate accumulation in vacuoles (Kovermann et al., 2007; Meyer et al., 2011). Later, ALMT9 was shown to be a Cl^- channel regulated by cytosol malate and to be required for the light-induced stomatal opening (De Angeli et al., 2013). As shown in **Figures 4A,B**, *almt6-1* mutant opened stomata with less efficiency in response to BL illumination and FC treatment, suggesting that ALMT6 is also required for BL- and FC-induced stomatal opening. Notably, *almt6-1* mutant showed significant impairment in BL-induced stomatal opening under low Cl^- condition (**Figure 4C**), suggesting that ALMT6, such as ALMT9, also contributes Cl^- influx to vacuole during stomatal opening. Since both *almt6* and *almt9* single mutants are impaired in the light-induced stomatal opening and there is no compensation of *ALMT9* expression in *almt6* (**Supplementary Figure 2**), it is possible that ALMT6 and ALMT9 function in an additive and/or cooperative manner. In the cooperative mode, a bold hypothesis is that ALMT6 and ALMT9 form heteromeric channels mediating anion accumulation in GC vacuoles as they were shown to form tetramer channels in heterosystems (Zhang et al., 2013). Future electrophysiological and genetic studies such as phenotyping using *almt6 almt9* double mutant are needed to clarify the contribution of ALMT6 and ALMT9 in stomatal opening.

In this study, we identified preferentially expressed genes in GCs and found that some uncharacterized genes are involved in stomatal movement. Especially, to our knowledge, AT5G18430 shows the most specific expression in GCs. In addition, we showed evidence that ALMT6 is important for BL- and FC-induced stomatal opening. Further detailed analyses of the uncharacterized GC-specific genes will provide novel understandings for stomatal movement.

DATA AVAILABILITY STATEMENT

The original contributions presented in the study are included in the article/**Supplementary Material**, further inquiries can be directed to the corresponding author/s.

AUTHOR CONTRIBUTIONS

WY, SK, and TK designed the experiments. WY, SK, YH, HJ, TO, KK, and TK performed the experiments. WY, SK, YH, and TK wrote the manuscript. All authors contributed to the article and approved the submitted version.

FUNDING

This study was supported by the Grants-in-Aid for Scientific Research from MEXT (Nos. 15H05956, 20H05687, and 20H05910 to TK).

ACKNOWLEDGMENTS

We would like to thank Koji Takahashi and Shin-ichiro Inoue for providing technical advice.

SUPPLEMENTARY MATERIAL

The Supplementary Material for this article can be found online at: https://www.frontiersin.org/articles/10.3389/fpls.2021.744991/full#supplementary-material

REFERENCES

Akoh, C. C., Lee, G., Liaw, Y., Huang, T., and Shaw, J. (2004). GDSL family of serine esterases/lipases. *Prog. Lipid Res.* 43, 534–552. doi: 10.1016/j.plipres.2004.09.002

Ando, E., and Kinoshita, T. (2018). Red light-induced phosphorylation of plasma membrane H^+-ATPase in stomatal guard cells. *Plant Physiol.* 178, 838–849. doi: 10.1104/pp.18.00544

Barbier-Brygoo, H., De Angeli, A., Filleur, S., Frachisse, J. M., Gambale, F., Thomine, S., et al. (2011). Anion channels/transporters in plants: from molecular bases to regulatory networks. *Annu. Rev. Plant Biol.* 62, 25–51. doi: 10.1146/annurev-arplant-042110-103741

Cominelli, E., Galbiati, M., Vavasseur, A., Conti, L., Sala, T., Vuylsteke, M., et al. (2005). A guard-cell-specific MYB transcription factor regulates stomatal movements and plant drought tolerance. *Curr. Biol.* 15, 1196–1200.

De Angeli, A., Zhang, J., Meyer, S., and Martinoia, E. (2013). AtALMT9 is a malate-activated vacuolar chloride channel required for stomatal opening in *Arabidopsis*. *Nat. Commun.* 4:1804.

Hashimoto, M., Negi, J., Young, J., Israelsson, M., Schroeder, J. I., and Iba, K. (2006). *Arabidopsis* HT1 kinase controls stomatal movements in response to CO2. *Nat. Cell Biol.* 8, 391–397. doi: 10.1038/ncb1387

Hayashi, M., Inoue, S., Takahashi, K., and Kinoshita, T. (2011). Immunohistochemical detection of blue light-induced phosphorylation of the plasma membrane H^+-ATPase in Stomatal Guard Cells. *Plant Cell Physiol.* 52, 1238–1248. doi: 10.1093/pcp/pcr072

Hayashi, Y., Nakamura, S., Takemiya, A., Takahashi, Y., Shimazaki, K., and Kinoshita, T. (2010). Biochemical characterization of in vitro phosphorylation and dephosphorylation of the plasma membrane H^+-ATPase. *Plant Cell Physiol.* 51, 1186–1196. doi: 10.1093/pcp/pcq078

Horrer, D., Flütsch, S., Pazmino, D., Matthews, J. S. A., Thalmann, M., Nigro, A., et al. (2016). Blue light induces a distinct starch degradation pathway in guard cells for stomatal opening. *Curr. Biol.* 26, 362–370. doi: 10.1016/j.cub.2015.12.036

Imlau, A., Truernit, E., and Sauer, N. (1999). Cell-to-cell and long-distance trafficking of the green fluorescent protein in the phloem and symplastic unloading of the protein into sink tissues. *Plant Cell* 11, 309–322. doi: 10.2307/3870862

Inoue, S., and Kinoshita, T. (2017). Blue light regulation of stomatal opening and the plasma membrane H+-ATPase. *Plant Physiol.* 174, 531–538. doi: 10.1104/pp.17.00166

Kinoshita, T., Doi, M., Suetsugu, N., Kagawa, T., Wada, M., and Shimazaki, K. (2001). phot1 and phot2 mediate blue light regulation of stomatal opening. *Nature* 414, 656–660. doi: 10.1038/414656a

Kovermann, P., Meyer, S., Hörtensteiner, S., Picco, C., Scholz-Starke, J., Ravera, S., et al. (2007). The *Arabidopsis* vacuolar malate channel is a member of the ALMT family. *Plant J.* 52, 1169–1180. doi: 10.1111/j.1365-313x.2007.03367.x

Lebaudy, A., Vavasseur, A., Hosy, E., Dreyer, I., Leonhardt, N., Thibaud, J. B., et al. (2008). Plant adaptation to fluctuating environment and biomass production are strongly dependent on guard cell potassium channels. *Proc. Natl. Acad. Sci. U.S.A.* 105, 5271–5276. doi: 10.1073/pnas.0709732105

Meyer, S., Mumm, P., Imes, D., Endler, A., Weder, B., Al-Rasheid, K. A. S., et al. (2010). AtALMT12 represents an R-type anion channel required for stomatal movement in *Arabidopsis* guard cells. *Plant J.* 63, 1054–1062. doi: 10.1111/j.1365-313x.2010.04302.x

Meyer, S., Scholz-Starke, J., De Angeli, A., Kovermann, P., Burla, B., Gambale, F., et al. (2011). Malate transport by the vacuolar AtALMT6 channel in guard cells is subject to multiple regulation. *Plant J.* 67, 247–257. doi: 10.1111/j.1365-313x.2011.04587.x

Munemasa, S., Hauser, F., Park, J., Waadt, R., Brandt, B., and Schroeder, J. I. (2015). Mechanisms of abscisic acid-mediated control of stomatal aperture. *Curr. Opin. Plant Biol.* 28, 154–162. doi: 10.1016/j.pbi.2015.10.010

Murata, Y., Mori, I. C., and Munemasa, S. (2015). Diverse stomatal signaling and the signal integration mechanism. *Annu. Rev. Plant Biol.* 66, 369–392. doi: 10.1146/annurev-arplant-043014-114707

Mustilli, A. C., Merlot, S., Vavasseur, A., Fenzi, F., and Giraudat, J. (2002). *Arabidopsis* OST1 protein kinase mediates the regulation of stomatal aperture by abscisic acid and acts upstream of reactive oxygen species production. *Plant Cell* 14, 3089–3099. doi: 10.1105/tpc.007906

Negi, J., Matsuda, O., Nagasawa, T., Oba, Y., Takahashi, H., Kawai-Yamada, M., et al. (2008). CO2 regulator SLAC1 and its homologues are essential for anion homeostasis in plant cells. *Nature* 452, 483–486. doi: 10.1038/nature06720

Okumura, M., Inoue, S., Kuwata, K., and Kinoshita, T. (2016). Photosynthesis activates plasma membrane H^+-ATPase via sugar accumulation. *Plant Physiol.* 171, 580–589. doi: 10.1104/pp.16.00355

Padmanaban, S., Chanroj, S., Kwak, J. M., Li, X., Ward, J. M., and Sze, H. (2007). Participation of endomembrane cation/H+ exchanger AtCHX20 in osmoregulation of guard cells. *Plant Physiol.* 144, 82–93. doi: 10.1104/pp.106.092155

Pascal, S., Bernard, A., Sorel, M., Pervent, M., Vile, D., Haslam, R. P., et al. (2013). The *Arabidopsis* cer26 mutant, like the cer2 mutant, is specifically affected in the very long chain fatty acid elongation process. *Plant J.* 73, 733–746. doi: 10.1111/tpj.12060

Santelia, D., and Lawson, T. (2016). Rethinking guard cell metabolism. *Plant Physiol.* 172, 1371–1392. doi: 10.1104/pp.16.00767

Sasaki, T., Mori, I. C., Furuichi, T., Munemasa, S., Toyooka, K., Matsuoka, K., et al. (2010). Closing plant stomata requires a homolog of an aluminum-activated malate transporter. *Plant Cell Physiol.* 51, 354–365. doi: 10.1093/pcp/pcq016

Shimazaki, K., Doi, M., Assmann, S. M., and Kinoshita, T. (2007). Light regulation of stomatal movement. *Annu. Rev. Plant Biol.* 58, 219–247. doi: 10.1146/annurev.arplant.57.032905.105434

Takahashi, Y., Ebisu, Y., Kinoshita, T., Doi, M., Okuma, E., Murata, Y., et al. (2013). bHLH transcription factors that facilitate K+ uptake during stomatal opening are repressed by abscisic acid through phosphorylation. *Sci. Signal.* 6:ra48. doi: 10.1126/scisignal.2003760

Tang, J., Yang, X., Xiao, C., Li, J., Chen, Y., Li, R., et al. (2020). GDSL lipase occluded stomatal pore 1 is required for wax biosynthesis and stomatal cuticular ledge formation. *New Phytol.* 228, 1880–1896. doi: 10.1111/nph.16741

Toh, S., Inoue, S., Toda, Y., Yuki, T., Suzuki, K., Hamamoto, S., et al. (2018). Identification and characterization of compounds that affect stomatal movements. *Plant Cell Physiol.* 59, 1568–1580. doi: 10.1093/pcp/pcy061

Tomiyama, M., Inoue, S., Tsuzuki, T., Soda, M., Morimoto, S., Okigaki, Y., et al. (2014). Mg-chelatase I subunit 1 and Mg-protoporphyrin IX methyltransferase affect the stomatal aperture in *Arabidopsis thaliana*. *J. Plant Res.* 127, 553–563. doi: 10.1007/s10265-014-0636-0

Vahisalu, T., Kollist, H., Wang, Y. F., Nishimura, N., Chan, W. Y., Valerio, G., et al. (2008). SLAC1 is required for plant guard cell S-type anion channel function in stomatal signalling. *Nature* 452, 487–491. doi: 10.1038/nature06608

Wang, Y., Noguchi, K., Ono, N., Inoue, S., Terashima, I., and Kinoshita, T. (2014). Overexpression of plasma membrane H+-ATPase in guard cells promotes light-induced stomatal opening and enhances plant growth. *Proc. Natl. Acad. Sci. U.S.A.* 111, 533–538. doi: 10.1073/pnas.1305438111

Yang, Y., Costa, A., Leonhardt, N., Siegel, R. S., and Schroeder, J. I. (2008). Isolation of a strong *Arabidopsis* guard cell promoter and its potential as a research tool. *Plant Methods* 4:6.

Zhang, J., Baetz, U., Krügel, U., Martinoia, E., and De Angeli, A. (2013). Identification of a probable pore-forming domain in the multimeric vacuolar anion channel AtALMT9. *Plant Physiol.* 163, 830–843. doi: 10.1104/pp.113.219832

Conflict of Interest: The authors declare that the research was conducted in the absence of any commercial or financial relationships that could be construed as a potential conflict of interest.

Publisher's Note: All claims expressed in this article are solely those of the authors and do not necessarily represent those of their affiliated organizations, or those of the publisher, the editors and the reviewers. Any product that may be evaluated in this article, or claim that may be made by its manufacturer, is not guaranteed or endorsed by the publisher.

frontiers in Plant Science

REVIEW
published: 11 October 2021
doi: 10.3389/fpls.2021.751852

Stomatal Lineage Control by Developmental Program and Environmental Cues

Soon-Ki Han[1], June M. Kwak[1] and Xingyun Qi[2]**

[1]Department of New Biology, DGIST, Daegu, South Korea, [2]Department of Biology, Rutgers University, Camden, NJ, United States

Stomata are micropores that allow plants to breathe and play a critical role in photosynthesis and nutrient uptake by regulating gas exchange and transpiration. Stomatal development, therefore, is optimized for survival and growth of the plant despite variable environmental conditions. Signaling cascades and transcriptional networks that determine the birth, proliferation, and differentiation of a stomate have been identified. These networks ensure proper stomatal patterning, density, and polarity. Environmental cues also influence stomatal development. In this review, we highlight recent findings regarding the developmental program governing cell fate and dynamics of stomatal lineage cells at the cell state- or single-cell level. We also overview the control of stomatal development by environmental cues as well as developmental plasticity associated with stomatal function and physiology. Recent advances in our understanding of stomatal development will provide a route to improving photosynthesis and water-stress resilience of crop plants in the climate change we currently face.

Keywords: stomatal lineage, development, transcription, environment

OPEN ACCESS

Edited by:
Wenxiu Ye,
Shanghai Jiao Tong University, China

Reviewed by:
Jin Suk Lee,
Concordia University, Canada
Eigo Ando,
The University of Tokyo, Japan

****Correspondence:***
Soon-Ki Han
soonhan@dgist.ac.kr
Xingyun Qi
xq67@camden.rutgers.edu

Specialty section:
This article was submitted to Plant Cell Biology, a section of the journal Frontiers in Plant Science

Received: *02 August 2021*
Accepted: *10 September 2021*
Published: *11 October 2021*

Citation:
Han S-K, Kwak JM and Qi X (2021) Stomatal Lineage Control by Developmental Program and Environmental Cues. Front. Plant Sci. 12:751852. doi: 10.3389/fpls.2021.751852

INTRODUCTION

When plants transition from water to land, they became more exposed to carbon dioxide (CO_2) and arid conditions. The evolution of stomata enabled plants to respond to the increased CO_2 availability and limit water loss, ensuring their survival on land. Stomata are micropores on plant surface that are surrounded by two guard cells. These stomata open and close to facilitate gas exchange between plant inner tissues and the environment. Optimal gas exchange and water usage require efficient allocation of leaf surface to stomata. Improper stomatal patterning and density result in a change in mesophyll tissues and the epidermal area, affecting photosynthesis (Chen et al., 2016). Stomatal development, therefore, is tightly regulated to ensure there is no loss in photosynthesis efficiency.

Stomata are found in most land plants (Duckett and Pressel, 2018), and the basic morphology is highly conserved (Chen et al., 2017). Most land plants, including Arabidopsis and grasses, undergo stomatal lineage progression and bear similar molecular components despite their substantial differences in morphology and arrangements (Raissig et al., 2016; Hepworth et al., 2018; Conklin et al., 2019; McKown and Bergmann, 2020). In dicotyledonous Arabidopsis, stomatal development initiates from a subset of protodermal cells, meristemoid mother cells (MMCs), which gain stem-cell fate (**Figure 1**). These MMCs undergo several rounds of amplifying division, where asymmetric division occurs in an inward spiral manner. Each round of asymmetric

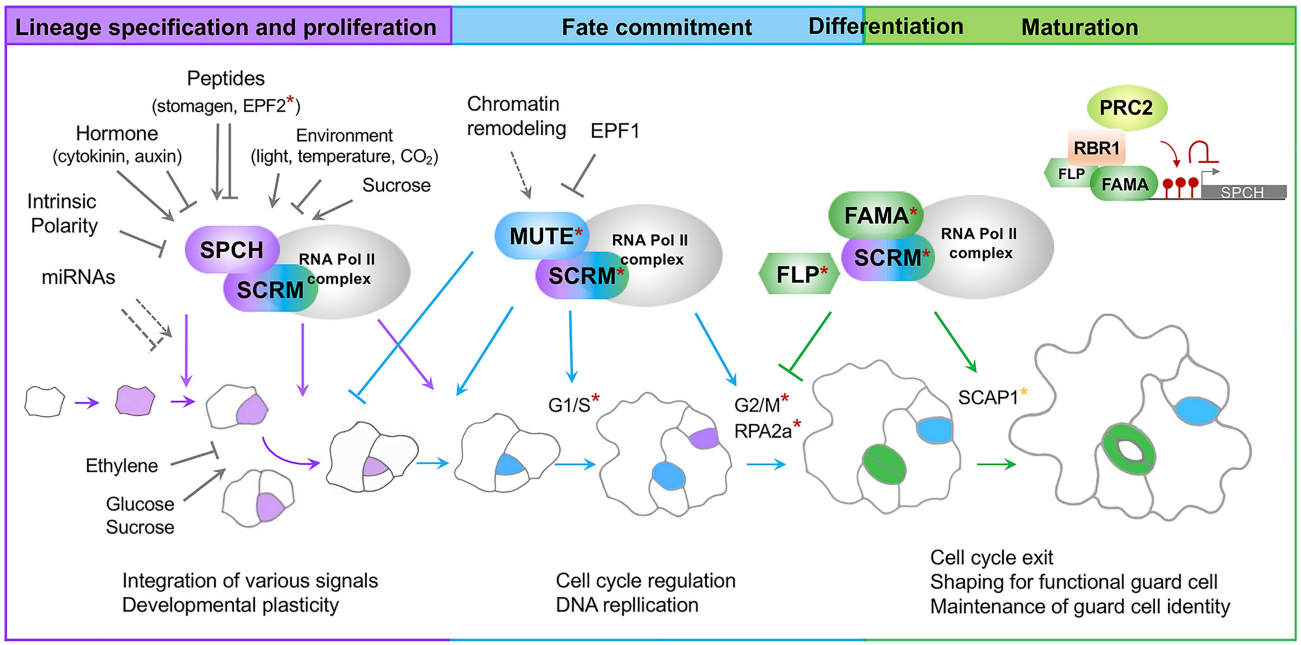

FIGURE 1 | A current model for Stomatal development in Arabidopsis. Stomatal lineage progression is mediated by a sequential action of the developmental stage-specific transcription factors. SPCH/SCRM are responsible for lineage specification and proliferation; MUTE/SCRM for fate commitment; FAMA/SCRM for differentiation and maturation. Developmental and environmental signals primarily modulate the first step mediated by SPCH/SCRM. A subunit of the RNA polymerase II complex and associated proteins interact with core transcription factors. Direct targets for MUTE and FAMA are denoted by asterisks in red and orange, respectively. Cells highlighted in purple indicate stomatal lineage precursors. Cells highlighted in blue are late meristemoids and GMCs. Cells highlighted in green are immature and mature guard cells. Colored arrows indicate positive regulation of transcription factors. Colored, inverted Ts indicate negative regulation of transcription factors. Arrows and closed lines in gray indicate developmental and environmental factors regulating transcription factors or stomatal lineage cells. A dotted line indicates potential regulation. SPCH, SPEECHLESS; SCRM, ICE1/SCRM2; FLP, FOUR LIPS; RPA2A, a core subunit of Replication Protein A complexes; SCAP1, STOMATAL CARPENTER 1; RBR1, RETINOBLASTOMA-RELATED 1; PRC2, Polycomb Repressive Complex 2; EPF, Epidermal Patterning Factor; G1/S G2M, phases of cell cycle.

division yields a small daughter cell, a meristemoid, and a large daughter cell, a stomatal lineage ground cell (SLGC). Meristemoids become guard mother cells (GMCs) which further undergo a single round of symmetric division and differentiation. This process produces two mirror-symmetric guard cells with a pore in the center. SLGCs can continue with spacing division, in which they divide asymmetrically to generate satellite stomata, or they can differentiate into pavement cells (Han and Torii, 2016; Lee and Bergmann, 2019). The stomatal complexes of monocotyledonous grass species are distinct from those in eudicot. Dumbbell-shaped guard cells are accompanied by subsidiary cells, arranged in parallel to the leaf vein, and develop without stem cell-like meristemoid cells. The initiation of stomatal lineage by an asymmetric division of the precursor cells directly produces GMCs. The neighboring cells of the newly formed GMCs acquire subsidiary mother cell (SMC) fate and establish polarity toward the adjacent GMC. After the SMCs asymmetrically divide and differentiate into subsidiary cells, the GMCs divide symmetrically to generate a pair of guard cells. Two guard cells and subsidiary cells together form a dumbbell-shaped stomatal complex (Hepworth et al., 2018; Nunes et al., 2020).

Stomatal development is sequentially controlled by three basic helix–loop–helix (bHLH) transcription factors, SPEECHLESS (SPCH), MUTE, and FAMA. These transcription factors work together with their heterodimeric partners SCRM (ICE1) and SCRM2 (Ohashi-Ito and Bergmann, 2006; MacAlister et al., 2007; Pillitteri et al., 2007; Kanaoka et al., 2008; **Figure 1**). The SPCH/SCRM heterodimer determines stomatal fate and maintains the proliferation step by promoting asymmetric division (MacAlister et al., 2007). The MUTE/SCRM dimer terminates the proliferative state initiated by SPCH/SCRM and drives differentiation of meristemoids to GMCs (Pillitteri et al., 2007). The FAMA/SCRM dimer induces guard cell differentiation and restricts the last symmetric division to form a pair of guard cells (Ohashi-Ito and Bergmann, 2006). Two closely related R2R3 MYB transcription factor genes, *FOUR LIPS (FLP)* and *MYB88,* function in a semi-redundant manner with FAMA in differentiation and coordination of the terminal symmetric cell division (Geisler et al., 1998).

bHLH genes regulating stomatal development are well conserved across the land plants (Liu et al., 2009). However, their function is alternatively wired among different species to accommodate the fundamental difference in the patterning and shape of stomatal complexes. In particular, two copies of *SPCH* that function redundantly at the entry of stomatal lineage are found in Brachypodium and rice (Raissig et al., 2016). In contrast to Arabidopsis, MUTE protein in grass species can

move from GMCs to the adjacent cells (Raissig et al., 2017; Wang et al., 2019; Wu et al., 2019). This lateral movement of MUTE establishes the identity of SMCs and drives the differentiation of subsidiary cells in a non-cell-autonomous fashion (Nunes et al., 2020).

Expression profiling of stomatal lineage cells at different developmental stages has revealed dynamic changes in the transcriptomes (Pillitteri et al., 2011; Adrian et al., 2015; Zhu et al., 2020; Ho et al., 2021). Moreover, direct target genes of the three master transcription factors have been identified (Hachez et al., 2011; Lau et al., 2014; Han et al., 2018). The recent advance in single-cell RNA-sequencing technology enables profiling spatiotemporal gene expression at the level of the individual stomatal lineage cells (Liu et al., 2020; Lopez-Anido et al., 2021). The systems-level analyses of stomatal lineage cells have deepened our understanding of how the developmental stage-specific transcriptional factors fulfill the developmental program.

Mitogen-Activated Protein Kinase (MAPK) cascades consist of YODA (YDA), MKK4/5/7/9, and MPK3/6. These cascades act upstream of the developmental stage-specific transcription factors (Bergmann et al., 2004; Wang et al., 2007). The activation of the MAPK cascade destabilizes SPCH and MUTE (Lampard et al., 2008; Qi et al., 2017). YDA-MPK3/6 MAPK signaling also plays a substantial role in establishing the cellular polarity required for asymmetric division and stomatal fate specification (Zhang et al., 2015, 2016). The molecular switch that either activates or suppresses the MAPK cascade, at least in part, consists of secreted epidermal patterning factor (EPF) peptides. EPF peptides are perceived by their corresponding cell-surface receptor complexes composed of the proteins belonging to the ERECTA family and their co-receptors TMM and SERK families (Torii, 2012). EPFs and their cognate receptors are conserved throughout the land plants (Caine et al., 2016; Hepworth et al., 2018). Functional studies of monocot species suggest that EPF1 and EPF2 inhibit, but EPFL9 enhances stomatal development, indicating that they are the functional ortholog of Arabidopsis EPFs (Franks et al., 2015; Hepworth et al., 2015; Wang et al., 2016; Hughes et al., 2017; Caine et al., 2019; Dunn et al., 2019; Mohammed et al., 2019). In addition, PANGLOSS1 and PANGLOSS 2 are Leucine-Rich-Repeat receptors in grasses and promote polarization of asymmetric SMC division (Cartwright et al., 2009; Facette and Smith, 2012; Facette et al., 2015). This result implies divergent receptor complexes perceive the extrinsic signal to modulate stomatal development.

Stomatal development is tightly controlled to ensure growth and survival and allows the plant to adapt to environmental changes. The current global climate changes could directly affect stomatal development and function and, thus, plant growth. CO_2 is a gas that exacerbates the greenhouse effect and, therefore, global climate change (Lindsey, 2020). Temperature increases are often accompanied by drought stress due to enhanced water evaporation and changing rain patterns. Both excessive heat and drought stress negatively impact plant production. A significant loss (80–90%) in grain yield can result from warm temperatures during the plant reproductive stage (Hatfield and Prueger, 2015). Given the role of stomata in plant growth, further investigation of stomatal development and their response to environmental changes would provide a strategy that could enhance plant performance and productivity despite global climate change (Dow and Bergmann, 2014; Buckley et al., 2019).

TRANSCRIPTIONAL CONTROL OF STOMATA DEVELOPMENT

Initiation and Maintenance of Stomatal Lineage Stem Cells

Stomatal lineage specification initiates with the *SPCH* expression in a subset of protodermal cells. This expression defines MMCs and continues through several rounds of asymmetric division. Persistent SPCH activity is found in meristemoids. The molecular signature of meristemoids was found *via* transcriptome analysis of stomatal development mutants overwhelmingly composed of meristemoids (Pillitteri et al., 2011). Pillitteri et al. identified the polarity protein POLAR and found that the cytokinin signaling pathway involving ARRs and CLEs, and ERECTA-family receptor-like kinases were part of the molecular feature of stem-cell populations.

How SPCH contributes to the specification and proliferation of stomatal lineage cells has been uncovered by identifying the targets of SPCH. Genome-wide profiling of SPCH targets was conducted by analyzing the transcriptome of transgenic plants harboring SPCH under the control of an inducible promoter and chromatin immunoprecipitation sequencing (Lau et al., 2014). The key regulatory genes, including *SCRMs, TMM, ERL2, EPF2, BASL, POLAR*, and the *ARK3/AtKINUa* kinesins, and brassinosteroid biosynthetic and response genes were found to be regulated by SPCH. The other genes identified as SPCH targets include *PHYTOCHROME-INTERACTING FACTOR 4 (PIF4;* Lau et al., 2018), *CLE9/10,* and *ARR16/17* (Vaten et al., 2018). These genes highlight the role of SPCH as an integrator conferring developmental flexibility of stomatal lineage in response to environmental or hormonal stimuli.

New Players and Refining the Paradigm

A recent study using single-cell transcriptome analysis of stomatal lineage cells has proposed an extended role for SPCH in reinforcing cell fate decisions (Lopez-Anido et al., 2021). *SPCH* appears to be expressed beyond the early stages of stomatal development and co-expressed with either *MUTE* or *FAMA*. This observation was supported by a reporter gene analysis showing the *SPCH* expression in GMCs and a small population of young guard cells. These findings contradict the existing paradigm that stomatal development proceeds with the sequential actions of the master transcription factors in each state of transition. Furthermore, the coding sequence of *SPCH* did not fully complement the *spch* null mutants due to the disrupted level and timing of SPCH expression. This lack of complement resulted in a reduced number of stomata and defects in fate commitment to GMCs. Similar defects were observed in knock-down mutants for *SPCH* by artificial microRNAs (miRNAs)

expressed under the *MUTE* promoter. Time-lapse imaging visualizing SPCH and MUTE protein expression showed overlapping expression patterns in late meristemoids (Davies and Bergmann, 2014). These studies indicate that SPCH activity is required for proper conversion of meristemoids to GMCs. It remains elusive, however, how SPCH functions in the later stages of stomatal development.

Another scRNA-seq analysis of stomatal lineage cells identified 11 cell clusters of epidermal cells, including two cell types that cannot be classified with known marker genes (Liu et al., 2020). One of the unclassified epidermal cell types highly expresses transcription factors and displays relatively similar patterns to early meristemoids in the developmental trajectory, suggesting that variable cell populations may exist at early stomatal developmental stages. This study also suggests potential regulators of stomatal development and a possible genetic network: *BASIC PENTACYSTEINE (BPC)* gene family and *WRKY33* genes are highly expressed in the MMC through GMC state. Higher-order BPC mutants exhibit defects in stomatal patterning and arrested precursors. Although SPCH was unaffected by the *bpc* sextuple mutants, the expression levels of SCRMs, MUTE, and FAMA were reduced. The detailed mechanism related to these transcription factors in stomatal development requires further investigation. Because the plant-specific BPCs family is involved in the recruitment of repressive histone-modifying complexes (Hecker et al., 2015; Mu et al., 2017; Xiao et al., 2017), it would be intriguing to test whether dynamic chromatin changes occur through the action of the BPC family during stomatal lineage progression.

MUTE, a Potent Inducer of Cell Cycle Regulators for Stomata

MUTE terminates the self-renewing meristemoid state initiated by SPCH. It triggers unidirectional differentiation accompanied by a single symmetric division to create a stomate surrounded by a pair of guard cells (Pillitteri et al., 2007). Genome-wide transcriptome analysis of transgenic plants in which *MUTE* is chemically induced (*iMUTE*) revealed a comprehensive MUTE-dependent gene expression profile (Han et al., 2018). MUTE shares the targets of stomatal genes with SPCH for continued lineage progression. MUTE directly induces SCRMs, ERL1, POLAR, and BASL-like SPCH. In contrast, the earlier EPF2 signal induced by SPCH is attenuated by MUTE activation. The expression of the common receptors (*ERLs*), however, is maintained to receive the EPF1 signal. These findings suggest that MUTE serves as a transcriptional switch for proper stomatal patterning. The majority of GO categories of genes up-regulated in the iMUTE plants include cell cycle and cell division, which is unique to the *iMUTE* transcriptome compared to that of *iSPCH*. MUTE directly induces expression of cell cycle activators, CDKs and cyclins, followed by the activation of cell cycle repressors, FAMA and FLP, which in turn ensures symmetric division occurs only once (Han et al., 2018).

The scRNA-seq analysis further defines the molecular signature of fate commitment at single-cell resolution by showing how cell state-specific transcription factors, chromatin remodelers, and cell cycle regulators are dynamically regulated (Lopez-Anido et al., 2021). After the onset of fate commitment is triggered by MUTE, phase transition of the cell cycle is observed in discrete clusters. There, MUTE (G1/S of the cell cycle) and FAMA (G2/M of the cell cycle) are exclusively expressed.

The R2R3-MYB transcription factor FLP functions redundantly with FAMA for stomatal differentiation and direct repression of the cell cycle genes (Xie et al., 2010; Lee et al., 2014b). Enhanced terminal symmetric division in a loss-of-function mutant of FLP exhibits paired stomata. Yang et al. have shown that the paired stomata phenotype of *flp* mutants can be suppressed by introducing the *rpa2a* mutation. The RPA2a subunit of the Replication Protein A (RPA) complexes is responsible for DNA replication, recombination, and repair, functions cooperatively with CDKB1s and CYCA2s in restricting terminal symmetric division and in maintaining DNA content and guard cell size. Therefore, phenotypic suppression of the *flp* mutant by *rpa2a* mutation is likely due to the failure of cell cycle checkpoints without RAP2a (Yang et al., 2019). Triggered by CDKB1s, RPA2a phosphorylation is associated with nuclear localization and function in DNA replication processes. It appears that the expression of RPA2a and genes involved in DNA replication is increased in the *iMUTE* plants (Han et al., 2018).

These findings indicate that during stomatal formation, MUTE contributes to timely coordination of the cell cycle. Further investigation is required to unveil how the cell cycle and the chromatin landscape are linked to the termination of a self-renewing state and fate commitment.

Fate Decision of Stomatal Lineage Ground Cells

SLGCs are large daughter cells derived from asymmetric divisions of MMCs or meristemoids. SLGCs bear bi-potency, meaning that they can either reenter asymmetric division to generate a satellite stomate or they can differentiate into a pavement cell.

Previously, it was shown that prolonged MUTE expression in 2-week-old *mute* mutants, where the meristemoids and SLGCs are arrested after several rounds of asymmetric division, resulted in clustered stomata (Trivino et al., 2013). In contrast, induced MUTE expression in wild-type plants did not show the clustered stomata phenotype due to full differentiation of stomatal lineage cells (Trivino et al., 2013). This result implies that SLGCs adjacent to the arrested meristemoid are competent to be a stomate. Additionally, it shows that SLGC differentiation to a pavement cell may require the MUTE activity in meristemoids.

Some molecular features of SLGCs were obtained from the transcriptome analyses of early stomatal lineage cells. It appears that SLGCs are enriched with genes associated with cell division and cytokinesis; they are poised between proliferation and endoreduplication-coupled differentiation (Ho et al., 2021). Fate decision to pavement cells or termination of proliferative SLGCs might also be linked to auxin-mediated onset of endoreduplication (John and Qi, 2008). It was reported that an auxin response gradient is formed and fluctuates within SLGCs, which helps to determine the fate and morphology of pavement cells

(Grones et al., 2020). Cytokinin signaling, however, preferentially promotes asymmetric divisions in SLGCs (spacing division) through the induction of SPCH expression. SPCH directly regulates genes encoding the cytokinin inhibitory effector ARR16 and the secreted peptide CLE9. ARR16 reduces the cytokinin sensitivity of SLGCs, and CLE9 suppresses SLGC division. A negative feedback regulatory circuit, therefore, is formed between cytokinin and SPCH to fine-tune SLGC divisions (Vaten et al., 2018).

Despite the recent findings, the mechanism allowing SLGCs to maintain proliferate-state or to differentiate remains unknown. Although it is challenging to define the characteristics of SLGCs due to their heterogeneity, asynchronous production, and lack of specific SLGC markers, a detailed molecular characterization of SLGCs should enhance the investigation.

Shaping Guard Cells and Maintenance of Guard Cell Fate

The final step of consecutive state transition in stomatal development is mediated by the transcription factor FAMA. It promotes guard cell differentiation and negatively controls symmetric division of GMCs (Ohashi-Ito and Bergmann., 2006). FAMA appears to be directly induced by MUTE. However, unlike other MUTE targets induced immediately, FAMA induction is delayed until just prior to symmetric division (Han et al., 2018). This delay implies there is an additional mechanism regulating FAMA expression. Hachez *et al* (Hachez et al., 2011) identified FAMA targets and regulators of guard cell development by transcript profiling of genes that are differentially modulated over chemically induced FAMA (*iFAMA*). These genes, regulated by FAMA, encode proteins with diverse functions, including transcription factors, cell cycle controllers, receptors, signaling proteins, and proteins associated with cell wall modification and metabolic processes (Hachez et al., 2011). This study supports the function of FAMA in differentiation of GMCs to guard cells and the maintenance of guard cell identity.

The loss-of-function mutant *stomatal carpenter 1* (*scap1*) develops skewed and dysfunctional guard cells. *SCAP1* encodes a Dof-type transcription factor and regulates the expression of key molecules in stomatal function and structure such as GORK (outward K^+ channel), MYB60, and PME6 (pectin methyltransferase; Negi et al., 2013). As a consequence, *scap1* mutants display impaired ion homeostasis and esterification of extracellular pectins responsible for cell wall maturation lining the pores (Negi et al., 2013). The loss-of-function mutant for PME6 displays dysfunctional guard cell dynamics due to the mechanical change in the guard cells (Amsbury et al., 2016). The expression of *FAMA* and *SCAP1* in guard cells and the rapid up-regulation of *SCAP1* upon *FAMA* induction (*iFAMA*; Ohashi-Ito and Bergmann, 2006; Hachez et al., 2011; Negi et al., 2013) suggest that SCAP1 is a potential target of FAMA. Despite the role of SCAP1 during stomata maturation, the expression of *SCAP1* is observed in young leaf primordia. Loss-of-function mutants display a reduced stomatal density and patterning defects (Castorina et al., 2016). The change in stomatal density and increased patterning defects suggests that SCAP1 plays an additional role in stomatal development.

A component of the RNA polymerase II complex plays a role in stomatal differentiation in concert with FAMA (Chen et al., 2016). The hypomorphic mutant for NRPB3, the third largest subunit of the RNA polymerase II complex, produces more stomatal lineage-, paired-, and non-stomatal cells. Interestingly, the *nrpb3* mutant synergistically produces a tumor-like structure when combined with *fama* and *flp*. NRPB3 physically interacts with FAMA and SCRM, but not with SPCH and MUTE. RPAP2 IYO MATE (RIMA) is another protein interacting with NRPB3. RIMA also physically interacts with SPCH, MUTE, FAMA, and SCRM (Chen et al., 2021). It appears that the state-specific transcription factors associated with the general transcription machinery give rise to the cell state-specific regulation of gene expression. Stomatal lineage cell divisions are thereby limited at later stages of stomatal development.

Guard cells are the terminal state of stomatal cell lineage. Fully differentiated guard cells must irreversibly lose their proliferation ability to maintain cellular identity for stomatal function. Failure in maintenance reverts a guard cell to a stomatal lineage precursor, leading to a re-initiation of early stomatal lineage from a differentiated stomate. Previous studies have shown that the RETINOBLASTOMA RELATED (RBR)-FAMA and RBR-FLP interactions play a critical role in freezing the guard cell identity upon completion of differentiation (Lee et al., 2014a,b; Matos et al., 2014). These interactions mediate the RBR-mediated recruitment of Polycomb Repressive Complex 2 (PRC2) and establish the repressive histone modification H3K27me3 of the stomatal lineage genes (Lee et al., 2014a,b; Matos et al., 2014). This mechanism is partly supported by an analysis of the single-cell type transcriptome and histone modification (H3K27me3 and H3K4me3) dynamics in normal guard cells compared to the guard cells in the reprogramming state ($FAMA^{LGK}$; Lee et al., 2019). When point mutations are introduced in the RBR binding motif (LxCxE) of FAMA (referred as $FAMA^{LGK}$), $FAMA^{LGK}$ is not capable of interacting with RBR and recruiting PRC2 (Matos et al., 2014). Modest changes in H3K27me3 peaks were observed between WT and $FAMA^{LGK}$. In $FAMA^{LGK}$ cells, the SPCH locus loses the H3K27me3 modification and its expression is concomitantly increased. The level of H3K27me3 at the MUTE and FAMA loci and their expression level, however, remained unchanged in the $FAMA^{LGK}$ guard cells. This finding suggests that de-repression of SPCH may contribute to the re-initiation of the stomatal lineage in $FAMA^{LGK}$ and that H3K27me3 is required to prevent guard cell fate from reverting to the precursor state. However, the MUTE expression level in $FAMA^{LGK}$ is contradictory to the previous report where MUTE is highly up-regulated in 15-day-old cotyledons of $FAMA^{LGK}$ (Matos et al., 2014).

SPCH expression alone is not capable of forming stomata (Davies and Bergmann, 2014). Ectopic SPCH expression results in more asymmetric divisions (Han et al., 2018). These results imply that the stomate in the stomate phenotype may not be solely attributable to the de-repression of SPCH. Knock-down of the PRC2 activity in guard cells mimics the stomate

in the stomate phenotype with a very low frequency compared to FAMA^{LGK}. This activity suggests a minor contribution of H3K27me3 and the presence of other mechanisms to maintain guard cell integrity. Indeed, H3K27me3 marks are increased on the locus of WOUND-INDUCED DEDIFFERENTIATION 1 (*WIND3*) during guard cell reprogramming (FAMA^{LGK}), thereby resulting in transcriptional down-regulation of WIND3. The ectopic expression of *WIND3* using the SPCH promoter enhances the FAMA^{LGK} phenotype. These results imply that guard cell integrity is maintained by complex mechanisms in addition to the known H3K27me3 reorganization at the loci of stomatal lineage genes.

Using the proximity labeling method that identifies spatial and temporal information in protein–protein interactions, the nuclear proteome of young guard cells and novel FAMA-interacting proteins were identified (Mair et al., 2019). The FAMA interactors include bHLH transcriptional factors SCRM, transcriptional co-activators that link transcriptional factors to RNA polymerase II, and histone acetyltransferases, which is consistent with the previous study showing a link between FAMA and RNA polymerase II (Chen et al., 2016). FAMA also interacts with the transcriptional co-repressor TOPLESS-related proteins that recruit histone deacetylases to transcriptional factors and their linker protein that mediates the interaction between the co-repressor complex with transcription factors (Long et al., 2006). Among the highly abundant proteins in the nuclei of young guard cells, SHL (SHORT LIFE) binds to both H3K27me3 and H3K4me3. SHL functions as a histone reader to direct a particular transcriptional outcome. It might be involved in the establishment of repressive chromatins in concert with the co-repressors to lock the guard cell identity in their terminally differentiated state. Overall, FAMA could positively or negatively regulate target genes in concert with the co-activators and the co-repressors. This regulation is likely mediated through histone acetylation/deacetylation in response to developmental or hormonal signals.

SIGNALING CASCADE CONVERGING TO TRANSCRIPTION FACTORS

Plant survival dictates that the level of expression and the activity of the master transcription factors in each state of stomatal development must be tightly regulated. SPCH expression is modulated directly by upstream transcription factors. These factors are induced by light, drought, and heat (Klermund et al., 2016; Lau et al., 2018; Qi et al., 2019). SPCH activity is crucial to determine the fate of bi-potent stomatal lineage cells after asymmetric division and is substantially modulated by various kinases. MAPK signaling cascades inhibit the SPCH activity (Lampard et al., 2008; Gudesblat et al., 2012; Yang et al., 2015; Han et al., 2020). The mechanism by which the expression and activity MUTE and FAMA are regulated, in contrast, is not fully understood yet.

The signaling pathway upstream of the bHLH transcription factors is initiated by the EPF-family ligands, ERECTA-family receptor-like kinases, TMM as a co-receptor, and the downstream MAPK signaling cascade. The EPF ligands belong to the peptide family secreted to the apoplast (Herrmann and Torii, 2020). Structural and biochemical analysis revealed that heterodimerization between the ER-family receptors and TMM is required for EPF1 and EPF2 ligand perception, but was not required for EPFL4/5/6 (Lin et al., 2017), which indicates that ligand-based selectivity of receptor heterodimerization specifies the downstream biological process. ER receptor-TMM modules can also associate with the co-receptors BRI1-ASSOCIATED RECEPTOR KINASE/SOMATIC EMBRYOGENESIS RECEPTOR KINASE (BAK/SERK) to form a ternary receptor complex. This complex contributes to the stabilization of a specific ligand–receptor pair and hence, confers higher specificity in signaling (Meng and Yao, 2015).

EPF1 and EPF2 peptide ligands negatively regulate stomatal formation (Hara et al., 2007, 2009; Hunt and Gray, 2009). EPF2 restricts the initiation of stomatal formation by reducing the stability of SPCH (Bergmann et al., 2004; Pillitteri et al., 2011; Robinson et al., 2011). Exaggerated EPF2 signaling leads to a plant leaf epidermis composed of only pavement cells, similar to the *spch* mutants (Hara et al., 2007; Rowe and Bergmann, 2010; Rychel et al., 2010). *EPF2* expression is directly regulated by SPCH and SCRM (Lau et al., 2014; Horst et al., 2015). It is repressed by MUTE activity when the stomatal fate is committed in GMCs. This regulation allows EPF1 to access the common receptor system (Han et al., 2018). Another EPF-family member, EPF1, inhibits stomatal formation by negatively regulating the stability of the MUTE protein (Hara et al., 2007; Lee et al., 2012, 2015; Lin et al., 2017; Qi et al., 2017, 2020). Enhanced EPF1 signaling causes the stomatal lineage to arrest at the meristemoid state, phenocopying the *mute* mutants. Unlike *EPF2*, *EPF1* expression is not directly regulated by MUTE (Qi et al., 2017). The transcription factors regulating *EPF1* expression are unknown.

EPF-like 9 (EPFL9), also known as STOMAGEN, promotes stomatal formation and is highly responsive to environmental cues (Kondo et al., 2010; Sugano et al., 2010). With a highly similar topology structure, STOMAGEN competes with EPF1 and EPF2 for the same receptor complex but does not activate the MAPK cascade (Ohki et al., 2011; Lee et al., 2015; Qi et al., 2017). An auxin-related transcription factor MONOPTEROS (MP) suppresses the expression of *STOMAGEN*. The light-inducible transcription factor *ELONGATED HYPOCOTYL 5* (*HY5*) induces *STOMATAGEN* expression (Wang et al., 2021).

SCRM functions as a scaffold protein and associates with MPK3/6 and SPCH (Putarjunan et al., 2019). MPK3/6 first binds to the bipartite SCRM-KRAAM motifs of SCRM, which bridges with SPCH. Then, it triggers the subsequent phosphorylation of SPCH, resulting in the degradation of SPCH-SCRM (Putarjunan et al., 2019). The KRAAM motif is distinct from the putative MAPK docking sites and is uniquely found in SCRMs and their orthologs. This distinction suggests a mechanism for MAPKs conferring substrate specificity in a developmental process.

The localization of the MAPK cascade is unevenly distributed in MMC and in the two daughter cells derived from an asymmetric division. This distribution is facilitated by the intrinsic polarity protein, BASL. BASL arranges the tethering of YDA-MPK signaling components at its polarized crescent of the membrane, which results in elevated SPCH phosphorylation/destabilization to reduce the concentration of SPCH protein in SLGCs (Zhang et al., 2015, 2016). YDA-MAPK signaling must be restricted to allow high division potential in MMCs. This process is mediated by the polarized POLAR-BRASSINOSTEROID-INSENSITIVE2 (BIN2) module at the polarity crescent. Polarized BIN2 can inhibit YDA, leading to the attenuation of the YDA-MAPK signaling (Houbaert et al., 2018; Guo and Dong, 2019). The protein phosphatase BRI1 SUPPRESSPR 1 (BSU1)-LIKE 1 (BSL1) associates with the polarity complex and subsequently triggers the translocation of BIN2 from the polar crescent to the nucleus. It also activates YDA-MAPK signaling in SLGCs. BIN2 in the nucleus directly phosphorylates and destabilizes SPCH. This destabilization further restricts asymmetric division and leads to differentiation (Gudesblat et al., 2012; Guo et al., 2021a,b).

MAP KINASE PHOSPHATASE1 (MKP1) fine-tunes the MAPK signaling by inactivating the MAPK cascade at the early stage of stomatal development (Tamnanloo et al., 2018). The *mkp1* mutants undergo the asymmetric entry division but fail to differentiate, resembling the *mute* mutant phenotype. Genetic analysis puts MKP1 upstream of MPK3/6 and downstream of YDA. Additionally, MPK3/6 signaling is hyperactivated when MKP1 is absent, suggesting MKP1 deactivates MPK3/6. Interestingly, MKP1 expression fully rescues the *mkp1*mutant phenotype only when the MPK1 expression is driven by the SPCH promoter. This result suggests that MKP1 has a significant role in controlling guard cell fate commitment in early stomatal precursor cells.

Phosphorylation on the SPCH protein usually leads to its degradation. Yet, phosphorylation on Thr49, Thr50, Ser51, and Ser52 of the SPCH protein has been shown to stabilize SPCH (Han et al., 2020). The accumulation of KIN10, a catalytic subunit of the conserved energy sensor kinase SnRK1, can be induced by sucrose and promotes stomatal development. *KIN10* is highly expressed in the nuclei of stomatal lineage cells where it phosphorylates and stabilizes SPCH to promote sucrose-induced stomatal formation (Han et al., 2020). Mutations in *KIN10* result in decreased stomatal index, while overexpression of KIN10 results in a higher stomatal index. This finding partly explains the previously observed stomatal phenotype when plants are treated with high doses of sucrose (Akita et al., 2013).

Multiple kinases phosphorylate SPCH, resulting in the destabilization of SPCH. Protein phosphatases that are responsible for dephosphorylating SPCH, however, have recently been discovered (Bian et al., 2020). The scaffolding A subunit of the PP2A heterotrimeric complex directly associates with SPCH. Loss-of-function mutations in PP2A or inactivation by PP2A inhibitors results in reduced stomata formation and round pavement cells. This result suggests that PP2A promotes stomatal development by positively regulating SPCH stability. Furthermore, undifferentiated precursors after asymmetric divisions and round pavement cells in the *pp2a* mutants increase the likelihood that PP2A may regulate other proteins such as MUTE or those involved in pavement cell differentiation.

ENVIRONMENTAL CUES AND DEVELOPMENTAL PLASTICITY

Given the essential role of stomata in photosynthesis and nutrient uptake, stomatal development is tightly controlled in response to a diverse range of environmental and phytohormonal signals (Qi and Torii, 2018). Plants have developed a highly coordinated regulatory mechanism that balances the need for photosynthesis and transpiration according to their specific environment (Hepworth et al., 2016). Atmospheric CO_2 concentration, water availability, environmental temperature, light intensity, and nutrients all influence the endogenous program (**Figure 2**).

Environmental Factors Affecting Stomata Development

Carbon Dioxide

Atmospheric CO_2 significantly influences stomatal formation and function. Evolutionary studies over geologic time scale as well as ecological studies imply that atmospheric CO_2 levels are inversely correlated with stomatal density and impacts on stomatal function (McElwain and Steinthorsdottir, 2017). Global climate impact assessments for crops have shown that elevated atmospheric CO_2 levels may be a preferable condition to mitigate yield losses due to climate changes. This preference is because low atmospheric CO_2 concentration imposes a negative repression on photosynthetic productivity (Sage and Coleman, 2001). In bread wheat, drought stress often causes reduction in seed yield, but this loss can be compensated by an elevated CO_2 level. This compensation is likely due to the high CO_2 concentration satisfying the photosynthesis needs more efficiently when stomatal conductance is limited by water shortage (Dunn et al., 2019). CO_2 enrichment often comes with other climate changes including rising temperatures and water shortages. The response of decreasing stomatal density at a high CO_2 level, therefore, implies that the ease in CO_2 uptake allows plants to respond to other limiting factors such as water availability.

The current understanding of how CO_2 regulates stomatal formation comes from a milestone study by Schroeder and his colleagues (Engineer et al., 2014; **Figure 2**). They found that *Arabidopsis* β-carbonic anhydrase double mutants (*ca1ca4*; Hu et al., 2010) display an increased stomata density at an elevated CO_2 level. This increase in stomata density was due to compromised *EPF2* expression. This study identified CO_2 RESPONSE SECRETED PROTEASE (CRSP), which is induced by elevated CO_2 level and encodes a protease that specifically cleaves the precursor of EPF2 to release the mature peptide into the apoplast. The processed, functional EPF2 inhibits stomatal initiation by destabilizing SPCH. Mutations in either *CRSP* or *EPF2* impair the stomatal development influenced by elevated CO_2 concentration (Engineer et al., 2014). Moreover, treatments with a high concentration of CO_2 promote

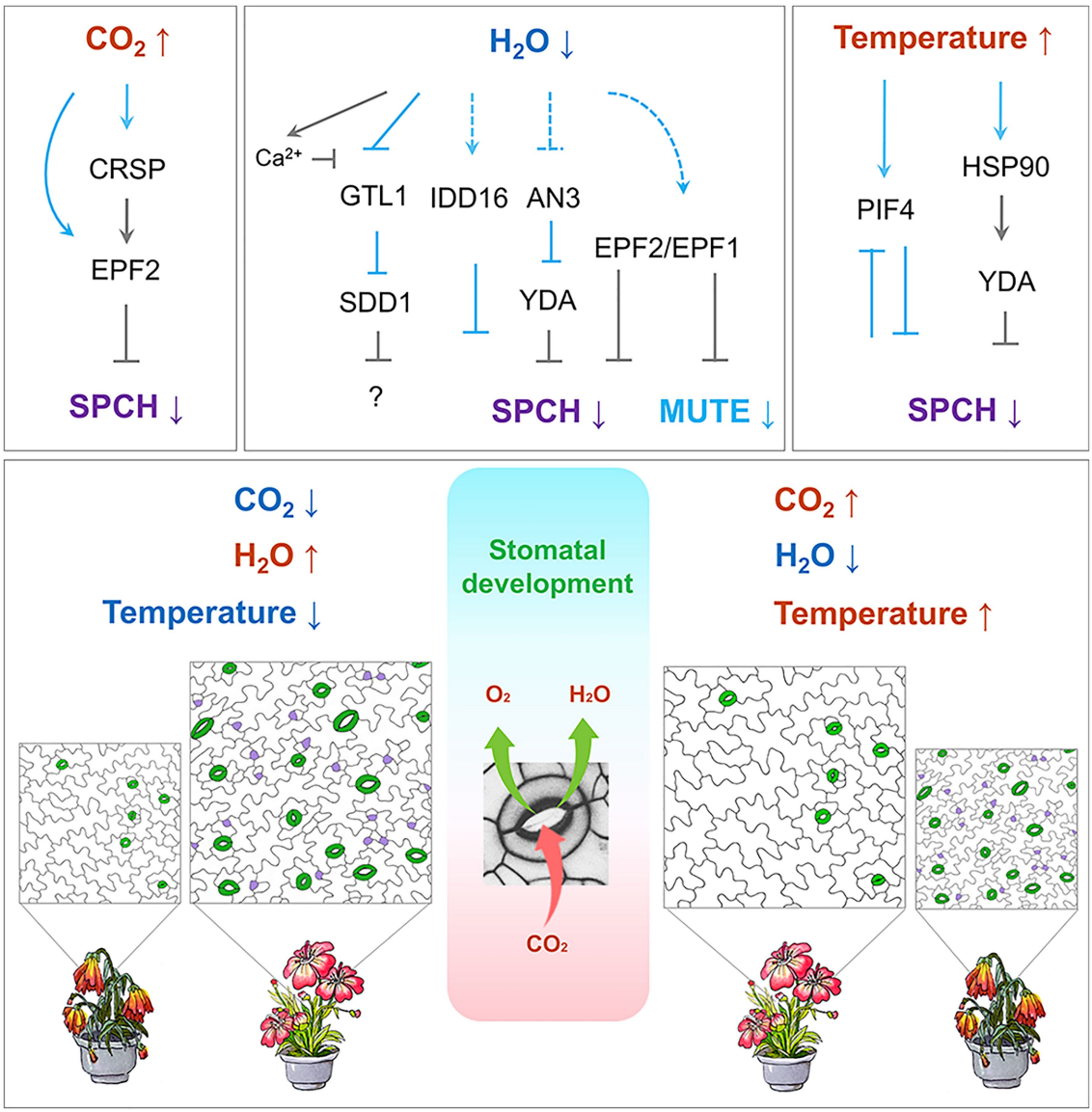

FIGURE 2 | Regulation of stomatal development by environmental cues. **Top:** Temperature, CO2, and water availability modulate the signaling cascade, which leads to the regulation of SPCH and MUTE. Arrows indicate positive regulation, and inverted Ts indicate negative regulation. Solid lines in light blue indicate transcriptional regulation, and solid grey lines indicate post-translational regulation. Dashed lines indicate potential regulation. **Bottom:** A stomate, formed by a pair of guard cells, takes up CO_2 (red arrow) for photosynthesis and releases the byproduct O_2 (green arrow) and water vapor (green arrow). On the left: low CO_2 concentration, sufficient water supply, and ambient temperature conditions prior to the global climate change. On the right: elevated CO_2 concentration, deficient water supply, and increased atmospheric temperature conditions after global climate change. Stomata are highlighted in green, and meristemoids in purple. The flowering plants underneath each of the stomatal images represent the growth and stress response of the plants along with the stomatal density. Color code: blue indicates decrease; red indicates increase.

satellite stomatal formation, leading to changes in stomatal distribution on abaxial cotyledons (Haus et al., 2018; Higaki et al., 2020). A detailed molecular mechanism and the benefits for plants to have satellite stomata under high CO_2 conditions are not fully understood.

Water Shortage

Water scarcity is a growing problem that correlates with global climate change. Drought conditions cause previously arable land to become unable to support crops. Increased drought conditions will cause crop yield reduction or even failure, which can result in starvation conditions for many populations. To avoid evaporative water loss, plants reduce stomatal conductance. This reduction in conductance ensures survival of the plant but causes a reduction in photosynthesis, yields, and productivity (Blum, 1996). Understanding how plants effectively use limited water resources is, therefore, crucial for future food security. Many studies on common crop plants indicate that reducing

transpiration by decreasing stomatal density is a feasible way to increase plant drought tolerance without compromising yield (Franks et al., 2015; Hepworth et al., 2015; Wang et al., 2016; Hughes et al., 2017; Caine et al., 2019; Dunn et al., 2019; Mohammed et al., 2019).

Molecules upstream of the core pathway controlling stomatal development are the current targets for genetic manipulation. In poplar, dehydration or ABA treatment causes up-regulation of *PdEPF1* (Wang et al., 2016). Overexpression of *PdEPF1* consistently results in a low stomatal density, high water use efficiency, and drought tolerance (Wang et al., 2016). In creeping bentgrass, overexpression of Osa-miR393 up-regulated *EPF* expression. This up-regulation leads to reduced stomatal density and enhanced plant drought tolerance (Zhao et al., 2019). Similarly, overexpression of *EPF2* in Arabidopsis, rice, and barley causes reduced stomatal density, decreased transpiration rate, and improved water use efficiency (Franks et al., 2015; Hepworth et al., 2015; Hughes et al., 2017; Dunn et al., 2019) (Caine et al., 2019; Mohammed et al., 2019). Reducing stomatal density by regulating EPFs, therefore, can be a promising tool for breeding crops that can better withstand drier environments without significant yield loss.

STOMATAL DENSITY AND DISTRIBUTION 1 (SDD1) could be another molecular target for improving drought tolerance in plants. Knockout mutants for *SDD1* display a noticeably increased stomatal density with severe stomatal clustering (Berger and Altmann, 2000; Von Groll et al., 2002). Because SDD1 belongs to the subtilisin-like serine protease family, it has been proposed that SDD1 cleaves a precursor of a mobile peptide that negatively regulates stomatal development (Berger and Altmann, 2000; Von Groll et al., 2002). EPF1 and EPF2, however, work independently of SDD1 (Hara et al., 2007, 2009). Manipulation of SDD1 can optimize WUE and thus improve plant drought tolerance. In Arabidopsis, *SDD1* expression is significantly up-regulated upon drought (Yoo et al., 2019). Overexpression of wild tomato *SchSDD1* in Arabidopsis and tomato results in higher productivity under drought conditions (Morales-Navarro et al., 2018). Further, it was found that *SDD1* expression is regulated by GT-2 LIKE 1 (GTL1), which is a transcription factor that binds the GT3 box in the *SDD1* promoter to trans-repress its transcription (Yoo et al., 2010). GTL1 is downregulated by drought stress. In *gtl1* loss-of-function mutants, *SDD1* expression is significantly increased, causing a 25% reduction in stomatal density (Yoo et al., 2010). Consequently, WUE is higher and drought tolerance is enhanced (Yoo et al., 2010). The Ca^{2+}-binding protein, calmodulin, upon binding of osmotic stress-induced Ca^{2+}, interacts with one of the N-terminal helices of GTL1 and inhibits GTL1 binding to the *SDD1* promoter. This inhibition thereby de-represses the *SDD1* expression and improves WUE (Yoo et al., 2019).

GTL1 is also known to regulate trichome development. This regulation would imply a correlation between the two epidermal cell types. Indeed, WUE was higher in four tomato lines with higher trichome density. Trichome density negatively correlates with stomatal density, and the ratio of trichomes to stomata shows a strong positive correlation with WUE (Galdon-Armero et al., 2018). The same observation was also reported in a wild-type population of Arabidopsis (Simon et al., 2020). Not surprisingly, many molecules regulating trichome development also play a role in stomatal development (Torii, 2021).

Many environmental conditions have a significant effect on SPCH (Chen et al., 2020; **Figures 1** and **2**). Qi and colleagues found that plants with a lower concentration of SPCH protein exhibit significantly increases in drought tolerance (Qi et al., 2019). Overexpression of the C2H2 zinc-finger transcription factor INDETERMINATE DOMAIN 16 (IDD16) caused a reduction in the SPCH transcription in a dose-dependent manner. The ChIP analysis indicates that IDD16 directly associates with the SPCH promoter, suggesting that SPCH is a direct downstream target of IDD16. In line with this, the IDD16 RNAi plants exhibit a higher stomatal density. Plants overexpressing *IDD16* displayed a reduced stomatal density and were hypo-sensitive to drought stress (Qi et al., 2019).

ANGUSTIFOLIA3 (AN3) is another transcription regulator involved in drought tolerance and stomatal development (Meng and Yao, 2015). Without AN3, fewer stomata were produced, transpiration was reduced, and the plants displayed improved drought tolerance. In *an3* mutants, a drastic increase was observed in the *YDA* transcript level. The ChIP analysis corroborated the theory that AN3 binds to the YDA promoter, indicating that AN3 acts as a transcriptional repressor of *YDA*.

Overall, drought stress modulates the stomatal formation pathway almost at every step, including the peptide ligands, the MAPK cascade, and the downstream transcription factors. Interestingly, all these targets appear to be regulated at the transcriptional level, indicating that transcriptional regulation is an efficient, effective way to deal with environmental stress.

High Temperature

Responding to environmental temperature, plants adjust their cooling capacity by controlling the rate of transpiration. Besides the quick response of stomatal apertures, control of stomatal formation contributes to plant body temperature. For instance, under ambient conditions, well-watered plants with more stomata (such as *epf1epf2*) maintain low body temperature, whereas those with fewer stomata (such as EPF1 overexpression lines) show higher body temperature (Hepworth et al., 2015; Caine et al., 2019). When water is restricted, however, EPF1 overexpression lines display more stable and lower leaf temperature than lines with a higher stomatal density. These effects are particularly notable during the reproductive stage (Hepworth et al., 2015; Caine et al., 2019; Mohammed et al., 2019). More interestingly, when the environmental temperature rises, stomatal pores of the EPF1 overexpression plants were significantly larger than those of the wild-type plants. This change allowed the plants to compensate for lower stomatal density. Plants are, therefore, dynamically balanced between evaporative cooling and water conservation. They maintain this delicate balance by regulating stomatal conductance. Plants with fewer stomata display improved initial water conservation, which allows them to more efficiently regulate stomatal movements. This improved regulation ensures adequate

evaporative cooling even under severe drought conditions at a high temperature.

When Arabidopsis plants grown at ambient temperature (22°C) are exposed to a high temperature (28°C), they develop fewer stomata (Crawford et al., 2012). PHYTOCHROME-INTERACTING FACTOR 4 (PIF4) is an essential component in this process. *PIF4* encodes a bHLH transcription factor involved in plant adaptation to high temperatures and is significantly up-regulated by elevated temperature (28°C; Koini et al., 2009). In stomatal lineage cells, high temperature stabilizes PIF4, which in turn binds to the *SPCH* promoter to repress its expression. This binding is responsible for inhibiting the entry of stomatal formation. Interestingly, *PIF4* was identified as an SPCH target, and the transcriptome data from the seedlings in which *SPCH* is conditionally expressed further indicate that SPCH protein also represses *PIF4* expression. Thus, at ambient temperature, SPCH promotes stomatal formation while blocking *PIF4* expression. When the temperature rises, *PIF4* is expressed and the stabilized PIF4 protein blocks *SPCH* transcription by binding to its promoter, therefore inhibiting stomatal formation through negative feedback (Lau et al., 2018).

HEAT SHOCK PROTEINS 90s (HSP90s) positively regulates YDA. Thus, YDA's targets, MPK3 and MPK6, cannot be activated when HSP90s is depleted. Lack of activation results in insufficient SPCH phosphorylation and destabilization. A higher concentration of stable SPCH protein eventually leads to clustered stomata (Samakovli et al., 2020). HSP90s also affects YDA polarization *via* physical interaction in stomatal lineage cells. Moreover, loss-of-function mutants of YDA or HSP90s altered the transcript levels of at least 18 SPCH target genes. This alteration indicates that the YDA-HSP90s module negatively affects the transcriptional activity of SPCH (Samakovli et al., 2020).

Similar to drought stress, heat stress modulates the stomatal entry transcription factor SPCH and the MAPK cascade. Additionally, heat stress impacts protein stability and/or function.

Light

Light, essential for growth and development, acts as an energy source and a developmental signal in plants. Stomatal development is a trait of photomorphogenesis and is positively regulated by light (Casson et al., 2009; Kang et al., 2009). Plants detect light through photoreceptors, including phytochromes and cryptochromes (Paik and Huq, 2019). Mutations in these photoreceptors cause reduced stomatal density within the corresponding light spectra (Kang et al., 2009). A common target of light signals is CONSTITUTIVE PHOTOMORPHOGENIC 1 (COP1), which is an E3 ubiquitin ligase. When COP1 is destabilized by light, it no longer activates the downstream YDA cascade, which leads to stomatal formation (Kang et al., 2009). In dark conditions, active COP1 can degrade SCRM *via* its E3 ubiquitin ligase activity, thereby preventing stomatal development. This pathway occurs in a YDA-independent manner and does not affect SPCH stability, suggesting a parallel pathway of COP1 that modulates the abundance of SCRM under unfavorable light conditions (Lee et al., 2017).

Additionally, light promotes stomatal formation by inducing *STOMAGEN* (Hronkova et al., 2015). MONOPTEROS/ARF5, a member of the AUXIN RESPONSE FACTORs family, has been reported to associate with the *STOMAGEN* promoter to suppress its expression (Zhang et al., 2014). Whether light exposure regulates this auxin-related MONOPTEROS is unknown. A recent study found an integration point where light signals impinge on stomatal development (Wang et al., 2021). The light-responsive HY5 plays a role in fundamental developmental processes such as photosynthetic machinery assembly, chloroplast development, pigment accumulation, and photomorphogenesis (Gangappa and Botto, 2016). The HY5 genomic binding sites have revealed its hierarchical role in the light regulation of plant development (Lee et al., 2007). Wang and colleagues found that HY5, a central transcriptional factor, directly binds to the promoter and activates *STOMAGEN* expression in mesophyll cells (Wang et al., 2021). HY5 is required for light regulation of SPCH. In *hy5* mutants, SPCH is marginally maintained. Compromising HY5 regulation results in stomatal formation that is unresponsive to light intensity. Light-stimulated HY5 directly activates *STOMAGEN* expression in mesophyll cells, which in turn acts in the epidermis to stabilize SPCH. Knock-down or overexpression of *STOMAGEN* results in stomatal production insensitive to light intensity (Wang et al., 2021). The direct regulation of *STOMAGEN* expression by HY5 was also detected in a previous report by Zoulias et al. (Zoulias et al., 2020). The up-regulation of STOMAGEN by HY5 represents a regulatory mechanism of how an environmental signal is integrated into the developmental program. It provides a correlation between the CO_2 uptake from stomata and the photosynthetic mesophyll cells.

Nutrients

Because nutrient uptake by roots is directly affected by transpiration, a correlation analysis of root and stomatal development in plants under drought conditions could be of interest. When plants are well watered, root area and the stomatal density are positively correlated. For example, *epf1epf2* mutants have an increased number of stomata and produce a larger root system than wild-type plants and thus, display improved phosphate and nitrogen accumulation (Hepworth et al., 2016). In contrast, plants with fewer stomata, such as transgenic plants overexpressing *EPF2,* share comparable root hair development and have a similar phosphate uptake capacity compared to wild-type plants (Hepworth et al., 2015, 2016). When water is restricted, a large decrease in stomatal density shows no significant effect on nitrogen accumulation (Hepworth et al., 2016). High transpiration rates due to increased stomatal density promote root development under water-sufficient conditions. When water shortage occurs, this correlation is altered, which implies that there is a complex interplay between root development and stomatal density.

miRNAs play a crucial role in plant development and environmental regulation (Song et al., 2019). It is surprising,

then, that no miRNAs appear to target known stomatal regulators, especially given the considerable number of transcriptional factors and signaling proteins that modulate stomatal development. Loss-of-function mutations in *AGO1* (*ARGONAUTE 1*), however, drastically impact stomatal patterning and morphology of epidermal cells. This implies that miRNAs play some role in stomatal development (Yang et al., 2014). Recently, expression profiling of miRNAs in stomatal lineage cells was carried out using the cell state-specific promoters of *SPCH*, *EPF2*, *MUTE*, *EPF1*, and *FAMA* (Zhu et al., 2020). Most of the identified miRNAs appear to be expressed at the entry state of stomatal development and target genes involved in nutrient homeostasis, metabolism, and light response (Zhu et al., 2020). Up- or down-regulation of miRNAs results in defective stomatal patterning and density. Together with previous data, Zhu et al. suggest that stomatal lineage miRNAs and their dynamic changes constitute another layer of stomatal development regulation and may play a role in response to developmental factors, environmental cues, and nutritional status for proper lineage specification and/or progression at the entry of stomatal lineage.

Sugar status and ethylene signaling appear to fine-tune the intrinsic polarity and division potential of stomatal lineage precursor cells (Gong et al., 2021). CONSTITUTIVE TRIPLE RESPONSE (CTR1) is a core component that negatively regulates ethylene signaling. In the *crt1* mutants, the stomatal-specific polar protein BREVIS RADIX-LIKE 2 (BRX2) becomes depolarized, which reduces the amplifying asymmetric division. This phenotype can be alleviated by glucose or sucrose treatment, suggesting an antagonistic effect of ethylene and sugar signaling on the self-renewing capacity of stomatal linage stem cells. Because sugar is produced by photosynthesis occurring in mesophyll cells, the effect of nutritional status and environment on the overall leaf size and epidermal patterning suggests active communication between the epidermis and mesophyll cells.

CONCLUSION AND PERSPECTIVES

Significant progress has been made in stomatal development over the past two decades. The discovery of key regulators and a core developmental pathway in stomatal lineage has contributed to the current understanding of stomatal development. Technical advances have identified genome-wide transcriptomes at the bulk-tissue, single-cell types, or single-cell level. ChIP-sequencing data of the master transcription factors are also accumulating. Despite the recent discoveries, there are open questions to be addressed: How are the stomatal lineage cells first established? How is the expression of master transcription factors initiated and coordinated at the chromatin level? How is intrinsic polarity complex targeted to the cortical membrane and integrated into the extrinsic signaling pathway? What are the molecular links between the environmental and hormonal control of stomatal development? Given the wealth of genetic resources and various types of omics data, one should explore novel factors and investigate comprehensive gene networks in stomatal lineage.

Single-cell RNA-seq can be applied to profile responses to environmental or hormonal perturbations, which could reveal whether the cell identity and cells at different developmental stages differentially respond to stress or hormone. Profiling chromatin accessibility such as Assay for Transposase Accessible Chromatin Sequencing and deoxyribonuclease I hypersensitive sequencing at the single-cell level would further the current understanding of the transcriptional program when combined with the single-cell transcriptome. Additionally, advanced live-cell imaging and quantitative image analysis make it easier to keep track of lineage and monitor the cellular events at single-cell resolution, which will help to pave the way to applying the single-cell approach to crop species.

We are currently facing an environmental crisis as global climate change caused by the greenhouse gases accelerates the temperature rise and water shortage. Each of these factors will negatively impact plant ecosystems, sustainability, and food supply. Stomata can directly influence the atmospheric CO_2 level, water evaporation, and even the surface temperature of the earth. Future challenges in stomatal development research, therefore, include addressing the open questions as well as translating discoveries made in Arabidopsis to agriculturally important crops. Many studies have demonstrated that stomatal morphology, density, size, distribution, and specialized cell type in grasses determine stomatal conductance. Stomatal development, then, significantly influences plant behavior in response to environmental changes. Genetic manipulation of stomatal development and physiology may contribute to better survival of plants and maintain agricultural productivity despite unfavorable conditions. Studies of stomatal development in monocots have started mostly by the comparative analysis of the genes in Arabidopsis. Because monocots bear linear arrangement of guard cells in specific cell files and four-celled stomatal complex, which enables "speedy stomata," the investigation of stomatal development and their regulation is a key to the breeding guidance. As transcriptional regulation is the major mechanism in environmental regulation on stomatal development, the rapidly responding transcription factors could form a useful toolbox for genetic manipulation. The use of CRISPR/Cas9 genome-editing technology in a cell type-specific manner could overcome deleterious effects caused by the ubiquitous disruption of essential genes. It is necessary to collect useful stomatal traits for plants to better adapt to global climate changes, which will allow us to see the outcome of current efforts.

AUTHOR CONTRIBUTIONS

S-KH, JK, and XQ wrote the manuscript. All authors read and approved this version of the manuscript.

FUNDING

The work in the authors' laboratories was supported by grants from National Research Foundation (2019R1A2C3007376 and

2020R1A4A1019408). S-KH was supported by the Brin Pool Program funded by the Ministry of Science and ICT through the National Research Foundation (2020H1D3A2A02110999). XQ was supported by Rutgers University.

ACKNOWLEDGMENTS

We would like to thank Shu Wu for providing the flower artwork in **Figure 2**.

REFERENCES

Adrian, J., Chang, J., Ballenger, C. E., Bargmann, B. O., Alassimone, J., Davies, K. A., et al. (2015). Transcriptome dynamics of the stomatal lineage: birth, amplification, and termination of a self-renewing population. *Dev. Cell* 33, 107–118. doi: 10.1016/j.devcel.2015.01.025

Akita, K., Hasezawa, S., and Higaki, T. (2013). Breaking of plant stomatal one-cell-spacing rule by sugar solution immersion. *PLoS One* 8:e72456. doi: 10.1371/journal.pone.0072456

Amsbury, S., Hunt, L., Elhaddad, N., Baillie, A., Lundgren, M., Verhertbruggen, Y., et al. (2016). Stomatal function requires pectin De-methyl-esterification of the guard Cell Wall. *Curr. Biol.* 26, 2899–2906. doi: 10.1016/j.cub.2016.08.021

Berger, D., and Altmann, T. (2000). A subtilisin-like serine protease involved in the regulation of stomatal density and distribution in Arabidopsis thaliana. *Genes Dev.* 14, 1119–1131

Bergmann, D. C., Lukowitz, W., and Somerville, C. R. (2004). Stomatal development and pattern controlled by a MAPKK kinase. *Science* 304, 1494–1497. doi: 10.1126/science.1096014

Bian, C., Guo, X., Zhang, Y., Wang, L., Xu, T., DeLong, A., et al (2020). Protein phosphatase 2A promotes stomatal development by stabilizing SPEECHLESS in Arabidopsis. *Proc. Natl. Acad. Sci.* 117, 13127–13137. doi: 10.1073/pnas.1912075117

Blum, A. (1996). Crop responses to drought and the interpretation of adaptation. *Plant Growth Regul.* 20, 135–148. doi: 10.1007/BF00024010

Buckley, C. R., Caine, R. S., and Gray, J. E. (2019). Pores for thought: can genetic manipulation of stomatal density protect future Rice yields? *Front. Plant Sci.* 10:1783. doi: 10.3389/fpls.2019.01783

Caine, R. S., Chater, C. C., Kamisugi, Y., Cuming, A. C., Beerling, D. J., Gray, J. E., et al. (2016). An ancestral stomatal patterning module revealed in the non-vascular land plant Physcomitrella patens. *Development* 143, 3306–3314. doi: 10.1242/dev.135038

Caine, R. S., Yin, X., Sloan, J., Harrison, E. L., Mohammed, U., Fulton, T., et al. (2019). Rice with reduced stomatal density conserves water and has improved drought tolerance under future climate conditions. *New Phytol.* 221, 371–384. doi: 10.1111/nph.15344

Cartwright, H. N., Humphries, J. A., and Smith, L. G. (2009). PAN1: a receptor-like protein that promotes polarization of an asymmetric cell division in maize. *Science* 323, 649–651. doi: 10.1126/science.1161686

Casson, S. A., Franklin, K. A., Gray, J. E., Grierson, C. S., Whitelam, G. C., and Hetherington, A. M. (2009). Phytochrome B and PIF4 regulate stomatal development in response to light quantity. *Curr. Biol.* 19, 229–234. doi: 10.1016/j.cub.2008.12.046

Castorina, G., Fox, S., Tonelli, C., Galbiati, M., and Conti, L. (2016). A novel role for STOMATAL CARPENTER 1 in stomata patterning. *BMC Plant Biol.* 16, 172. doi: 10.1186/s12870-016-0851-z

Chen, Z. H., Chen, G., Dai, F., Wang, Y., Hills, A., Ruan, Y. L., et al. (2017). Molecular evolution of grass stomata. *Trends Plant Sci.* 22, 124–139. doi: 10.1016/j.tplants.2016.09.005

Chen, L., Guan, L., Qian, P., Xu, F., Wu, Z., Wu, Y., et al. (2016). NRPB3, the third largest subunit of RNA polymerase II, is essential for stomatal patterning and differentiation in Arabidopsis. *Development* 143, 1600–1611. doi: 10.1242/dev.129098

Chen, L., Wu, Z., and Hou, S. (2020). SPEECHLESS speaks loudly in stomatal development. *Front. Plant Sci.* 11:114. doi: 10.3389/fpls.2020.00114

Chen, L., Zhao, M., Wu, Z., Chen, S., Rojo, E., Luo, J., et al. (2021). RNA polymerase II associated proteins regulate stomatal development through direct interaction with stomatal transcription factors in Arabidopsis thaliana. *New Phytol.* 230, 171–189. doi: 10.1111/nph.17004

Conklin, P. A., Strable, J., Li, S., and Scanlon, M. J. (2019). On the mechanisms of development in monocot and eudicot leaves. *New Phytol.* 221, 706–724. doi: 10.1111/nph.15371

Crawford, A. J., McLachlan, D. H., Hetherington, A. M., and Franklin, K. A. (2012). High temperature exposure increases plant cooling capacity. *Curr. Biol.* 22, R396–R397. doi: 10.1016/j.cub.2012.03.044

Davies, K. A., and Bergmann, D. C. (2014). Functional specialization of stomatal bHLHs through modification of DNA-binding and phosphoregulation potential. *Proc. Natl. Acad. Sci.* 111, 15585–15590. doi: 10.1073/pnas.1411766111

Dow, G. J., and Bergmann, D. C. (2014). Patterning and processes: how stomatal development defines physiological potential. *Curr. Opin. Plant Biol.* 21, 67–74. doi: 10.1016/j.pbi.2014.06.007

Duckett, J. G., and Pressel, S. (2018). The evolution of the stomatal apparatus: intercellular spaces and sporophyte water relations in bryophytes-two ignored dimensions. *Philos. Trans. R. Soc. Lond. Ser. B Biol. Sci.* 373:20160498. doi: 10.1098/rstb.2016.0498

Dunn, J., Hunt, L., Afsharinafar, M., Meselmani, M. A., Mitchell, A., Howells, R., et al. (2019). Reduced stomatal density in bread wheat leads to increased water-use efficiency. *J. Exp. Bot.* 70, 4737–4748. doi: 10.1093/jxb/erz248

Engineer, C. B., Ghassemian, M., Anderson, J. C., Peck, S. C., Hu, H., and Schroeder, J. I. (2014). Carbonic anhydrases, EPF2 and a novel protease mediate CO2 control of stomatal development. *Nature* 513, 246–250. doi: 10.1038/nature13452

Facette, M. R., Park, Y., Sutimantanapi, D., Luo, A., Cartwright, H. N., Yang, B., et al. (2015). The SCAR/WAVE complex polarizes PAN receptors and promotes division asymmetry in maize. *Nat Plants* 1, 1–8. doi: 10.1038/nplants.2014.24

Facette, M. R., and Smith, L. G. (2012). Division polarity in developing stomata. *Curr. Opin. Plant Biol.* 15, 585–592. doi: 10.1016/j.pbi.2012.09.013

Franks, P. J. W., Doheny-Adams, T., Britton-Harper, Z. J., and Gray, J. E. (2015). Increasing water-use efficiency directly through genetic manipulation of stomatal density. *New Phytol.* 207, 188–195. doi: 10.1111/nph.13347

Galdon-Armero, J., Fullana-Pericas, M., Mulet, P. A., Conesa, M. A., Martin, C., and Galmes, J. (2018). The ratio of trichomes to stomata is associated with water use efficiency in Solanum lycopersicum (tomato). *Plant J.* 96, 607–619. doi: 10.1111/tpj.14055

Gangappa, S. N., and Botto, J. F. (2016). The multifaceted roles of HY5 in plant growth and development. *Mol. Plant* 9, 1353–1365. doi: 10.1016/j.molp.2016.07.002

Geisler, M., Yang, M., and Sack, F. D. (1998). Divergent regulation of stomatal initiation and patterning in organ and suborgan regions of the Arabidopsis mutants too many mouths and four lips. *Planta* 205, 522–530. doi: 10.1007/s004250050351

Gong, Y., Alassimone, J., Varnau, R., Sharma, N., Cheung, L. S., and Bergmann, D. C. (2021). Tuning self-renewal in the Arabidopsis stomatal lineage by hormone and nutrient regulation of asymmetric cell division. *elife* 10:e63335. doi: 10.7554/eLife.63335

Grones, P., Majda, M., Doyle, S. M., Van Damme, D., and Robert, S. (2020). Fluctuating auxin response gradients determine pavement cell-shape acquisition. *Proc. Natl. Acad. Sci.* 117, 16027–16034. doi: 10.1073/pnas.2007400117

Gudesblat, G. E., Schneider-Pizon, J., Betti, C., Mayerhofer, J., Vanhoutte, I., van Dongen, W., et al. (2012). SPEECHLESS integrates brassinosteroid and stomata signalling pathways. *Nat. Cell Biol.* 14, 548–554. doi: 10.1038/ncb2471

Guo, X., and Dong, J. (2019). To divide or differentiate: it is about scaffolding. *Trends Plant Sci.* 24, 481–484. doi: 10.1016/j.tplants.2019.03.007

Guo, X., Park, C. H., Wang, Z. Y., Nickels, B. E., and Dong, J. (2021a). A spatiotemporal molecular switch governs plant asymmetric cell division. *Nat Plants* 7, 667–680. doi: 10.1038/s41477-021-00906-0

Guo, X., Wang, L., and Dong, J. (2021b). Establishing asymmetry: stomatal division and differentiation in plants. *New Phytol.* 232, 60–67. doi: 10.1111/nph.17613

Hachez, C., Ohashi-Ito, K., Dong, J., and Bergmann, D. C. (2011). Differentiation of Arabidopsis guard cells: analysis of the networks incorporating the basic helix-loop-helix transcription factor, FAMA. *Plant Physiol.* 155, 1458–1472. doi: 10.1104/pp.110.167718

Han, C., Liu, Y., Shi, W., Qiao, Y., Wang, L., Tian, Y., et al. (2020). KIN10 promotes stomatal development through stabilization of the SPEECHLESS transcription factor. *Nat. Commun.* 11, 1–10. doi: 10.1038/s41467-020-18048-w

Han, S. K., Qi, X., Sugihara, K., Dang, J. H., Endo, T. A., Miller, K. L., et al. (2018). MUTE directly orchestrates cell-state switch and the single symmetric division to create stomata. *Dev. Cell* 45, 303–315 e305. doi: 10.1016/j.devcel.2018.04.010

Han, S. K., and Torii, K. U. (2016). Lineage-specific stem cells, signals and asymmetries during stomatal development. *Development* 143, 1259–1270. doi: 10.1242/dev.127712

Hara, K., Kajita, R., Torii, K. U., Bergmann, D. C., and Kakimoto, T. (2007). The secretory peptide gene EPF1 enforces the stomatal one-cell-spacing rule. *Genes Dev.* 21, 1720–1725. doi: 10.1101/gad.1550707

Hara, K., Yokoo, T., Kajita, R., Onishi, T., Yahata, S., Peterson, K. M., et al. (2009). Epidermal cell density is autoregulated via a secretory peptide, EPIDERMAL PATTERNING FACTOR 2 in Arabidopsis leaves. *Plant Cell Physiol.* 50, 1019–1031. doi: 10.1093/pcp/pcp068

Hatfield, L. J., and Prueger, H. J. (2015). Temperature extremes: effect on plant growth and development. *Weather and Climate Extremes* 10, 4–10. doi: 10.1016/j.wace.2015.08.001

Haus, M. J., Li, M., Chitwood, D. H., and Jacobs, T. W. (2018). Long-distance and trans-generational stomatal patterning by CO2 Across Arabidopsis organs. *Front. Plant Sci.* 9:1714. doi: 10.3389/fpls.2018.01714

Hecker, A., Brand, L. H., Peter, S., Simoncello, N., Kilian, J., Harter, K., et al. (2015). The Arabidopsis GAGA-binding factor BASIC PENTACYSTEINE6 recruits the POLYCOMB-REPRESSIVE COMPLEX1 component LIKE HETEROCHROMATIN PROTEIN1 to GAGA DNA motifs. *Plant Physiol.* 168, 1013–1024. doi: 10.1104/pp.15.00409

Hepworth, C., Caine, R. S., Harrison, E. L., Sloan, J., and Gray, J. E. (2018). Stomatal development: focusing on the grasses. *Curr. Opin. Plant Biol.* 41, 1–7. doi: 10.1016/j.pbi.2017.07.009

Hepworth, C., Doheny-Adams, T., Hunt, L., Cameron, D. D., and Gray, J. E. (2015). Manipulating stomatal density enhances drought tolerance without deleterious effect on nutrient uptake. *New Phytol.* 208, 336–341. doi: 10.1111/nph.13598

Hepworth, C., Turner, C., Landim, M. G., Cameron, D., and Gray, J. E. (2016). Balancing water uptake and loss through the coordinated regulation of stomatal and root development. *PLoS One* 11:e0156930. doi: 10.1371/journal.pone.0156930

Herrmann, A., and Torii, K. U. (2020). Shouting out loud: Signaling modules in the regulation of stomatal development. *Plant Physiol.* 185, 765–780. doi: 10.1093/plphys/kiaa061

Higaki, T., Akita, K., and Hasezawa, S. (2020). Elevated CO2 promotes satellite stomata production in young cotyledons of Arabidopsis thaliana. *Genes Cells* 25, 475–482. doi: 10.1111/gtc.12773

Ho, C. K., Bringmann, M., Oshima, Y., Mitsuda, N., and Bergmann, D. C. (2021). Transcriptional profiling reveals signatures of latent developmental potential in Arabidopsis stomatal lineage ground cells. *Proc. Natl. Acad. Sci.* 118:e2021682118. doi: 10.1073/pnas.2021682118

Horst, R. J., Fujita, H., Lee, J. S., Rychel, A. L., Garrick, J. M., Kawaguchi, M., et al. (2015). Molecular framework of a regulatory circuit initiating two-dimensional spatial patterning of stomatal lineage. *PLoS Genet.* 11:e1005374. doi: 10.1371/journal.pgen.1005374

Houbaert, A., Zhang, C., Tiwari, M., Wang, K., de Marcos Serrano, A., Savatin, D. V., et al. (2018). POLAR-guided signalling complex assembly and localization drive asymmetric cell division. *Nature* 563, 574–578. doi: 10.1038/s41586-018-0714-x

Hronkova, M., Wiesnerova, D., Simkova, M., Skupa, P., Dewitte, W., Vrablova, M., et al. (2015). Light-induced STOMAGEN-mediated stomatal development in Arabidopsis leaves. *J. Exp. Bot.* 66, 4621–4630. doi: 10.1093/jxb/erv233

Hu, H., Boisson-Dernier, A., Israelsson-Nordstrom, M., Bohmer, M., Xue, S., Ries, A., et al. (2010). Carbonic anhydrases are upstream regulators of CO2-controlled stomatal movements in guard cells. *Nat. Cell Biol.* 12, 87–93. doi: 10.1038/ncb2009

Hughes, J., Hepworth, C., Dutton, C., Dunn, J. A., Hunt, L., Stephens, J., et al. (2017). Reducing stomatal density in barley improves drought tolerance without impacting on yield. *Plant Physiol.* 174, 776–787. doi: 10.1104/pp.16.01844

Hunt, L., and Gray, J. E. (2009). The signaling peptide EPF2 controls asymmetric cell divisions during stomatal development. *Curr. Biol.* 19, 864–869. doi: 10.1016/j.cub.2009.03.069

John, P. C., and Qi, R. (2008). Cell division and endoreduplication: doubtful engines of vegetative growth. *Trends Plant Sci.* 13, 121–127. doi: 10.1016/j.tplants.2008.01.004

Kanaoka, M. M., Pillitteri, L. J., Fujii, H., Yoshida, Y., Bogenschutz, N. L., Takabayashi, J., et al. (2008). SCREAM/ICE1 and SCREAM2 specify three cell-state transitional steps leading to arabidopsis stomatal differentiation. *Plant Cell* 20, 1775–1785. doi: 10.1105/tpc.108.060848

Kang, C. Y., Lian, H. L., Wang, F. F., Huang, J. R., and Yang, H. Q. (2009). Cryptochromes, phytochromes, and COP1 regulate light-controlled stomatal development in Arabidopsis. *Plant Cell* 21, 2624–2641. doi: 10.1105/tpc.109.069765

Klermund, C., Ranftl, Q. L., Diener, J., Bastakis, E., Richter, R., and Schwechheimer, C. (2016). LLM-Domain B-GATA transcription factors promote stomatal development downstream of light Signaling pathways in Arabidopsis thaliana hypocotyls. *Plant Cell* 28, 646–660. doi: 10.1105/tpc.15.00783

Koini, M. A., Alvey, L., Allen, T., Tilley, C. A., Harberd, N. P., Whitelam, G. C., et al. (2009). High temperature-mediated adaptations in plant architecture require the bHLH transcription factor PIF4. *Curr. Biol.* 19, 408–413. doi: 10.1016/j.cub.2009.01.046

Kondo, T., Kajita, R., Miyazaki, A., Hokoyama, M., Nakamura-Miura, T., Mizuno, S., et al. (2010). Stomatal density is controlled by a mesophyll-derived signaling molecule. *Plant Cell Physiol.* 51, 1–8. doi: 10.1093/pcp/pcp180

Lampard, G. R., Macalister, C. A., and Bergmann, D. C. (2008). Arabidopsis stomatal initiation is controlled by MAPK-mediated regulation of the bHLH SPEECHLESS. *Science* 322, 1113–1116. doi: 10.1126/science.1162263

Lau, O. S., Davies, K. A., Chang, J., Adrian, J., Rowe, M. H., Ballenger, C. E., et al. (2014). Direct roles of SPEECHLESS in the specification of stomatal self-renewing cells. *Science* 345, 1605–1609. doi: 10.1126/science.1256888

Lau, O. S., Song, Z., Zhou, Z., Davies, K. A., Chang, J., Yang, X., et al. (2018). Direct control of SPEECHLESS by PIF4 in the high-temperature response of stomatal development. *Curr. Biol.* 28, 1273–1280 e1273. doi: 10.1016/j.cub.2018.02.054

Lee, L. R., and Bergmann, D. C. (2019). The plant stomatal lineage at a glance. *J. Cell Sci.* 132:jcs228551. doi: 10.1242/jcs.228551

Lee, J., He, K., Stolc, V., Lee, H., Figueroa, P., Gao, Y., et al. (2007). Analysis of transcription factor HY5 genomic binding sites revealed its hierarchical role in light regulation of development. *Plant Cell* 19, 731–749. doi: 10.1105/tpc.106.047688

Lee, J. S., Hnilova, M., Maes, M., Lin, Y. C., Putarjunan, A., Han, S. K., et al. (2015). Competitive binding of antagonistic peptides fine-tunes stomatal patterning. *Nature* 522, 439–443. doi: 10.1038/nature14561

Lee, J. H., Jung, J. H., and Park, C. M. (2017). Light inhibits COP1-mediated degradation of ICE transcription factors to induce stomatal development in Arabidopsis. *Plant Cell* 29, 2817–2830. doi: 10.1105/tpc.17.00371

Lee, J. S., Kuroha, T., Hnilova, M., Khatayevich, D., Kanaoka, M. M., McAbee, J. M., et al. (2012). Direct interaction of ligand-receptor pairs specifying stomatal patterning. *Genes Dev.* 26, 126–136. doi: 10.1101/gad.179895.111

Lee, E., Lucas, J. R., Goodrich, J., and Sack, F. D. (2014a). Arabidopsis guard cell integrity involves the epigenetic stabilization of the FLP and FAMA transcription factor genes. *Plant J.* 78, 566–577. doi: 10.1111/tpj.12516

Lee, E., Lucas, J. R., and Sack, F. D. (2014b). Deep functional redundancy between FAMA and FOUR LIPS in stomatal development. *Plant J.* 78, 555–565. doi: 10.1111/tpj.12489

Lee, L. R., Wengier, D. L., and Bergmann, D. C. (2019). Cell-type-specific transcriptome and histone modification dynamics during cellular reprogramming in the Arabidopsis stomatal lineage. *Proc. Natl. Acad. Sci.* 116, 21914–21924. doi: 10.1073/pnas.1911400116

Lin, G., Zhang, L., Han, Z., Yang, X., Liu, W., Li, E., et al. (2017). A receptor-like protein acts as a specificity switch for the regulation of stomatal development. *Genes Dev.* 31, 927–938. doi: 10.1101/gad.297580.117

Lindsey, R. (2020). Climate Change: Atomospheric Carbon Dioxide. *NOAA. Climate.gov.* https://www.climate.gov/print/8431

Liu, T., Ohashi-Ito, K., and Bergmann, D. C. (2009). Orthologs of Arabidopsis thaliana stomatal bHLH genes and regulation of stomatal development in grasses. *Development* 136, 2265–2276. doi: 10.1242/dev.032938

Liu, Z., Zhou, Y., Guo, J., Li, J., Tian, Z., Zhu, Z., et al. (2020). Global dynamic molecular profiling of stomatal lineage cell development by single-cell RNA sequencing. *Mol. Plant* 13, 1178–1193. doi: 10.1016/j.molp.2020.06.010

Long, J. A., Ohno, C., Smith, Z. R., and Meyerowitz, E. M. (2020). TOPLESS regulates apical embryonic fate in Arabidopsis. *Science* 312, 1520–1523. doi: 10.1126/science.1123841

Lopez-Anido, C. B., Vaten, A., Smoot, N. K., Sharma, N., Guo, V., Gong, Y., et al. (2021). Single-cell resolution of lineage trajectories in the Arabidopsis stomatal lineage and developing leaf. *Dev. Cell* 56, 1043–1055 e1044. doi: 10.1016/j.devcel.2021.03.014

MacAlister, C. A., Ohashi-Ito, K., and Bergmann, D. C. (2007). Transcription factor control of asymmetric cell divisions that establish the stomatal lineage. *Nature* 445, 537–540. doi: 10.1038/nature05491

Mair, A., Xu, S. L., Branon, T. C., Ting, A. Y., and Bergmann, D. C. (2019). Proximity labeling of protein complexes and cell-type-specific organellar proteomes in Arabidopsis enabled by TurboID. *elife* 8:e47864. doi: 10.7554/eLife.47864

Matos, J. L., Lau, O. S., Hachez, C., Cruz-Ramirez, A., Scheres, B., and Bergmann, D. C. (2014). Irreversible fate commitment in the Arabidopsis stomatal lineage requires a FAMA and RETINOBLASTOMA-RELATED module. *elife* 3:e03271. doi: 10.7554/eLife.03271

McElwain, J. C., and Steinthorsdottir, M. (2017). Paleoecology, ploidy, Paleoatmospheric composition, and developmental biology: A review of the multiple uses of fossil stomata. *Plant Physiol.* 174, 650–664. doi: 10.1104/pp.17.00204

McKown, K. H., and Bergmann, D. C. (2020). Stomatal development in the grasses: lessons from models and crops (and crop models). *New Phytol.* 227, 1636–1648. doi: 10.1111/nph.16450

Meng, L. S., and Yao, S. Q. (2015). Transcription co-activator Arabidopsis ANGUSTIFOLIA3 (AN3) regulates water-use efficiency and drought tolerance by modulating stomatal density and improving root architecture by the transrepression of YODA (YDA). *Plant Biotechnol. J.* 13, 893–902. doi: 10.1111/pbi.12324

Mohammed, U., Caine, R. S., Atkinson, J. A., Harrison, E. L., Wells, D., Chater, C. C., et al. (2019). Rice plants overexpressing OsEPF1 show reduced stomatal density and increased root cortical aerenchyma formation. *Sci. Rep.* 9, 1–13. doi: 10.1038/s41598-019-41922-7

Morales-Navarro, S., Pérez-Díaz, R., Ortega, A., de Marcos, A., Mena, M., Fenoll, C., et al. (2018). Overexpression of a SDD1-Like Gene From wild tomato decreases stomatal density and enhances dehydration avoidance in Arabidopsis and cultivated tomato. *Front. Plant Sci.* 9:940. doi: 10.3389/fpls.2018.00940

Mu, Y., Zou, M., Sun, X., He, B., Xu, X., Liu, Y., et al. (2017). BASIC PENTACYSTEINE proteins repress ABSCISIC ACID INSENSITIVE4 expression via direct recruitment of the Polycomb-repressive complex 2 in Arabidopsis root development. *Plant Cell Physiol.* 58, 607–621. doi: 10.1093/pcp/pcx006

Negi, J., Moriwaki, K., Konishi, M., Yokoyama, R., Nakano, T., Kusumi, K., et al. (2013). A Dof transcription factor, SCAP1, is essential for the development of functional stomata in Arabidopsis. *Curr. Biol.* 23, 479–484. doi: 10.1016/j.cub.2013.02.001

Nunes, T. D. G., Zhang, D., and Raissig, M. T. (2020). Form, development and function of grass stomata. *Plant J.* 101, 780–799. doi: 10.1111/tpj.14552

Ohashi-Ito, K., and Bergmann, D. C. (2006). Arabidopsis FAMA controls the final proliferation/differentiation switch during stomatal development. *Plant Cell* 18, 2493–2505. doi: 10.1105/tpc.106.046136

Ohki, S., Takeuchi, M., and Mori, M. (2011). The NMR structure of stomagen reveals the basis of stomatal density regulation by plant peptide hormones. *Nat. Commun.* 2, 1–7. doi: 10.1038/ncomms1520

Paik, I., and Huq, E. (2019). Plant photoreceptors: multi-functional sensory proteins and their signaling networks. *Semin. Cell Dev. Biol.* 92, 114–121. doi: 10.1016/j.semcdb.2019.03.007

Pillitteri, L. J., Peterson, K. M., Horst, R. J., and Torii, K. U. (2011). Molecular profiling of stomatal meristemoids reveals new component of asymmetric cell division and commonalities among stem cell populations in Arabidopsis. *Plant Cell* 23, 3260–3275. doi: 10.1105/tpc.111.088583

Pillitteri, L. J., Sloan, D. B., Bogenschutz, N. L., and Torii, K. U. (2007). Termination of asymmetric cell division and differentiation of stomata. *Nature* 445, 501–505. doi: 10.1038/nature05467

Putarjunan, A., Ruble, J., Srivastava, A., Zhao, C., Rychel, A. L., Hofstetter, A. K., et al. (2019). Bipartite anchoring of SCREAM enforces stomatal initiation by coupling MAP kinases to SPEECHLESS. *Nat Plants* 5, 742–754. doi: 10.1038/s41477-019-0440-x

Qi, X., Han, S. K., Dang, J. H., Garrick, J. M., Ito, M., Hofstetter, A. K., et al. (2017). Autocrine regulation of stomatal differentiation potential by EPF1 and ERECTA-LIKE1 ligand-receptor signaling. *elife* 6:24102. doi: 10.7554/eLife.24102

Qi, S. L., Lin, Q. F., Feng, X. J., Han, H. L., Liu, J., Zhang, L., et al. (2019). IDD16 negatively regulates stomatal initiation via trans-repression of SPCH in Arabidopsis. *Plant Biotechnol. J.* 17, 1446–1457. doi: 10.1111/pbi.13070

Qi, X., and Torii, K. U. (2018). Hormonal and environmental signals guiding stomatal development. *BMC Biol.* 16, 21. doi: 10.1186/s12915-018-0488-5

Qi, X., Yoshinari, A., Bai, P., Maes, M., Zeng, S. M., and Torii, K. U. (2020). The manifold actions of signaling peptides on subcellular dynamics of a receptor specify stomatal cell fate. *elife* 9:e58097. doi: 10.7554/eLife.58097

Raissig, M. T., Abrash, E., Bettadapur, A., Vogel, J. P., and Bergmann, D. C. (2016). Grasses use an alternatively wired bHLH transcription factor network to establish stomatal identity. *Proc. Natl. Acad. Sci.* 113, 8326–8331. doi: 10.1073/pnas.1606728113

Raissig, M. T., Matos, J. L., Anleu Gil, M. X., Kornfeld, A., Bettadapur, A., Abrash, E., et al. (2017). Mobile MUTE specifies subsidiary cells to build physiologically improved grass stomata. *Science* 355, 1215–1218. doi: 10.1126/science.aal3254

Robinson, S., Barbier de Reuille, P., Chan, J., Bergmann, D., Prusinkiewicz, P., and Coen, E. (2011). Generation of spatial patterns through cell polarity switching. *Science* 333, 1436–1440. doi: 10.1126/science.1202185

Rowe, M. H., and Bergmann, D. C. (2010). Complex signals for simple cells: the expanding ranks of signals and receptors guiding stomatal development. *Curr. Opin. Plant Biol.* 13, 548–555. doi: 10.1016/j.pbi.2010.06.002

Rychel, A. L., Peterson, K. M., and Torii, K. U. (2010). Plant twitter: ligands under 140 amino acids enforcing stomatal patterning. *J. Plant Res.* 123, 275–280. doi: 10.1007/s10265-010-0330-9

Sage, R. F., and Coleman, J. R. (2001). Effects of low atmospheric CO(2) on plants: more than a thing of the past. *Trends Plant Sci.* 6, 18–24. doi: 10.1016/S1360-1385(00)01813-6

Samakovli, D., Ticha, T., Vavrdova, T., Ovecka, M., Luptovciak, I., Zapletalova, V., et al. (2020). YODA-HSP90 module regulates phosphorylation-dependent inactivation of SPEECHLESS to control stomatal development under acute heat stress in Arabidopsis. *Mol. Plant* 13, 612–633. doi: 10.1016/j.molp.2020.01.001

Simon, N. M. L., Sugisaka, J., Honjo, M. N., Tunstad, S. A., Tunna, G., Kudoh, H., et al. (2020). Altered stomatal patterning accompanies a trichome dimorphism in a natural population of. *Plant Direct* 4:e00262. doi: 10.1002/pld3.262

Song, X., Li, Y., Cao, X., and Qi, Y. (2019). MicroRNAs and their regulatory roles in plant-environment interactions. *Annu. Rev. Plant Biol.* 70, 489–525. doi: 10.1146/annurev-arplant-050718-100334

Sugano, S. S., Shimada, T., Imai, Y., Okawa, K., Tamai, A., Mori, M., et al. (2010). Stomagen positively regulates stomatal density in Arabidopsis. *Nature* 463, 241–244. doi: 10.1038/nature08682

Tamnanloo, F., Damen, H., Jangra, R., and Lee, J. S. (2018). MAP KINASE PHOSPHATASE1 controls cell fate transition during stomatal development. *Plant Physiol.* 178, 247–257. doi: 10.1104/pp.18.00475

Torii, K. U. (2012). Mix-and-match: ligand-receptor pairs in stomatal development and beyond. *Trends Plant Sci.* 17, 711–719. doi: 10.1016/j.tplants.2012.06.013

Torii, K. U. (2021). Stomatal development in the context of epidermal tissues. *Ann. Bot.* 128, 137–148. doi: 10.1093/aob/mcab052

Trivino, M., Martin-Trillo, M., Ballesteros, I., Delgado, D., de Marcos, A., Desvoyes, B., et al. (2013). Timely expression of the Arabidopsis stoma-fate master regulator MUTE is required for specification of other epidermal cell types. *Plant J.* 75, 808–822. doi: 10.1111/tpj.12244

Vaten, A., Soyars, C. L., Tarr, P. T., Nimchuk, Z. L., and Bergmann, D. C. (2018). Modulation of asymmetric division diversity through Cytokinin and SPEECHLESS regulatory interactions in the Arabidopsis stomatal lineage. *Dev. Cell* 47, 53–66. doi: 10.1016/j.devcel.2018.08.007

Von Groll, U., Berger, D., and Altmann, T. (2002). The subtilisin-like serine protease SDD1 mediates cell-to-cell signaling during Arabidopsis stomatal development. *Plant Cell* 14, 1527–1539. doi: 10.1105/tpc.001016

Wang, H., Guo, S., Qiao, X., Guo, J., Li, Z., Zhou, Y., et al. (2019). BZU2/ZmMUTE controls symmetrical division of guard mother cell and specifies neighbor cell fate in maize. *PLoS Genet.* 15:e1008377. doi: 10.1371/journal.pgen.1008377

Wang, C., Liu, S., Dong, Y., Zhao, Y., Geng, A., Xia, X., et al. (2016). PdEPF1 regulates water-use efficiency and drought tolerance by modulating stomatal density in poplar. *Plant Biotechnol. J.* 14, 849–860. doi: 10.1111/pbi.12434

Wang, H., Ngwenyama, N., Liu, Y., Walker, J. C., and Zhang, S. (2007). Stomatal development and patterning are regulated by environmentally responsive mitogen-activated protein kinases in Arabidopsis. *Plant Cell* 19, 63–73. doi: 10.1105/tpc.106.048298

Wang, S., Zhou, Z., Rahiman, R., Lee, G. S. Y., Yeo, Y. K., Yang, X., et al. (2021). Light regulates stomatal development by modulating paracrine signaling from inner tissues. *Nat. Commun.* 12, 1–13. doi: 10.1038/s41467-021-23728-2

Wu, Z., Chen, L., Yu, Q., Zhou, W., Gou, X., Li, J., et al. (2019). Multiple transcriptional factors control stomata developmentin rice. *New Phytol.* 223, 220–232. doi: 10.1111/nph.15766

Xiao, J., Jin, R., Yu, X., Shen, M., Wagner, J. D., Pai, A., et al. (2017). Cis and trans determinants of epigenetic silencing by Polycomb repressive complex 2 in Arabidopsis. *Nat. Genet.* 49, 1546–1552. doi: 10.1038/ng.3937

Xie, Z., Lee, E., Lucas, J. R., Morohashi, K., Li, D., Murray, J. A., et al. (2010). Regulation of cell proliferation in the stomatal lineage by the Arabidopsis MYB FOUR LIPS via direct targeting of core cell cycle genes. *Plant Cell* 22, 2306–2321. doi: 10.1105/tpc.110.074609

Yang, K., Jiang, M., and Le, J. (2014). A new loss-of-function allele 28y reveals a role of ARGONAUTE1 in limiting asymmetric division of stomatal lineage ground cell. *J. Integr. Plant Biol.* 56, 539–549. doi: 10.1111/jipb.12154

Yang, K. Z., Jiang, M., Wang, M., Xue, S., Zhu, L. L., Wang, H. Z., et al. (2015). Phosphorylation of serine 186 of bHLH transcription factor SPEECHLESS promotes stomatal development in Arabidopsis. *Mol. Plant* 8, 783–795. doi: 10.1016/j.molp.2014.12.014

Yang, K., Zhu, L., Wang, H., Jiang, M., Xiao, C., Hu, X., et al. (2019). A conserved but plant-specific CDK-mediated regulation of DNA replication protein A2 in the precise control of stomatal terminal division. *Proc. Natl. Acad. Sci.* 116, 18126–18131. doi: 10.1073/pnas.1819345116

Yoo, C. Y., Mano, N., Finkler, A., Weng, H., Day, I. S., Reddy, A. S. N., et al. (2019). A Ca. *Sci. Rep.* 9:12282. doi: 10.1038/s41598-019-47529-2

Yoo, C. Y., Pence, H. E., Jin, J. B., Miura, K., Gosney, M. J., Hasegawa, P. M., et al. (2010). The Arabidopsis GTL1 transcription factor regulates water use efficiency and drought tolerance by modulating stomatal density via transrepression of SDD1. *Plant Cell* 22, 4128–4141. doi: 10.1105/tpc.110.078691

Zhang, U., He, S. B., Li, L., and Yang, H. Q. (2002). The subtilisin-like serine protease SDD1 mediates cell-to-cell signaling during Arabidopsis stomatal development. *Proc. Natl. Acad. Sci.* 111, 3015–3023. doi: 10.1073/pnas.1400542111

Zhang, J. Y., Guo, X., and Dong, J. (2016). Auxin inhibits stomatal development through MONOPTEROS repression of a mobile peptide gene STOMAGEN in mesophyll. *Curr. Biol.* 26, 2957–2965. doi: 10.1016/j.cub.2016.08.066

Zhang, Y., Wang, P., Shao, W., Zhu, J. K., and Dong, J. (2015). The BASL polarity protein controls a MAPK signaling feedback loop in asymmetric cell division. *Dev. Cell* 33, 136–149. doi: 10.1016/j.devcel.2015.02.022

Zhao, J., Yuan, S., Zhou, M., Yuan, N., Li, Z., Hu, Q., et al. (2019). Transgenic creeping bentgrass overexpressing Osa-miR393a exhibits altered plant development and improved multiple stress tolerance. *Plant Biotechnol. J.* 17, 233–251. doi: 10.1111/pbi.12960

Zhu, J., Park, J. H., Lee, S., Lee, J. H., Hwang, D., Kwak, J. M., et al. (2020). Regulation of stomatal development by stomatal lineage miRNAs. *Proc. Natl. Acad. Sci.* 117, 6237–6245. doi: 10.1073/pnas.1919722117

Zoulias, N., Brown, J., Rowe, J., and Casson, S. A. (2020). HY5 is not integral to light mediated stomatal development in Arabidopsis. *PLoS One* 15:e0222480. doi: 10.1371/journal.pone.0222480

Conflict of Interest: The authors declare that the research was conducted in the absence of any commercial or financial relationships that could be construed as a potential conflict of interest.

Publisher's Note: All claims expressed in this article are solely those of the authors and do not necessarily represent those of their affiliated organizations, or those of the publisher, the editors and the reviewers. Any product that may be evaluated in this article, or claim that may be made by its manufacturer, is not guaranteed or endorsed by the publisher.

frontiers in Plant Science

ORIGINAL RESEARCH
published: 27 October 2021
doi: 10.3389/fpls.2021.740534

Stomatal Responses to Light, CO_2, and Mesophyll Tissue in *Vicia faba* and *Kalanchoë fedtschenkoi*

Mauro G. Santos[1†], *Phillip A. Davey*[1], *Tanja A. Hofmann*[2], *Anne Borland*[3], *James Hartwell*[4] *and Tracy Lawson*[1*]

[1] School of Life Sciences, University of Essex, Wivenhoe Park, Colchester, United Kingdom, [2] OSFC, Scrivener Dr, Pinewood, Ipswich, United Kingdom, [3] School of Natural and Environmental Sciences, Devonshire Building, Newcastle University, Newcastle upon Tyne, United Kingdom, [4] Department of Biochemistry and Systems Biology, Institute of Systems, Molecular and Integrative Biology, University of Liverpool, Liverpool, United Kingdom

OPEN ACCESS

Edited by:
Wenxiu Ye,
Shanghai Jiao Tong University, China

Reviewed by:
Scott McAdam,
Purdue University, United States
Caspar Christian Cedric Chater,
Royal Botanic Gardens, Kew, United Kingdom
Ichiro Terashima,
The University of Tokyo, Japan
Dr. Eigo Ando,
Japan Society for the Promotion of Science, in collaboration with reviewer IT

***Correspondence:**
Tracy Lawson
tlawson@essex.ac.uk

†Present address:
Mauro G. Santos,
Botany Department, Federal University of Pernambuco, Recife, Brazil

Specialty section:
This article was submitted to Plant Cell Biology, a section of the journal Frontiers in Plant Science

Received: *13 July 2021*
Accepted: *22 September 2021*
Published: *27 October 2021*

Citation:
Santos MG, Davey PA, Hofmann TA, Borland A, Hartwell J and Lawson T (2021) Stomatal Responses to Light, CO_2, and Mesophyll Tissue in Vicia faba and Kalanchoë fedtschenkoi. Front. Plant Sci. 12:740534. doi: 10.3389/fpls.2021.740534

The responses of stomatal aperture to light intensity and CO_2 concentration were studied in both *Vicia faba* (C_3) and *Kalanchoë fedtschenkoi* (Crassulacean acid metabolism; CAM), in material sampled from both light and dark periods. Direct comparison was made between intact leaf segments, epidermises grafted onto exposed mesophyll, and isolated epidermal peels, including transplantations between species and between diel periods. We reported the stomatal opening in response to darkness in isolated CAM peels from the light period, but not from the dark. Furthermore, we showed that C_3 mesophyll has stimulated CAM stomata in transplanted peels to behave as C_3 in response to light and CO_2. By using peels and mesophyll from plants sampled in the dark and the light period, we provided clear evidence that CAM stomata behaved differently from C_3. This might be linked to stored metabolites/ions and signalling pathway components within the guard cells, and/or a mesophyll-derived signal. Overall, our results provided evidence for both the involvement of guard cell metabolism *and* mesophyll signals in stomatal responses in both C_3 and CAM species.

Keywords: stomata, CAM, mesophyll, *Vicia faba, Kalanchoë fedtschenkoi*, conductance, stomatal dynamics

INTRODUCTION

The waxy leaf surface is almost impermeable to carbon dioxide and water and therefore nearly all gaseous exchange between the leaf interior and the external environment passes through the stomatal pores on the leaf surface (Lawson, 2009). Stomata open and close in response to changes in both external environmental and internal plant signals (e.g., Mott, 1988; Outlaw, 2003; Vavasseur and Raghavendra, 2005; Shimazaki et al., 2007; Lawson, 2009). The nuanced control of stomatal aperture ensures sufficient carbon dioxide (CO_2) uptake for photosynthesis, as well as maintaining an appropriate water (H_2O) status and leaf temperature (Lawson and Blatt, 2014). In species with C_3 and C_4 photosynthetic metabolism, stomata open in response to low CO_2 concentration, high light, and low VPD, whereas closure is driven by the reverse, high CO_2 concentration, low light, and high VPD (Outlaw, 2003; Vavasseur and Raghavendra, 2005; Shimazaki et al., 2007; Lawson, 2009).

It is well-established that stomatal conductance (g_s) correlates with mesophyll rates of photosynthesis under a range of different conditions (Farquhar and Wong, 1984; Wong et al., 1979; Mansfield et al., 1990; Buckley et al., 2003). This helps to maintain an appropriate balance of CO_2 uptake with water loss (often referred to as instantaneous water use efficiency). Until recently it was thought that [CO_2] concentration in the sub-stomatal cavity, internal [CO_2] (C_i) co-ordinated stomatal behaviour with mesophyll demands for CO_2. For example, when irradiance increases CO_2 consumption by the mesophyll, stomata will respond to the decrease in C_i by opening (Mott, 1988). Conversely, when photosynthesis is reduced due to a changing environmental factor, the higher C_i results in stomatal closure. However, several studies have suggested that stomatal responses to changing C_i are too small to account for the differences in observed g_s in response to light (Raschke, 1975; Farquhar et al., 1978; Sharkey and Raschke, 1981; Farquhar and Sharkey, 1982; Morison and Jarvis, 1983; Ramos and Hall, 1983; Mott, 1988). These findings had led to the proposal that there must be an alternative signal (see Lawson et al., 2018).

Stomata in Crassulacean acid metabolism (CAM) plants operate differently. They open at night when there is no light, and this facilitates CO_2 uptake when evaporative demand is low. In addition, they close during the day when light intensity and ambient temperatures are high, thereby minimising water loss through transpiration and optimising water use efficiency (Males and Griffiths, 2017). During the night in a CAM photosynthetic tissue, phosphoenolpyruvate carboxylase (PEPC or PPC) in the mesophyll draws down CO_2, as it functions as the primary nocturnal carboxylase for atmospheric CO_2 fixation (Borland et al., 2009). This nocturnal draw-down is hypothesised to drive stomatal opening in the dark. Atmospheric and respiratory CO_2 fixed at night by PPC is stored as malic acid in the vacuole, reaching a maximum concentration at dawn (Borland et al., 2009). During the light period, the stored malate is transported out of the vacuole and decarboxylated, and the CO_2 released increases C_i (Males and Griffiths, 2017). This increase in the light period in C_i due to malate decarboxylation has been proposed to drive stomatal closure in the light (Cockburn et al., 1979; Spalding et al., 1979; Borland et al., 1998; von Caemmerer and Griffiths, 2009). In general, as in C_3 plants, stomatal responses in CAM plants have been attributed to changes in C_i (von Caemmerer and Griffiths, 2009; Males and Griffiths, 2017).

In addition, it is increasingly clear that the circadian clock is likely to play an important role in CAM stomatal regulation (Boxall et al., 2005, 2020; Hubbard and Webb, 2015). In a seminal paper, von Caemmerer and Griffiths (2009) manipulated external CO_2 concentration and demonstrated stomatal closure in CAM-performing *Kalanchoë daigremontiana* leaves in the light period. The fact that the stomata closed in the light despite low C_i suggested that C_i was not the sole factor driving CAM stomatal responses and that another signal, possibly from the endogenous circadian clock, interacted with C_i to influence stomatal behaviour (von Caemmerer and Griffiths, 2009).

There is evidence that metabolites also play an important role in stomatal regulation. For example, when nocturnal CO_2 fixation and associated malic acid synthesis and accumulation were reduced by restricting CO_2 supply to *K. daigremontiana* leaves in the dark period, it was discovered that the adjusted metabolic status of the leaf could override the dawn-phased, circadian clock-controlled disappearance of the regulatory protein kinase responsible for making PPC less sensitive to feedback inhibition by malate, namely PPC kinase (PPCK) (Borland et al., 1999). In addition, transgenic gene silencing approaches have been used to generate CAM loss-of-function mutants in the CAM model species *Kalanchoë fedtschenkoi* and *Kalanchoë laxiflora* (e.g., Hartwell et al., 2016). Physiological, metabolic, and molecular phenotypic responses have been characterised for *Kalanchoë* mutants lacking the primary carboxylase PPC1, its circadian clock-controlled, nocturnal regulator PPCK1, plastidic α-glucan phosphorylase (PHS1) required for starch breakdown for PEP provision in the dark, and two key steps in the malate decarboxylation pathway that operates in the light period (Dever et al., 2015; Boxall et al., 2017, 2020; Ceusters et al., 2021). These mutants displayed either no dark atmospheric CO_2 fixation, or reduced nocturnal CO_2 fixation, but they still displayed decreased stomatal conductance in the middle of the light period (e.g., Boxall et al., 2020). The CAM mutants also revealed likely cross-talk between CAM-associated metabolites and both the leaf circadian clock and the light/dark regulation of guard cell genes known to be involved in stomatal opening and closing (Boxall et al., 2020).

Further evidence that questioned the role of C_i in stomatal behaviour in C_3 plants came from experiments in which stomata responded to increasing light even when C_i was held constant (Messinger et al., 2006; Lawson et al., 2008).

Together, these findings led to the hypothesis that a diffusible mesophyll signal co-ordinates stomatal behaviour with mesophyll demands for CO_2 (Lee and Bowling, 1992, 1995; Mott et al., 2008; Mott, 2009). The idea for a mesophyll signal was initially proposed by Heath and Russell in 1954, who postulated that stomatal behaviour was influenced by an indirect chemical or electrical signal transmitted from mesophyll or epidermal cells. Further support for a diffusible signal from the mesophyll was provided by the study of Lee and Bowling (1993), who demonstrated a stomatal response when isolated peels were incubated in the presence of mesophyll cells or chloroplasts from an illuminated leaf, but not when mesophyll tissue was not present, or when chloroplasts were used from dark-adapted material (see Lawson et al., 2018). Later studies suggested a photosynthetic intermediate or metabolite (Wong et al., 1979; Grantz and Schwartz, 1988; Lee and Bowling, 1992), specifically one that balances photosynthesis between Rubisco and electron transport limitation (Wong et al., 1979; Messinger et al., 2006). Support for the role of an active mesophyll-driven signal in stomatal responses has been provided from experiments carried out on epidermal peels in which the influence of the mesophyll had been removed. These studies have demonstrated either no effect or a slower response, of stomata to red light and/or [CO_2] (Lee and Bowling, 1992; Olsen and Junttila, 2002; Roelfsema et al., 2002), as compared with responses reported in intact leaves (Mott et al., 2008).

However, as pointed out by the study of Fujita et al. (2013), utilising isolated epidermises floated on buffer solutions makes

it difficult to track the same stoma due to movement in the buffer and the buffer permeating into sub-stomatal cavities, which are normally in contact with air. To overcome this, the study of Fujita et al. (2013) used a solid gellan gum matrix incorporating buffers, which was believed to mimic a leaf structure more closely. These experiments showed that buffer-filled cavities affected stomatal responses due to a lack of gaseous diffusion. To overcome the problems associated with using peels floated on the buffer, the study of Mott et al. (2008) used a unique epidermis–mesophyll transplantation experimental approach. The epidermis from one leaf was peeled and placed on the mesophyll belonging to either the same species or another species. Stomatal responses to changes in irradiance and [CO_2] were different when the epidermises were assayed in isolation as compared to those in contact with mesophyll tissue (Mott et al., 2008). By injecting various solutions into the leaf, the work of Sibbernsen and Mott (2010) suggested that the mesophyll signal must be gaseous, and, following later experiments, proposed vapour phase ions as the entities responsible for mesophyll control of guard cells and stomatal aperture (Mott and Peak, 2013; Mott et al., 2014). The study of Fujita et al. (2013) further tested this hypothesis by using different combinations of cellophane and polyethylene films inserted between an epidermal peel and the gel-based support medium. Only aqueous solutes could pass through the cellophane, whereas only gases could pass through the polyethylene film. No stomatal response to CO_2 was observed when using polyethylene films. However, a response was reported when using cellophane film, which led the authors to conclude that the mesophyll to guard cell signal must be aqueous (Fujita et al., 2013).

Several studies have examined stomatal behaviour in epidermises from one leaf placed onto mesophyll from a different leaf or species (Mott et al., 2008; Shope et al., 2008; McAdam and Brodribb, 2012; Fujita et al., 2013). The study of McAdam and Brodribb (2012) used a grafting approach (called xenografts) to assess differential influences of mesophyll on seed plants relative to ferns and showed that stomatal closing in response to light was impaired in isolated peels of seed plants but not the older ferns or lycophytes (McAdam and Brodribb, 2012). However, to date, no study has investigated the stomatal responses of an epidermis transplanted onto mesophyll of a species with different photosynthetic metabolism. Specifically, we examined stomatal responses to changes in irradiance and [CO_2] in the epidermis of the C_3 plant *Vicia faba* when placed on the mesophyll of the CAM species *K. fedtschenkoi* and *vice versa*. This unique approach has several distinct advantages. Each photosynthetic type exhibits an opposing stomatal response to the light and dark periods, and the photosynthetic mesophyll cells of C_3 and CAM species have markedly different metabolite pools at different times in the light and dark. Thus, we established an experimental system that provided novel insights into the question of whether or not a mesophyll-derived signal influences stomatal aperture responses. For example, the question "Will C_3 epidermal stomata sampled in the light still open in response to light when transplanted onto CAM mesophyll from the light?" was investigated in this study.

MATERIALS AND METHODS

Plant Material and Growth Conditions

Vicia faba (L.) (C_3) seed and *Kalanchoë fedtschenkoi* (Hamet et Perrier) (CAM) clonal stem cuttings were grown in two identical controlled environments (PG660, Sanyo, UK) using 24 h cycles of 12-h light [390 ($\pm$10) μmol m^{-2} s^{-1} at the top of the canopy], 25°C, and 12-h dark, 18°C, and a constant vapour pressure deficit of 1($\pm$0.1) kPa in the light and dark. In the first controlled environment, the 12-h light period was from 8:00 a.m. to 8:00 p.m., which will be known as the "light" chamber. The second controlled environment chamber had an inverted light and dark cycle, such that the 12-h light period was from 8:00 p.m. to 8:00 a.m., and thus, the chamber was in the 12-h dark period when the "light chamber" was in its 12-h light period from 8:00 a.m. to 8:00 p.m. This second chamber is hereafter referred to as the "dark" growth chamber. Plants were grown in 0.5 L pots containing peat-based compost (Levington F2+S, ICL, UK) and were watered daily. *V. faba* plants used during the experimental period were at least 4-weeks post-emergence, and *K. fedtschenkoi* were at least 2 months old and had acclimated to their respective controlled environment for at least 2 months. The youngest fully expanded leaves were used from the *V. faba*, whilst mature leaves (older than 6 leaf pairs down from the apical meristem) were used from *K. fedtschenkoi* to ensure the leaves were CAM, as younger leaves have been shown to operate as C_3, with a gradual developmental progression to full CAM in leaf pair six and older (Jones, 1975; Hartwell et al., 1999; Borland et al., 2009; Boxall et al., 2020).

Preparation of Leaf Material

Leaf segments at 11 × 15 mm in size were cut from the central mid lamina of selected leaves and exposed mesophyll was generated by peeling away the abaxial epidermis with the aid of broad-tip tweezers. Isolated epidermises were prepared in the same way from the lower surface of leaves of both species and were washed with distilled water after peeling. Visual examination of these epidermises showed that essentially no mesophyll cells remained. The prepared material was immediately placed on a 3 cm diameter philtre paper saturated with distilled water, or if used as an isolated epidermis, placed on philtre paper saturated with incubation media following the methods of Mott et al., 2008 (3 ml of 50 mM KCl and 1 mM $CaCl_2$). It should be noted that no buffers were used to prevent counteraction of the membrane H^+-ATPase, which could influence stomatal movements.

Incubation Chamber Design and Microenvironment

The prepared leaf materials were mounted into a gas-tight cuvette (Type 7937, ADC Bioscientific, UK) attached to a microscope (Leica, Leitz, DMRX, Wetzlar, Germany) (**Supplementary Figure 1**). The cuvette was constructed from two aluminium blocks, similar to that described in the study by Shope et al. (2008), giving a total sample volume of 6 cm^3. The upper section of the cuvette was connected to the microscope lens with a condom, which allowed stomatal images to be recorded

whilst maintaining the gaseous environment. The lower section of the cuvette contained a 3.5 cm diameter optical window to allow sample illumination. The cuvette was unstirred, using an internal plenum around the diameter of the cuvette to deliver mixed gas flow. The temperature of the cuvette was maintained at 23 ± 1°C by a chilled water bath supplying integral water jackets in both the upper and lower cuvette sections. The concentration of CO_2 inside the cuvette was controlled using an infrared gas analyser (IRGA 6400, Licor, NE, USA) at a flow rate of 500 μmol s^{-1} and vapour pressure deficit of 1 ± 0.1 KPa.

The segment of intact leaf and epidermal-mesophyll transfer material was illuminated through the optical window of the lower cuvette section. A white light source (XBO 75 W/HBO 100 W, Leica, Wetzlar, Germany) delivered a light intensity of 400 ± 10 μmol m^{-2} s^{-1} PAR at the surface of the epidermal peel. However, to allow measurements of stomatal opening during dark experimental periods, this was switched to a green LED light source (Luxeon Star, Lumileds Holding B.V., CA, USA) at an actinic intensity of 100 ± 10 μmol m^{-2} s^{-1} PAR which resulted in an intensity of 10 μmol m^{-2} s^{-1} on the abaxial surface (as shown in **Supplementary Figure 2**). Greenlight was selected in order to minimise photosynthesis and the associated changes in [CO_2], and although several studies have suggested that stomata can respond to green light, these are mostly associated with reversal of blue light responses (Talbott et al., 2002) or minimal opening responses compared with other wavelengths (Wang et al., 2011). One stoma was measured per day, and all response curves were started between 8:30 and 8:40 a.m. and finished between 2:45 and 3:00 p.m., respectively.

In all of the experiments, the light was changed sequentially from 400 to 0 μmol m^{-2} s^{-1} for 60 min and then returned back to 400 μmol m^{-2} s^{-1}, at a stable [CO_2] of 120 μmol mol^{-1}, after which [CO_2] was changed sequentially from 120 to 650 μmol mol^{-1} for 60 and then back to 120 μmol mol^{-1}. Afterward, 60 min was allowed for stomata to respond to darkness or higher [CO_2]. A low initial [CO_2] was used to ensure that stomata in all tissues experienced a similar [CO_2], as [CO_2] in intact leaves or grafted material would have reduced internal CO_2 due to photosynthetic CO_2 drawdown.

Determination of Stomatal Aperture

Stomatal apertures were measured using a camera (Bresser-Mikrocam 5-megapixel camera, 2,592 × 1,944, Rhede, Germany) attached to the microscope and connected to a personal computer (**Supplementary Figure 2**). Digital imaging software (Image J; U.S. National Institutes of Health, MD, USA, https://imagej.nih.gov/ij/) was used to measure apertures following calibration with a stage graticule. Each figure shows the results from three to four experiments conducted on different plants of the same age maintained under identical growth environments. As only a single stoma could be measured in the field of view, measurements were conducted over multiple days (3–4) and the data was used to generate mean responses.

Statistical Analyses

The data are shown as the means ± SE of three or four independent experiments. Possible differences among the mean values of data were analysed using ANOVA-factorial, and the means were compared with a Newman-Keuls test. The data were analysed using Statistica 8 (StatSoft. Inc., Tulsa, OK 74104, USA).

RESULTS

Titratable Acidity

In Crassulacean acid metabolism species, titratable acidity (TA) correlated directly with nocturnal CO_2 fixation and associated malic acid accumulation, and light period malate decarboxylation (Borland et al., 2009). Therefore, we measured titratable acid (TA) at dawn and dusk in order to determine the degree of CAM. As a direct confirmation that the *K. fedtschenkoi* leaves were operating the CAM pathway, the TA content was highest at dawn in the CAM leaves, approximately double the content of CAM leaves at dusk (**Supplementary Figure 3**). By contrast, only a negligible quantity of TA was measured in C_3 *V. faba* leaves, and the level did not vary markedly between dawn and dusk (**Supplementary Figure 3**). No significant differences were observed in the temporal variations in TA for the plants grown in either of the two chambers ("light" and "dark"), demonstrating that the key metabolic correlates of CAM in the *K. fedtschenkoi* leaf mesophyll were likely to be identical regardless of whether the plants were experiencing their dark period between 8:00 p.m. and 08:00 a.m. ("light" chamber), or between 8:00 a.m. and 8:00 p.m. ("dark" chamber).

C_3 and CAM Stomatal Responses of Plants in the "Light" Growth Chamber

To examine the C_3 physiology of *V. faba*, peeled epidermises transplanted back onto exposed *V. faba* mesophyll, stomatal responses in both intact leaf segments (**Figure 1A**), and abaxial epidermal peels placed onto the exposed mesophyll of a different leaf (**Figure 1B**) were assessed. In addition, epidermal peels in which the mesophyll was completely removed were also measured (**Figure 1C**). Stomata of *V. faba* sampled from the "light" chamber responded to light intensity as expected for a C_3 species (**Figure 1**). Stomatal aperture increased during the first incubation phase with 400 μmol m^{-2} s^{-1} light intensity, with apertures reaching about 8 μm, followed by a decrease in aperture to *ca.* 4 μm when the light was turned off (**Figure 1**). Restoration of the light to 400 μmol m^{-2} s^{-1} resulted in apertures returning to values close to those before the dark treatment. Exposure to 1 h high CO_2 (650 μmol mol^{-1}) decreased aperture by around 42%, returning to initial values when [CO_2] was returned to the original level of 120 μmol mol^{-1} (**Figure 1**). The magnitude of the changes in the stomatal aperture in response to changing light intensity was similar in both the intact leaf segments and the epidermal-mesophyll peeled and transplanted material, illustrating that removing the epidermis from *V. faba* and transplanting it onto exposed mesophyll of an equivalent leaf had little effect on the ability of stomata to function or any influence on a potential putative mesophyll signal (**Figure 1B**). Isolated epidermis responded to both changing light intensity and [CO_2] concentration, similar to the intact leaf segments (**Figure 1C**),

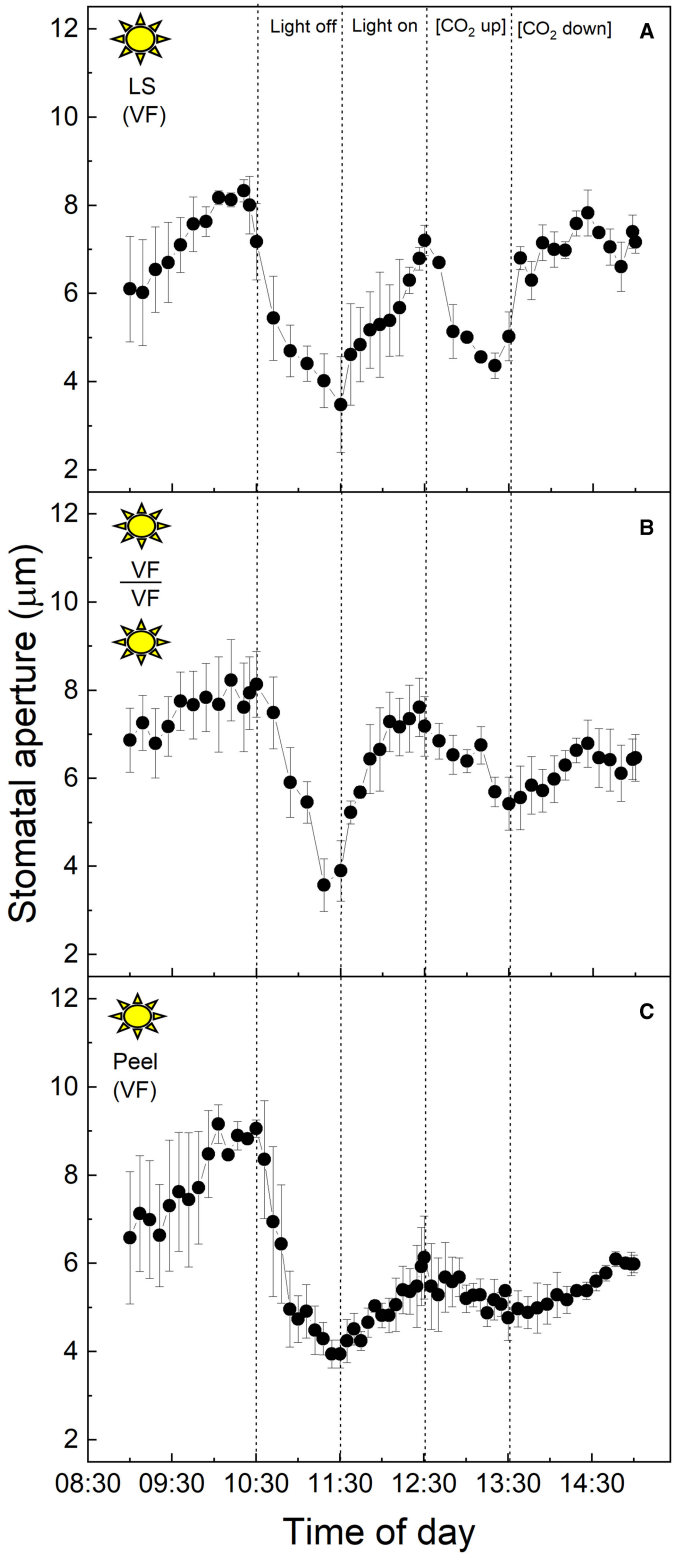

FIGURE 1 | (A) *Vicia faba* leaf segment; **(B)** Abaxial peeled epidermis of *Vicia faba* leaf on abaxial exposed mesophyll of *Vicia faba*, from the "light" growth chamber; **(C)** Abaxial isolated epidermis of *Vicia faba* leaf, from the "light" growth chamber (normal light period 8:00 a.m. to 8:00 p.m.). Light intensity was changed from photon flux density of 400 ± 10 μmol m^{-2} s^{-1} to darkness, as indicated, and [CO_2] was changed from 120 to 650 μmol mol^{-1}, as indicated. The temperature of the chamber was maintained at 23 ± 1°C. The values are means of four repetitions (± SE). The sun symbol represents plants taken from the light-grown chamber.

although the responses in the latter part of the experiment were dampened.

The equivalent experiment to that described above was performed using full CAM leaves of *K. fedtschenkoi* sampled from the "light" chamber (**Figure 2**). In this species, stomatal apertures increased by ∼40% upon dark treatment of the intact leaf segment (**Figure 2A**), or when the abaxial epidermis from one leaf was transplanted onto the mesophyll of a different, but equivalent leaf, and switched into darkness (**Figure 2B**). The aperture returned to the initial lower value of about 4 μm when the light was turned on again (**Figure 2B**). Increasing [CO_2] from 120 to 650 μmol mol^{-1} resulted in a slight decrease in the aperture in the epidermal-mesophyll transfer material in the light (**Figure 2B**), but the little stomatal movement was observed in the intact leaf segment (**Figure 2A**). As discussed above, stomata within leaf epidermal peels placed on exposed mesophyll showed similar responses to the intact leaf segment, supporting the conclusion that peeling the epidermis and transplanting it onto exposed mesophyll resulted in the expected stomatal responses for a CAM species, which were observed for the intact leaf segments (*cf.* **Figures 2A,B**). Interestingly, under these experimental conditions, stomata of the CAM species appeared to be less sensitive to changing [CO_2] as compared with their response to light intensity, and when compared with stomatal responses to [CO_2] in C_3 *V. faba* (**Figure 1**). Isolated epidermises again showed similar responses to both changing light intensity and [CO_2] concentration as an intact leaf segment, although the initial dark and low [CO_2] induced opening was dramatically more pronounced (**Figure 2C**).

To investigate the influence of CAM mesophyll tissue on epidermal peels from the C_3 species *V. faba*, isolated epidermises of the C_3 species were grafted onto the exposed mesophyll of CAM *K. fedtschenkoi* leaves, and *vice versa* (**Figure 3**). When C_3 *V. faba* epidermises were transplanted onto *K. fedtschenkoi* mesophyll, the *V. faba* stomata proceeded to close in response to "light off" and opened when the light was switched on again (**Figure 3A**). This was consistent with the result observed when *V. faba* epidermis was transplanted onto the exposed *V. faba* mesophyll of an equivalent leaf (**Figure 1B**). Stomata in epidermal peels from CAM leaves of *K. fedtschenkoi* exhibited a different behaviour when transplanted onto exposed C_3 mesophyll from *V. faba* (**Figure 3B**). Under these conditions, the *K. fedtschenkoi* CAM stomata closed in response to darkness, which was the opposite of the behaviour of CAM intact leaves, peels, or when CAM peels were placed on CAM mesophyll (**Figure 2**). When light intensity was increased, a strong increase in the aperture was observed, which was reduced under high [CO_2] (albeit less than in the C_3 responses in **Figure 1**), and, once again, aperture increased when [CO_2] was lowered (**Figure 3B**).

C_3 and CAM Stomatal Apertures in the Reverse Growth Chamber

All of the experiments outlined above were carried out using leaves from plants grown in the "light" chamber, lights came on at 8:00 a.m. and switched off at 8:00 p.m. As described above, CAM physiology is very different from that of C_3 plants, with stomata opening for atmospheric CO_2 uptake and primary fixation during the nocturnal phase of the diel cycle. Due to this, the next set of experiments were performed on plants entrained in a reverse phase "dark" growth chamber in which the 12-h dark period (8:00 a.m. to 8:00 p.m.) corresponded with the 12-h light period in the "light" chamber, and vice versa. The light period was from 8:00 p.m. to 8:00 a.m. in the "dark" chamber, when the normal chamber had 12-h dark (**Figures 4–6**).

Vicia faba C_3 stomata in the intact leaf segments showed the same behaviour as in the first experiment using the plants from the "light" chamber, although here aperture values were near zero at the start of the experiments, which was consistent with the dark conditions inside the growth chamber prior to the sampling of the leaves for the experiments (cf. **Figure 4A** with **Figure 1A**). Furthermore, the *V. faba* epidermal peel without mesophyll showed a similar response to the intact leaf fragment, with the exception of the start of the experiment, when the peels showed a high and stable conductance compared with the leaf segment, which initially had much lower apertures and increased with time in the light (**Figure 4A**). It was notable that the responses to light in the dark period samples were faster and of a greater magnitude (**Figure 4B**) when compared with the epidermal peels from plants entrained in the "light" chamber (**Figure 1C**).

At the start of the experiment, *K. fedtschenkoi* CAM stomata in the intact leaf segments from the "dark" cabinet showed some of the highest initial stomatal aperture values observed among the treatments (*ca.* 8 μm, **Figure 5A**). Stomata responded to the higher light intensity of the cuvette by closing, then opened slightly when the light was turned off, and subsequently closed during the latter part of the experiment when [CO_2] was altered. Surprisingly, no response to either light intensity or [CO_2] was observed in the dark sampled CAM epidermal peels from the "dark" chamber (**Figure 5B**).

When the epidermis was removed at the start of the dark period from plants grown in the "dark" growth conditions and placed on the mesophyll of plants grown in the "dark" conditions, stomata of the C_3 *V. faba* epidermis were placed onto *K. fedtschenkoi* exposed mesophyll performing CAM showed the same behaviour as stomata in C_3 intact leaves in the dark (**Figures 4A**, **6A**). In contrast, stomata in the CAM epidermis exposed to C_3 mesophyll from the "dark" chamber showed limited response to changes in light intensity (**Figure 6B**), unlike plants grown in the "light" cabinets (**Figure 3B**). A dampened, but typical C_3 CO_2 response was observed, with aperture decreasing slightly with increasing [CO_2] and opening when [CO_2] was lowered (**Figure 6B**), which was similar to the CO_2 response observed in the light-grown material (**Figure 3B**).

Finally, when the epidermis from CAM *K. fedtschenkoi* leaves grown in the "light" cabinet was placed on mesophyll from the "dark" cabinet and subjected to changes in light intensity and [CO_2], stomata showed the typical CAM response to light by increasing aperture in darkness and decreasing aperture when light intensity was increased (**Figure 7A**). In response to high [CO_2], stomata closed, although this response was not of the same magnitude as the response to light (**Figure 7A**). However, when the epidermis from dark sampled CAM leaves grown in the "dark" cabinet was placed on mesophyll from the "light"

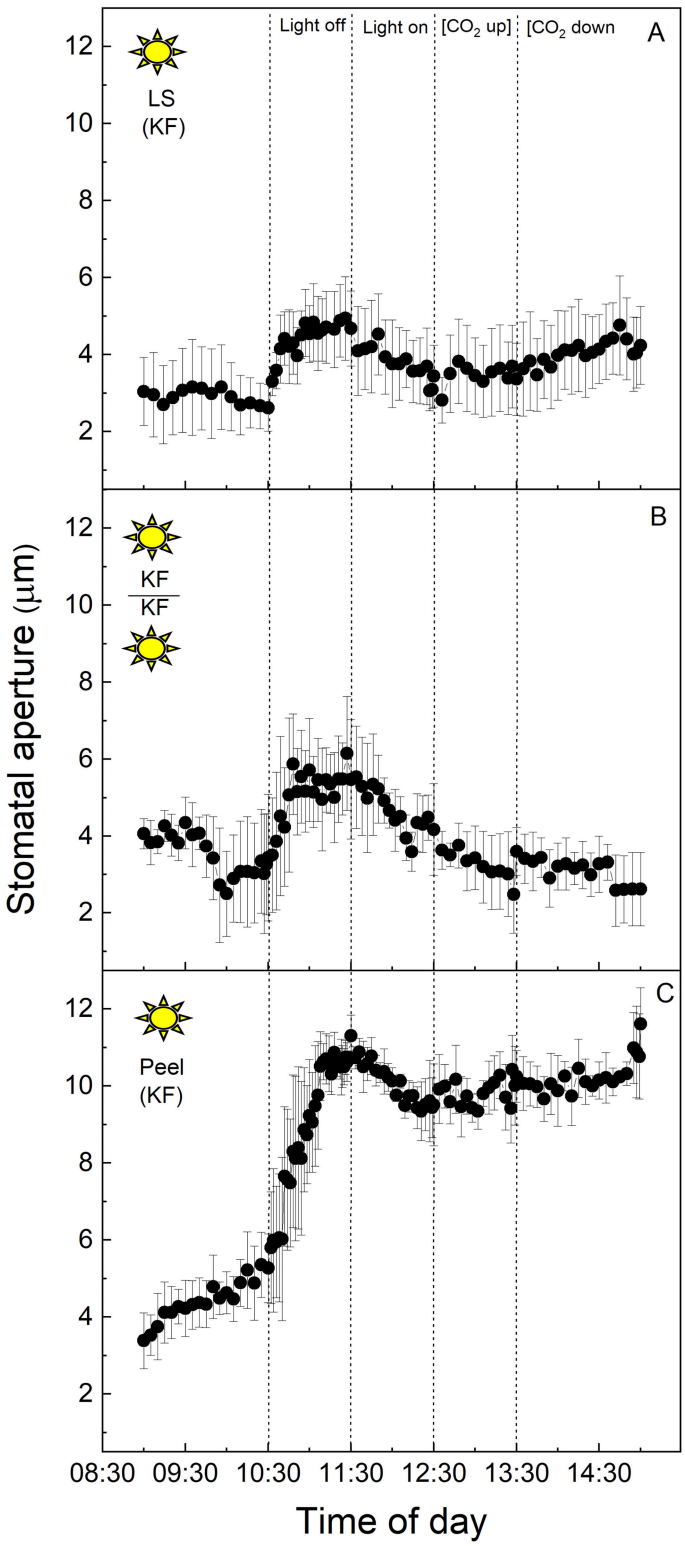

FIGURE 2 | (A) *Kalanchoë fedschenkoi* leaf segment; **(B)** Abaxial peeled epidermis of *Kalanchoë fedschenkoi* leaf on abaxial exposed mesophyll of *Kalanchoë fedschenkoi*, from the "light" growth chamber; **(C)** Abaxial isolated epidermis of *Kalanchoë fedschenkoi* leaf, from "light" growth chamber (light period 8:00 a.m. to 8:00 p.m.). Light intensity was changed from photon flux density of 400 ± 10 μmol m^{-2} s^{-1} to darkness, as indicated, and [CO_2] was changed from 120 to 650 μmol mol^{-1}, as indicated. The temperature of the chamber was maintained at 23 ± 1°C. The values are means of four repetitions (± SE). The sun symbol represents plants taken from the light-grown chamber.

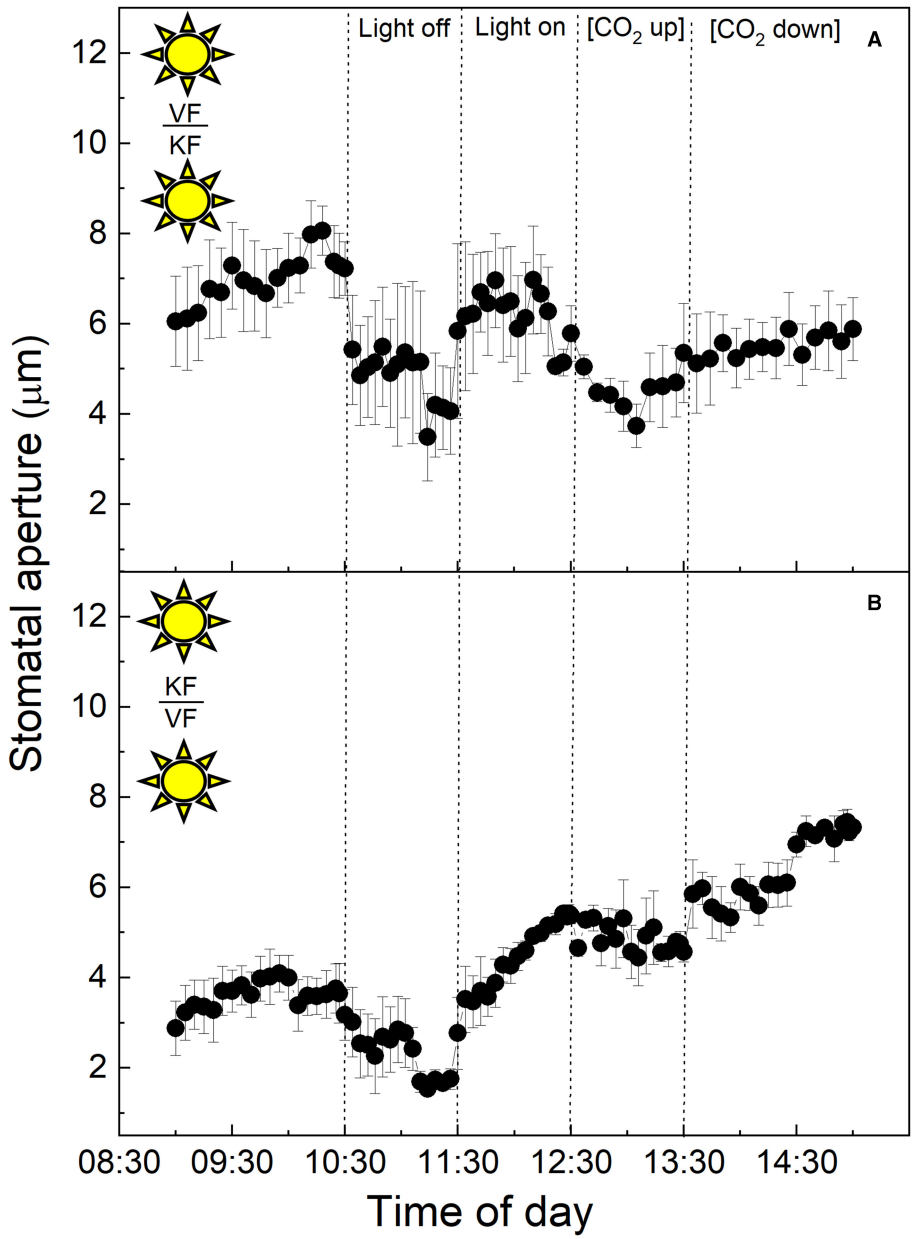

FIGURE 3 | (A) Abaxial peeled epidermis of *Vicia faba* leaf on abaxial exposed mesophyll of *Kalanchoë fedschenkoi* leaf from the "light" growth chamber; **(B)** Abaxial peeled epidermis of *Kalanchoë fedschenkoi* leaf on abaxial exposed mesophyll of *Vicia faba* leaf, from the "light" growth chamber (light period 8:00 a.m. to 8:00 p.m.). Light intensity was changed from photon flux density of 400 ± 10 μmol m^{-2} s^{-1} to darkness, as indicated, and [CO_2] was changed from 120 to 650 μmol mol^{-1}, as indicated. The temperature of the chamber was maintained at 23 ± 1°C. The values are means of four repetitions (± SE). The sun symbol represents plants taken from the light-grown chamber.

cabinet and subjected to the same light and CO_2 changes, stomata showed no response to light or changing [CO_2], with stomatal aperture maintained <4 μm (**Figure 7B**).

DISCUSSION

In this study, we compared stomatal responses and the influence of mesophyll on stomatal aperture in two species with different types of photosynthetic metabolism, namely *V. faba* (C_3) and *K. fedtschenkoi* (CAM). We showed that stomata from isolated peels (in which the influence of mesophyll had been removed) behaved in a similar manner (although sometimes with different magnitudes for response) to both intact leaf segments and epidermal transfers, with exception of those from the CAM "dark" chamber (**Figure 5B**). Stomatal responses observed in the C_3 *V. faba* samples were as expected (Olsen et al., 2002; Fujita et al., 2013), with a characteristic opening in response to increasing light intensity, closure in response to dark, and

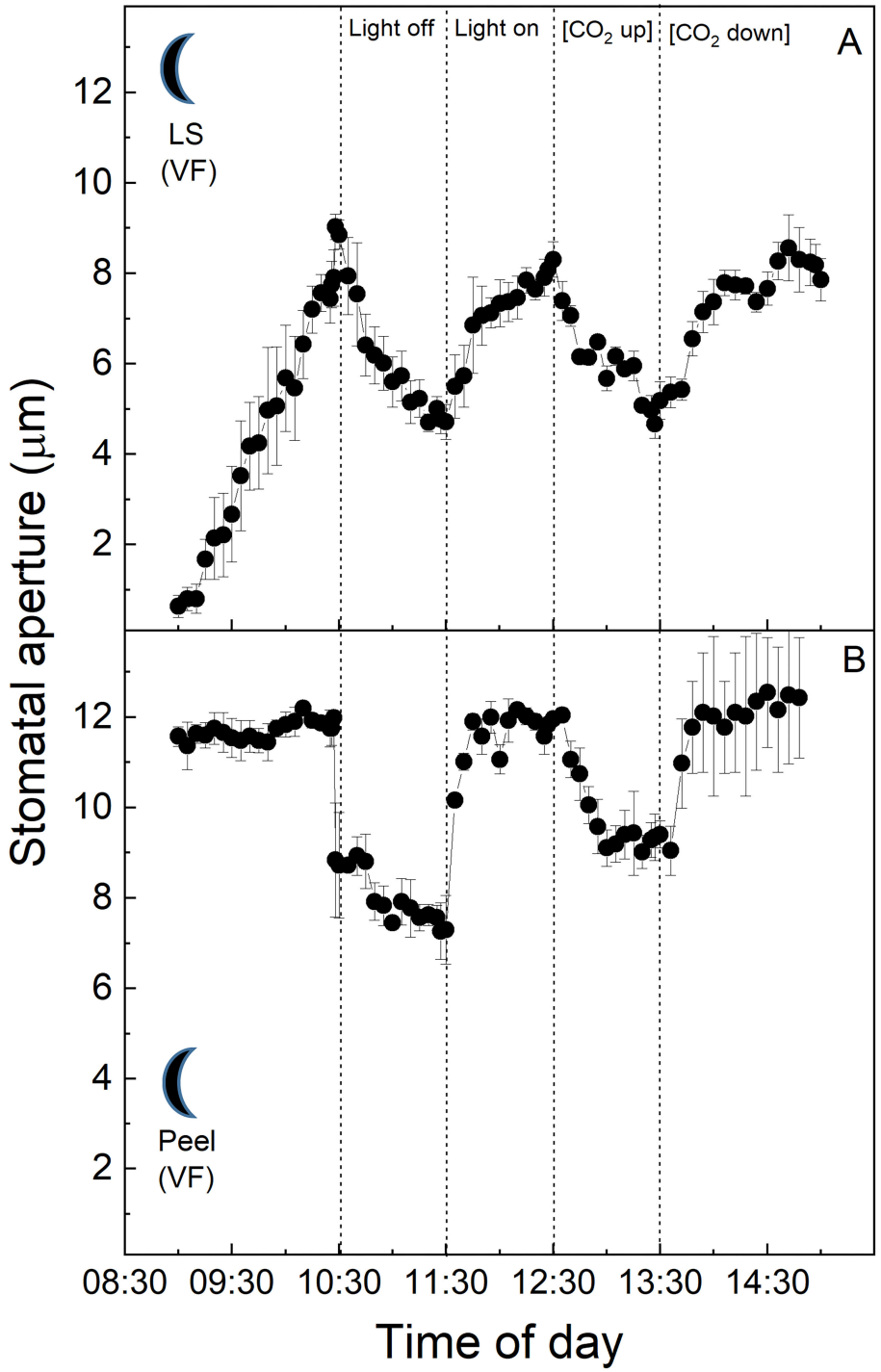

FIGURE 4 | (A) *Vicia faba* leaf fragment from the "dark" cabinet.; **(B)** Abaxial isolated epidermis of *Vicia faba* leaf from the "dark" growth chamber (reverse light period 8:00 p.m. to 8:00 a.m.). Light intensity was changed from photon flux density of 400 ± 10 μmol m^{-2} s^{-1} to darkness, as indicated, and [CO_2] was changed from 120 to 650 μmol mol^{-1}, as indicated. The temperature of the chamber was maintained at 23 ± 1°C. The values are means of four repetitions (± SE). The moon symbol represents plants taken from the dark-grown chamber.

closure at high [CO_2] (Lawson and Blatt, 2014). In contrast, the stomatal aperture in the CAM leaf sections/peels sampled in the light, as well as intact leaf segments sampled in the dark, increased in response to darkness (**Figures 2**, **5A**), although it was noteworthy that dark sampled *K. fedtschenkoi* epidermal peels did not respond to changes in light or [CO_2] (**Figure 5B**).

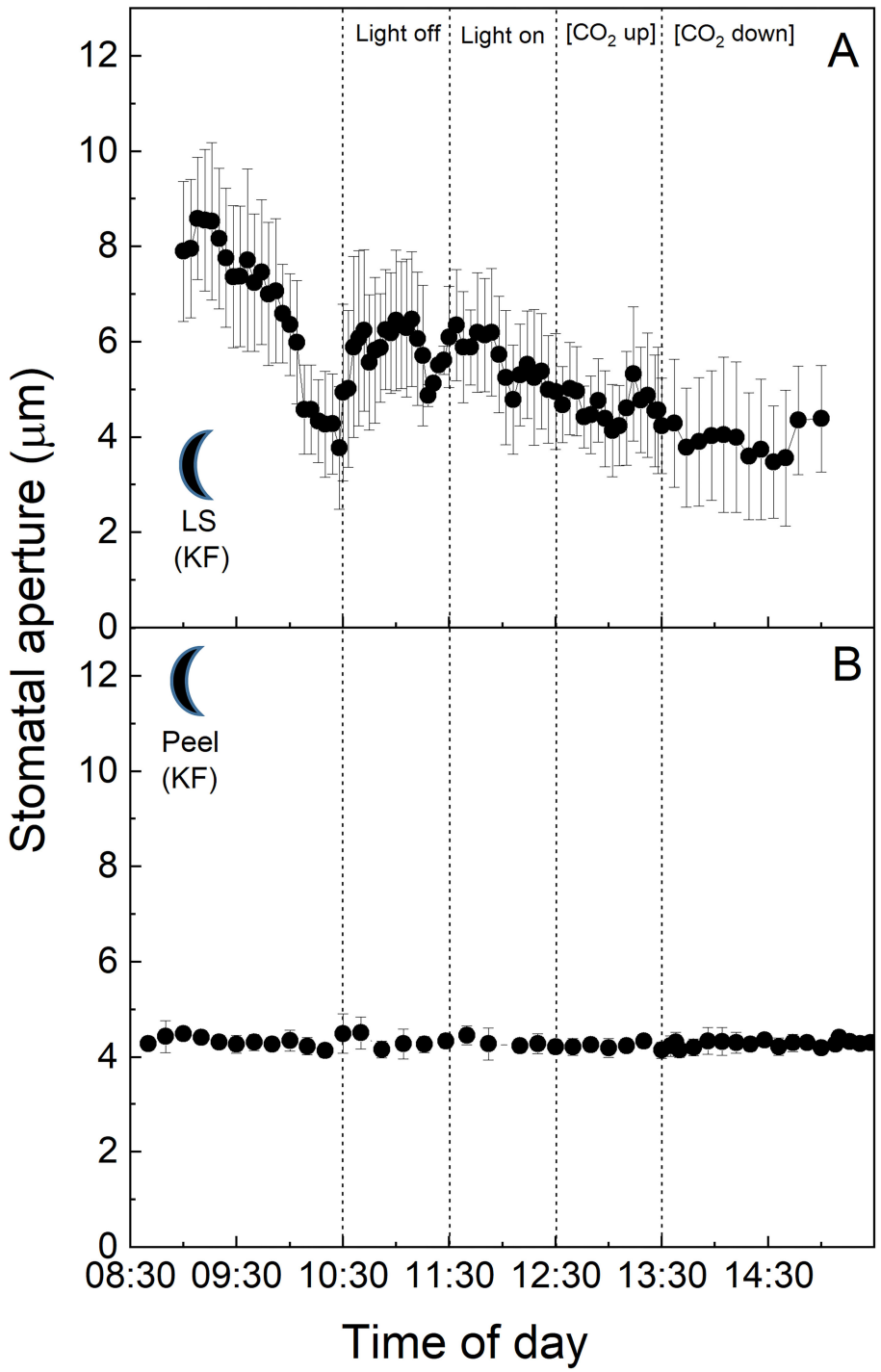

FIGURE 5 | (A) *Kalanchoë fedschenkoi* leaf segment from the "dark" growth chamber; **(B)** Abaxial isolated epidermis of *Kalanchoë fedschenkoi* leaf, from the "dark" growth chamber (light period 8:00 p.m. to 8:00 a.m.). Light intensity was changed from photon flux density of 400 ± 10 μmol m^{-2} s^{-1} to darkness, as indicated, and [CO_2] was changed from 120 to 650 μmol mol^{-1}, as indicated. The temperature of the chamber was maintained at 23 ± 1°C. The values are means of four repetitions (± SE). The moon symbol represents plants taken from the dark-grown chamber.

To date, we are unaware of any previous studies that reported stomatal opening as a direct response to darkness in CAM plants, and the fact that this could be observed in isolated peels from CAM leaves sampled in the light (**Figure 2C**) suggested that light intensity is perceived by the guard cells themselves. Although it was well established that CAM plants open stomata in the

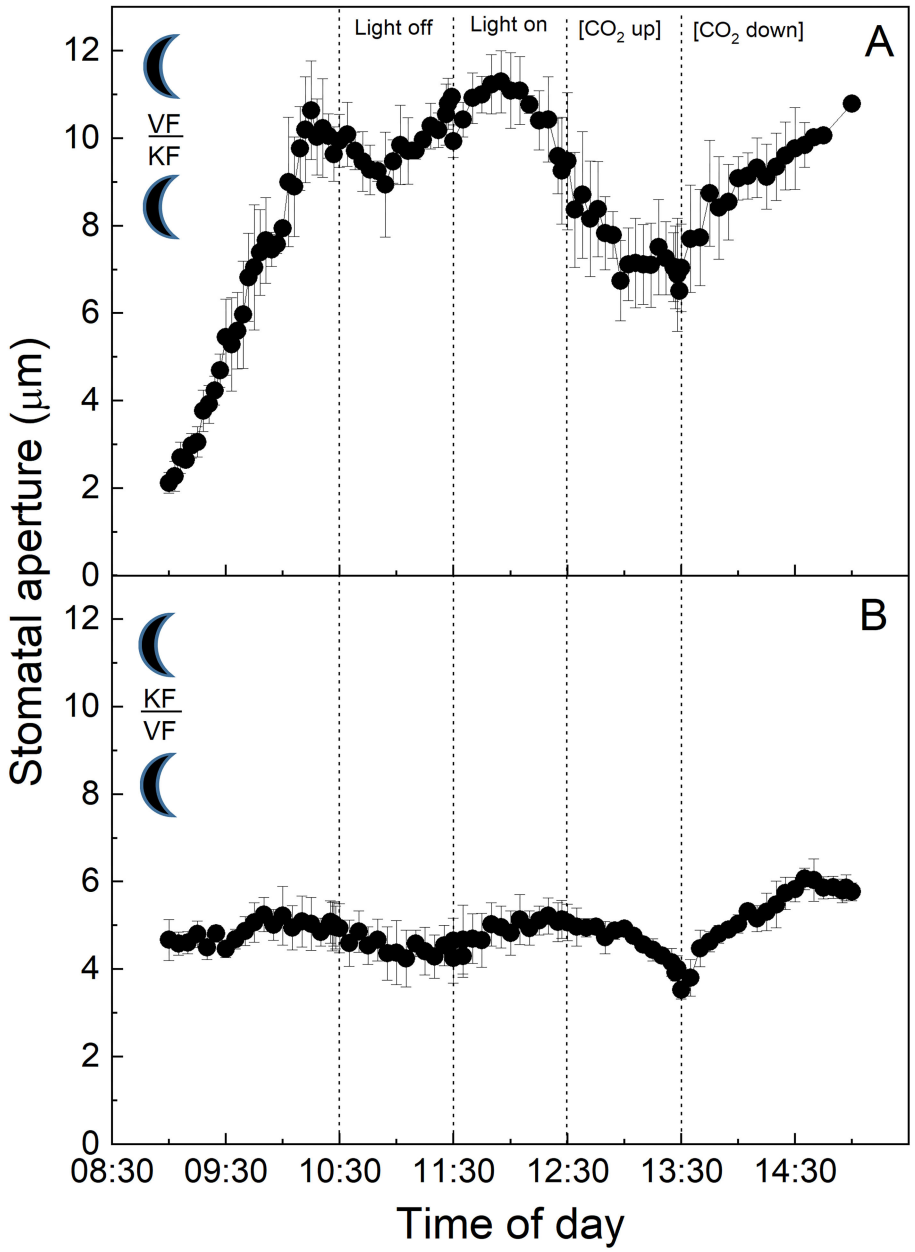

FIGURE 6 | (A) Abaxial peeled epidermis of *Vicia faba* leaf on abaxial exposed mesophyll of *Kalanchoë fedschenkoi* leaf both from the "dark" growth chamber; **(B)** Abaxial peeled epidermis of *Kalanchoë fedschenkoi* leaf on abaxial exposed mesophyll of *Vicia faba* leaf from the "dark" growth chamber (reverse light period 8:00 p.m. to 8:00 a.m.). Light intensity was changed from photon flux density of 400 μmol m^{-2} s^{-1} to darkness, as indicated, and [CO_2] was changed from 120 to 650 μmol mol^{-1}, as indicated. The temperature of the chamber was maintained at 23°C. The values are means of four repetitions (± SE). The moon symbol represents plants taken from the dark-grown chamber.

dark period (Cockburn, 1983), this has been associated with the reduction in C_i when PPC activity in the mesophyll increases at dusk (Wyka et al., 2005; Griffiths et al., 2007; von Caemmerer and Griffiths, 2009). Similarly, stomatal closure during the light period was thought to be driven by the generation of internal CO_2 (increased C_i) due to the decarboxylation of stored malic acid (Cockburn et al., 1979; Spalding et al., 1979). The above theoretical framework for understanding the physiological responses of stomata in CAM species implied that a mesophyll signal (including C_i) was required for stomatal responses to changes in light and [CO_2], which was not fully supported by our findings.

Specifically, the findings presented here suggest the presence of additional autonomous guard cell behaviour

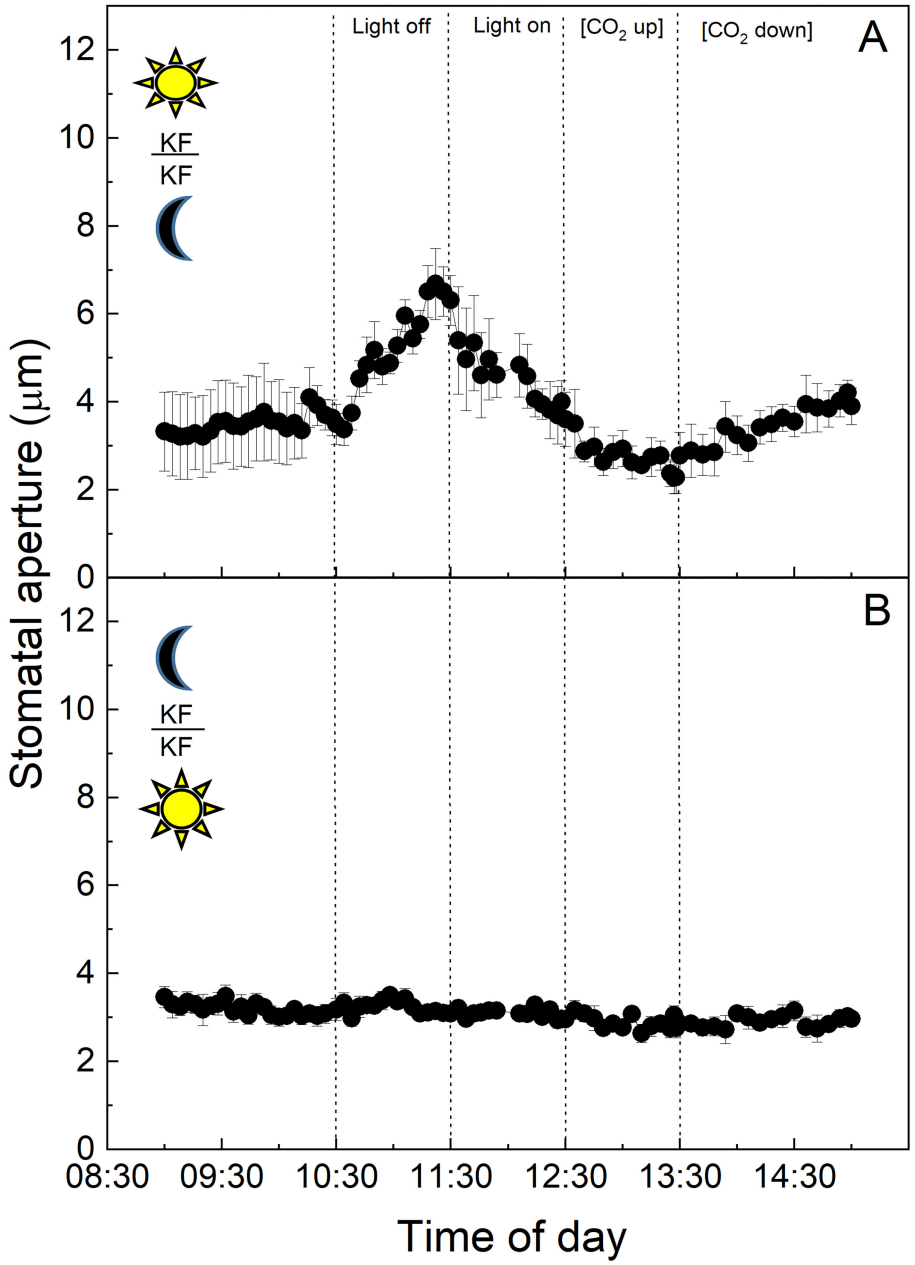

FIGURE 7 | (A) Abaxial peeled epidermis of *Kalanchoë fedschenkoi* leaf from the "light" growth chamber, on abaxial exposed mesophyll of *Kalanchoë fedschenkoi* leaf, from the "dark" growth chamber; **(B)** Abaxial peeled epidermis of *Kalanchoë fedschenkoi* leaf from the "dark" growth chamber, on abaxial exposed mesophyll of *Kalanchoë fedschenkoi* leaf from the "light" growth chamber (light period 8:00 a.m. to 8:00 p.m.), and from the "dark" growth chamber (reverse light period 8:00 p.m. to 8:00 a.m.). Light intensity was changed from photon flux density of 400 ± 1 0 μmol m^{-2} s^{-1} to darkness, as indicated, and [CO_2] was changed from 120 to 650 μmol mol^{-1}, as indicated. The temperature of the chamber was maintained at 23 ± 1°C. The values are means of four repetitions (± SE). The sun symbol represents plants taken from the light-grown chamber and the moon symbol represents plants taken from the dark-grown chamber.

in the guard cell pairs of CAM leaves of *K. fedtschenkoi*. However, this can be overridden by the presence of C_3 mesophyll (**Figure 3B**), indicating that stomatal behaviour in CAM plants can be influenced by a signal transmitted from the mesophyll in stomatal responses to light intensity, as has been proposed for C_3 and C_4 plants (Shimazaki et al., 2007).

Stomatal Responses to Changes in Light Intensity

In C_3 and C_4 plants, stomatal responses to light are divided into two categories (Matthews et al., 2020). The first is the red light or photosynthetic response, which is dependent on mesophyll and/or guard cell chloroplasts (Mott et al., 2008; Suetsugu et al., 2014), and is often closely associated with

stomatal responses to C_i as described above (although other signals have been suggested; see Lawson et al., 2014, 2018). The second is the blue light (BL) response. This is independent of photosynthesis and the result of a signalling cascade that starts with the perception of low fluence rates of BL in the guard cells by phototropin (Kinoshita et al., 2001, 2003; Inoue et al., 2008) which triggers the action of the plasmalemma H^+-ATPase pumps, resulting in hyperpolarization of the plasma membrane and stomatal opening. Interestingly a recent study has shown that guard cell H^+ -ATPase pumps were also activated by red light and their action correlates with the stomatal opening. However, DCMU abolished this response indicating that a photosynthetic factor in the mesophyll was also required (Ando and Kinoshita, 2018). A subsequent study confirmed red light-driven stomatal opening in epidermal peels of *Commelina communis*, although mesophyll involvement was not essential. However, the presence of mesophyll tissue accelerated stomatal opening (Fujita et al., 2019). The stomatal BL response is species-specific (Vialet-Chabrand et al., 2021), and has been reported to be absent in the facultative CAM species *Mesembryanthemum crystallinum* when the plant shifts from C_3 metabolism to CAM (Tallman et al., 1997). In contrast to this, a recent study reported BL-dependent stomatal opening in the obligate CAM plants *K. pinnata* and *K. daigremontiana,* and that BL-induced opening was not linked to CO_2 assimilation (Gotoh et al., 2019). Since our study was conducted using white light on peels, our findings could support CAM guard cell perception of blue (or red) light in *K. fedtschenkoi* leading to a change in aperture (in a different direction to C_3 and depending on whether the CAM leaf was sampled from the light or dark period). Even more intriguing was the fact that *V. faba* C_3 mesophyll overrode the stomatal response of the *K. fedtschenkoi* CAM epidermis sampled in the light. This finding supported the proposal that a mesophyll-derived signal can dominate over a guard cell signal resulting in stomata in CAM peels behaving as C_3 in response to light (**Figure 3B**). Interestingly, CAM mesophyll was unable to override the C_3 stomatal response in peels from *V. faba* (**Figure 3A**).

The Influence of Mesophyll on Stomatal Responses

Several studies in C_3 species have shown that a mesophyll signal other than $[CO_2]$ is required to drive stomatal responses (Mott et al., 2008; Fujita et al., 2013, 2019), and the same may also be true for CAM stomata. Isolated C_3 epidermal peels responded to changing light intensity and $[CO_2]$, at a slower and reduced magnitude of response (**Figure 1C**) supporting the involvement of a mesophyll signal (Mott et al., 2008), but indicated that this is not essential. Other studies have shown that the speed of stomatal responses to light in peels also depends on epidermal turgor pressures (as shown in Zeiger et al., 1987 and references therein). The nature of a mesophyll signal remains unclear, some studies have suggested that guard cell chloroplastic photosynthetic electron transport is involved in C_3 stomatal behaviour (Olsen et al., 2002; Lawson et al., 2002, 2003; Lawson, 2009), while others suggested a vapour ion (Mott et al., 2014) or aqueous signal (Fujita et al., 2013).

The study of Mott et al. (2008) reported no stomatal responses to light and $[CO_2]$ in epidermal peels from *Vicia, Tradescantia,* or *Pisum*. However, they also showed that stomatal responses were restored in *Tradescantia* and *Pisum,* but not *Vicia,* when the peels were grafted back onto the underlying mesophyll. The authors used these data to suggest that the mesophyll is responsible for detecting changes in light and $[CO_2]$ and a mesophyll-driven signal coordinates changes in stomatal aperture. These findings did not entirely agree with our data since we demonstrated a stomatal response in both *Vicia* epidermal peels with and without the mesophyll, although the stomatal response to $[CO_2]$ was greatly dampened in some peel experiments, suggesting that a mesophyll signal plays a role in the CO_2 response. A major difference between our experiments and those conducted by Mott et al. (2008) was their use of a 12-h incubation time of epidermal peel samples before use, which may have altered any stored carbohydrates, e.g., starch, within the guard cells, and/or lead to greater stomatal apertures in peels due to hydro-passive effects both of which could have influenced stomatal behaviour. The study of McAdam and Brodribb (2012), using a similar xenografting approach to ours demonstrated that stomata responded to increasing light intensity in isolated peels of angiosperms but closure to decreasing light was not observed and only restored when they were placed back onto their own mesophyll or the mesophyll from ferns. Although our data for the isolated epidermises of *V. faba* illustrated stomata closing in response to decreasing light, the response to increasing light and $[CO_2]$ after this closure were somewhat dampened. The lower ambient $[CO_2]$ used in our experiment could explain some of the differences between our experiments and those of McAdam and Brodribb (2012).

In this study, we had shown that CAM stomatal responses to changing $[CO_2]$ (particularly in material with attached *K. fedtschenkoi* mesophyll) were somewhat dampened compared with the C_3 response in *V. faba* (**Figures 1**, **2**), and whether the plant was sampled from the dark period or the light period prior to measurements did not influence the responses (**Figures 4**, **5**). The fact that these measurements were performed under illumination and stomata responded to changes in light intensity may suggest that light signals override other signals including those driven by changing $[CO_2]$ (Lawson et al., 2010). However, when CAM epidermal peels were placed on C_3 mesophyll (from either light or dark chamber) stomata opened in response to a decrease $[CO_2]$ (**Figures 3B**, **6B**). The greater sensitivity to $[CO_2]$ of CAM stomata when grafted onto C_3 mesophyll could be explained by an enhanced CO_2 draw-down from C_3 metabolism, which for *V faba* has photosynthetic rates of around 20 $\mu mol\ m^{-2}\ s^{-1}$ (e.g., Lawson and Blatt, 2014), which was generally greater than *K. fedtschenkoi* which has been reported to be somewhere between 5 and 8 $\mu mol\ m^{-2}\ s^{-1}$ (e.g., Boxall et al., 2020; Ceusters et al., 2021). These findings could also suggest that signals in the CAM mesophyll are *preventing* stomatal opening supporting a role for mesophyll signals as well as C_i in stomatal responses. Several studies

support the suggestion, that C_i is not the only and major signal to which CAM stomata respond and that other signals must be involved (von Caemmerer and Griffiths, 2009 Males and Griffiths, 2017).

Stomatal Aperture Responses Using Leaves Sampled From the Dark seriod

Crassulacean acid metabolism has a completely different diel pattern of gas exchange physiology and associated mesophyll metabolism in comparison with C_3 plants, plus both the circadian clock, along with malic acid content stored in the mesophyll vacuole, are believed to play important roles in CAM stomatal responses (Wilkins, 1991; Nimmo, 2000; Dodd et al., 2002; Borland et al., 2006; Hartwell, 2006). Due to this distinctive temporal regulation of stomatal physiology associated with CAM, we also repeated the epidermal peel transfer experiments using plants in which the lighting regime had been swapped and grown under a "dark" regime and sampled at the start of the dark period (**Figures 4**–**7**). When grown in the "dark" growth chamber, stomata on leaf segments from C_3 *V. faba* plants showed little difference in their responses compared with the "light" conditions (**Figures 1**, **4**). However, stomatal responses in the isolated epidermis from the "dark" grown plants showed much more rapid responses compared with the whole leaf segment of plants sampled from the "light" regime (**Figure 4B**). It is noteworthy that maximum stomatal aperture was initially observed in *V. faba* peels from the dark material, which might be due to pre-dawn stomatal opening, or due to biological or technical differences when sampling dark material. Surprisingly stomata in CAM epidermal peels from the "dark" chamber (**Figure 5B**) were unresponsive to both light and [CO_2] and this response was not restored by placing the epidermal peels onto CAM mesophyll from the light period (**Figure 7B**). Stomata in C_3 *V. faba* peels sampled in the dark period and placed onto dark sampled *K. fedtschenkoi* CAM mesophyll (**Figure 6A**), showed a typical C_3 type stomatal response, with relatively large magnitudes of change. The second and third light switch events showed some deviation from the expected results with stomata starting to open even though the light was off, and this is most likely due to lags in stomatal behaviour (Lawson and Matthews, 2020) and/or sluggish stomatal responses in peels that have been reported previously (Lee and Bowling, 1992; Roelfsema et al., 2002). These findings could also indicate a slow CAM mesophyll response. When CAM *K. fedtschenkoi* epidermises sampled from the dark were placed on C_3 *V. faba* mesophyll from the dark period, the stomatal aperture showed very little response to changing light intensity and remained at a steady aperture (**Figure 6B**). However, a typical, although small, C_3 type response was observed with changing [CO_2]. These data and those from the other experiments presented indicated strongly that stomatal responses to [CO_2] are influenced by the presence of the mesophyll.

These findings could be explained solely by changes in C_i, as light would trigger activation of Calvin cycle enzymes in C_3 which would drive the mesophyll consumption of CO_2, reducing C_i, which should have elicited changes in stomatal aperture during light-dark transitions (Roelfsema et al., 2002) which were not observed. It is worth noting that, unlike leaves from the "light" growth chamber (**Figure 3B**), C_3 mesophyll from plants grown in the "dark" chamber was unable to drive a stomatal response to light (**Figure 6B**). This provided strong support for the proposal that in the plants from the "dark" chamber, there was a factor missing from either the guard cells themselves, or such a factor needs to be provided from the CAM "dark" mesophyll and is essential for light-driven stomatal behaviour.

To further investigate the influence of the CAM mesophyll/photosynthetic signals on stomatal responses, we conducted a reciprocal epidermal peel transfer experiment in which epidermis from *K. fedtschenkoi* grown in the "light" chamber was placed on CAM mesophyll from plants in the "dark" chamber, and vice versa (**Figure 7**). In the first part of this experiment, stomata in epidermal peels from the light transplanted onto exposed mesophyll from the dark displaying a typical CAM response (*cf.* **Figures 2**, **7**) to light although the CO_2 response was dampened. However, when *K. fedtschenkoi* CAM leaf epidermal peels from the dark period were transplanted onto the CAM mesophyll from the "light" cabinet, no stomatal responses to light or [CO_2] were observed (**Figure 7B**). Under the first conditions, the *K. fedtschenkoi* mesophyll had just experienced a 12-h dark period and would therefore be transitioning through Phases II and III of CAM, producing internal CO_2 through decarboxylation of stored malate, which could explain the lack of a stomatal response. However, this was not the case when dark period *V. faba* epidermal peels were placed on dark period CAM mesophyll (**Figure 6A**), suggesting that C_3 *V. faba* guard cells in the dark period were not influenced by the *K. fedtschenkoi* CAM mesophyll that they were transplanted onto.

Our findings suggested both a direct mesophyll influence and a guard cell-specific response, depending on the growth environment. The guard cell-specific component was demonstrated for CAM peels sampled from the light period, which responded to light, whereas the lack of any stomatal response in epidermal peels taken from CAM leaves of *K. fedtschenkoi* plants sampled in the dark (**Figures 5B**, **7B**) has supported the requirement for a mesophyll signal, as demonstrated for the intact leaf segment (**Figure 5A**). Furthermore, the fact *K. fedtschenkoi* peels from the "light" chamber grown plants were able to respond to both light off and the light was switched back on (**Figure 2C**), suggesting that the light period *K. fedtschenkoi* guard cells had the required stores and/or metabolites and other regulatory/signalling components required for guard cell osmoregulation and that these might be lacking in guard cells sampled from the "dark"'chamber plants (see Lawson et al., 2014, 2018).

Under the conditions of the present study, a logical hypothesis was that stomata would be less responsive, particularly to changes in light intensity, due to the fact that CAM leaves sampled from the "light" growth chamber would possess high levels of malic acid, Furthermore, we hypothesised that leaves

sampled from the "dark" growth chamber would open stomata more readily due to the low malic acid content early in the dark period when the experiments were started. However, our findings demonstrated that the mechanism is not as simple as this, as CAM mesophyll sampled from both the light and the dark period stimulated stomatal responses in C_3 and CAM peels sampled from the light period. Conversely, stomata in *K. fedtschenkoi* epidermal peels from the dark period had no response, supporting the conclusion that both stored products in guard cells and signals from mesophyll cells influence stomatal responses.

In summary, we concluded that guard cells can respond independently of the mesophyll, but this was greatly dampened when underlying mesophyll signals were removed. These results further highlighted the importance of the mesophyll for both the rapidity and the magnitude of the observed stomatal aperture responses. Furthermore, we had demonstrated that mesophyll signals could alter the typical CAM stomatal response, with C_3 *V. faba* mesophyll tissue able to stimulate the stomata in *K. fedtschenkoi* epidermal peels from CAM leaves sampled in the light growth chamber to behave like those of a C_3 plant (**Figure 3B**). Therefore, both mesophyll and guard cell metabolism and/or cell signalling machinery contributed to stomatal responses. Additionally, mesophyll influences were not solely through changes in C_i (although these clearly play an important role) but also through some other unknown signal.

DATA AVAILABILITY STATEMENT

The raw data supporting the conclusions of this article will be made available by the authors, without undue reservation.

AUTHOR CONTRIBUTIONS

MS, AB, JH, and TL discussed and plan the work. MS, PD, and TH conducted the experiments. MS carried out the data analysis, created the figures, and drafted the initial manuscript. MS, TL, JH, and TH wrote the manuscript. All authors commented, made corrections, and approved the submitted version.

ACKNOWLEDGMENTS

MS is grateful to Conselho Nacional de Desenvolvimento Científico e Tecnológico (CNPq) for a fellowship (Proc. 239228/2012-0). TL would like to acknowledge BBSRC for funding through the BBSRC IWYP programme (BB/S005080/1) and the Global Challenges Research Fund as part of TIGR2ESS: Transforming India's Green Revolution by Research and Empowerment for Sustainable food supplies (BB/P027970/1). JH and AB were supported by the U.S. Department of Energy (DOE) Office of Science, Genomic Science Program under Award Number DE-SC0008834, and JH was also supported in part by the Biotechnology and Biological Sciences Research Council, U.K. (BBSRC grant no. BB/F009313/1). The contents of this article are solely the responsibility of the authors and do not necessarily represent the official views of the DOE.

SUPPLEMENTARY MATERIAL

The Supplementary Material for this article can be found online at: https://www.frontiersin.org/articles/10.3389/fpls.2021.740534/full#supplementary-material

Supplementary Figure 1 | Photograph of the microscope system along with leaf section chambers.

Supplementary Figure 2 | Examples of images taken using the microscopy system. Image of stoma taken from intact leaf segments from **(A)** *Kalanchoë fedtschenkoi* **(B)** *Vicia faba*, and from epidermal peels of **(C)** *Kalanchoë fedtschenkoi* and **(D)** *Vicia faba*. All scale bars represent 10 mm.

Supplementary Figure 3 | Changes in titratable acidity of *Vicia faba* (C_3) and *Kalanchoë fedschenkoi* (CAM) grown in a "light" growth chamber (light period 8:00 a.m. to 8:00 p.m.) and in reverse time "dark" cabinet (light period 8:00 p.m. to 8:00 a.m.) for local time. All other variables were the same in both chambers: light intensity of 390 μmol m^{-2} s^{-1}, the temperature of 18°C (night) and 25°C (day), and air humidity of 60%. The dawn moment was 7:30 a.m. and dusk was 7:30 p.m. The values are means of three repetitions (± SE). Means followed by different letters denote differences among treatments ($P < 0.005$).

REFERENCES

Ando, E., and Kinoshita, T. (2018). Red light-induced phosphorylation of plasma membrane H+-ATPase in stomatal guard cells. *Plant Physiol.* 178, 838–849. doi: 10.1104/pp.18.00544

Borland, A., Elliott, S., Patterson, S., Taybi, T., Cushman, J., Pater, B., et al. (2006). Are the metabolic components of crassulacean acid metabolism up-regulated in response to an increase in oxidative burden? *J. Exp. Bot.* 57, 319–328. doi: 10.1093/jxb/erj028

Borland, A., Hartwell, J., Jenkins, G., Wilkins, M., and Nimmo, H. (1999). Metabolite control overrides circadian regulation of phosphoenolpyruvate carboxylase kinase and CO2 fixation in crassulacean acid metabolism. *Plant Physiol.* 121, 889–896. doi: 10.1104/pp.121.3.889

Borland, A. M., Griffiths, H. G., Hartwell, J., and Smith, J. A. C. (2009). Exploiting the potential of plants with Crassulacean acid metabolism for bioenergy production on marginal lands. *J. Exp. Bot.* 60, 2879–2896. doi: 10.1093/jxb/erp118

Borland, A. M., Técsi, L. I., Leegood, R. C., and Walker, R. P. (1998). Inducibility of crassulacean acid metabolism (CAM) in Clusia species; physiological/biochemical characterisation and intercellular localization of carboxylation and decarboxylation processes in three species which exhibit diferent degrees of CAM. *Planta* 205, 342–351. doi: 10.1007/s004250050329

Boxall, S. F., Dever, L. V., Kneřřov,á J., Gould, P. D., and Hartwell, J. (2017). Phosphorylation of phosphoenolpyruvate carboxylase is essential for maximal and sustained dark CO2 fixation and core circadian clock operation in the obligate crassulacean acid metabolism species kalanchoë fedtschenkoi. *Plant Cell* 29, 2519–2536. doi: 10.1105/tpc.17.00301

Boxall, S. F., Foster, J. M., Bohnert, H. J., Cushman, J. C., Nimmo, H. G., and Hartwell, J. (2005). Conservation and divergence of circadian clock operation in a stress-inducible Crassulacean acid metabolism species reveals clock compensation against stress. *Plant Physiol.* 137, 969–982. doi: 10.1104/pp.104.054577

Boxall, S. F., Kadu, N., Dever, L. V., Kneřová, J., Waller, J. L., Gould, P. D., et al. (2020). Kalanchoë PPC1 is essential for crassulacean acid metabolism and the regulation of core circadian clock and guard cell signaling genes. *Plant Cell* 32, 1136–1160. doi: 10.1105/tpc.19.00481

Buckley, T. N., Mott, K. A., and Farquhar, G. D. (2003). A hydromechanical and biochemical model of stomatal. *Plant Cell Environ*. 26, 1767–1785. doi: 10.1046/j.1365-3040.2003.01094.x

Ceusters, N., Ceusters, J., Hurtado-Castano, N., Dever, L. V., Boxall, S. F., Kneřová, J., et al. (2021). Phosphorolytic degradation of leaf starch via plastidic α-glucan phosphorylase leads to optimized plant growth and water use efficiency over the diel phases of Crassulacean acid metabolism, Journal of Experimental *Botany* 72, 4419–4434. doi: 10.1093/jxb/erab132

Cockburn, W. (1983). Stomatal mechanism as the basis of the evolution of CAM and C4 photosynthesis. *Plant Cell Environ*. 6, 275–279. doi: 10.1111/1365-3040.ep11611925

Cockburn, W., Ting,. I. P., and Sternberg, L. O. (1979). Relationships between stomatal behavior and internal carbon dioxide concentration in crassulacean acid metabolism plants. *Plant Physiol*. 63, 1029–1032 doi: 10.1104/pp.63.6.1029

Dever, L. V., Boxall, S. F., Kneřová, J., and Hartwell, J. (2015). Transgenic perturbation of the decarboxylation phase of crassulacean acid metabolism alters physiology and metabolism but has only a small effect on growth. *Plant Physiol*. 167, 44–59. doi: 10.1104/pp.114.251827

Dodd, A. N., Borland, A. M., Haslam, R. P., Griffiths, H., and Maxwell, K. (2002). Crassulacean acid metabolism: plastic, fantastic. *J. Exp. Bot.* 53, 569–580. doi: 10.1093/jexbot/53.369.569

Farquhar, D. G., and Sharkey, T. D. (1982). Stomatal conductance and photosynthesis. *Annu. Rev. Plant Physiol.* 33, 317–345. doi: 10.1146/annurev.pp.33.060182.001533

Farquhar, G. D., Dubbe, D. R., and Raschke, K. (1978). Gain of the feedback loop involving carbon dioxide and stomata. *Theory Measure. Plant Physiol*. 62, 406–412. doi: 10.1104/pp.62.3.406

Farquhar, G. D., and Wong, S. C. (1984). An empirical model of stomatal conductance. *Aust. J. Plant Physiol*. 11, 191–210. doi: 10.1071/PP9840191

Fujita, T., Noguchi, K., Ozaki, H., and Terashima, I. (2019). Confirmation of mesophyll signals controlling stomatal responses by a newly devised transplanting method. *Funct. Plant Biol*. 46, 467–481. doi: 10.1071/FP18250

Fujita, T., Noguchi, K., and Terashima, I. (2013). Apoplastic mesophyll signals induce rapid stomatal responses to CO2 in Commelina communis. *New Phytol*. 2, 395–406. doi: 10.1111/nph.12261

Gotoh, E., Oiwamoto, K., Inoue, S. I., Shimazaki, K. I., and Doi, M. (2019). Stomatal response to blue light in crassulacean acid metabolism plants Kalanchoe pinnata and Kalanchoe daigremontiana. *J. Exp. Bot*. 70, 1367–1374. doi: 10.1093/jxb/ery450

Grantz, D. A., and Schwartz, A. (1988). Guard cells of *Commelina communis* L. do not respond metabolically to osmotic stress in isolated epidermis: implications for stomatal responses to drought and humidity. *Planta* 174, 166–173 doi: 10.1007/BF00394768

Griffiths, H., Cousins, A., Badger, M., and von Caemmerer, S. (2007). Discrimination in the dark: resolving the interplay between metabolic and physical constraints to PEPC activity during the CAM cycle. *Plant Physiol*. 147, 1055–1067. doi: 10.1104/pp.106.088302

Hartwell, J. (2006). "The circadian clock in CAM plants," in *Endogenous Plant Rhythms*, eds A. J. W. Hall and H. G. McWatters (Oxford: Blackwell Publishing), 211–236. doi: 10.1002/9780470988527.ch9

Hartwell, J., Dever, L. V., and Boxall, S. F. (2016). Emerging model systems for functional genomics analysis of Crassulacean acid metabolism. *Curr. Opin. Plant Biol*. 31, 100–108. doi: 10.1016/j.pbi.2016.03.019

Hartwell, J., Gill, A., Nimmo, G. A., Wilkins, M. B., Jenkins, G. L., and Nimmo, H. G. (1999). Phosphoenolpyruvate carboxylase kinase is a novel protein kinase regulated at the level of expression. *Plant J.* 20, 333–342 doi: 10.1046/j.1365-313X.1999.t01-1-00609.x

Heath, O. V. S., and Russell, J. (1954). Studies in stomatal behavior. VI. an investigation of the light responses of wheat stomata with the attempted elimination of control by the mesophyll. Part 1. effects of light independent of carbon dioxide and the transmission from one part of the leaf to another. *J. Exp. Bot*. 5, 1–15. doi: 10.1093/jxb/5.1.1

Hubbard, K. E., and Webb, A. A. R. (2015). "Circadian rhythms in stomata: physiological and molecular aspects," in *Rhythms in Plants*, eds S. Mancuso, and S. Shabala (Cham: Springer), 231–255. doi: 10.1007/978-3-319-20517-5_9

Inoue, S. I., Kinoshita, T., Matsumoto, M., Nakayama, K. I., Doi, M., and Shimazaki, K. I. (2008). Blue light-induced autophosphorylation of phototropin is a primary step for signaling. *Proc. Natl. Acad. Sci. U.S.A*. 105, 5326–5631. doi: 10.1073/pnas.0709189105

Jones, M. B. (1975). The effect of leaf age on leaf resistance and CO2 exchange of the CAM plant Bryophyllum fedtschenkoi. *Planta* 123, 91–96. doi: 10.1007/BF00388063

Kinoshita, T., Doi, M., Suetsugu, N., Kagawa, T., Wada, M., and Shimazaki, K. (2001). Phot1 and phot2 mediate blue light regulation of stomatal opening. *Nature* 414, 656–660. doi: 10.1038/414656a

Kinoshita, T., Emi, T., Tominaga, M., Sakamoto, K., Shigenaga, A., Doi, M., et al. (2003). Blue-light- and phosphorylationdependent binding of a 14-3-3 protein to phototropins in stomatal guard cells of broad bean. *Plant Physiol*. 133, 1453–1463. doi: 10.1104/pp.103.029629

Lawson, T. (2009). Guard cell photosynthesis and stomatal function. *New Phytol*. 181, 13–34. doi: 10.1111/j.1469-8137.2008.02685.x

Lawson, T., and Blatt, M. R. (2014). Stomatal size, speed, and responsiveness impact on photosynthesis and water use efficiency. *Plant Physiol*. 164, 1556–1570. doi: 10.1104/pp.114.237107

Lawson, T., Lefebvre, S., Baker, N. R., Morison, J. I. L., and Raines, C. A. (2008). Reductions in mesophyll and guard cell photosynthesis impact on the control of stomatal responses to light and CO2. *J. Exp. Bot*. 59, 3609–3619. doi: 10.1093/jxb/ern211

Lawson, T., and Matthews, J. (2020). Guard cell metabolism and stomatal function. *Ann Rev Plant Biol*. 71, 273–302. doi: 10.1146/annurev-arplant-050718-100251

Lawson, T., Oxborough, K., Morison, J. I. L., and Baker N. R. (2002). Responses of photosynthetic electron transport in stomatal guard cells and mesophyll cells in intact leaves to light, CO_2 and humidity. *Plant Physiol.* 128, 52–62. doi: 10.1104/pp.01

Lawson, T., Oxborough, K., Morison, J. I. L., and Baker, N. R. (2003). The response of guard cell photosynthesis to CO_2, O_2, light and water stress in a range of species are similar. *J. Exp. Bot.* 54, 1743–1752. doi: 10.1093/jxb/erg186

Lawson, T., Simkin, A. J., Gilor, K., and Grant, D. A. (2014). Mesophyll photosynthesis and guard cell metabolism impacts on stomatal behaviour. Tansley review. *New Phytol.* 203, 1064–1081. doi: 10.1111/nph.12945

Lawson, T., Terashima, I., Fujita, T., and Wang, Y. (2018). "Coordination between photosynthesis and stomatal behavior," in *The Leaf: A Platform for Performing Photosynthesis. Advances in Photosynthesis and Respiration (Including Bioenergy and Related Processes)*, Vol 44, eds W. Adams III and I. Terashima (Cham: Springer), 141–161. doi: 10.1007/978-3-319-93594-2_6

Lawson, T., vonCaemmerer, S., and Baroli, I. (2010). Photosynthesis and stomatal behaviour. *Prog. Bot.* 72, 265–304. doi: 10.1007/978-3-642-13145-5_11

Lee, J. S., and Bowling, D. J. F. (1992). Effect of the mesophyll on stomatal opening in Commelina communis. *J. Exp. Bot*. 43, 951–957 doi: 10.1093/jxb/43.7.951

Lee, J. S., and Bowling, D. J. F. (1993). The effect of a mesophyll factor on the swelling of guard cell protoplasts of Commelina communis L. *J. Plant Physiol*. 142, 203–207. doi: 10.1016/S0176-1617(11)80964-8

Lee, J. S., and Bowling, D. J. F. (1995). Influence of the mesophyll on stomatal opening. *Aust. J. Plant Physiol*. 22, 357–363. doi: 10.1071/PP9950357

Males, J., and Griffiths, H. G. (2017). Stomatal biology of CAM plants. *Plant Physiol*. 174, 550–560. doi: 10.1104/pp.17.00114

Mansfield, T. A., Hetherington, A. M., and Atkinson, C. J. (1990). Some Current Aspects of Stomatal Physiology. *Ann Rev Plant Biol*. 41, 55–75. doi: 10.1146/annurev.pp.41.060190.000415

Matthews, J. S., Vialet-Chabrand, S., and Lawson, T. (2020). Role of blue and red light in stomatal dynamic behaviour. *J. Exp. Bot.* 71, 2253–2269. doi: 10.1093/jxb/erz563

McAdam, S. A., and Brodribb, T. J. (2012). Stomatal innovation and the rise of seed plants. *Ecol. Lett*. 15, 1–8. doi: 10.1111/j.1461-0248.2011.01700.x

Messinger, S. M., Buckley, T. N., and Mott, K. A. (2006). Evidence for involvement of photosynthetic processes in the stomatal response to CO2. *Plant Physiol*. 140,771–778. doi: 10.1104/pp.105.073676

Morison, J. I. L., and Jarvis, P. G. (1983). Direct and indirect effects of light on stomata II. in *Commelina communis L. Plant Cell Environ*. 6, 106–109. doi: 10.1111/j.1365-3040.1983.tb01882.x

Mott, K. (1988). Do stomata respond to CO2, concentrations other than intercellular? *Plant Physiol*. 86, 200–203. doi: 10.1104/pp.86.1.200

Mott, K. A. (2009). Opinion: stomatal responses to light and CO2 depend on the mesophyll. *Plant Cell Environ*. 32, 1479–1486. doi: 10.1111/j.1365-3040.2009.02022.x

Mott, K. A., Berg, D. G., Hunt, S. M., and Peak, D. (2014). Is the signal from the mesophyll to the guard cells a vapour-phase ion? *Plant Cell Environ*. 37, 1184–1191. doi: 10.1111/pce.12226

Mott, K. A., and Peak, D. (2013). Testing a vapour-phase model of stomatal responses to humidity. *Plant Cell Environ*. 36, 936–944. doi: 10.1111/pce.12026

Mott, K. A., Sibbernsen, E. D., and Shope, J. C. (2008). The role of the mesophyll in stomatal responses to light and CO2. *Plant Cell Environ*. 31, 1299–1306. doi: 10.1111/j.1365-3040.2008.01845.x

Nimmo, H. G. (2000). The regulation of phosphoenolpyruvate carboxylase in CAM plants. *Trends Plant Sci*. 5, 75–80. doi: 10.1016/S1360-1385(99)01543-5

Olsen, J. E., and Junttila, O. (2002). Far red end-of-day treatment restores wild type-like plant length in hybrid aspen overexpressing phytochrome A. *Physiol. Plant*. 115, 448–457. doi: 10.1034/j.1399-3054.2002.1150315.x

Olsen, R. L., Pratt, R. B., Gump, P., Kemper, A., and Tallman, G. (2002). Red light activates a chloroplast-dependent ion uptake mechanism for stomatal opening under reduced CO2 concentrations in Vicia spp. *New Phytol*. 153, 497–508. doi: 10.1046/j.0028-646X.2001.00337.x

Outlaw, W. H. Jr. (2003). Integration of cellular and physiological functions of guard cells. *Crit. Rev. Plant. Sci*. 22, 503–529. doi: 10.1080/713608316

Ramos, C., and Hall, A. E. (1983). Effects of photon fluence rate and intercellular CO2 partial pressure on leaf conductance and CO2 uptake rate in Capsicum and Amaranthus. *Photosynthetica* 17, 34–42.

Raschke, K. (1975). Stomatal action. *Annu. Rev. Plant Physiol.* 26, 309–340. doi: 10.1146/annurev.pp.26.060175.001521

Roelfsema, M. R. G., Hanstein, S., Felle, H. H., and Hedrich, R. (2002). CO_2 provides an intermediate link in the red light response of guard cells. *Plant J. Cell Mol. Biol*. 32, 65–75. doi: 10.1046/j.1365-313X.2002.01403.x

Sharkey, T. D., and Raschke, K. (1981). Separation and measurement of direct and indirect effects of light on stomata. *Plant Physiol*. 68, 33–40. doi: 10.1104/pp.68.1.33

Shimazaki, K., Doi, M., Assmann, S. M., and Kinoshita, T. (2007). Light regulation of stomatal movement. *Annu. Rev. Plant Biol*. 58, 219–247. doi: 10.1146/annurev.arplant.57.032905.105434

Shope, J. C., Peak, D., and Mott, K. A. (2008). Stomatal responses to humidity in isolated epidermis. *Plant Cell Environ*. 31, 1290–1298. doi: 10.1111/j.1365-3040.2008.01844.x

Sibbernsen, E., and Mott, K. A. (2010). Stomatal responses to flooding of the intercellular air spaces suggest a vapor-phase signal between the mesophyll and the guard cells. *Plant Physiol*. 153, 1435–1442. doi: 10.1104/pp.110.157685

Spalding, M. H., Stumpf, D. K., Ku, M. S. B., Burris, R. H., and Edwards, G. E. (1979). Crassulacean Acid Metabolism and Diurnal Variations of Internal CO, and 0, Concentrations in Sedum pvaealtum DC. *Aust. J. Plant Physiol*. 6, 557–567. doi: 10.1071/PP9790557

Suetsugu, N., Takami, T., Ebisu, Y., Watanabe, H., Iiboshi, C., Doi, M., et al. (2014). Guard cell chloroplasts are essential for blue light-dependent stomatal opening in Arabidopsis. *PLoS ONE* 9:e108374. doi: 10.1371/journal.pone.0108374

Talbott, L. D., Nikolova, G., Ortiz, A., Shmayevich, I., and Zeiger, E. (2002). Green light reversal of blue-light-stimulated stomatal opening is found in a diversity of plant species. *Am. J. Bot*. 89, 366–368. doi: 10.3732/ajb.89.2.366

Tallman, G., Zhu, J. X., Mawson, B. T., Amodeo, G., Nouhi, Z., et al. (1997). Induction of CAM in Mesembryanthemum crystallinum abolishes the stomatal response to blue light and light-dependent zeaxanthin formation in guard cell chloroplasts. *Plant Cell Physiol*. 38, 236–242. doi: 10.1093/oxfordjournals.pcp.a029158

Vavasseur, A., and Raghavendra, A. (2005). Guard cell metabolism and CO2 sensing. *New Phytol*.165, 665–682. doi: 10.1111/j.1469-8137.2004.01276.x

Vialet-Chabrand, S., Matthews, J. S. A., and Lawson, T. (2021). Light, power, action! Interaction of respiratory energy and blue light induced stomatal movements. *New Phytol*. 231, 2231–2246. doi: 10.1111/nph.17538

von Caemmerer, S., and Griffiths, H. (2009). Stomatal responses to CO2 during a diel Crassulacean acid metabolism cycle in Kalanchoe daigremontiana and Kalanchoe pinnata. *Plant Cell Environ*. 32, 567–576. doi: 10.1111/j.1365-3040.2009.01951.x

Wang, Y., Noguchi, K., and Terashima, I. (2011). Photosynthesis-dependent and -independent responses of stomata to blue, red and green monochromatic light: differences between the normally oriented and inverted leaves of sunflower. *Plant Cell Physiol.* 52, 479–489. doi: 10.1093/pcp/pcr005

Wilkins, M. (1991). The role of the epidermis in the generation of the circadian rhythm of carbon dioxide fixation in leaves of Bryophyllum fedtschenkoi. *Planta* 185, 425–431. doi: 10.1007/BF00201067

Wong, S. C., Cowan, I. R., and Farquhar, G. D. (1979). Stomatal conductance correlates with photosynthetic capacity. *Nature* 282, 424–426. doi: 10.1038/282424a0

Wyka, T. P., Duarte, H. M., and Luttge, U. (2005). Redundancy of stomatal control for the circadian photosynthetic rhythm in Kalanchoe daigremontiana Hamet et Perrier. *Plant Biol*. 7, 176–181. doi: 10.1055/s-2005-837541

Zeiger, E., Farquhar, G. D., and Cowan, I. R. (1987). *Stomatal Function*. Stanford, CA: Stanford University Press.

Conflict of Interest: The authors declare that the research was conducted in the absence of any commercial or financial relationships that could be construed as a potential conflict of interest.

Publisher's Note: All claims expressed in this article are solely those of the authors and do not necessarily represent those of their affiliated organizations, or those of the publisher, the editors and the reviewers. Any product that may be evaluated in this article, or claim that may be made by its manufacturer, is not guaranteed or endorsed by the publisher.

frontiers in Plant Science

ORIGINAL RESEARCH
published: 26 November 2021
doi: 10.3389/fpls.2021.766037

Overexpression of Plasma Membrane H⁺-ATPase in Guard Cells Enhances Light-Induced Stomatal Opening, Photosynthesis, and Plant Growth in Hybrid Aspen

Shigeo Toh[1,2†‡], Naoki Takata[3†], Eigo Ando[2,4], Yosuke Toda[5,6,7], Yin Wang[8,9], Yuki Hayashi[2], Nobutaka Mitsuda[10,11], Soichiro Nagano[12], Toru Taniguchi[3,13] and Toshinori Kinoshita[2,6*‡]*

[1]Department of Environmental Bioscience, Meijo University, Nagoya, Japan, [2]Division of Biological Science, Graduate School of Science, Nagoya University, Nagoya, Japan, [3]Forest Bio-Research Center, Forestry and Forest Products Research Institute, Hitachi, Japan, [4]Department of Biological Sciences, Graduate School of Science, The University of Tokyo, Tokyo, Japan, [5]Japan Science and Technology Agency, Saitama, Japan, [6]Institute of Transformative Bio-Molecules (WPI-ITbM), Nagoya University, Nagoya, Japan, [7]Phytometrics co., ltd., Shizuoka, Japan, [8]Institute for Advanced Research, Nagoya University, Nagoya, Japan, [9]Institute of Ecology, College of Urban and Environmental Sciences and Key Laboratory for Earth Surface Processes of Ministry of Education, Peking University, Beijing, China, [10]Bioproduction Research Institute, National Institute of Advanced Industrial Science and Technology (AIST), Tsukuba, Japan, [11]Global Zero Emission Research Center, National Institute of Advanced Industrial Science and Technology (AIST), Tsukuba, Japan, [12]Forest Tree Breeding Center, Forestry and Forest Products Research Institute, Hitachi, Japan, [13]Tohoku Regional Breeding Office, Forest Tree Breeding Center, Forestry and Forest Products Research Institute, Takizawa, Japan

Stomata in the plant epidermis open in response to light and regulate CO_2 uptake for photosynthesis and transpiration for uptake of water and nutrients from roots. Light-induced stomatal opening is mediated by activation of the plasma membrane (PM) H⁺-ATPase in guard cells. Overexpression of PM H⁺-ATPase in guard cells promotes light-induced stomatal opening, enhancing photosynthesis and growth in *Arabidopsis thaliana*. In this study, transgenic hybrid aspens overexpressing Arabidopsis PM *H⁺-ATPase* (*AHA2*) in guard cells under the strong guard cell promoter Arabidopsis *GC1* (*AtGC1*) showed enhanced light-induced stomatal opening, photosynthesis, and growth. First, we confirmed that *AtGC1* induces GUS expression specifically in guard cells in hybrid aspens. Thus, we produced *AtGC1::AHA2* transgenic hybrid aspens and confirmed expression of *AHA2* in *AtGC1::AHA2* transgenic plants. In addition, *AtGC1::AHA2* transgenic plants showed a higher PM H⁺-ATPase protein level in guard cells. Analysis using a gas exchange system revealed that transpiration and the photosynthetic rate were significantly increased in *AtGC1::AHA2* transgenic aspen plants. *AtGC1::AHA2* transgenic plants showed a > 20% higher stem elongation rate than the wild type (WT). Therefore, overexpression of PM H⁺-ATPase in guard cells promotes the growth of perennial woody plants.

Keywords: PUMP, PM H⁺-ATPase, guard cell, stomatal conductance, hybrid aspen

OPEN ACCESS

Edited by:
Mamoru Okamoto,
University of Adelaide, Australia

Reviewed by:
Mikael Brosché,
University of Helsinki, Finland
Karl H. Hasenstein,
University of Louisiana at Lafayette, United States

***Correspondence:**
Shigeo Toh
stoh@meijo-u.ac.jp
Toshinori Kinoshita
kinoshita@bio.nagoya-u.ac.jp

†These authors share first authorship
‡These authors share co-corresponding authorship

Specialty section:
This article was submitted to Plant Physiology, a section of the journal Frontiers in Plant Science

Received: *28 August 2021*
Accepted: *15 October 2021*
Published: *26 November 2021*

Citation:
Toh S, Takata N, Ando E, Toda Y, Wang Y, Hayashi Y, Mitsuda N, Nagano S, Taniguchi T and Kinoshita T (2021) Overexpression of Plasma Membrane H⁺-ATPase in Guard Cells Enhances Light-Induced Stomatal Opening, Photosynthesis, and Plant Growth in Hybrid Aspen. Front. Plant Sci. 12:766037. doi: 10.3389/fpls.2021.766037

INTRODUCTION

In an era of global climate change and food shortages, finding ways to improve the absorption of CO_2 by land plants is becoming an increasingly important issue. Stomatal pores in the epidermis are surrounded by two guard cells and are important for capturing CO_2. Stomata are found mainly on the surface of leaves in land plants. Because the leaf surface is almost impermeable to air and water, the stomatal pores are the primary pathway for diffusion of CO_2, O_2, and water vapour between the atmosphere and interior of the leaf (Willmer and Fricker, 1995). Enhancement of gas exchange by stomatal opening is essential for photosynthesis and transpiration (Shimazaki et al., 2007). Stomatal transpiration limits photosynthesis in rice (Kusumi et al., 2012). Therefore, increasing the stomatal opening and transpiration could enhance photosynthesis and thus plant growth. Condon et al. (1987) examined diverse wheat genotypes and found that increasing stomatal conductance, especially abaxial stomatal conduct, enhanced crop biomass. Transgenic *Arabidopsis thaliana* (Arabidopsis) overexpressing plasma membrane (PM) H^+-ATPase, a key enzyme for stomatal opening, in guard cells promotes light-induced stomatal aperture opening, photosynthetic activity, and plant growth (Wang et al., 2014). Furthermore, the overexpression of PM H^+-ATPase in rice increases stomatal opening, nutrient uptake, and photosynthesis, thus enhancing grain yield in paddy fields (Zhang et al., 2021). Therefore, we propose designating plants overexpressing PM H^+-ATPase as Promotion and Upregulation of plasma Membrane Proton-ATPase (PUMP) plants.

Light stimulates the stomatal opening, and there are several mechanisms of stomatal opening in response to light of different wavelengths (Shimazaki et al., 2007; Inoue and Kinoshita, 2017). Blue light is a major stimulator of the stomatal opening. The blue light receptors, phototropins (phot1 and phot2), activate PM H^+-ATPase in the PM by binding 14-3-3 protein to the phosphorylated penultimate residue, threonine (Thr; Kinoshita and Shimazaki, 1999; Kinoshita et al., 2001). Following activation by blue light, PM H^+-ATPase induces hyperpolarisation of the PM, allowing K^+ uptake through inwardly rectifying K^+ (K^+_{in}) channels (Shimazaki et al., 2007). The accumulation of K^+ causes guard cells to swell and pores to open. Several signal components – such as blue light signalling 1 (BLUS1), type 1 protein phosphatase, and blue light-dependent H^+-ATPase phosphorylation (BHP) – mediate blue light-dependent signalling in guard cells (Takemiya et al., 2013; Hayashi et al., 2017). Red light opens stomata by decreasing the intercellular CO_2 concentration (Ci) and photosynthesis in leaf chloroplasts and stomata (Sharkey and Ogawa, 1987; Roelfsema and Hedrich, 2005; Vavasseur and Raghavendra, 2005). However, the mechanism of the stomatal response to red light is unclear (Baroli et al., 2008; Wang et al., 2011). Red light induces stomatal opening in whole leaves by activating PM H^+-ATPase *via* photosynthesis-dependent phosphorylation of its penultimate residue, Thr (Ando and Kinoshita, 2018).

Forest trees fix atmospheric CO_2 mainly into wood biomass. Indeed, forest products, such as timber, contain large amounts of carbon, contributing to mitigation of climate change. *Populus* is one of the fastest growing trees in the Northern Hemisphere and is ideal for furniture, paper pulp, and biofuel production. The genomic sequence of *Populus trichocarpa* was published in 2006 (Tuskan et al., 2006), facilitating transgenic approaches to improving the growth and wood properties of *Populus* species. Enhancement of tree growth and biomass production is typically accomplished by overexpression of endogenous and exogenous *Populus* genes and by RNAi repression of *Populus* endogenous genes (reviewed in Dubouzet et al., 2013). For example, photosynthetic yield and assimilation have been modified to increase plant biomass in *Populus*. In *P. trichocarpa*, the overexpression of *Populus Photoperiod Response 1*, which is associated with starch accumulation, enhances starch accumulation in transgenic plants, thereby increasing biomass production in stem and root (Zawaski et al., 2012). Because the PUMP plant's strategy is effective in eudicotyledonous and monocotyledonous plants, it may also be useful for enhancing photosynthetic activity and biomass production in perennial woody plants.

In this study, the PUMP plant's strategy was applied to hybrid aspen (*Populus tremula* × *Populus tremuloides*), a perennial woody plant, to enhance plant growth and biomass production. Overexpression of Arabidopsis PM *H+-ATPase* (*AHA2*) under *CaMV35S* promoter could not be achieved in hybrid aspen. Therefore, we used the guard cell-specific promoter Arabidopsis *GC1* (*AtGC1*) to overexpress *AHA2* in hybrid aspen. *AtGC1* was active in guard cells in hybrid aspen as in Arabidopsis. *AtGC1::AHA2* transgenic hybrid aspens showed higher stomatal conductance and photosynthetic rate compared to wild-type (WT) plants. The transgenic plants were taller and had more biomass than WT plants when grown in a greenhouse for 2 months. Therefore, the PUMP plant's strategy can increase growth and biomass production in perennial plants.

MATERIALS AND METHODS

Phylogenetic Tree and Bioinformatics

Plasma membrane *H+-ATPase* genes were retrieved from genomic databases for *A. thaliana* (The *Arabidopsis* Information Resource, TAIR) and *P. trichocarpa* (Phytozome v. 12.1). Amino acid sequences were aligned using ClustalW. Evolutionary distances were computed using the Jones-Taylor-Thornton (JTT) matrix-based method with the complete-deletion option (Jones et al., 1992). Phylogenetic trees were constructed by the neighbour-joining (NJ; Saitou and Nei, 1987) and maximum-likelihood (ML) methods. Bootstrap values were calculated with 1,000 replications using the NJ (Felsenstein, 1985) and ML methods in MEGA7 software (Kumar et al., 2016).

Tissue-specific gene expression patterns of 13 *Populus* PM *H+-ATPase* genes were examined by re-analysing the RNA sequencing data (Shi et al., 2017). We normalised the raw count data set obtained by RNA sequencing (GSE81077) for xylem, phloem, leaf, shoot, and root with trimmed mean M-values using edgeR v. 3.18.1 (Robinson et al., 2010) in R software v. 3.3.2 (R Core Team, 2018; Hori et al., 2020).

Plant Materials and Growth

Populus tremula×*Populus tremuloides* (WT clone T89) seedlings were cultured in 0.8% (w/v) agar box containing 0.5× Murashige and Skoog medium (pH 5.7) at 25°C under a cycle of 16-h white light (50 μmol m^{-2} s^{-1})/8-h dark. Cultured hybrid aspens were transferred to the soil mix (3:1 fertilised peat moss: vermiculite, v/v) and grown in two different conditions. One is a greenhouse, and the other is an indoor plant growth room. Greenhouse temperatures were maintained at 21.5 ± 8°C, and natural light was supplemented with metal halide lamps (KI Holdings, Yokohama, Japan) to achieve an 18-h daylength (PAR ≥ 200 μmol m^{-2} s^{-1})/6-h dark. The indoor plant growth was maintained at 20°C, and plants were grown under a cycle of 16-h white light (80 μmol m^{-2} s^{-1})/8-h dark. Plants were watered and fertilised once weekly with 2,000-fold diluted Hyponex 6-10-5 solution (HYPONeX Japan, Osaka, Japan) for all conditions.

Generation of Transgenic Hybrid Aspens

For *AtGC1::GUS* and *CaMV35S::AHA2* constructs, *AtGC1* and *AHA2* were cloned into the pCR8/GW/TOPO vector (Thermo Fisher Scientific, Waltham, MA, United States) and transferred to the pGWB433 and pGWB402 vectors *via* the Gateway LR reaction (Nakagawa et al., 2007). Construction of *AtGC1::AHA2* was described previously (Wang et al., 2014). The binary vectors (pGWB433-*AtGC1::GUS*, pGWB402-*CaMV35S::AHA2*, and pPZP211-*AtGC1::AHA2*) were transformed into *Agrobacterium tumefaciens* strain GV3101 (pMP90). Transgenic hybrid aspens were generated using the vectors, essentially as described by Eriksson et al. (2000).

GUS Staining of Transgenic Hybrid Aspen

Samples were thoroughly rinsed in distilled water and placed in cold 90% acetone on ice for 5 min. Acetone was removed, and GUS staining solution was added for 20 min, followed by incubation overnight at 37°C. GUS staining solution consisted of 10 mM Na_2EDTA, 50 mM phosphate buffer (pH 7.0), 1 mM $K_4Fe(CN)_6$, 1 mM $K_3Fe(CN)_6$, 0.5 mg/ml X-Gluc (5-bromo-4-chloro-3-indolyl β-D-glucuronide), and 0.1% Triton X-100. Stained samples were soaked in 70% (v/v) ethanol to remove chlorophyll.

Reverse Transcription PCR for Gene Expression

Total RNA was extracted from epidermal fragments using the NucleoSpin RNA Plant kit (TaKaRa Bio, Shiga, Japan). Epidermal fragments from whole leaves were isolated from 10-week-old plants as described previously (Hayashi et al., 2011). First-strand cDNAs were synthesised from total RNA using the QuantiTect Reverse Transcription Kit (Qiagen, Hilden, Germany). Reverse transcription PCR was performed using 2 μl of cDNA template with Ex Taq PCR Mix (TaKaRa Bio) and specific primers. Primers were shown in **Supplementary Table 1**. Master mix of PCR reaction was prepared for each gene of interest, and 20 μl of reaction mix, including the cDNA template, was pipetted into each tube. The conditions were 1 cycle at 95°C for 2 min; 24 (*UBQ*), 28 (*AHA2* and *Pt*×*tHA2*) cycles of 95°C for 15 s, 57°C for 30 s, and 72°C for 30 s; and a final incubation at 72°C for 2 min. Amplified cDNA was detected by electrophoresis.

Immunohistochemical Detection of Plasma Membrane H+-ATPase in Guard Cells

Immunohistochemical detection was performed as described previously (Hayashi et al., 2011). Polyclonal antibodies against the conserved catalytic domain of the plasma membrane H+-ATPase of Arabidopsis (AHA2) were raised in rabbits. The AHA2 DNA fragment was amplified from first-strand Arabidopsis cDNA with PCR using the specific primers 5′-GCCGGATCC ATGGATGTCCTGTGCAGTGAC-3′ and 5′-GCCGGATCCTC AAGCACCACGAGCAGC-3′. The resulting amplified DNA fragment of 967–1,845 bp of AHA2, which contains BamHI sites at both ends, was cloned into the BamHI site of the pET30a vector (Merck, Darmstadt, Germany). The purified proteins from *E. coli* (BL21) were used as an antigen. The antiserum was used for immunoblots in Arabidopsis (1:1,000 dilution; Hayashi et al., 2010). PM H+-ATPase was detected in guard cells using epidermis isolated from hybrid aspen leaf. The amount of PM H+-ATPase was estimated using antiserum against the catalytic domain of AHA2. Fluorescence intensity was quantified according to Ando and Kinoshita (2018).

Gas Exchange Measurements

Gas exchange measurements were performed as described previously (Wang et al., 2014) using the LI-6400 system (Li Cor Biosciences, Lincoln, NE, United States), and parameters were calculated with the software supplied by the manufacturer. White light (1,000 μmol·m^{-2}·s^{-1}) was provided by a fibre optic illuminator with a halogen projector lamp (15 V/150 W; Moritex, Saitama, Japan) as a light source and a MHAB-150W; power supply (Moritex). Light was attenuated by a series of optical crown glass metallic neutral density filters (Newport Japan, Hakuto, Japan). The molar flow rate of air entering the leaf chamber, leaf temperature, and relative humidity was maintained at 500 μmol·s^{-1}, 24°C, and 40–50% (Pa/Pa), respectively. After the initial 10 min of dark adaptation, the plants were exposed to white light (1,000 μmol·m^{-2}·s^{-1}) for 30 min.

Growth Analyses and Biomass Assays

Plant height was measured weekly from 21 days after potting in a greenhouse. Once trees had reached 20 cm in height, the stem diameters were measured weekly at 10 cm above the soil. The elongation growth rate of plants was evaluated by a curve-fitting procedure (Buchwald, 2007; Edwards et al., 2018). The radial growth rate was calculated by fitting to a linear function. These procedures were conducted in KaleidaGraph v. 4.1 (Synergy Software, Reading, PA, United States). Leaf number and size (leaves 16–25) were measured when sampling leaves. Leaves were imaged using a scanner (Perfection V700 Photo; Epson, Nagano, Japan) at 600 dpi, and leaf size was evaluated by ImageJ 1.51 software.[1] Leaves, stems, and roots were collected from each plant and

[1]https://imagej.net/

weighed to calculate the fresh weight. Following 3 days of drying at 60°C, the leaves, stems, and roots were weighed again to determine the dry weight (DW). The index of stem volume (volumetric index) was calculated as (diameter ÷ 2)^2 × height × π, from the final diameter (cm) and height (cm) of an individual tree. A 1 cm length of stem segment was sampled from 2 cm above the soil to determine wood density. Xylem tissues were obtained by peeling off the bark and were then filled with ultrapure water. The weight increase by increased water volume (V) was measured by a balance at 20°C. The xylem samples were dried in an oven at 105°C for 72 h, and DW was measured using a balance. The wood density was calculated by the formula: Wood density = DW ÷ V.

Statistical Analysis

Statistical significance was evaluated by Student's *t* test followed by the multiple testing correction procedure of Benjamini and Hochberg (1995), performed using Excel (Microsoft Corp., Redmond, WA, United States).

RESULTS

Phylogeny and Protein Structure of PM H$^+$-ATPase Homologs in *Populus*

The *P. trichocarpa* genome has 13 PM H$^+$-ATPase (HA) homologs with high amino acid similarity to *A. thaliana* HA2 (AHA2; **Figure 1; Supplementary Table 2**). We designated the *P. trichocarpa* isoforms PotriHA1–PotriHA13. The *Populus* isoforms have a highly conserved characteristic sequence, GDGVNDAPALKKA, in the catalytic domain of the P-type ATPase (Axelsen and Palmgren, 1998), supporting our proposal that these isoforms are functional homologs in *Populus*. The C-terminal region of PM H$^+$-ATPases is important for catalytic regulation (Palmgren, 2001; Haruta et al., 2015; Falhof et al., 2016; Inoue and Kinoshita, 2017). All *Populus* isoforms conserve regions I and II, which are important for autoinhibition, in the C-terminal region (Axelsen et al., 1999), and Thr as a penultimate residue, which is important for its activation *via* phosphorylation (**Figure 1A**). Several phosphorylation sites in the C-terminal domain (Thr-881, Ser-899, and Ser-931), in addition to Thr as a penultimate residue, are also highly conserved in *Populus* PM H$^+$-ATPases.

Phylogenetic analysis using full-length amino acid sequences showed that PotriHAs were classified into classes I–V (**Figure 1B**), as defined in Arango et al. (2003). PotriHA10 and PotriHA11 formed a clade with AHA4 and AHA11 in class I. PotriHA1, PotriHA2, PotriHA3, and PotriHA4 formed a clade with AHA1, AHA2, AHA3, and AHA5 in class II. PotriHA13 formed a clade with AHA10 in class III. PotriHA5, PotriHA6, PotriHA7, PotriHA8, and PotriHA9 formed a clade with AHA6, AHA8, and AHA9 in class IV. PotriHA12 formed a clade with AHA7 in class V. PM H$^+$-ATPases in class II, including *A. thaliana* AHA1 and AHA2 and rice OSA7, have a major role in plants (Haruta et al., 2010; Toda et al., 2016). In *P. trhichocarpa*, *PotriHA2*, *PotriHA3*, and *PotriHA4* (class II) showed higher expression than the other class genes in xylem, phloem, leaf, shoot, and root (**Figure 1C**), suggesting that those isoforms are major PM H$^+$-ATPases in *Populus* species.

Overexpression of *AHA2* Under Arabidopsis *GC1* Promoter in Hybrid Aspen

We first attempted to introduce *CaMV35S::AHA2* into hybrid aspen to ectopically overexpress *AHA2*. However, no transgenic hybrid aspens were generated, even using 109 stem segments for *Agrobacterium*-mediated transformation. Therefore, we used the guard cell-specific promoter in *A. thaliana*, *AtGC1*, to express *AHA2* in hybrid aspen. To investigate *AtGC1* activity in hybrid aspen, we generated *AtGC1::GUS* transgenic plants and examined their GUS activity. As shown in **Figure 2A**, GUS staining was observed in guard cells of the leaf epidermis of *AtGC1::GUS* transgenic plants, similar to *AtGC1::GUS*-expressing *A. thaliana* (Yang et al., 2008). We next transformed the *AtGC1::AHA2* construct into hybrid aspen to overexpress *AHA2* in guard cells and generated at least three independent transgenic events (#3, #5, and #9; **Figure 2B**). In the transgenic plants, *AHA2* was expressed in leaf epidermis, as was *Pt* × *tHA2*, a major PM H$^+$-ATPase in *Populus*. To examine whether the introduction of *AtGC1::AHA2* elevated the PM H$^+$-ATPase protein level in guard cells, immunohistochemical analysis using an anti-AHA2 antibody was conducted in the leaf epidermis of transgenic and WT plants. Immunofluorescence was brighter in guard cells of *AtGC1::AHA2* transgenic plants than WT plants (**Figures 2C,D**). Fluorescence intensity relative to the WT showed that the protein level of PM H$^+$-ATPase was enhanced in guard cells of transgenic plants (70% for #3, 75% for #5, and 150% for #9), indicating that *AtGC1::AHA2* transgenic plants over-accumulated PM H$^+$-ATPase in guard cells. The density of stomata in *AtGC1::AHA2* transgenic plants was comparable to that in WT plants (196 stomata mm^{-2} for WT, 203 for #3, 217 for #5, and 203 for #9; **Supplementary Table 3**). Therefore, the introduction of *AtGC1::AHA2* increased its protein levels in guard cells without affecting stomatal development in hybrid aspen, similar to *A. thaliana* expressing *AtGC1::AHA2* (Wang et al., 2014).

Stomatal Conductance and Photosynthetic Rate in *AtGC1::AHA2* Transgenic Hybrid Aspens

To investigate photosynthetic activity in *AtGC1::AHA2* transgenic plants, stomatal conductance and the photosynthetic rate (CO_2 assimilation rate) were measured in intact leaves of transgenic and WT plants grown in an indoor-growth room for 82–94 days. The *AtGC1::AHA2* transgenic plants showed higher stomatal conductance in the dark compared to the WT (0.07 for WT, 0.22 for #3, 0.15 for #5, and 0.16 for #9 mol·m^{-2}·s^{-1}. In the WT, white light at 1,000 μmol·m^{-2}·s^{-1} increased stomatal conductance. Similarly, light illumination increased stomatal conductance in *AtGC1::AHA2* transgenic plants. Stomatal conductance was saturated within 10 min of the start of light illumination in the transgenic and WT plants. The average

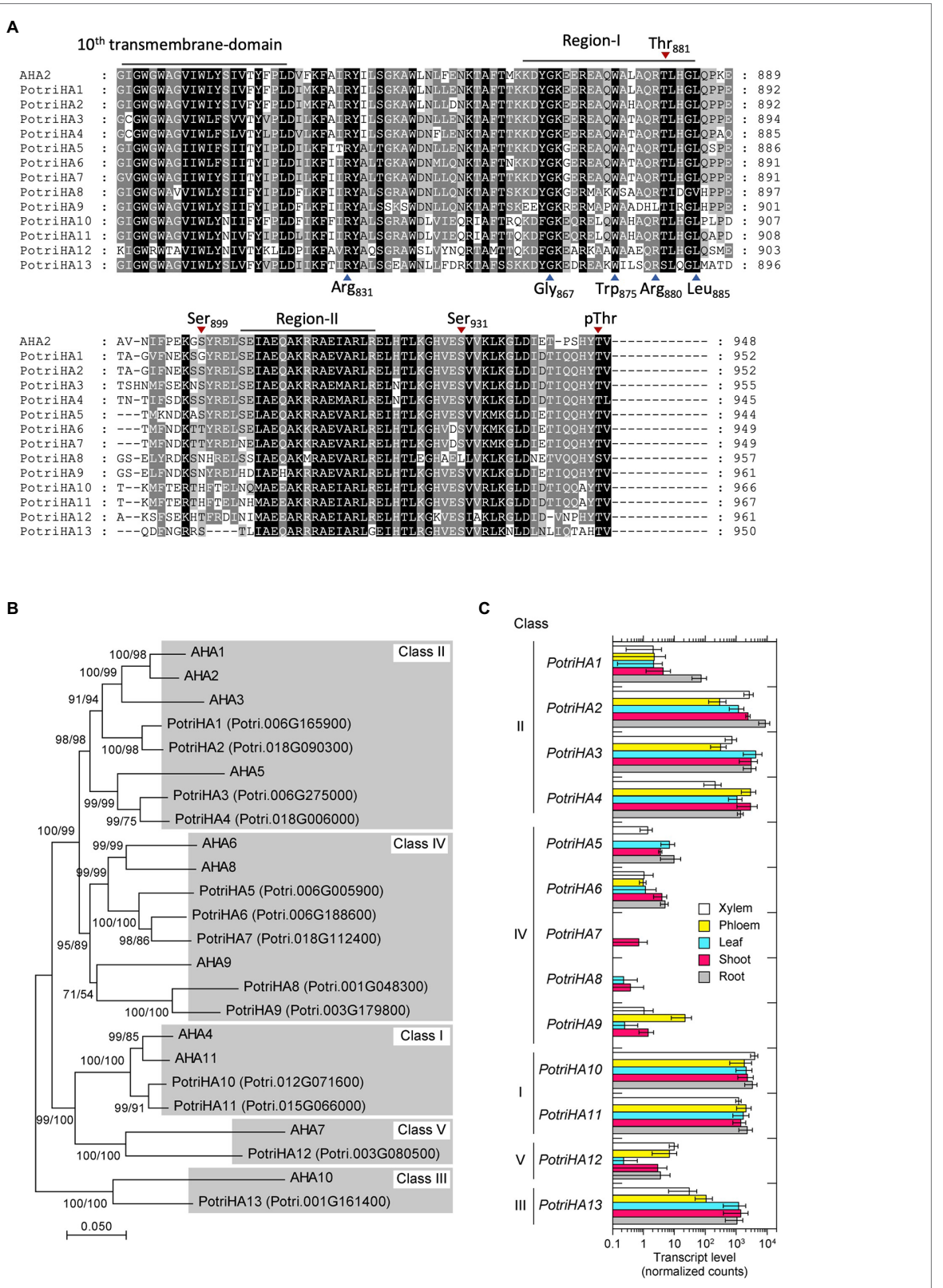

FIGURE 1 | Amino acid sequence similarity and gene expression of *Populus PM H⁺-ATPases*. **(A)** Amino acid sequence alignment of *P. trichocarpa* H⁺-ATPases with the C-terminal inhibition domain of Arabidopsis PM *H⁺-ATPase* (AHA2). The 10th transmembrane domain and the inhibitory motifs (regions I and II) in

(continued)

FIGURE 1 | the C-terminal inhibitory domain are shown. Identical and similar amino acid residues are highlighted by black and grey backgrounds, respectively. Blue arrowheads below the sequence alignment indicate amino acids important for the function of the inhibitory domain of AHA2 (Axelsen et al., 1999) Red arrowheads above the sequence alignment indicate phosphorylation target sites of AHA2 (Fuglsang et al., 2007; Niittylä et al., 2007; Haruta et al., 2014). **(B)** Phylogenetic tree of PM H+-ATPases in *A. thaliana* and *P. trichocarpa*. Phylogenetic trees were reconstructed by the neighbour-joining (NJ) and maximum-likelihood (ML) methods based on the alignment of full-length amino acid sequences. The phylogenetic topology was the same in trees reconstructed by the NJ and ML methods. Bootstrap values were calculated by the NJ method with 1,000 replications (left) and by the ML method with 1,000 replications (right). Roman numerals indicate classes, as defined by Arango et al. (2003). **(C)** The expression pattern of *P. trichocarpa H+-ATPase*s in xylem, phloem, leaf, shoot, and root tissues. The raw count data set obtained by tissue-specific RNA sequencing (GSE81077, Shi et al., 2017) was reanalysed to calculate normalised read counts as gene expression level of each gene. Error bars represent the SD with three sample replicates.

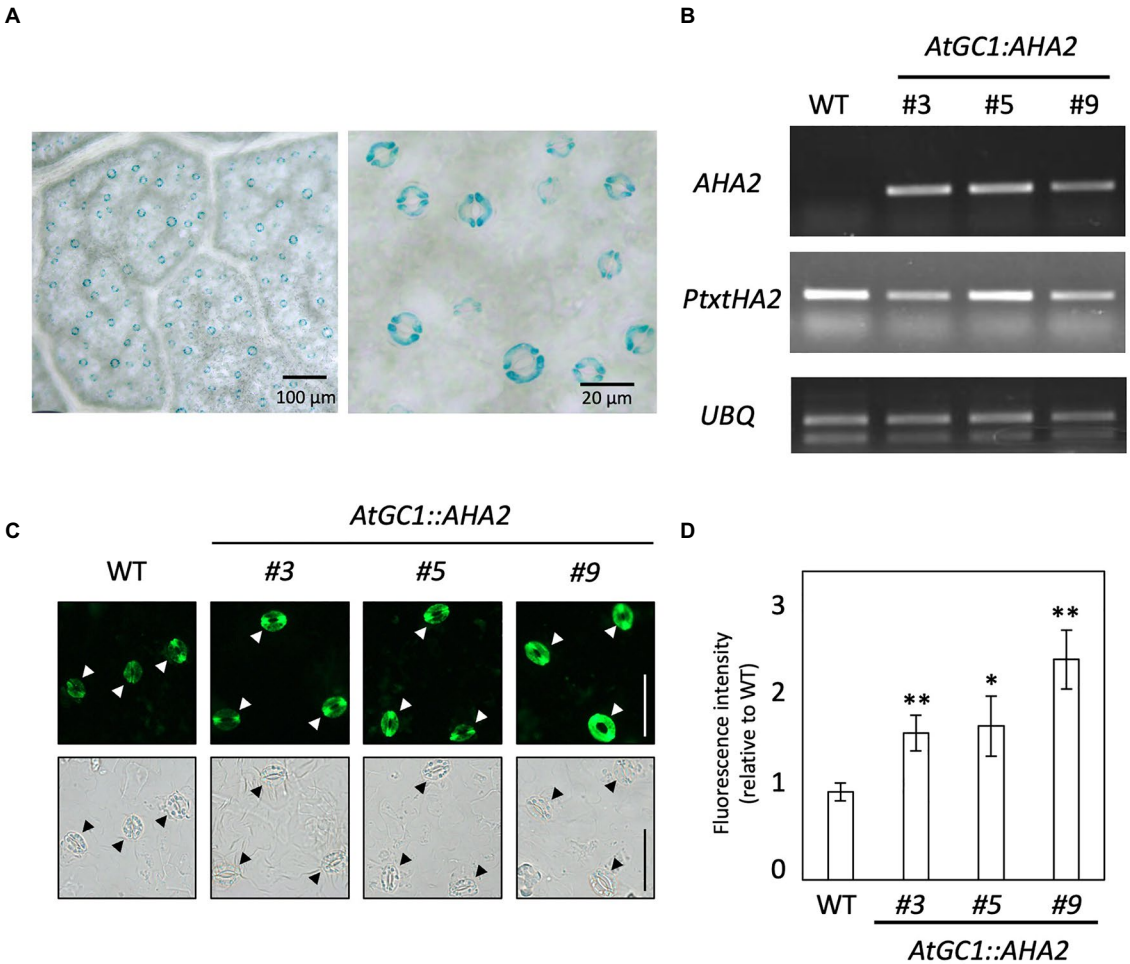

FIGURE 2 | Promoter activity of *AtGC1* in hybrid aspen and generation of *AtGC1::AHA2* transgenic hybrid aspens. **(A)** Histochemical GUS analysis of *AtGC1::GUS* transgenic hybrid aspens. Images are of the abaxial side of the leaf. A high-magnification image is shown in the right panel. Scale bar = 100 µm (left panel) and 20 µm (right panel). **(B)** Expression level of *AHA2* and *P. tremula* × *P. tremuloides* (*Pt* × *t*) *H+-ATPase* in transgenic hybrid aspens and wild type (WT). The expression of *AHA2* and *Pt* × *tHA2* was analysed by reverse transcription PCR. *Ubiquitin 11* (*UBQ*, Takata et al., 2009) was used as the internal control. **(C)** Immunohistochemical analysis of PM H+-ATPase in guard cells of transgenic hybrid aspens and WT. Isolated abaxial leaf epidermis was immunolabeled with antiserum raised against the catalytic domain of AHA2. Fluorescence (upper panel) and bright-field images (lower panel) were captured by a fluorescence microscope. Arrowheads indicate guard cells. Scale bar = 50 µm. **(D)** Immunofluorescence intensity in guard cells of transgenic hybrid aspens and WT. Fluorescence intensities in transgenic plants were normalised to those in WT plants. Data are means ± SD of three independent measurements. Asterisks denote a mean significantly higher than the WT (set to 1.0; Student's *t* test followed by the Benjamini and Hochberg multiple test correction; $^{**}p < 0.01$ and $^{*}p < 0.05$).

stomatal conductance in the transgenic plants was approximately 3-fold higher than in the WT (**Figure 3A**). Under identical conditions, photosynthetic rates were saturated 20 min after the start of light illumination in WT and *AtGC1::AHA2* transgenic plants. The photosynthetic rate was 45% higher in the transgenic compared to the WT plants (**Figure 3B**). Although stomatal aperture is used to estimate stomatal conductance and photosynthetic activity, determining the average stomatal aperture is more problematic in hybrid aspen compared to *A. thaliana*, because stomatal size varies in the abaxial epidermis of the

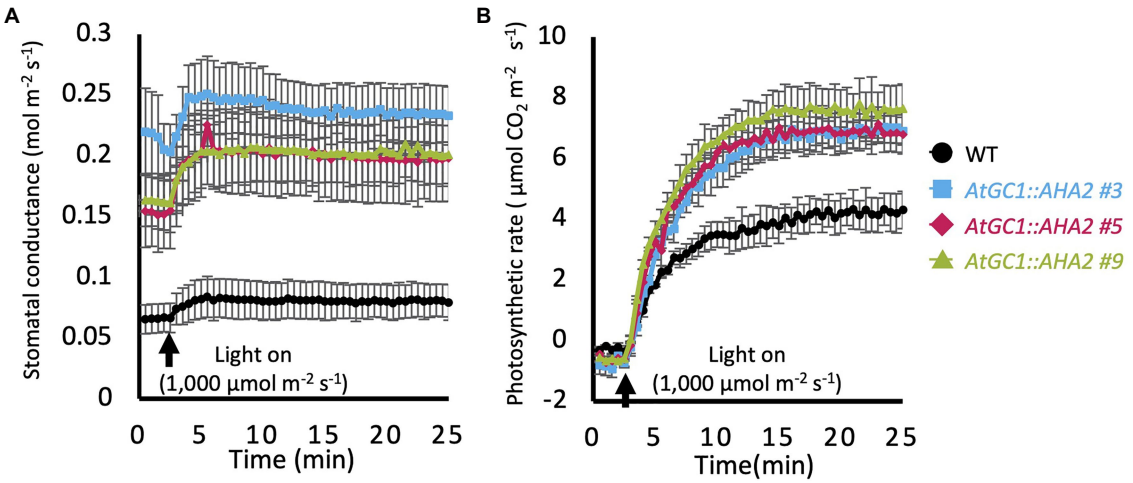

FIGURE 3 | Gas exchange properties of *AtGC1::AHA2* transgenic and wild-type (WT) plants. **(A)** Light responses of stomatal conductance and **(B)** the photosynthetic rate in transgenic and WT plants. Measurements were conducted under dark conditions followed by 1,000 µmol·m^{-2}·s^{-1} light. Black arrows indicate the time of light-on. Data were plotted every 30 s. Measurements were conducted on three different plants for each transgenic event. Error bars represent SE and are not shown if smaller than the symbols.

former (**Supplementary Figure 1; Figure 2A**). Taken together, our results indicate that the introduction of AHA2 protein to guard cells increased stomatal conductance and the photosynthetic rate in hybrid aspen.

Growth Phenology and Biomass Production of *AtGC1::AHA2* Transgenic Hybrid Aspens

Enhancement of photosynthetic activity in *AtGC1::AHA2* transgenic plants was expected to promote growth and biomass production. When *AtGC1::AHA2* transgenic plants and WT plants were grown in a greenhouse for 63 days, the transgenic plants showed 14–21% greater height compared to the WT (**Figure 4**). The elongation rates were 11–15% higher in transgenic than WT plants. The stem diameter and radial growth rates were similar between the transgenic and WT plants. The leaf number per plant was increased 7–16% in the transgenic compared to WT plants, although the area of mature leaves was decreased 14–28%. For biomass production, the volumetric index of stem-trunk biomass was enhanced 14–23% in the transgenic compared to WT plants. Furthermore, the DW of leaves, stems, and roots was non-significantly increased in the transgenic compared to WT plants. However, the stem wood density of the transgenic plants (0.37 ± 0.02 g·cm^{-3} for #3, 0.36 ± 0.03 g·cm^{-3} for #5, and 0.38 ± 0.01 g·cm^{-3} for #9) was similar to that of WT plants (0.37 ± 0.01 g·cm^{-3}). The increment of tree height in the transgenic plants was observed in the indoor-growth room (**Supplementary Figure 2**), indicating that the enhancement of growth phenology was stable under different light intensities. Together, our results indicate that *AtGC1::AHA2* transgenic hybrid aspens had a higher stem elongation rate and greater biomass production than the WT, likely due to the enhanced stomatal opening and photosynthetic rate.

DISCUSSION

In this study, the PUMP plant's strategy was used to enhance the photosynthetic rate and growth of *Populus* species. PM H$^+$-ATPases are highly conserved among plant species, and their gene numbers vary among plant species (e.g., 11 isoforms in *A. thaliana*, nine in *Nicotiana plumbaginifolia*, and 10 in *O. sativa*; Arango et al., 2003). In the genome of *P. trichocarpa*, there were 13 PM H$^+$-ATPases, PotriHA1–PotriHA13, with high similarity to *A. thaliana* PM H$^+$-ATPase (**Figure 1**). All isoforms in *P. trichocarpa* had domains typical of plant PM H$^+$-ATPases. We overexpressed Arabidopsis *AHA2* under the control of *CaMV35S* or *AtGC1* promoter in hybrid aspens. However, we could not generate *CaMV35S::AHA2* plants. *AtGC1* was specifically expressed in guard cells of hybrid aspens (**Figure 2A**), indicating that we developed a stomatal-specific promoter in *Populus* species. The *AtGC1::AHA2* transgenic hybrid aspens showed enhanced light-induced stomatal opening (**Figure 3**). This suggests that PM H$^+$-ATPase is the limiting factor in stomatal opening in *Populus* species, as in *A. thaliana* (Wang et al., 2014). Furthermore, the *AtGC1::AHA2* transgenic hybrid aspens had an enhanced photosynthetic rate and growth (**Figures 3, 4**), indicating that the PUMP plant's strategy is applicable for perennial trees using a guard cell-specific promoter and PM H$^+$-ATPase.

The *AtGC1::AHA2* transgenic hybrid aspens had enhanced stomatal conductance and photosynthetic rate compared to WT plants, increasing plant height, volumetric index, and stem biomass production (**Figure 4**). The number of leaves and leaf biomass also increased in the transgenic hybrid aspens as elongation growth accelerated, whereas the size of leaves decreased. However, the stem diameter and wood density of the transgenic plants were comparable to those of WT plants. These phenotypic changes imply that improvement of the

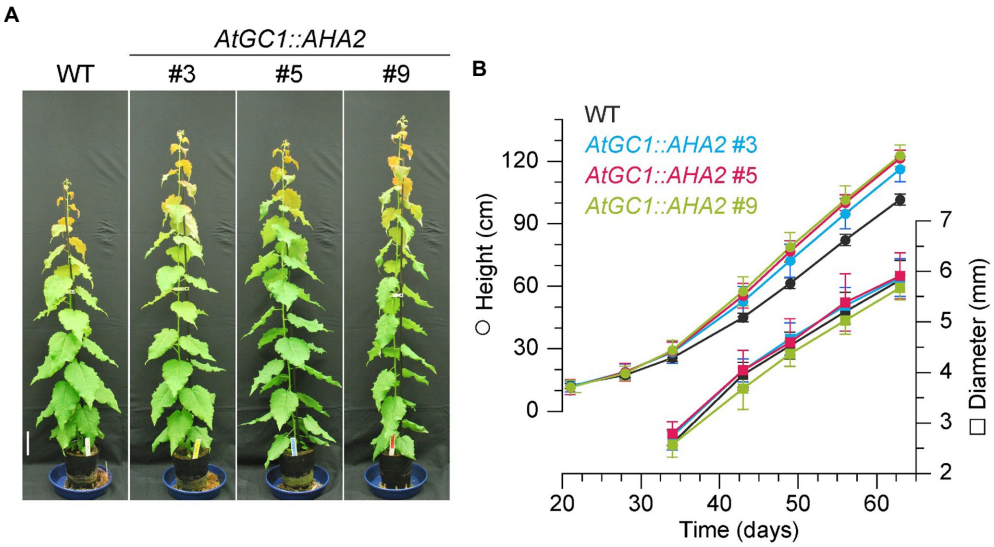

C

Genotype	Height (cm)	Diameter (mm)	Elongation growth rate (cm/day)	Radial growth rate (mm/day)	Leaf number	Leaf size (cm^2)
WT	101.6 ± 2.7	5.8 ± 0.4	2.90 ± 0.05	0.11 ± 0.01	30.5 ± 1.3	119.1 ± 11.8
AtGC1::AHA2#3	**116.3 ± 6.1****	5.9 ± 0.4	3.23 ± 0.31	0.11 ± 0.02	32.5 ± 1.3	102.4 ± 17.1
AtGC1::AHA2#5	**121.5 ± 3.9****	5.9 ± 0.5	3.33 ± 0.35	0.11 ± 0.02	**34.8 ± 0.5****	100.1 ± 20.9
AtGC1::AHA2#9	**122.8 ± 5.2****	5.7 ± 0.2	**3.28 ± 0.11****	0.11 ± 0.01	**35.3 ± 1.5****	**86.7 ± 11.8****

Genotype	volumetric index	Fresh weight (FW) (g)			Dry weight (DW) (g)			Wood density (g/cm3)
		leaf	stem	root	leaf	stem	root	
WT	27.3 ± 4.3	35.9 ± 2.2	22.0 ± 3.6	34.8 ± 11.6	8.0 ± 0.5	5.6 ± 0.9	4.2 ± 1.2	0.37 ± 0.01
AtGC1::AHA2#3	31.8 ± 5.3	36.2 ± 5.6	25.3 ± 4.0	35.1 ± 3.6	8.3 ± 1.3	6.2 ± 1.1	4.4 ± 0.7	0.37 ± 0.02
AtGC1::AHA2#5	33.5 ± 5.6	40.8 ± 7.6	26.9 ± 4.6	43.8 ± 6.8	9.4 ± 1.2	6.6 ± 0.9	4.9 ± 1.1	0.36 ± 0.03
AtGC1::AHA2#9	31.2 ± 3.9	34.8 ± 3.9	24.8 ± 3.2	36.2 ± 6.1	9.0 ± 0.9	6.4 ± 0.9	4.9 ± 0.4	0.38 ± 0.01

FIGURE 4 | Growth and biomass production of *AtGC1::AHA2* transgenic and wild-type (WT) plants. **(A)** Growth phenotypes of 63-day-old transgenic and WT plants. Scale bar = 10 cm. **(B)** Height (circles) and diameter (squares) of the transgenic and WT plants against time over 63 days of growth. **(C)** Growth rates and biomass production of transgenic and WT plants. Values are means ± SD ($n = 4$). Double asterisk indicates $p < 0.01$ by Student's t test followed by the Benjamini and Hochberg multiple test correction.

photosynthetic rate (**Figure 3**) increased assimilation products, resulting in morphological changes in different tissues of *AtGC1::AHA2* transgenic plants. The allocation of assimilation products varies depending on, for instance, the plant species, plant size, environment, and season. In young cottonwood trees (*Populus deltoides*), younger middle leaves transport assimilation products acropetally and basipetally, while older bottom leaves transport them primarily to lower stem and roots in the growing season (Dickson, 1989). In the present study, hybrid aspens were grown for 2 months in a greenhouse and maintained rapid elongation growth. This implies that the increased assimilation products in *AtGC1::AHA2* transgenic hybrid aspens may have been used more for elongation than radial growth in young trees. Because trees grow for many years, develop many branches, and form a large trunk, further study is needed to examine whether carbon allocation changes seasonally and with age in *AtGC1::AHA2* transgenic plants and whether enhancement of the photosynthetic rate by the PUMP plant's strategy improves biomass production over several years.

The *AtGC1::AHA2* transgenic aspen plants showed basically higher stomatal conductance under both the dark and light than those in WT plants (**Figure 3A**). It should be noted that enhancement of stomatal opening basically decreases water-use efficiency (WUE). Then, we calculated intrinsic WUE (iWUE; the ratio of photosynthetic rate to stomatal conductance; μmol CO_2/μmol H_2O) based on the data from **Figure 4** (Leakey et al., 2019). The results showed that iWUE values of WT, *AtGC1::AHA2* transgenic plants #3, #5, and #9 were 52.6, 28.4, 34.4, and 38.4, indicating that the iWUE in *AtGC1::AHA2* transgenic plants was 27–46% lower than that in WT. These results suggest that the *AtGC1::AHA2* transgenic plants enhanced water consumption and required much more water than WT

for normal condition. In the case of *A. thaliana*, the *AtGC1::AHA2* transgenic plants showed normal sensitivity to plant hormone abscisic acid (ABA), an inducer of stomatal closing (Wang et al., 2014). Taken together, these results suggest that stomata in the *AtGC1::AHA2* transgenic aspen plants may also show normal sensitivity to ABA and drought responses.

We introduced *Arabidopsis AHA2*, as a typical plant PM H^+-ATPase, to hybrid aspen. *AtGC1::AHA2* transgenic hybrid aspens showed higher stomatal conductance compared to WT plants in the dark (**Figure 3**). Enhancement of stomatal opening decreases WUE, indicating that the *AtGC1::AHA2* transgenic hybrid aspens require more water than WT plants for normal growth. Arabidopsis and rice overexpressing endogenous PM *H^+-ATPase* do not show higher stomatal opening under dark conditions (Wang et al., 2014; Zhang et al., 2021). These results suggest that post-translational modification of Arabidopsis AHA2 in response to light is not fine-tuned in the *AtGC1::AHA2* transgenic hybrid aspens. Because *Populus* HA1, HA2, HA3, and HA4 have high similarities to Arabidopsis AHA2 (**Figure 1**), overexpressing *Populus* endogenous PM *H^+-ATPase* in class II may overcome this problem. Further study is needed to generate transgenic hybrid aspen expressing *Populus HA*s under *AtGC1* and to characterise the stomatal properties, light requirements, drought tolerance, and mechanical resilience of the transgenic plants.

Improving the efficiency of photosynthesis can enhance biomass yield. In addition to regulation of stomatal opening, other factors determine the photosynthetic uptake of CO_2 by plants. Examples include the photosynthetic machinery, carbon flux, photorespiration, photoinhibition, assimilation partitioning, and assimilation utilisation (Dubouzet et al., 2013). Rubisco evolved under conditions characterised by much higher CO_2 levels than the current ones (Whitney et al., 2011). Therefore, many plants thrive at higher CO_2 concentrations (Smith et al., 2013). In a study of a deciduous forest, carbon enrichment increased photosynthesis by >40% (Bader et al., 2010). Also, free-air CO_2 enrichment (FACE) in field plots increased biomass yield by 15–27% in three *Populus* species (Calfapietra et al., 2003). In this study, we promoted light-responsive stomatal opening in hybrid aspens. Thus, our results are consistent with the growth-promoting effect of CO_2 concentration. Synergistic effects may be obtained by combining these growth conditions with PUMP plants.

We used *AtGC1* for expression of PM H^+-ATPase in guard cells. The *AtGC1::AHA2* transgenic hybrid aspens showed superior growth for ≥2 months after potting. However, we did not investigate plant phenotypes over the long-term. Furthermore, we grew plants in a greenhouse or indoor plant growth room, so plant growth in the field is unknown. We are planning long-term field experiments to verify the usefulness of the PUMP plant's strategy in perennial woody plants. In addition, we produced *AtGC1::AHA2* transgenic plants; in future, when PM H^+-ATPase overexpression or activation can be achieved by non-transgenic techniques – for example, genome editing and chemical treatments – such plants could enhance tree biomass.

DATA AVAILABILITY STATEMENT

The original contributions presented in the study are included in the article/**Supplementary Materials**, further inquiries can be directed to the corresponding authors.

AUTHOR CONTRIBUTIONS

ST, NT, YT, YW, NM, TT, and TK designed the experiments. ST, NT, EA, YT, YW, YH, and SN performed the experiments. ST, NT, and TK wrote the manuscript. NM and TK contributed to the original idea of the project and supervised the study and prepared the manuscript. All authors contributed to the article and approved the submitted version.

FUNDING

This work was supported in part by the Advanced Low Carbon Technology Research and Development Program of the Japan Science and Technology Agency (JPMJAL1011 to TK; JPMJAL1107 to NM and TT) and Grants-in-Aid for Scientific Research on Innovative Areas (20H05687 and 20H05910 to TK).

ACKNOWLEDGMENTS

We are grateful to Shiho Kamikabeya (Forestry and Forest Products Research Institute) and Mami Uchida and Eri Asai (Nagoya University) for technical support.

SUPPLEMENTARY MATERIAL

The Supplementary Material for this article can be found online at: https://www.frontiersin.org/articles/10.3389/fpls.2021.766037/full#supplementary-material

REFERENCES

Ando, E., and Kinoshita, T. (2018). Red light-induced phosphorylation of plasma membrane H^+-ATPase in stomatal guard cells. *Plant Physiol.* 178, 838–849. doi: 10.1104/pp.18.00544

Arango, M., Gévaudant, F., Oufattole, M., and Boutry, M. (2003). The plasma membrane proton pump ATPase: the significance of gene subfamilies. *Planta* 216, 355–365. doi: 10.1007/s00425-002-0856-8

Axelsen, K. B., and Palmgren, M. G. (1998). Evolution of substrate specificities in the P-type ATPase superfamily. *J. Mol. Evol.* 46, 84–101. doi: 10.1007/pl00006286

Axelsen, K. B., Venema, K., Jahn, T., Baunsgaard, L., and Palmgren, M. G. (1999). Molecular dissection of the C-terminal regulatory domain of the plant plasma membrane H^+-ATPase AHA2: mapping of residues that when altered give rise to an activated enzyme. *Biochemistry* 38, 7227–7234. doi: 10.1021/bi982482l

Bader, M. K.-F., Siegwolf, R., and Körner, C. (2010). Sustained enhancement of photosynthesis in mature deciduous forest trees after 8 years of free air CO_2 enrichment. *Planta* 232, 1115–1125. doi: 10.1007/s00425-010-1240-8

Baroli, I., Price, G. D., Badger, M. R., and von Caemmerer, S. (2008). The contribution of photosynthesis to the red light response of stomatal conductance. *Plant Physiol.* 146, 737–747. doi: 10.1104/pp.107.110924

Benjamini, Y., and Hochberg, Y. (1995). Controlling the false discovery rate: a practical and powerful approach to multiple testing. *J. R. Stat. Soc. Series B. Stat. Methodol.* 57, 289–300. doi: 10.1111/j.2517-6161.1995.tb02031.x

Buchwald, P. (2007). A general bilinear model to describe growth or decline time profiles. *Math. Biosci.* 205, 108–136. doi: 10.1016/j.mbs.2006.08.013

Calfapietra, C., Gielen, B., Galema, A. N. J., Lukac, M., Angelis, P. D., Moscatelli, M. C., et al. (2003). Free-air CO_2 enrichment (FACE) enhances biomass production in a short-rotation poplar plantation. *Tree Physiol.* 23, 805–814. doi: 10.1093/treephys/23.12.805

Condon, A. G., Richards, R. A., and Farquhar, G. D. (1987). Carbon isotope discrimination is positively correlated with grain yield and dry matter production in field-grown wheat. *Crop Sci.* 27, 996–1001. doi: 10.2135/cropsci1987.0011183x002700050035x

Dickson, R. E. (1989). Carbon and nitrogen allocation in trees. *Ann. Des. Sci. For.* 46, 631s–647s. doi: 10.1051/forest:198905art0142

Dubouzet, J. G., Strabala, T. J., and Wagner, A. (2013). Potential transgenic routes to increase tree biomass. *Plant Sci.* 212, 72–101. doi: 10.1016/j.plantsci.2013.08.006

Edwards, K. D., Takata, N., Johansson, M., Jurca, M., Novák, O., Hényková, E., et al. (2018). Circadian clock components control daily growth activities by modulating cytokinin levels and cell division-associated gene expression in Populus trees. *Plant Cell Environ.* 41, 1468–1482. doi: 10.1111/pce.13185

Eriksson, M. E., Israelsson, M., Olsson, O., and Moritz, T. (2000). Increased gibberellin biosynthesis in transgenic trees promotes growth, biomass production and xylem fiber length. *Nat. Biotechnol.* 18, 784–788. doi: 10.1038/77355

Falhof, J., Pedersen, J. T., Fuglsang, A. T., and Palmgren, M. (2016). Plasma membrane H+-ATPase regulation in the center of plant physiology. *Mol. Plant* 9, 323–337. doi: 10.1016/j.molp.2015.11.002

Felsenstein, J. (1985). Confidence limits on phylogenies: an approach using the bootstrap. *Evolution* 39, 783–791. doi: 10.1111/j.1558-5646.1985.tb00420.x

Fuglsang, A. T., Guo, Y., Cuin, T. A., Qiu, Q., Song, C., Kristiansen, K. A., et al. (2007). Arabidopsis protein kinase PKS5 inhibits the plasma membrane H+-ATPase by preventing interaction with 14-3-3 protein. *Plant Cell* 19, 1617–1634. doi: 10.1105/tpc.105.035626

Haruta, M., Burch, H. L., Nelson, R. B., Barrett-Wilt, G., Kline, K. G., Mohsin, S. B., et al. (2010). Molecular characterization of mutant Arabidopsis plants with reduced plasma membrane proton pump activity. *J. Biol. Chem.* 285, 17918–17929. doi: 10.1074/jbc.m110.101733

Haruta, M., Gray, W. M., and Sussman, M. R. (2015). Regulation of the plasma membrane proton pump (H+-ATPase) by phosphorylation. *Curr. Opin. Plant Biol.* 28, 68–75. doi: 10.1016/j.pbi.2015.09.005

Haruta, M., Sabat, G., Stecker, K., Minkoff, B. B., and Sussman, M. R. (2014). A peptide hormone and its receptor protein kinase regulate plant cell expansion. *Science* 343, 408–411. doi: 10.1126/science.1244454

Hayashi, M., Inoue, S., Takahashi, K., and Kinoshita, T. (2011). Immunohistochemical detection of blue light-induced phosphorylation of the plasma membrane H+-ATPase in stomatal guard cells. *Plant Cell Physiol.* 52, 1238–1248. doi: 10.1093/pcp/pcr072

Hayashi, M., Inoue, S., Ueno, Y., and Kinoshita, T. (2017). A Raf-like protein kinase BHP mediates blue light-dependent stomatal opening. *Sci. Report.* 7:45586. doi: 10.1038/srep45586

Hayashi, Y., Nakamura, S., Takemiya, A., Takahashi, Y., Shimazaki, K., and Kinoshita, T. (2010). Biochemical characterization of in vitro phosphorylation and dephosphorylation of the plasma membrane H+-ATPase. *Plant Cell Physiol.* 51, 1186–1196. doi: 10.1093/pcp/pcq078

Hori, C., Takata, N., Lam, P. Y., Tobimatsu, Y., Nagano, S., Mortimer, J. C., et al. (2020). Identifying transcription factors that reduce wood recalcitrance and improve enzymatic degradation of xylem cell wall in *Populus*. *Sci. Report.* 10:22043. doi: 10.1038/s41598-020-78781-6

Inoue, S., and Kinoshita, T. (2017). Blue light regulation of stomatal opening and the plasma membrane H+-ATPase. *Plant Physiol.* 174, 531–538. doi: 10.1104/pp.17.00166

Jones, D. T., Taylor, W. R., and Thornton, J. M. (1992). The rapid generation of mutation data matrices from protein sequences. *Bioinformatics* 8, 275–282. doi: 10.1093/bioinformatics/8.3.275

Kinoshita, T., Doi, M., Suetsugu, N., Kagawa, T., Wada, M., and Shimazaki, K. (2001). phot1 and phot2 mediate blue light regulation of stomatal opening. *Nature* 414, 656–660. doi: 10.1038/414656a

Kinoshita, T., and Shimazaki, K. (1999). Blue light activates the plasma membrane H+-ATPase by phosphorylation of the C-terminus in stomatal guard cells. *EMBO J.* 18, 5548–5558. doi: 10.1093/emboj/18.20.5548

Kumar, S., Stecher, G., and Tamura, K. (2016). MEGA7: molecular evolutionary genetics analysis version 7.0 for bigger datasets. *Mol. Biol. Evol.* 33, 1870–1874. doi: 10.1093/molbev/msw054

Kusumi, K., Hirotsuka, S., Kumamaru, T., and Iba, K. (2012). Increased leaf photosynthesis caused by elevated stomatal conductance in a rice mutant deficient in SLAC1, a guard cell anion channel protein. *J. Exp. Bot.* 63, 5635–5644. doi: 10.1093/jxb/ers216

Leakey, A. D. B., Ferguson, J. N., Pignon, C. P., Wu, A., Jin, Z., Hammer, G. L., et al. (2019). Water use efficiency as a constraint and target for improving the resilience and productivity of C3 and C4 crops. *Annu. Rev. Plant Biol.* 70, 781–808. doi: 10.1146/annurev-arplant-042817-040305

Nakagawa, T., Suzuki, T., Murata, S., Nakamura, S., Hino, T., Maeo, K., et al. (2007). Improved gateway binary vectors: high-performance vectors for creation of fusion constructs in transgenic analysis of plants. *Biosci. Biotechnol. Biochem.* 71, 2095–2100. doi: 10.1271/bbb.70216

Niittylä, T., Fuglsang, A. T., Palmgren, M. G., Frommer, W. B., and Schulze, W. X. (2007). Temporal analysis of sucrose-induced phosphorylation changes in plasma membrane proteins of Arabidopsis. *Mol. Cell. Proteomics* 6, 1711–1726. doi: 10.1074/mcp.m700164-mcp200

Palmgren, M. G. (2001). Plant plasma membrane H+-ATPases: powerhouses for nutrient uptake. *Annu. Rev. Plant Physiol.* 52, 817–845. doi: 10.1146/annurev.arplant.52.1.817

R Core Team (2018). *R: A language and environment for statistical computing*. R Found. Stat. Comput. Vienna, Austria. Available at: https://www.r-project.org/

Robinson, M. D., McCarthy, D. J., and Smyth, G. K. (2010). edgeR: a Bioconductor package for differential expression analysis of digital gene expression data. *Bioinformatics* 26, 139–140. doi: 10.1093/bioinformatics/btp616

Roelfsema, M. R. G., and Hedrich, R. (2005). In the light of stomatal opening: new insights into 'the Watergate'. *New Phytol.* 167, 665–691. doi: 10.1111/j.1469-8137.2005.01460.x

Saitou, N., and Nei, M. (1987). The neighbor-joining method: a new method for reconstructing phylogenetic trees. *Mol. Biol. Evol.* 4, 406–425. doi: 10.1093/oxfordjournals.molbev.a040454

Sharkey, T. D., and Ogawa, T. (1987). "Stomatal response to light," in *Stomatal Function*. ed. E. Zeiger (California: Stanford University Press), 195–208.

Shi, R., Wang, J. P., Lin, Y.-C., Li, Q., Sun, Y.-H., Chen, H., et al. (2017). Tissue and cell-type co-expression networks of transcription factors and wood component genes in *Populus trichocarpa*. *Planta* 245, 927–938. doi: 10.1007/s00425-016-2640-1

Shimazaki, K., Doi, M., Assmann, S. M., and Kinoshita, T. (2007). Light regulation of stomatal movement. *Plant Biol.* 58, 219–247. doi: 10.1146/annurev.arplant.57.032905.105434

Smith, A. R., Lukac, M., Hood, R., Healey, J. R., Miglietta, F., and Godbold, D. L. (2013). Elevated CO_2 enrichment induces a differential biomass response in a mixed species temperate forest plantation. *New Phytol.* 198, 156–168. doi: 10.1111/nph.12136

Takata, N., Saito, S., Saito, C. T., Nanjo, T., Shinohara, K., and Uemura, M. (2009). Molecular phylogeny and expression of poplar circadian clock genes, LHY1 and LHY2. *New Phytol.* 181, 808–819. doi: 10.1111/j.1469-8137.2008.02714.x

Takemiya, A., Sugiyama, N., Fujimoto, H., Tsutsumi, T., Yamauchi, S., Hiyama, A., et al. (2013). Phosphorylation of BLUS1 kinase by phototropins is a primary step in stomatal opening. *Nat. Commun.* 4:2094. doi: 10.1038/ncomms3094

Toda, Y., Wang, Y., Takahashi, A., Kawai, Y., Tada, Y., Yamaji, N., et al. (2016). *Oryza sativa* H+-ATPase (OSA) is involved in the regulation of dumbbell-shaped guard cells of rice. *Plant Cell Physiol.* 57, 1220–1230. doi: 10.1093/pcp/pcw070

Tuskan, G. A., DiFazio, S., Jansson, S., Bohlmann, J., Grigoriev, I., Hellsten, U., et al. (2006). The genome of black cottonwood, *Populus trichocarpa* (Torr. & Gray). *Science* 313, 1596–1604. doi: 10.1126/science.1128691

Vavasseur, A., and Raghavendra, A. S. (2005). Guard cell metabolism and CO_2 sensing. *New Phytol.* 165, 665–682. doi: 10.1111/j.1469-8137.2004.01276.x

Wang, Y., Noguchi, K., Ono, N., Inoue, S., Terashima, I., and Kinoshita, T. (2014). Overexpression of plasma membrane H+-ATPase in guard cells promotes light-induced stomatal opening and enhances plant growth. *Proc. Natl. Acad. Sci. U. S. A.* 111, 533–538. doi: 10.1073/pnas.1305438111

Wang, Y., Noguchi, K., and Terashima, I. (2011). Photosynthesis-dependent and -independent responses of stomata to blue, red and green monochromatic light: differences between the normally oriented and inverted leaves of sunflower. *Plant Cell Physiol.* 52, 479–489. doi: 10.1093/pcp/pcr005

Whitney, S. M., Houtz, R. L., and Alonso, H. (2011). Advancing our understanding and capacity to engineer nature's CO_2-sequestering enzyme, rubisco. *Plant Physiol.* 155, 27–35. doi: 10.1104/pp.110.164814

Willmer, C., and Fricker, M. (1995). *Stomata (Topics in Plant Functional Biology). 2nd Edn.* UK: Springer.

Yang, Y., Costa, A., Leonhardt, N., Siegel, R. S., and Schroeder, J. I. (2008). Isolation of a strong Arabidopsis guard cell promoter and its potential as a research tool. *Plant Methods* 4:6. doi: 10.1186/1746-4811-4-6

Zawaski, C., Ma, C., Strauss, S. H., French, D., Meilan, R., and Busov, V. B. (2012). PHOTOPERIOD RESPONSE 1 (PHOR1)-like genes regulate shoot/root growth, starch accumulation, and wood formation in *Populus*. *J. Exp. Bot.* 63, 5623–5634. doi: 10.1093/jxb/ers217

Zhang, M., Wang, Y., Chen, X., Xu, F., Ding, M., Ye, W., et al. (2021). Plasma membrane H+-ATPase overexpression increases rice yield via simultaneous enhancement of nutrient uptake and photosynthesis. *Nat. Commun.* 12:735. doi: 10.1038/s41467-021-20964-4

Conflict of Interest: YT was employed by Phytometrics, co., ltd.

The remaining authors declare that the research was conducted in the absence of any commercial or financial relationships that could be construed as a potential conflict of interest.

Publisher's Note: All claims expressed in this article are solely those of the authors and do not necessarily represent those of their affiliated organizations, or those of the publisher, the editors and the reviewers. Any product that may be evaluated in this article, or claim that may be made by its manufacturer, is not guaranteed or endorsed by the publisher.

frontiers in Plant Science

ORIGINAL RESEARCH
published: 20 December 2021
doi: 10.3389/fpls.2021.735271

Identification of Abscisic Acid-Dependent Phosphorylated Basic Helix-Loop-Helix Transcription Factors in Guard Cells of *Vicia faba* by Mass Spectrometry

Yuki Hayashi[1], Yohei Takahashi[2,3], Kohei Fukatsu[1], Yasuomi Tada[4], Koji Takahashi[1], Keiko Kuwata[3], Takamasa Suzuki[5] and Toshinori Kinoshita[1,3]**

[1]Division of Biological Science, Graduate School of Science, Nagoya University, Nagoya, Japan, [2]Cell and Developmental Biology Section, Division of Biological Sciences, University of California San Diego, San Diego, CA, United States, [3]Institute of Transformative Bio-Molecules (WPI-ITbM), Nagoya University, Nagoya, Japan, [4]Center for Gene Research, Nagoya University, Nagoya, Japan, [5]Department of Biological Chemistry, College of Bioscience and Biotechnology, Chubu University, Kasugai, Japan

OPEN ACCESS

Edited by:
Jin Chen,
University of Kentucky, United States

Reviewed by:
Tong Zhang,
Pacific Northwest National Laboratory (DOE), United States
Yun Zheng,
Kunming University of Science and Technology, China

***Correspondence:**
Yohei Takahashi
ytakahashi@itbm.nagoya-u.ac.jp
Toshinori Kinoshita
kinoshita@bio.nagoya-u.ac.jp

Specialty section:
This article was submitted to Plant Physiology, a section of the journal Frontiers in Plant Science

Received: 02 July 2021
Accepted: 24 November 2021
Published: 20 December 2021

Citation:
Hayashi Y, Takahashi Y, Fukatsu K, Tada Y, Takahashi K, Kuwata K, Suzuki T and Kinoshita T (2021) Identification of Abscisic Acid-Dependent Phosphorylated Basic Helix-Loop-Helix Transcription Factors in Guard Cells of Vicia faba by Mass Spectrometry. Front. Plant Sci. 12:735271. doi: 10.3389/fpls.2021.735271

An unknown 61 kDa protein is phosphorylated by abscisic acid (ABA)-activated protein kinase in response to ABA and binds to 14-3-3 protein in a phosphorylation-dependent manner in guard-cell protoplasts (GCPs) from *Vicia faba*. Subsequently, ABA-dependent phosphorylated proteins were identified as basic helix–loop–helix transcription factors, named ABA-responsive kinase substrates (AKSs) in GCPs from *Arabidopsis thaliana*. However, whether the 61 kDa protein in *Vicia* GCPs is an AKS is unclear. We performed immunoprecipitation of ABA-treated *Vicia* GCPs using anti-14-3-3 protein antibodies and identified several AKS isoforms in *V. faba* (VfAKSs) by mass spectrometry. The 61 kDa protein was identified as VfAKS1. Phosphoproteomic analysis revealed that VfAKSs are phosphorylated at Ser residues, which are important for 14-3-3 protein binding and monomerisation, in response to ABA in GCPs. Orthologs of AtABCG40, an ABA importer in guard cells, and CHC1, a clathrin heavy chain and a regulator of stomatal movement, also co-immunoprecipitated with 14-3-3 protein from guard cells.

Keywords: abscisic acid, Arabidopsis, bHLH transcription factor, protein phosphorylation, stomata, *Vicia faba*, 14-3-3 protein, mass spectrometry

INTRODUCTION

Stomata in plant epidermis consist of a pair of guard cells. The stomatal aperture is regulated by environmental signals—such as light, drought and CO_2—and controls CO_2 uptake for photosynthesis and transpiration (Shimazaki et al., 2007; Inoue and Kinoshita 2017). The plant hormone abscisic acid (ABA) promotes plant adaptation to drought stress by regulating gene expression, ion transport and enzyme activities (Cutler et al., 2010; Dejonghe et al., 2018). ABA induces stomatal closure to prevent water loss by transpiration (Kim et al., 2010; Munemasa et al., 2015). Analysis of the core complex of the ABA-dependent early signalling pathway showed that the ABA receptor

PYRABACTIN RESISTANCE/PYRABACTIN RESISTANCE-LIKE/REGULATORY COMPONENTS OF ABA RECEPTOR (PYR/PYL/RCAR) inhibits type 2C protein phosphatases (PP2Cs), which negatively regulate ABA signalling in the core complex in response to ABA (Ma et al., 2009; Melcher et al., 2009; Miyazono et al., 2009; Nishimura et al., 2009; Park et al., 2009). SNF1-related protein kinases 2 (SnRK2s) are activated by inhibition of PP2C and phosphorylate their substrates, such as the SLOW ANION CHANNEL-ASSOCIATED 1 anion channel in the plasma membrane, which is important for stomatal closure, and basic region/Leu zipper motif transcription factors of ABA-responsive element (ABRE)-binding proteins (AREBs)/ABRE-binding factors (Yoshida et al., 2006; Fujii et al., 2009; Geiger et al., 2009; Lee et al., 2009; Umezawa et al., 2009; Vlad et al., 2009; Kline et al., 2010).

It has been demonstrated that protein phosphorylation and phosphorylation-dependent binding of 14-3-3 protein have important roles for stomatal movements (Zhang et al., 2014; Cotelle and Leonhardt, 2016). A 61 kDa protein is phosphorylated in response to ABA according to protein-blot analysis using recombinant glutathione S-transferase (GST)-14-3-3 protein as the probe. The 61 kDa protein binds to 14-3-3 protein in a phosphorylation-dependent manner in guard-cell protoplasts (GCPs) from *V. faba* (Takahashi et al., 2007). Further characterisation suggested that the 61 kDa protein is soluble and phosphorylated by ABA-activated protein kinase (AAPK; Li and Assmann, 1996; Li et al., 2000; Takahashi et al., 2007). However, the gene encoding the 61 kDa protein is unknown.

Using a similar approach, three ABA-dependent phosphorylated proteins were found in Arabidopsis guard cells and were identified by mass spectrometry (MS) as basic helix–loop–helix (bHLH) transcription factors, named ABA-responsive kinase substrate (AKS) 1 to AKS3 (Takahashi et al., 2013). AKSs possess two 14-3-3 protein-binding sites in which Ser residues (Ser-30 and -157 in AKS1) are phosphorylated in response to ABA, resulting in binding of 14-3-3 protein. AKSs facilitate stomatal opening by stimulating transcription of genes encoding K^+_{in} channels, including *KAT1*, in guard cells by binding to their promoter regions, and their function is counteracted by ABA-dependent phosphorylation of the AKS proteins downstream of the PYR/PYL/RCAR ABA receptor (Takahashi et al., 2013). AKS1 is likely to bind to DNA as a dimer, and AKS1 dimer formation is reportedly disrupted by phosphorylation at Ser-284, -288 and-290 in AKS1 (Takahashi et al., 2016). AKSs are phosphorylated by SnRK2 kinases in response to ABA *in vivo*. (Takahashi et al., 2017). Furthermore, ABA-induced AKS1 monomerisation and detachment from the *KAT1* promoter have been reconstituted *in vitro* using recombinant PYR1 ABA receptor, HAB1 PP2C, and OST1/SnRK2.6 protein-kinase proteins, suggesting the minimal signalling mechanism from the ABA receptor to DNA (Takahashi et al., 2017). Therefore, AKSs play pivotal roles in ABA-induced repression of potassium-channel gene expression in Arabidopsis guard cells.

The *Vicia* 61 kDa protein shows similar properties to Arabidopsis AKS proteins, including ABA-induced phosphorylation and 14-3-3 protein binding (Takahashi et al., 2007). However, the 61 kDa protein in *Vicia* GCPs has not been identified because of the difficulty identifying *V. faba* proteins by mass spectrometry. To overcome this issue, we constructed an RNA-sequencing (RNA-seq) expression database of *V. faba* for identification of proteins. We subsequently purified and identified the 61 kDa protein as a bHLH transcription factor of *V. faba* (VfAKS) by MS. Furthermore, we mapped *in vivo* phosphorylation sites in VfAKS proteins in response to ABA using 1 mg of protein from *Vicia* GCPs.

MATERIALS AND METHODS

Plant Materials and Isolation of GCPs

Vicia faba (Broad bean; Ryosai Issun) was cultivated hydroponically in a greenhouse as described previously (Shimazaki et al., 1992). GCPs were isolated enzymatically from lower epidermis of 4- to 6-week-old leaves as described elsewhere (Kinoshita and Shimazaki, 1999). Protein concentrations were determined using a Bradford kit according to the manufacturer's instructions (Bio-Rad Laboratories, Hercules, CA).

Protein Blotting With a Glutathione S-Transferase–14-3-3 Protein and Immunoblotting

Protein-blot analysis was performed using a GST–GF14phi fusion protein as described (Takahashi et al., 2007; Minami et al., 2019). GF14phi is an Arabidopsis 14-3-3 protein (Kinoshita and Shimazaki, 1999). Immunoblotting was performed using an antibody for *Vicia* 14-3-3 protein (Vf14-3-3a) as described previously (Emi et al., 2001; Takahashi et al., 2007).

Co-immunoprecipitation of 14-3-3 Binding Protein and Liquid Chromatography–Tandem Mass Spectrometry

To purify 14-3-3 binding proteins, GCPs from *V. faba* (330–500 μg) in suspension buffer (5 mM MES-NaOH [pH 6.0], 10 mM KCl, 0.4 M mannitol and 1 mM $CaCl_2$) were treated with 10 μM ABA for 10 min in the dark. The 14-3-3 binding proteins were co-immunoprecipitated from the supernatant using an antibody against vf14-3-3a (Kinoshita and Shimazaki, 1999; Takahashi et al., 2013). The precipitated proteins were separated by sodium dodecyl sulphate-polyacrylamide gel electrophoresis (SDS-PAGE). The sample lanes were excised into 7 to 10 segments and subsequently subjected to in-gel digestion according to previous method (Shevchenko et al., 2006). The digested peptides were analysed by nano-liquid chromatography–tandem mass spectrometry (LC-MS/MS). Nano-LC-MS/MS was performed using a Dionex U3000 Gradient Pump (Thermo Fisher Scientific) connected to a Q-Exactive Hybrid Quadrupole-Orbitrap Mass Spectrometer (Thermo Fisher Scientific). Peptides were loaded into a trap column [L-column ODS (300 μM internal diameter [ID] × 5 mM, 5 μM particle size), CERI] and separated at 500 nl/min using a 5–40% buffer B gradient over 100 min on a nano-HPLC capillary column [NTCC-360 (100 μM I.D. × 125 mM, 3 μM particle size), Nikkyo

Technos]. The composition of the LC buffer A was 0.5% (v/v) acetic acid in water and LC buffer B was of 80% (v/v) acetonitrile, 0.5% (v/v) acetic acid. The Xcalibur 3.0.63 system (Thermo) was used to record peptide spectra over the mass range of m/z 350–1800 (70,000 resolution, 3e6 AGC, 60 ms injection time), followed by ten data-dependent high-energy collisional dissociations (HCD) MS/MS spectra generated from ten highest-intensity precursor ions (17,500 resolution, 1e5 AGC, 60 ms injection time, 27 NCE).

Peptides and proteins were identified by means of automated database searching using Proteome Discoverer v. 2.2.0.388 (Thermo Fisher Scientific) against the *V. faba* expression database. The following search parameters were employed as: peptide mass range (m/z), 350–1,800 Da; enzyme specificity, trypsin or LysC with up to two missed cleavages; and precursor ion and peptide fragment mass tolerances, ± 10 ppm and ± 0.02 Da, respectively. Peptide validation was performed using the Percolator algorithm, and only high-confidence peptides were used for peptide identification and quantification. The identified peptides in each sample lane were summarised (**Table 1**).

RNA-Seq Analysis and Construction of an Expression Database of *Vicia faba*

Total RNA was extracted from GCPs and leaves of 4- to 6-week-old *V. faba* using a TRIzol Plus RNA Purification Kit (Thermo Fisher Scientific). Three independent biological samples of each tissue type were harvested and snap-frozen in liquid nitrogen. Complementary DNA (cDNA) libraries were constructed from 1 µg of total RNA using the TruSeq RNA Sample Prep Kit v. 2 (Illumina) and sequenced on an NextSeq 500 (Illumina), yielding 13.0 to 19.8 million paired-end sequence reads per sample. Adapter sequences were trimmed with bcl2fastq2 (Illumina) and bases with low-quality scores were masked by N with the original script. In total, 288 million reads, which contained >50 non-masked bases, were used for *de novo* assembly by Trinity (Grabherr et al., 2011), yielding 134,130 contigs. The contigs were functionally annotated by BLASTX analysis against an Arabidopsis database (TAIR10). For MS determination of the amino acid sequences, these contigs were translated in six-frame and used for reference. To calculate expression levels, filtered reads were mapped to these contigs by Bowtie (Langmead et al., 2009).

In vitro Translation of *VfAKSs*

In vitro transcription and translation were performed as described previously (Nomoto and Tada, 2018). First-strand cDNA was synthesised from total RNA of GCPs using SuperScript II reverse transcriptase (Invitrogen, Carlsbad, CA) with oligo(dT)$_{12–18}$ as the primer and was used as the template for *in vitro* transcription. The PCR products were sequenced. To attach an N-terminal FLAG tag to the coding sequences of VfAKSs (VfAKS1-3), two-step PCR was carried out using the primers listed in **Supplementary Table S2**. *In vitro* transcription was carried out using a transcription kit (NUProtein). For *in vitro* translation, the resulting RNA solutions were mixed with wheat germ extract and amino acid mix (NUProtein) and incubated at 16°C for 10 h. The synthesised proteins were solubilised and separated by SDS-PAGE and detected by immunoblotting using an anti-FLAG antibody (Sigma).

Phosphoproteomic Analysis of GCPs

GCPs from *V. faba* (1.3–1.6 mg of proteins) in suspension buffer were treated with 10 µM ABA for 10 min in the dark. The GCPs were disrupted by addition of trichloroacetic acid to a final concentration of 20% (v/v), followed by centrifugation. The precipitated guard-cell proteins were suspended in digestion buffer (8 M urea, 250 mM ammonium bicarbonate, 1× PhosSTOP [Roche]). The suspensions were reduced with Tris (2-carboxyethyl) phosphine hydrochloride, alkylated by iodoacetamide and digested with LysC (FUJIFILM), followed by tryptic digestion. Digestions were performed with the enhancer ProteaseMAX™ Surfactant (Promega). The digested samples were acidified and desalted on MonoSpin C18 columns (GL Sciences). Phosphopeptides were enriched by IMAC (Agilent) from 100 µg of digested peptides and diluted with 0.1% (v/v)

TABLE 1 | List of bHLH DNA-binding superfamily proteins in Vicia GCPs.

Accession	Protein length (aa)	Estimated molecular mass (kDa)	14–3-3 IP (PSMs)						
			Experiment 1		Experiment 2		Experiment 3		Number of unique peptides
			−ABA	+ABA	−ABA	+ABA	−ABA	+ABA	
VfAKS1	423	47.7	–	37	3	32	–	20	5
VfAKS2	442	48.0	–	12	1	8	–	7	1
VfAKS3	384	41.9	–	3	–	3	–	6	2
VfAKS4	326	35.4	2	22	4	22	–	13	6
VfAKS5	190	21.5	–	2	–	4	–	–	1
VfAKS6	376	42.5	–	–	–	–	–	–	–
VfAKS7	345	39.2	–	–	–	–	–	–	–

Protein length (number of amino acid) and estimated molecular mass of VfAKSs are listed. Peptide spectrum matches (PSMs), the total number of identified peptide spectra matched for the protein, of each protein in the immunoprecipitation using the antibody against Vicia 14–3-3a are indicated. –: not detected. Number of unique peptides from each VfAKSs in the immunoprecipitation of Experiment 1 is listed.

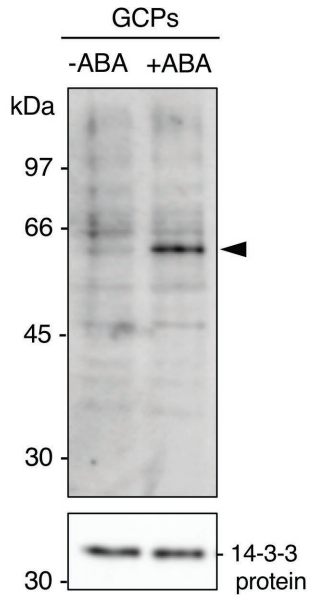

FIGURE 1 | Detection of the 61 kDa protein in guard cell protoplasts (GCPs) from *Vicia faba* in response to ABA. ABA-dependent binding of 14-3-3 protein to the 61 kDa protein. GCPs were treated with 0.5% dimethyl sulphoxide as a solvent (–ABA) or 10 μM ABA (+ABA) and 20 μg of guard-cell proteins were separated by sodium dodecyl sulphate-polyacrylamide gel electrophoresis. Upper panel: 61 kDa protein detected by protein blotting using GST-14-3-3 protein as the probe. Lower panel: 14-3-3 protein detected by immunoblotting with an anti-14-3-3 antibody as the loading control. Arrowhead, the 61 kDa protein. Numbers at left indicate molecular weight markers.

TFA, 2% (v/v) AcCN in distilled water for nano-LC–MS/MS. Nano-LC–MS/MS was performed as described above.

Peptides and proteins were identified by means of automated database searching using Proteome Discoverer 2.2.0.388 (Thermo Fisher Scientific) against an expression database of *V. faba*. The following search parameters were employed as: peptide mass range (m/z), 350–1,800 Da; enzyme specificity, trypsin or LysC with up to two missed cleavages; precursor ion and peptide fragment mass tolerances, ± 10 ppm and ± 0.02 Da, respectively; static modification, carbamidomethyl (Cys); and dynamic modifications, phosphorylation (Ser, Thr and Tyr) and oxidation (Met). Peptide validation was performed using the Percolator algorithm, and only high-confidence peptides were used for peptide identification and quantification. The resulting dataset, which included information on annotated sequences, modifications, master protein accession, peptide spectrum matches (PSMs) and the total number of identified peptide spectra, for each identified peptide, was imported into Microsoft Excel. Using the filter function of Excel, peptides with no phosphorylated residues were excluded from the list. PSMs, the total number of identified peptide spectra matched for the protein, of each protein were compared between the datasets.

Accession Numbers

Sequence data can be found in the Arabidopsis genome database TAIR10 under the following accession numbers: AKS1 (AT1G51140.1), AKS2 (AT1G05805.1), AKS3 (AT2G42280.1), AKS4 (AT2G43140.1), AKS5 (AT4G09180.1), AKS6 (AT1G35460.1), AtABCG40 (AT1G15520) and CHC1 (AT3G11130).

Data Availability

RNA-seq data supporting the findings of this work have been deposited in the DNA Data Bank of Japan (DDBJ) under accession number DRA012337. The raw MS data have been deposited in the ProteomeXchange Consortium *via* the PRIDE partner repository under accession numbers, PXD027057 for immunoprecipitation and PXD027058 for phosphoproteomics.

RESULTS

The 61 kDa Protein Bound to the 14-3-3 Protein From Guard Cells

GCPs from *V. faba* were treated with ABA at 10 μM for 10 min in the dark. A 61 kDa protein was confirmed as a 14-3-3 protein-binding protein in response to ABA by protein blot using a recombinant GST-14-3-3 fusion protein (**Figure 1**; Takahashi et al., 2007). GST alone did not show a prominent 61 kDa band (Kinoshita et al., 2003; Takahashi et al., 2007). Therefore, 14-3-3 protein specifically binds to the 61 kDa protein in an ABA-dependent manner.

AKS Orthologs in *V. faba*

In Arabidopsis, ABA-dependent phosphorylated proteins were identified as bHLH transcription factors, named ABA-responsive kinase substrate 1 (AKS1) to AKS3 in GCPs (Takahashi et al., 2013). AKSs possess two 14-3-3 protein-binding sites. However, there is no sequence information regarding AKSs in *V. faba*. Therefore, we performed RNA-seq analysis using GCPs and leaves from *V. faba* and constructed an expression database of *V. faba* by *de novo* assembly. At least seven AKS-like proteins, which possessed 14-3-3 binding sites and a bHLH domain, as well as Arabidopsis AKSs were expressed in *V. faba*. We named these proteins VfAKS1 to VfAKS7 (**Figure 2A**; **Table 1**). In addition, we identified AT2G43140, AT4G09180 and AT1G35460 as AKS homologs in *A. thaliana,* and designated them AKS4, AKS5 and AKS6, respectively (**Figure 2A**). **Figure 2B** shows a phylogenetic analysis based on the full-length amino acid sequences of AKSs from *V. faba* and *A. thaliana*. VfAKS1 and VfAKS2 were similar to AKS1, and VfAKS3 to AKS3. All possessed two 14-3-3 protein-binding motifs at the N-terminus and middle of the sequence. Previous *in vitro* experiments suggested that phosphorylation of AKS1 at Ser-284, −288 and −290 induces monomerisation of AKS1 and inhibits its transactivation activity (Takahashi et al., 2017). VfAKS1, VfAKS2, VfAKS3 and AKS3 also possess Ser or Thr upstream of the bHLH domain (**Figures 2A,B**). In contrast, VfAKS5, AKS5 and AKS6 lack the corresponding Ser or Thr and their sequences were shorter than other AKSs. Of these, VfAKS5 was the shortest and lacked the middle 14-3-3 binding motif. VfAKS4 was similar to AKS2 and AKS4. In contrast, no ortholog of VfAKS6 and VfAKS7 lacking the 14-3-3

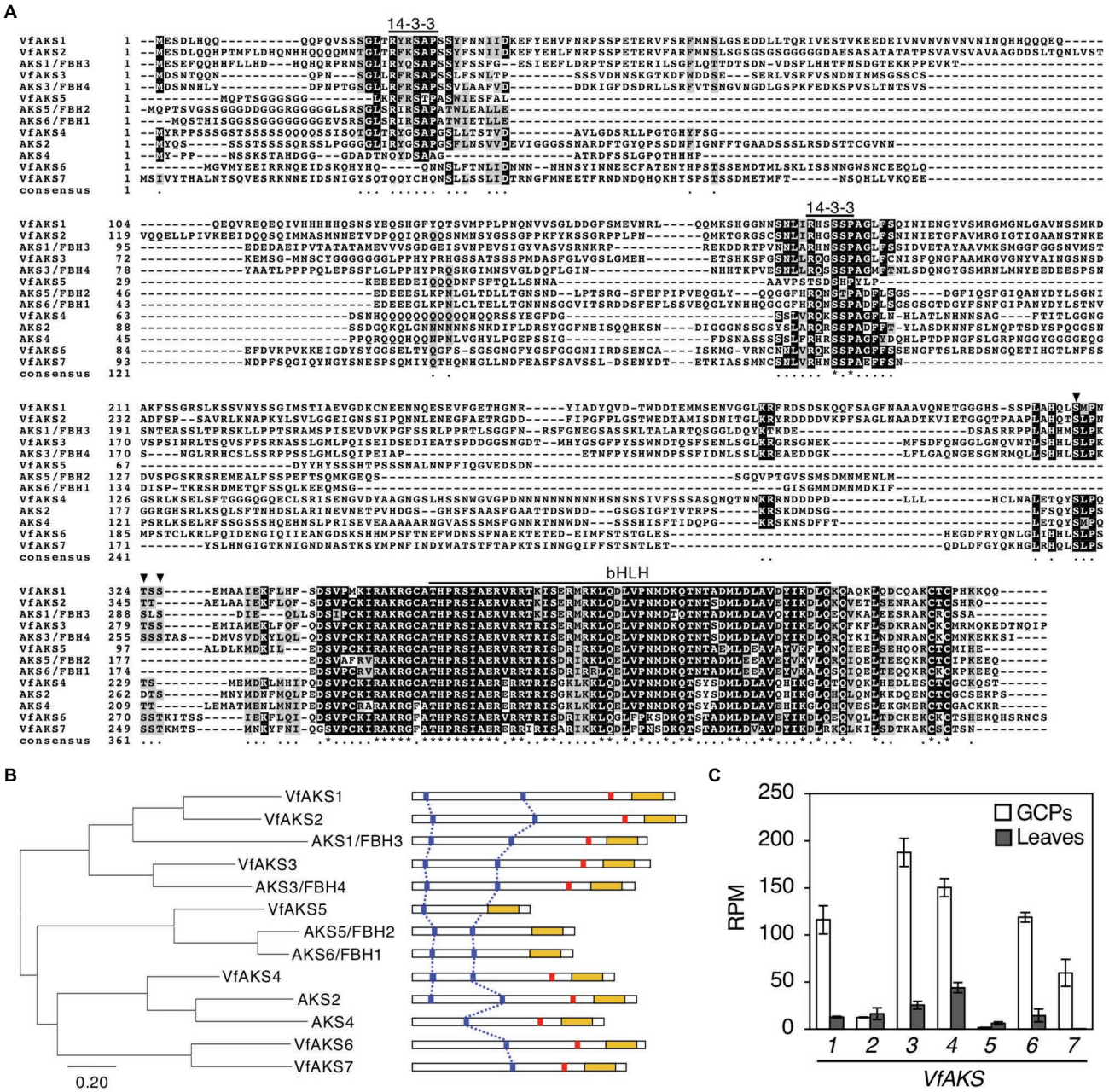

FIGURE 2 | Evolutionary analysis of VfAKSs and AtAKSs. (A), Alignment of AKSs from *Vicia faba* (VfAKS1–VfAKS7) and *Arabidopsis thaliana* (AKS1–AKS6) generated using ClustalW (Thompson et al., 1994) with manual modification. Black boxes indicate highly conserved residues. Grey boxes indicate conservative residues. Consensus symbols "*" and "." indicate perfect alignment and a site belonging to a group exhibiting weak similarity, respectively. Binding motifs for 14-3-3 protein (RXXpSXP) and bHLH motifs are indicated by lines. Phosphorylation sites that induce monomerisation of AKS1 and inhibit the transactivation activity of AKS1 are indicated by arrowheads. Dashes indicate gaps introduced to enable optimal sequence alignment. **(B)**, Phylogenetic tree of AKSs from *V. faba* and *A. thaliana.* Alignment for the phylogenetic tree was performed as described in **(A)**. The phylogenetic tree with the highest log likelihood (9768.99) was created by the maximum-likelihood method and JTT matrix-based model with MEGAX software. Structures of the AKS proteins are shown at right. 14-3-3 protein-binding motifs (blue lines), phosphorylation sites leading to inhibition of monomerisation (red lines) and bHLH domains (yellow boxes) are indicated. **(C)**, Expression levels of VfAKSs assayed by RNA-seq in GCPs and leaves. RPM values of VfAKS1–VfAKS7 are shown ($n = 3$, means ± SD).

protein-binding motif at the N-terminus was found in *A. thaliana*. AKS1, AKS3, AKS5 and AKS6 are identical to FLOWERING BHLH3 (FBH3), FBH4, FBH2 and FBH1, respectively (Ito et al., 2012).

Next, we investigated the expression of VfAKS1–VfAKS7 in GCPs and leaves based on RNA-seq data. The expression levels of VfAKS1, VfAKS3, VfAKS4, VfAKS6 and VfAKS7 were higher in GCPs compared to leaves (**Figure 2C**). This is consistent

with a report that the response is specific to guard cells and is not found in other cell types, such as mesophyll cell protoplasts and root and leaf cells (Takahashi et al., 2007). In addition, previous promoter GUS assay of *AKS1* in *Arabidopsis thaliana* also revealed preferential expression of *AKS1* in guard cells and vascular tissues (Takahashi et al., 2013).

Identification of Proteins Co-immunoprecipitated With 14-3-3 Protein by MS

ABA-dependent 14-3-3 binding proteins were isolated by co-immunoprecipitation using anti-14-3-3 protein antibodies from Arabidopsis GCPs (Takahashi et al., 2013). Next, we performed immunoprecipitation of ABA-treated *Vicia* GCPs using anti-14-3-3 protein antibodies against *Vicia* 14-3-3a (Emi et al., 2001) and LC–MS/MS using gel segments after resolving the immunoprecipitate by SDS-PAGE. Immunoprecipitates from control and ABA-treated GCPs contained >507 proteins, including those annotated as 14-3-3 proteins, plasma membrane H^+-ATPases, vacuolar ATP synthase subunit A, pleiotropic drug resistance 12 and clathrin heavy chain (**Supplementary Table S1**). The number of peptides from VfAKS1–VfAKS5 increased in response to ABA (**Table 1**).

The 61 kDa Protein Is the bHLH DNA-Binding Superfamily Protein VfAKS1

VfAKS1–VfAKS5 immunoprecipitated with GCPs, suggesting that one may be the 61 kDa protein. However, the estimated molecular masses of VfAKS1–VfAKS5 based on the amino acid sequences were < 61 kDa (**Table 1**). Next, we synthesised FLAG-VfAKS1, VfAKS2 and VfAKS3, which had high estimated molecular masses (**Table 1**), by *in vitro* translation assay and determined their molecular masses by SDS-PAGE. As shown in **Figure 3A**, full-length CDSs of *VfAKSs* were amplified by RT-PCR from cDNAs of *Vicia* GCPs. Finally, we detected FLAG-VfAKS1 (61.4 kDa), FLAG-VfAKS2 (54.3 kDa) and FLAG-VfAKS3 (43.9 kDa) proteins by Western blotting (**Figure 3B**). The FLAG tag is around 1.0 kDa. These results indicated that the 61 kDa protein is VfAKS1.

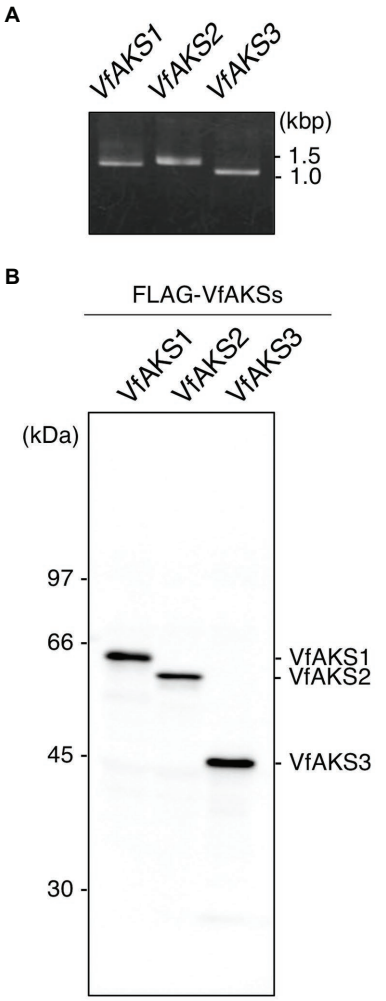

FIGURE 3 | *In vitro* translation of VfAKSs. **(A)**, First PCR of *VfAKSs* for *in vitro* translation. The cording sequences of *VfAKSs* were amplified with adaptor sequences for *in vitro* translation using specific primers. **(B)**, Western blotting of FLAG-VfAKSs. VfAKSs were expressed with a FLAG tag using an *in vitro* translation system and detected with anti-FLAG antibody. Numbers at left indicate molecular weight markers.

Phosphoproteomic Analyses Revealed ABA-Dependent Phosphorylation Sites of the VfAKSs

To confirm ABA-dependent phosphorylation of VfAKSs, we performed phosphoproteomic analyses using GCPs treated with ABA. We detected 7,459 phosphopeptides belonging to 2,938 proteins. Of these, 929 phosphopeptides (12.5%) showed at least 2-fold increase in ABA-treated GCPs compared to ABA-untreated GCPs, whereas 489 phosphopeptides (6.6%) showed at least 2-fold decrease.

We detected multiple phosphorylation sites in VfAKS1, VfAKS2, VfAKS3, VfAKS4 and VfAKS6 (**Table 2**). The conserved Ser residues in the 14-3-3 protein-binding motifs (**Figure 2A**; **Table 2**; single asterisk) were phosphorylated in response to ABA (in the case of VfAKS1, Ser-23 and Ser-177). Moreover, ABA-dependent phosphorylation of the conserved Ser or Thr leading to monomerisation and inactivation of transactivation in AKS1 (Takahashi et al., 2016) was observed (**Table 2**; double asterisks; in the case of VfAKS2, Ser-341 and Thr-345). Ser-182 in VfAKS3 was phosphorylated in response to ABA. Interestingly, Ser-47 of VfAKS1 and Ser-57 of VfAKS2, corresponding to Ser-52 of AKS1, were highly phosphorylated in untreated and ABA-treated GCPs.

Other 14-3-3-Binding Proteins Were Also Phosphorylated in Response to ABA

Interestingly, we detected ABA-dependent phosphorylation of proteins annotated as pleiotropic drug resistance 12 (PDR12) and clathrin heavy chain, both of which immunoprecipitated with 14-3-3 protein (**Table 3**; **Supplementary Table S1**).

TABLE 2 | List of phosphorylation sites of VfAKSs detected by phosphoproteomic analyses.

	Phospho-site	PSMs			
		Experiment 1		Experiment 2	
		−ABA	+ABA	−ABA	+ABA
VfAKS1	S23*	5	44	8	31
	S47	43	46	51	40
	S63	11	8	20	12
	S177*	–	24	–	15
	S294	1	1	–	–
VfAKS2	S33*	–	11	–	8
	S57	17	16	13	10
	S341**	–	8	–	6
	T345**	–	2	–	–
VfAKS3	S19*	–	9	–	11
	S19 or S22 (S23)*	–	9	–	8
	S22 (or S23)*	–	3	–	2
	S182	4	13	4	15
	S275**	–	7	–	3
VfAKS4	S33*	42	66	41	73
	S225**	–	2	–	–
VfAKS6	S266**	–	8	–	5
	S266 or S271**	–	–	–	1
	S271**	–	–	–	3

PSMs of each phosphopeptides and phosphorylation sites are indicated.
**represent the phosphorylation site in 14-3-3 binding sites.*
***represent the phosphorylation sites corresponding to the sites for monomerisation and inactivation of transactivation in AKS1. –: not detected.*

TABLE 3 | List of phosphorylation sites of VfABCG40 and VfCHC1 detected by phosphoproteomic analyses.

	Phosphosite	PSMs			
		Experiment 1		Experiment 2	
		−ABA	+ABA	−ABA	+ABA
VfABCG40	S12	4	–	3	4
	S17 or S18 or T19	23	33	41	43
	S30 or S32 or S33	152	210	121	152
	T51	26	30	20	26
	T62 or S64	71	114	61	81
	S804	1	1	1	1
	S812 or S814 or S815	4	1	2	4
VfCHC1	T67	2	6	2	4

PSMs of each phosphopeptides and phosphorylation sites are indicated. -: not detected.

Arabidopsis AtPDR12 encodes ATP-binding cassette (ABC) transporter (ABCG40), which is an ABA importer expressed in guard cells. We designated the ortholog in *V. faba* as VfABCG40. VfABCG40 showed high sequence similarity (72%) with AtABCG40. The phosphorylation sites of VfABCG40 detected by phosphoproteomics were located at the N- and C-termini (**Figure 4A**). Most phospho-Ser and -Thr at the N-terminus were conserved in Arabidopsis ABCG40, but those at the C-terminus were not. At the N-terminus sites, phosphorylation of Ser-30/ Ser-32/ Ser-33 and Thr-62/Ser-64 was slightly upregulated in response to ABA (**Table 3**).

Clathrin heavy chain protein showed high sequence similarity (91%) with Arabidopsis clathrin heavy chain 1 (CHC1; Blackbourn and Jackson, 1996), and we designated its ortholog in *V. faba* as VfCHC1. The phosphorylation site at Thr-67 in VfCHC1 is conserved in AtCHC1 (**Figure 4B**). ABA induced phosphorylation of Thr-67 (**Table 3**).

DISCUSSION

In the present study, RNA-seq-based transcriptome data and targeted 14-3-3 protein-binding protein analyses using highly purified GCPs from *V. faba* revealed that the unknown 61 kDa protein, which is rapidly phosphorylated in response to ABA in *Vicia* guard cells (Takahashi et al., 2007), is a bHLH transcription factor, named *V. faba* ABA-responsive kinase substrate (VfAKS; **Figure 2**). The AKS family was originally identified in *A. thaliana* as a substrate of ABA-activated OST1/SnRK2 protein kinases (Takahashi et al., 2013; Wang et al., 2013). We identified seven AKS-family genes in *V. faba* and demonstrated rapid ABA-induced AKS phosphorylation and binding to 14-3-3 proteins in guard cells.

VfAKS1 and VfAKS2 had similar SDS-PAGE mobilities to the 61 kDa protein (**Figures 1**, **3**), although their theoretical molecular weights were 47.7 and 48.0 kDa, respectively. The amino acid sequences of these proteins might affect their SDS-PAGE mobilities. Based on the mobility of 61.4 kDa recombinant FLAG-VfAKS1 protein (**Figure 3B**), VfAKS1 is likely to be the 61 kDa protein of Takahashi et al. (2007). In that study, 43 and 39 kDa proteins were also identified as 14-3-3 protein-binding proteins in response to ABA in *Vicia* guard cells (Takahashi et al., 2007). The molecular mass of FLAG-VfAKS3 by SDS-PAGE was 43.9 kDa, suggesting that the previously reported 43 kDa protein is VfAKS3.

MS identified *in vivo* ABA-dependent phosphorylation sites of VfAKS-family members, including VfAKS2 Ser-341 and Thr-345 (**Table 2**), corresponding to Arabidopsis AKS1 (AtAKS1) Ser-284 and -288. *In vitro*, AtAKS1 phosphorylation at these serine residues is mediated by OST1/SnRK2.6 protein kinase and inhibits DNA binding by AtAKS1 by disrupting AtAKS1 dimer formation (Takahashi et al., 2016). This may be the mechanism by which ABA represses the expression of genes, including Arabidopsis *KAT1* inward-rectifying potassium channel, which functions in stomatal opening in guard cells (Takahashi et al., 2017). However, it is unclear whether these phosphorylations are induced in response to ABA in plant cells. Our results provide *in vivo* evidence supporting the proposed model of phosphorylation-dependent control of AKS transcription factor function (**Table 2**). In addition, amino acid alignment analyses suggest that these phosphorylation sites are conserved in many AKS-family members in *A. thaliana* and *V. faba* (**Figure 2A**). Note that we did not detect phosphorylation of VfAKS1 at Ser-320 and Thr-324, corresponding to AtAKS1

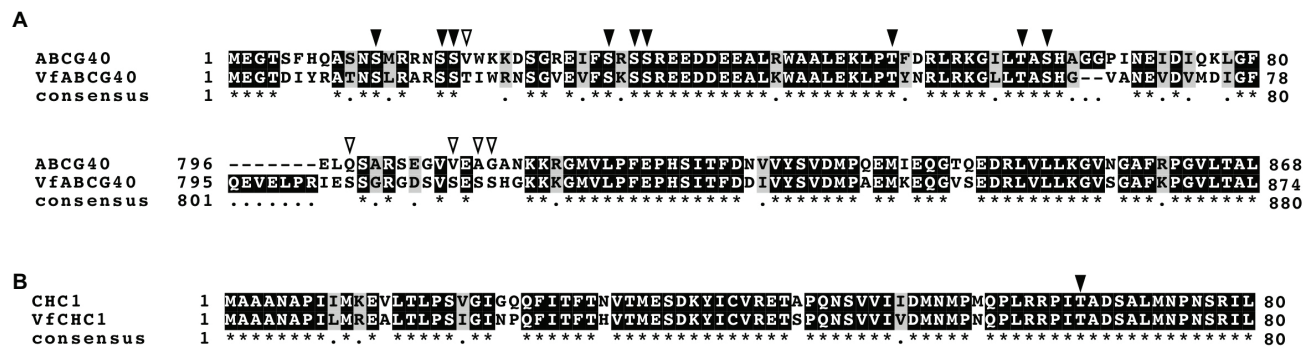

FIGURE 4 | Alignment of ABCG40 and CHC1 from *Vicia faba* and *Arabidopsis thaliana*. **(A)**, Alignment of ABCG40s from *V. faba* (VfABCG40) and *A. thaliana* (AtABCG40) generated with ClustalW (Thompson et al., 1994) using full-length amino acid sequences (VfABCG40 1430 aa and AtABCG40 1423 aa). Black boxes indicate highly conserved residues. Grey box indicates conservative residues. Consensus symbols "*" and "." indicate perfect alignment and a site belonging to a group exhibiting weak similarity, respectively. Phosphorylation sites detected by phosphoproteomic analysis are indicated by arrowheads; black arrowheads, conserved residues in both *A. thaliana* and *V. faba*; and open arrowheads, non-conserved residues. **(B)**, Alignment of CHC1s from *V. faba* (VfCHC1) and *A. thaliana* (AtCHC1) was generated with ClustalW (Thompson et al., 1994) using full-length amino acid sequences (VfCHC1 1701 aa and AtCHC1 1705 aa). Others are the same as **(B)**.

Ser-284 and Ser-288, despite sufficient phosphopeptides from the 14-3-3 binding site (**Table 2**). Moreover, phosphoproteomic analyses revealed new phosphorylation residues in GCPs from *V. faba*. Ser-47 of VfAKS1 and Ser-57 of VfAKS2, phosphorylation of which was detected in control and ABA-treated GCPs, were conserved in AKS1 (**Table 2**; **Figure 2A**). Other physiological signals may regulate phosphorylation of these residues.

In this study, we identified >500 proteins that co-immunoprecipitated with 14-3-3 proteins in GCPs from *V. faba*. Of them, orthologs of Arabidopsis ABCG40 and CHC1 in *V. faba* were detected as phosphorylated proteins by phosphoproteomic analysis. Arabidopsis ABCG40 expressed in stomatal guard cells imports ABA, synthesised in the vascular bundle in response to drought stress, into guard cells, leading to stomatal closure (Kang et al., 2010). In this study, ABA-dependent phosphorylation of ABCG40 at Ser-30/Ser-32/Ser-33 and Thr-62/Ser-64, corresponding to Ser-30/Ser-32/Ser-33 and Thr-62/Ser-64 in AtABCG40, was slightly upregulated in response to ABA in 10 min (**Figure 4**; **Table 3**). The function of CHC1 in stomatal movement has been investigated using *A. thaliana*. Plessis et al. (2011) isolated a *hot ABA-deficient suppressor 1* (*has1*) suppressor mutant of *ABA deficient3* (*aba3-1*) by infrared imaging. The *has1* mutant showed a closed stomatal phenotype in response to a low concentration of exogenous ABA and drought tolerance. Larson et al. (2017) identified *CHC1* as responsible for *has1* mutant and found that *chc1* and *chc2* affect endocytosis, exocytosis and stomatal movement. To our knowledge, this is the first report that CHC1 is phosphorylated in response to ABA. Further investigation is needed of the roles of ABA-dependent phosphorylation of ABCG40 and CHC1.

V. faba is used for research on stomatal movement (Willmer and Fricker, 1996). However, the limited genomic information on *V. faba* because of its large genome (13 Gb; Kaur et al., 2012) had hampered identification of the 61 kDa protein in *Vicia* GCPs by MS (Takahashi et al., 2007). We constructed an expression database of *V. faba* from RNA-seq data and identified VfAKS1 as the 61 kDa protein. Furthermore, the database allows phosphoproteomic analysis of *Vicia* GCPs in response to various signals.

DATA AVAILABILITY STATEMENT

The datasets presented in this study can be found in online repositories. The names of the repository/repositories and accession number(s) can be found at: http://www.proteomexchange.org/, PXD027057 and PXD027058, and DNA Data Bank of Japan (https://www.ddbj.nig.ac.jp/index-e.html) under accession number DRA012337.

AUTHOR CONTRIBUTIONS

YH, YoT, and TK designed the experiments and wrote the manuscript. YH, YoT, KF, YaT, KT, KK, TS, and TK performed the experiments. All authors reviewed the manuscript.

FUNDING

This research was supported by the Grants-in-Aid for Scientific Research from MEXT (15H05956, 20H05687 and 20H05910 to TK) and PRESTO, Japan Science and Technology Agency (Grant Number JPMJPR21D8 to YoT).

SUPPLEMENTARY MATERIAL

The Supplementary Material for this article can be found online at: https://www.frontiersin.org/articles/10.3389/fpls.2021.735271/full#supplementary-material

REFERENCES

Blackbourn, H. D., and Jackson, A. P. (1996). Plant clathrin heavy chain: sequence analysis and restricted localisation in growing pollen tubes. *J. Cell Sci.* 109, 777–786. doi: 10.1242/jcs.109.4.777

Cotelle, V., and Leonhardt, N. (2016). 14-3-3 proteins in guard cell signaling. *Front. Plant Sci.* 6:1210. doi: 10.3389/fpls.2015.01210

Cutler, S. R., Rodriguez, P. L., Finkelstein, R. R., and Abrams, S. R. (2010). Abscisic acid: emergence of a core signaling network. *Annu. Rev. Plant Biol.* 61, 651–679. doi: 10.1146/annurev-arplant-042809-112122

Dejonghe, W., Okamoto, M., and Cutler, S. R. (2018). Small molecule probes of ABA biosynthesis and signaling. *Plant Cell Physiol.* 59, 1490–1499. doi: 10.1093/pcp/pcy126

Emi, T., Kinoshita, T., and Shimazaki, K. (2001). Specific binding of vf14-3-3a isoform to the plasma membrane H^+-ATPase in response to blue light and fusicoccin in guard cells of broad bean. *Plant Physiol.* 125, 1115–1125. doi: 10.1104/pp.125.2.1115

Fujii, H., Chinnusamy, V., Rodrigues, A., Rubio, S., Antoni, R., Park, S. Y., et al. (2009). *In vitro* reconstitution of an abscisic acid signaling pathway. *Nature* 462, 660–664. doi: 10.1038/nature08599

Geiger, D., Scherzer, S., Mumm, P., Stange, A., Marten, I., Bauer, H., et al. (2009). Activity of guard cell anion channel SLAC1 is controlled by drought-stress signaling kinase- phosphatase pair. *Proc. Natl. Acad. Sci. U. S. A.* 106, 21425–21430. doi: 10.1073/pnas.0912021106

Grabherr, M. G., Haas, B. J., Yassour, M., Levin, J. Z.,Thompson, D. A., Amit, I., et al. (2011). Full-length transcriptome assembly from RNA-Seq data without a reference genome. *Nat. Biotechnol.* 29, 644–652. doi: 10.1038/nbt.1883

Inoue, S., and Kinoshita, T. (2017). Blue light regulation of stomatal opening and the plasma membrane H+-ATPase. *Plant Physiol.* 174, 531–538. doi: 10.1104/pp.17.00166

Ito, S., Song, Y. H., Josephson-Day, A. R., Miller, R. J., Breton, G., Olmstead, R. G., et al. (2012). FLOWERING BHLH transcriptional activators control expression of the photoperiodic flowering regulator CONSTANS in Arabidopsis. *Proc. Natl. Acad. Sci. U. S. A.* 109, 3582–3587. doi: 10.1073/pnas.1118876109

Kang, J., Hwang, J. U., Lee, M., Kim, Y. Y., Assmann, S. M., Martinoia, E., et al. (2010). PDR-type ABC transporter mediates cellular uptake of the phytohormone abscisic acid. *Proc. Natl. Acad. Sci. U. S. A.* 107, 2355–2360. doi: 10.1073/pnas.0909222107

Kaur, S., Pembleton, L. W., Cogan, N. O., Savin, K. W., Leonforte, T., and Paull, J. (2012). Transcriptome sequencing of field pea and faba bean for discovery and validation of SSR genetic markers. *BMC Genomics* 13:104. doi: 10.1186/1471- 2164-13-104

Kim, T. H., Böhmer, M., Hu, H., Nishimura, N., and Schroeder, J. I. (2010). Guard cell signal transduction network: advances in understanding abscisic acid, CO_2, and Ca^{2+} signaling. *Annu. Rev. Plant Biol.* 61, 61–591. doi: 10.1146/annurev-arplant-042809-112226

Kinoshita, T., Emi, T., Tomonaga, M., Sakamoto, K., Shigenaga, A., Doi, M., et al. (2003). Blue light- and phosphorylation-dependent binding of a 14-3-3 protein to phototropins in stomatal guard cells of broad bean. *Plant Physiol.* 133, 1453–1463. doi: 10.1104/pp.103.029629

Kinoshita, T., and Shimazaki, K. (1999). Blue light activates the plasma membrane H^+-ATPase by phosphorylation of the C-terminus in stomatal guard cells. *EMBO J.* 18, 5548–5558. doi: 10.1093/emboj/18.20.5548

Kline, K. G., Barrett-Wilt, G. A., and Sussman, M. R. (2010). *In planta* changes in protein phosphorylation induced by the plant hormone abscisic acid. *Proc. Natl. Acad. Sci. U. S. A.* 107, 15986–15991. doi: 10.1073/pnas.1007879107

Langmead, B., Trapnell, C., Pop, M., and Salzberg, S. L. (2009). Ultrafast and memory-efficient alignment of short DNA sequences to the human genome. *Genome Biol.* 10:R25. doi: 10.1186/gb-2009-10-3-r25

Larson, E. R., Zelm, E. V., Roux, C., Marion-Poll, A., and Blatt, M. R. (2017). Clathrin heavy chain subunits coordinate endo- and exocytic traffic and affect stomatal movement. *Plant Physiol.* 175, 708–720. doi: 10.1104/pp.17.00970

Lee, S. C., Lan, W., Buchanan, B. B., and Luan, S. (2009). A protein kinase-phosphatase pair interacts with an ion channel to regulate ABA signaling in plant guard cells. *Proc. Natl. Acad. Sci. U. S. A.* 106, 21419–21424. doi: 10.1073/pnas.0910601106

Li, J., and Assmann, S. M. (1996). An abscisic acid-activated and calcium-independent protein kinase from guard cells of fava bean. *Plant Cell* 8, 2359–2368. doi: 10.2307/3870474

Li, J., Wang, X. Q., Watson, M. B., and Assmann, S. M. (2000). Regulation of abscisic acid-induced stomatal closure and anion channels by guard cell AAPK kinase. *Science* 287, 300–303. doi: 10.1126/science.287.5451.300

Ma, Y., Szostkiewicz, I., Korte, A., Moes, D., Yang, Y., Christmann, A., et al. (2009). Regulators of PP2C phosphatase activity function as abscisic acid sensors. *Science* 324, 1064–1068. doi: 10.1126/science.1172408

Melcher, K., Ng, L. M., Zhou, X. E., Soon, F. F., Xu, Y., Suino-Powell, K. M., et al. (2009). A gate-latch-lock mechanism for hormone signalling by abscisic acid receptors. *Nature* 462, 602–608. doi: 10.1038/nature08613

Minami, A., Takahashi, K., Inoue, S., Tada, Y., and Kinoshita, T. (2019). Brassinosteroid induces phosphorylation of the plasma membrane H+-ATPase during hypocotyl elongation in Arabidopsis thaliana. *Plant Cell Physiol.* 60, 935–944. doi: 10.1093/pcp/pcz005

Miyazono, K., Miyakawa, T., Sawano, Y., Kubota, K., Kang, H. J., Asano, A., et al. (2009). Structural basis of abscisic acid signalling. *Nature* 462, 609–614. doi: 10.1038/nature08583

Munemasa, S., Hauser, F., Park, J., Waadt, R., Brandt, B., and Schroeder, J. I. (2015). Mechanisms of abscisic acid-mediated control of stomatal aperture. *Curr. Opin. Plant Biol.* 28, 154–162. doi: 10.1016/j.pbi.2015.10.010

Nishimura, N., Hitomi, K., Arvai, A. S., Rambo, R. P., Hitomi, C., Cutler, S. R., et al. (2009). Structural mechanism of abscisic acid binding and signaling by dimeric PYR1. *Science* 326, 1373–1379. doi: 10.1126/science.1181829

Nomoto, M., and Tada, Y. (2018). Cloning-free template DNA preparation for cell-free protein synthesis via two-step PCR using versatile primer designs with short 3′-UTR. *Genes Cells* 23, 46–53. doi: 10.1111/gtc.12547

Park, S. Y., Fung, P., Nishimura, N., Jensen, D. R., Fujii, H., Zhao, Y., et al. (2009). Abscisic acid inhibits type 2C protein phosphatases via the PYR/PYL family of START proteins. *Science* 324, 1068–1071. doi: 10.1126/science.1173041

Plessis, A., Cournol, R., Effroy, D., Silva, P. V., Botran, L., Kraepiel, Y., et al. (2011). New ABA-hypersensitive Arabidopsis mutants are affected in loci mediating responses to water deficit and *Dickeya dadantii* infection. *PLoS One* 6:e20243. doi: 10.1371/journal.pone.0020243

Shevchenko, A., Tomas, H., Havli, J., Olsen, J. V., and Mann, M. (2006). In-gel digestion for mass spectrometric characterization of proteins and proteomes. *Nat. Protoc.* 1, 2856–2860. doi: 10.1038/nprot.2006.468

Shimazaki, K., Doi, M., Assmann, S. M., and Kinoshita, T. (2007). Light regulation of stomatal movement. *Annu. Rev. Plant Biol.* 58, 219–247. doi: 10.1146/annurev.arplant.57.032905.105434

Shimazaki, K., Kinoshita, T., and Nishimura, M. (1992). Involvement of calmodulin and calmodulin-dependent myosin light chain kinase in blue light-dependent H^+ pumping by guard cell protoplasts from *Vicia faba* L. *Plant Physiol.* 99, 1416–1421. doi: 10.1104/pp.99.4.1416

Takahashi, Y., Ebisu, Y., Kinoshita, T., Doi, M., Okuma, E., Murata, Y., et al. (2013). bHLH transcription factors that facilitate K^+ uptake during stomatal opening are repressed by abscisic acid through phosphorylation. *Sci. Signal.* 6:ra48. doi: 10.1126/scisignal.2003760

Takahashi, Y., Ebisu, Y., and Shimazaki, K. (2017). Reconstitution of abscisic acid signaling from the receptor to DNA via bHLH transcription factors. *Plant Physiol.* 174, 815–822. doi: 10.1104/pp.16.01825

Thompson, J. D., Higgins, D. G., and Gibson, T. J. (1994). CLUSTAL W: improving the sensitivity of progressive multiple sequence alignment through sequence weighting, position-specific gap penalties and weight matrix choice. *Nucleic Acids Res.* 22, 4673–4680. doi: 10.1093/nar/22.22.4673

Takahashi, Y., Kinoshita, T., Matsumoto, M., and Shimazaki, K. (2016). Inhibition of the Arabidopsis bHLH transcription factor by monomerization through abscisic acid-induced phosphorylation. *Plant J.* 87, 559–567. doi: 10.1111/tpj.13217

Takahashi, Y., Kinoshita, T., and Shimazaki, K. (2007). Protein phosphorylation and binding of a 14-3-3 protein in *Vicia* guard cells in response to ABA. *Plant Cell Physiol.* 48, 1182–1191. doi: 10.1093/pcp/pcm093

Umezawa, T., Sugiyama, N., Mizoguchi, M., Hayashi, S., Myouga, F., Yamaguchi-Shinozaki, K., et al. (2009). Type 2C protein phosphatases

directly regulate abscisic acid-activated protein kinases in Arabidopsis. *Proc. Natl. Acad. Sci. U. S. A.* 106, 17588–17593. doi: 10.1073/pnas.0907095106

Vlad, F., Rubio, S., Rodrigues, A., Sirichandra, C., Belin, C., Robert, N., et al. (2009). Protein phosphatases 2C regulate the activation of the Snf1-related kinase OST1 by abscisic acid in Arabidopsis. *Plant Cell* 21, 3170–3184. doi: 10.1105/tpc.109.069179

Wang, P., Xue, L., Batelli, G., Lee, S., Hou, Y.-J., Van Oosten, M. J., et al. (2013). Quantitative phosphoproteomics identifies SnRK2 protein kinase substrates and reveals the effectors of abscisic acid action. *Proc. Natl. Acad. Sci. U. S. A.* 110, 11205–11210. doi: 10.1073/pnas.1308974110

Willmer, C., and Fricker, M. (1996). *Stomata. 2nd Edn.* (Florida: Chapman & Hill).

Yoshida, R., Umezawa, T., Mizoguchi, T., Takahashi, S., Takahashi, F., and Shinozaki, K. (2006). The regulatory domain of SRK2E/OST1/SnRK2.6 interacts with ABI1 and integrates abscisic acid (ABA) and osmotic stress signals controlling stomatal closure in Arabidopsis. *J. Biol. Chem.* 281, 5310–5318. doi: 10.1074/jbc.M509820200

Zhang, T., Chen, S., and Harmon, A. C. (2014). Protein phosphorylation in stomatal movement. *Plant Signal. Behav.* 9:e972845. doi: 10.4161/15592316.2014.972845

Conflict of Interest: The authors declare that the research was conducted in the absence of any commercial or financial relationships that could be construed as a potential conflict of interest.

Publisher's Note: All claims expressed in this article are solely those of the authors and do not necessarily represent those of their affiliated organizations, or those of the publisher, the editors and the reviewers. Any product that may be evaluated in this article, or claim that may be made by its manufacturer, is not guaranteed or endorsed by the publisher.

frontiers in Plant Science

REVIEW
published: 22 December 2021
doi: 10.3389/fpls.2021.749337

Promotion and Upregulation of a Plasma Membrane Proton-ATPase Strategy: Principles and Applications

Zirong Ren[1†], Bazhen Suolang[1†], Tadashi Fujiwara[2], Dan Yang[3], Yusuke Saijo[2], Toshinori Kinoshita[4] and Yin Wang[1*]*

[1]*Institute of Ecology, College of Urban and Environmental Sciences and Key Laboratory for Earth Surface Processes of Ministry of Education, Peking University, Beijing, China,* [2]*Division of Biological Sciences, Nara Institute of Science and Technology, Nara, Japan,* [3]*College of Urban and Environmental Sciences, Peking University, Beijing, China,* [4]*Institute of Transformative Bio-Molecules (WPI-ITbM), Nagoya University, Nagoya, Japan*

OPEN ACCESS

Edited by:
Adriano Nunes-Nesi, Universidade Federal de Viçosa, Brazil

Reviewed by:
Anja Thoe Fuglsang, University of Copenhagen, Denmark
Agepati S. Raghavendra, University of Hyderabad, India

***Correspondence:**
Toshinori Kinoshita
kinoshita@bio.nagoya-u.ac.jp
Yin Wang
wangyinpku@pku.edu.cn

†These authors have contributed equally to this work

Specialty section:
This article was submitted to Plant Physiology, a section of the journal Frontiers in Plant Science

Received: *29 July 2021*
Accepted: *26 November 2021*
Published: *22 December 2021*

Citation:
Ren Z, Suolang B, Fujiwara T, Yang D, Saijo Y, Kinoshita T and Wang Y (2021) Promotion and Upregulation of a Plasma Membrane Proton-ATPase Strategy: Principles and Applications. Front. Plant Sci. 12:749337. doi: 10.3389/fpls.2021.749337

Plasma membrane proton-ATPase (PM H^+-ATPase) is a primary H^+ transporter that consumes ATP *in vivo* and is a limiting factor in the blue light-induced stomatal opening signaling pathway. It was recently reported that manipulation of PM H^+-ATPase in stomatal guard cells and other tissues greatly improved leaf photosynthesis and plant growth. In this report, we review and discuss the function of PM H^+-ATPase in the context of the promotion and upregulation H^+-ATPase strategy, including associated principles pertaining to enhanced stomatal opening, environmental plasticity, and potential applications in crops and nanotechnology. We highlight the great potential of the promotion and upregulation H^+-ATPase strategy, and explain why it may be applied in many crops in the future.

Keywords: *Arabidopsis*, environmental plasticity, plasma membrane proton ATPase, rice, stomata

INTRODUCTION

The growth of terrestrial plants by fixing CO_2 from the atmosphere plays an important role as a carbon sink in global change. As the world population increases year by year and urbanization intensifies, areas available for vegetation are becoming more limited. There is a pressing need to improve plant growth efficiency in order to neutralize CO_2 emissions caused by human activities worldwide. Recent studies on the manipulation of plasma membrane proton-ATPase (PM H^+-ATPase) in an *Arabidopsis thaliana* plant model have suggested a new strategy to enhance plant growth (Young et al., 1998; Robertson et al., 2004; Wang et al., 2014a; Hoffmann et al., 2019; Zhang et al., 2021). Because PM H^+-ATPase is a key enzyme for regulating membrane potential and is conserved in most plant species, the promotion and upregulation of a PM-ATPase strategy are expected to be applied outside the laboratory. The current review discusses the main details of the promotion and upregulation H^+-ATPase strategy, including the fundamentals of PM H^+-ATPase involved in stomatal opening; evidence on how overexpression of PM H^+-ATPase enhances plant growth, aspects of environmental plasticity associated with promotion and upregulation H^+-ATPase, and provides examples of applications in crops and nanotechnology.

FUNCTION OF PM H+-ATPase

PM H+-ATPase Family

PM H+-ATPase is a member of the P-type ATPase super family and is the primary active transport system in plants and fungi (Sussman, 1994). The activated state of PM H+-ATPase results in an electrochemical gradient that is the driving force behind the transport of other solutes across the cell membrane (Palmgren, 2001; Pedersen et al., 2018). This process involves the hyperpolarization of the plasma membrane and the hydrolysis of ATP, and these two steps occur almost simultaneously (Morsomme and Boutry, 2000). PM H+-ATPase extrudes H+ from the cell, generating a proton motive force with a membrane potential of −120 to −160 mV (negative inside) and a pH gradient of 1.5 to 2.0 units (acidic outside; Sze et al., 1999). Thus, PM H+-ATPase facilitates efficient transport and normal physiological functioning of the plant cell. In several species, PM H+-ATPase is encoded by a gene family composed of multiple genes, such as the PM H+-ATPase gene family of *Nicotiana tabacum* which contains nine genes (Duby and Boutry, 2009). *A. thaliana* H+-ATPase (AHA) is encoded by a family of 11 genes, and *Oryza sativa* H+-ATPase (OSA) is encoded by a family of 10 genes (Arango et al., 2003; Baxter et al., 2003; Toda et al., 2016). Distinct subtypes of the same plant may have different expression levels, expression sites, and modes of phosphorylation regulation, but there is also overlapping expression and functional redundancy. Phylogenetic analysis of the H+-ATPases in several primary C3 crops indicates that the evolutionary processes of different H+-ATPase isoforms in the same species are inconsistent (**Figure 1**). Notably however, all plant isoforms are included in the five subfamilies classified by Arango et al. (2003). Interestingly, the isoforms of *O. sativa* and *Triticum aestivum* were adjacent to each other but separate from other plants, suggesting a conserved H+-ATPase evolution between them (**Figure 1**).

Structure and Regulation of PM H+-ATPase

Given the important role of H+-ATPase in plant physiology and biochemistry, many researchers have studied the molecular structure, function, and regulatory mechanisms associated with the enzyme. PM H+-ATPase has a molecular mass of approximately 100 kDa and is structurally highly conserved in plants and fungi (Sussman, 1994). The structures all share 10 transmembrane segments, as well as C-terminal and N-terminal domains extending into the cytosolic side of the plasma membrane (Morsomme and Boutry, 2000; Pedersen et al., 2007; Falhof et al., 2016). Autoinhibitory C-terminal domains have been identified in both plant and fungal PM H+-ATPases (Pedersen et al., 2018). The autoinhibitory domain is a key region with respect to the regulation of H+-ATPase activity (Palmgren et al., 1990; Axelsen et al., 1999; Ekberg et al., 2010). N-terminal and C-terminal residues are considered essential for the regulation and targeting of PM H+-ATPases. Phosphorylation of the C terminus of PM H+-ATPase provides binding sites for 14-3-3 proteins (Gaxiola et al., 2007; Falhof et al., 2016). Inactivated PM H+-ATPases usually exist as dimers and are converted into dodecamers when activated by phosphorylation of threonine on the C-terminal autoinhibitory domain and binding to 14-3-3 proteins (Olsson et al., 1998; Bobik et al., 2010; Falhof et al., 2016; Fuglsang and Palmgren, 2021). More interestingly, the quaternary structure of the yeast *Kluyveromyces lactis* PM H+-ATPase is a hexamer, and there is evidently a relationship between ATPase function and the aggregation state of the hexamer. The aggregated H+-ATPase hexamers are reportedly the activated state of the enzyme (Ruiz-Granados et al., 2019).

The protein kinases involved in PM H+-ATPase phosphorylation have not yet been identified (Falhof et al., 2016) and many details of PM H+-ATPase regulation are still unknown, although various studies have revealed some of the details of PM H+-ATPase regulation. It is well established that the fungal toxin fusicoccin is an effective activator of PM H+-ATPase (Marrè, 1979) and that vanadate is an inhibitor of PM H+-ATPase (Zhu et al., 2015). PKS5 blocks interaction between H+-ATPase and 14-3-3 proteins *via* phosphorylation of Ser-931in *A. thaliana* (Fuglsang et al., 2007). Small auxin UP-RNA proteins reportedly inhibit the activity of a family of type 2C protein phosphatases, which in turn modulates the Thr-947 phosphorylation status of PM H+-ATPases (Spartz et al., 2014). There is evidence of differences in regulation between different subfamilies. Bobik et al. (2010) reported that cold stress led to different PMA2 and PMA4 responses in *N. tabacum*, specifically that PMA2 was dephosphorylated within a few minutes, whereas PMA4 was not. Notably however, the regulatory mechanism distinguishing these two isoforms is unknown.

Physiological Roles of PM H+-ATPase

PM H+-ATPase is active throughout the entire life process in plants, including seed germination, plant growth and defense, and pollen tube elongation, among other processes. According to acid growth theory PM H+-ATPase promotes proton efflux, acidifying the apoplast and facilitating the uptake of solutes and water, thus driving plant cell expansion and eventually resulting in hypocotyl elongation and root elongation (Spartz et al., 2014). AHA1 is reportedly a slow-wave potential regulator that activates the jasmonate defense pathway in distal leaves in response to wounding (Kumari et al., 2019). Recent reports indicate that there is a pH gradient in pollen tubes and that three members of the AHA family (AHA6, AHA8, and AHA9) are redundantly involved in the formation of a proton gradient and cell-wall patterning in the pollen tubes and are essential for polar growth in the pistil (Chen et al., 2020b; Hoffmann et al., 2020).

PM H+-ATPase IS THE LIMITING FACTOR IN LIGHT-INDUCED STOMATAL OPENING

Function of Stomata

Stomata are a special structure on the surface of terrestrial plants that consists of a pore surrounded by two guard cells. Stomata control gas exchange between the atmosphere and plants, which is required for CO_2 uptake in photosynthesis and the loss of H_2O in transpiration. Plants can regulate the size of stomatal

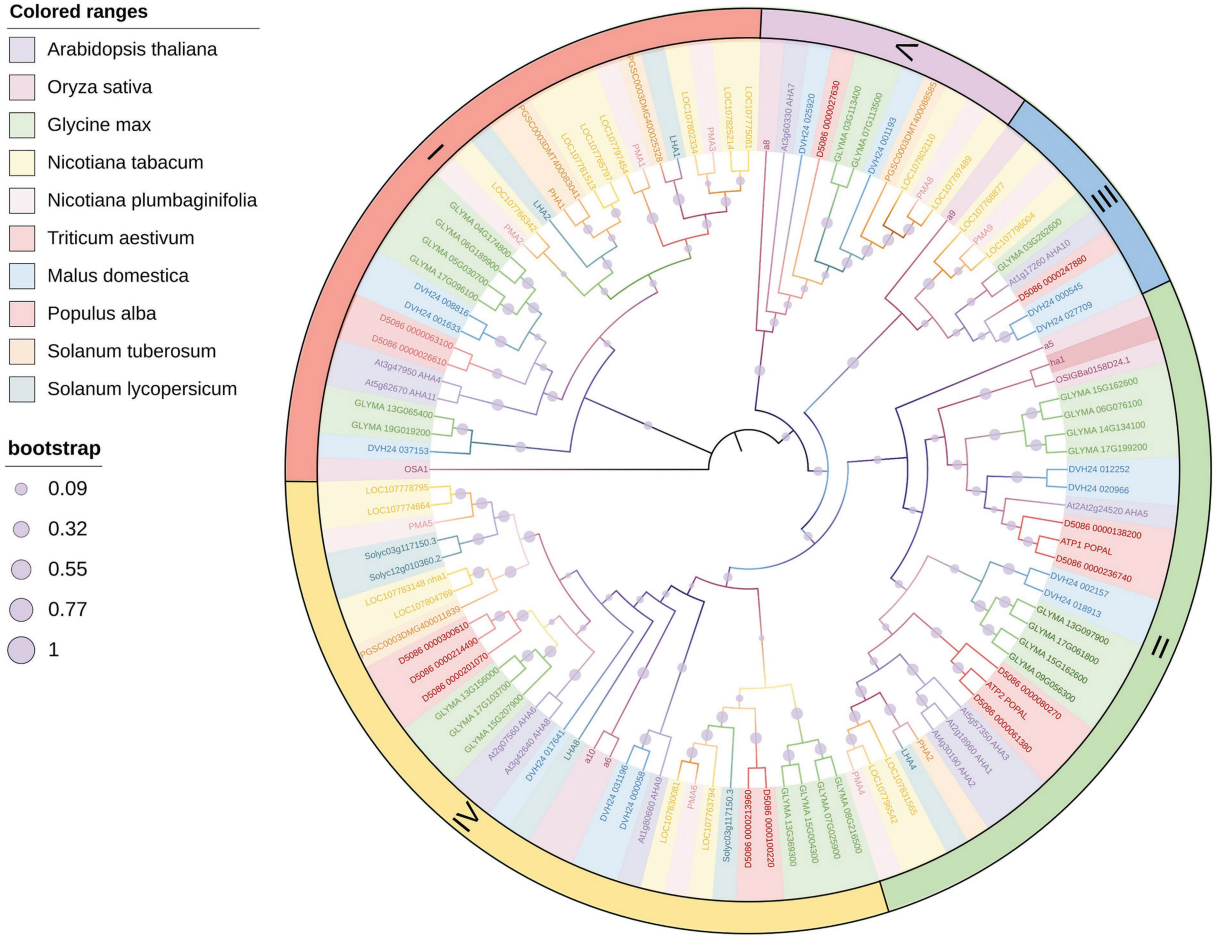

FIGURE 1 | Phylogenetic tree of main crop PM H⁺-ATPases. The phylogenetic tree was constructed using PM H⁺-ATPase amino acid sequences. Different colored ranges represent different species as shown in the top legend. Different sized purple circles represent the bootstrap of every branch as shown in the bottom legend. Roman numerals indicate subfamilies defined by Arango et al. (2003). The main part of the figure was drawn by iTOL (https://itol.embl.de/).

pores in response to environment changes, which can further coordinate photosynthesis with transpiration and also affect other physiological activities. Plant photosynthesis and transpiration are a significant component of global water and carbon cycles in atmospheric modeling. Excessive emission of CO_2 by humankind has made the global carbon cycle imbalanced, causing a serious climate problem-global warming. Humankind is also facing a severe food crisis whereby globally a large number of people do not have access to enough food. As a result, stomata have drawn more attention, and improving the ability of plants to fix CO_2 by manipulating stomata constitutes a potential means of addressing global climate changes and food insufficiency.

Light-Induced Stomatal Opening

Light can stimulate stomatal opening *via* at least two mechanistically different pathways, the red-light pathway and the blue light pathway (Zeiger, 1983; Shimazaki et al., 2007). Blue light induces stomatal opening *via* a photosynthesis-independent signal pathway. A study in *Arabidopsis* suggests that blue light-induced stomatal opening is mediated by at least three key components: the blue light receptor phototropins, H⁺-ATPase, and plasma membrane inward-rectifying K^+ channels (K^+_{in} channels; Wang et al., 2014b). The phototropins phot1 and phot2 can be activated by blue light, and transmit signals downstream that activate PM H⁺-ATPase (Kinoshita et al., 2001). Activated PM H⁺-ATPase binds the 14-3-3 protein, phosphorylating the penultimate threonine on its C terminus, and pumps H^+ out of the plasma membrane leading its hyperpolarization (Assmann et al., 1985; Shimazaki et al., 1986; Kinoshita and Shimazaki, 1999, 2002). It then evokes K^+_{in} channels, promoting the uptake of K^+ into the guard cells (Schroeder et al., 1987; Lebaudy et al., 2008). Simultaneously, some anions are required to compensate for the positively charged K^+ in guard cells, mainly Cl^-, malate^{2-}, and NO^{3-} (Shimazaki, et al., 2007). Cl^- is taken up into the vacuole *via* the major vacuole chloride channel AtALMT9, which takes precedence over the accumulation of other ions (De Angeli et al., 2013). Malate^{2-} is required in the process, some of which is synthesized from starch degradation in the chloroplast, and some of which is transported in guard cells through the

ABC transporter AtABCB14 (Shimazaki, et al., 2007; Lee et al., 2008). Blue light also induces starch degradation, which is activated *via* the phot1/phot2-dependent signaling pathway and associated with PM H^+-ATPase activity, as evidenced by the observation that the *Arabidopsis* blue light-signaling mutants *phot1phot2* and *blus1* exhibit altered starch degradation in guard cells (Horrer et al., 2016). Some of the starch is used to produce malate^{2-}, and some is converted to sucrose or hexose sugars which act as osmolytes or are used for respiration. The accumulated osmolytes including K^+ and sugars reduce water potential and drive water uptake into the guard cell, significantly increasing its volume. Because the inner side of the guard cell wall is thicker than the outer side, the turgor of guard cells widens the stomatal pore and causes stomatal opening (Shimazaki et al., 2007).

Stomatal opening in response to red light can be inhibited by the photosynthetic electron transport inhibitor DCMU, indicating that it is related to photosynthesis (Sharkey and Raschke, 1981; Doi and Shimazaki, 2008; Wang et al., 2011; Suetsugu et al., 2014). Red light-induced stomatal opening is an indirect response to intercellular CO_2 concentration. A high concentration of CO_2 activates anion channels and outward-rectifying K^+ channels (Brearley et al., 1997; Roelfsema et al., 2002). Red light promotes photosynthesis and reduces the intercellular CO_2 concentration, relieving the negative effect of a high CO_2 concentration on stomata opening. Conversely, a low CO_2 concentration as a signal directly induces the protein kinase high leaf temperature 1, inhibiting S-type anion channels *via* convergence of blue light and CO_2 (CBC)1 and CBC2 (Hashimoto et al., 2006; Hiyama et al., 2017). This promotes the uptake of K^+ and stomatal opening. Under red-light illumination mesophyll cells and guard cells produce starch *via* photosynthesis, some of which is degraded into sucrose. Guard cells also take up sucrose from apoplasts. Sucrose can increase osmolytes and is used for the formation of ATP and malate^{2-} (Daloso et al., 2016). Photosynthesis in guard cells and mesophyll cells can also promote the accumulation of ATP, which is required for activated H^+-ATPase (Tominaga et al., 2001; Wang et al., 2014a). Red light can reportedly induce photosynthesis-dependent phosphorylation of PM H^+-ATPase in guard cells, which further promotes the absorption of K^+ and stomatal opening. Notably however, neither sucrose nor CO_2 as photosynthetic products are responsible for phosphorylation of H^+-ATPase. It is currently unclear what mediates the photosynthesis-dependent phosphorylation of H^+-ATPase (Ando and Kinoshita, 2018).

Although the details of signaling pathways involving phototropins and PM H^+-ATPase have not been entirely clarified, the following important steps pertaining to relevant signal transduction have recently been reported as:

1. Phototropins function as blue light receptors *via* the chromophore flavin. In the N terminus of phototropins, there are two so-called light, oxygen, and voltage domains which act as binding sites for flavin mononucleotide and absorb blue light (Christie et al., 1999). After receiving a light signal phototropins are activated *via* autophosphorylation, with subsequent binding of 14-3-3 protein in response to blue light (Kinoshita et al., 2003). Blue light-activated phototropins are phosphorylated and transmit the signal downstream *via* the blue light-signaling 1 (BLUS1) protein kinase (Takemiya et al., 2013). It has also been reported that phototropins may be involved in another BLUS1-independent signaling pathway which inhibits stomatal opening by mediating dephosphorylation of PM H^+-ATPase (Hosotani et al., 2021).
2. BLUS1 is a Ser/Thr protein kinase expressed in the cytoplasm of guard cells. It can be phosphorylated by phototropins and indirectly activate PM H^+-ATPase, which transduces blue light signal from phototropins to type 1 protein phosphatase (PP1). The loss of blue light-dependent stomatal opening has been observed in BLUS1 mutants *via* infrared thermography (Takemiya et al., 2013). There is a Ser/Thr kinase domain in the N-terminal of BLUS1 and a regulatory domain in the C-terminal which inhibit its kinase activity. Phototropins phosphorylate Ser-348 within the C-terminal domain of BLUS1, alleviating auto-inhibition of the C-terminal domain and transmitting the signal downstream (Takemiya et al., 2013; Hosotani et al., 2021).
3. Blue light-dependent H^+-ATPase phosphorylation (BHP) is a Raf-like protein kinase that indirectly activates PM H^+-ATPase and functions in the cytosol of guard cells. It was identified by screening kinase inhibitors that suppress blue light-dependent H^+-ATPase phosphorylation and stomatal opening in guard cells. It has been suggested that BHP can interact with both BLUS1 and PP1 *in vitro*, but only interaction between BHP and BLUS1 has been observed *in vivo* – thus whether or not BLUS1 phosphorylates BHP is uncertain (Hayashi et al., 2017).
4. PP1 and its regulatory subunit PRSL1 transmit signals between phototropin and PM H^+-ATPase. The function of PP1 has been demonstrated by the transformation of guard cells with PP1c isoforms and inhibitors, which specifically reduces PP1 activity and suppresses stomatal opening. Tutomycin, an inhibitor of PP1, affects the phosphorylation of PM H^+-ATPase but does not affect phototropins (Takemiya et al., 2006).

PROMOTION AND UPGREGULATION H^+-ATPase STRATEGY ENHANCES PHOTOSYNTHESIS AND PLANT GROWTH

Principles

Stomatal conductance is always proportional to the degree of stomatal aperture and is one of the main limiting factors in C3 photosynthesis (Farquhar and Sharkey, 1982), thus improving stomatal conductance is predicted to enhance photosynthesis and crop yield when there are no other stresses affect plant performance. Because stomatal conductance depends on both stomatal density and property, manipulations mainly focus on these two things. Sugano et al. (2010) reported that *STOMAGEN*, which encodes a secretory peptide involved in stomatal differentiation, regulates

stomatal density. In that study overexpression of *STOMAGEN* in *Arabidopsis* increased stomatal density and enhanced the rate of photosynthesis by 30% compared to wild-type (WT) plants. Notably however, *STOMAGEN* overexpression also increased net water loss, and the whole plant biomass did not change (Tanaka et al., 2013). Similar results were observed in a mutant of *slow anion channel 1*, which had defects in the stomatal closing pathway resulting in constantly open stomata (Kusumi et al., 2012). These two methods successfully enhanced stomatal conductance and promoted photosynthesis rates, but significantly increased water loss was not beneficial with respect to accumulating biomass. From this perspective, increasing the aperture of stomata under light conditions and maintaining normal closure under stress and dark conditions are likely to be more favorable for plant growth.

Recent studies have attempted to modify several key components involved in stomatal light responses to investigate their effects on stomatal traits and plant growth. As a component involved in stomatal opening induced by red and blue light, PM H^+-ATPase reportedly has the potential to increase plant production *via* genetic modification. Wang et al. (2014a) used the strong guard cell promoter *GC1*, and Yang et al. (2008) overexpressed key genes in blue light-induced stomatal opening and reported that *AHA2* (*A. thaliana* H^+-ATPase 2) was the limiting factor in this process. In *GC1::AHA2*-overexpressing plants, the levels of *AHA2* transcription and translation were increased, in conjunction with elevation of H^+-ATPase phosphorylation (**Figure 2A**) and further hyperpolarization of the plasma membrane. Overexpression of PM H^+-ATPase also affects the downstream K^+ channel. *Via* sodium hexanitrocobaltate III staining of K^+, it was determined that K^+ uptake in *GC1::AHA2*-overexpressing plants was significantly higher than it was in WT plants under both light and exposure to fusicoccin conditions (Green et al., 1990; **Figure 2B**). The K^+ channel current in *GC1::AHA2* was similar to that in WT at the same voltage however (**Figure 2C**), indicating that manipulating PM H^+-ATPase in guard cells did not alter the properties of K^+ channels. Moreover, the expression level of *potassium channel in Arabidopsis thaliana 1* (*KAT1*), a major guard cell K^+ channel gene, also exhibited no significant change in *GC1::AHA2*-overexpressing plants (**Figure 2D**). Together these results indicated that the *GC1::AHA2*-overexpressing plant absorbed more K^+ through the K^+ channel without altering its expression level or properties. Eventually the ions and osmoticum accumulated, increasing the stomatal aperture.

Improving stomatal conductance is associated with increased photosynthetic rates and leads to greater biomass in *GC1::AHA2*-overexpressing plants. In light response curve studies, when light intensity was higher than 200 $\mu mol\, m^{-2}\, s^{-1}$, stomatal conductance and the CO_2 assimilation rate of *GC1::AHA2*-overexpressing plants were strikingly higher than those of WT. At a light intensity of nearly 200 $\mu mol\, m^{-2}\, s^{-1}$, the growth of *GC1::AHA2*-overexpressing plants was increased, and the fresh and dry weights of rosettes and flower stems were significantly higher than those of WT (Wang et al., 2014a). The relationship between stomatal phenotypes and plant production has also been clarified. Because plants preferentially fix ^{12}C during photosynthesis, an increase in stomatal conductance could lead to a decrease in the $^{13}C/^{12}C$ ratio ($\delta^{13}C$; Farquhar et al., 1989). *GC1::AHA2*-overexpressing plants had lower $\delta^{13}C$ (Wang et al., 2014a), demonstrating that stomatal opening increased the intercellular CO_2 concentration, which ultimately contributed to the plant growth. Moreover, it is reported that PM H^+-ATPase also involved in plant root hair elongation and pollen tube growth (Axelsen and Palmgren, 2001; Hoffmann et al., 2019, 2020). Further studies are needed to exam whether *GC1::AHA2*-overexpression also affects root hair and pollen tube growth.

In one study, light-induced stomatal opening was disrupted by modifying certain components, but plant growth did not change. In *GC1::AHA2*-overexpressing plants with a Pro68-to-Ser point mutation at the AHA2 first transmembrane domain (*GC1::AHA2-P68S*), PM H^+-ATPase was constitutively activated. *GC1::AHA2-P68S*-overexpressing plants exhibited continuous stomatal opening under light and dark conditions, and after the addition of abscisic acid (ABA), but there was no significant difference in plant growth compared to WT (Wang et al., 2014a). These results indicated that the functional integrity of PM H^+-ATPase is essential for maintaining stomatal responses to light and promoting plant growth. Moreover, in plants overexpressing the stomatal opening positive regulator *flowering locus T*, stomata opened constantly under light and dark conditions, but closed normally with the application of ABA (Kinoshita et al., 2011). Compared with WT, *flowering locus T*-overexpression did not enhance plant growth (Wang et al., 2014a). These results may be partly due to the constant stomatal opening which led to lower water use efficiency, or it may be that PM H^+-ATPase consumed ATP while the stomata remained open (Palmgren, 2001). Collectively, these results indicate that continuously open stomata under dark or stressed conditions probably hinder plant growth.

Environmental Plasticity

The aforementioned transgenic plants were all cultivated under suitable environmental conditions. In sessile organisms however, the ability to adapt to environmental changes directly affects their probability of survival. Therefore, the responses of modified plants under various conditions are a useful indicator of their merits.

Plants always face different environmental conditions, such as changes in day length and light conditions over time, high CO_2 conditions due to increased global CO_2 concentrations. The performance of *GC1::AHA2*-overexpressing plants under these conditions warrants attention. Under short-day conditions, the stomatal aperture of *GC1::AHA2*-overexpressing plants was notably higher than that of WT, as was their fresh and dry aboveground weight (**Figures 3A,B**). The stomatal aperture of the long-day plant *A. thaliana* was significantly reduced when the daylight duration was shortened (Aoki et al., 2019). Therefore, the enlarged stomatal aperture in *GC1::AHA2*-overexpressing plants may compensate for its reduction. The light intensity in this experiment was suitable (150 $\mu mol\, m^{-2}\, s^{-1}$), which led to the stomatal aperture becoming the main limiting factor of photosynthesis under light. Therefore, the increased CO_2 absorption through open stomata ultimately increased

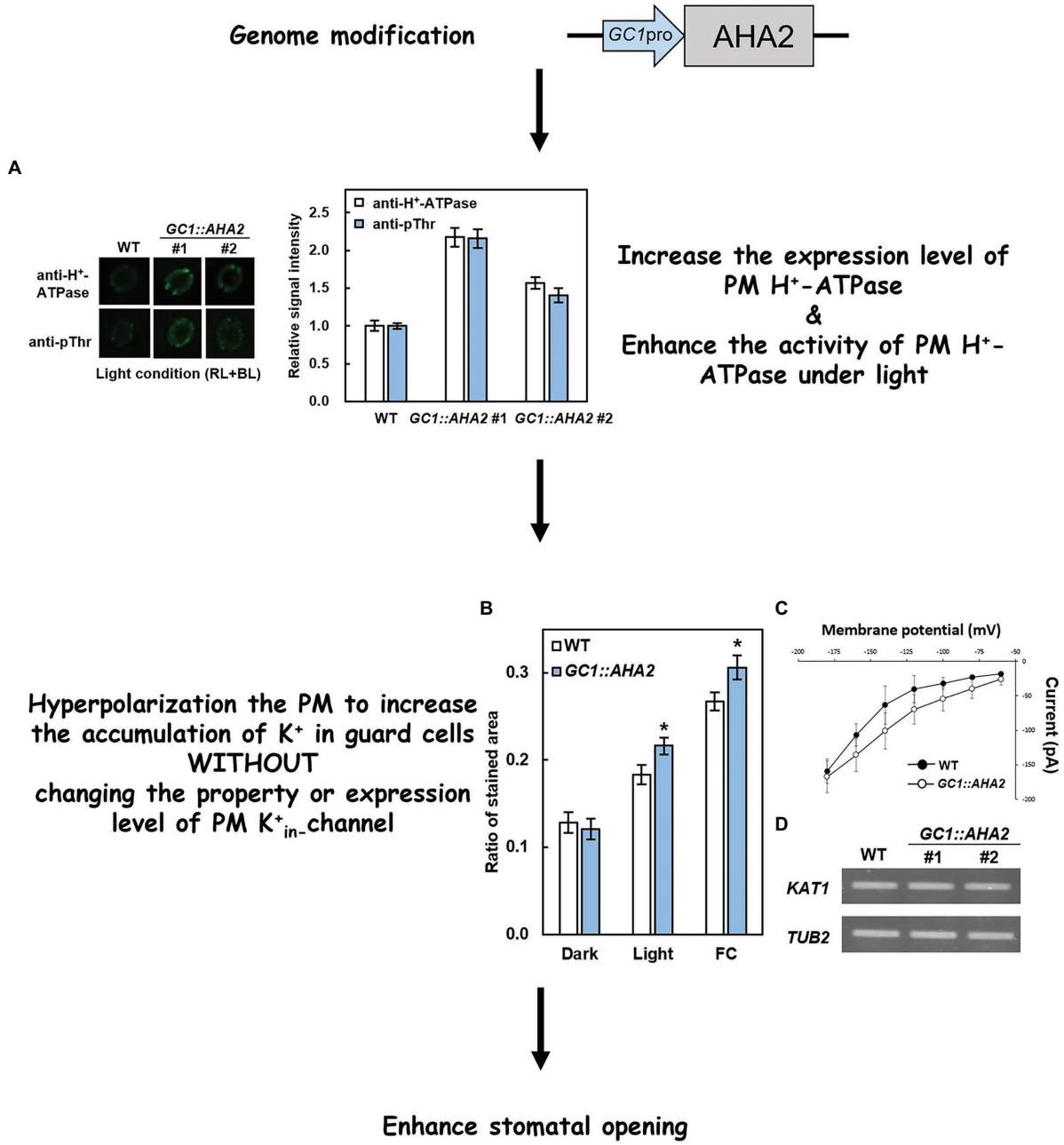

FIGURE 2 | Principle of overexpression of PM H+-ATPase to enhance stomatal opening. **(A)** Immunohistochemical detection of PM H+-ATPase (anti-H+-ATPase) and its phosphorylation level (anti-pThr) in guard cells of WT and *GC1::AHA2* (the same lines used in Wang et al., 2014a). **(B)** K^+ uptake in wild-type (WT) and *AHA2*-overexpressing guard cells. Bars indicate the average of three replicates, and error bars indicate the standard error ($n = 3$). Asterisks indicates a significant difference from WT ($p < 0.05$, Student's *t*-test). **(C)** Current–voltage relationships in guard cell protoplasts of WT and *GC1::AHA2* detected by patch-clamp analysis. Solid circles represent WT, and hollow circles represent *AHA2*-overexpressing plants. Bars indicate the average of 4 replicates, and error bars indicate the standard deviation ($n = 4$ cells). **(D)** *KAT1* expression levels were comparable in WT plants and *AHA2*-overexpressing plants.

the biomass of the plants. Under low light conditions, the production of transgenic plants was identical to that of WT, although the stomatal aperture increased (Wang et al., 2014a). It may be that intercellular CO_2 concentration affected the photosynthetic rate under low light, but electron transport was still a limiting factor in this process (Farquhar et al., 1980). Similarly, under elevated CO_2 conditions, *GC1::AHA2*-overexpressing plants also exhibited increased stomatal apertures and an unchanged biomass (**Figures 3C,D**). It may be that stomatal restriction was not the main limiter of intracellular CO_2 concentration (Farquhar et al., 1980; Busch et al., 2020).

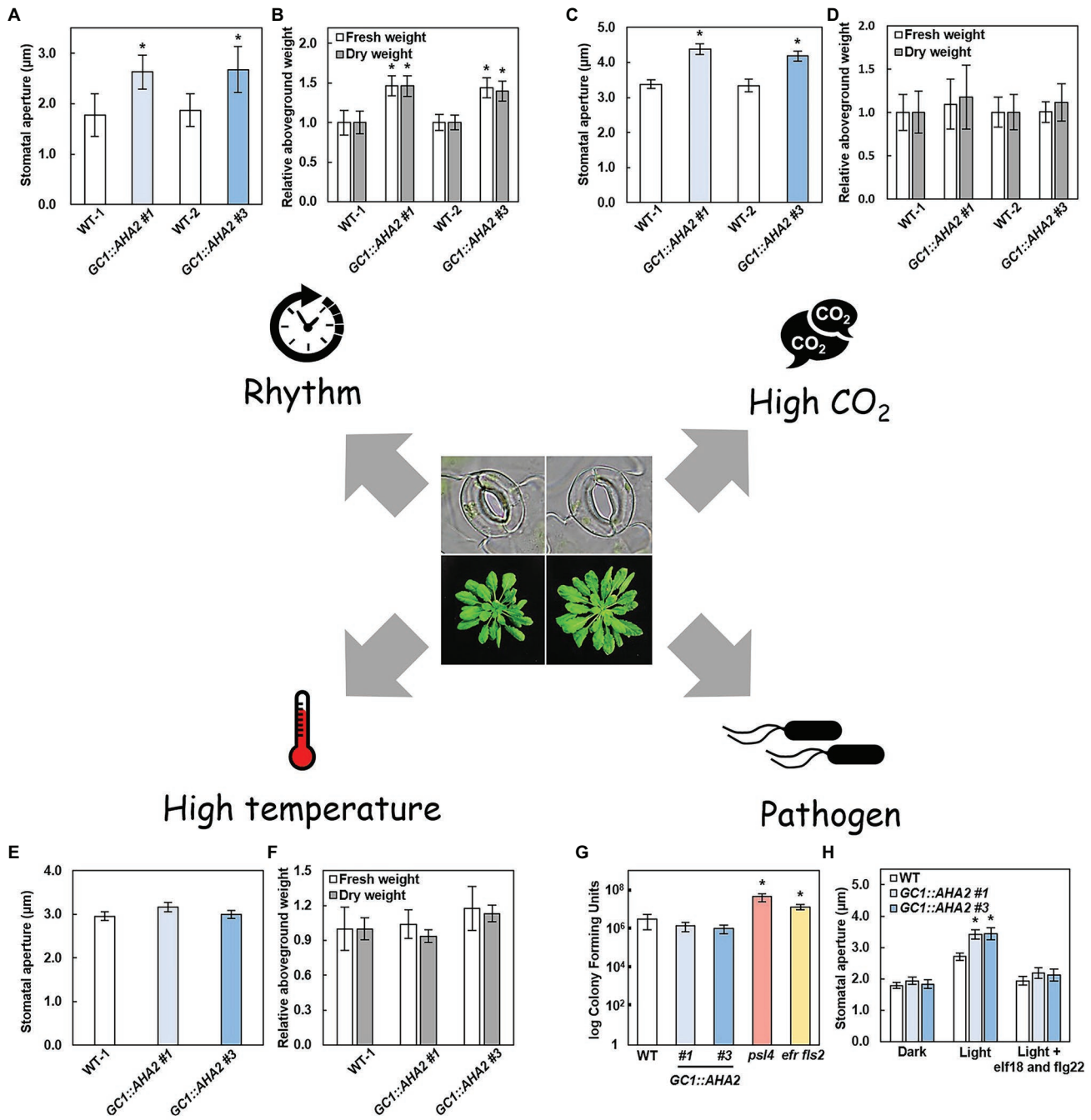

FIGURE 3 | Environmental plasticity of *AHA2*-overexpressing plants. **(A–F)** Stomatal aperture **(A,C,E)** and relative aboveground weight **(B,D,F)** of WT and *AHA2*-overexpressing plants grown under short day (**A,B**, 8 h/16 h), high CO_2 concentration (**C,D**, 800 ppm), and high temperature (**E,F**, 27°C) conditions. Bars indicate the average of 3 replicates, and error bars indicate the standard error ($n = 3$). Asterisks indicate a significant difference from WT ($p < 0.05$, Student's *t*-test). **(G,H)** Responses of *AHA2*-overexpressing plants to biotic stress. **(G)** Colony-forming units of different plants. Four-week-old plants were sprayed with a *Pst* DC3000 suspension (OD600 of 1) in 10 mM $MgCl_2$ with 0.02% silwet L-77. Leaf surfaces were sterilized with 70% ethanol for 1 min, then washed with water twice. Four leaf disks were ground in 1 ml of 10 mM $MgCl_2$. The mutant plants *psl4* and *efr fls2* are insensitive to *Pst* DC3000. **(H)** Stomatal responses to bacterial epitopes. The concentration of elf18 and flg22 were 5 μM, respectively. Bars indicate the average of three independent samples with two replicates each, and error bars indicate the standard deviation ($n = 3$). Asterisks indicate a significant difference from WT ($p < 0.01$, Student's *t*-test).

Because *AHA2* overexpression alters stomatal traits, the biotic and abiotic stress associated with stomata may affect plant traits. The most deleterious abiotic sources of stress in plants are drought and heat. Under severe drought stress, plants mainly produced the phytohormone ABA to induce stomatal closure (Roelfsema et al., 2004). As well as inducing the activation of

TABLE 1 | Summary of PM H+-ATPase-overexpression plant characteristics under different conditions.

Condition	Stomatal aperture	Plant growth
Well condition* (High light, long day, well watered, ambient CO_2)	Increase	Increase
Short-day	Increase	Increase
Low light*	Increase	Normal as WT
High CO_2	Increase	Normal as WT
Drought*	Normal as WT	Normal as WT
High temperature	Normal as WT	Normal as WT
Pathogen	Normal as WT	-

*WT means the wide type of Arabidopsis thaliana. *Data are from Wang et al. (2014a).*

R-type and S-type anion channels, ABA also inhibited the capacity of PM H+-ATPase to maintain membrane depolarization which led to stomatal closure (Goh et al., 1996; Roelfsema et al., 2004). *GC1*::*AHA2*-overexpressing plants exhibited more PM H+-ATPase expression but were still regulated by ABA, resulting in the same stomatal and biomass phenotypes as WT. Under mild drought conditions, *GC1*::*AHA2*-overexpressing plants also exhibited the same performance as WT (Wang et al., 2014a). When land plants are exposed to high temperature they generally facilitate leaf cooling by opening stomata to increasing transpiration. It has been reported that components of the blue light-signaling pathway, including PM H+-ATPase and its upstream and downstream substances, are involved in high-temperature-induced stomatal opening (Kostaki et al., 2020). Notably however, the phenotype of *GC1*::*AHA2*-overexpressing plants was the same as WT (**Figures 3E,F**). It may be that the stomatal aperture of WT also increased at high temperature, eliminating the difference between them (Rogers, 1979).

The main source of biotic stress in plants is pathogen infection. One form of plant defense against bacterial invasion is closing stomata (Melotto et al., 2006). When *GC1*::*AHA2*-overexpressing plants were sprayed with *Pst* DC3000 (*Pseudomonas syringae* pv. *tomato* DC3000), the number of pathogenic bacteria entering the leaves through stomata remained unchanged compared to WT, indicating that the *GC1*::*AHA2*-overexpressing plants were normally susceptible to pathogens (**Figures 3G,H**). After adding a mixture of the bacterial epitopes elf18 and flg22, the stomatal apertures of the *GC1*::*AHA2*-overexpressing plants were similar to those of WT. This may be a result of a normal phytohormone pathway (such as the ABA pathway) in *GC1*::*AHA2*-overexpressing plants, which regulated stomatal closure to inhibit the entry of pathogenic bacteria. These results indicate that transgenic plants have a normal capacity to resist biotic stress.

Collectively, the above-describe observations suggest that under favorable conditions, especially when the stomatal aperture is the main limiting factor of photosynthesis, the CO_2 assimilation rate and plant production of *GC1*::*AHA2*-overexpressing plants may be superior to WT. Under stress conditions, whether it was biotic or abiotic, *GC1*::*AHA2*-overexpressing plants showed neither advantages nor inferiority, and grew as well as WT (**Table 1**). These advantages of the technology enable it to be used in combination with other methods to further enhance photosynthesis and plant growth.

APPLICATIONS OF PROMOTION AND UPGREGULATION H+-ATPase PLANTS

Overexpression of PM H+-ATPase Promotes Grain Yield in Rice

O. sativa is one of the most important crops worldwide and is the staple food of 3 billion people (Woolston, 2014). As a monocotyledon its stomata are formed as pairs of dumbbell-shaped guard cells surrounded by two subsidiary cells. Because of the difference in guard cell morphology between rice and *Arabidopsis*, whether modifying PM H+-ATPase could lead to a breakthrough in crop production warrants investigation.

There are 10 isoforms of OSA located on the plasma membrane, most of which are involved in light-induced stomatal opening. Like PM H+-ATPase in kidney-shaped guard cells, the activity of most OSAs is regulated *via* phosphorylation of penultimate threonine. Among them, OSA7 is the dominant isoform in rice guard cells and plays an indispensable role in plant growth. The stomatal conductance of the mutant *osa7* was significantly lower than that of WT, and plant growth was severely restricted – to the extent that the plants were unable to develop to the reproductive stage. OSA7 is involved in blue light-induced stomatal opening (Toda et al., 2016). Other homologous genes involved in the blue light-signaling pathway in kidney-shaped guard cells have also been identified in rice (Kanegae et al., 2000; Takemiya et al., 2013), but the specific components and mechanism of the pathway in dumbbell-shaped guard cells remain to be determined.

OSA1 is one of the main isoforms in rice. A recent study on *osa1* mutants and overexpressing rice plants improved our understanding of *OSA* genetically modified plants (Zhang et al., 2021). Because there is no guard cell-specific promoter in rice Zhang et al. (2021) used the *CaMV-35S* promoter to constitutively express *OSA1*. Stomatal conductance and the CO_2 assimilation rate of *OSA1*-overexpressing plants were significantly higher than those of WT. Because active PM H+-ATPase could facilitate the absorption of ammonium (NH_4^+) in root, the NH_4^+ absorption rate in *OSA1*-overexpressing plants was also significantly increased. Moreover, because NH_4^+ absorption and assimilation occur almost simultaneously in plant roots (Xu et al., 2012), compared with both WT and mutants, the total amount of nitrogen in *OSA1*-overexpressing plants also increased (Zhang et al., 2021). Carbon and nitrogen are both associated with the rate of photosynthesis in leaves and root nitrogen assimilation, and both were significantly increased in *OSA1*-overexpressing plants.

The above-mentioned physiological changes were only short-term processes, and the final change in plant biomass also depended on a series of downstream genes. Long-term cultivation of *OSA1*-overexpressing plants increased the expression of genes associated with plant growth. Remarkably, *via* differentially expressed gene analysis, it was determined that overexpressing PM H+-ATPase activated a series gene involved in ammonia assimilation, amino acid metabolism, photosynthesis, and GRF4, a key transcription factor that integrates nitrogen assimilation, carbon fixation, and plant growth in rice (Li et al., 2018; Zhang et al., 2021). Positive feedback between the physiological process and gene expression eventually results in the crop yield of *OSA1*-overexpressing plants under different fertilization

conditions being notably higher than that of WT, indicating that overexpression of PM H+-ATPase in rice has the potential to facilitate reduced use of nitrogen fertilizer. It also provides a new direction for the coordination of the N and C assimilation pathway, and to emphasize the importance of PM H+-ATPase (also known as proton pump), Zhang et al. (2021) suggested to define the "promotion and upregulation of PM H+-ATPase plants" as "PUMP" plants.

Nanomaterials Benefit Plants by Increasing PM H+-ATPase Expression

Nanomaterial science can be used to increase the expression of PM H+-ATPase in plants, and its effects are similar to those of genetic manipulation. Engineered nanomaterials have been widely applied in environmental remediation, agriculture, and other fields, and have specific effects on PM H+-ATPase in plants. The effects of engineered nano zerovalent iron (nZVI) on PM H+-ATPase have been investigated. In studies on nZVI in *Arabidopsis*, the surface of nZVI was oxidized to iron oxide-hydroxide, which was hydrolyzed resulting in OH^- and increased rhizosphere pH, and the activation and expression of PM H+-ATPase were promoted. Remarkably, the treated plants maintained satisfactory water use efficiency while increasing the stomatal aperture (Kim et al., 2015). In another study, nZVI was investigated in cucumber plants, and under favorable conditions, the photosynthetic capacity of plants was enhanced (Yoon et al., 2019). Moreover, when carbon nanoparticles were added to tobacco plant cell suspensions the expression of PM H+-ATPase was significantly upregulated, and plant growth was also increased (Chen et al., 2020a). These technologies constitute a potential new method for increasing PM H+-ATPase in plants to improve plant production.

CONCLUSION

PM H+-ATPase occurs in numerous plants, especially crops, and PM H+-ATPase manipulation has a wide range of potential applications in various crops under certain conditions. In the future, the application of gene-editing tools, such as the Crispr/cas9 system to edit the promoter region of PM H+-ATPase to enhance PM H+-ATPase expression, may facilitate the breeding of non-transgenic promotion and upregulation H+-ATPase plants. Chemical compounds that induce PM H+-ATPase activity, such as plant hormones, auxin (Takahashi et al., 2012), and brassinosteroid (Minami et al., 2019), and stomatal opening (Toh et al., 2018) is also candidates for incorporation into promotion and upregulation H+-ATPase strategies.

AUTHOR CONTRIBUTIONS

YW and TK conceived the idea. YW, TF, and ZR conducted experiments and performed data analyses. ZR, BS, DY, and YW wrote the manuscript. YS, TK, and YW reviewed and edited the manuscript. All authors contributed to the article and approved the submitted version.

FUNDING

This study was financially supported by the National Natural Science Foundation of China (grant number 31972937 to YW), the Youth Fund of the Ministry of Education Laboratory for Earth Surface Processes, Peking University (to YW), Grants-in-Aid for Scientific Research from MEXT (20H05687 and 20H05910 to TK), and the Advanced Low Carbon Technology Research and Development Program from the Japan Science and Technology Agency (JPMJAL1011 to TK).

ACKNOWLEDGMENTS

We sincerely thank Julian Schroeder (University of California, San Diego, United States) for supporting the patch-clamp analyses.

REFERENCES

Ando, E., and Kinoshita, T. (2018). Red light-induced phosphorylation of plasma membrane H+-ATPase in stomatal guard cells. *Plant Physiol.* 178, 838–849. doi: 10.1104/pp.18.00544

Aoki, S., Toh, S., Nakamichi, N., Hayashi, Y., Wang, Y., Suzuki, T., et al. (2019). Regulation of stomatal opening and histone modification by photoperiod in *Arabidopsis thaliana*. *Sci. Rep.* 9:10054. doi: 10.1038/s41598-019-46440-0

Arango, M., Gevaudant, F., Oufattole, M., and Boutry, M. (2003). The plasma membrane proton pump ATPase: the significance of gene subfamilies. *Planta* 216, 355–365. doi: 10.1007/s00425-002-0856-8

Assmann, S. M., Simoncini, L., and Schroeder, J. I. (1985). Blue-light activates electrogenic ion pumping in guard-cell protoplasts of *Vicia faba*. *Nature* 318, 285–287. doi: 10.1038/318285a0

Axelsen, K. B., and Palmgren, M. G. (2001). Inventory of the superfamily of P-type ion pumps in *Arabidopsis*. *Plant Physiol.* 126, 696–706. doi: 10.1104/pp.126.2.696

Axelsen, K. B., Venema, K., Jahn, T., Baunsgaard, L., and Palmgren, M. G. (1999). Molecular dissection of the C-terminal regulatory domain of the plant plasma membrane H+-ATPase AHA2: mapping of residues that when altered give rise to an activated enzyme. *Biochemistry* 38, 7227–7234. doi: 10.1021/bi982482l

Baxter, I., Tchieu, J., Sussman, M. R., Boutry, M., Palmgren, M. G., Gribskov, M., et al. (2003). Genomic comparison of P-type ATPase ion pumps in *Arabidopsis* and rice. *Plant Physiol.* 132, 618–628. doi: 10.1104/pp.103.021923

Bobik, K., Duby, G., Nizet, Y., Vandermeeren, C., Stiernet, P., Kanczewska, J., et al. (2010). Two widely expressed plasma membrane H+-ATPase isoforms of *Nicotiana tabacum* are differentially regulated by phosphorylation of their penultimate threonine. *Plant J.* 62, 291–301. doi: 10.1111/j.1365-313X. 2010.04147.x

Brearley, J., Venis, M. A., and Blatt, M. R. (1997). The effect of elevated CO_2 concentrations on K^+ and anion channels of *Vicia faba* L. guard cells. *Planta* 203, 145–154. doi: 10.1007/s004250050176

Busch, F. A., Tominaga, J., Muroya, M., Shirakami, N., Takahashi, S., Yamori, W., et al. (2020). Overexpression of BUNDLE SHEATH DEFECTIVE 2 improves the efficiency of photosynthesis and growth in *Arabidopsis*. *Plant J.* 102, 129–137. doi: 10.1111/tpj.14617

Chen, L., Yang, J., Li, X., Liang, T., Nie, C., Xie, F., et al. (2020a). Carbon nanoparticles enhance potassium uptake via upregulating potassium channel expression and imitating biological ion channels in BY-2 cells. *J. Nanobiotechnology* 18:21. doi: 10.1186/s12951-020-0581-0

Chen, W., Jia, P. F., Yang, W. C., and Li, H. J. (2020b). Plasma membrane H+-ATPases-mediated cytosolic proton gradient regulates pollen tube growth. *J. Integr. Plant Biol.* 62, 1817–1822. doi: 10.1111/jipb.12981

Christie, J. M., Salomon, M., Nozue, K., Wada, M., and Briggs, W. R. (1999). LOV (light, oxygen, or voltage) domains of the blue-light photoreceptor phototropin (nph1): binding sites for the chromophore flavin mononucleotide. *Proc. Natl. Acad. Sci. U. S. A.* 96, 8779–8783. doi: 10.1073/pnas.96.15.8779

Daloso, D. M., Dos Anjos, L., and Fernie, A. R. (2016). Roles of sucrose in guard cell regulation. *New Phytol.* 211, 809–818. doi: 10.1111/nph.13950

De Angeli, A., Zhang, J. B., Meyer, S., and Martinoia, E. (2013). AtALMT9 is a malate-activated vacuolar chloride channel required for stomatal opening in *Arabidopsis*. *Nat. Commun.* 4:1804. doi: 10.1038/ncomms2815

Doi, M., and Shimazaki, K. I. (2008). The stomata of the fern *Adiantum capillus-veneris* do not respond to CO_2 in the dark and open by photosynthesis in guard cells. *Plant Physiol.* 147, 922–930. doi: 10.1104/pp.108.118950

Duby, G., and Boutry, M. (2009). The plant plasma membrane proton pump ATPase: a highly regulated P-type ATPase with multiple physiological roles. *Pflugers Arch.* 457, 645–655. doi: 10.1007/s00424-008-0457-x

Ekberg, K., Palmgren, M. G., Veierskov, B., and Buch-Pedersen, M. J. (2010). A novel mechanism of P-type ATPase autoinhibition involving both termini of the protein. *J. Biol. Chem.* 285, 7344–7350. doi: 10.1074/jbc.M109.096123

Falhof, J., Pedersen, J. T., Fuglsang, A. T., and Palmgren, M. (2016). Plasma membrane H+-ATPase regulation in the Center of Plant Physiology. *Mol. Plant* 9, 323–337. doi: 10.1016/j.molp.2015.11.002

Farquhar, G., Ehleringer, J., and Hubick, K. (1989). Carbon isotope discrimination and photosynthesis. *Annu. Rev. Plant Physiol. Plant Mol. Biol.* 40, 503–537. doi: 10.1146/annurev.pp.40.060189.002443

Farquhar, G., and Sharkey, T. (1982). Stomatal conductance and photosynthesis. *Annu. Rev. Plant Physiol.* 33, 317–345. doi: 10.1146/annurev.pp.33.060182.001533

Farquhar, G., von Caemmerer, S., and Berry, J. (1980). A biochemical model of photosynthetic CO_2 assimilation in leaves of C3 species. *Planta* 149, 78–90. doi: 10.1007/BF00386231

Fuglsang, A. T., Guo, Y., Cuin, T. A., Qiu, Q., Song, C., Kristiansen, K. A., et al. (2007). *Arabidopsis* protein kinase PKS5 inhibits the plasma membrane H+-ATPase by preventing interaction with 14-3-3 protein. *Plant Cell* 19, 1617–1634. doi: 10.1105/tpc.105.035626

Fuglsang, A. T., and Palmgren, M. G. (2021). Proton and calcium pumping P-type ATPases and their regulation of plant responses to the environment. *Plant Physiol.* 0, 1–20. doi: 10.1093/plphys/kiab330

Gaxiola, R. A., Palmgren, M. G., and Schumacher, K. (2007). Plant proton pumps. *FEBS Lett.* 581, 2204–2214. doi: 10.1016/j.febslet.2007.03.050

Goh, C., Kinoshita, T., Oku, T., and Shimazaki, K. (1996). Inhibition of blue light-dependent H+ pumping by abscisic acid in vicia guard-cell protoplasts. *Plant Physiol.* 111, 433–440. doi: 10.1104/pp.111.2.433

Green, D., Dodge, S., Lee, J., and Tallman, G. (1990). Effect of sodium hexanitrocobaltate (III) decomposition on its staining of intracellular potassium ions. *Stain. Technol.* 65, 14–24. doi: 10.3109/10520299009105603

Hashimoto, M., Negi, J., Young, J., Israelsson, M., Schroeder, J. I., and Iba, K. (2006). *Arabidopsis* HT1 kinase controls stomatal movements in response to CO_2. *Nat. Cell Biol.* 8, 391–352. doi: 10.1038/ncb1387

Hayashi, M., Inoue, S., Ueno, Y., and Kinoshita, T. (2017). A Raf-Like protein kinase BHP mediates blue light-dependent stomatal opening. *Sci. Rep.* 7:45586. doi: 10.1038/srep45586

Hiyama, A., Takemiya, A., Munemasa, S., Okuma, E., Sugiyama, N., Tada, Y., et al. (2017). Blue light and CO_2 signals converge to regulate light-induced Stomatal opening. *Nat. Commun.* 8:1284. doi: 10.1038/s41467-017-01237-5

Hoffmann, R. D., Olsen, L. I., Ezike, C. V., Pedersen, J. T., Manstretta, R., Lopez-Marques, R. L., et al. (2019). Roles of plasma membrane proton ATPases AHA2 and AHA7 in normal growth of roots and root hairs in *Arabidopsis thaliana*. *Physiol. Plant.* 166, 848–861. doi: 10.1111/ppl.12842

Hoffmann, R. D., Portes, M. T., Olsen, L. I., Damineli, D. S. C., Hayashi, M., Nunes, C. O., et al. (2020). Plasma membrane H+-ATPases sustain pollen tube growth and fertilization. *Nat. Commun.* 11:2395. doi: 10.1038/s41467-020-16253-1

Horrer, D., Flutsch, S., Pazmino, D., Matthews, J. S. A., Thalmann, M., Nigro, A., et al. (2016). Blue light induces a distinct starch degradation pathway in guard cells for stomatal opening. *Curr. Biol.* 26, 362–370. doi: 10.1016/j.cub.2015.12.036

Hosotani, S., Yamauchi, S., Kobayashi, H., Fuji, S., Koya, S., Shimazaki, K. I., et al. (2021). A BLUS1 kinase signal and a decrease in intercellular CO_2 concentration are necessary for stomatal opening in response to blue light. *Plant Cell* 33, 1813–1827. doi: 10.1093/plcell/koab067

Kanegae, H., Tahir, M., Savazzini, F., Yamamoto, K., Yano, M., Sasaki, T., et al. (2000). Rice NPH1 homologues, OsNPH1a and OsNPH1b, are differently photoregulated. *Plant Cell Physiol.* 41, 415–423. doi: 10.1093/pcp/41.4.415

Kim, J., Oh, Y., Yoon, H., Hwang, I., and Chang, Y. (2015). Iron nanoparticle-induced activation of plasma membrane H+-ATPase promotes stomatal opening in *Arabidopsis Thaliana*. *Environ. Sci. Technol.* 49, 1113–1119. doi: 10.1021/es504375t

Kinoshita, T., Doi, M., Suetsugu, N., Kagawa, T., Wada, M., and Shimazaki, K. (2001). Phot1 and Phot2 mediate blue light regulation of stomatal opening. *Nature* 414, 656–660. doi: 10.1038/414656a

Kinoshita, T., Emi, T., Tominaga, M., Sakamoto, K., Shigenaga, A., Doi, M., et al. (2003). Blue-light- and phosphorylation-dependent binding of a 14-3-3 protein to phototropins in stomatal guard cells of broad bean. *Plant Physiol.* 133, 1453–1463. doi: 10.1104/pp.103.029629

Kinoshita, T., Ono, N., Hayashi, Y., Morimoto, S., Nakamura, S., Soda, M., et al. (2011). FLOWERING LOCUS T regulates stomatal opening. *Curr. Biol.* 21, 1232–1238. doi: 10.1016/j.cub.2011.06.025

Kinoshita, T., and Shimazaki, K. (1999). Blue light activates the plasma membrane H+-ATPase by phosphorylation of the C-terminus in stomatal guard cells. *EMBO J.* 18, 5548–5558. doi: 10.1093/emboj/18.20.5548

Kinoshita, T., and Shimazaki, K. (2002). Biochemical evidence for the requirement of 14-3-3 protein binding in activation of the guard-cell plasma membrane H+-ATPase by blue light. *Plant Cell Physiol.* 43, 1359–1365. doi: 10.1093/pcp/pcf167

Kostaki, K., Coupel-Ledru, A., Bonnell, V., Gustavsson, M., Sun, P., McLaughlin, F., et al. (2020). Guard cells integrate light and temperature signals to control stomatal aperture. *Plant Physiol.* 182, 1404–1419. doi: 10.1104/pp.19.01528

Kumari, A., Chételat, A., Nguyen, C. T., and Farmer, E. E. (2019). *Arabidopsis* H+-ATPase AHA1 controls slow wave potential duration and wound-response jasmonate pathway activation. *Proc. Natl. Acad. Sci. U. S. A.* 116, 20226–20231. doi: 10.1073/pnas.1907379116

Kusumi, K., Hirotsuka, S., Kumamaru, T., and Iba, K. (2012). Increased leaf photosynthesis caused by elevated stomatal conductance in a Rice mutant deficient in SLAC1, a guard cell anion channel protein. *J. Exp. Bot.* 63, 5635–5644. doi: 10.1093/jxb/ers216

Lebaudy, A., Hosy, E., Simonneau, T., Sentenac, H., Thibaud, J. B., and Dreyer, I. (2008). Heteromeric K+ channels in plants. *Plant J.* 54, 1076–1082. doi: 10.1111/j.1365-313X.2008.03479.x

Lee, M., Choi, Y., Burla, B., Kim, Y. Y., Jeon, B., Maeshima, M., et al. (2008). The ABC transporter AtABCB14 is a malate importer and modulates stomatal response to CO_2. *Nat. Cell Biol.* 10, 1217–1223. doi: 10.1038/ncb1782

Li, S., Tian, Y., Wu, K., Ye, Y., Yu, J., Zhang, J., et al. (2018). Modulating plant growth-metabolism coordination for sustainable agriculture. *Nature* 560, 595–560. doi: 10.1038/s41586-018-0415-5

Marrè, E. (1979). Fusicoccin: a tool in plant physiology. *Annu. Rev. Plant Physiol.* 30, 273–288. doi: 10.1146/annurev.pp.30.060179.001421

Melotto, M., Underwood, W., Koczan, J., Nomura, K., and He, S. (2006). Plant stomata function in innate immunity against bacterial invasion. *Cell* 126, 969–980. doi: 10.1016/j.cell.2006.06.054

Minami, A., Takahashi, K., Inoue, S., Tada, Y., and Kinoshita, T. (2019). Brassinosteroid induces phosphorylation of the plasma membrane H+-ATPase during hypocotyl elongation in *Arabidopsis thaliana*. *Plant Cell Physiol.* 60, 935–944. doi: 10.1093/pcp/pcz005

Morsomme, P., and Boutry, M. (2000). The plant plasma membrane H+-ATPase: structure, function and regulation. *Biochim. Biophys. Acta Biomembr.* 1465, 1–16. doi: 10.1016/S0005-2736(00)00128-0

Olsson, A., Svennelid, F., Ek, B., Sommarin, M., and Larsson, C. (1998). A phosphothreonine residue at the C-terminal end of the plasma membrane H+-ATPase is protected by fusicoccin-induced 14-3-3 binding. *Plant Physiol.* 118, 551–555. doi: 10.1104/pp.118.2.551

Palmgren, M. G. (2001). Plant plasma memberane H+-ATPases: powerhouses for nutrient uptake. *Annu. Rev. Plant Physiol. Plant Mol. Biol.* 52, 817–845. doi: 10.1146/annurev.arplant.52.1.817

Palmgren, M. G., Larsson, C., and Sommarin, M. (1990). Proteolytic activation of the plant plasma membrane H+-ATPase by removal of a terminal segment. *J. Biol. Chem.* 265, 13423–13426. doi: 10.1016/S0021-9258(18)77361-4

Pedersen, B. P., Buch-Pedersen, M. J., Morth, J. P., Palmgren, M. G., and Nissen, P. (2007). Crystal structure of the plasma membrane proton pump. *Nature* 450, 1111–1114. doi: 10.1038/nature06417

Pedersen, J. T., Kanashova, T., Dittmar, G., and Palmgren, M. (2018). Isolation of native plasma membrane H+-ATPase (Pma1p) in both the active and basal activation states. *FEBS Open Bio.* 8, 774–783. doi: 10.1002/2211-5463.12413

Robertson, W. R., Clark, K., Young, J. C., and Sussman, M. R. (2004). An *Arabidopsis thaliana* plasma membrane proton pump is essential for pollen development. *Genetics* 168, 1677–1687. doi: 10.1534/genetics.104.032326

Roelfsema, M. R., Hanstein, S., Felle, H. H., and Hedrich, R. (2002). CO_2 provides an intermediate link in the red light response of guard cells. *Plant J.* 32, 65–75. doi: 10.1046/j.1365-313X.2002.01403.x

Roelfsema, M., Levchenko, V., and Hedrich, R. (2004). ABA depolarizes guard cells in intact plants, through a transient activation of R- and S-type anion channels. *Plant J.* 37, 578–588. doi: 10.1111/j.1365-313X.2003.01985.x

Rogers, C. (1979). Relationship of temperature to Stomatal aperture and potassium accumulation in guard cells of *Vicia Faba*. *Plant Physiol.* 63, 388–391. doi: 10.1104/pp.63.2.388

Ruiz-Granados, Y. G., De La Cruz-Torres, V., and Sampedro, J. G. (2019). The oligomeric state of the plasma membrane H+-ATPase from *Kluyveromyces Lactis*. *Molecules* 24:958. doi: 10.3390/molecules24050958

Schroeder, J. I., Raschke, K., and Neher, E. (1987). Voltage dependence of K+ channels in guard-cell protoplasts. *Proc. Natl. Acad. Sci. U. S. A.* 84, 4108–4112. doi: 10.1073/pnas.84.12.4108

Sharkey, T. D., and Raschke, K. (1981). Effect of light quality on stomatal opening in leaves of *xanthium Strumarium* L. *Plant Physiol.* 68, 1170–1174. doi: 10.1104/pp.68.5.1170

Shimazaki, K., Doi, M., Assmann, S. M., and Kinoshita, T. (2007). Light regulation of stomatal movement. *Annu. Rev. Plant Biol.* 58, 219–247. doi: 10.1146/annurev.arplant.57.032905.105434

Shimazaki, K., Iino, M., and Zeiger, E. (1986). Blue light-dependent proton extrusion by guard-cell protoplasts of *Vicia-Faba*. *Nature* 319, 324–326. doi: 10.1038/319324a0

Spartz, A. K., Ren, H., Park, M. Y., Grandt, K. N., Lee, S. H., Murphy, A. S., et al. (2014). SAUR inhibition of PP2C-D phosphatases activates plasma membrane H+-ATPases to promote cell expansion in *Arabidopsis*. *Plant Cell* 26, 2129–2142. doi: 10.1105/tpc.114.126037

Suetsugu, N., Takami, T., Ebisu, Y., Watanabe, H., Iiboshi, C., Doi, M., et al. (2014). Guard cell chloroplasts are essential for blue light-dependent stomatal opening in *Arabidopsis*. *PLoS One* 9:e108374. doi: 10.1371/journal.pone.0108374

Sugano, S., Shimada, T., Imai, Y., Okawa, K., Tamai, A., Mori, M., et al. (2010). Stomagen positively regulates stomatal density in *Arabidopsis*. *Nature* 463, 241–244. doi: 10.1038/nature08682

Sussman, M. R. (1994). Molecular analysis of proteins in the plant plasma membrane. *Annu. Rev. Plant Physiol. Plant Mol. Biol.* 45, 211–234. doi: 10.1146/annurev.pp.45.060194.001235

Sze, H., Li, X., and Palmgren, M. G. (1999). Energization of plant cell membranes by H+-pumping. *Plant Cell* 11, 677–689. doi: 10.1105/tpc.11.4.677

Takahashi, K., Hayashi, K., and Kinoshita, T. (2012). Auxin activates the plasma membrane H+-ATPase by phosphorylation during hypocotyl elongation in *Arabidopsis thaliana*. *Plant Physiol.* 159, 632–641. doi: 10.1104/pp.112.196428

Takemiya, A., Kinoshita, T., Asanuma, M., and Shimazaki, K. I. (2006). Protein phosphatase 1 positively regulates stomatal opening in response to blue light in *Vicia faba*. *Proc. Natl. Acad. Sci. U.S.A.* 103, 13549–13554. doi: 10.1073/pnas.0602503103

Takemiya, A., Sugiyama, N., Fujimoto, H., Tsutsumi, T., Yamauchi, S., Hiyama, A., et al. (2013). Phosphorylation of BLUS1 kinase by phototropins is a primary step in stomatal opening. *Nat. Commun.* 4:2094. doi: 10.1038/ncomms3094

Tanaka, Y., Sugano, S., Shimada, T., and Hara-Nishimura, I. (2013). Enhancement of leaf photosynthetic capacity through increased stomatal density in *Arabidopsis*. *New Phytol.* 198, 757–764. doi: 10.1111/nph.12186

Toda, Y., Wang, Y., Takahashi, A., Kawai, Y., Tada, Y., Yamaji, N., et al. (2016). *Oryza Sativa* H+-ATPase (OSA) is involved in the regulation of dumbbell-shaped guard cells of Rice. *Plant Cell Physiol.* 57, 1220–1230. doi: 10.1093/pcp/pcw070

Toh, S., Inoue, S., Toda, Y., Yuki, T., Suzuki, K., Hamamoto, S., et al. (2018). Identification and characterization of compounds that affect stomatal movements. *Plant Cell Physiol.* 59, 1568–1580. doi: 10.1093/pcp/pcy061

Tominaga, M., Kinoshita, T., and Shimazaki, K. (2001). Guard-cell chloroplasts provide ATP required for H+ pumping in the plasma membrane and stomatal opening. *Plant Cell Physiol.* 42, 795–802. doi: 10.1093/pcp/pce101

Wang, Y., Noguchi, K., Ono, N., Inoue, S., Terashima, I., and Kinoshita, T. (2014a). Overexpression of plasma membrane H+-ATPase in guard cells promotes light-induced stomatal opening and enhances plant growth. *Proc. Natl. Acad. Sci. U. S. A.* 111, 533–538. doi: 10.1073/pnas.1305438111

Wang, Y., Noguchi, K., and Terashima, I. (2011). Photosynthesis-dependent and -independent responses of stomata to blue, red and green monochromatic light: differences between the normally oriented and inverted leaves of sunflower. *Plant Cell Physiol.* 52, 479–489. doi: 10.1093/pcp/pcr005

Wang, Y., Shimazaki, K., and Kinoshita, T. (2014b). Multiple roles of the plasma membrane H+-ATPase and its regulation. *Enzymes* 35, 191–211. doi: 10.1016/B978-0-12-801922-1.00008-7

Woolston, C. (2014). Rice. *Nature* 514:49. doi: 10.1038/514s49a

Xu, G., Fan, X., and Miller, A. (2012). Plant nitrogen assimilation and use efficiency. *Annu. Rev. Plant Biol.* 63, 153–182. doi: 10.1146/annurev-arplant-042811-105532

Yang, Y., Costa, A., Leonhardt, N., Siegel, R., and Schroeder, J. (2008). Isolation of a strong *Arabidopsis* guard cell promoter and its potential as a research tool. *Plant Methods* 4:6. doi: 10.1186/1746-4811-4-6

Yoon, H., Kang, Y., Chang, Y., and Kim, J. (2019). Effects of zerovalent iron nanoparticles on photosynthesis and biochemical adaptation of soil-grown *Arabidopsis thaliana*. *Nano* 9:1543. doi: 10.3390/nano9111543

Young, J. C., DeWitt, N. D., and Sussman, M. R. (1998). A transgene encoding a plasma membrane H+-ATPase that confers acid resistance in *Arabidopsis thaliana* seedlings. *Genetics* 149, 501–507. doi: 10.1093/genetics/149.2.501

Zeiger, E. (1983). The biology of stomatal guard-cells. *Annu. Rev. Plant Physiol.* 34, 441–475. doi: 10.1146/annurev.pp.34.060183.002301

Zhang, M., Wang, Y., Chen, X., Xu, F., Ding, M., Ye, W., et al. (2021). Plasma membrane H+-ATPase overexpression increases rice yield via simultaneous enhancement of nutrient uptake and photosynthesis. *Nat. Commun.* 12:735. doi: 10.1038/s41467-021-20964-4

Zhu, C., Yang, N., Ma, X., Li, G., Qian, M., Ng, D., et al. (2015). Plasma membrane H+-ATPase is involved in methyl jasmonate-induced root hair formation in lettuce (*Lactuca sativa* L.) seedlings. *Plant Cell Rep.* 34, 1025–1036. doi: 10.1007/s00299-015-1762-4

Conflict of Interest: The authors declare that the research was conducted in the absence of any commercial or financial relationships that could be construed as a potential conflict of interest.

Publisher's Note: All claims expressed in this article are solely those of the authors and do not necessarily represent those of their affiliated organizations, or those of the publisher, the editors and the reviewers. Any product that may be evaluated in this article, or claim that may be made by its manufacturer, is not guaranteed or endorsed by the publisher.

Advantages of publishing in Frontiers

OPEN ACCESS
Articles are free to read for greatest visibility and readership

FAST PUBLICATION
Around 90 days from submission to decision

HIGH QUALITY PEER-REVIEW
Rigorous, collaborative, and constructive peer-review

TRANSPARENT PEER-REVIEW
Editors and reviewers acknowledged by name on published articles

Frontiers
Avenue du Tribunal-Fédéral 34
1005 Lausanne | Switzerland

Visit us: www.frontiersin.org
Contact us: frontiersin.org/about/contact

REPRODUCIBILITY OF RESEARCH
Support open data and methods to enhance research reproducibility

DIGITAL PUBLISHING
Articles designed for optimal readership across devices

FOLLOW US
@frontiersin

IMPACT METRICS
Advanced article metrics track visibility across digital media

EXTENSIVE PROMOTION
Marketing and promotion of impactful research

LOOP RESEARCH NETWORK
Our network increases your article's readership